Behaviour and Design of Structures using Thin-Walled Cold-Formed Sections

by

Spiridione Buhagiar

A thesis submitted for the degree of Doctor of Philosophy
In the Faculty of Engineering of the University of London

Engineering Structures Section

Civil Engineering Department

Imperial College of Science, Technology and Medicine

University of London

June 1993

BIBL. LONDEN. UNIV.

To

Denise

and

our children

Kenneth and *Kristina*

Behaviour and Design of Structures using Thin-Walled Cold-Formed Sections



ABSTRACT

Cold formed steel sections have usually been used by the construction industry as secondary members e.g. sheeting, decking and purlins. In recent years several attempts have been made to manufacture pre-engineered structural systems using only cold-formed sections. This thesis is concerned with the overall and local behaviour of a novel form of space frame structure constructed entirely of thin-wall cold-formed channel sections and tubes.

In order to obtain a better understanding of the complex behaviour of this system using doubly lipped channel sections a program of experiments on full size frames and individual components was undertaken. In addition to this a series of numerical solutions were obtained by using a non-linear elasto-plastic finite element program for both critical buckling and the ultimate capacity of doubly lipped channel sections.

New and modified design methods based on the experimental and numerical results and on theoretical investigations of the various buckling phenomena encountered are proposed for the following:

(a) *Lip buckling (Deformational buckling);* Not presently treated in BS 5950: Part 5 (1987). A design model for predicting the ultimate axial or bending capacity is given.

(b) *Torsional flexural buckling of singly symmetric sections;* A new approach to predicting the ultimate compressive resistance based on small displacement theory is presented.

(c) *Lateral torsional buckling of a singly symmetric section bent about the minor axis;* This form of failure is not considered in any code of practice. Numerical and theoretical analysis shows that failure in this mode is possible. Design recommendations for predicting the ultimate bending capacity are given.

(d) *Beam/Column interactive buckling including the effects of torsional flexural buckling;* Not presently accounted for in the British standard. Design recommendations based on a numerical parametric study are made for members subject to combined torsional-flexural and lateral-torsional buckling, and torsional-flexural buckling and bending.

(e) *Web crippling;* modifications are proposed to existing design formulations for non uniform local loading in the presence of biaxial bending and axial compression.

(f) *Connection design;* modifications are given to the current treatment of bearing in connected parts, bolt forces and washer plate moment.

Most of the design recommendations presented are applicable to any structure utilizing doubly lipped channel sections.

ACKNOWLEDGEMENTS

I would like to start by thanking my wife Denise for her patience and understanding. Words cannot begin to express my real gratitude to her. In addition I would also like to express my deep gratitude to my parents who have always supported me in everything I have done. Thanks also go to Denise's parents. Were it not for the continual support and encouragement given to me by these people I would not have achieved so much, and I am sure they will derive as much joy from this achievement as I shall.

The work presented in this thesis was supervised by Professor John C. Chapman and Professor Patrick J. Dowling in the Civil Engineering Department of Imperial College. I am deeply grateful to Professor Chapman for the many hours spent in fruitful discussion, for his expert advice and his unrelenting commitment to this research project. I would also like to express my sincere gratitude to Professor Dowling, Head of the Civil Engineering for his kind support and constant encouragement throughout the duration of my studies.

Words of thanks also go to Professor Roger E. Hobbs, Head of the Structures Section. My sincere gratitude also goes to Dr Marios Chryssanthopoulos for his warm friendship.

Sincere thanks also go to Dr Alex Torpiano, Head of the Building and Civil Engineering Department of the Faculty of Architecture and Civil Engineering, University of Malta for all his support and understanding during my absence from the Department.

The work presented in this thesis, as well as my attendance to the 10th and 11th Specialty Conferences held in St. Louis, Missouri, was made possible through the financial support of the following organizations:

- The Association of Commonwealth Universities in the United Kingdom
- The University of Malta

- Conder Group Plc
- Chapman Dowling Associates
- The Royal Academy of Engineers
- The Department of Civil Engineering, Imperial College

Their support is gratefully acknowledged.

Other members of staff who I would like to thank are Sue Wright, Fionnuala Donovan, Colin Kerr, George Scopes, Clive Hargreaves, Andrew Chipling, Richard Packer (for producing the numerous photographs presented in this thesis), the library staff Kay Crooks and Sussannah Parry, and Elizabeth Sandland the departmental computing officer, for accommodating my rather large computational requirements.

Word of thanks also go to all the lab staff; Tony Boxall, Jack Neale, Joe Finn, (the late) Bob Phillpot, Ron Day, Alex Laidlaw, James Mullord, Alan Roberts, and especially to Ron Millward for all his patience and dedication. Thank you all for making my stay in the structures lab an enjoyable one.

At Imperial, I was fortunate to have had the company of many colleagues, all from very different ethnic backgrounds. Their friendship over the past few years has enabled me to look at life with a much wider perspective. I would particularly like to thank my colleagues in Room 429, my fellow countryman Dr Marc Bonello, Fadi Hamdan, Gili Shanit, and Dr Navil Shetty for making my stay a memorable one. Special thanks go to Frederick Tsui for extending the capabilities of FINASIC.

Other colleagues of the structures section who deserve a word of thanks for their friendship are Dr Vangelis Vassilikos, Dr Kim Ki Du, Harsha Subbarao, Mark Manzocchi, Tatjana Micic, Dr Khurram Wadee, Pariatmono and Dr Bao Ruiquing.

I would also like to thank Dr Ray Vella and his wife Lucienne for all their help during my stay in London.

A final word of thanks goes to my children Kenneth and Kristina, I hope that you will someday understand why I had to be away from home.

CONTENTS

ABSTRACT iv

ACKNOWLEDGEMENTS v

CONTENTS vii

NOTATION xiii

Chapter One
INTRODUCTION

1.1 Preamble 1-1
1.2 Cold Formed Sections 1-1
1.3 An Overview of Research and Design Code Development 1-2
1.4 A Space Frame System using Cold Formed Sections 1-3
1.5 Structural Behaviour 1-6
1.6 Design of Section 1-6
1.7 The Approach Adopted 1-7

Chapter Two
FRAME ANALYSIS

2.1 İntroduction 2-1
2.2 Numerical Analysis 2-1
2.2.1 Pin Jointed Frame Analysis 2-3
2.2.2 Frame Analysis with Eccentricity and Continuity 2-4
2.2.3 Comparison Between Numerical and Experimental Results 2-10
2.3 Effective Length of Continuous Members 2-12
2.4 Conclusions 2-15

Chapter Three

FRAME TESTS

3.1 Introduction 3-1

3.2 Test Arrangement 3-2

3.3 Instrumentation 3-10

3.4 Material Tests 3-10

3.5 Experimental Procedure 3-12

3.6 Experimental Behaviour 3-13

3.6.1 Tests 1a-1b 3-13

3.6.2 Tests 2a-2c 3-17

3.6.3 Tests 3a-3e 3-21

3.6.4 Tests 4a-4c 3-25

3.6.5 Tests 5a-5d 3-27

3.6.6 Tests 6a-6c 3-29

3.6.7 Tests 7a-7d 3-31

3.6.8 Summary of Tests Results. 3-35

3.7 Conclusions 3-38

Chapter Four

COMPRESSIVE BUCKLING OF SECTION ELEMENTS

4.1 Introduction 4-1

4.2 Critical Buckling of Section Elements 4-2

Method (A) 4-4

Method (B) 4-4

Method (C) 4-6

4.2.1 Finite Element Analysis of Doubly Lipped Channel Sections 4-6

4.3 Post-Buckling Capacity of Plate Elements in Compression 4-9

4.4 Ultimate Local Buckling Capacity of Doubly Lipped Channel Sections 4-13

4.4.1 Experimental Investigation 4-14

4.4.2 Non-Linear Elasto-Plastic Finite Element Analysis 4-16

4.4.3 Comparison of Current Design Recommendations with Experimental and Numerical Results 4-18

4.5 Conclusions 4-19

Chapter Five

LIP BUCKLING OF DOUBLY LIPPED CHANNELS

5.1 Introduction 5-1

5.2 Critical Lip Buckling 5-3

5.2.1 Buckling of Doubly Lipped Channel 5-4

5.2.2 Finite Element Analysis of Doubly Lipped Channel 5-8

5.3 Lip Buckling Resistance 5-12

5.3.1 Buckling Resistance of Doubly Lipped Channel 5-12

5.3.2 Non-Linear Finite Element Analysis of Doubly Lipped Channel 5-14

5.3.3 Experiments 5-20

5.3.4 Comparison Between Experiments and Various Methods of Design 5-24

5.4 Proposed Design Model 5-25

5.5 Conclusions 5-26

Chapter Six

FLEXURAL BUCKLING OF AXIALLY LOADED DOUBLY LIPPED CHANNELS AND TUBES

6.1 Introduction 6-1

6.2 Critical Flexural Buckling 6-2

6.2.1 Finite Element Analysis of Doubly Lipped Channel 6-3

6.3 Flexural Buckling Resistance of Imperfect Channel Members 6-6

6.3.1 The Perry Formulation 6-6

6.3.2 Buckling Resistance of Singly Symmetric Sections 6-8

6.3.3 Buckling Resistance of Doubly Lipped Channels in the Presence of Local and Lip Buckling 6-10

6.3.4 Non-Linear Elasto-Plastic Finite Element Analysis of Imperfect Doubly Lipped Channels 6-13

6.3.5 Experiments 6-19

6.3.6 Comparison Between Experiments and Various Design Methods 6-23

6.4 Proposed Design Model for Singly Symmetric Channels 6-26

6.5 Flexural Buckling Resistance of Imperfect Tubular Members 6-26

Overall Buckling Check 6-28

Chapter Six (cont)

FLEXURAL BUCKLING OF AXIALLY LOADED DOUBLY LIPPED CHANNELS AND TUBES

Local Capacity Check 6-30

6.5.1 Experiments 6-31

6.5.2 Comparison Between Experiments and Various Design Methods 6-33

6.6 Proposed Design Model for Tubular Diagonals 6-34

6.7 Conclusions 6-35

Chapter Seven

TORSIONAL-FLEXURAL BUCKLING OF DOUBLY LIPPED CHANNELS

7.1 Introduction 7-1

7.2 Critical Torsional and Torsional-Flexural Buckling 7-2

7.2.1 Governing Equations for Torsional-Flexural Buckling 7-3

7.2.2 Critical Buckling of An I-Section 7-5

7.2.3 Critical Buckling of Doubly Lipped Channels 7-7

7.2.4 Shear Centre and Warping Constant 7-9

7.2.5 Finite Element Critical Buckling Analysis of Double Lipped Channel. 7-12

7.3 Ultimate Torsional-Flexural Buckling Resistance 7-14

7.3.1 Torsional Buckling of Imperfect Doubly Symmetric Sections 7-15

7.3.2 Torsional-Flexural Buckling of Imperfect Doubly Lipped Channel Sections 7-20

7.3.3 Non-Linear Elasto-Plastic Analysis of Imperfect Members 7-30

7.3.4 Experimental Behaviour 7-34

7.3.5 Effect Of Warping Restraint on The Ultimate Torsional-Flexural Buckling Resistance . 7-36

Kw for Connection Torsional Stiffness 7-37

Kw for Continuous Members With End Warping Restraint 7-42

Kw for Combined Connection Torsional Stiffness and End Warping Restraint 7-42

7.5 Proposed Design Method 7-43

7.5.1 Comparison Between Experiments and Current and Proposed Design Methods 7-44

7.6 Conclusions 7-46

Chapter Eight

LATERAL-TORSIONAL BUCKLING OF DOUBLY LIPPED CHANNELS

8.1 Introduction 8-1

8.2 Critical Lateral-Torsional Buckling 8-3

8.2.1 Critical Buckling of Doubly Symmetric Sections 8-3

8.2.2 Critical Buckling of Doubly Lipped Channels 8-8

8.2.3 Finite Element Buckling Analysis of Doubly Lipped Channel. 8-16

8.3 Lateral-Torsional Buckling Resistance of Imperfect Members 8-18

8.3.1 Buckling Resistance of Imperfect Doubly Symmetric Sections 8-18

8.3.2 Buckling Resistance of Imperfect Doubly Lipped Channels 8-23

8.3.3 Non-Linear Elasto-Plastic Finite Element Analysis of Doubly Lipped Channels 8-28

8.4 Proposed Design Method 8-35

8.4.1 Critical Lateral-Torsional Buckling 8-35

8.4.2 Minor Axis Lateral-Torsional Buckling Resistance 8-36

8.5 Conclusions 8-39

Chapter Nine

INTERACTION BETWEEN AXIAL FORCE AND MINOR AXIS BENDING

9.1 Introduction 9-1

9.2 Combined Bending and Compression 9-2

9.2.1 Local Capacity Check 9-3

9.2.2 Overall Buckling Check 9-3

9.3 Non-Linear, Elasto-Plastic Finite Element Analysis Of Double Lipped Channels 9-7

9.4 Proposed Design Method 9-10

Members Subject to Torsional-Flexural Buckling and Bending Causing Lip Tension. 9-11

Members Subject to Torsional-Flexural and Lateral-Torsional Buckling Causing Lip Compression. 9-12

9.5 Comparison Between the Proposed Design Method and Experiments 9-13

9.6 Conclusions 9-16

Chapter Ten
CONNECTION DESIGN

10.1 Introduction **10-1**
10.2 Web Crippling of Channel Sections **10-2**
10.2.1 Unreinforced Connection **10-4**
10.2.2 Connection with Reinforcing Sleeves **10-8**
10.2.3 Experiments **10-11**
10.2.4 Proposed Design Method for Combined Web Crippling and Bending **10-18**
10.3 Bearing Strength of Connected Elements **10-19**
10.3.1 Experiments **10-20**
10.3.2 Comparison Between Experiments and Design Methods **10-30**
10.3.3 Proposed Design Method **10-32**
10.4 Bolt and Washer Plate Design **10-32**
10.4.1 Transfer of Forces **10-32**
10.4.2 Joint Model for Bolt Design **10-34**
10.4.3 Joint Model for Washer Plate Design **10-39**
10.4.4 Experiments **10-40**
10.4.5 Proposed Design Method **10-45**
Bolts Subjected to Combined Tension And Shear **10-45**
Washer Plate Bending **10-46**
10.5 Conclusions **10-46**

Chapter Eleven
GENERAL COMMENTS AND CONCLUSIONS **11-1**

REFERENCES **R-1**

Appendix A
Description of the Finite Element Program Finasic, the Elements used and the Initial Convergence Study. **A-1**

Appendix B
The Differential Equations of Static Equilibrium **B-1**

Appendix C
End Bearing Test Results **C-1**

NOTATION

The following notation is used in this thesis. Usually, only one meaning is assigned to each symbol, but in those cases where more meanings than one are possible, then the correct one will be evident from the context in which it is used. Other symbols not listed are defined in the main text.

A	area of cross section
A_b	shank area of bolt
A_{eff}	effective area
A_L	effective area of lip
A_t	tensile area of bolt
B	breadth to mid thickness
B_L	breadth of lip to mid thickness
B_w	breadth of washer plate
b	width of plate
b_{eff}	effective width of plate
C_b	equivalent moment coefficient
C_w	warping constant
c	the distance from the end of the member to the load or reaction
D	depth to mid thickness
D_c	length of diagonal tab crease in top chord connection
D_{eff}	effective depth of web
D_L	depth of lip to mid thickness
D_s	length of supported diagonal tab crease in top chord connection
d	bolt diameter
d_e	end distance measured from centre of bolt hole
E	modulus of elasticity (205 kN/mm^2)
$e\%$	percentage elongation of material at failure

e_B	top chord tab eccentricity
e_c	the distance between the gross and effective neutral
e_H	the distance between the centroid of the section and the mid plane of the connection
e_{LU}, e_{LD}	the distance between the intersection point of the diagonals and the centroidal axes of the lips up and lips down top chord members
F	lip disturbing force
G	shear modulus (78.8 kN/mm^2)
H	distance between the mid thickness of the table and the centroid of the lip
I	moment of inertia
I_L	second moment of area of lip about a vertical axis
I_s	second moment of lip stiffener
I_y, I_z	second moment of area about Y and Z axes
J	St. Venant torsion constant
K	plate buckling coefficient, or bearing constant (0.78)
K_B	buckling coefficient of table
K_{BF}	buckling coefficient of table obtained numerically
K_{BL}	buckling coefficient of lip table
K_c	connection torsional stiffness
K_{cr}	crippling constant
K_D	buckling coefficient of web
K_{DL}	buckling coefficient of lip downturn
K_M	flexural stiffness of member
K_R	stiffness of elastic end restraint
K_T	warping stiffness of cross section
K_w	warping restraint factor
k	$\sigma_d/_{228}$, in which σ_d is the design stress
L	length of member
L_B	minimum critical lip buckling half wave length, or the distance between bolts
L_c	the distance between diagonal creases measured at mid thickness of the tab
L_{cr}	critical lip buckling halfwave length
L_{eff}	effective length of member
L_R	the distance between effective restraints, or the distance between reactions

L_T	distance between bolts
L_w	the length of the washer plate
ℓ	lip halfwave length of buckling
M	applied bending moment
$\overline{M}$	equivalent moment
M_{Bx}, M_{By}	are the lateral-torsional buckling capacities of the section to cause first yield
M_{ec}	elastic bending capacity of the crease in the presence of axial load
M_{LT}	critical lateral-torsional buckling moment
M_{LTy},M_{LTz}	critical lateral-torsional buckling moments about Y and Z axes
M_o	the moment capacity of a fully effective section
M_{oy}, M_{oz}	the moment capacity of a fully effective section about the Y and Z axes
M_p	plastic moment capacity
M_u	the moment capacity of the section at first yield
M_{uy},M_{uz}	are the moment capacities of the section about the Y and Z axes at first yield
M_y, M_z	applied moments about Y and Z axes
m	number of half waves along the length of the member
N	is the patch length of stiff bearing (L_w/3)
P	applied axial force
P_B	the bolt force (the lesser of the shear capacity of the bolt or the bearing capacity of the thinner ply
P_{bs}	bearing strength
P_{crF}	critical buckling resistance obtained numerically
P_{cs}	the short strut capacity of the section
P_D	diagonal force
P_{Dmax}	maximum diagonal force in a connection
P_E	Euler critical buckling load
P_{exp}	component failure load
P_{Ey},P_{Ez}	Euler buckling load about Y and Z axes
P_{JK}	central jack load
P_o	squash load of fully effective section
P_{oF}	lip resistance at first surface yield obtained numerically
P_R	reaction between washer plate and table
P_T	critical torsional buckling load

P_{tb}	tensile force in bolt
P_{TEST}	frame failure load
P_{TF}	critical torsional-flexural buckling load
P_{TFY}	axial load to cause first yield due to torsional-flexural buckling
P_u	ultimate axial resistance
P_{uBS}	ultimate axial resistance given by BS 5950: Part 5: 1987
P_{uF}	ultimate axial load on member obtained numerically
P_{us}	the shear capacity of table
P_{usb}	shear capacity of bolt
P_{ut}	tensile capacity of bolt
P_{uw}, P_{uw}'	the crippling capacity in the absence of bending moments
P_w	the patch load
P_{wc}	patch load on channel
P_{ws}	patch load on sleeve insert
P_Y	axial load to cause first yield caused by flexural buckling
Q	the ratio of the effective area to the gross area of the section
R	radius of curvature
r	radius of gyration, or the inside bend radius ($r/t \leq 6$)
r_L	radius of gyration of lip about a vertical axis
r_o	polar radius of gyration about the shear centre
r_y, r_z	radius of gyration about Y and Z axes
t, t_s	thickness of section
t_w	thickness of washer plate
u	longitudinal displacement
V	vertical force
V_c	vertical force in the web of a channel
V_s	the vertical force on sleeve
V_u	ultimate vertical force
V_{wk}	vertical force at working load ($V_{wk} = 2/3\, V_u$)
v	horizontal displacement
v_l	additional horizontal displacement
$v_{l\theta}$	additional horizontal displacement due to rotation about shear centre
v_{lT}	additional horizontal displacement of the shear centre
v_{max}	maximum horizontal displacement
v_o	initial horizontal displacement
v_{oL}	initial horizontal imperfection of lip

v_θ	lateral displacement due to rotation about shear centre
$v_{\theta o}$	initial horizontal displacement due to rotation about the shear centre
v_T	horizontal translation of shear centre
v_{To}	initial horizontal displacement of shear centre
w	vertical displacement
w_1	additional vertical displacement
w_{max}	maximum vertical displacement
w_o	initial out-of-plane displacement
w_{ov}	initial overall vertical imperfection of member
y_o, z_o	shear centre co-ordinates with respect to CG
$\bar{y}$	the greater distance from the vertical lip centroidal axis to the vertical surface of the lip, or the greater distance from the NA position of a section to the outer most fibre
Z_ℓ, Z_t	section modulii at lip and table
Z_p	plastic section modulus
Z_y	section modulus about Y axis
$\bar{z}_\ell$	distance between neutral axis and mid thickness of lip table
$\bar{z}_{max}$	distance from neutral axis to outermost fibre in the Z plane
$\bar{z}_{sc}$	distance between shear centre and mid-thickness of table element
$\bar{z}_t$	distance between neutral axis and mid thickness of table.
α	geometric constant, or the angle between the diagonal and the top chord viewed, in plan.
β	foundation modulus based on transverse stiffness of cross section
β_y, β_z	Geometric properties of section
ε	axial strain
ε_{max}	maximum axial strain
ε_o	yield stain
ϕ	the angle between the diagonal and the bottom chord
γ_m	partial safety factor on yield stress (γ_m=1.1)
η	imperfection parameter
$\eta, \eta', \eta_{To}, \eta_{\theta o}$	imperfection constants
φ	the relative angle between the bottom and top chord creases
λ	slenderness ratio

ν	Poisson's ratio (0.3)
θ	is the angle between the plane of the web and the bearing surface
θ	rotation about shear centre
θ_1	additional rotation about longitudinal axis
θ_{max}	maximum rotation about the shear centre
θ_o	initial rotation about shear centre
ρ	critical stress ratio
σ	stress in longitudinal direction
σ_A	axial stress
σ_{av}	average stress on member
σ_B	bending stress which causes first yield
σ_{By}	bending stress about the Y axis which causes first yield
σ_{cr}	critical stress
σ_{crF}	critical buckling stress obtained numerically
σ_{crL}	elastic critical lip buckling stress
σ_d	design strength (the smaller of σ_{uL}, σ_o or 0.84 σ_u)
σ_E	Euler buckling stress
σ_{ed}	edge stress
σ_{exp}	failure stress obtained from experiments
σ_{Ey}, σ_{Ez}	Euler buckling stress about Y, and Z axes
σ_{LTy}, σ_{LTz}	critical lateral-torsional buckling stress about Y and Z axis
σ_o	yield stress of material
σ_{oF}	axial stress to cause first yield in lip obtained numerically
σ_T	torsional buckling stress
σ_{TF}	critical torsional-flexural buckling stress
σ_{TFY}	axial stress to cause first yield due to torsional-flexural buckling
σ_u	ultimate stress of material
σ_{uF}	ultimate stress of lip obtained from finite element analysis
σ_{uL}	ultimate lip buckling stress
σ_{uT}	ultimate stress in lip obtained from tests
σ_Y	average longitudinal stress which causes first yield
σ_{YF}	axial stress to cause first surface yield obtained numerically
ω_{av}	average warping constant

Chapter One

INTRODUCTION

1.1 PREAMBLE

The thesis describes the experimental, theoretical and numerical studies which were undertaken to enable a new space frame system to be designed with confidence, understanding and with reasonable economy. It was necessary to consider the behaviour and analysis of all members and connections, under the combinations of axial load and moment which would be encountered in practice. In general, the existing design codes did not include, or did not adequately treat, the required arrangements and force combinations.

The thesis is therefore unusual, in that the scope is rather wide, and as a consequence it was necessary to resist a natural inclination to pursue each topic to the extent which seemed desirable. Nevertheless several new insights, facts and methods have been achieved, and doors have been opened to the pursuit of further studies.

1.2 COLD-FORMED SECTIONS

Cold-formed steel sections have mostly been used by the construction industry as secondary members e.g. sheeting, decking and purlins. Cold-formed steel sections can be rolled from a relatively small stockpile of steel strip into a variety of shapes with consistent and accurate profile dimensions. The capital and production costs associated with this type of manufacture are relative low. In recent years there has been a trend towards the replacement of hot rolled main members by cold-formed steel component and several attempts have been made to manufacture pre-engineered structural systems using only cold-formed sections.

The design of cold-formed structures entails rather complex calculations to avoid various forms of instability associated with thin-walled open sections. Space frames typically consist of several thousand members and for a cold-formed system, computer aided design and analysis becomes essential for member and connection design as well as for frame analysis.

1.3 AN OVERVIEW OF RESEARCH AND DESIGN CODE DEVELOPMENT

Extensive experimental and analytical work into the structural behaviour of cold-formed sections has been carried out world wide. Research in North America has been carried out continuously since 1939 at Cornell University, where basic design methods for lateral buckling of beams, flexural buckling of thin-walled columns, torsional-flexural buckling of concentric and eccentric loaded columns, as well as the interaction of local and overall buckling were developed. The University of Missouri-Rolla, has also contributed to design development in the area of web crippling, bolted connections and limit state design.

The first edition of the American Iron and Steel Institute (AISI) specification for the design of cold-formed steel members was published in 1946. This AISI specification has subsequently had seven revisions, reflecting the results of continued research and technical development achieved during this period. This specification is used extensively, and has also served as a basis for design codes in many other countries. An informative explanation of the design philosophies adopted in the AISI recommendations is given by Yu(1991).

In Europe, research and development into the structural behaviour of cold-formed steel members, connections and structural systems has been actively conducted at many institutions. Research in the UK into the behaviour of cold-formed steel structures has been concentrated on the behaviour of top hat and singly lipped columns, purlin systems, bolted connections, members subject to combined loading, and most notably on the use of sheet cladding to brace industrial buildings. By the early 1950's a substantial amount of research development had taken place, and the first design proposals for a specification were put forward in 1951. However, it was to be some ten years before the first specification was published. Subsequently, a new British specification was published, Addendum No.1 to BS449 (1975) .

During recent years there has been a great deal of activity in many European countries to produce new cold-formed steel design specifications based on current research findings. In the UK the design and use of cold-formed steel structures in buildings is dealt with in BS 5950: Part 5 (1987), though the code is more strongly oriented towards secondary load carrying members as opposed to primary structural members. More recently the engineering community has seen the introduction of European recommendations for the design of steel structures ENV 1993-1-1 (1992). The design recommendations pertaining to the use of cold-formed steel structures EC3: Part 1.3 (1992) are still being drafted.

All these codes give design recommendations for the use of cold-formed steel sections in buildings subjected to:

(a) Local buckling
(b) Members in bending
(c) Members in axial compression/combined bending and axial compression
(d) Members in tension
(e) Members subject to web crippling/combined crippling and bending
(f) Connections

Because of the broad nature of the thesis no attempt to survey the comprehensive list of all research publications pertaining to cold-formed steel structures has been made, and only key publications directly relevant to the particular phenomenon being investigated are cited. Extensive literature surveys have been made by LaBoube (1986), Yu (1991) and Rhodes (1991).

1.4 A SPACE FRAME SYSTEM USING COLD FORMED SECTIONS

Space frames have long provided architects and engineers with a structural solution which combines simplicity of construction with inherent flexibility of plan shape and support arrangement. In the last decade space structures have influenced the architectural scene all over the world and have become an integral part of modern architecture and progressive engineering. In their search for new forms, architects and engineers have discovered that space structures not only offer them many structural advantages, but also produce striking simplicity of form, a pleasing appearance and frequently, unusual beauty.

Traditionally space frames are constructed from hot rolled tubing and special nodal connections which are usually patented and require specialised manufacturing equipment and high cost materials. All the members are connected concentrically to a special node as shown for example in Figure 1.1, to avoid joint moments. It is because of this that the members can be assumed to be pin jointed, and axial forces are the only action which need to be considered during the design process. The high cost of connections has resulted in space frames being used predominantly for "feature" buildings where the cost is not a prime consideration.

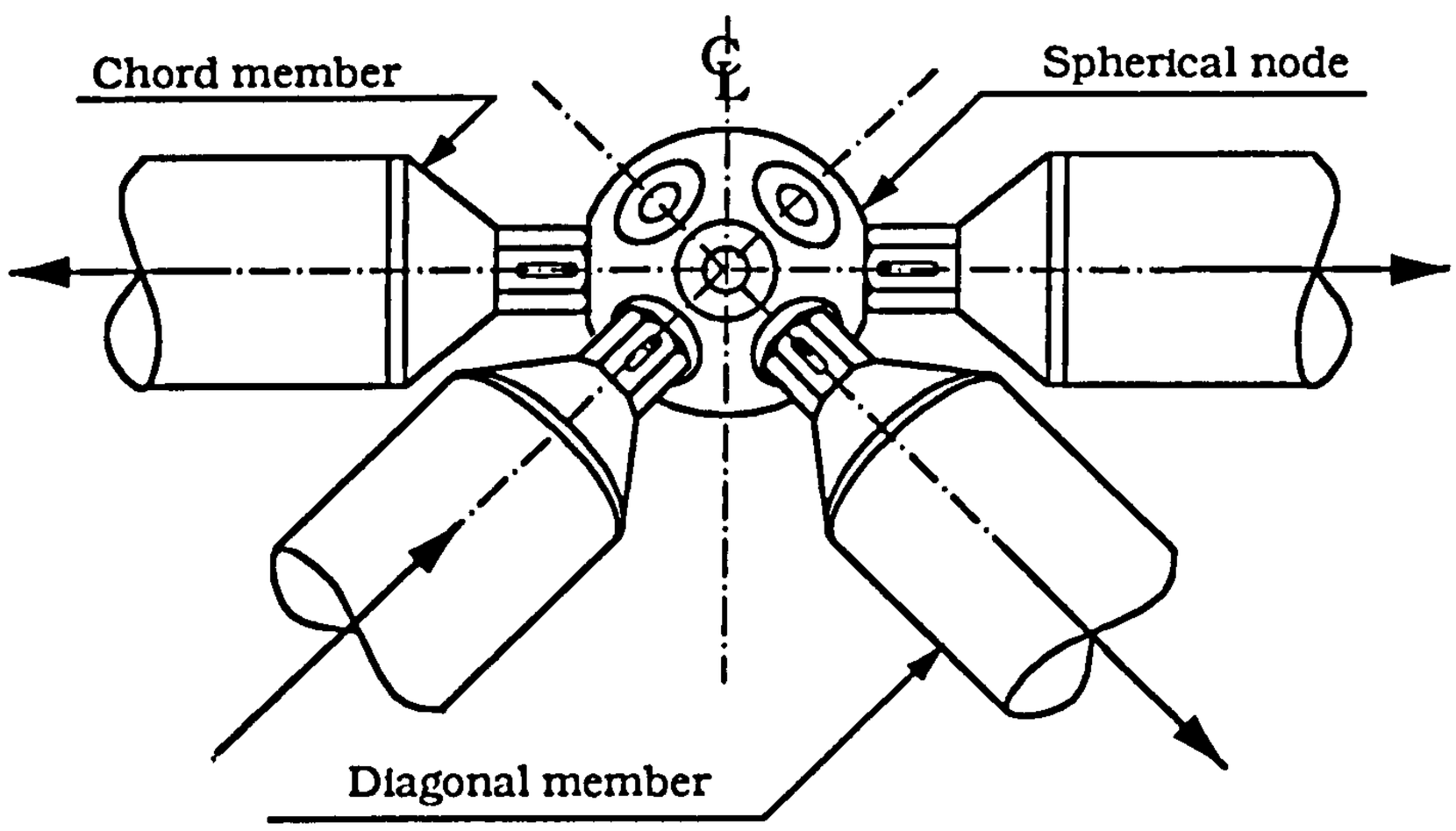


Figure 1.1 Pin jointed space frame connection

It is therefore a major objective in the design of space structures to reduce the cost per connection. This can be achieved by using cold-formed sections which are continuous across connections. The system studied in this thesis uses typically 12 metre lengths of channel for the chord members, which are manufactured from standard pre-galvanised cold-rolled steel strip, continuously cold-formed and if required, powder-coated on line. The diagonal members are made from standard circular hollow tubing with flattened ends pre-punched with a single hole, providing connection with the chord members. An architecturally neat connection is obtained by clamping and bolting the ends of the diagonals between the orthogonally intersecting back-to-back channel sections. A bottom chord and top chord connection for a diagonal on square frame is shown in Figure 1.2. Many structures using this system have been built in Australia and the Far East (Codd 1991).

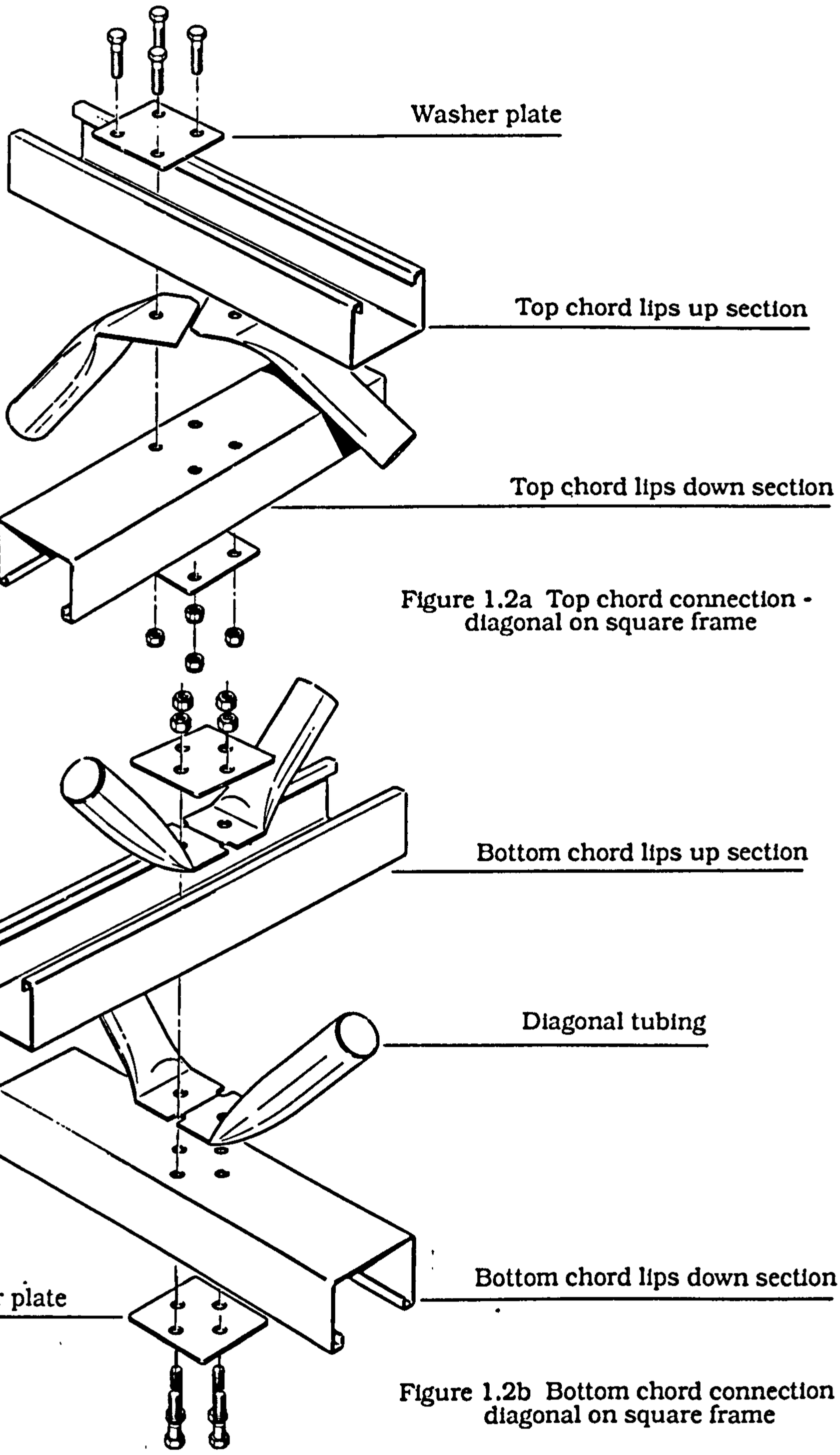


Figure 1.2a Top chord connection - diagonal on square frame

Figure 1.2b Bottom chord connection - diagonal on square frame

Figure 1.2 Top and bottom chord connections - diagonal on square frame

1.5 STRUCTURAL BEHAVIOUR

Though easily assembled, the joint configuration requires special attention early on in the design stage because of the eccentricity moments generated by this particular configuration. The intersection points of the diagonal members do not coincide with the centroids of the chords, and neither do the centroids of the chords in orthogonal directions coincide. As a result, moments are induced at the nodes, the magnitudes of which depend on the diagonal member forces and the relative eccentricities at the joint. These moments are not secondary moments in the usual sense as they do not arise only from changes in geometry of the structure, and they must therefore be taken into account in design. These moments are in general just as important as the axial forces. The continuity of the chords through the connection enables the eccentricity moments to be resisted, and a rather robust structure results.

The combination of axial loads and moments coupled with the cross-sectional geometry of the chord members gives rise to flexural and torsional-flexural instabilities. The joint configuration also subjects the diagonal members to combined axial loads and end moments caused by the unsupported portion of the tab. Analysis of this type of double layer space frame is particularly complex as several design checks are required for every connection and every member. It is only through the use of computers that this method of construction can be considered to be a practicable structural solution.

1.6 DESIGN OF SECTION

The cross-sectional dimensions of the channel sections used as chord members in a diagonal on square space frame were governed by several geometric and practical considerations which required providing for sufficient end distance for the diagonal tabs, bolt installation and maximising the section modulus and inertia to resist beam/column actions and lip buckling.

Making the channel wider increases the joint moments with a relatively modest increase in the bending resistance. Making the section deeper increases the joint moment but the increase on this account is less than the increase in bending resistance. It should be remarked that deeper sections are prone to lip buckling and have a reduced resistance to both local element and web crippling. Nevertheless, it

is useful to increase the depth of the section in respect of both strut buckling and bending moment resistance.

To provide a satisfactory section inertia and modulus, the lip should be as wide as possible. However the minimum bolt spacing is determined by the diagonal tab end distance and the lips must permit the shaft of the torque wrench to be positioned vertically above the bolt. These requirements led to a lip width of 20mm. In order for the lip table to remain stable it must be supported by a lip downturn. This downturn also improves the section properties. The maximum downturn is limited by the need to insert the bolts and sockets under the downturn, and by the painting process.

The depth of section chosen for the first structures in the UK was 100mm as this was the maximum depth that could be rolled by existing rolls. This depth also satisfied all the practical constraints associated with the type of joint configuration. For a typical span of 3000mm a section depth of 100mm gives a span to depth ratio of 30, which is fairly slender for a beam/column in which the thrust and moment are of approximately equal importance. The width of the section was determined by the tab end distance in the bottom chord connection, coupled with the need for a reasonable lip width. A narrower section reduces the moment, but restricts the end length of the diagonal tabs.

The external dimensions of the doubly lipped channel sections finally adopted for the experimental and numerical investigations presented in this thesis were: 125mm wide, 100mm deep, with a lip table 20mm wide and a lip downturn 20mm deep (Figure 3.2). The external dimensions of the channel section are kept constant throughout a structure while the thickness varies according to the forces and moments present. Diagonal sizes vary according to the forces.

1.7 THE APPROACH ADOPTED

It was apparent from the outset that BS5950: Part5 (1987) did not consider all the phenomena associated with the structural behaviour of the system being investigated. Clarification and/or modification of the following design criteria was felt to be necessary:

(a) Lip buckling (deformational buckling)

(b) Lateral torsional buckling about the minor axis

(c) Beam/Column interaction including torsional flexural buckling

(d) Web crippling combined with biaxial bending and axial compression

(e) Design of connections

Because of the exigency for devising interim design methods for this system frame and component tests were carried out in preference to conducting a literature search directed at the various phenomena listed above. Experiments were undertaken with the general intention of clarifying member behaviour by causing failure by each of the phenomena. This involved progressive strengthening to attain higher failure modes. In some cases the strengthening devices were also designed to have practical application.

The initial design methods were based on reasoning supported by tests. Subsequently, critical buckling, linear and non-linear finite element analyses were carried out to supplement the experimental data and also to gain a better physical appreciation of the various observed buckling phenomena. The overall force distributions for different test frame configurations discussed in Chapter Two were obtained using the general purpose finite element program LUSAS (1992). The local and overall critical buckling behaviour and the non-linear elasto-plastic behaviour of the doubly lipped channel section was investigated using the finite element programme FINASIC (1990), developed at Imperial College, described in Appendix A.

Refinement of the earlier interim design proposals, and various newly developed proposed design recommendations were made based on the theoretical, experimental and numerical investigations carried out on the various buckling and other phenomena. The design proposals were validated against the numerical and experimental data obtained.

Chapter Two

FRAME ANALYSIS

2.1 INTRODUCTION

Frame analysis programs have a facility whereby joint eccentricities can be taken into account. This is done by taking the global co-ordinates of the frame at the intersection points of the diagonal tubes, and the local member axes at the centroids of the chord sections. The analysis which has been used enables the member forces and moments to be determined according to the assumptions of linear analysis - namely that the displacements coupled with the axial forces are not sufficient to cause significant additional moments, i.e. PΔ moments can be neglected; also that the member stiffness, and hence the distribution of moments are not affected by the axial forces.

In this chapter the effects of frame geometry, member size, loading arrangement and joint eccentricity on the frame displacements and member forces will be discussed considering results obtained from a limited numerical study. Comparisons between experimental and numerical results are made. The later part of this chapter deals with the effects of member continuity on effective length. A method for determining the effective lengths for members in a continuous member is described.

2.2 NUMERICAL ANALYSIS

A series of finite element analyses were carried out to determine the overall behaviour of pin jointed and eccentrically jointed space frames using the general purpose finite element program LUSAS (1992). Two different frame geometries were analysed. These were the square on square and diagonal on square frames shown in Figures 2.1 and 2.2 which consisted of a 3 x 3 bay bottom grid, with an overall

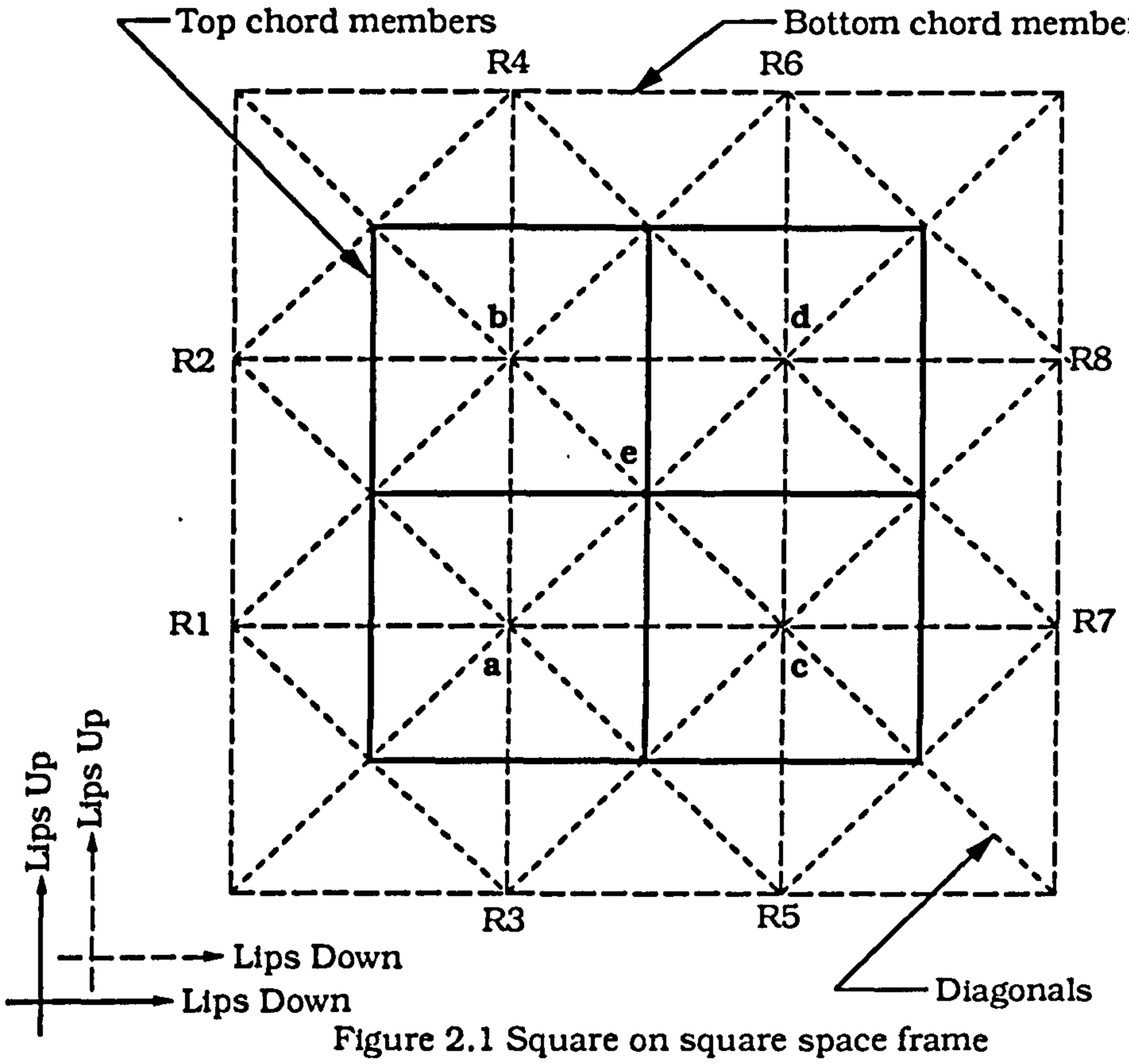


Figure 2.1 Square on square space frame

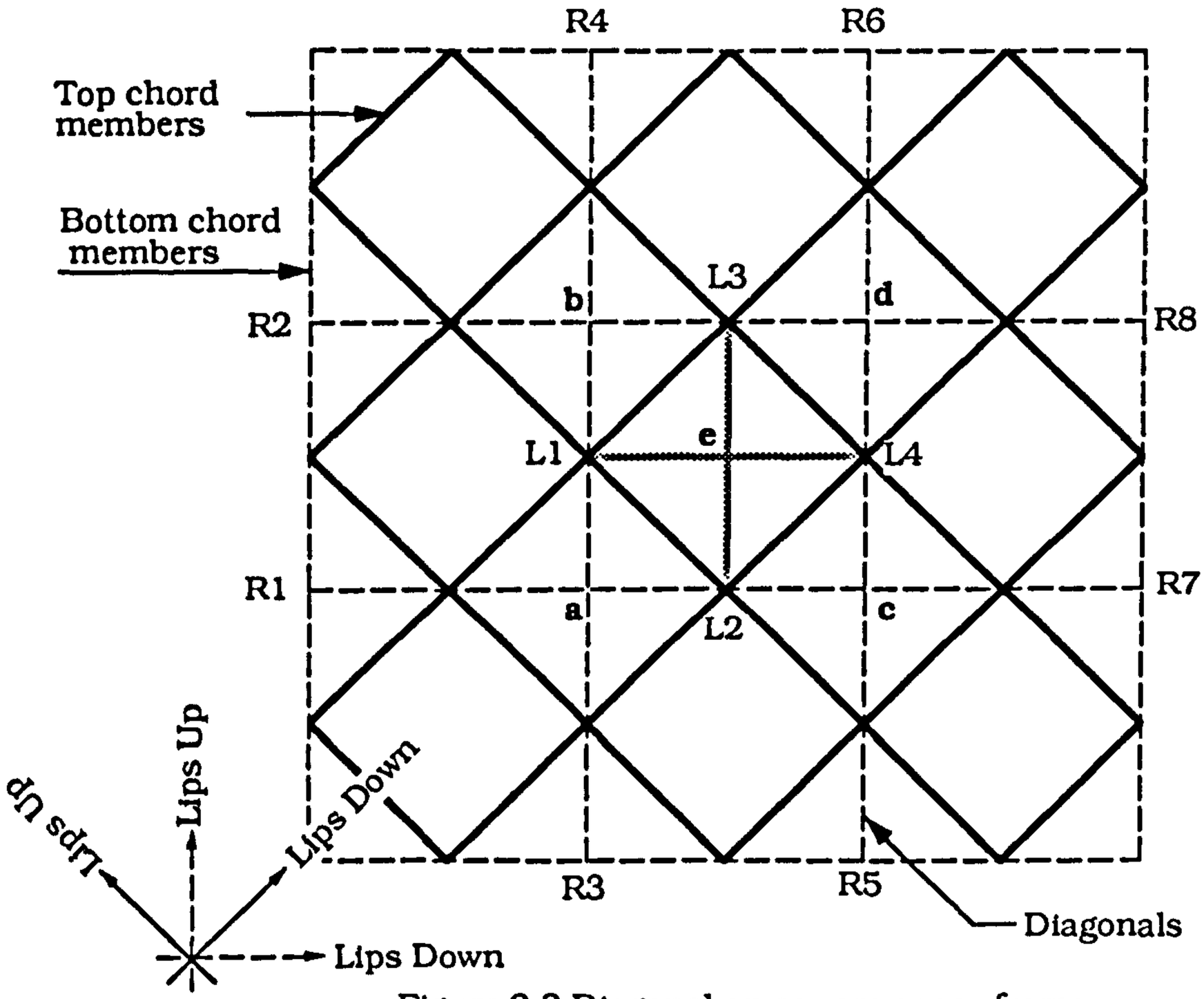


Figure 2.2 Diagonal on square space frame

(a,b,c,d) - Bottom chord connections, e - Top chord connections/cruciform

base dimension of 9000mm x 9000mm, and a frame depth between diagonal intersection points, of 1772mm. Both frames were centrally loaded in an upward direction and reacted at eight points around the perimeter of the frame. The reactions are denoted as R1 through to R8 in Figures 2.1 and 2.2. This particular loading arrangement was chosen as it represents a point of internal support in a large frame where high top and bottom chord forces due to a reversed moment are coupled with high diagonal forces. This situation is considered to be critical for the geometries considered.

The chord members were modelled with three dimensional beam elements of constant cross-section. Eccentric loading of the beam elements was permitted. The ends of each beam element were either pinned or continuous through the frame connection. It is important to note that the beam elements used in the analysis do not account for local buckling and warping effects. The diagonals consisted of bar elements.

The square on square frames were loaded by an upward force at the central node of the top chord. The diagonal on square frames were loaded either through a cruciform member, modelled with the same cross sectional properties as the one subsequently used during testing, or by four equal point loads located at the central nodes of the top grid. The points of load application are denoted as L1 through to L4 in Figures 2.1 and 2.2. The overall behaviour of square on square and of diagonal on square frames was investigated by systematically varying the thickness of the chords, the diameter and thickness of the diagonals and the location of the joint eccentricities in either the top or bottom chords, or both.

2.2.1 PIN JOINTED FRAME ANALYSIS

In order to demonstrate the effects of chord continuity the frames shown in Figures 2.1 and 2.2 were first analysed as pin jointed frames with various combinations of chord and diagonal members. Chord member intersections were assumed to occur at the intersection of the diagonal members. The vertical displacements of the bottom chord nodes located around the central bay of each frame (**a**,**b**,**c**,**d**), along with the maximum chord and diagonal forces are given in Table 2.1. The axial force distribution in the diagonal on square frame remains unchanged with variations in chord and diagonal cross-sectional properties; this is because the pin jointed system is statically determinate.

FRAME TYPE	LOAD TYPE	Chord Thickness	Diagonal	†Max Chd. force (kN)	††Max Diag. force (kN)	*Disp (mm)
FRM1-S/S	B	3.0	48.4 x 2.0	160.4	‡156.0	10.4
FRM2-D/S	A	1.5	48.4 x 2.0	127.0	65.5	12.7
FRM3-D/S	A	1.5	60.1 x 4.0	127.0	65.5	8.8
FRM4-D/S	A	3.0	48.4 x 2.0	127.0	65.5	9.6
FRM5-D/S	A	3.0	60.1 x 4.0	127.0	65.5	5.8

D/S - Diagonal on square S/S - Square on square A - Four 100kN point loads B- 400kN point load

* Displacements measured in central bay, bottom chord (points a, b, c, d see Figures 2.1 and 2.2)

† Central bay bottom chord †† Perimeter diagonal, ‡ Central diagonal

Table 2.1 Variation in member forces, and vertical displacement for pin jointed frames with different geometries obtained from numerical analysis (LUSAS 1992)

2.2.2 FRAME ANALYSIS WITH ECCENTRICITY AND CONTINUITY

The effects of joint eccentricity, chord continuity and member size on the member forces and displacements for the square on square and diagonal on square frames were also investigated numerically. The joint eccentricies used in the frame analyses were modelled on the joint configuration of Figure 2.3 which is described fully in Chapter One. The frame used in the numerical analysis consisted of 125x100x20x20-3.0mm thick double lipped channel sections for the chord members, and 48mm dia-2mm thick diagonal tubing. Joint eccentricities were first introduced in the bottom grid, then in the top grid and finally in both grids. The same loading arrangements used for the pin jointed frame analysis were again employed. The reaction and cruciform force distributions for different frame geometries, joint eccentricities and load arrangements are given in Table 2.2 and Figure 2.4.

If a square on square frame is eccentrically jointed in the bottom grid, the reactions are no longer equal, but are distributed symmetrically about the centre lines of the bottom grid, with the larger reactions located at the ends of the members with the smaller joint eccentricity. When the eccentric joints are located in the top grid the

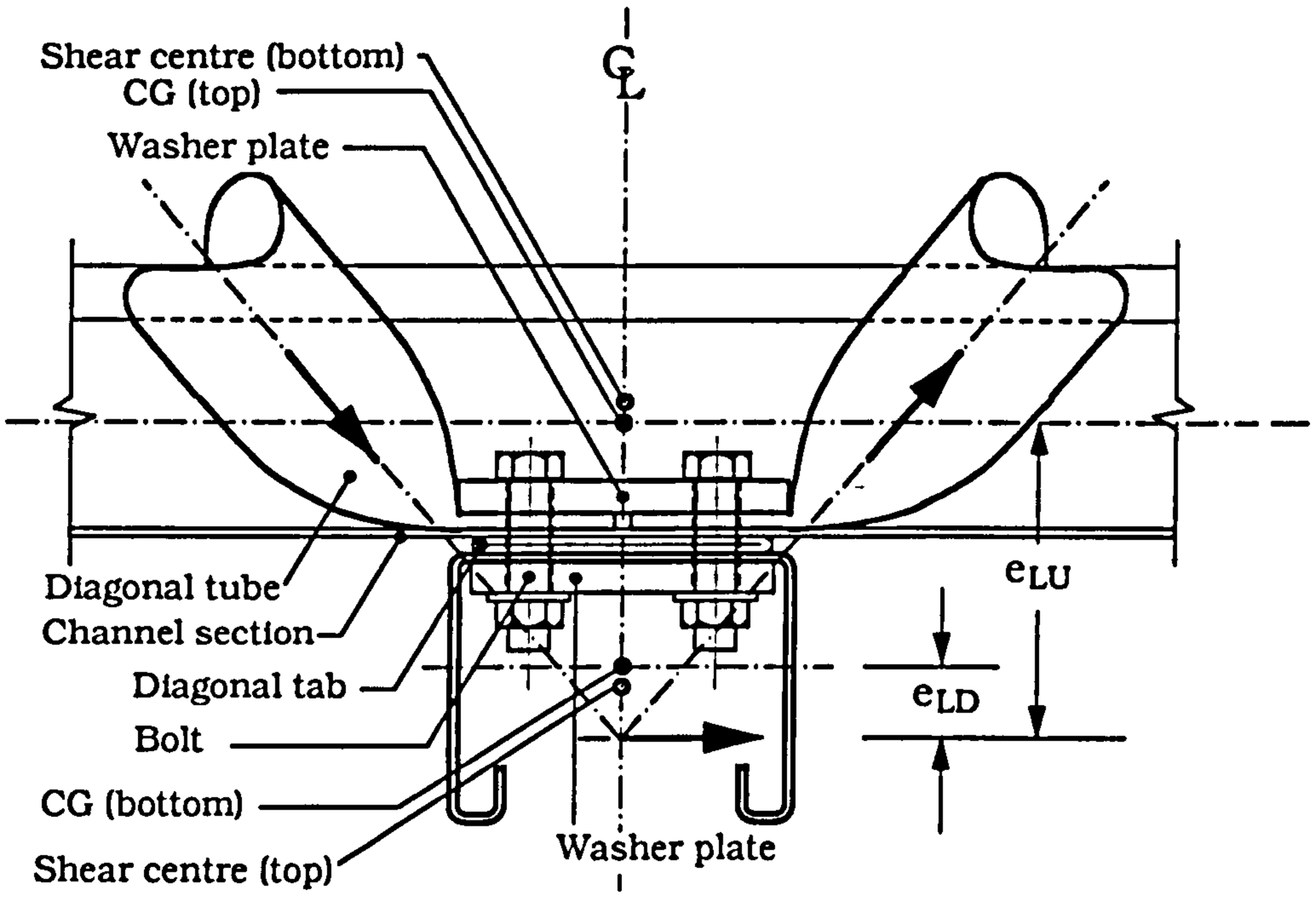


Figure 2.3 Eccentric space frame joint (Conder-Harley)

FRAME TYPE	LOAD TYPE	Ecc btm	Ecc top	R1-R7 (kN)	R2-R8 (kN)	R3-R6 (kN)	R4-R5 (kN)	L1-L4 (kN)	L2-L3 (kN)
† **FRM1**-S/S	B			**50.0**	**50.0**	**50.0**	**50.0**	-	-
FRM1A-S/S	B	●		**58.3**	**58.3**	41.7	41.7	-	-
FRM1B-S/S	B		●	38.7	38.7	**61.3**	**61.3**	-	-
FRM1C-S/S	B	●	●	46.6	46.6	**53.4**	**53.4**	-	-
† **FRM4**-D/S	A			**50.0**	**50.0**	**50.0**	**50.0**	-	-
FRM4A-D/S	A	●		**52.2**	**52.2**	47.8	47.8	-	-
FRM4B-D/S	A		●	48.1	**51.9**	48.1	**51.9**	-	-
FRM4C-D/S	A	●	●	50.2	**54.3**	45.8	49.8	-	-
† **FRM4D**-D/S	C			**50.0**	**50.0**	**50.0**	**50.0**	100.0	100.0
FRM4E-D/S	C	●		**52.0**	**52.0**	48.0	48.0	111.8	88.2
FRM4F-D/S	C		●	48.1	**51.9**	48.1	**51.9**	100.0	100.0
FRM4G-D/S	C	●	●	50.0	**54.1**	45.9	49.9	112.5	87.5

D/S - Diagonal on square S/S - Square on square A - Four 100kN point loads B- 400kN point load C-400kN point load transferred through cruciform † Pin jointed frames Chords (Top & Bottom)- 125x100x20x20-3.0 mm thick Diagonals-48mm dia x 2.0mm thick

Table 2.2 Reactions and cruciform loads for eccentrically and pin jointed frames obtained from numerical analysis (LUSAS 1992) (See Figure 2.4)

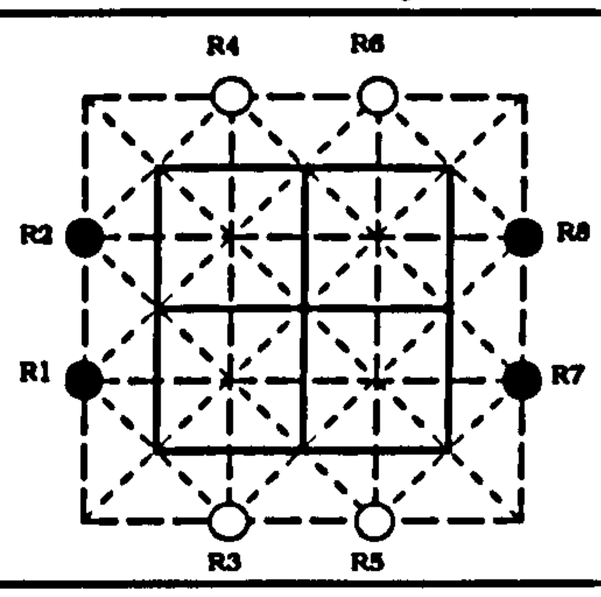
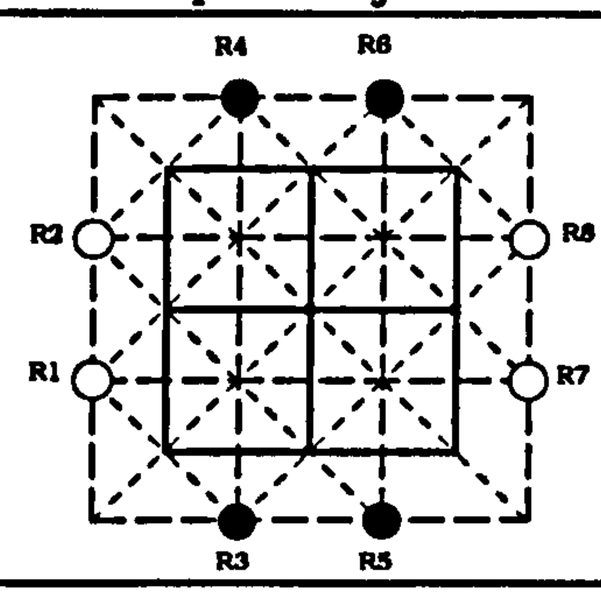
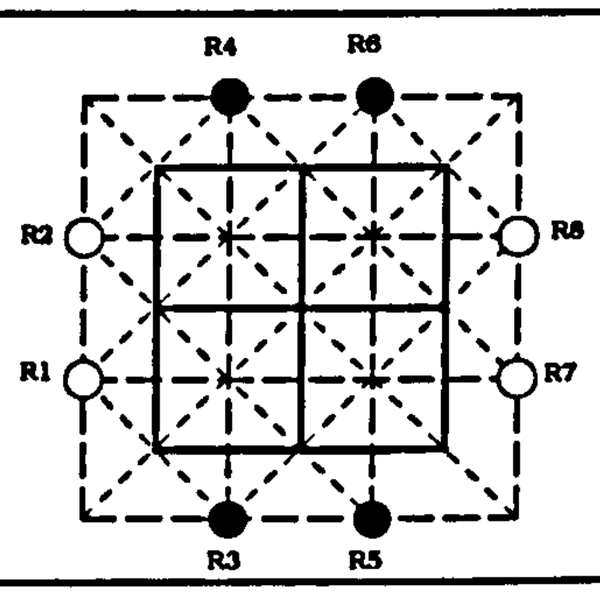
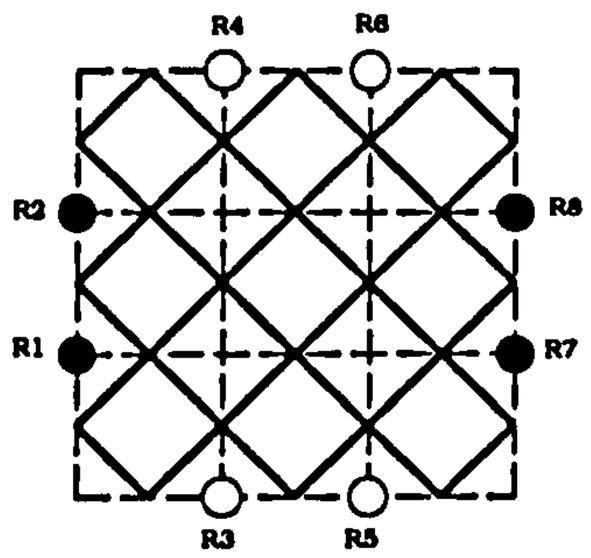
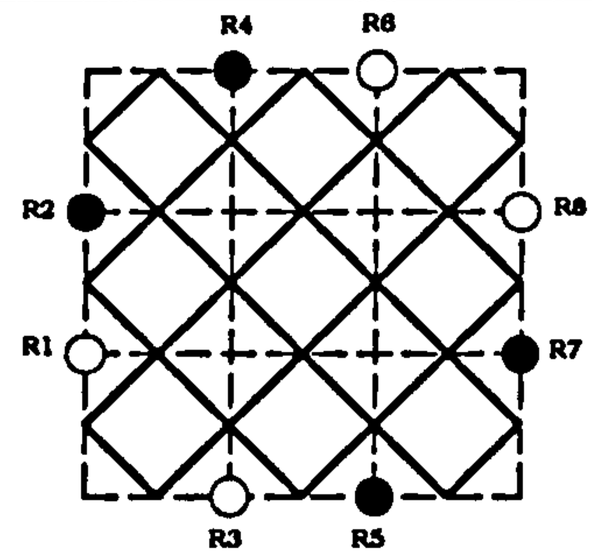
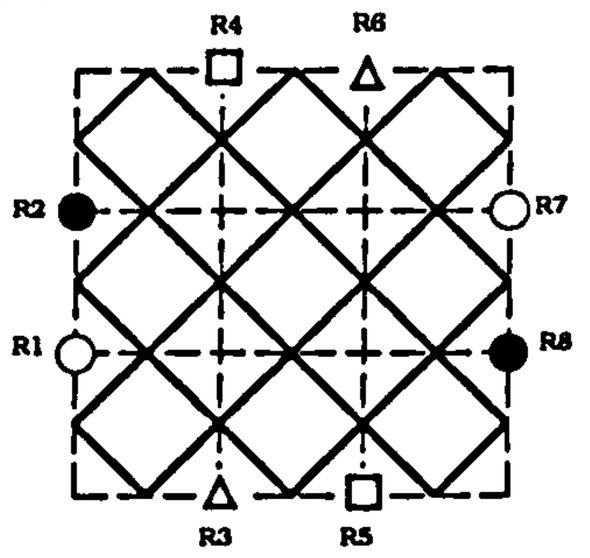
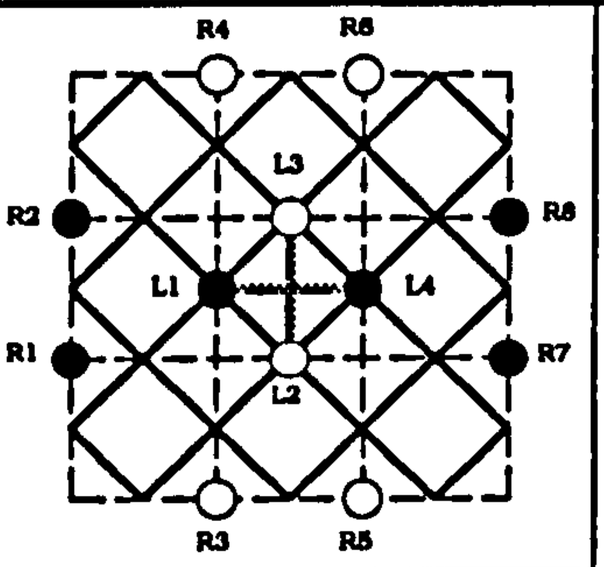
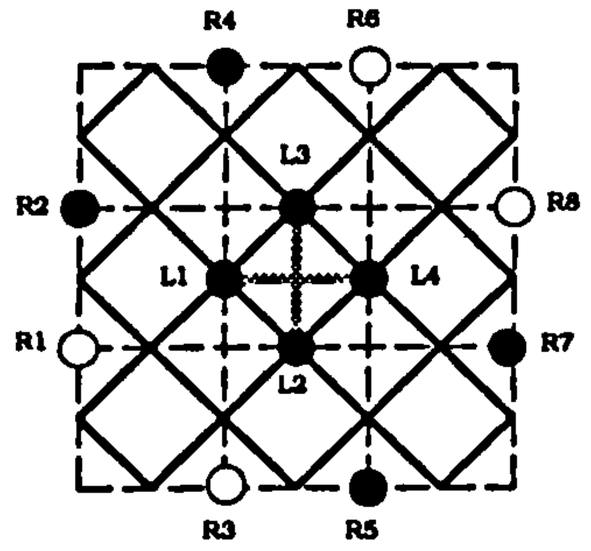
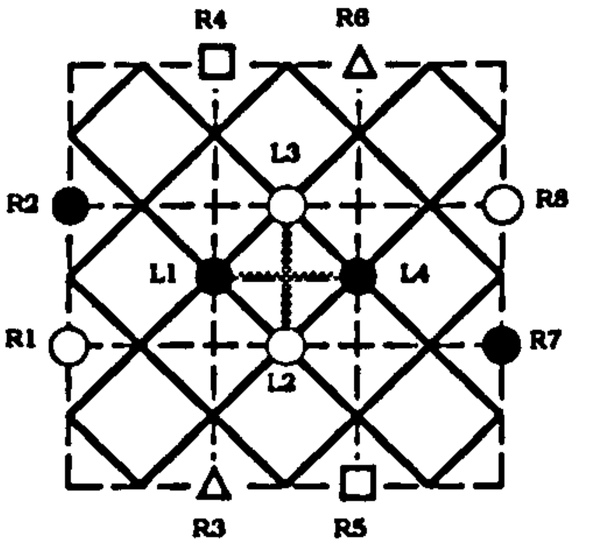
Eccentric bottom chord joints	Eccentric top chord joints	All joint eccentric
		
FRM1A	**FRM1B**	**FRM1C**
		
FRM4A	**FRM4B**	**FRM4C**
		
FRM4E	**FRM4F**	**FRM4G**

Figure 2.4 Variation in support reactions and cruciform forces with frame geometry and joint eccentricity (see Table 2.2)

larger reactions occur at the ends of the diagonals connected to the top chord members with the smaller joint moments. If the square on square frame is eccentrically jointed in both the top and bottom grids the distribution of reactions remains symmetrical about the centre lines of the bottom grid with the larger reactions at the ends of the bottom chord members with the smaller joint eccentricity. The distribution and magnitude of reactions is also seen to be more uniform (Table 2.2). The degree of uniformity in the distribution of reactions depends on the relative stiffnesses in the vertical planes of the chord members. The joint moments cause a loss in stiffness in the affected chord members. Consequently, the chords with the smaller joint moments attract more load. Displacement of the internal nodes of a chord relative to the supports nodes also induces additional vertical reactive forces at the supports.

In Table 2.2 and Figure 2.4 it can be seen that the reactions around the perimeter of a diagonal on square frame having eccentric joints in the bottom grid, are distributed in a pattern similar to that observed for the eccentrically jointed square on square frame. It is interesting to note that the bottom chord joint eccentricities also affect the distribution of forces around the cruciform. The larger forces occur at the ends of the cruciform directly above the chord members with the larger joint moments. The unequal distribution of cruciform forces is due to shears induced by the eccentric joint moments which cause the bottom chords to bend in the direction of the loading. When the diagonal on square frame is eccentrically jointed in the top grid, the reactions are symmetrical about axes at 45 degrees to the centre lines of the bottom grid. Top chord eccentricities do not affect the distribution of cruciform forces. When the bottom and top chords are both eccentrically jointed the reactions are point symmetric about the centre of the bottom grid. The bending shears caused by the bottom chord joint moments are again seen to influence the distribution of cruciform forces. The maximum axial force in the chord and diagonal members, maximum chord moment, reactions and overall displacements for various eccentrically jointed square on square and diagonal on square frames are given in Tables 2.3 and 2.4.

It is evident that when a frame is eccentrically jointed in both the top and bottom chord, the distribution of reactions and cruciform forces is influenced by the magnitude of the eccentricity at the nodes and the orientation of the top and bottom grids relative to each another. The largest reactions occur at the supports of the chords having the smaller joint eccentricities.

FRAME TYPE	LOAD TYPE	Chord Thickness (mm)	Diagonal	†Max Chd. force (kN)	‡Max Chd. Mnt (kNm)	Max Diag. force (kN)	Disp.* (mm)	Disp.(e) (mm)
FRM1C-S/S	B	3.0	48.4 x 2.0	175.3	5.5	160.6	15.6	31.5
FRM2A-D/S	A	1.5	48.4 x 2.0	136.4	3.8	74.8	21.7	-
FRM2B-D/S	C	1.5	48.4 x 2.0	144.8	3.4	81.5	21.5	30.4
FRM3A-D/S	A	1.5	60.1 x 4.0	136.7	3.7	74.8	17.0	-
FRM3B-D/S	C	1.5	60.1 x 4.0	148.4	3.2	86.9	16.8	23.5
FRM4E-D/S	A	3.0	48.4 x 2.0	135.9	3.9	74.7	15.0	-
FRM4G-D/S	C	1.5	48.4 x 2.0	140.7	3.6	75.5	15.1	22.5
FRM5A-D/S	A	3.0	60.1 x 4.0	136.6	3.8	74.8	10.4	-
FRM5B-D/S	C	3.0	60.1 x 4.0	143.6	3.4	79.4	10.4	15.8

D/S - Diagonal on square S/S - Square on square A - Four 100kN point loads B- 400kN point load C-400kN point load transfered through cruciform

† Maximum chord force in central bay of bottom grid ‡ Maximum moment in central bay of bottom grid * Displacements at points a, b, c, d.

Table 2.3 Frame geometry, chord and diagonal forces, and displacements for eccentrically jointed frames obtained from numerical analysis (LUSAS 1992)

The vertical displacements for the eccentrically jointed frame are seen to be significantly larger (Table 2.3) than those obtained for a similar pin jointed frame (Table 2.1). This increase in displacement is largely due to eccentricity moments at the joints and partly due to the difference in the lever arm between the top and bottom chord members in the two frames-that is 1600mm compared to 1772mm. Changing the thickness of the chords and/or the diameter and thickness of the diagonal members has little or no effect on the member forces.

FRAME TYPE	R1-R8 (kN)	R2-R7 (kN)	R3-R6 (kN)	R4-R5 (kN)	L1-L4 (kN)	L2-L3 (kN)
FRM1-S/S	46.6	46.6	53.4	53.4	-	-
FRM2A-D/S	50.2	54.3	45.8	49.8	-	-
FRM2B-D/S	49.9	54.1	45.9	50.1	121.1	78.9
FRM3A-D/S	50.2	54.4	45.8	49.8	-	-
FRM3B-D/S	49.9	53.9	46.1	50.1	128.5	71.5
FRM4C-D/S	50.2	54.3	45.8	49.8	-	-
FRM4G-D/S	50.0	54.1	45.9	49.9	112.5	87.5
FRM5A-D/S	50.4	54.3	45.8	49.8	-	-
FRM5B-D/S	49.9	54.1	45.9	49.9	117.3	82.7

Table 2.4 Reactions and cruciform loads for frames with eccentrically jointed top and bottom chords.

From the limited parametric study carried out it has been shown that the effects of joint eccentricity must be taken into account in the design process. They significantly influence the force distribution and displacements in the frame. Moments arising from eccentric joints must be considered as primary moments when determining the member capacities. It was also observed that the joint eccentricity affects the distribution of the forces passing from the frame to a supporting structure such as the cruciform or tree structure. In the frame analysis the stiffness of the cruciform also has a significant effect on the distribution of these forces. In general, the supporting structure must be included in the analysis in order to take account for the its flexibility and consequently, its influence on the force distribution.

2.2.3 COMPARISON BETWEEN NUMERICAL AND EXPERIMENTAL RESULTS

Test 5c reported in Chapter Three forms the basis for comparison between numerical and experimental values of axial forces in the diagonal members, the force distribution in the cruciform and the variation of vertical displacement with load. The diagonal on square frame consisted of 3.0mm thick doubly lipped channel sections for the chords, with 60mm dia-2.5mm thick diagonal tubing around the external perimeter of the frame and 76mm dia-3.0mm thick diagonal tubing internally. Two 60mm dia-2.5mm thick diagonals were also fitted internally. All top and bottom chord joints were fitted with 340x100mm-3.0mm thick nodal inserts. Displacements and strains were measured using linear transducers and strain gauges at pre-selected positions. The test frame was loaded through a central cruciform (Figure 3.4).

A linear elastic analysis was carried out for the same frame configuration. It should be mentioned that the finite element model does not take account of the additional local bending and torsional stiffness provided by the nodal insert, or the restraint provided by the diagonal members. A comparison between experimental and numerical values of axial force in the diagonal members meeting supported joints around the perimeter are given in Table 2.6. The distribution of cruciform forces is given in Table 2.7.

Diagonal @	TEST 5c (kN)	LUSAS / TEST 5c †	LUSAS / TEST 5c
R1	62.9	0.88	0.98
R2	60.0	0.92	1.06
R3	59.8	0.92	1.02
R4	66.4	0.84	0.94
R5	57.4	0.97	1.09
R6	62.3	0.89	0.98
R7	65.8	0.84	0.96
R8	59.3	0.93	1.04

† Diagonal forces for pin jointed frame.

Table 2.6 Numerical and experiments diagonal forces. (P_{TEST} = 340kN)

If the frame is analysed as a pin jointed structure the diagonal forces in the test frame are underestimated by between 3% and 16% while the diagonal forces

obtained from a frame analysis with eccentric joints and continuous chords vary between -6% and +9% of the experimental results.

The distribution of cruciform forces obtained experimentally and numerically are compared in Table 2.7. The cruciform forces from the frame test were obtained by taking the axial strain readings in the tensile diagonals located at the ends of the cruciform and resolving them vertically; the chord shears were not measured. It is evident that the load is not equally distributed to all points of contact on the cruciform. The difference in load at L1 and L3 (Table 2.7) obtained from the frame tests is not as large as that given by the numerical analysis (Table 2.4).

Cruciform Force @	TEST 5c* (kN)	$\frac{\text{LUSAS}}{\text{TEST 5c}}$ †	$\frac{\text{LUSAS}}{\text{TEST 5c}}$
L1	80.8	1.05	0.87
L3	89.3	0.95	1.11

† cruciform forces for pin jointed frame. * See Chapter Three

Table 2.7 Numerical and experiments values of cruciform force (P_{TEST} = 340kN).

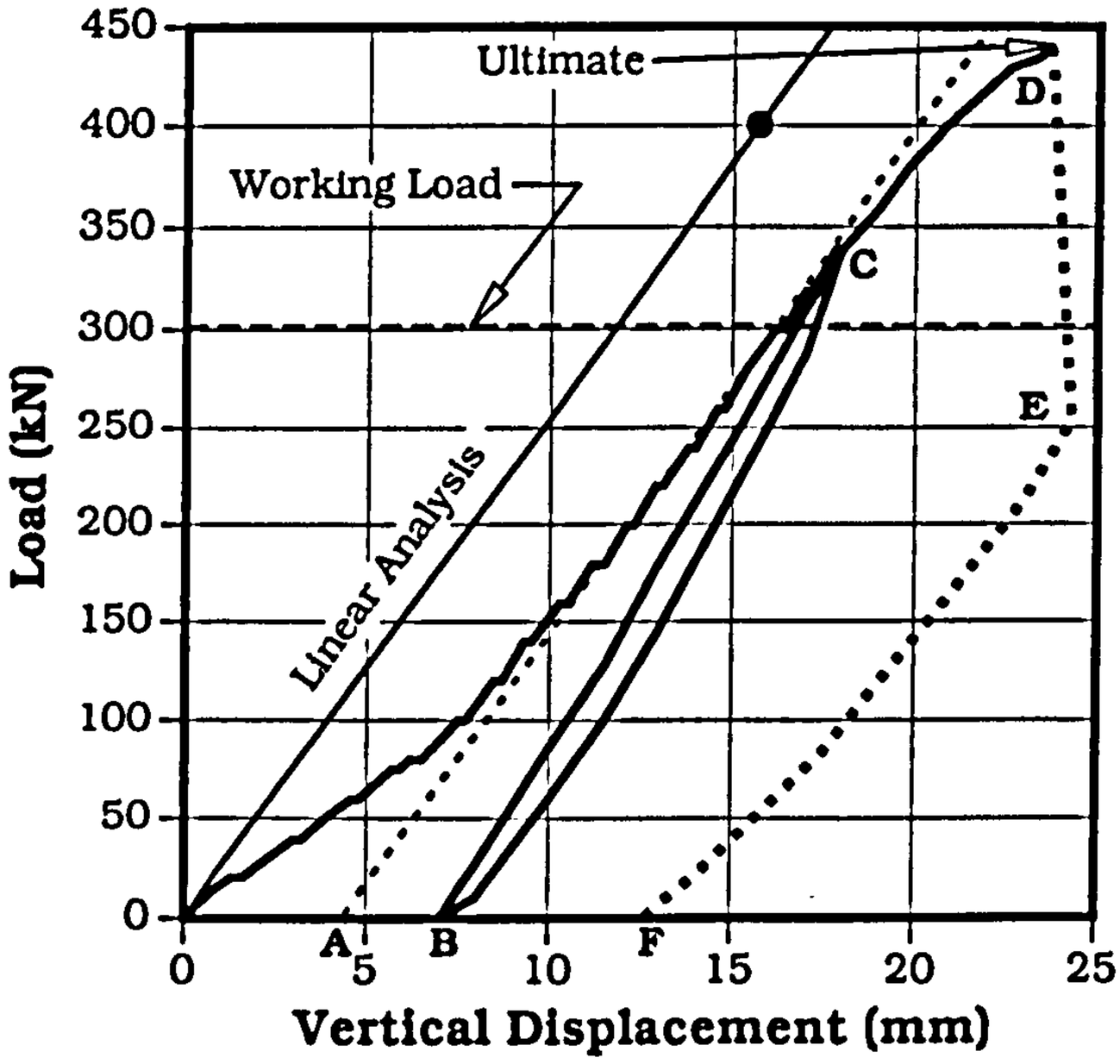


Figure 2.5 Comparison between vertical displacements at point e obtained experimentally and from a linear frame analysis (see Figure 2.2)

If the force is assumed to be equally distributed to all points on the cruciform then this would result in an overestimation of force in one pair of the supports and an underestimation in the other. The variation in central displacement of the cruciform (point **e**) with load obtained numerically and experimentally is shown in Figure 2.5.

During testing, the frame was loaded in increments of 20kN up to 340kN (point **C**), and at each load increment the load was held constant for a time to allow bedding of the joints. Appreciable bedding was observed at lower frame loads and is characterised by the saw toothed appearance of the curve shown in Figure 2.5. The frame was unloaded at 340kN. A permanent vertical displacement of 7mm was recorded (point **B**).

The load/displacement relationship of the frame neglecting bedding of the joints may be approximated by passing a line through point **C** drawn back to point **A** (Figure 2.5). It can be seen that the vertical displacement at 300kN due to joint bedding is approximately 4mm compared to 12mm given by the linear analysis. At a load of 340kN the central vertical frame displacement obtained from the numerical analysis underestimates the actual frame displacement about 30%. If the additional vertical displacement due to bedding of the joints is neglected, the vertical displacement obtained from the linear elastic analysis compares well with the test frame. Further load was applied to the frame, up to failure, which occurred suddenly at a load of 440kN caused by diagonal buckling (point **D**). It is interesting to observe that after failure of the diagonal occurred the frame was still able to carry a residual load of 250kN (point **E**).

2.3 EFFECTIVE LENGTH OF CONTINUOUS MEMBERS

In design, it is usual to make the conservative assumption that the effective length is equal to the nodal distance, regardless of the relative stiffness and forces in adjacent spans. When interpreting test results however, it is necessary to take account of the actual forces; otherwise it is possible to draw unsafe conclusions.

When more than one span of a continuous member is loaded, the critical load can be determined by analysing the interaction between segments. Consider the continuous member of constant stiffness shown in Figure 2.6, loaded by unequal compressive axial loads between simple supports. The stability of the lightly loaded spans is reduced owing to the flexural restraint which it provides for the more

heavily loaded span, while the stability of the latter is increased. The result of this is to increase the effectiveness of the more heavily loaded member, and hence the axial capacity of the continuous member.

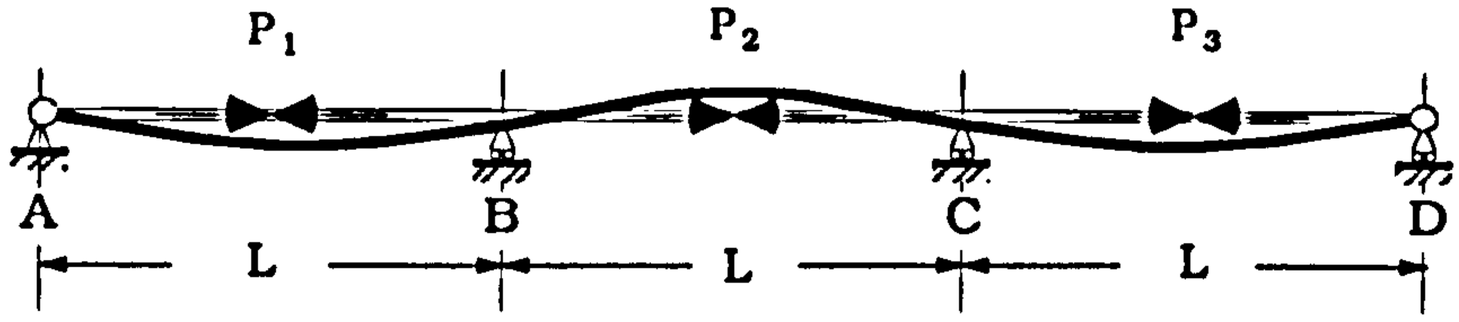


Figure 2.6 Axially loaded three span continuous column

The buckling mode for a continuous three span column depends on the distribution of force in the system and on the support conditions. Figure 2.7 shows the three primary modes of buckling for symmetrical loading. If the central span is unloaded the points of inflexion occur in the outer spans; when the outer spans are unloaded the inflexion points are located in the central span. If all three spans are equally loaded then the points of inflexion coincide with the supports and there is no interaction between spans. The effective length of each span can be found by obtaining the critical load of the system.

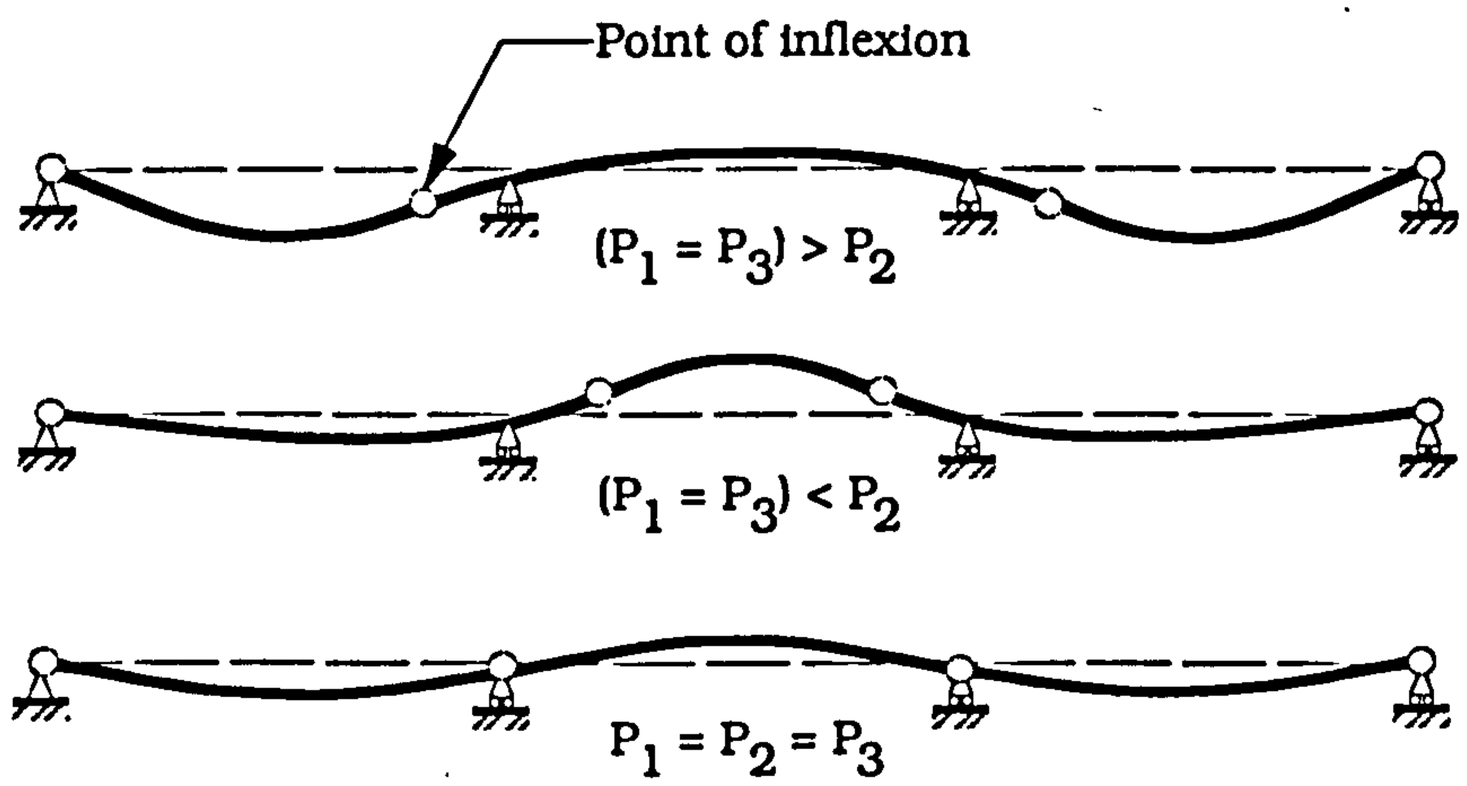


Figure 2.7 Buckling modes for continuous column of constant cross-section

Timoshenko and Gere (1961) provides the theoretical background in the form of a three moment equation for continuous beams with axial loads, which has been used to produce Figures 2.8 and 2.9. They show the variation in effective length for the central span with the load ratios P_1/P_2 and P_3/P_2 for both simply supported and fixed ended support conditions. The effective length of the more heavily loaded

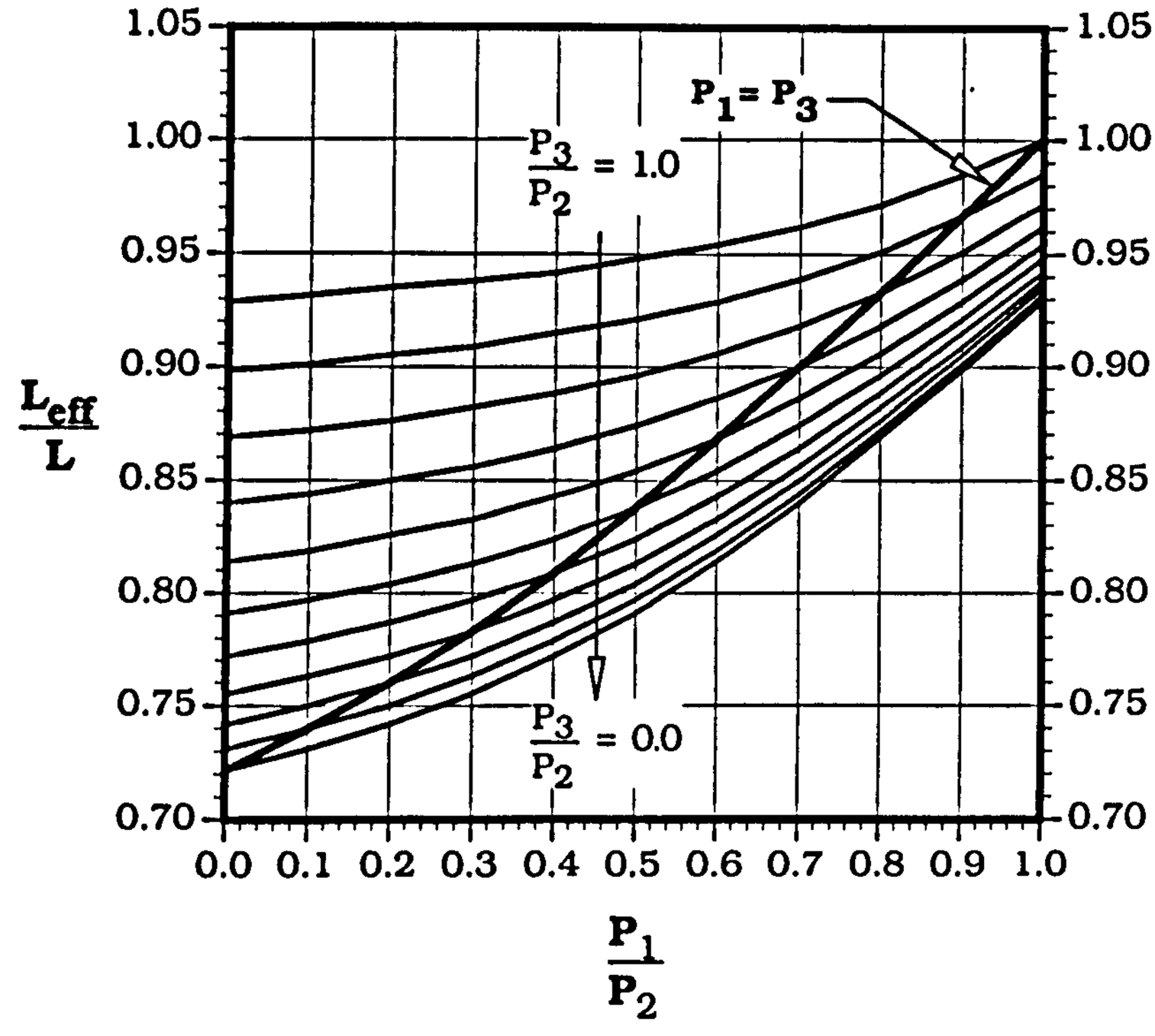


Figure 2.8 Effective length ratio for three span continuous column with simply supported ends

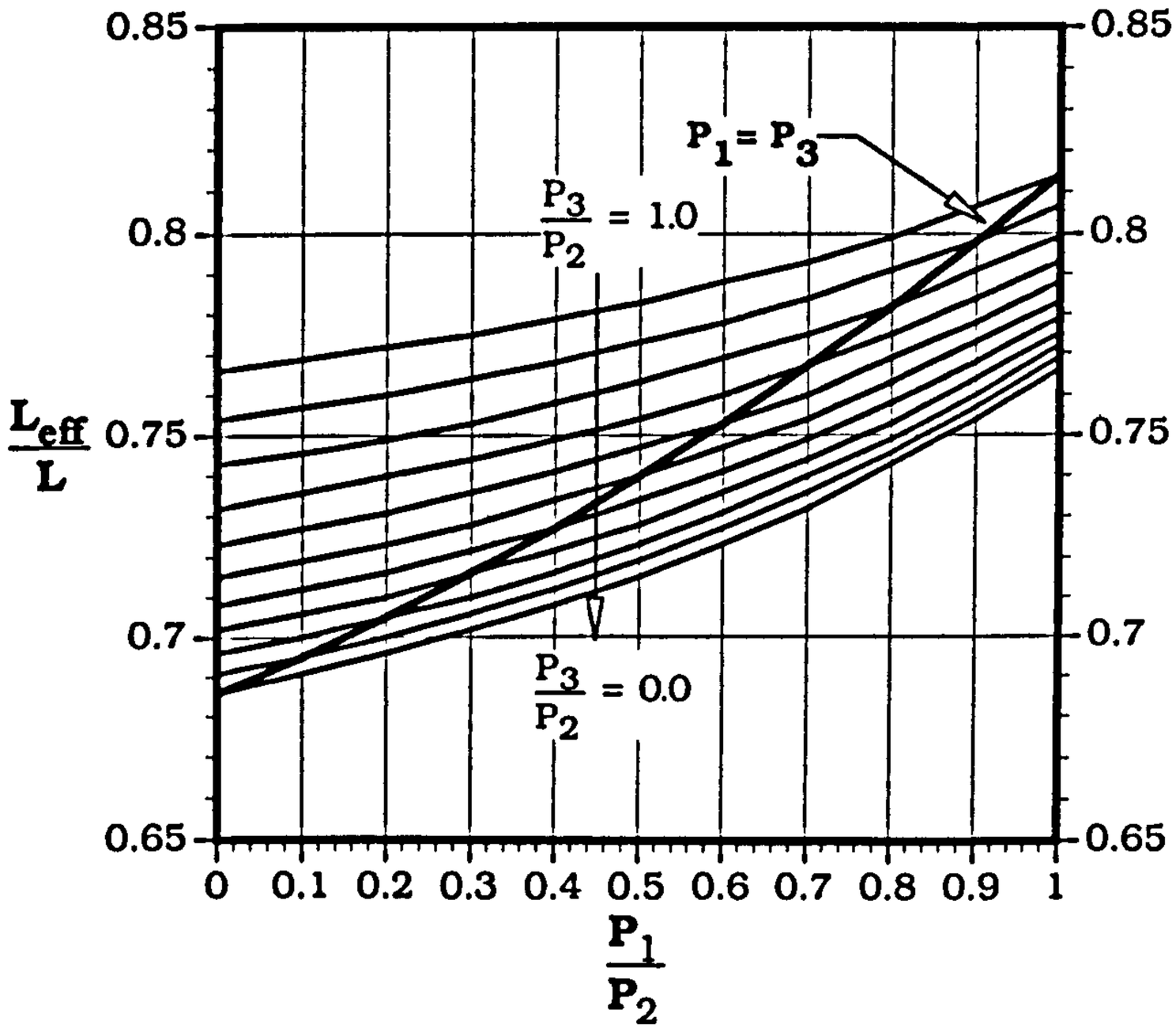


Figure 2.9 Effective length ratio for three span continuous column with fixed end supports at the extremities

central span for a simply supported continuous column with both outer spans equally loaded, (that is (P_1=P_3) ≤ P_2) varies between 0.72L and 1.0L. If one of the outer spans is unloaded (P_1=0) the effective length of the critical central span varies between 0.72L and 0.93L when $P_2 \geq P_3$. If the continuous member is fixed ended the effective length of the central span is further reduced and if the restraining spans are then both equally loaded such that ($P_1 = P_3$) ≤ P_2 the effective length of the central span varies between 0.686L and 0.814L. If one of the outer spans is unloaded then the effective length of the central span varies between 0.686L and 0.767L. Figure 2.8 will be used to determining the effective length of the critically loaded bottom chord central spans of the test frame subjected to flexural and torsional-flexural buckling, while Figure 2.9 will be used to interpret the results obtained from the torsional-flexural buckling component tests described in Chapter Seven.

2.4 CONCLUSIONS

(1) The effects of frame geometry, member size, loading arrangement and joint eccentricity on the displacements and forces were investigated numerically. The distribution of member forces from a pin jointed analysis were shown to be symmetric, whereas when eccentricities were taken into account, the distribution became unsymmetric due to a loss of stiffness in the vertical planes of the chords caused by bending induced by the chord eccentricities.

(2) If an eccentrically jointed frame is assumed to be pin jointed the member forces obtained from a linear-elastic analysis underestimate the actual forces. It is necessary to take account of the joint eccentricities.

(3) The distribution of load in a supporting structure such as a tree support is also influenced by the presence of joint eccentricity and the stiffness of the supporting members. It is important when carrying out an analysis on an eccentrically jointed frame that the supporting structure be included in order to obtain realistic estimates of member forces.

(4) Comparison between numerical and experimental results shows that bedding of the connections can increase the deflection by about 30% at working load.

(5) If the axial loads in a continuous chord member vary significantly between spans, then it is possible to reduce the effective length of the more heavily loaded member because of the flexural restraint provided by the lighter loaded adjacent members. The reduction in effective length of the heavily loaded central member can vary by a factor of 0.72 and 1.00 of the distance between nodes.

Chapter Three

FRAME TESTS

3.1 INTRODUCTION

Experiments were conducted on seven full size frames subjected to vertical load. Their purpose was to obtain a better understanding of the overall and local behaviour of the diagonal on square space frame, and to verify existing or new design procedures. In general, tests were conducted with the intention of replacing failed components with a stronger component. In this way a succession of failures could be achieved from a single frame. The frames are designated by a number, and the successive tests on the frame are designated by letters.

Frames 1a-1b were constructed from readily available 127 x 63.5 x 12.7-2.0mm single lip channel sections (Figure 3.1), and 60mm dia.-2.5mm thick circular tubing. The tests on this frame were intended to be exploratory. They provided experience of the general behaviour of the system, and demonstrated three modes of failure. It was not envisaged that the 63.5 deep channel sections would be suitable for the proposed joint spacing (the slenderness ratio L/r was 130). The tests did however provide insight which greatly assisted the design of the section which would be used in production.

The chord slenderness was reduced by increasing the depth of the channel to 100mm, and a more balanced section, better able to resist bending, was achieved by increasing the lip area by means of a downturn. This also stabilised the lip table against wrinkling, and increased the lateral stiffness of the effective lip against lip buckling. Increasing the width of the section would have increased the joint eccentricity moment, whilst the internal width between downturns had to be sufficient to allow bolt tightening. The eccentricity moment produces local vertical forces, and it was foreseen that increasing the depth of the section would

necessitate local reinforcement in regions of high shear, to prevent web crippling. The section adopted is shown in Figure 3.2.

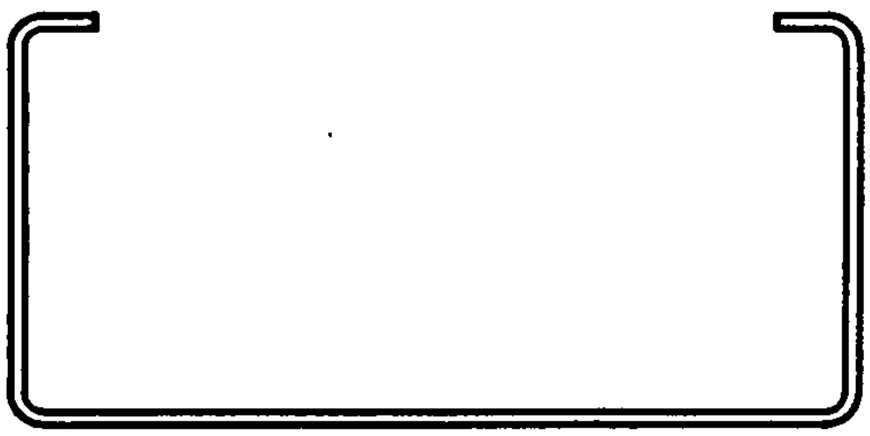


Figure 3.1 127 x 63.5 x 12.7 thick simple lipped channel

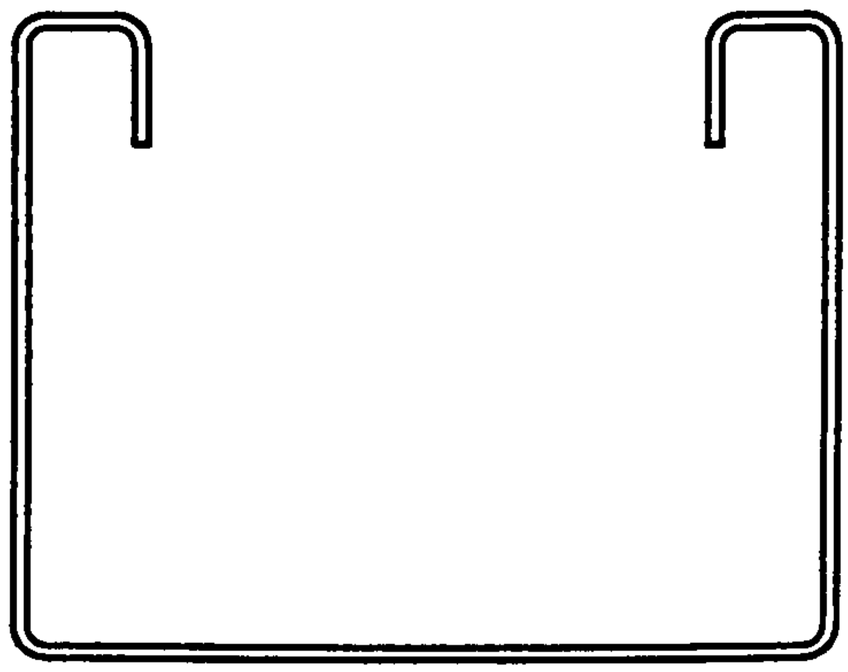


Figure 3.2 125 x 100 x 20 x 20 doubly lipped channel section

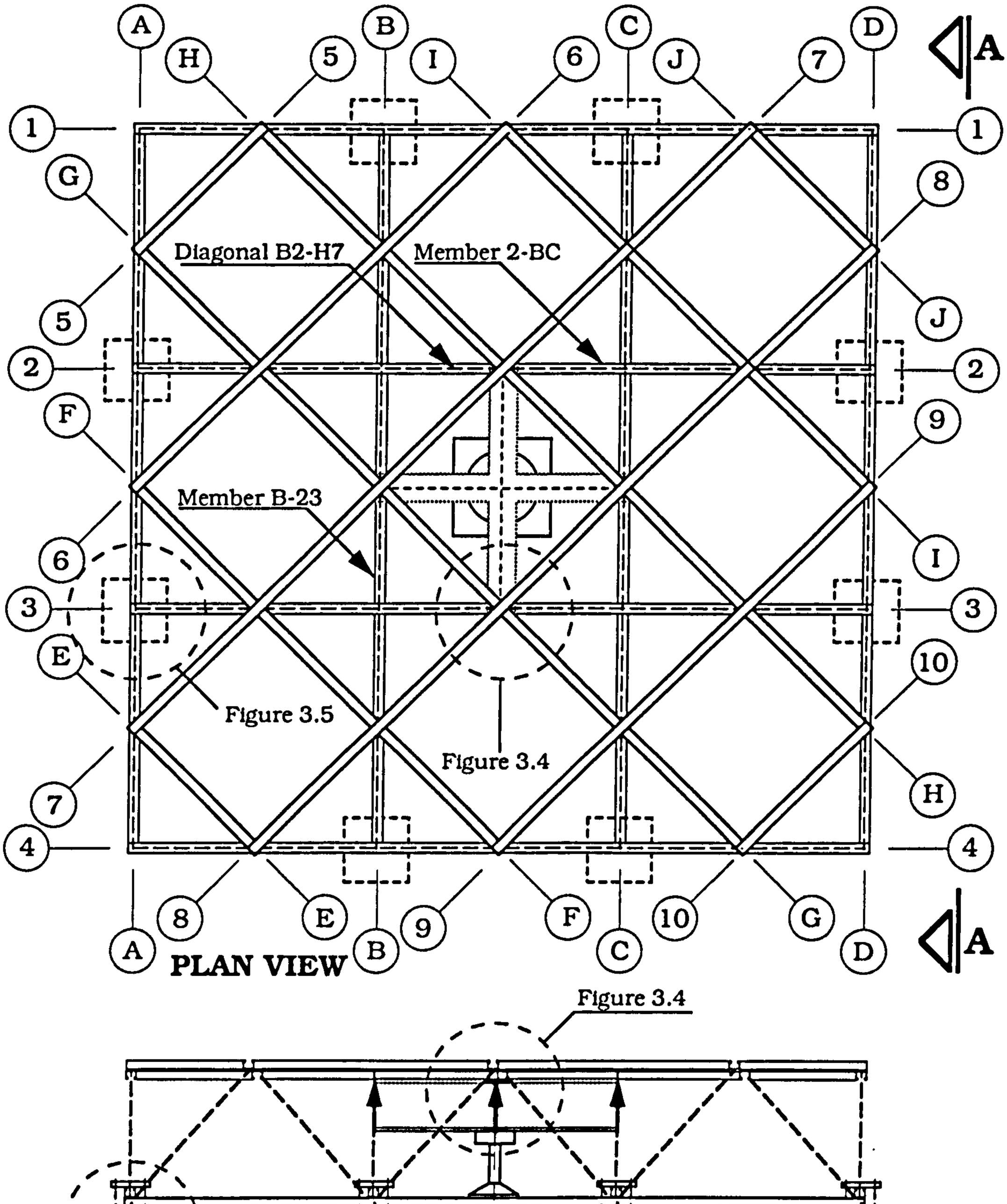
Frames 2 to 7 were constructed from specially manufactured 125 x 100 x 20 x 20 doubly lipped channel sections 1.5 and 3.0mm thick and diagonal tubes whose diameter varied between 42mm and 76mm. Various modes of failure were observed in these frame tests, some of which were further investigated by component tests which are reported within the relevant chapters in this thesis.

This chapter describes the test arrangement, instrumentation and methodology which was adopted for the frame tests. A description of the loading sequence, frame behaviour and failure mode for each test is presented. The correlation of the test results with theory and with proposed design methods will be given in the chapters dealing with each mode of failure.

3.2 TEST ARRANGEMENT

The frames were constructed using the diagonal on square arrangement shown in Figure 3.3. The frames consist of top and bottom grids 1600mm apart, where the top chords are at 45° to the bottom chords. The top joints are vertically above mid points of the bottom chord members. Bottom chord members are $\sqrt{2}$ times the length of the top chord members. The diagonal members are in the same vertical planes as the bottom chord members; they are shown in Figure 3.3 as broken lines.

The grid reference system shown in Figure 3.3 was used to describe the location of individual members of the test frame. Grid lines A to D are located along lips-down



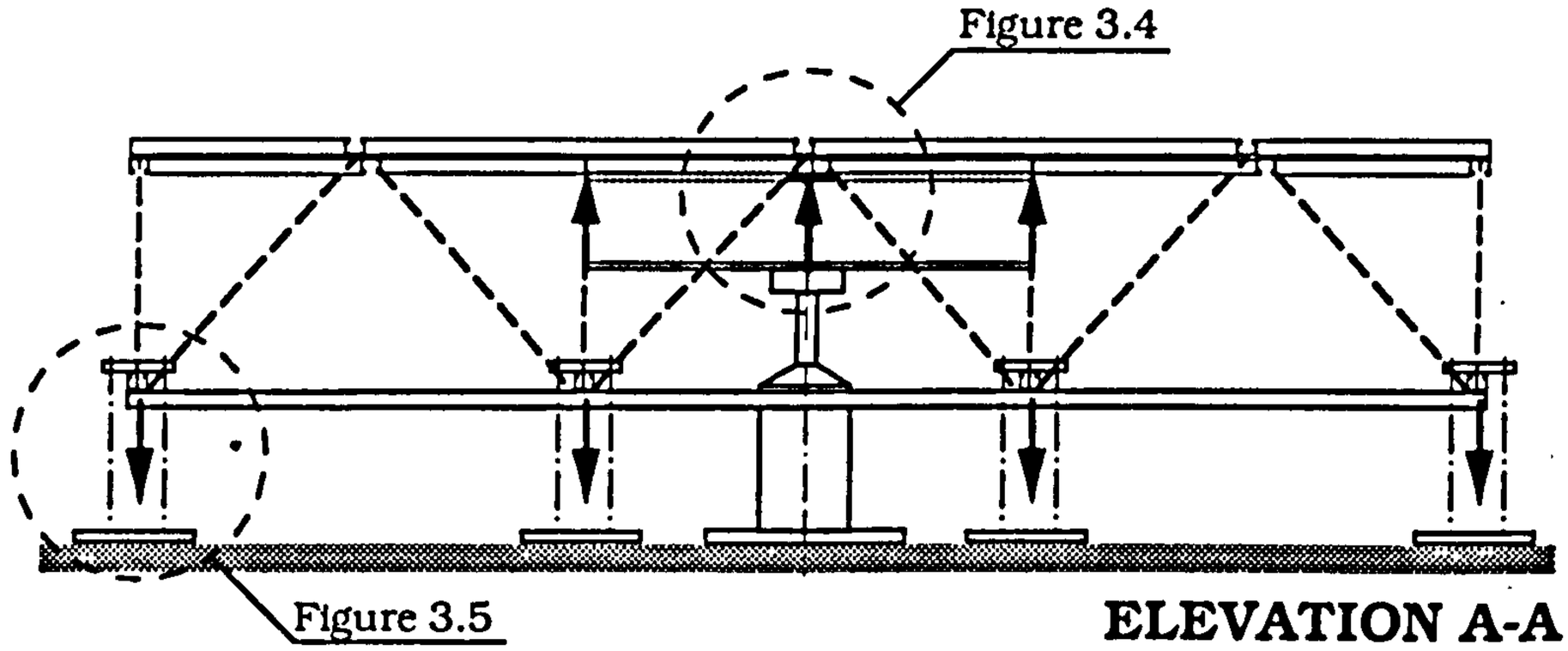


Figure 3.3 Test Frame

bottom chord members and lines 1 to 4 along the lips-up bottom chord members. The position of each chord member can then be defined by giving the chord grid line followed by the grid lines of the intersecting members at each end of the member.

For example, the bottom chord lips-down member B-23, and a bottom chord lips-up member 2-BC, are indicated in Figure 3.3. Grid lines E to J are located along the lips-up top chord members and grid lines 5 to 10 are along the top chord lips-down members. The diagonal members can be located by referring to the bottom chord and top chord intersecting chord members at each end of the diagonal, for example B2-H7.

In a space frame with internal supports, bending moments and shear forces both have maximum values at the support. Because of the eccentricity between chord and diagonal forces, the bottom chord members adjacent to the internal support are subject to a combination of large axial forces and large bending moments. The bending moment is greater in the lips up members, but the bending causes lip tension. In the lips down members the moment is smaller but causes lip compression. Consequently, the lips down members fail as a result of a combination of torsional-flexural and lateral-torsional buckling, whereas the lips up members fail by flexural buckling, and the loads which cause failure in the central lips-up and lips-down members are approximately equal. The above considerations along with the numerical analysis described in Chapter Two led to the choice of a test rig which would represent part of a frame surrounding an internal column. The perimeter of the frame approximates to the region of zero bending moment in a frame having equally spaced internal columns and typical spans.

In the test rig shown in Figure 3.3 the column force is applied by a centrally located 100 ton jack, acting through a cruciform member, to four central top chord joints (Figure 3.4). Neither the force nor the vertical displacements at the four joints are equal. Their relative magnitudes depend on the relative flexibilities of the cruciform beam and the frame and also the magnitude of the chord shears present in the bottom chord. The load was reacted through eight perimeter joints to the laboratory floor (Figure 3.5). The extension of the tie rods was small compared to the central deflection of the frame.

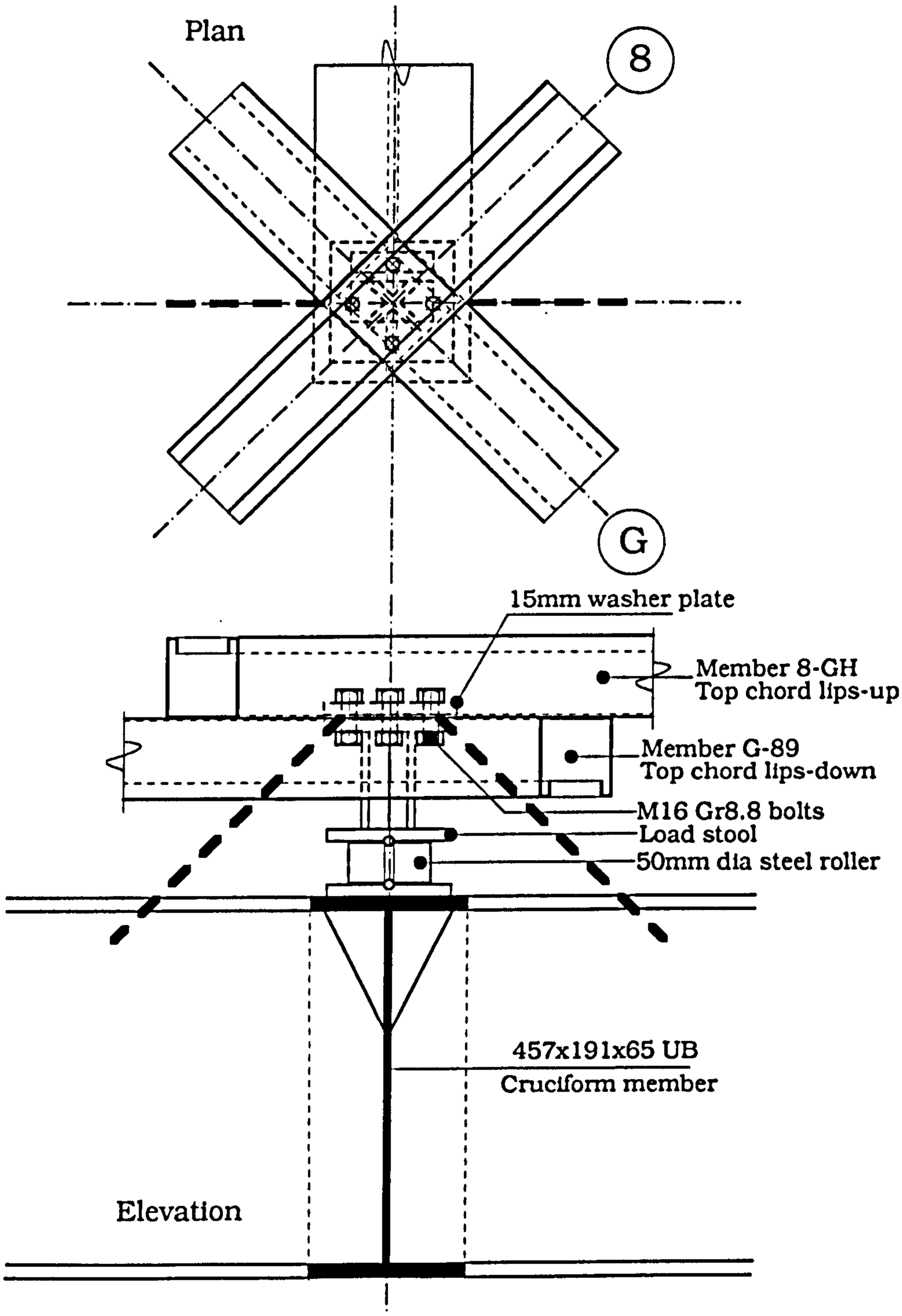


Figure 3.4 Cruciform and load stool arrangement

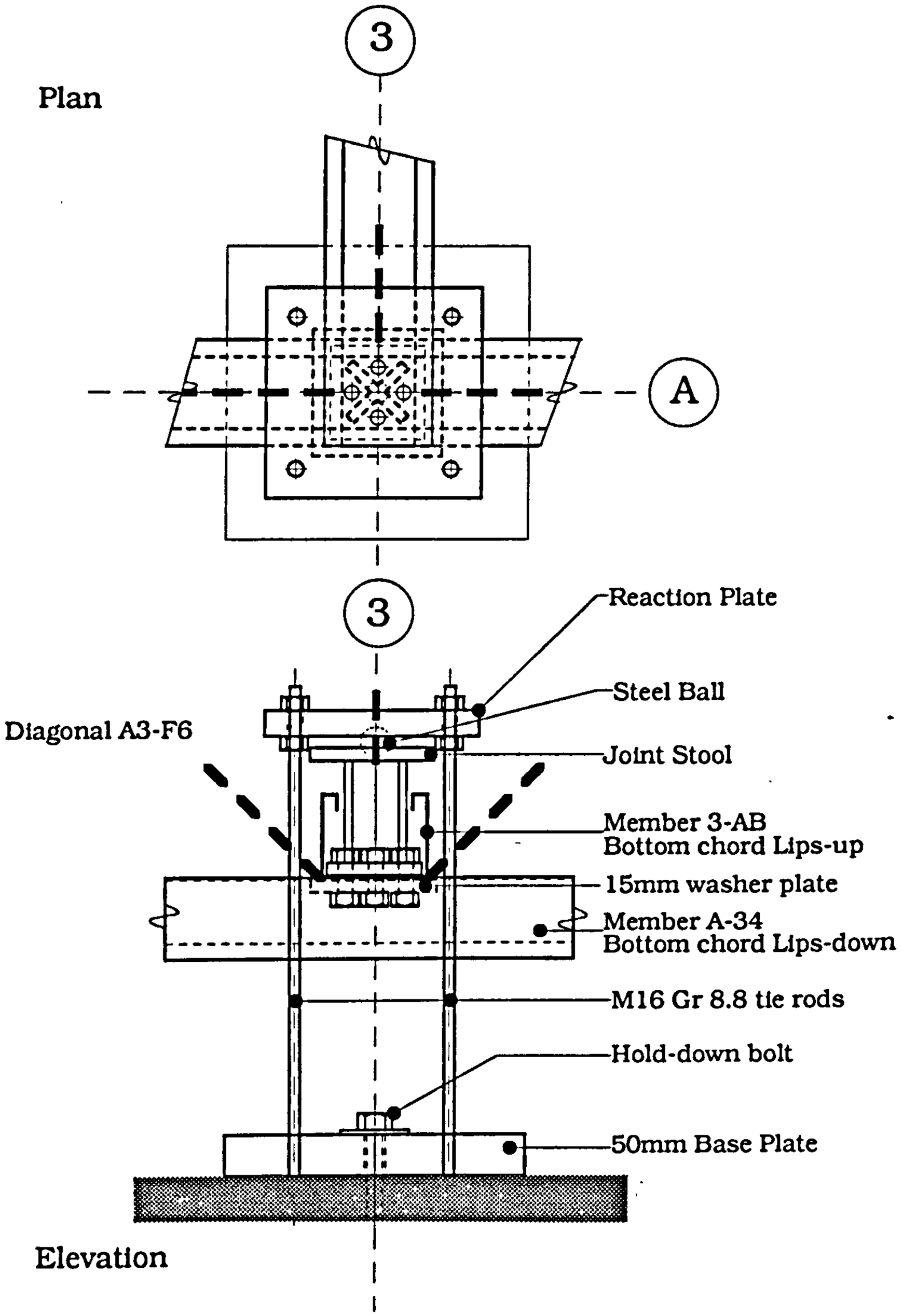


Figure 3.5 Frame anchorage point

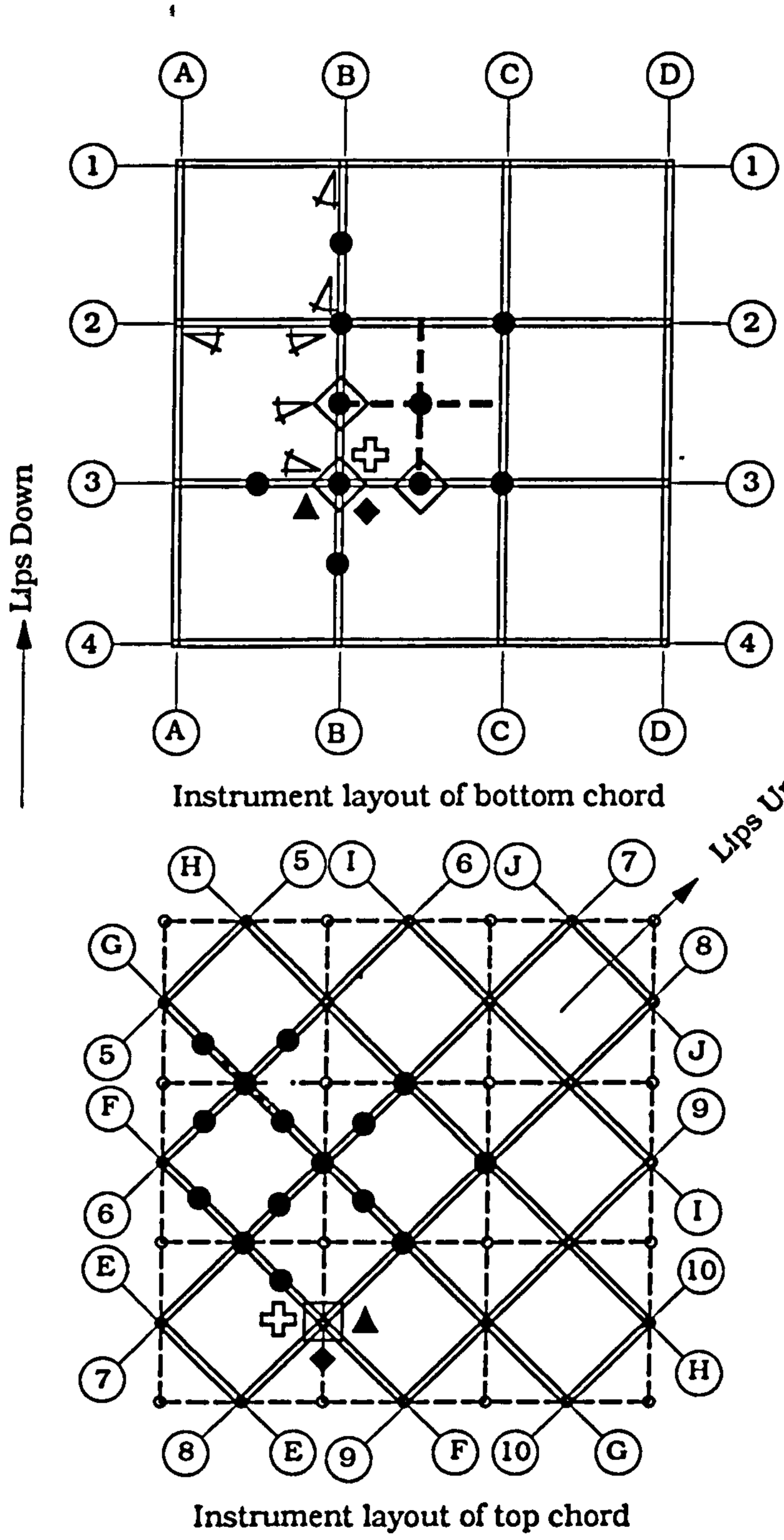


Figure 3.6 General Layout of Instrumentation

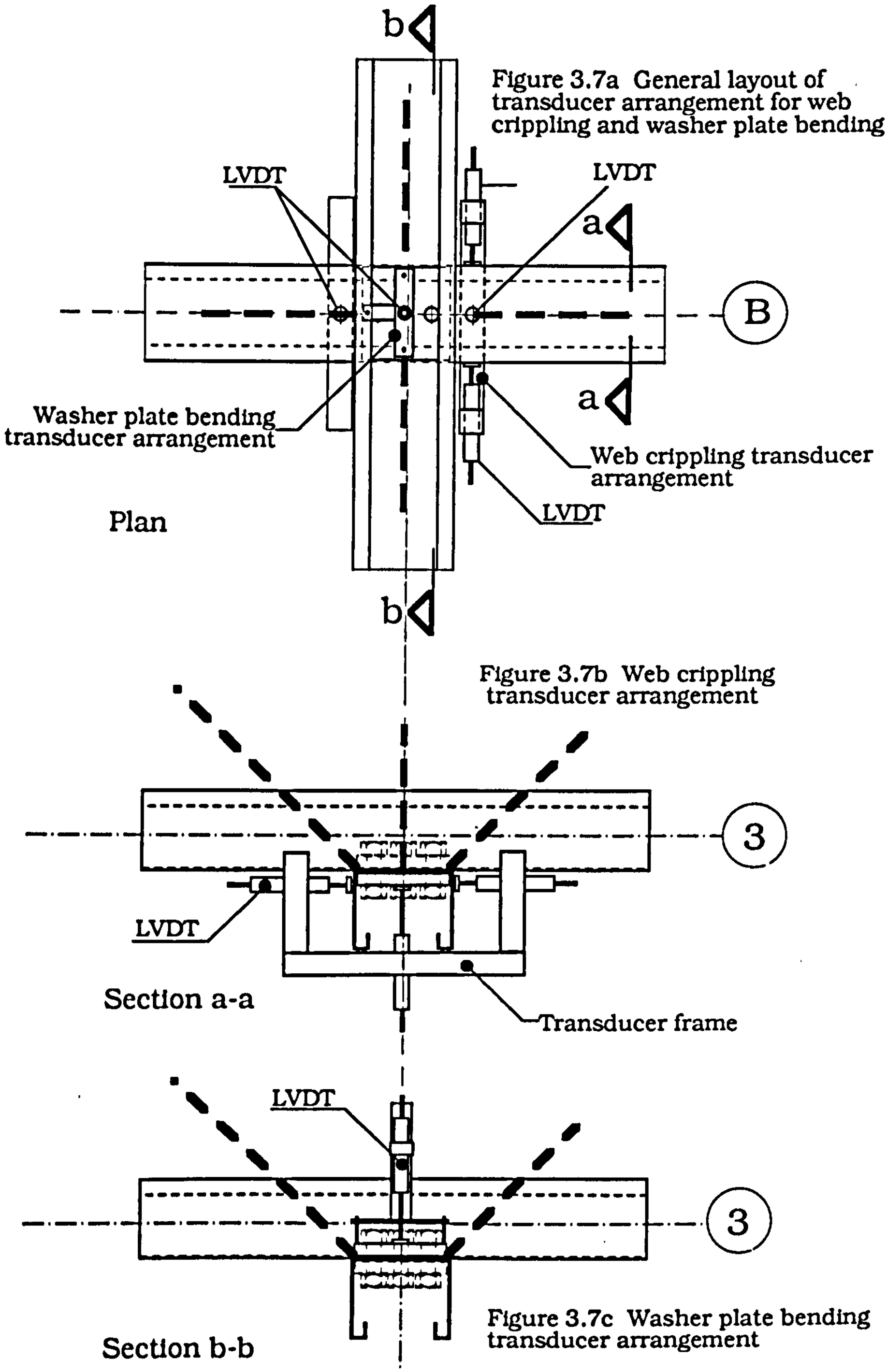


Figure 3.7a General layout of transducer arrangement for web crippling and washer plate bending

Figure 3.7b Web crippling transducer arrangement

Figure 3.7c Washer plate bending transducer arrangement

Figure 3.7 Web crippling and washer plate bending transducer arrangements

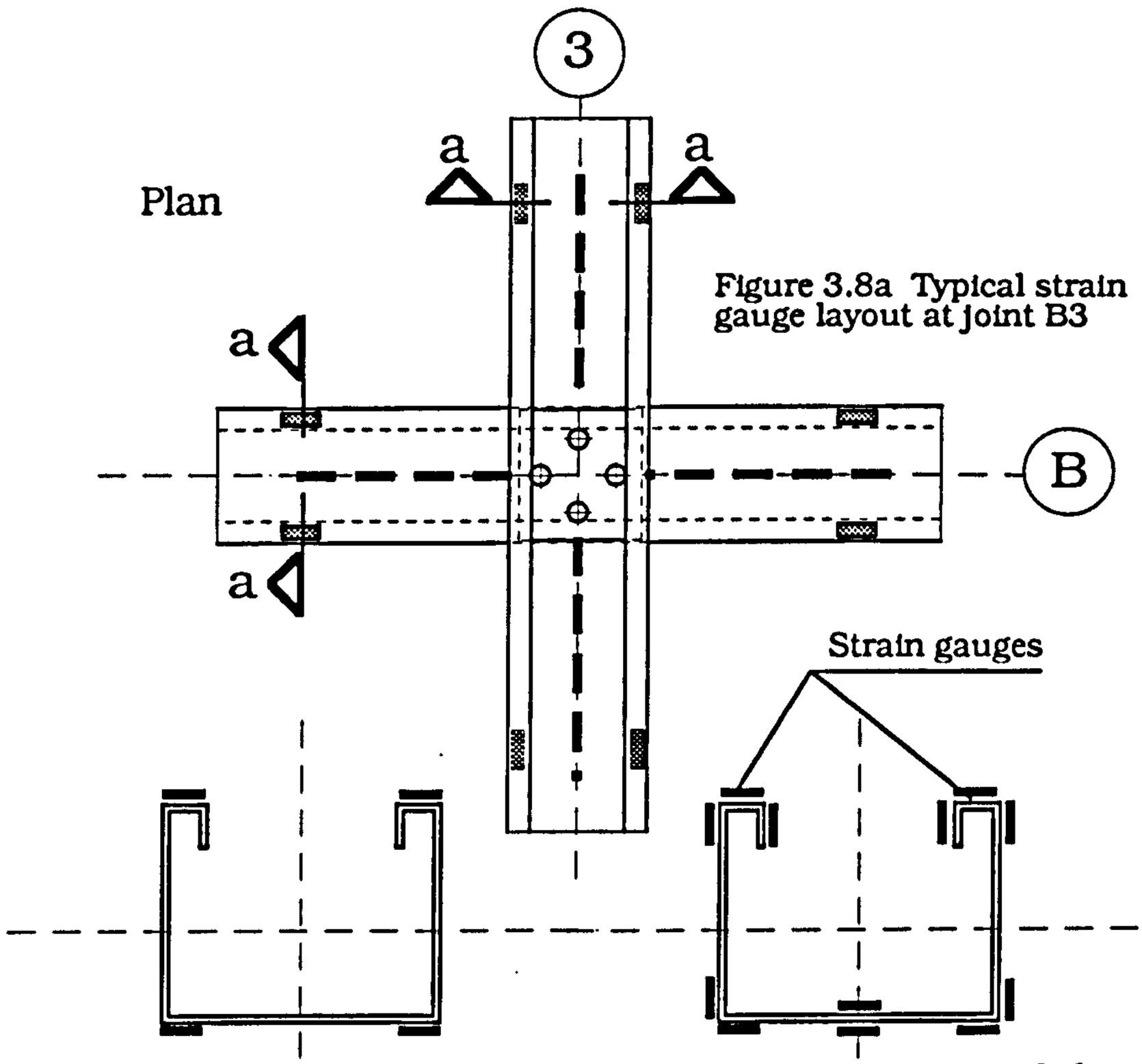
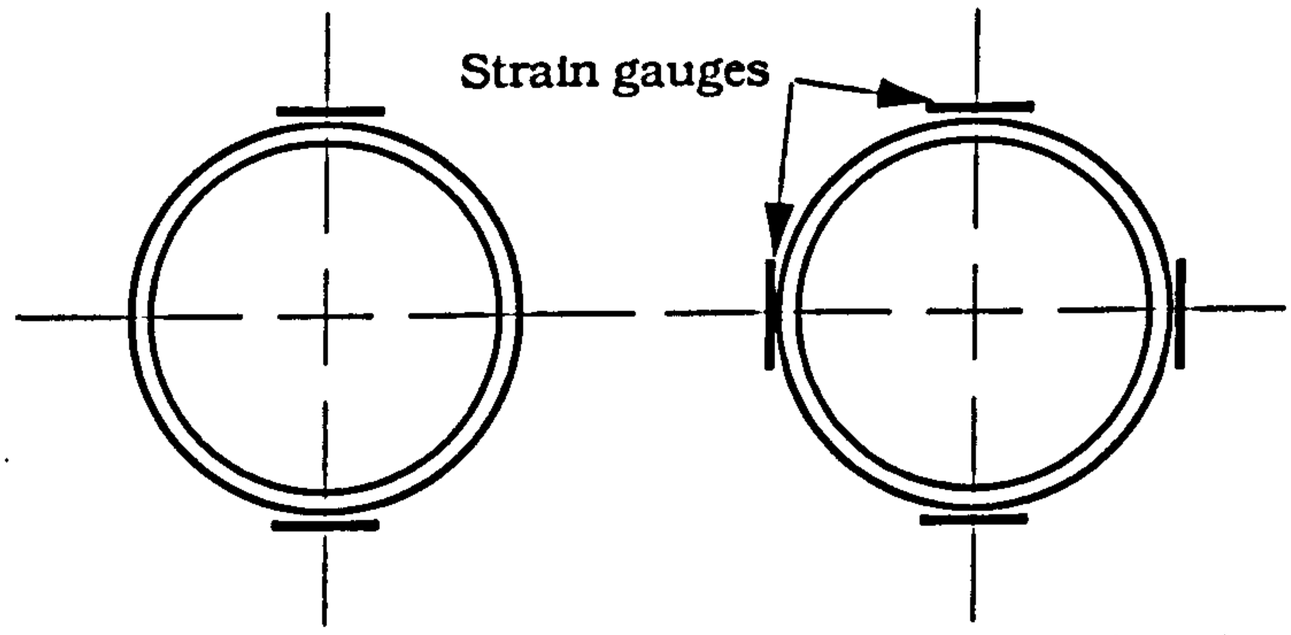


Figure 3.8a Typical strain gauge layout at joint B3

Figure 3.8b Typical strain gauge layout at mid span of chord

Figure 3.8 Strain gauage layout for channel section



(Vertical axis parallel to bottom chord members)

Figure 3.9 Typical strain gauge layout for diagonal members

3.3 INSTRUMENTATION

Transducers were used to record the vertical displacements at the centre of the frame as well as at joints and mid-span locations of both bottom and top chord members. Torsional rotations were measured at the mid-span locations and ends of selected bottom and top chord members. A typical layout of the instrumentation used is shown in Figure 3.6. Lip buckling deformations were measured by means of micrometer. Web crippling and washer plate bending deformations were recorded by using the transducer arrangements shown in Figure 3.7. Longitudinal strains were given by strain gauges located around the perimeter of the channel and tube cross-sections as shown in Figures 3.8 and 3.9 respectively. Computer data acquisition equipment was used to record automatically and store all transducer and strain gauge measurements during testing for later reference.

3.4 MATERIAL TESTS

The channel sections shown in Figures 3.1 and 3.2 as well as all the tubing, nodal inserts and some of the angle reinforcement used in constructing the test frames were manufactured from cold-reduced zinc coated steel. The washer plates were fabricated from hot rolled Grade 43 steel plate.

The tensile specimens taken from various chord and diagonal members were prepared and tested in accordance with BS 18 (1987). Tensile coupons 450 x 50mm, were cut out of the table and web elements of each of the channel sections, whilst 450mm lengths of tubing were cut from individual diagonal members and plugged. All the tensile specimens were then prepared with gauge marks 200mm apart. Each specimen was tested to failure. The materials used in manufacturing the chord and diagonal members were high yield ductile steels with variations in yield stress between 350 N/mm^2 and 510 N/mm^2 and elongations determined at fracture were between 20% to 27% of the original gauge length of 200mm. The yield (σ_o) and ultimate (σ_u) strengths as well as the percentage elongations (%e) obtained for each of the specimens are given in Tables 3.1a to 3.1c. Typical stress-strain curves for the various components are shown in Figure 3.10.

Description		σ_o N/mm^2	σ_u N/mm^2	%e
127x63.5x12.7-2.0mm	table	363	468	22
125x100x20x20-1.5mm	web	384	449	27
	web *	350	512	25
	web*	355	508	27
	table	370	488	26
	table *	360	513	25
125x100x20x20-3.0mm	web	468	516	22
	table	511	562	20

* Specimen edges machined parallel

Table 3.1a Material properties of channel sections

Description	σ_o N/mm^2	σ_u N/mm^2	%e
48mm dia-2.0mm thick	426	450	23
	415	491	19
	415	491	20
60mm dia-2.0 mm thick	395	439	19
60mm dia-2.5 mm thick	427	453	21
	421	450	26
60mm dia-4.0mm thick	497	577	15
70mm dia-3.0mmthick	475	554	22
76mm dia-3.0mm thick	451	420	15

Table 3.1b Material Properties of diagonal tubing

Description		σ_o N/mm^2	σ_u N/mm^2	%e
10mm plate	test1a-1b	297	488	43
15mm plate	test1a-1b	246	451	34
10mm plate	test 2-7	232	292	-
15mm plate	test 2-7	268	297	-

Table 3.1c Material Properties of washer plates (Hounsfield Tests)

For steels which display a definite transition from elastic to plastic deformation the yield stress is taken to be equal to the lower yield value. For steels for which the transition in not clearly evident but occurs progressively, the yield stress has been taken to equal the stress at which the stress-strain relationship becomes non-linear (Figure 3.10).

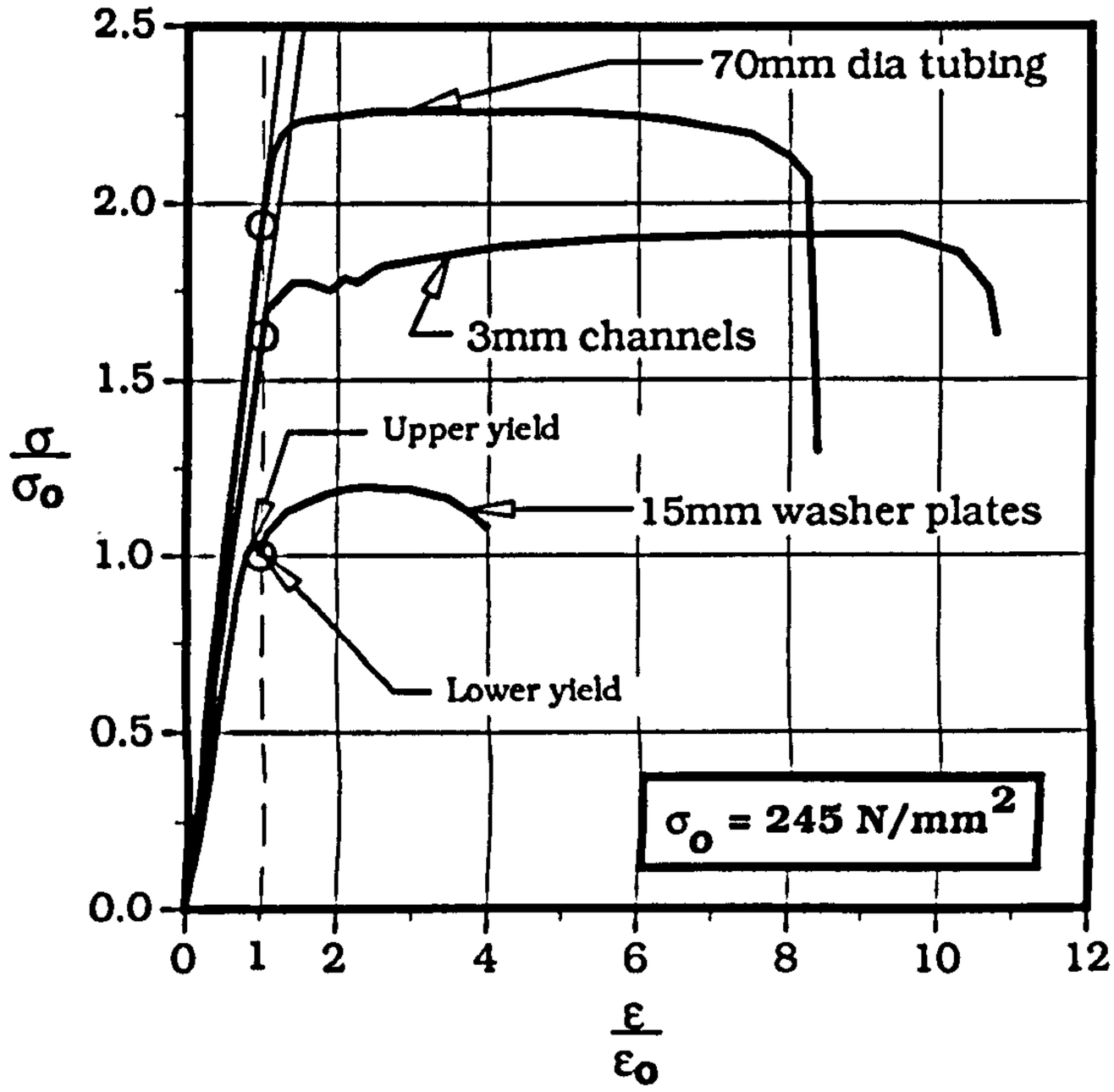


Figure 3.10 Typical stress/strain curves for various component materials

Throughout this thesis the ultimate section resistance has been evaluated by setting the design stress (σ_d) equal to the average yield stress obtained from tensile tests (Table 3.1). The values for Young's modulus of Elasticity (E) and Poisson's ratio (v) are assumed to be equal to 205kN/mm^2 and 0.3 respectively.

3.5 EXPERIMENTAL PROCEDURE

The test frames were constructed by placing the bottom chord lips-down members on trestles approximately 700mm above the laboratory floor. The bottom chord lips-up members were then placed on the lips-down members at right angles. After the bolt holes had been aligned, individual diagonal tube members were inserted into the joints and loosely bolted.

The top chord lips-down channels were then laced between the diagonal members and loosely fastened. The lips-up top chord channels were then placed upon the lips-down members. After the entire frame had been loosely connected each connection was torqued up to a predetermined pre-load (40% of the proof load). The eight reaction points were then levelled horizontally with the aid of a theodolite.

The cruciform member was then raised to engage the four central top chord joints of the frame. The instrumentation was checked for any errors. Each test frame was then subjected to a number of load cycles. So far as possible each test was discontinued when member or joint failure was imminent to prevent general damage to the frame. This was not possible when sudden failure occurred; however, the load was removed as quickly as possible in order to restrict further displacement of the loading ram. In some tests displacement restraints were introduced to limit post-failure damage. The affected members were then either replaced or reinforced. The test frame was loaded to failure after all the desired failure phenomena had been observed.

3.6 EXPERIMENTAL BEHAVIOUR

Seven full size diagonal on square frames were tested with the purpose of observing the mode of failure and obtaining the ultimate load. The frames were all of the same configuration, but constructed of different sized chord and diagonal members. Various methods of reinforcing the frame were also investigated. The various frame arrangements, instrumentation, loading sequence and observed buckling modes as well as the associated failure load for each frame are described in this section. The results from these tests will be used in comparisons made elsewhere in this thesis between existing codes of practice, proposed design recommendations and numerical analyses. The ultimate load and mode of failure for each test are summarised in Table 3.2.

3.6.1 TESTS 1a-1b

Tests 1a and 1b were conducted with the purpose of identifying the predominant modes of failure associated with the diagonal on square space frame. Subsequently, modifications to the design were made based on the preliminary findings of tests 1a and 1b, and on design calculations.

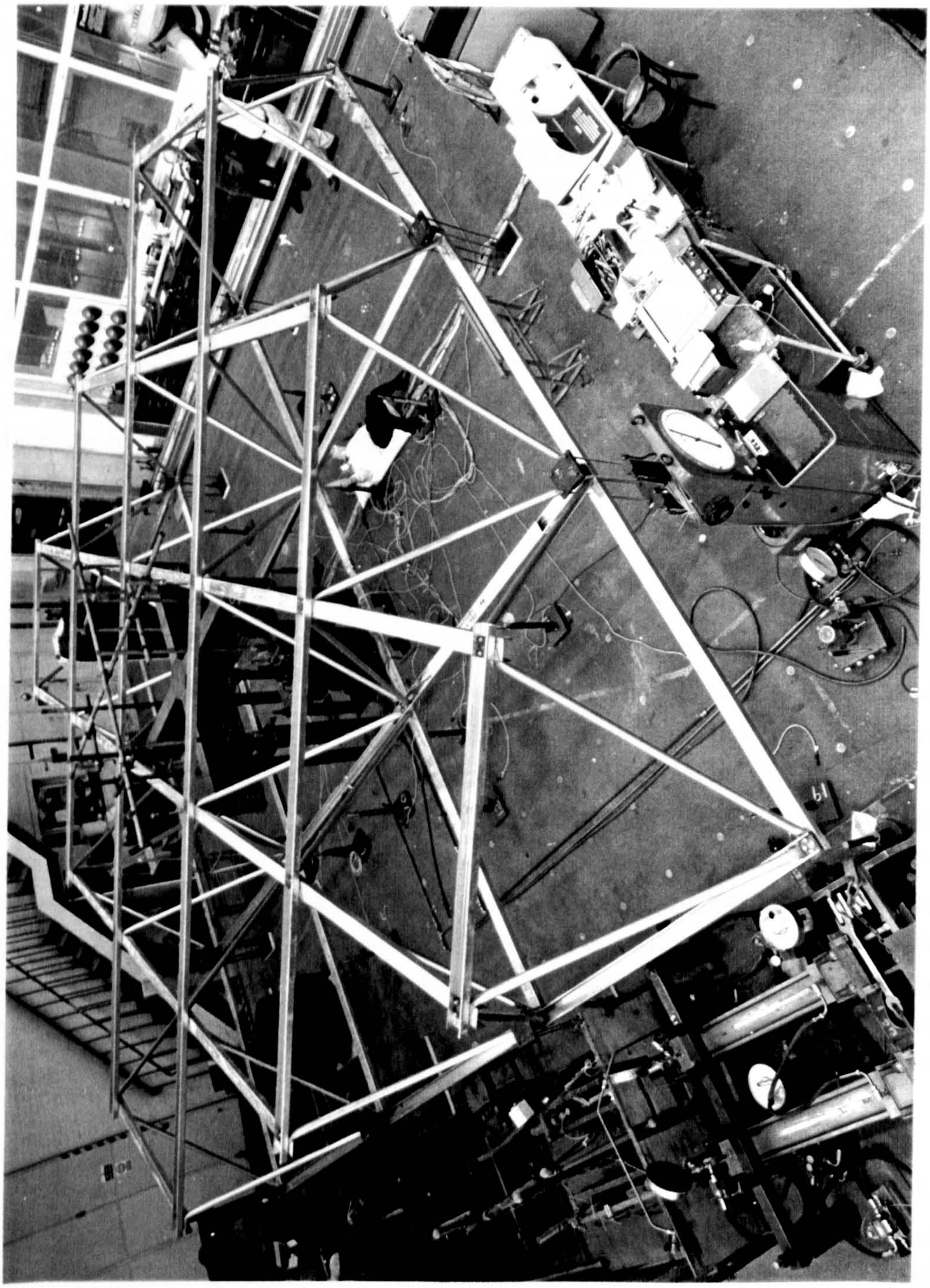


Figure 3.11 Test frame arrangement - Tests 1a - 1b

Test 1a

●*Construction:* 127 x 63.5 x 12.7-2mm thick single lip channels were used for the bottom and top chords of the test frame. All diagonal members were 60mm dia-2.5mm thick tubing. M16 Gr.8.8 bolts and 10mm washer plates were fitted in all joints. All bolts were hand tightened. A general view of the test frame can be seen in Figure 3.11.

●*Instrumentation:* Vertical displacements were measured by using transducers located at predetermined joints and mid-span positions in the bottom chord. Strain gauges were fixed at the mid-span position of members B-23 and 2-BC. End rotations in a vertical plane parallel to the longitudinal axis of two mutually perpendicular members in the bottom chord were monitored by using electro-levels at joints B1, B2 and A2.

●*Observations:* The frame was initially loaded and unloaded in increments of 2.5kN. Vertical displacements, strains and rotations were recorded at the beginning and end of each load cycle. At 140kN the frame was subjected to a constant load for 3 minutes, it was noted that the lips-down member (B-23) had rotated noticeably about its longitudinal axis. During this time interval it was also observed that the overall vertical displacement of the frame continued to increase slowly. Further load was then applied to the frame in increments of 2.5kN up to a load of 150kN and in increments of 1kN up to failure. Flexural buckling of the bottom chord lips-up member (2-BC) occurred at a load of 163kN. Failure was sudden but contained. The frame sustained a residual load of approximately 110kN. Further load was applied to the partially failed frame; this resulted in torsional failure of the bottom chord lips-down member (B-23) as shown in Figure 3.12.

Test 1b

●*Construction:* The bottom chord members B-23, C-23, 2-BC and 3-BC of test 1a were reinforced with 127 x 63.5-2.0mm thick channel capping pieces and 50 x 50-5mm thick hot rolled angles. M16 Gr.8.8 bolts and 15mm washer plates were fitted in all bottom chord joints. With the exception of joints G6 and F8 all top chord joints were fitted with M16 Gr.8.8 bolts and 4-10mm thick washer plates. Joints G6 and F8 were fitted with M16 Gr.8.8 bolts and 2-10mm washer plates.

●*Instrumentation:* Vertical displacements were measured by using transducers fitted at selected joints and at mid-span positions of both the top and bottom chord members. Bending deformation of the 10mm washer plates fitted into joints G6 and F8 were monitored using the transducer arrangement shown in Figure 3.7. The two orthogonal channel sections common to joint G6 were strain gauged as shown in Figures 3.8(a) and 3.8(c). Eight M16 Gr. 8.8 bolts had internal concentric strain

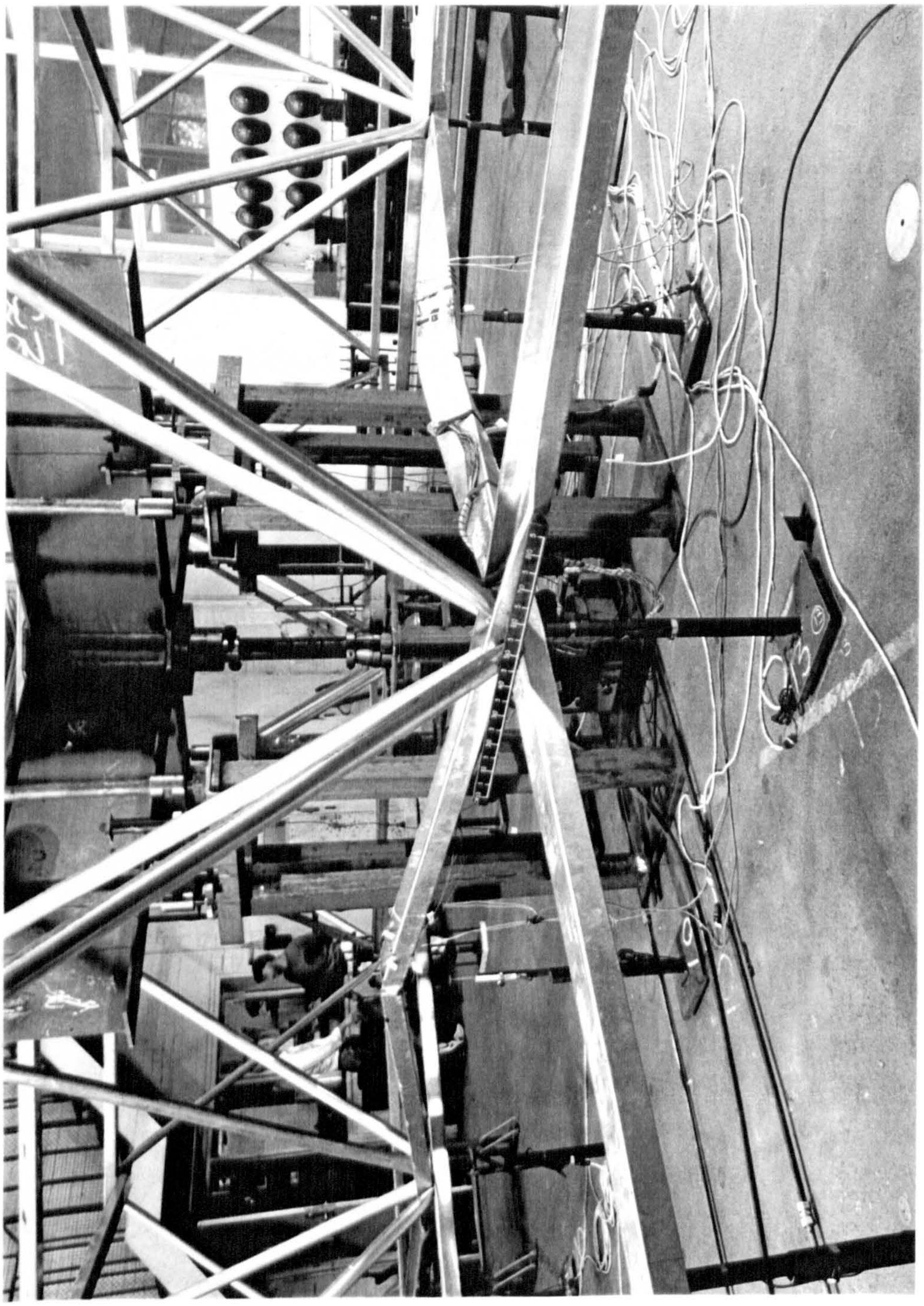


Figure 3.12 Bottom chord failure - Test 1a

gauges located in joints C3 and F8. End rotations in the vertical plane of the two orthogonal members common to joint F8 were also recorded.

●*Observations:* The frame was loaded in increments of 10kN and unloaded after two successive load increments. Vertical displacements, strains, and rotations were measured at each load cycle. Failure of the frame occurred at a load of 250kN caused by web crippling and table tearing in joint F8 as shown in Figure 3.13. No damage to either the 10mm washer plate or the M16 Gr8.8 bolts was observed.

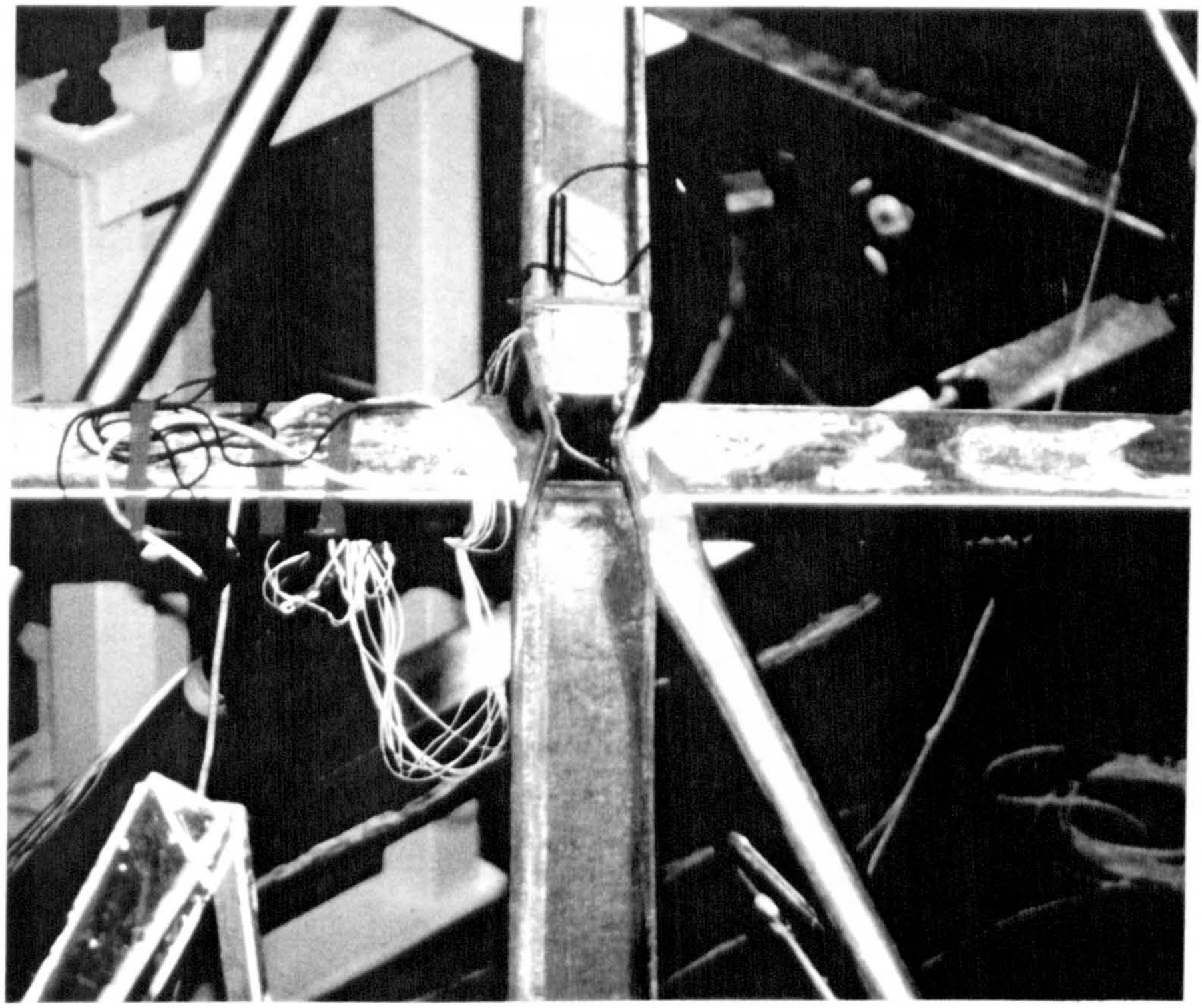


Figure 3.13 Top chord web crippling failure (F8) (See Figure 10.7)

3.6.2 TESTS 2a-2c

The modified channel section shown in Figure 3.2 was better suited to resisting bending moments in the vertical plane caused by the eccentricity between chord and diagonal forces. Increasing the depth of the section increases the eccentricity but reduces the stress caused by the moment and the axial force, and the axial capacity is much increased. The web crippling resistance is reduced.

The tests described in this section were carried out first to determine the web crippling/table shearing capacity of the 3.0mm thick doubly lipped channel section. Having found the web crippling resistance, all joints were then reinforced with 340 x 100-3mm thick nodal inserts (Figure 3.14). Further tests were then carried out to determine both the flexural, and combined torsional-flexural, lateral-torsional buckling resistance of the chord members. The buckling capacity of the 60mm dia-2.5mm thick diagonal tube was also obtained during this test series.

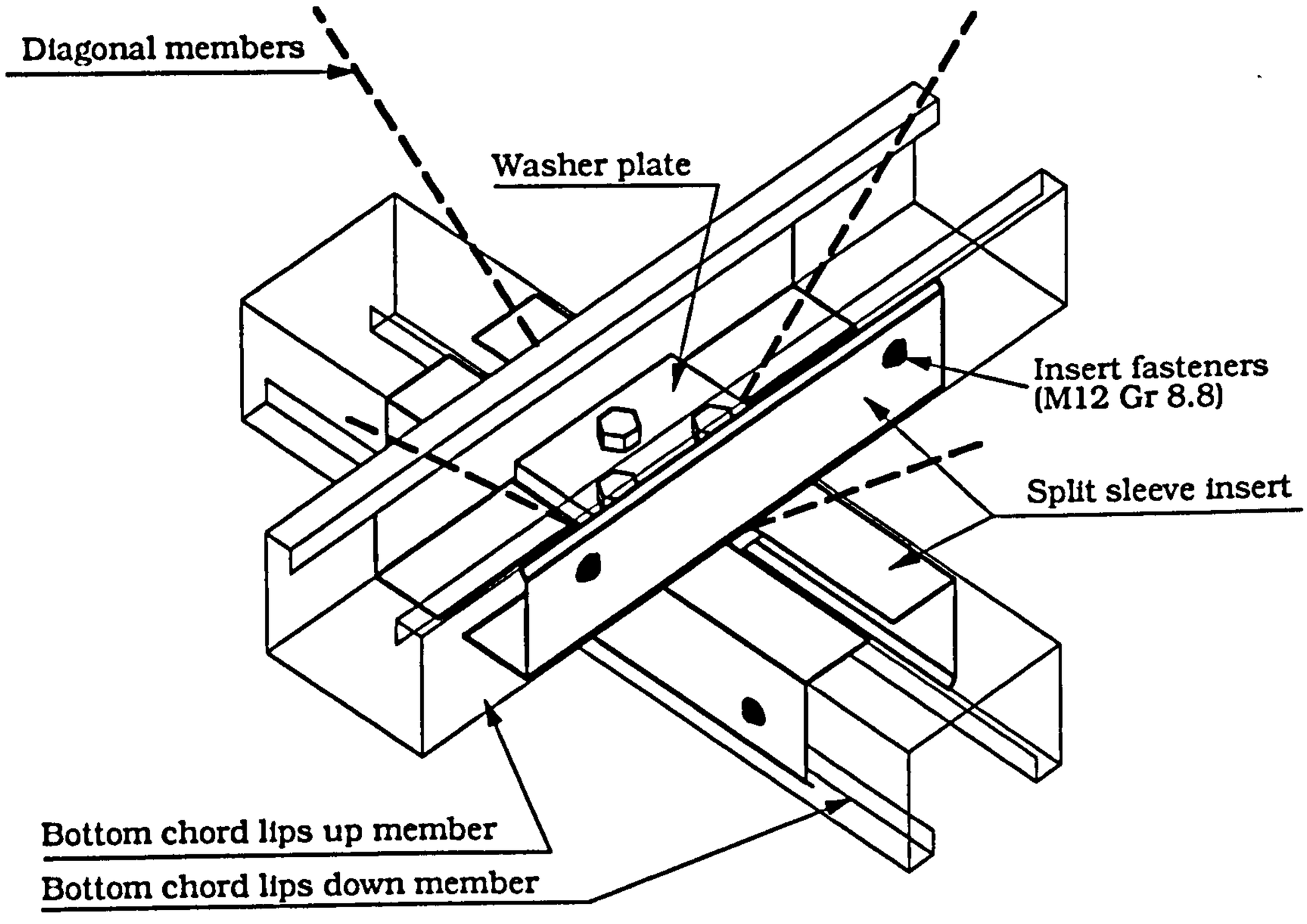


Figure 3.14 Nodal reinforcement

Test 2a

●*Construction:* The bottom and top chords of the test frame were 125 x 100 x 20 x 20-3mm thick double lipped channel sections. All diagonal members along grids B, C, 2 and 3 were 60mm dia, 2.5mm thick tubes. All perimeter diagonals were 48mm dia-2.0mm thick tubes. M16, Gr. 8.8 bolts were fitted in all 48mm dia-2.0mm thick diagonal members and all 60mm dia-2.5mm thick compression diagonals. M20, Gr.8.8 bolts were fitted in all 60mm dia-2.5mm thick tensile tabs. All M16 and M20 bolts were torqued to 120 Nm and 240 Nm respectively. With the

exception of joints B3 and F8 all top and bottom chord joints were fitted with 15mm washer plates and 340 x 100-3.0mm thick nodal inserts (Figure 3.14). 10mm washer plates were fitted at joints B3 and F8. A general view of the test frame can be seen in Figure 3.15.

●*Instrumentation:* Vertical displacements were recorded using transducers located at selected mid-span and joint positions both in the top and bottom chords. The 10mm washer plates in joints B3 and F8 were monitored for possible bending deformations. End rotations of members B-12 and 2-AB were also recorded at each load increment. Strain gauges were fixed at mid-span of members B-23 and 3-BC, and at nodes B3 and F8. The 60mm dia-2.0mm thick diagonal member located at grid B3-F8 was also strain gauged at mid length. Strain gauged M16 Gr 8.8 bolts were introduced into joints B3 and F8.

●*Observations:* The frame was loaded in 10kN increments and unloaded after every second successive increment. Vertical displacements, strains and rotations were measured at each load cycle. At a load of 330kN it was observed that the web of the unreinforced lips-down member at joint B3 had deformed appreciably due to web crippling. The frame was unloaded and joints B3 and F8 were dismantled. After inspection it was observed that the 10mm thick washer plates in joint B3 were bent. Because of the web crippling joints B3 and F8 were reinforced.

Test 2b

●*Construction:* As for test 2a. Joints B3 and F8 now reinforced with 340x100-3.0mm thick nodal inserts and 10mm washer plates replaced by 15mm washer plates.

●*Instrumentation:* As for test 2a

●*Observations:* The frame was loaded and unloaded in increments of 50kN up to a load of 300kN, then in increments of 10kN up to 370kN and finally in load steps of 1kN up to 373kN. Vertical displacements, strains and rotations were measured at each load cycle. A load of 373kN was maintained on the frame for 15 minutes. The load was then increased to 374kN and kept on the frame for a further 15 minutes. At this load a strain of 2000 με and a displacement of 4.5mm were recorded at mid length of the 60mm dia-2.5mm thick diagonal member B3-F8, indicating that first surface yield (ε_o=2300 με) was imminent. The bottom chord lips down member at this load had rotated about its longitudinal axis by 4.2°. The test was suspended and the frame unloaded. All 60mm dia-2.5mm thick compression diagonals were replaced with 76mm dia-3.0mm thick tubes, with M20 Gr. 8.8 bolts.

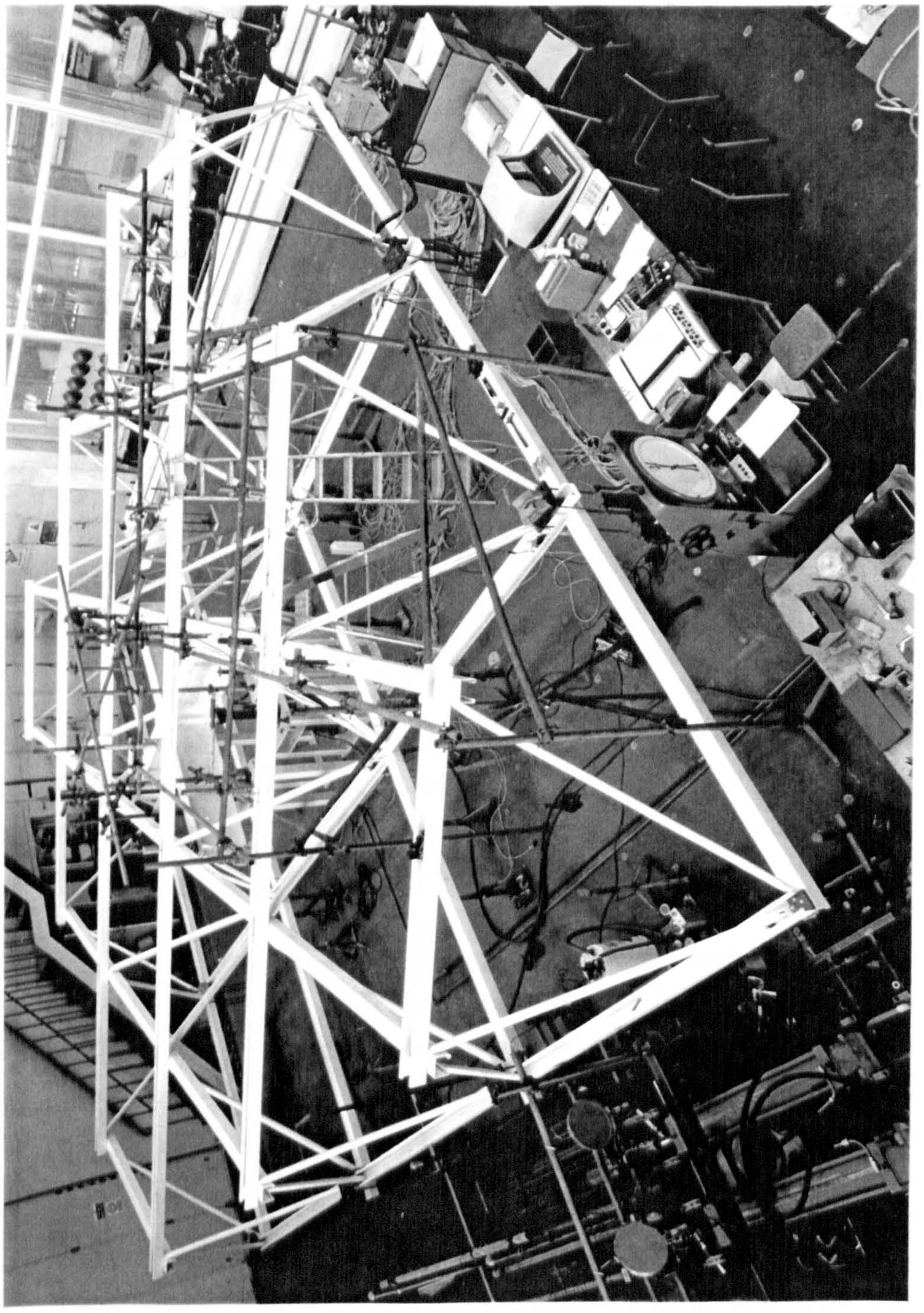


Figure 3.15 Test frame arrangement - Tests 2 - 7

Test 2c

●*Construction:* Same as for test 2a and 2b. All 60mm dia-2.5mm thick compression diagonals were replaced with 76mm dia-3.0mm thick tubes.

●*Instrumentation:* As for test 2a and 2b.

●*Observations:* The frame was loaded and unloaded in increments of 50kN up to a load of 300kN, then in increments of 10kN with unloading taking place after every fifth increment of load. At loads greater than 400kN unloading of the test frame took place at every second increment. Failure occurred suddenly at a load of 460kN and was caused by tab bearing and tearing at the crease of the tab of a 60mm dia-2.5mm thick tension diagonal located at joint B1 (Figure 3.16). This sudden tab failure prompted an extensive study into the bearing behaviour of the diagonal tabs. The results of this study are reported in Chapter Ten and in CESLIC Report CFS1 (1991). Just before failure the torsional rotation of member B-23 about its longitudinal axis was observed to be 6.7^{o}.

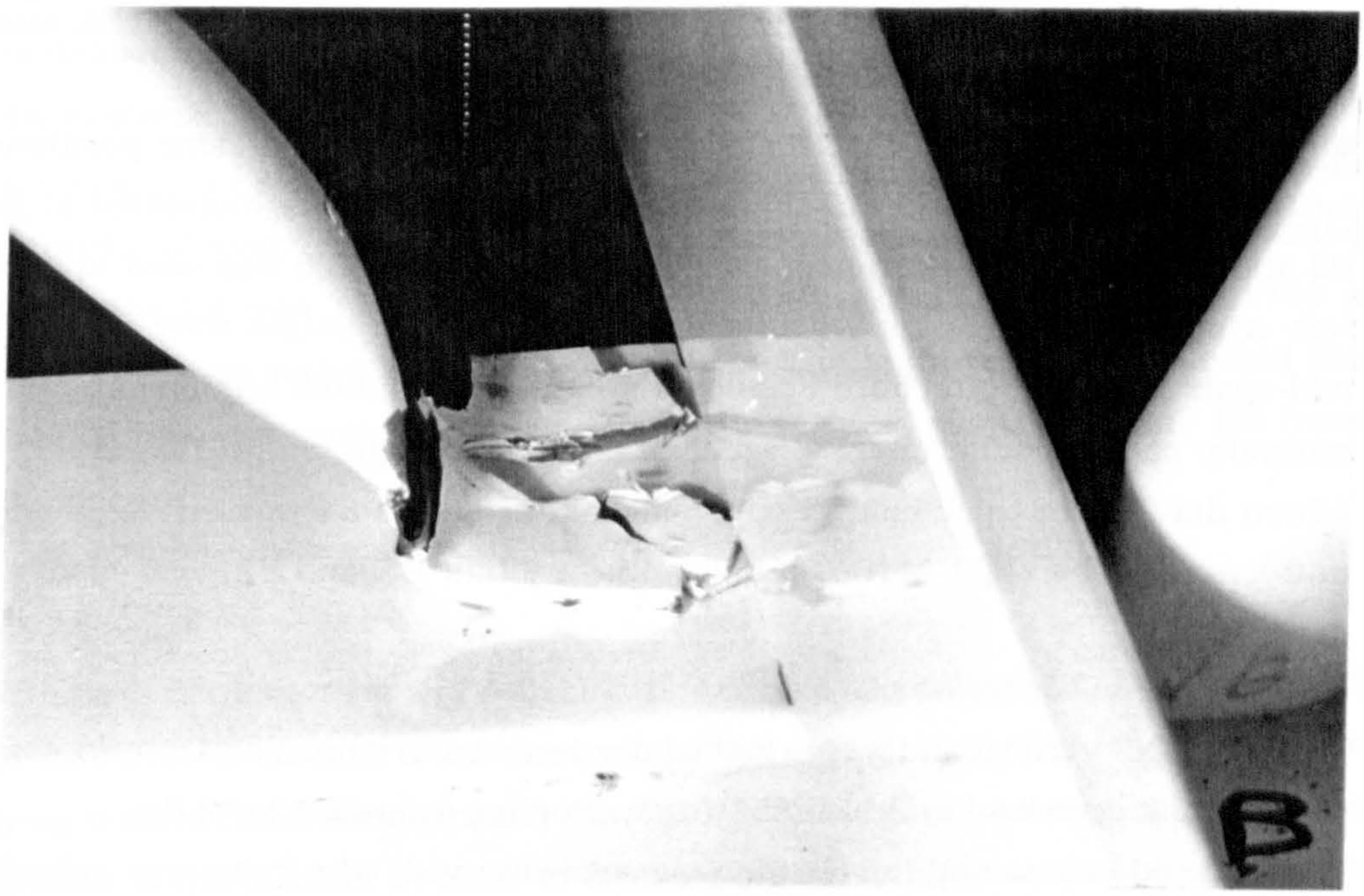


Figure 3.16 Tab bearing failure

3.6.3 TESTS 3a-3e

The tests reported in this section were carried out with the purpose of determining the web crippling/table shearing capacity, the flexural buckling resistance and the

combined torsional-flexural and lateral-torsional buckling resistance of the 1.5mm thick section. Both local element and distortional lip buckling of the cross-section were observed during testing. Tests were also carried out to determine the efficiency of internal diaphragms used to prevent lip buckling and to obtain the ultimate capacity of the bottom chord members. The test procedures adopted in tests 2a to 2c were again repeated for this series of tests.

Test 3a

●*Construction:* The bottom and top chords of the frame were 125 x 100 x 20 x 20-1.5mm thick double lipped channel sections. 48mm dia-2.0mm thick diagonal tubes were used for all tension and perimeter members. With the exception of two compression diagonals located at B3-F8 and B3-F7 all other compression diagonals were 60mm dia-2.5mm thick tubing. 48mm dia-2.0 mm thick tubing was used for members B3-F8 and B3-F7. All the frame joints with the exception of joints B3 and F8 were reinforced with 340 x 100-3.0mm thick nodal inserts. 10mm thick washer plates were fitted in all joints.

●*Instrumentation:* Vertical displacements were measured in the same positions as for tests 2a and 2b. Washer plate bending displacements were monitored at joints B3 and F8. The transducer arrangement shown in Figure 3.8 was used to monitor web crippling deformations at joints B3 and F8. Strain gauges were fitted at the mid-span of the bottom chord lips-down and lips-up channel sections and on two mutually perpendicular channel sections passing through joints B3 and F8. The 48mm dia-2.0mm thick compressive diagonal at grid B-34 was strain gauged at mid-length. The eight M16 Gr. 8.8 bolts in joints B3 and F8 were also strain gauged.

●*Observations:* The frame was loaded and unloaded in increments of 5kN up to a load of 85kN. Vertical and web crippling displacements, strains and rotations were measured at each load cycle. At 85kN web crippling deformations of the unreinforced bottom and top chord joints were observed. The frame was unloaded and joints B3 and F8 were reinforced.

Test 3b

●*Construction:* As for test 3a with additional 340 x 100-3.0mm thick nodal inserts fitted in joints B3 and F8.

●*Instrumentation:* As for test 3a.

●*Observations:* The frame was initially loaded in increments of 10kN up to a load of 80kN and unloaded after two successive increments of load. Further load was applied to the frame in 5kN increments up to 110kN, and then in 1kN increments

thereafter. At loads greater than 100kN the frame was unloaded at 110kN, 120kN, 130kN and 140kN. Vertical displacements, strains and rotations were recorded at each load cycle. Micrometer readings across the open side of the channel section were taken at every 300mm along members B-23 and 2-BC. Local buckling of the table element of the bottom chord lips-up member was observed at 115kN. At 140kN it was observed that substantial cross-sectional deformation was occurring in the vicinity of the bottom chord lips up connections in members 2-AB, 2-CD, 3-AB and 3-CD. It was also observed that at this load a three halfwave distortional lip buckle had formed along the length member B-23.

Test 3c

●*Construction:* As for tests 3a and 3b. The bottom chord lips-up members along grids 2 and 3 were stiffened against distortion of the cross-section with 125 x 100-3.0mm thick diaphragms inserted, 300mm from centre of nodes B2, B3, C2 and C3.

●*Instrumentation:* As for tests 3a and 3b.

●*Observations:* The load on the frame was taken directly to 140kN, then increased in increments of 1kN up to failure. The frame was unloaded after ten successive increments of load. At 160kN the average strain reading at mid-span of member B-23 in the lip was 1161 με (290 N/mm^2), with a maximum stress of 1759 με (360 N/mm^2) occurring in the lip downturn. The stain readings indicated that failure of the cross-section was imminent. The test was suspended and the frame was unloaded.

Test 3d

●*Construction:* As for tests 3a to 3c. 125x100-3 mm thick diaphragms were inserted into members B-23 and C-23 between grids 2 and 3 at a pitch of 600mm. The lips-up bottom chord members BC-2 and BC-3 had beams spanning between nodes and close to the member in order to control post failure displacements, should this occur before failure of the lips-down bottom chord members.

●*Instrumentation:* As for tests 3a to 3c

●*Observations:* The frame was loaded directly to 160kN. Further load was then applied in increments of 2kN up to 180kN and finally in increments of 1kN up to failure. The frame was unloaded after ten successive increments of load. Failure of the frame occurred at a load of 188kN caused by flexural buckling of the bottom chord lips-up member 3-BC.

Test 3e

●*Construction:* As for tests 3a to 3d. Members 2-BC and 3-BC were reinforced with 127x63.5-2.0mm thick channel sections and 50x50-5mm hot rolled angle.

●*Instrumentation:* As for tests 3a to 3d

●*Observations:* The frame was loaded directly to 160kN, then increased in increments of 2kN up to a load of 180kN, and in 1kN increments thereafter up to failure. The frame was unloaded after every multiple of 10kN was attained. Vertical displacements, strains and torsional rotations were measured at the beginning and end of each load cycle. Failure occurred at a load of 200kN, caused by buckling of the 48mm dia-2.0mm thick compression diagonal located at grid B3-F7, shown in Figure 3.17. The frame was unloaded and the buckled diagonal member was straightened and reinforced with angle sections. The load was again increased to 200kN and incremented in steps of 1kN. Failure occurred at a load of 210kN, caused by a combination of torsional-flexural and lateral torsional-buckling of member B-23 (Figure 3.18). Prior to failure the rotation about the longitudinal axis of member B-23 was 10°.



Figure 3.17 Diagonal buckling failure of 48mm dia - 2.0mm thick tubing

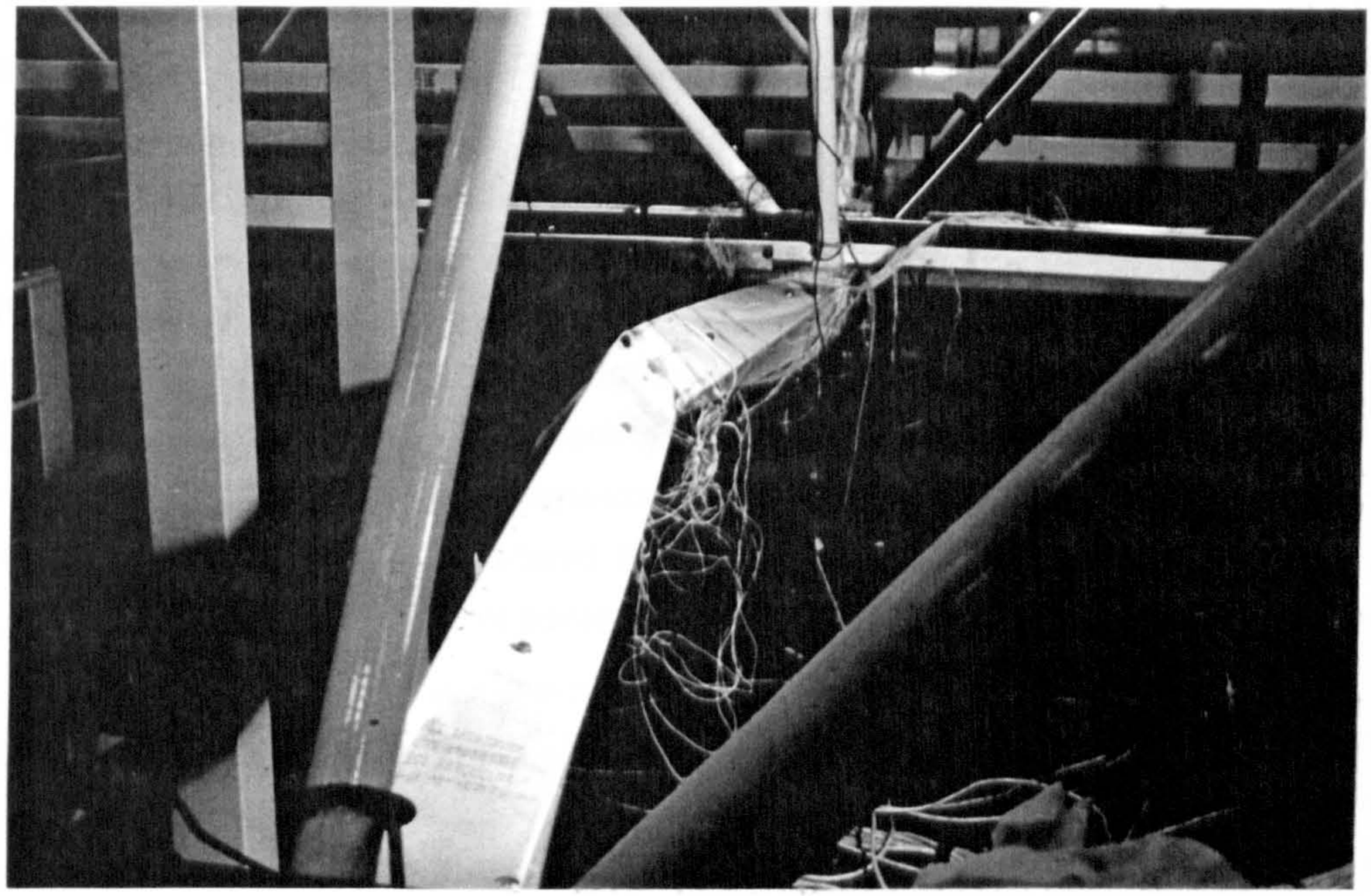


Figure 3.18 Torsional-flexural/lateral-torsional buckling failure of bottom chord lips down member

3.6.4 TESTS 4a-4c

The tests described in this section were carried out to observe and to obtain a better understanding of the behaviour of the top chord connections and members, and to determine the ultimate load capacity. During the tests web crippling of the 1.5mm thick section, washer plate bending and bottom chord tab bearing/tab tearing were all observed.

Test 4a

- *Construction:* The perimeter of the test frame was constructed of 125 x 100 x 20 x 20-1.5mm thick sections while 3mm thick sections were used along grid lines B, C, 2 and 3. The top chord consisted entirely of 125 x 100 x 20 x 20-1.5mm thick sections. 48mm dia-2.0mm thick diagonal tubes were used in all tension diagonals. 60mm dia-2.5mm thick diagonal tubes were used in all compression diagonals. M16 Gr.8.8 bolts were used in all joints. With the exception of joint F8 all top and bottom chord joints were fitted with 10mm washer plates and reinforced with 340 x 100-3.0mm nodal inserts. Joint F8 was fitted with 6mm washer plates.

●*Instrumentation:* Vertical displacements were measured in the same positions as for the test series three. An additional 8 strain gauges were fixed to the two orthogonally intersecting members at joint F8. The four M16 Gr.8.8 bolts in joint F8 were strain gauged. Washer plate bending deformations at joint F8 were recorded. Web crippling deformations were measured at joints B3 and F8.

●*Observations:* The load was applied to the frame in 10kN increments up to a load of 140kN, and unloaded after two successive load increments. After a load of 100kN was attained, unloading was carried out after each increment. At a load of 140kN web crippling deformations were observed in member 8-EF adjacent to joint F8. The frame was unloaded and joint F8 was reinforced with nodal inserts. The 6mm washer plates in joint F8 were inspected for bending deformations. As no washer plate deformations were evident they were retained in joint F8 for further testing.

Test 4b

●*Construction:* As for test 4a. Joint F8 now reinforced with nodal inserts.

●*Instrumentation:* As for test 4a.

●*Observations:* The frame was loaded in increments of 20kN up to 240kN then in 10kN increments up to failure. The frame was unloaded after every second successive increment of load. The load was maintained on the test frame for approximately 5 minutes at every increment of load greater than 260kN. Readings were taken at the beginning and end of each load increment. It became evident during this test that the 6.0mm washer plates were bending. At a load of 300kN further loading was suspended and the frame was unloaded. The 6mm washer plates were removed and replaced with 10mm plates.

Test 4c

●*Construction:* As for test 4b. Joint F8 fitted with 10mm washer plates.

●*Instrumentation:* As for tests 4a and 4b.

●*Observations:* The frame was loaded in increments of 20kN up to 280kN then in 10kN increments up to 300kN and finally in increments of 5kN to failure. Unloading was carried out after each increment of load up to 300kN then in increments of 10kN. At a load of 310kN the load was maintained on the frame for a period of approximately 5 minutes. Measurements were taken at the beginning and end of this interval. At 320kN, 330kN, 340kN, 350kN and 360kN the load was maintained on the frame for 5 minutes. Frame failure occurred at a load of 360kN caused by tab bearing and tearing along the crease of the 48 dia-2.0mm thick tension diagonal tube located at node B1.

3.6.5 TESTS 5a-5d

The purpose of this series of tests was to obtain the bolt capacity for combined shear and tension. Various grades of bolt were used during this test series i.e. Gr. 4.6, Gr. 8.8, Gr. 10.9 and Gr. 12.0, while the diameter was either M12 or M16, thereby ensuring that several bolt failures would occur. The predominant mode of failure observed was bolt bending. Additional tests were carried out to obtain the ultimate buckling resistance for a 60mm dia compression tube, and the bottom chord tab bearing capacity for a 76mm-3.0mm thick tension diagonal tube.

Test 5a

●*Construction:* The frame was constructed entirely of 3.0mm thick channel sections. With the exception of joints B2, B3 and H6 all the joints were sleeved with nodal inserts. Joints C3, I7 and G9 were fitted with 10mm washer plates, whilst the remaining joints in both the top and bottom chords were fitted with 15mm washer plates. M16 Gr.4.6 bolts were fitted and torqued to 40 Nm in joints C3, I7 and G9. M16 Gr. 8.8 bolts were fitted and torqued to 120Nm in all remaining joints. Two 60mm dia-2.5mm thick compression diagonals were located at grids B3-F7 and B3-F8. The remainder of the compression diagonals and all internally located tensile diagonals consisted of 76mm dia-3.0mm thick tubes. The bottom chord tabs of the 76mm dia-3.0mm thick diagonals were machined at their edges in order to permit insertion into the locally reinforced bottom chord lips-up joints B2, B3, C2 and C3. All perimeter diagonals were 60mm dia-2.5mm tubes.

●*Instrumentation:* Vertical displacements were measured at selected mid-span and joint positions both in the top and bottom chords. Strain gauges were located at mid-span of members B-23 and 2-BC. All diagonal members along grid lines B and 2 were strain gauged at their mid length. Strain gauges were fitted to tensile diagonal members A3-F7, D3-H9, C4-G9 and C1-H7. The M16 Gr. 4.6 internally strain gauged bolts (Figure 10.21) were fitted into joints C3 and I7. The elongation of each M16 Gr.4.6 bolt was measured with a specially adapted micrometer. Web crippling deformations were monitored at joints B3 and H6.

●*Observations:* The frame was loaded in increments of 20kN up to a load of 320kN then in increments of 10kN thereafter. Measurements were recorded at each load increment. Bolt elongations were read at every multiple of 60kN. When the load on the frame reached 330kN it was held for 10 minutes. It was then increased to 340kN and held for a further 10 minutes. Instrument readings were taken at the beginning and end of each interval. The frame was then unloaded. The M16 Gr.4.6

bolts in joints C3 and G9 were inspected for visible damage. The four bolts in joint C3 were found to have bent. Further inspection of the frame revealed that the 76mm dia-3.0mm thick tensile diagonals had begun to crack along the tab crease. Web crippling deformations were also observed in the unreinforced joints B2, B3 and H6.

Test 5b

- *Construction:* As for test 5a. All joints reinforced with 340x100-3.0mm thick nodal inserts. All 10mm washer plates replaced with 15mm washer plates. Four M12 Gr.8.8 bolts were introduced into joint C3 and torqued to 45 Nm, while the M16 Gr.4.6 bolts in joints I7 and G9 were retained .
- *Instrumentation:* As for test 5a
- *Observations:* The frame was subjected to the same load sequence used in test 5a. When the load reached 340kN it was held for 10 minutes. Instrument readings were taken at the beginning and end of this load increment. The load was then increased to 380kN. Failure occurred shortly after reaching 380kN, caused by transverse tearing along the crease of a machined 76mm dia-3.0mm thick tensile tab located at joint B3. The frame was unloaded and the remaining 76mm dia-3.0mm thick tensile tabs were reinforced with weld beads along the machined sides of the tab. The M12 Gr.8.8 bolts in joint C3 were inspected and found to be bent, they were replaced with M12 Gr.10.9 bolts. The M16 Gr.4.6 bolts in joint I7 were also inspected for deformations. As no deformations were observed they were retained in joint I7 for further testing.

Test 5c

- *Construction:* No change from tests 5a and 5b. M12 Gr.10.9 bolts were fitted into joint C3, and torqued to 65Nm. M16 Gr.4.6 bolts retained in node I7. M16 Gr.4.6 bolts in joint G9 were replaced with M12 Gr.8.8.
- *Instrumentation:* As from tests 5a and 5b.
- *Observations:* Initially 20kN increments of load were applied to the frame up to 340kN. Instrument readings were taken at each increment of load, while bolt elongations were read at 60kN, 120kN, 180kN, 240kN and 300kN. When the load reached 340kN it was held for 10 minutes. It was then increased to 380kN in increments of 10kN. Bolt elongations were also recorded at loads of 360kN and 380kN. At 380kN the lateral displacement at mid-length of the 60mm dia-2.5mm thick compressive diagonal was observed to be approximately 11mm with a maximum strain of 1300 $\mu\varepsilon$. The load was then slowly increased in 5kN increments. Failure occurred at 440kN caused by buckling of the 60mm dia-2.5mm thick

diagonal (B3-F7). The frame was unloaded and inspected. The M16 Gr.4.6 bolts in joint G9 as well as the M12 Gr.10.9 bolts in joint C3 were observed to be slightly bent. These bolts were retained for further testing.

Test 5d

●*Construction:* As for test 5a to 5c. The two 60mm dia-2.5mm thick diagonals from test 5c were replaced with 76mm dia-3.0mm thick diagonals. Member C-23 was reinforced with a 127x65-2.0mm thick channel section, while member BC-3 was reinforced internally with four lengths of two metre cold-formed angle sections, spliced at mid-span.

●*Instrumentation:* As for tests 5a to 5c. Torsional rotations about the longitudinal axis of both the reinforced (C-23) and unreinforced (B-23) lips-down bottom chord sections were measured and recorded..

●*Observations:* The load was applied to the frame in 20kN increments up to a load of 440kN. Instrument readings were taken at each increment of load. The frame was unloaded after increments of 100kN were attained. Bolt elongations were recorded prior to unloading. At 340kN the load was held on the frame for 10 minutes. It was then slowly increased to 440kN; the torsional rotations at mid-span of members C-23 and B-23 were 2.62^{o} and 5.3^{o} respectively. Additional load was then applied in increments of 10kN up to 490kN, and in 5kN increments thereafter. At 510kN the 76mm dia-3.0mm thick diagonal failed due to tab bearing and tearing along the tab crease located at joint B1.

3.6.6 TESTS 6a-6c

This series of tests were carried out to obtain the tab bearing and or tab tearing capacity of various diameters of tensile diagonal tubing. The 3mm thick members bottom chord members of the frame were reinforced to prevent flexural, torsional-flexural and lateral-torsional buckling. Diagonal buckling was also observed during these tests.

Test 6a

●*Construction:* The top and bottom chords were 125 x 100 x 20 x 20-3.0mm thick sections. Members B-23, C-23, 2-BC and 3-BC were reinforced internally with cold-formed angle sections. All joints were reinforced with nodal inserts and fitted with 15mm washer plates. M16 Gr.8.8 bolts were fitted into all joints. All bolts were torqued to 120Nm. The perimeter diagonals were 60mm dia-2.5mm thick tubes.

Compression diagonals were 70mm dia-3.0mm thick while all tension diagonals were 60mm dia-4.0mm thick. Two 48mm dia-2.0mm thick tension diagonals were located at B1-H6 and C1-I7. Whilst assembling the frame it was observed that the bolt holes in the top chord tabs of the 60mm dia-4.0mm tension diagonals did not align with the holes of the top chord members. Consequently, some of the tab bolt holes were reamed.

●*Instrumentation:* Vertical displacements were measured at the same transducer positions as for tests 5a to 5e. Strain gauges were located at the mid-span of the bottom chord lips-down and lips-up channel sections along grids B-23 and 2-BC. The 48mm dia-2.0mm thick tension diagonal member located along grid B1-H6 was strain gauged at mid length of the member. Bolt hole elongation of the two 48mm dia tabs at joints B1 and C1 were recorded during testing.

●*Observations:* Load increments of 20kN were applied to the frame up to a load of 320kN. The frame was unloaded after each increment. At a load of 200kN it was observed that the 48mm dia tensile tabs had begun to lift away from the bottom chord at joints B1 and C1. Additional load was applied to the frame at 340kN in 10kN increments up to a load of 370kN. Unloading of the frame was carried out after two successive increments of load and also at 370kN. No bolt hole elongations were observed in either of the 48mm dia-2.0mm thick tabs at 370kN. Further load was then applied in increments of 5kN. At 420kN the bolt hole elongation of tab C1-I7 at joint C1 had increased to 3.0mm. This load was maintained on the frame for a period of 10 minutes. At the end of this load increment the bolt hole elongations were observed to have increased to 6.0mm indicating that failure of the 48mm dia-2.5mm thick tab was imminent and the test was suspended. Diagonals B1-H6 and C1-I7 were removed for inspection. The bolt holes were observed to have elongated by 4.6mm and 9.2mm respectively (Figure 3.19).

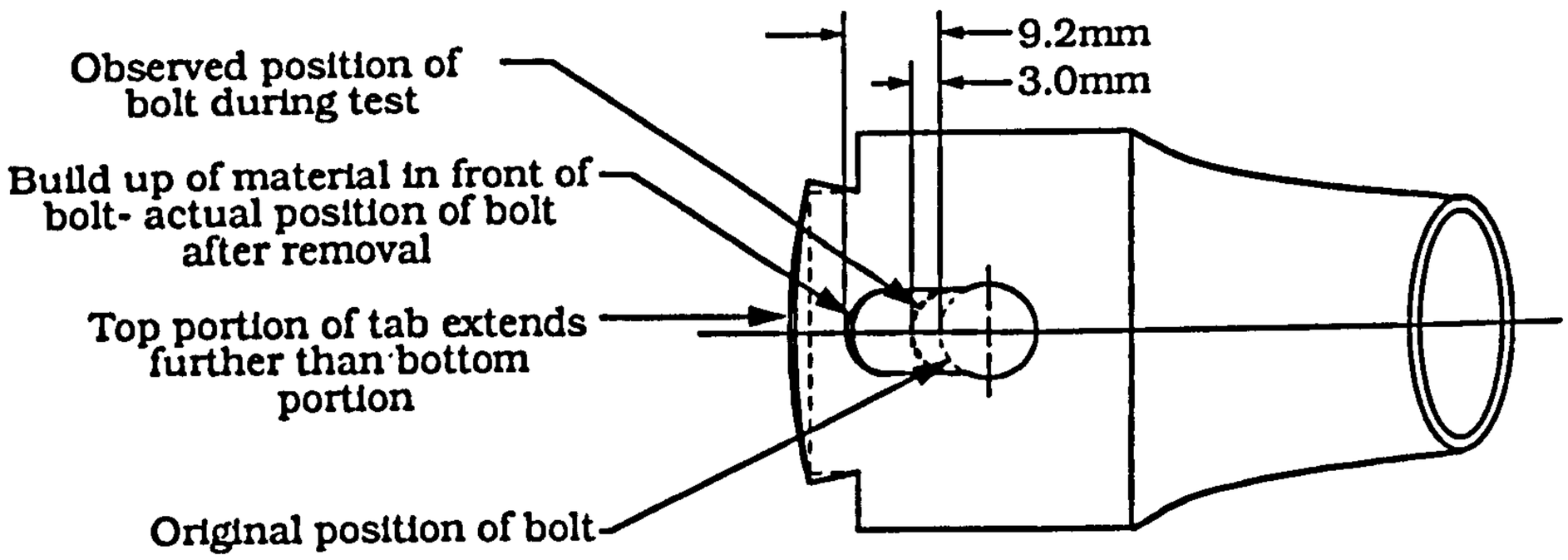


Figure 3.19 Bolt hole elongation in 48mm dia-2.0mm thick diagonal tubing (P=420kN)

Test 6b

Construction: Same as for test 6a. The 48mm dia-2.0mm thick tension diagonals B1-H6 and C1-I7 were replaced with 60mm dia-2.5mm thick tubes.

●*Instrumentation:* No change from test 6a

●*Observations:* The load was applied to the frame in 20kN increments up to 380kN. At 380kN the load was maintained on the frame for 10 minutes. No visible bolt hole elongations were observed at joints B1 and C2. Further load was applied in increments of 10kN up to failure. The load was held for 5 minutes at 470kN, 500kN, 520kN, 530kN, 540kN, 560kN and 570kN. Instrument readings were taken at the beginning and end of each load increment. At 480kN some bolt hole elongation was observed. When the load reached 570kN it was observed that the bolt hole elongation had increased to 6.0mm. The test was suspended at 570kN due to the imminence of tensile tab failure of the 60mm dia-2.5mm tube.

Test 6c

●*Construction:* As for test 6a and 6b. The 60mm dia-2.5mm thick tension diagonals B1-H6 and C1-I7 were replaced with 70mm dia-3.0mm thick tubes.

●*Instrumentation:* Six additional strain gauges were fixed to the top chord member along grid 8 near to joints F8.

●*Observations:* The frame was loaded up to 500kN in increments of 50kN. Unloading was carried out at every 100kN. Instrument readings were taken at each load increment. At 500kN the bolt hole elongation recorded at joints B1 and C1 were approximately 2.0mm. The load was then increased in increments of 10kN up to failure. At 580kN and 590kN the load was maintained on the frame for 5 minute and for 10 minutes at 600kN. Failure occurred at 600kN, caused by compressive buckling of a 70mm dia-3.0mm thick diagonal (B3-F7). The failed member was removed and replaced with a 76mm dia-3.0mm thick tube. The frame was again loaded to failure. Failure occurred at 630kN, caused again by buckling of a 70mm dia-3.0mm thick diagonal (C2-I8). The test was repeated for a third time. Failure occurred at 650kN caused by buckling of a 70mm dia-3.0mm thick diagonal (B2-G6).

3.6.7 TESTS 7a-7d

This final series of tests were carried out with the purpose of observing the torsional-flexural/lateral-torsional buckling behaviour and to obtaining the ultimate

capacity for torsionally reinforced doubly-lipped 1.5mm and 3.0mm thick channel sections having various reinforcement arrangements. A number of tests were firstly carried out to determine the optimum position and the number of anti-twist battens required (Figure 3.20). The optimum arrangement was then used in the frame tests. It was observed that by providing ant-twist battens along the length of a bottom chord member that the torsional rotation at mid-span could be suppressed, while substantially increasing the ultimate failure load of the member. Tests were also carried out to obtain the compressive buckling capacity of both the 60mm dia-4.0mm thick, and 76mm dia-3.0mm thick compression diagonals. During testing tab bearing failure of a 70mm 3.0mm thick tension diagonal was also recorded.

Test 7a

- *Construction:* Same as tests 6c with member B-23 replaced with a 1.5 thick section and reinforced with anti-twist battens, as shown in Figure 3.20. All 70mm dia-3.0mm thick compression diagonals replaced with 76mm-3.0mm thick tubes. All joints were reinforced with nodal inserts and fitted with 15mm washer plates. M16 Gr.8.8 bolts were fitted into all joints.
- *Instrumentation:* As for tests 6a to 6c.
- *Observations:* The torsional behaviour of 34 different torsional stiffener arrangements was observed by systematically changing the length, number of bolts used to fasten each batten to the channel, and the location of the anti-twist battens. Three lengths of 3mm thick anti-twist batten, 340mm, 510mm and 670mm, were used to reinforce the channel section. The anti-twist battens were fastened to the channel section with either four or eight M12 Gr.8.8 bolts located just below the level of the lip down-turn as shown in Figure 3.20. Maximum restraint against torsional rotation of the section was obtained by locating three battens along member B-23. Two 510mm lengths were located at 594mm from the centre of the joints B2 and B3, the third, a 340mm length of stiffener located at mid-span of B-23. This batten arrangement was adopted for further testing. The frame was again loaded incrementally with instrument readings, torsional rotations and lip displacements taken at 100kN, 150kN, 180kN, 200kN, 220kN, 230kN and 240kN. At 240kN the torsional rotation about the longitudinal axis of member B-23 was recorded to be 3°. Member B-23 failed at a load of 240kN, caused by a combination of torsional-flexural and lip buckling.

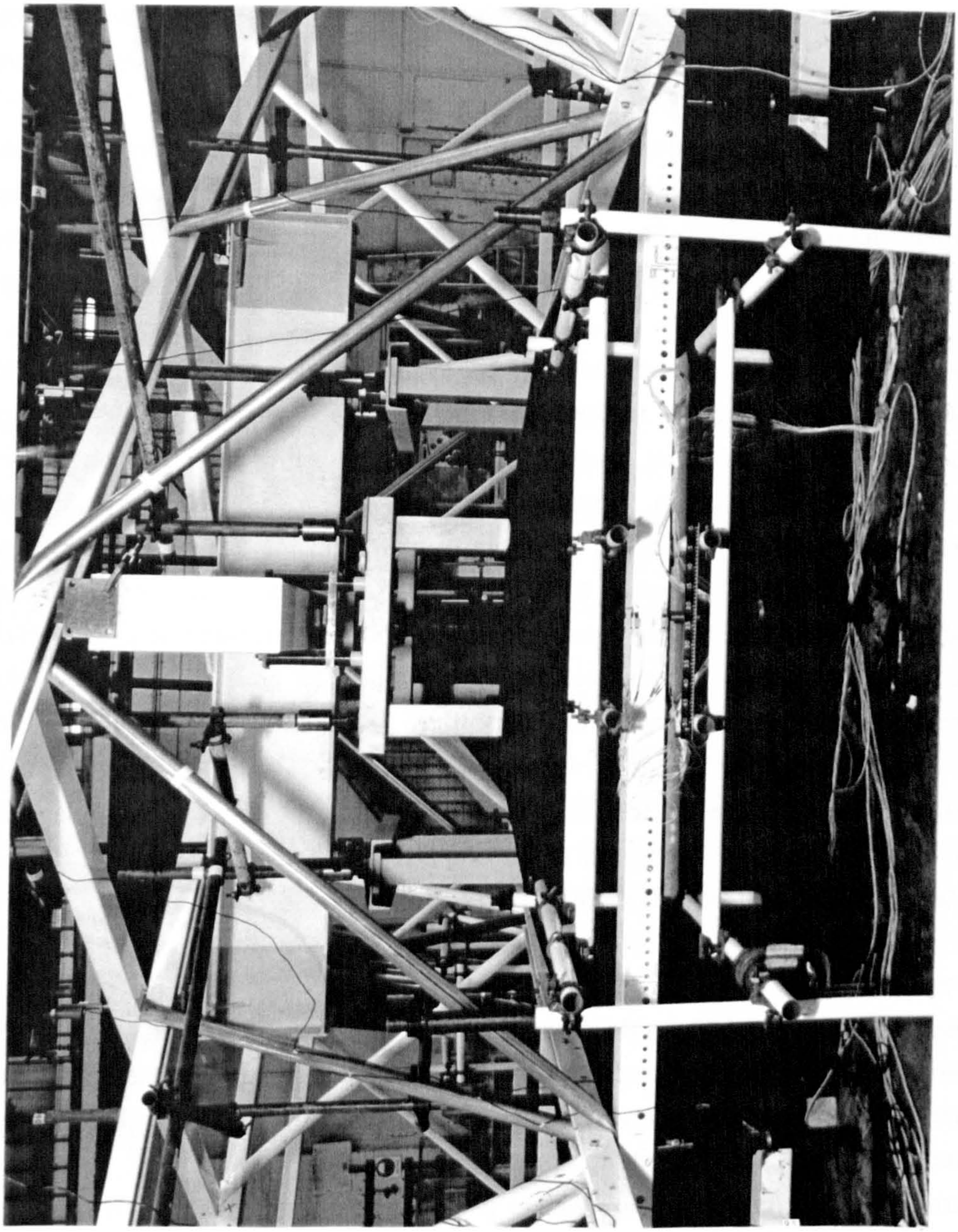


Figure 3.20 Anti-twist arrangement - bottom chord lips down member

Test 7b

●*Construction:* The failed 1.5mm channel section was replaced with a 3.0mm thick section with two 510mm-3.0mm thick anti-twist battens located 594mm from the centre of joints B2 and B3. Four M12 Gr.8.8 bolts in 13mm holes were used to fasten each torsional stiffener to member B-23. Two 60mm dia-4.0mm thick compression diagonals were located at B3-F8 and B3-F7. Tensile diagonal members B1-H7, C1-I7 and D2-I8 were 70mm dia-3.0mm thick tubes.

●*Instrumentation:* No change in the position of the bottom and top grid transducers. No change in strain gauge locations. Lip displacements were measured by micrometer along member B-23 at a pitch of 300mm. Torsional rotations about the longitudinal axis of member B-23were measured at joints B2 and B3, and at mid-span.

●*Observations:* The frame was initially loaded in increments of 100kN up to 300kN, then in increments of 50kN to 500kN. Instrument readings, rotations and lip displacements were taken at each load increment. At 500kN the frame was unloaded and readings taken. The load on the frame was again taken to 500kN, further load was then applied in increments of 10kN. At 540kN the torsional rotation at mid-span of member B-23 was 8°. As the torsional rotations were considered to be excessive the test was suspended and an additional four M12 Gr.8.8 bolts were fitted 68mm from the first set of M12 bolts. Load was again applied to the frame in increments of 100kN up to 500kN and then in increments of 10kN up to failure. The torsional rotation of member B-23 at 540kN was 5°. This represented a decrease in torsional rotation of 40% over the previous bolt arrangement. The frame eventually failed at a load of 630kN caused by buckling of the 60mm dia-4.0mm thick diagonal compression tube B3-F7.

Test 7c

●*Construction:* The two 60mm dia-4.0mm thick compression diagonals used in test 7b were replaced with 76mm dia-3.0mm thick tubing. The nodal inserts and 15mm washer plates in node F7 were removed and replaced with 8mm purlin support washer plates. M16 Gr.8.8 bolts were used in all nodes.

●*Instrumentation:* As for test 7a. Washer plate bending were measured by means of micrometer.

●*Observations:* Load increments of 50kN were applied to the frame up to a load of 250kN, then in 10kN increments up to 320kN. Instrument and micrometer readings were taken at each load increment. The test was suspended at 320kN as web crippling of the 3mm chord member previously occurred at 330kN. The washer plates located in joint F7 were removed and inspected for permanent deformations.

As some deformation was evident joint F7 was subsequently fitted with 15mm washer plates and nodal inserts The frame was again loaded for a second time in increments of 100kN up to 600kN, then in increments of 10kN thereafter. Failure of the frame occurred at 700kN caused by tab bearing and tab tearing along the crease of a 70mm dia-3.0mm thick tensile diagonal located at joint C1.

Test 7d

●*Construction:* Member B-23 was reinforced with 3mm thick angle inserts which were spliced at mid-span. A 12mm purlin washer plate was fitted into joint F7. The remaining 70mm dia-3.0mm tension diagonals were all replaced with 60mm dia-4.0mm tension members.

●*Instrumentation:* No change in instrumentation. Member torsional rotations at joint F7 were recorded.

●*Observations:* The load was applied to the frame in increments of 100kN up to 600kN, then in increments of 10kN up to 650kN, and 5kN increments thereafter. At 670kN the mid-span longitudinal rotation of member B-23 was approximately 21°. At 675kN it was observed that the strain gauge fixed to the lip-downturn of member B-23 had in fact exceeded the material yield strain (2300 με). The test was suspended and the frame unloaded. Member B-23 was then capped with a 127 x 65-2.0mm thick channel section. The frame was again loaded to 600kN in increments of 100kN, then in 10kN load steps up to 700kN. The load was held on the frame for 5 minutes at each load increment greater than 660kN. Instrument readings were taken at the beginning and end of each load increment. On reaching 670kN for a second time the longitudinal rotation measured at mid-span of member B-23 was approximately 11°. Further load was applied to the frame in increments of 5kN up to failure. At 750kN it was observed that the unsupported portion of the tabs at then ends of the 76mm dia-3.0mm thick compression tube had deformed appreciably. The frame failed at 760kN caused by buckling of the 76mm dia-3.0mm thick diagonal (C2-I8).

3.6.8 SUMMARY OF TESTS RESULTS.

The failure loads and the mode of failure observed for each of the frame tests can be found in Table 3.2.

TEST FAILURE	1a	1b	2a	2b	2c	3a	3b	3c	3d	3e	4a	4b	4c
Lip Buckling							140	160					
Section Web Crippling		250	330[1]			85					140		
B.Col-Flexural Failure	163 [1]								188				
B.Col -Torsional Failure	125[2] †									210[2]			
Diagonal Buckling				374						200[1]			
Tab end Bearing					460								360
Washer Plate Bending			330[2]									300	
Bolt Bending													

FAILED COMPONENT
48mm dia-2.5mm, B1-H6
6mm washer plate, F8
125x100x20x20-3.0mm, F8
(1) 48mm dia-2.0mm , B3-F8 (2) 125x100x20x20-1.5mm, B-23
125x100x20x20-1.5mm, 3-BC
125x100x20x20-1.5mm, B-23
125x100x20x20-1.5mm B2,B3,C2 and C3
125x100x20x20-1.5mm, B3, F8
60mm dia-2.5mm, B1-H6
60mm dia-2.5mm, B3-F8
(1) 125x100x20x20-1.5, B3 (2) 10mm washer plate, B3
127x65x12.5-2.0mm, F8
(1) 127x65x12.5-2.0mm, 2-BC (2) 127x65x12.5-2.0mm, B-23

† Failure after reloading partially failed frame.

Table 3.2 Summary of frame test results (Values given in table correspond to jack loads in kN)

TEST / FAILURE	5a	5b	5c	5d	6a	6b	6c	7a	7b	7c	7d
Lip Buckling											
Section Web Crippling	340(1)									320(1)	
B.Col-Flexural Failure											
B.Col -Torsional Failure								240			675(1)
Diagonal Buckling			440(1)				600‡		630		760(3)
Tab end Bearing		380(1)*		510	420	570				700(2)	750(2)
Washer Plate Bending											
Bolt Bending	340(2)	380(2)	440(2)								

FAILED COMPONENT

(1) 125x100x20x20-3.0mm, B-23
(2) All Top Chord Tabs
(3) 76mm dia-3.0mm, 2-CD

(1) 125x100x20x20-3.0mm, F7
(2) 70mm dia-3.0mm, C1-I7

60mm dia-4.0mm, 3-CD

125x100x20x20-1.5, B-23

70mm dia-3.0mm, B3-H7

60mm dia-2.5mm, C1-I7

48mm dia-2.0mm, B1-H6

76mm dia-3.0mm, B1-H6

(1) 60mm dia-2.5mm, B3-F7
(2) M12 Gr.10.9, C3
(2) M16 Gr.4.6, G9

(1) 76mm dia-3.0mm, B3-C8
(2) M12 Gr8.8, C3

(1)125x100x20x20-3.0mm B2, B3 and H6
(2) M16 Gr.4.6

* Premature failure due to tearing of tab crease. ‡ Value of first 70mm dia. diagonal buckling failure recorded, other failures @ 630kN and 650kN

Figure 3.2 (Cont) Summary of frame test results

3.7 CONCLUSIONS

(1) From the outset it was apparent that various phenomena observed while testing the frame were not covered by the British design code BS5950 (1987). A series of experiments on frames and components were conducted concurrently with numerical analysis and with the formulation of design rules.

(2) The frame tests presented in this chapter were carried out with the purpose of obtaining a better understanding of the overall and local behaviour of the diagonal on square space frame. Various methods of member and joint reinforcement were also investigated. Individual component tests were also carried out to provide test data for members subjected to singular load conditions.

(3) The results obtained provided basic information needed for the assessment of design recommendations discussed in later Chapters.

(4) The various modes of failure observed in these frame tests were;

(a) Flexural buckling of the bottom chord lips-up member
(b) Lip buckling of the 1.5mm thick chord members
(b) Combined torsional-flexural and lateral torsional buckling of the bottom chord lips down member
(c) Compressive buckling of diagonal tubes
(d) Tab bearing and or tab crease tearing
(e) Web crippling /table shearing
(f) Bolt failure
(g) Washer plate failure

(5) Some of the observed phenomena were specific to the test frame, but several phenomena can occur in other structures consisting of similar cold-formed components.

Chapter Four

COMPRESSIVE BUCKLING OF SECTION ELEMENTS

4.1 INTRODUCTION

Many structural steel compression members are made up of a number of flat plate elements which are rigidly connected along common edges. Cold-formed thin-walled steel sections are one such example. When thin plates are loaded in compression the possibility of local buckling may arise. Local buckling is so called because the half wavelength of buckle that forms is of the same order of magnitude as the cross-sectional dimensions of the structural component and is therefore usually small, when compared to the overall dimension of the member.

The occurrence of local element buckling depends on the slenderness ratio (b/t) of each element, the mode and magnitude of the initial imperfection, the level of residual stress and the support boundary conditions at the junctions between elements in a cross-section. All these factors have a significant effect on the ultimate compressive resistance. In recognition of the importance of local plate buckling and its effects on the ultimate compressive resistance extensive research has been carried out over the past fifty years. This has resulted in numerous methods for obtaining an estimate of the failure load

This chapter briefly discusses the critical buckling behaviour of thin plates with particular emphasis being given to the interaction between web and table buckling of a doubly lipped channel section (Figure 4.1). A number of finite element analyses were carried out to investigate the critical buckling behaviour of the doubly lipped channel subject to axial compression and to validate current design recommendations. The post buckling behaviour of thin plates and the application of plate buckling theory to the analysis of imperfect thin-walled cold-formed sections is

discussed. Further validation was provided through tests carried out on 125x100x20x20, 1.5mm and 3.0mm thick stub columns.

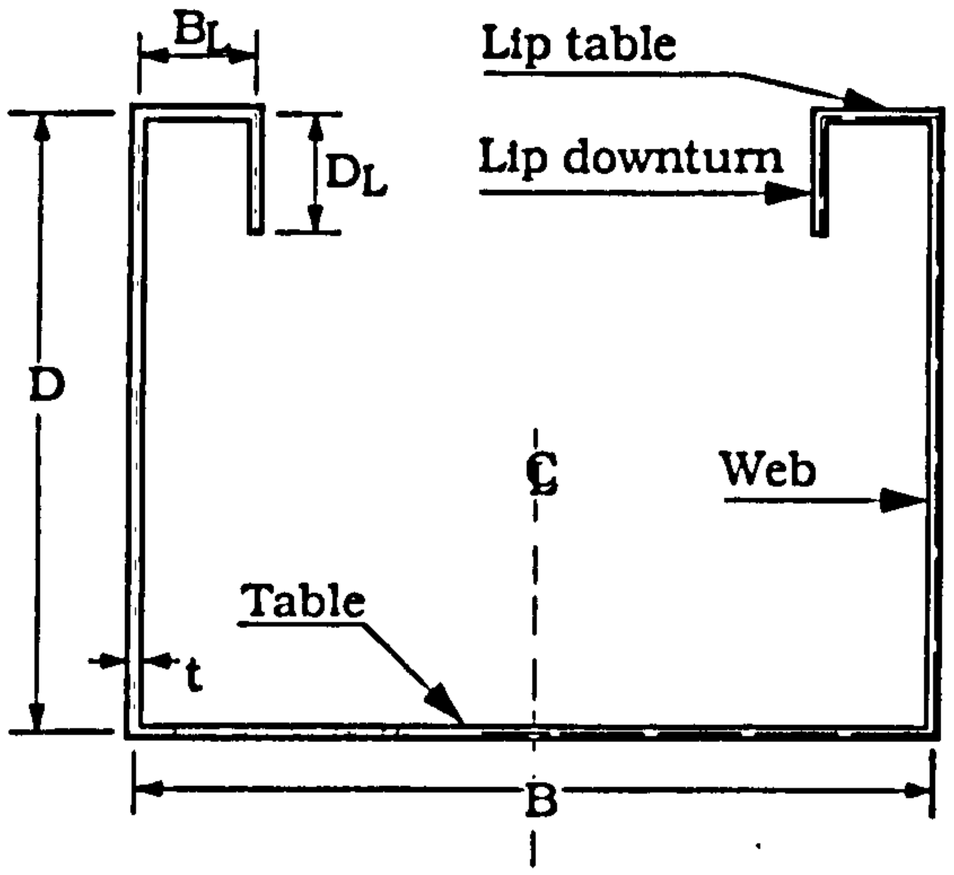


Figure 4.1 Doubly Lipped Channel Section

4.2 CRITICAL BUCKLING OF SECTION ELEMENTS

When a number of plates are joined along longitudinal edges to form a thin-walled structural member, short lengths of such a member can suffer local instability if subjected to axial compressive loading. The following assumptions are normally associated with this form of buckling:

(a) common edges of component plates remain straight
(b) the original angle between adjacent plates at their common edge is maintained during buckling,
(c) the wavelengths of the buckles, which (for critical buckling) occur in all plates simultaneously, are the same.

The subject of local buckling of plated elements is well documented and can be found in many standard texts such as Timoshenko and Gere (1961), Bleich (1952), Bulson (1970) and Allen and Bulson (1980). The critical buckling stress for a thin flat plate subjected to axial compressive loading is given by the familiar equation derived by Bryan (1891)

$$\sigma_{cr} = \frac{K\pi^2 E}{12\,(1-\nu^2)}\left(\frac{t}{b}\right)^2 \qquad (4.1)$$

where

b width of plate element

E elastic modulus (E=205 kN/mm^2)

K plate buckling coefficient

t thickness of section

ν Poisson's ratio (ν= 0.3)

The value of the plate buckling coefficient K for a given plate slenderness (b/t) is dependent on the support conditions. The plate buckling coefficients for various support conditions are given in Figure 4.2. The critical buckling stress for local buckling of thin-walled cold-formed channel sections may be obtained by idealising the elements of the cross-section as individual thin flat plates, with a varying degree of rotational restraint along the common longitudinal edges.

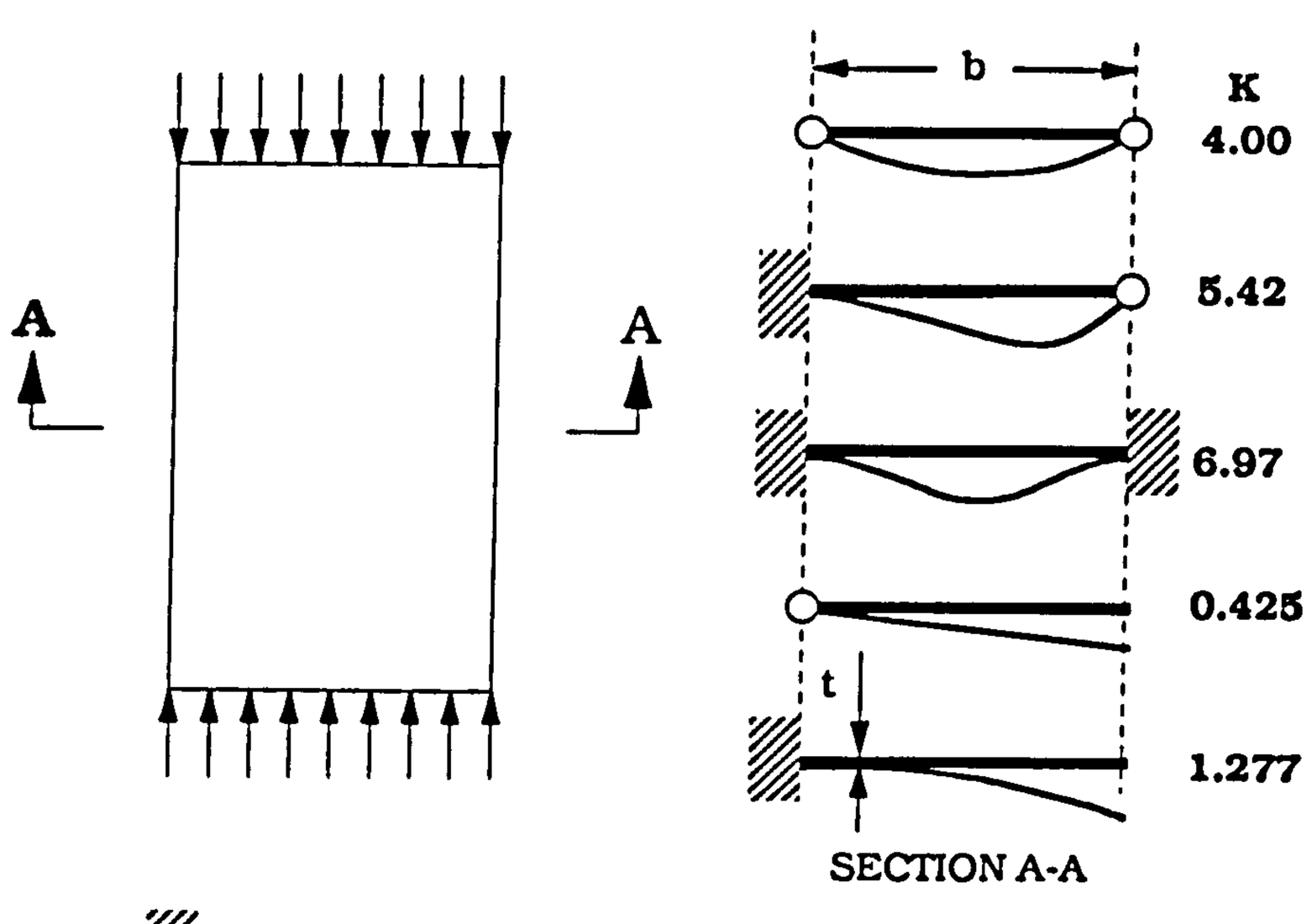


Figure 4.2 Buckling Coefficient K for various support conditions (Equation 4.1)

In Figure 4.2 it can be seen that the buckling coefficient K varies between 4.0 for simple supported plates and 6.97 for fixed edges. When a section such as the channel is subjected to a compressive load the elements adjoining either side of an element provide a degree of rotational restraint. The buckling coefficient of the most slender element will therefore lie between the limits $4.0 \leq K \leq 6.97$.

For the purpose of estimating the critical buckling stress of a section, individual elements may be classified as; "supported elements" where all four edges of the element are simply supported and "partially supported elements" where the element is simply supported at both ends and along only on longitudinal edge. The table, web and lip table elements of the doubly lipped channel section shown in Figure 4.1, are supported elements, whilst the lip downturn is considered to be a partially supported element.

Codes of practice tend to adopt one of three approaches for determining the critical buckling coefficient K for each element in a cross-section. These methods can be summarized as follows;

Method (a) The critical buckling stress of supported and partially supported elements in a section can be estimated by assuming that no rotational restraint is provided by the adjoining elements and that each element is hinged along the element junctions in the cross-section. The critical buckling coefficient for a supported element can then be taken to equal a value of 4.0 and the buckling coefficient for an partially supported element, equal to 0.425. This is a rather simple approach to a very complex buckling problem, yet this method forms the basis of design recommendations given in AISI (1989), EC3: Part 1.3 (1990) and BS 5950: Part 5 (1987). The separate strengths are then added.

Method (b) An accurate estimation of the buckling coefficients for each element in a cross-section may be found by employing analytical techniques similar to those used in the solution of flat plates whereby the equations of equilibrium for the complete section are solved. This method of analysis results in rather complicated arithmetic which for practical reasons is not suitable for use in design. Bulson (1970) uses this approach to provide exact values for the buckling coefficients for a variety of structural shapes. His work forms the basis for the design curves and approximate formulae given in Appendix B: BS5950: Part 5 (1987) for a number of commonly used cold-formed sections.

Consider a singly lipped channel section in which the table is the more slender element. The buckling coefficient for the table element, K_B, can be obtained from the appropriate equation given in Appendix B of BS5950, which is

$$K_B = 7 - \frac{1.8\left(\frac{D}{B}\right)}{0.15+\left(\frac{D}{B}\right)} - 1.43\left(\frac{D}{B}\right)^3 \qquad (4.2)$$

If the elements are affected equally when the section buckles, then it would be reasonable to assume that all elements in the cross-section buckle sympathetically with the more slender element. The buckling coefficient K_D for the web element taking into account the loss of stability due to the restraint which it provides for the table element may be obtained from Equation 4.1 by setting σ_{cr} equal to the critical buckling stress for the table element given by Equation 4.2. The buckling coefficient K_D for the web element of a singly lipped channel section, where $D < B$, is given by

$$\frac{K_D \pi^2 E}{12(1-\nu^2)}\left(\frac{t}{D}\right)^2 = \frac{K_B \pi^2 E}{12(1-\nu^2)}\left(\frac{t}{B}\right)^2$$

$$K_D = K_B\left(\frac{D}{B}\right)^2 \qquad (4.3)$$

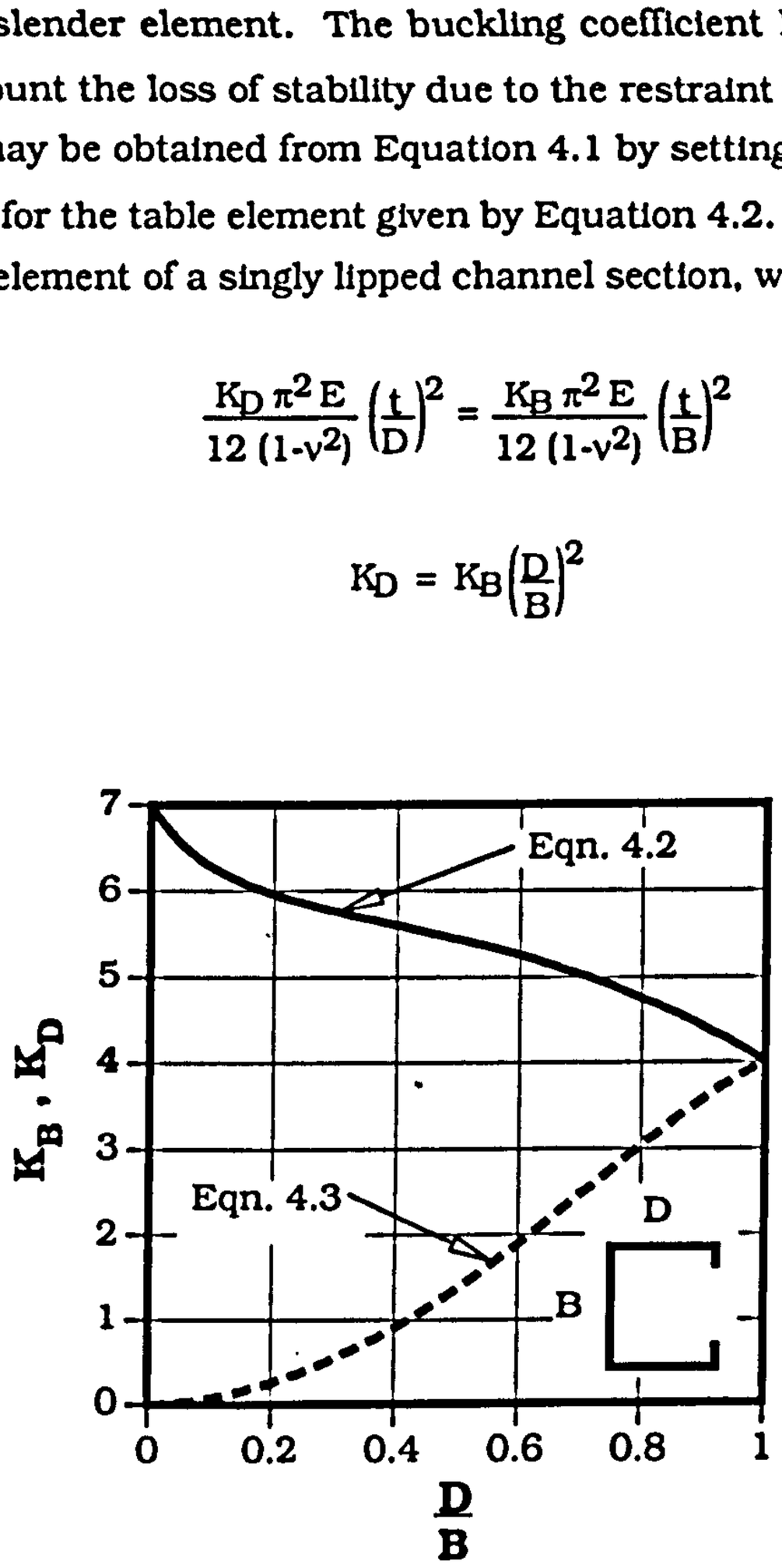


Figure 4.3 Buckling coefficients K_B and K_D for singly-lipped channel section given by Equations 4.2 and 4.3 (BS5950: Part 5 (1987))

Figure 4.3 shows the variation in K_B and K_D obtained from Equations 4.2 and 4.3 with the depth for the singly lipped channel sections. It can be seen that as the depth of the channel decreases, the value of K_B increases while K_D decreases such that $6.97 \geq K_B \geq 4.0$ when $0.0 \leq K_D \leq 4.0$.

In the absence of any design guidance for the doubly lipped channel section, Equation 4.2 for singly lipped channels may be adopted for the purpose of obtaining the buckling coefficient K_B and K_D. Use of this equation is justified since the additional rotational restraint provided by the lip downturn to the web and table elements of the section will tend to increase the web and table buckling coefficients. Equation 4.2 should give a conservative estimate of the buckling coefficient of the table element.

Method (c) Rhodes (1991) argues that the above method may lead to a very conservative estimate of the critical buckling strength of the section since;

> *"..it has been observed (Rhodes 1987) that for restraining elements the effects of premature local buckling are negligible. Only when the applied loading is sufficient to attain the natural (simply supported) buckling stress of such elements do these elements suffer the effects of local buckling to any substantial degree."*

This observation forms the basis for the alternative recommendations given in Appendix B of BS 5950: Part 5 (1987), where K_B for the table element can be found using method (b), and the buckling coefficient K_D of the restraining element can be taken to equal 4.0. This enhancement of K_B with no reduction in K_D because of the rotational restraint at the common edge of two adjoining plate elements, is only permitted in BS 5950: Part 5 (1987), and has not been adopted in the design recommendations for the system discussed in this thesis.

4.2.1 FINITE ELEMENT ANALYSIS OF DOUBLY LIPPED CHANNEL SECTIONS

In order to assess the different approaches described in the preceding section, a series of critical buckling analyses were carried for a range of web depths ($47mm \leq D \leq 122mm$) using the non-linear elasto-plastic finite element package FINASIC (1990). Two lengths of 125x100x20x20, 1.5mm and 3.0mm thick channel

section were modelled and analysed, a short stub column 375mm, and a longer member 1220mm long.

The finite element mesh used to model the cross-section of the doubly lipped channel consisting of eight noded shell elements, and the aspect ratio of the elements was chosen to conform with the recommendations made in Appendix A- that is, that each local buckle should be described by at least a 4 x 4 finite element mesh. The entire cross-section of the of the 375mm stub column was modelled (Figure 4.4) using four elements in the table and webs of the channel, one element in the lip table and one element in the lip downturn, with twelve elements along the length. The same finite element aspect ratios were again employed to model the 1220mm long member. However, due to symmetry of both the buckled shape and the cross-section only half cross-section of the channel was modelled. Boundary conditions at the ends of the member prevented deformation of the cross-section. Lateral displacement of the web/lip table junction along the length was also suppressed. The members were subjected to a uniform compressive load applied at both ends of the channel. Figure 4.4 shows the lowest critical buckling mode for a 1.5mm thick stub column.

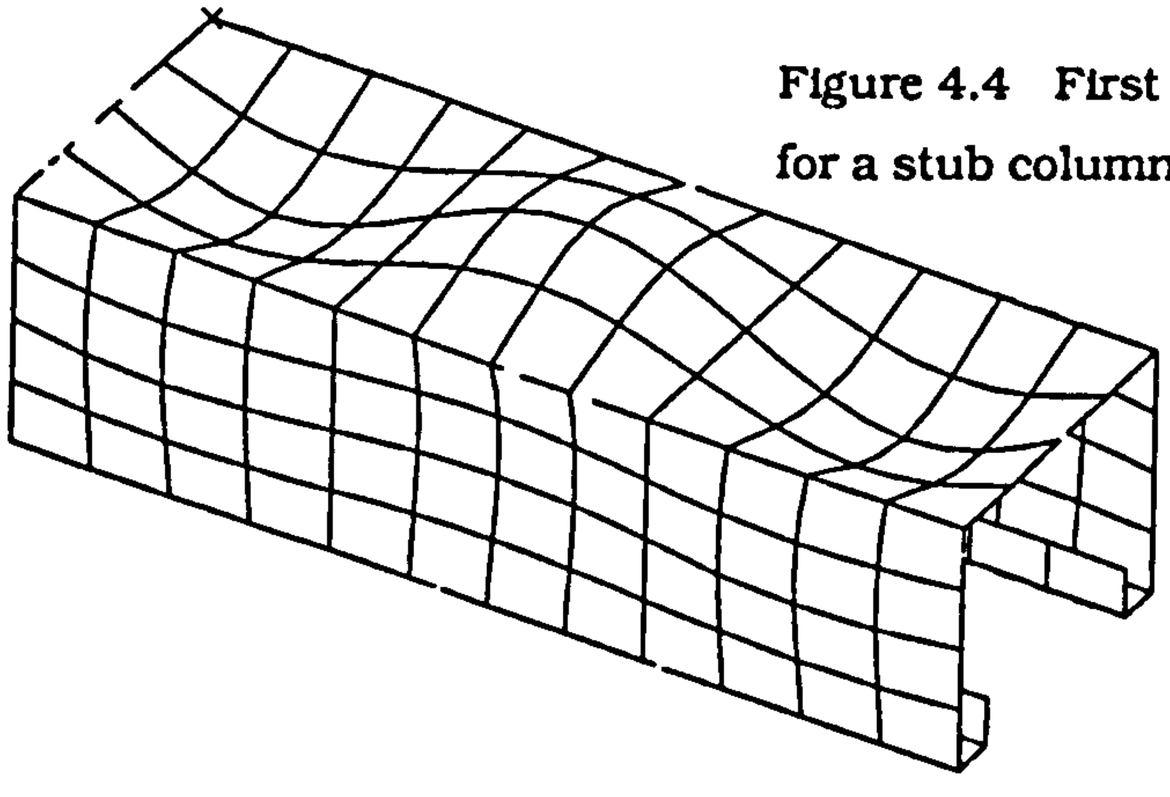


Figure 4.4 First critical buckling mode for a stub column - 375mm long, 1.5mm thick

$$\frac{\sigma_{crF}}{\sigma_o} = 0.37$$

t (mm)	$\frac{D}{B}$	σ_{crF} (N/mm^2)	K_{BF}	$\frac{K_{BF}}{K_B}$
1.5	0.795	144	5.3	**1.11**
3.0	0.795	563	5.0	**1.05**

Table 4.1 Comparison between buckling coefficients K_B for doubly lipped channel section obtained from numerical analysis and from Equation 4.2 when L = 375mm

t (mm)	$\frac{D}{B}$	σ_{crF} (N/mm^2)	K_{BF}	$\frac{K_{BF}}{K_B}$
1.5	0.389	160.1	5.7	1.01
	0.615	152.2	5.4	1.03
	0.795	143.3	5.1	1.07
	1.000	130.4	4.7	1.17
2.0	0.389	282.8	5.7	1.01
	0.615	269.5	5.4	1.03
	0.795	253.6	5.1	1.07
	1.000	220.3	4.4	1.10
3.0	0.389	628.6	5.6	1.00
	0.615	598.8	5.3	1.02
	0.795	559.4	5.0	1.04
	1.000	473.1	4.2	1.05
4.0	0.389	1091.2	5.5	0.98
	0.615	1041.2	5.2	0.99
	0.795	965.6	4.8	1.00
	1.000	786.6	4.0	1.00

Table 4.2 Comparison between buckling coefficients K_B for doubly lipped channel section obtained from numerical analysis and from Equation 4.2 when L =1220mm

The results of the critical buckling analysis for the stub column and the 1220mm long member are given in Tables 4.1 and 4.2 respectively. Comparisons between the finite element results obtained for the doubly lipped channel section and Equation 4.2 for the singly lipped channel are made in Table 4.1, Table 4.2, and in Figure 4.5. The values of K_{BF} for each section, given in Tables 4.1 and 4.2 were obtained by equating the critical buckling stresses obtained from the finite element analyses and the plate buckling Equation 4.1, and solving for the buckling coefficient K. It can be seen in Table 4.1 and Figure 4.5 that Equation 4.2 gives a conservative estimate of the critical buckling coefficient K_B.

For a doubly lipped channel of varying depth and thickness the buckling coefficients K_B are seen to be between -2% and 17% of the values given by Equation 4.2 (Figure 4.5). This increase in the value of the critical buckling coefficients is due to

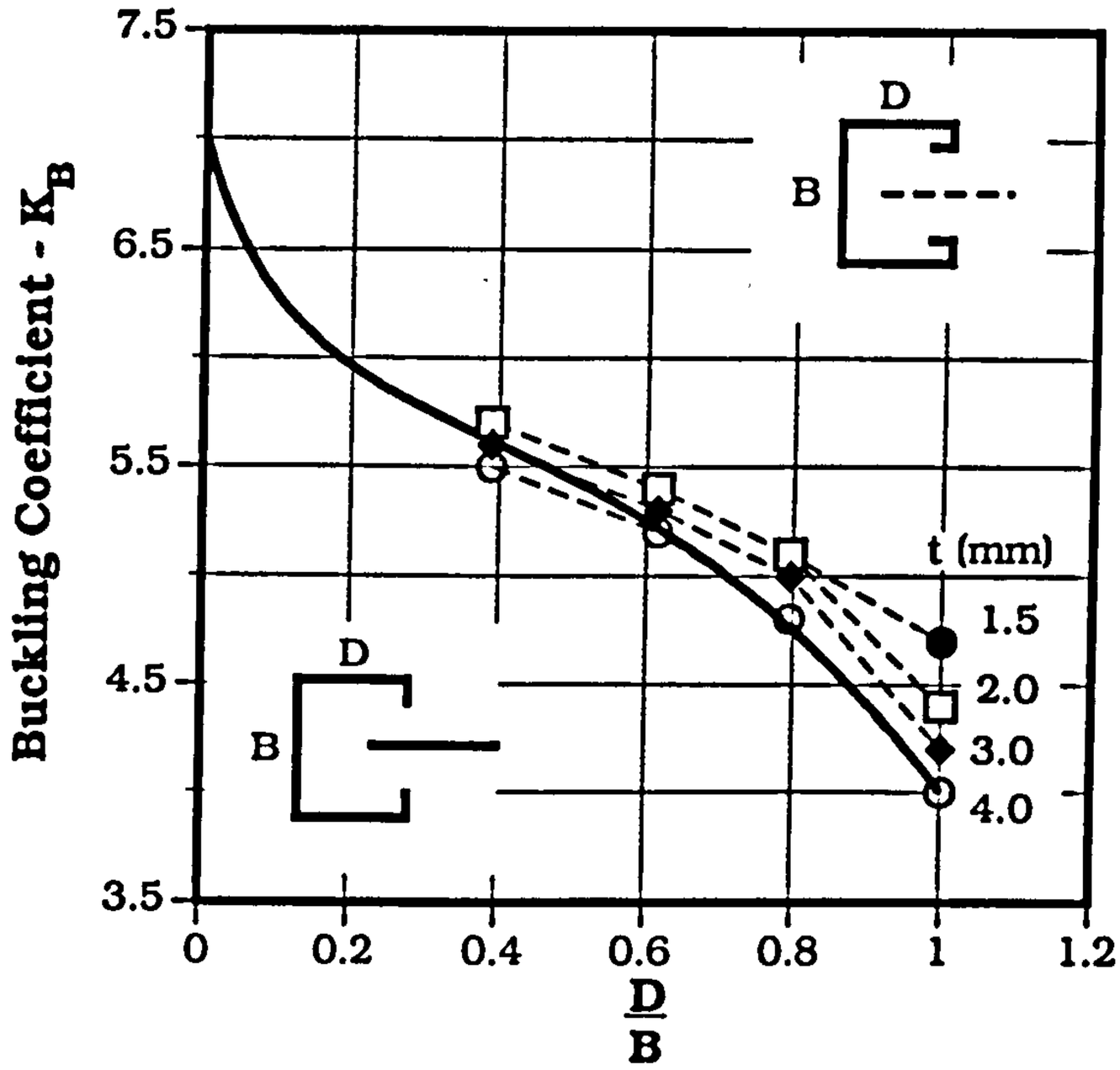


Figure 4.5 Comparison between critical buckling coefficients obtained from finite element analysis for the doubly lipped channel section with Equation 4.2
B = 122mm, B_L = 17mm, D_L = 18.5mm

the inplane bending stiffness of the lip downturn which enables the lip to provide some rotational restraint to the web and table elements of the section. However, the downturn vertical bending stiffness is proportional to the thickness whilst the bending stiffness of the webs and flanges vary as the square of the thickness, so the downturn has less effect for the thicker sections.

The validity of methods (a),. (b) and (c) for determining the web buckling coefficient K_D can only be ascertained after carrying out a series of non-linear elasto-plastic finite element analysis and comparing the numerical results with the ultimate capacities obtained from the three alternative methods.

4.3 POST-BUCKLING CAPACITY OF PLATE ELEMENTS IN COMPRESSION

Local buckling does not normally result in the failure of the section as does the Euler buckling of a column. A thin plate can support loads significantly greater that its critical load before failure occurs. The post buckling strength of a plate is due to

the fact that the deflected shape of the buckled plate cannot develop unless redistribution of the in-plane stress occurs. Redistribution of these stresses is dependent on the inplane boundary conditions at the loaded and unloaded edges of the plate. Stress redistribution continues after buckling with increasing load until the yield stress σ_o is reached at the supported edges; yielding then spreads rapidly, resulting in failure of the plate.

The analytical determination of the post buckling strength of flat thin plates is very difficult, several methods exist which allow for the rigorous analysis of plates under many conditions of loading and support. These range from numerical methods such as finite element and finite difference, to others making use of perturbation techniques. An alternative to these is the effective width concept.

This method first proposed by von Kármán et al (1932) assumes that the actual ultimate stress distribution in a simply supported plate is replaced by a simplified distribution in which the central portion of the plate is considered to carry no load while the remaining portion of plate b_{eff} carries the yield stress σ_o (Figure 4.6). The effective portion of plate of width b_{eff} is considered to be equivalent to a notional rectangular plate of overall width b_{eff}. Failure then occurs when the critical buckling stress of the notional plate reaches σ_o.

From Equation 4.1

$$\sigma_o = \frac{K\pi^2 E}{12\left(1-\nu^2\right)}\left(\frac{t}{b_{eff}}\right)^2 \qquad (4.4)$$

as the critical buckling stress of the original plate is given by

$$\sigma_{cr} = \frac{K\pi^2 E}{12\left(1-\nu^2\right)}\left(\frac{t}{b}\right)^2 \qquad (4.5)$$

Equating Equations 4.4 and 4.5

$$\frac{b_{eff}}{b} = \sqrt{\frac{\sigma_{cr}}{\sigma_o}} \qquad (4.6)$$

where

b	plate width
b_{eff}	effective width of plate
σ_{cr}	plate critical buckling stress
σ_o	material yield stress

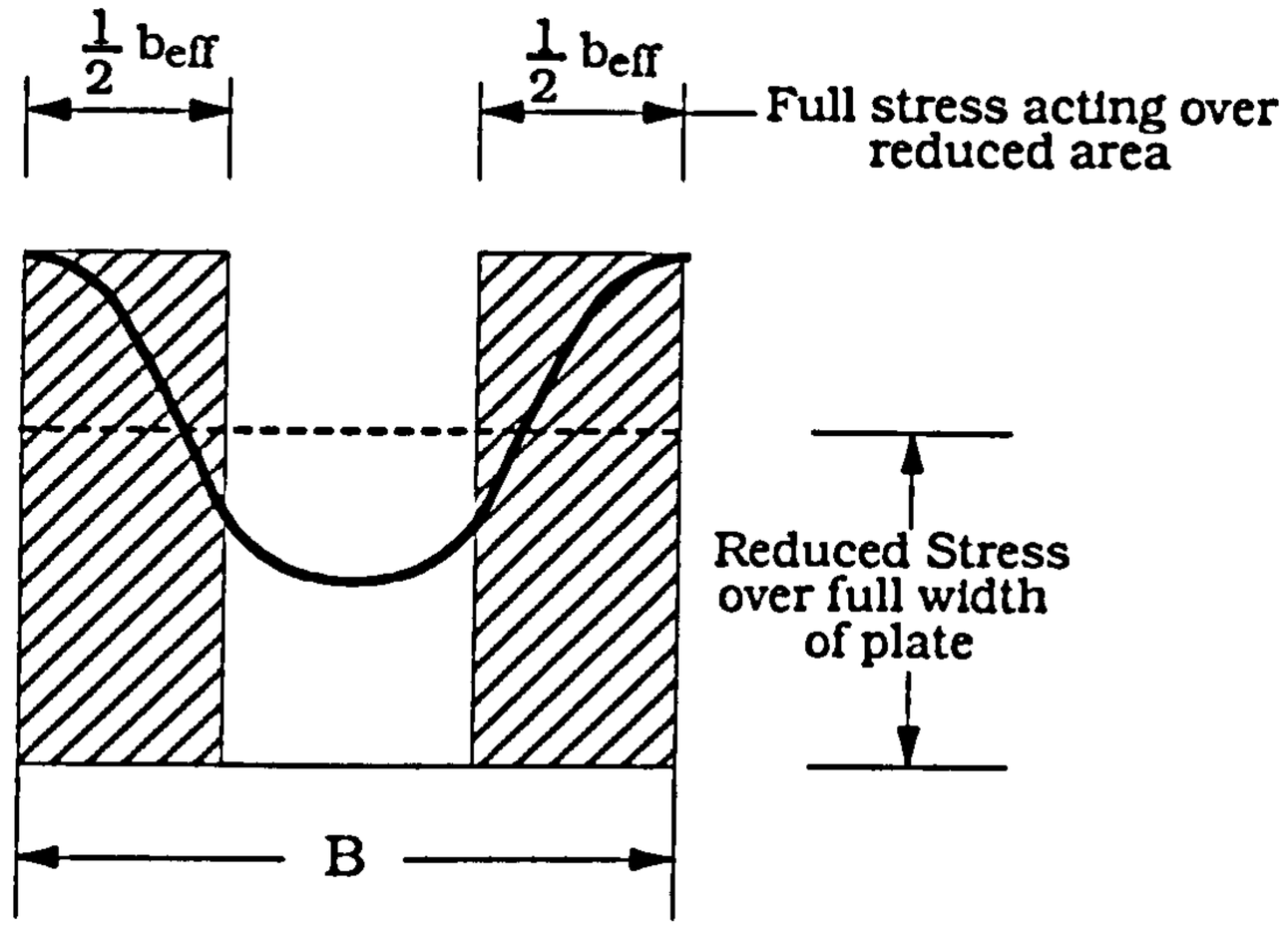


Figure 4.6 Effective Width of Plate

Comparison of Equation 4.6 with published experimental data (Rhodes 1991) suggests that the von Kármán equation which take no account of initial imperfection or residual stresses, describes the post buckling behaviour of thin plates adequately. Further research into the buckling behaviour of plated structures has over the past fifty years lead to numerous effective width formulations. An extensive summary of these developments is provided by Faulkner (1975) and Rhodes (1982).

Research into local buckling of cold-formed steel sections began largely in the United States at Cornell University by Winter. Winter (1946) published an experimental variation of the von Kármán equation based on tests carried out on beam flanges. Subsequent test were carried out on other types of cold-formed compression elements. The original equation proposed by Winter, is

$$\frac{b_{eff}}{b} = \sqrt{\frac{\sigma_{cr}}{\sigma_o}} \left[1 - 0.25 \sqrt{\frac{\sigma_{cr}}{\sigma_o}} \right] \qquad (4.7)$$

The original von Kármán equation can be obtained from Equation 4.7 by setting the term within the brackets to unity. The empirical formulation obtained by Winter allowed implicitly for the effects of initial imperfection and the presence of residual stresses.

Equation 4.7 was subsequently modified as more data became available and has remained unchanged to this day (Equation 4.8). This equation has been incorporated into AISI (1989) and EC3: Part 1.3 (1992).

$$\frac{b_{eff}}{b} = \sqrt{\frac{\sigma_{cr}}{\sigma_o}}\left[1 - 0.22\sqrt{\frac{\sigma_{cr}}{\sigma_o}}\right] \tag{4.8}$$

The problem of estimating the post buckling strength of plate elements was approached differently in Britain. Rhodes (1991) points out that explicit expressions for the buckling behaviour of simply supported thin square plates were obtained by Walker (1969), and that his work forms the basis for the approach adopted in the first British code of practice for the use of cold-formed sections, BS 449: Addendum No.1 (1975). This approach assumes that a reduced stress acts over the full width of plate, and is therefore aptly known as the reduced stress approach (CL Factor). In many ways this is similar to the effective width method which assumes that the full stress acts over a reduced area as shown in Figure 4.6.

The British code was subsequently revised in 1987, and during the drafting process an effective width formulation was adopted in preference to the reduced stress method, as it was considered that the former gave a better representation of the actual stress state of the buckled plate. An effective width formulation (Rhodes 1984) based on an empirical curve fit to existing data, giving conservative predictions of the effective plate width when compared to the CL approach of Addendum No1 to BS 449 (1975) has been adopted for use in BS5950: Part5 (1987) and is given by

$$\frac{b_{eff}}{b} = \left[1 + 14\left\{\left(\frac{\sigma}{\sigma_{cr}}\right)^{1/2} - 0.35\right\}^4\right]^{-0.2} \tag{4.9a}$$

where

σ is the compressive edge stress on the affected element

σ_{cr} is the local buckling stress of the element given by

$$\sigma_{cr} = 185\,000\,K\left(\frac{t}{b}\right)^2 \tag{4.9b}$$

K is the local buckling coefficient

t is the material thickness

Figure 4.7 shows a comparison of the basic effective width expressions given by Equation 4.8 (assuming that K = 4.0), Equations 4.9 and von Kármán's original effective width equation.

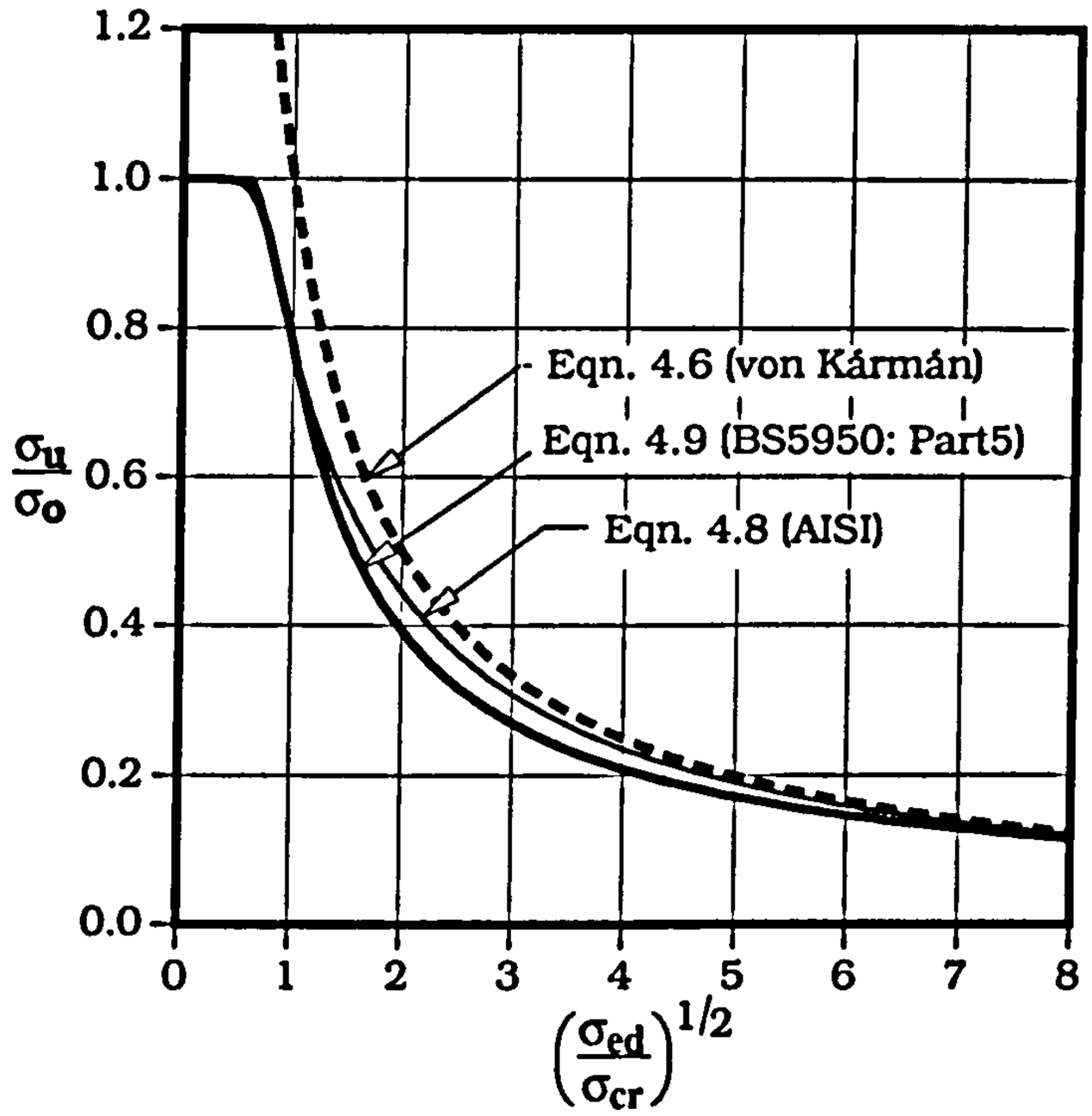


Figure 4.7 Comparison of effective formulations

4.4 ULTIMATE LOCAL BUCKLING CAPACITY OF DOUBLY LIPPED CHANNEL SECTIONS

The ultimate compressive resistance of a doubly lipped channel section is influenced by the degree of inplane and rotational restraint provided at junctions between elements in the cross-section, the level of imperfection and the residual stress pattern around the cross-section. The combined effect of all these parameters on the ultimate compressive resistance of the section is difficult to quantify. Because of this, the ultimate compressive resistance of a section is usually based on a variety of simplifying assumptions, leading to design recommendations which tend to be rather conservative.

The effects of local buckling on the ultimate load carrying capacity of a thin-walled section are dealt with in AISI (1989), EC3:Part1.3 (1990) and BS 5950: Part5 (1987). All three codes recommend a simplified approach to estimating the ultimate strength of individual plate elements by setting the buckling coefficient K to either

4.0 for supported elements or 0.425 for partially supported elements (method a). One exception is the alternative approach presented in Appendix B BS5950: Part 5 (1987) which permits the enhancement of K_B for the critical table element and no reduction in K_D of the web restraining element (methods c).

The following sections sets out to determine the validity of the various methods of estimating the local buckling capacity of the doubly lipped channel section and to this end a number of experimental and numerical analyses were carried out on short lengths of channel.

4.4.1 EXPERIMENTAL INVESTIGATION

Two stub columns, 1.5mm and 3.0mm thick, 375mm in length were axially loaded in pairs as shown in Figure 4.8. The yield and ultimate stress of the parent material was determined by tensile tests carried out on 450x50mm coupons taken from the web and table of the channel prior to testing. The material and geometric properties are give in Tables 4.3.

t mm	B mm	D mm		B_L mm		D_L mm		σ_o N/mm^2	σ_u N/mm^2
		D1	D2	B_{L1}	B_{L2}	D_{L1}	D_{L2}		
1.5	125.4	99.0	99.0	20.5	20.5	18.5	20.5	364	484
3.0	125.2	100.9	100.0	20.0	20.5	18.5	18.3	489	539

Table 4.3 Section geometric and material properties

The local imperfections in the web and table elements for both the 1.5mm and 3.0mm thick sections were measured and found to be in the order of ±0.12mm (B/1042) and ±0.05mm (B/2500) respectively.

The 3.0mm channel section was loaded in increments of 5kN up to 800kN and the 1.5mm section in increments of 2kN up to 200kN. Both sections were then loaded in increments of 1kN up to failure. Failure of the sections resulted through local buckling of the cross-section, the wavelength of buckling being approximately equal to the width of the table element (Figure 4.8). The end-shortening of each test

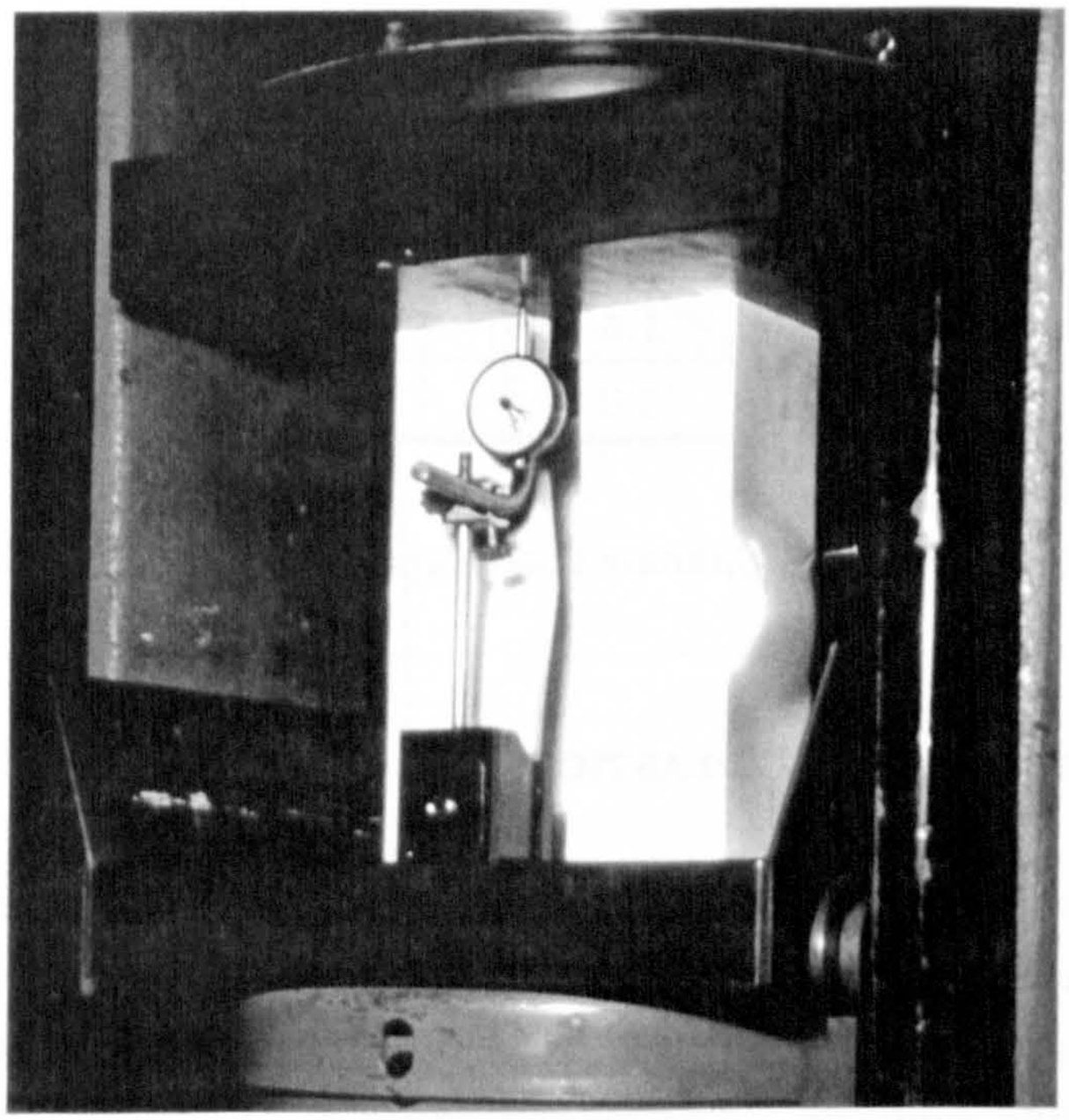


Figure 4.8 Local buckling test arrangement

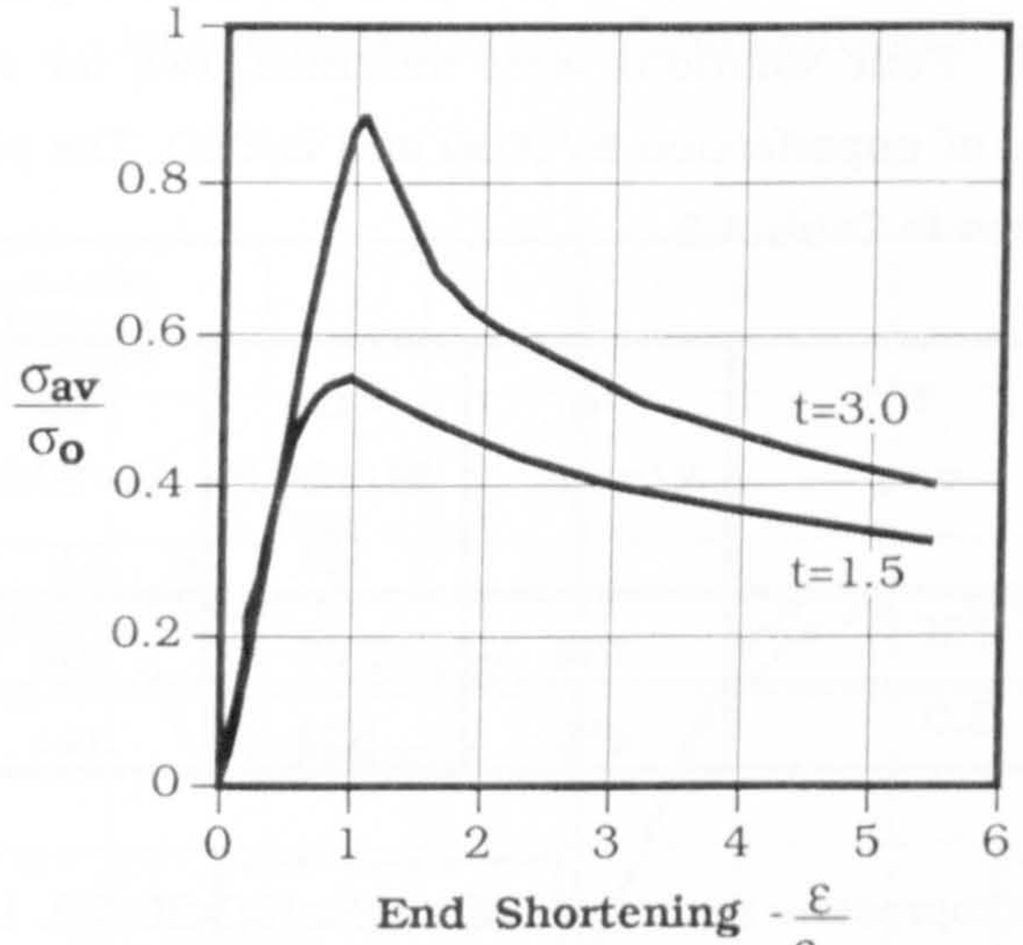


Figure 4.9 Load vs. End shortening Stub column tests

specimen was recorded at each increment of load (Figure 4.9). The ultimate axial resistance of each channel is given in Table 4.4.

t (mm)	P_{exp} kN
1.5	117
3.0	504

Table 4.4 Experimental Ultimate Load Capacity for 375mm Stub Columns

4.4.2 NON-LINEAR ELASTO-PLASTIC FINITE ELEMENT ANALYSIS

The ultimate capacity of an axially loaded doubly-lipped channel sections was also obtained numerically using FINASIC (1990). The cross-section of the channel was modelled using the same mesh and boundary conditions as those used for the critical buckling analysis. The loaded edges were constrained, using spring elements, ensuring uniform end displacement. The lowest critical buckling mode for each thickness of section was scaled to provide the initial imperfections needed for the analyses. It is worth mentioning at this point that in all the numerical analyses presented in this thesis, the effects of material strain hardening and residual stress have been neglected. Four solutions were obtained, two for each thickness of section, for two levels of imperfection B/1000 and B/500. The results of the non-linear analysis are given in Table 4.5.

t mm	σ_o N/mm^2	P_{uF} (B/1000) kN	P_{uF} (B/500) kN
1.5	364	107	106
3.0	489	533	511

Table 4.5 Ultimate compressive resistance of a 125x100x20x20, 1.5mm and 3.0mm thick doubly lipped channels section (FINASIC).

Increasing the level of imperfection from B/1000 to B/500 has the effect of reducing the ultimate compressive resistance of the 1.5 mm section and the 3.0mm thick by 1% and 4% respectively. Figure 4.10 shows the cross-sectional deformation at

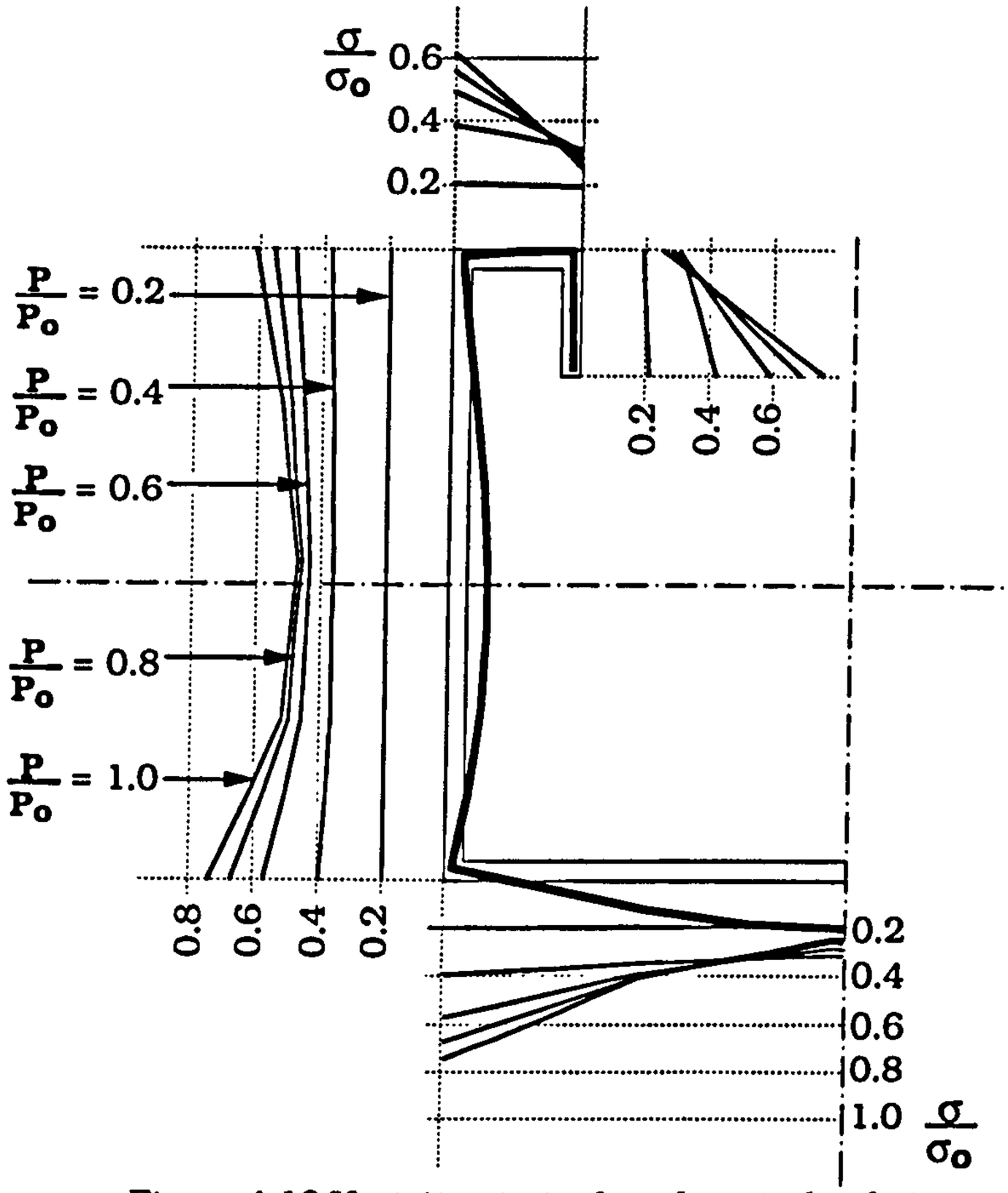


Figure 4.10 Variation in inplane longitudinal stress with load and cross-sectional deformation at ultimate load

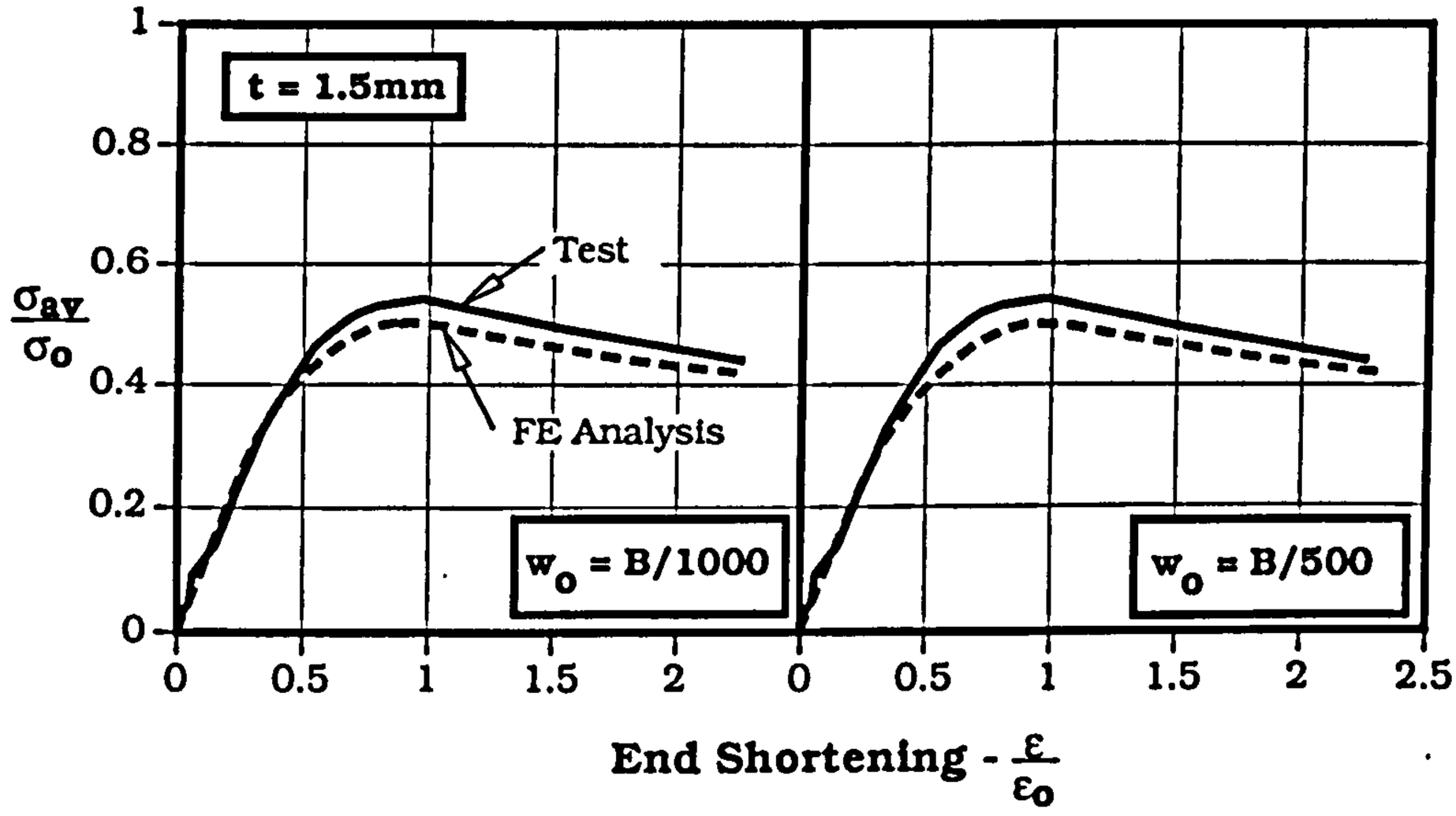


Figure 4.11 Comparison between numerical and experimental Load vs. end shortening behaviour of a 1.5mm thick doubly lipped channel stub column.

ultimate load for a 1.5mm thick section, as well as the variation in longitudinal stress around the cross-section at various levels of load. The load end-shortening behaviour of both the experimental and non-linear analysis are compared in Figures 4.11 and 4.12.

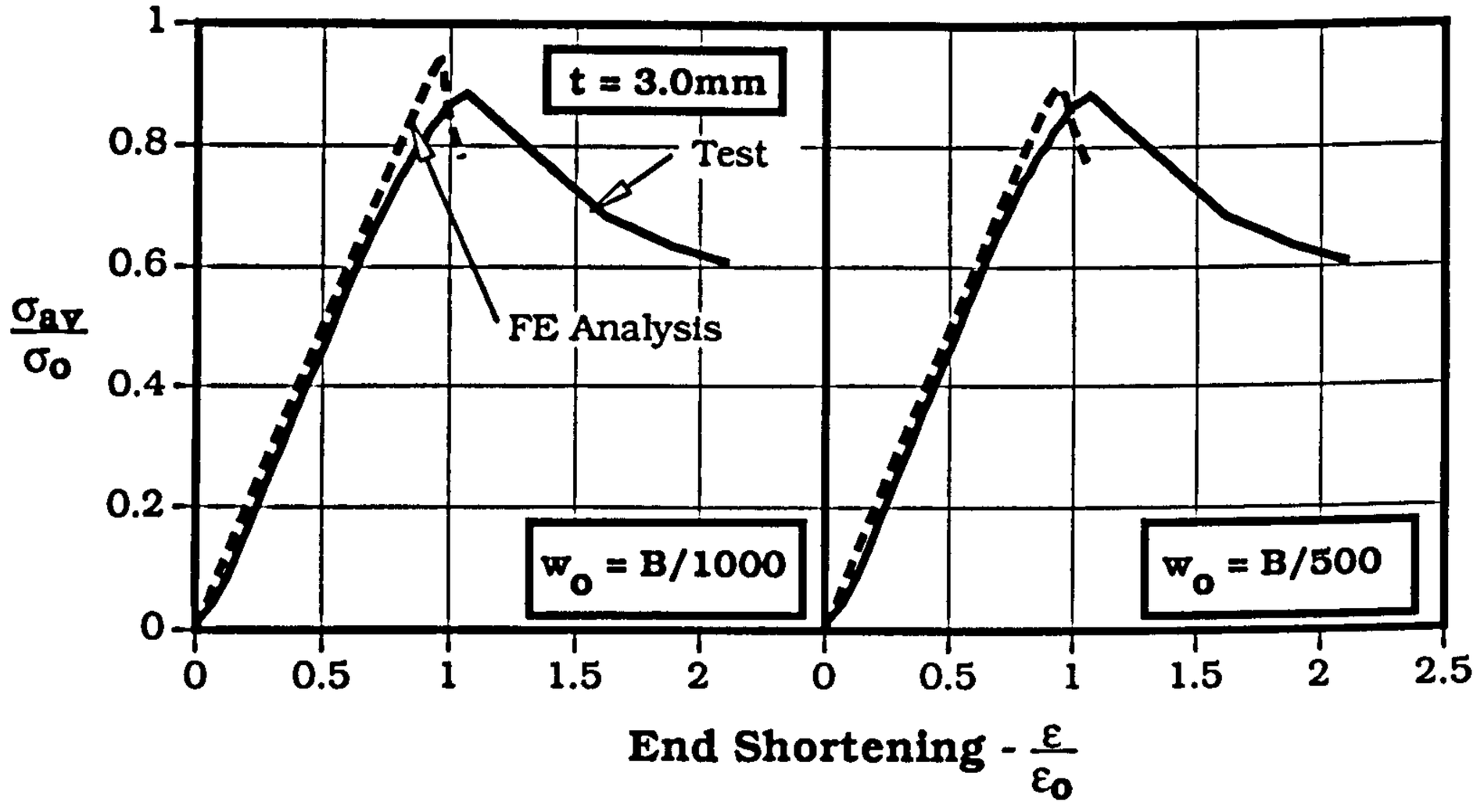


Figure 4.12 Comparison between numerical and experimental Load vs. end shortening behaviour of a 3.0mm thick doubly lipped channel stub column.

4.4.3 COMPARISON OF CURRENT DESIGN RECOMMENDATIONS WITH EXPERIMENTAL AND NUMERICAL RESULTS.

The compressive resistance for both the 122x97x17x18.5, 1.5mm and 3.0mm thick doubly lipped channel sections have been evaluated according to the three methods previous described in section 4.2.1 The axial capacity of the channel is given by

$$P_{cs} = A_{eff}\,\sigma_d \qquad (4.10)$$

where

A_{eff} is the effective area of the cross-section due to local buckling defined as

$$A_{eff} = \sum_{i=1}^{n} \left(\frac{b_{eff}}{b}\right)_i t_i$$

σ_d is the design stress (the smaller of σ_o or 0.84 σ_u)

Comparisons between the axial capacities obtained from methods a, b and c, given in BS5950: Part 5 (1987) the experimental results and numerical results are given in Table 4.6. From Table 4.6 is would seem that for the 1.5mm thick section the three methods over estimate the ultimate axial resistance of the doubly lipped channels section, however method (b) gives the best estimate for both the numerical and experimental results. The three methods are seen to under estimate the ultimate axial resistance of the 3.0mm thick section, with method (c) giving the better estimate.

t (mm)	P_{uF}* (kN)	P_{exp} (kN)	K_B	K_D	K_{BL}	K_{DL}	$\frac{A_{eff}}{A}$	$\frac{P_{uF}}{P_{cs}}$	$\frac{P_{exp}}{P_{cs}}$	Method
1.5	107	117	4.00	4.00	4.0	0.425	0.59	0.84	0.92	(a)
			4.76	3.02	4.0	0.425	0.56	0.89	0.97	(b)
			4.76	4.00	4.0	0.425	0.60	0.82	0.90	(c)
3.0	533	504	4.00	4.00	4.0	0.425	0.85	1.11	1.05	(a)
			4.76	3.02	4.0	0.425	0.84	1.11	1.05	(b)
			4.76	4.00	4.0	0.425	0.89	1.06	1.00	(c)

* $w_o = B/1000$

Table 4.6 Comparison between the various methods given in BS 5950: Part 5 (1987) for determining the short strut axial resistance P_{cs} with numerical and experimental results for the doubly-lipped channel section 122x97x17x18.5.

A variation of +18% to -11% is observed in the ratio of the finite element results to the predicted axial capacity, while the ratio of the experimental results to the predicted failure capacities is on the whole much better where a variation of between +10% and -5% is observed.

4.5 CONCLUSIONS

(1) Various methods for determining the critical buckling coefficients of individual elements in a thin-walled cold formed cross-sections and subsequently the axial resistance of the cross-section, based on recommendations given in AISI (1989), EC3: Part 1.3 (1990) and BS 5950: Part 5 (1987) were compared with finite element solutions and experimental results. As a limited number of test and numerically analyses were carried out it would be unwise to draw any conclusion as to which method is best

suited for estimating the values for K_B and K_D needed for the purpose of obtaining the failure load caused by local buckling for a doubly lipped channel section.

(2) Method (a) will be adopted for the purpose of estimating the short strut capacity of the doubly lipped channel section throughout the remainder of this thesis.

(3) The approximate equations for determining the critical buckling coefficient K_B for the singly lipped channel, given in Appendix B of BS 5950: Part 5 (1987), are shown to give a reasonable estimate of the short strut capacity of the doubly lipped channel section.

(4) From a comparison between the critical buckling and non-linear elasto-plastic analyses with experimental results, the mesh employed to model the cross-section of the doubly lipped channel gave reasonable results. On the basis of this as well as the recommendations given in Appendix A, it is proposed that the mesh of Figure 4.5 be adopted where possible for any further finite element analyses, in which the occurrence of local buckling is to be expected.

Chapter Five

LIP BUCKLING OF DOUBLY LIPPED CHANNELS

5.1 INTRODUCTION

When the lips of a channels, such as that shown in Figure 5.1, are in compression they are liable to buckle sideways, as shown in Figure 5.2. This phenomenon is referred to as "lip buckling". Restraint against lip buckling is provided by the transverse bending stiffness of the section and lip buckling entails deformation (distortion) of the section. Lip buckling can therefore alternatively be referred to as "deformational" or "distortional" buckling.

The lip can be regarded as a strut supported by an elastic foundation. The relation between the stiffness of the strut, the stiffness of the foundation, and the wavelength of buckling is well known (Timoshenko and Gere 1961). The stiffer the foundation in relation to the strut flexural stiffness, the shorter the wavelength and the higher the buckling stress. It will be noticed that in the section considered, the lateral stiffness EI of the "strut" (the "lip" in Figure 5.1) depends predominantly on the thickness t, whereas the stiffness of the foundation (expressed as the "foundation modulus" β) depends on cube of the thickness.

For the section of Figure 5.1, for the 3000mm spans adopted in the bottom chord, and the range of thicknesses employed in practice and in the test frames, the wavelength of buckling varies between about 700mm and 1100mm, and the critical lip buckling stress varies between 135 N/mm^2 and 515 N/mm^2. It is apparent therefore that when the initial imperfections are taken into account, lip buckling is a phenomenon which must be considered as part of the design process.

BS 5950: Part5 (1987) specifies a width of lip which is deemed to ensure that the webs may be treated as plate elements supported on both longitudinal edges.

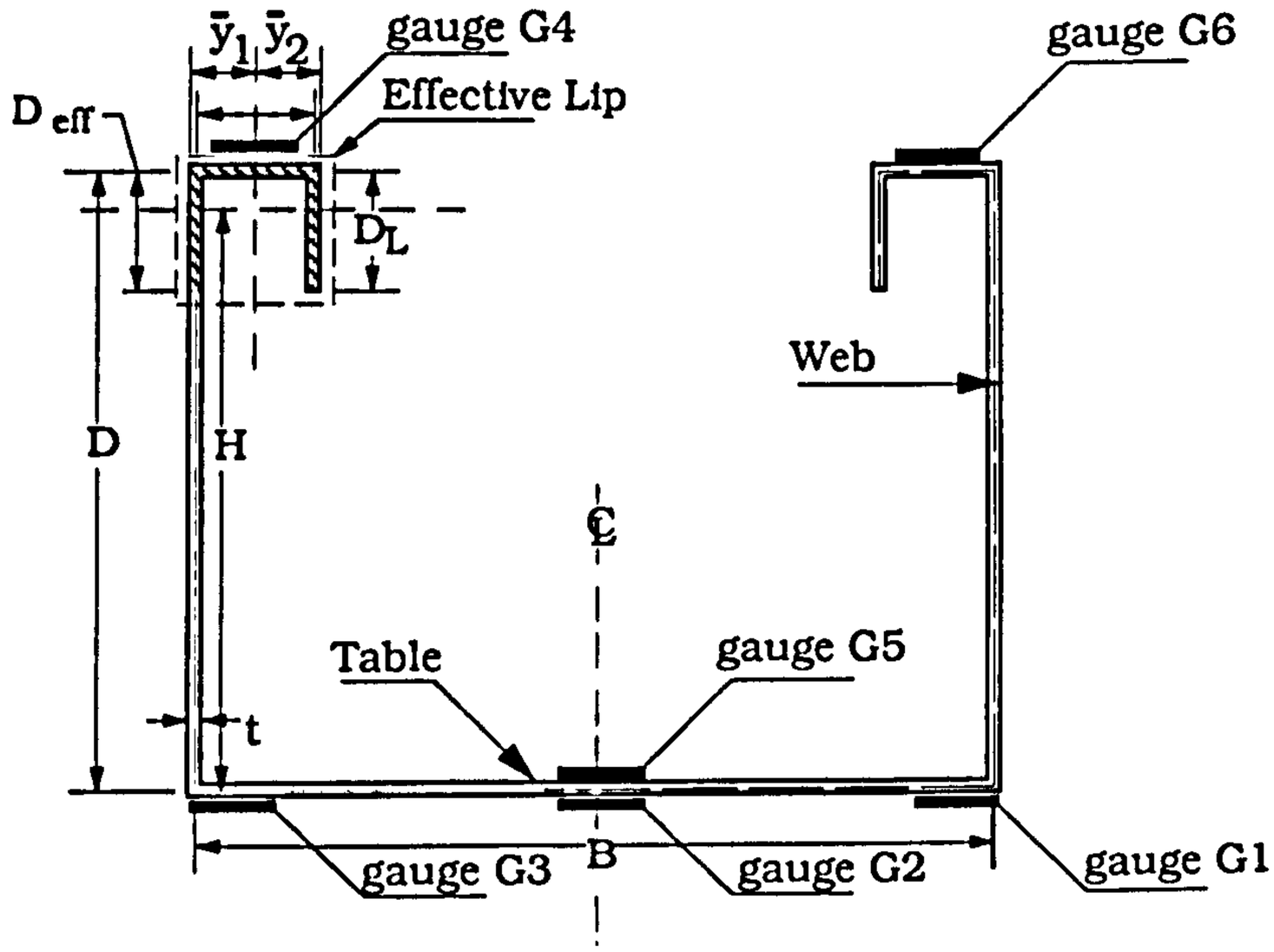


Figure 5.1 Channel section - strain gauge positions

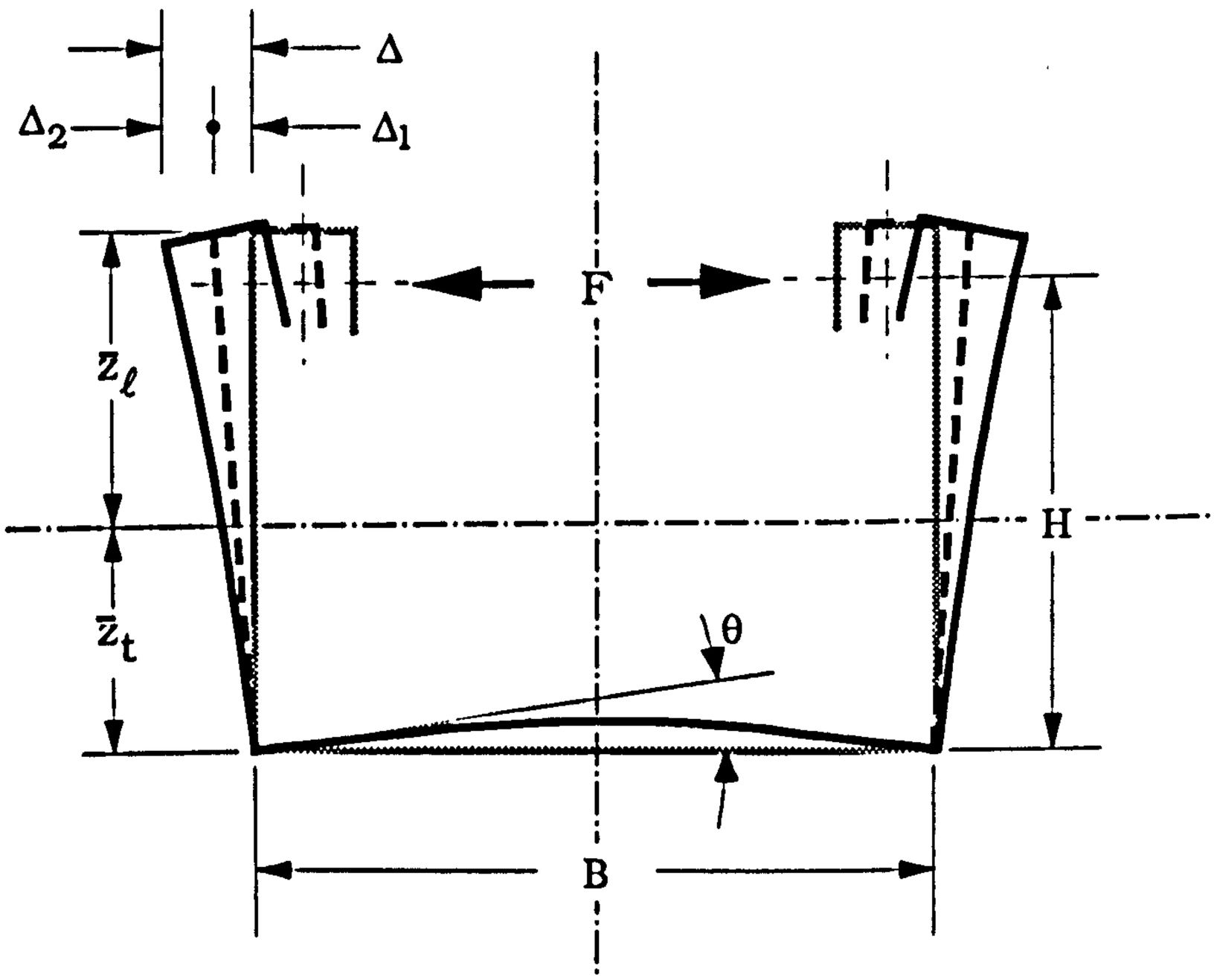


Figure 5.2 Lip buckling deformation

However, lip buckling is not treated, and neither is the specified width sufficient to prevent lip buckling.

In this chapter, a simple approximate model for determining the critical lip buckling stress, based on a "strut on elastic foundation" is proposed. The lip buckling resistance is estimated on the basis of a notional imperfection consistent with normal design tolerances. The principal uncertainties were the extent of the lip which should be taken as the "strut", the modelling of the foundation (the stiffness is calculated on the basis of unconnected transverse strips), the influence of local plate element buckling on transverse stiffness, and the appropriate magnitude of the imperfection.

A design method was required to meet the exigencies of the development programme, and time did not permit literature searches and studies. Initial verification was provided by tests, and more systematic verification on the basis of the design model was provided subsequently by non-linear elasto-plastic finite element studies in which the assumed imperfections were incorporated. When time permitted, existing literature was reviewed, and similarities to and differences from the above approach could then be noted. It was found in fact that the effect of initial imperfections had not previously been considered.

Several researchers have proposed a variety of methods for determining lip adequacy and the critical buckling resistance for various types of lips. Douty (1962) and Haussler (1964) idealised the lip as a strut on an elastic foundation to determine the critical lip buckling stress (Yu 1991). Desmond et al (1981), Hancock (1985), Lau and Hancock (1988), Seah and Rhodes (1990), Rhodes and Seah (1992), Seah et al (1991) have all suggested variations of a modified effective width approach, whilst explicit analytical expressions based on an approximate distortional buckling model have been derived to predict the ultimate lip buckling stress of thin-walled columns and beams by Lau and Hancock (1987) and Serrette and Pekoz (1991, 1992).

5.2 CRITICAL LIP BUCKLING

The lip can be idealised as a strut with continuous elastic restraint. The "strut" is not of course a separate entity, and its assumed effective extent requires verification. The mid-thickness dimensions of the section are used in evaluating the lip buckling stress. In the channel section, the "elastic foundation" is provided by

the stiffness of the cross-section in response to a horizontal disturbing force applied at the lips. The torsional rigidities of the web and lip are neglected and the deformational stiffness has been assumed to be that of uncoupled transverse strips of unit width. No distinction is made between lip stress caused by axial compression or by bending; the validity of this simple model will be examined by means of finite element analysis.

5.2.1 BUCKLING OF DOUBLY LIPPED CHANNEL

Consider the doubly lipped channel section shown in Figures 5.1 and 5.2. The "effective strut" consists of the lip downturn, lip table and a portion of each web. The effective portion of the web was taken to be equal to 0.2D; this assumption is compared with the empirical equation for a singly lipped channel section given by Douty (1962) (Yu 1991)

$$D_{eff} = \frac{[(3\bar{z}_\ell - \bar{z}_t)]}{12\bar{z}_\ell} D \qquad (5.1)$$

D (mm)	$\frac{0.2D}{\text{Eqn. 5.1}}$
125	1.07
100	0.96
75	0.90
50	0.85

Table 5.1 Comparison between assumed effective portion of web (0.2D) and Equation 5.1 for a 3mm thick doubly lipped channel section.

for the section considered in Table 5.1.

If a disturbing force F is assumed to act at the centroid of the effective lip section, this results in a unit deflection Δ (Figure 5.2). The deflection at the lip caused by the force F per unit length, acting at the centroid of the effective strut, at a distance H above the table of the section, is given by

$$\Delta_1 = \frac{F H^3 12(1 - \nu^2)}{3 E t^3} \qquad (5.2)$$

and

$$\Delta_2 = \theta H = \frac{F\, H^2 B\, 12(1 - \nu^2)}{2\, E\, t^3} \tag{5.3}$$

The total deflection at the lip is

$$\Delta_{total} = \Delta_1 + \Delta_2 = \frac{2\, F\, H^2 (1 - \nu^2)}{E\, t^3}[3B + 2H] \tag{5.4}$$

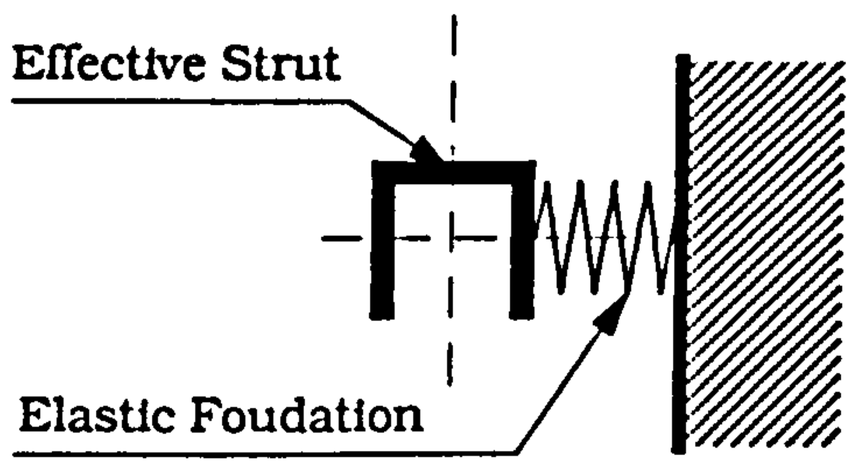


Figure 5.3 Lip buckling model

The elastic restraint given by the deformational stiffness can be expressed as a "foundation modulus", shown as a linear spring in Figure 5.3, where β is

$$\beta = \frac{F}{\Delta} \tag{5.5a}$$

and

$$\beta = \frac{E t^3}{2H^2 (1-\nu^2)[3B+2H]} \tag{5.5b}$$

where

B breadth of section to mid thickness
F disturbing force per unit length
H height of the lip centroid above the mid thickness of the table
E modulus of elasticity (205 kN/mm^2)
t thickness of section
Δ transverse deflection caused by force F
ν Poisson's Ratio

The critical buckling stress for a long strut on an elastic foundation, in which the preferred wave length is free to develop, is given by Timosenko and Gere (1961), and

is

$$\sigma_{crL} = \frac{2\,(E\,I_L\,\beta)^{1/2}}{A_L} \tag{5.6}$$

Alternatively

$$\sigma_{crL} = 2\,r_L\left(\frac{E\,\beta}{A_L}\right)^{1/2} \tag{5.7}$$

where

A_L effective area of lip
I_L second moment of area of lip about the local Y axis of effective lip
r_L radius of gyration of lip about z axis
σ_{crL} elastic critical lip buckling stress

It can be seen from Equation 5.7 that for a given β and A_L, σ_{cr} is proportional to r_L. The preferred half wave length of buckling for a long strut is

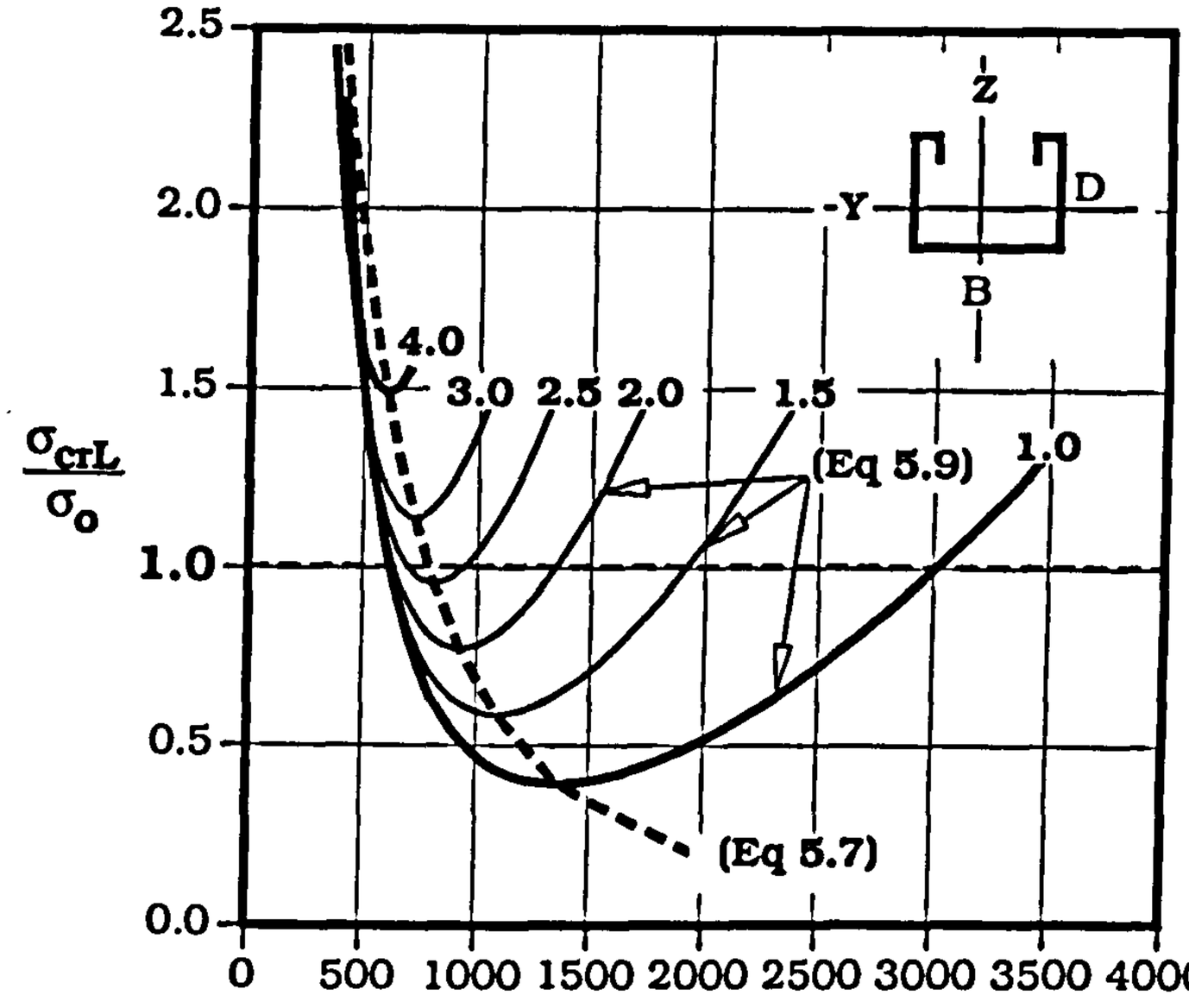
$$L_B = \left(\frac{\pi^4\,E\,I_L}{\beta}\right)^{1/4} \tag{5.8}$$

For a finite length of member, the number of half waves m must be an integer. The preferred number of half waves is then obtained by minimising the critical elastic lip buckling stress given by Equation 5.9 with respect to L_{cr}.

$$\sigma_{crL} = \frac{\pi^2 E}{\left(\frac{L_{cr}}{r_L}\right)^2}\left(1+\frac{\beta\,L_{cr}^4}{\pi^4\,E\,I_L}\right) = \frac{\pi^2 E}{\left(\frac{L_{cr}}{r_L}\right)^2}\left(1+\left(\frac{L_{cr}}{L_B}\right)^4\right) \tag{5.9}$$

where L_{cr} is the half wave length for lip buckling, and $L_{cr} = L/m$. The variation in critical lip buckling stress with length for various thickness of section is shown in Figure 5.4. The minima of each of the curves may be found from Equations 5.7 and 5.8, and represents the critical stress and the corresponding halfwave length for a member having a length for which the preferred mode of buckling is free to develop, for a particular thickness of cross section. It can be seen that the least critical stress varies from 1.5 σ_o for t = 4mm to 0.4 σ_o for t = 1mm.

Figure 5.5 shows the variation in the critical lip buckling stress with depth and breadth. It can be seen that the critical lip buckling stress is more sensitive to change in web depth for a given table breadth, than to a change in table breadth for a constant depth.



B=122mm, D=97mm, B_L=17mm, D_L=18.5mm, σ_o = 390 N/mm^2

Figure 5.4 Variation in critical lip buckling stress with length given by Equations 5.7 and 5.9

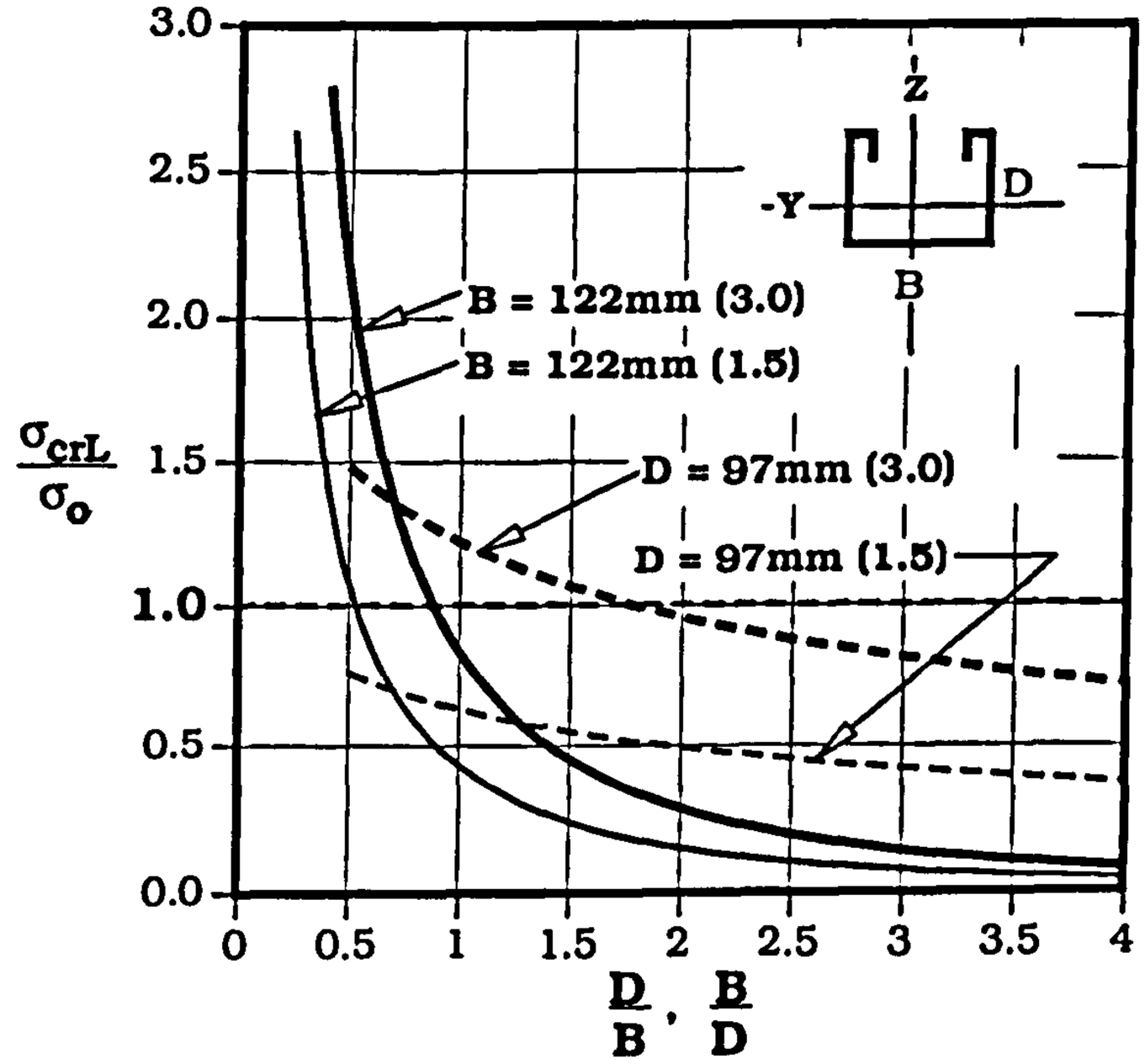


Figure 5.5 Variation in critical lip buckling stress with depth and breadth given by Equation 5.7

B = 122mm or D = 97mm, B_L = 17, D_L = 18.5, σ_o = 390 N/mm^2

Thickness of section in brackets

The critical lip buckling stress of a section may be increased by providing point restraints to the lip L_R apart, where L_R is less than L_{cr}. The critical lip buckling stress can then be found from Equation 5.9, writing $L_{cr} = L_R$.

5.2.2 FINITE ELEMENT ANALYSIS OF DOUBLY LIPPED CHANNEL

Critical buckling solutions were obtained using finite element analyses. The first member analysed was 122mm wide and 1220mm long. The depth and thickness were varied. The purpose was to examine the validity of Equations 5.6 to 5.9. The aspect ratios of the elements in the finite element mesh adopted for this series of analyses were the same as that used in Chapter Four. The length of member was chosen such that local table and web buckling, and lip buckling were free to develop. Possible interaction between the two buckling modes would then be revealed in subsequent non-linear solutions for initially imperfect members. The symmetric nature of the buckling modes permitted modelling of half the cross-section. For axially loaded members, overall bending and rotation of the section were prevented, whilst for sections subject to uniform bending, overall rotation was prevented. Deformation of the cross-section was prevented at each end. However, the lip was allowed to rotate in plan.

For sections having large width to thickness ratios the first and many subsequent buckling modes (eigenvectors) correspond to local buckling of the table, with smaller carry-over deformations of the webs and lips. The critical lip buckling stress is given by the first eigenvector which displays overall lip buckling. The lowest mode (local buckling), as well as the critical lip buckling modes for a 122mm x 97mm, 1.5mm thick section, are illustrated in Figure 5.6. Overall lip buckling of this section occurred as the 22nd mode. Figure 5.7 shows a comparison between the critical lip buckling stresses obtained from the numerical analysis corresponding to m = 1, 2, 3 with Equation 5.9. As the pre-buckling stress distribution is uniform, the critical lip buckling stress is given by the axial load divided by the gross cross-sectional area.

Bending solutions were also obtained for four different thicknesses. The results are compared with Equation 5.9 in Figure 5.8. The critical bending stress is taken as the critical moment divided by the gross section modulus at the mid thickness of the lip table. As expected, the critical stresses (so calculated) for bending are higher than for axial loading.

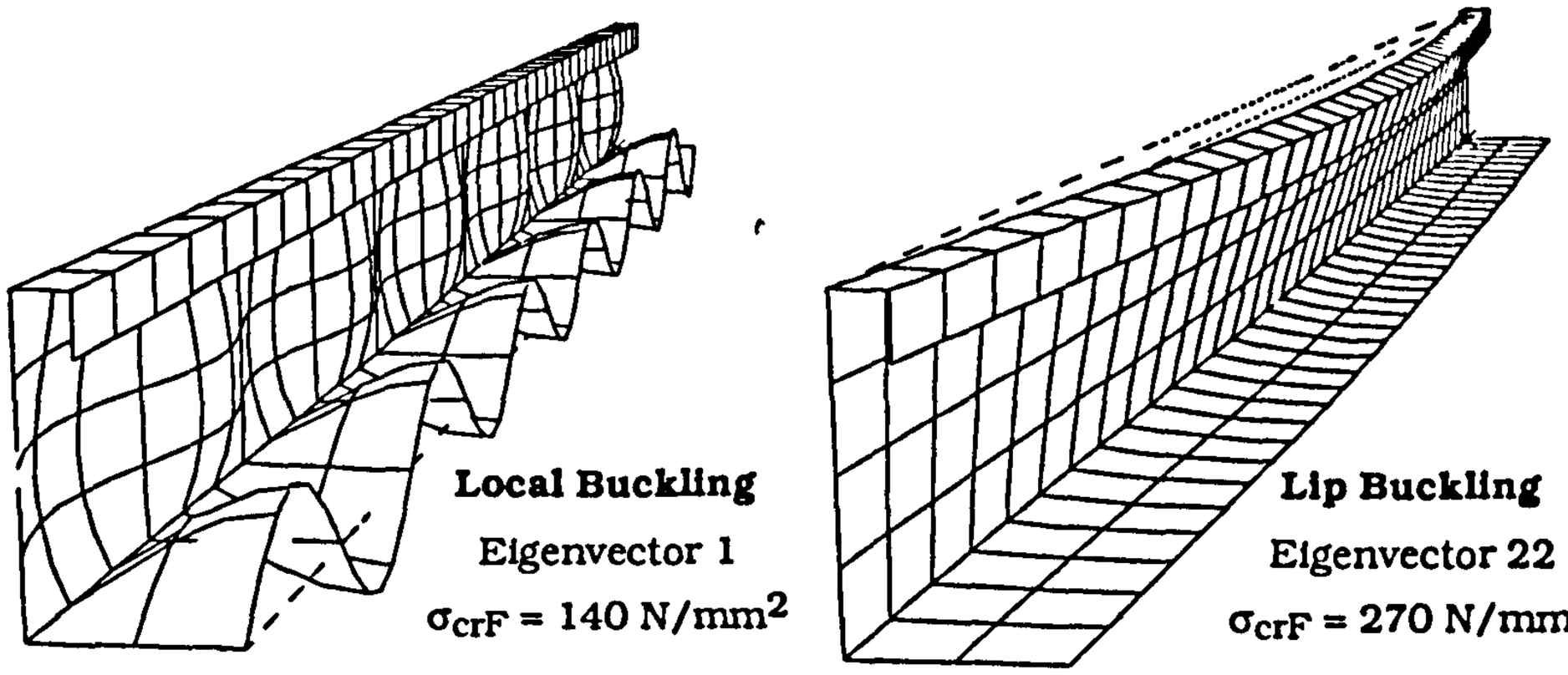


Figure 5.6 Critical buckling modes for a 122x97x17x18.5 - 1.5mm thick doubly lipped channel, L = 1220mm

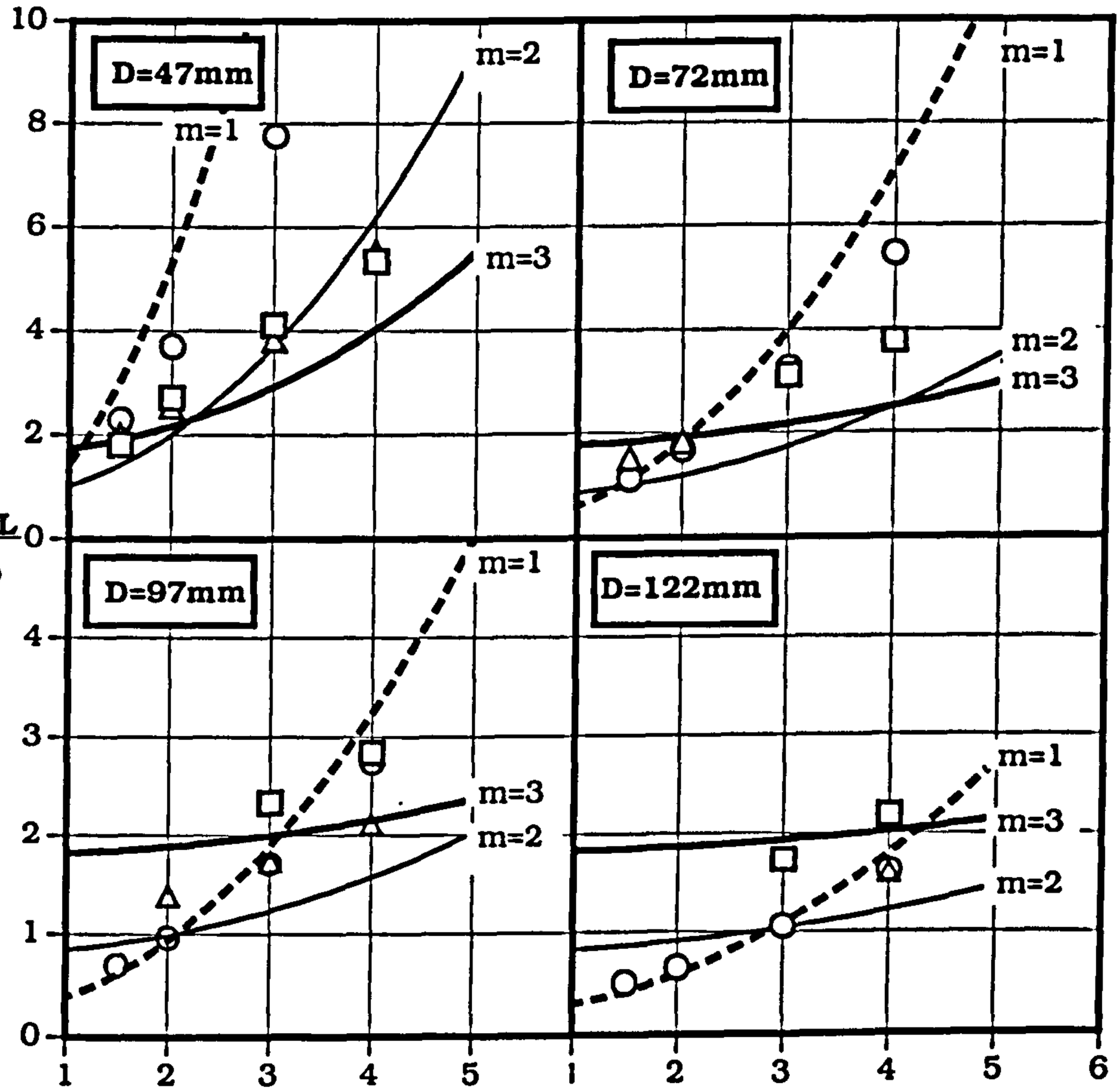
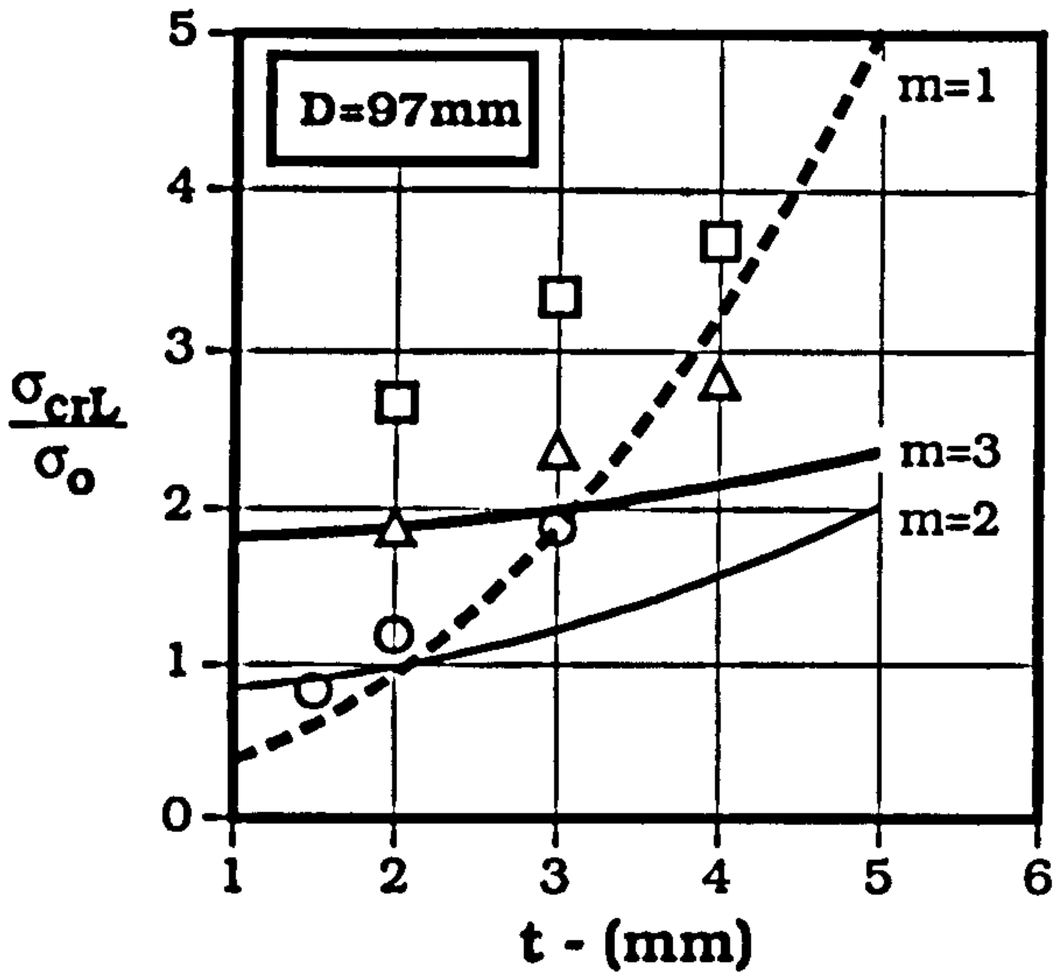


Figure 5.7 Comparison Equation 5.9 with Finite Element Analysis, Axial Loading

B=122mm, B_L=17mm, D_L=18.5mm, L=1220mm, σ_o = 390 N/mm^2



FINASIC (1990)

○ m=1 △ m=2 □ m=3

Figure 5.8 Comparison Equation 5.9 with Finite Element Analysis, Bending.

B=122mm, B_L=17mm, D_L=18.5mm, L=1220mm, σ_o = 390 N/mm^2

For axially loaded members, the lip buckling displacement described by the eigenvector was in most cases inwards but in some instances the displacement was outward, while for members subject to bending the lip displacement was always inwards. If the effective lip is symmetric about the vertical axis, the centroid and the shear centre of the lip will both be on that axis, and the lip will have no preferred direction of buckling. If the shear centre is not on the centroidal axis the tendency for torsional buckling will predispose the lip to rotate in one direction or the other. For the lip considered, where the downturn is 20mm, it might be supposed that the direction of buckling is not strongly predisposed. The effect of variations in thickness for a given depth, and of variations in depth for a given thickness, on the preferred wave length and on the corresponding critical stress, according to Equations 5.7 and 5.9, are shown in Figure 5.9.

An axially loaded 122mm x 97mm-3mm thick channel section, 3000mm long was also analysed. The first lip buckling mode had three half waves (P_{crF} = 674 kN) whilst the second had four half waves (P_{crF} = 684 kN). The critical stresses for both the lip buckling modes are compared with Equation 5.9 in Table 5.2.

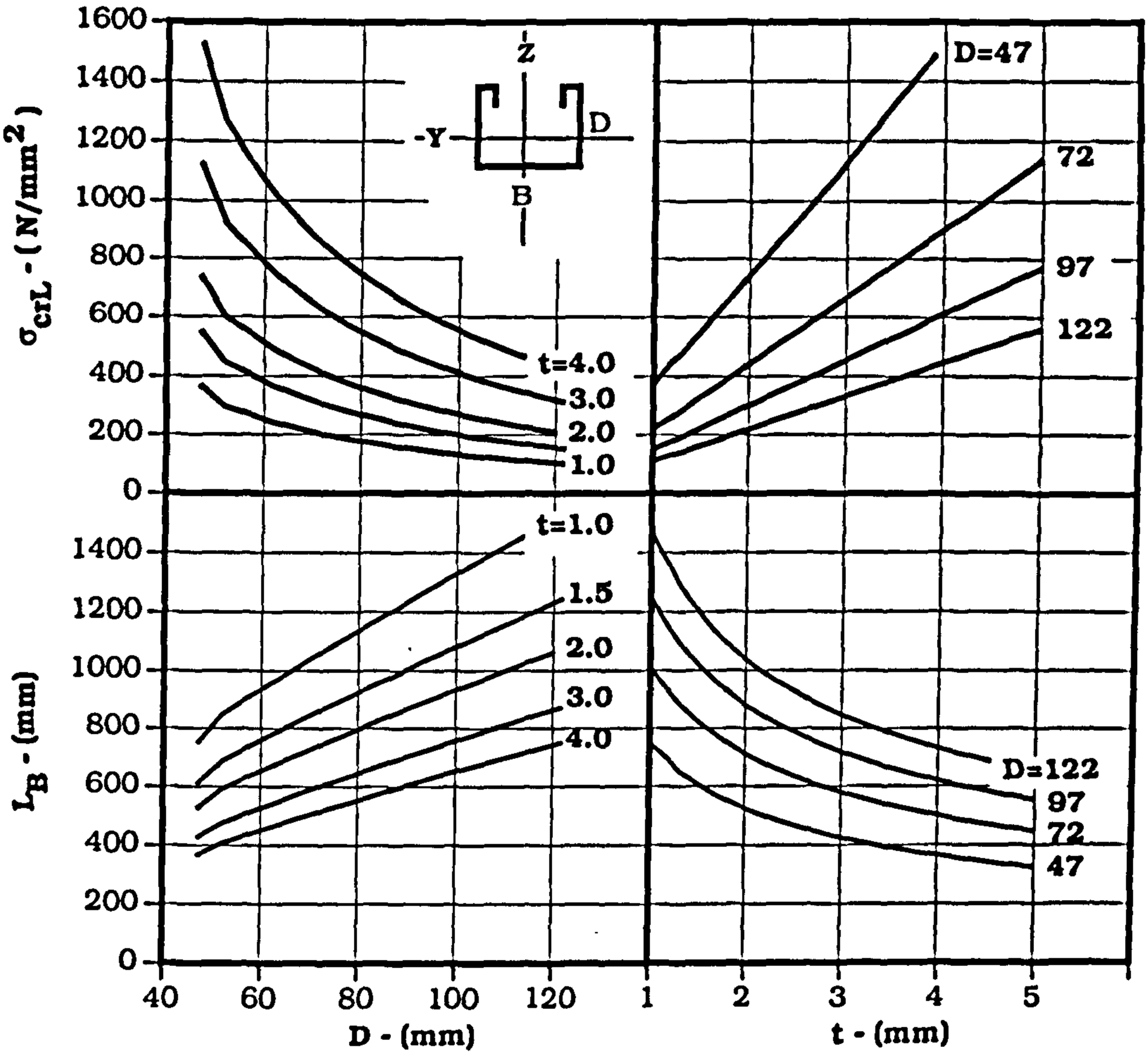


Figure 5.9 Variation of Critical Buckling Stress and Critical Lip Buckling Length with D and t (Equations 5.7 and 5.8) (B=122mm, B_L=17mm, D_L=18.5mm)

m	$\frac{L}{m}$ (mm)	σ_{crF} (N/mm2)	$\frac{\sigma_{crF}}{\text{Eqn 5.9}}$
3	1000	581	1.08
4	750	589	1.32

Table 5.2 Comparison of critical lip buckling stress (FE analysis) with Equation 5.9
B = 122mm, D = 97mm, B_L = 17mm, D_L = 18.5mm, t = 3.0, L = 3000mm

The agreement between Equation 5.9 and the finite element solutions (Figures 5.7 and 5.8) could probably be improved by adjusting the assumed extent of the web contributing to the effective lip, the level at which the disturbing forces is assumed to act, and the level at which the bending stress is calculated. The effect of coupling the transverse strips might also be included at the cost of complicating the model. Nevertheless, the present model is shown to be conservative and satisfactory for the sections considered.

5.3 LIP BUCKLING RESISTANCE

5.3.1 BUCKLING RESISTANCE OF DOUBLY LIPPED CHANNEL

Any formulation adopted for the purposes of determining the lip buckling resistance of a cross-section should take account of imperfections. Consider the elastically restrained axially loaded "lip" strut of length L shown in Figure 5.10.

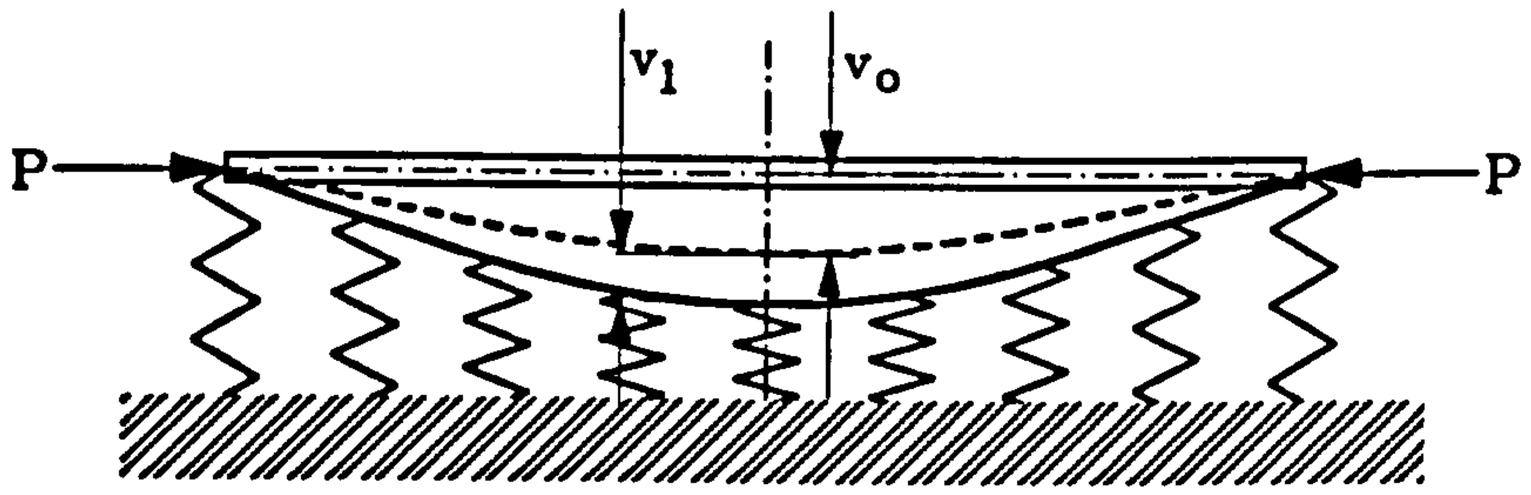


Figure 5.10 Elastically restrained, axially loaded strut

Assuming that initial imperfection (v_o) has the same effects on an elastically supported lip as it has for purely flexural buckling of a simply supported strut, then the load-displacement relationship can be defined by

$$v_1 = \frac{v_o}{\left(1 - \frac{\sigma_A}{\sigma_{crL}}\right)} - v_o \qquad (5.10)$$

The lateral displacement of the lip can be assumed to be described by

$$v_{1x} = v_1 \sin \frac{\pi x}{L} \qquad (5.11)$$

The moment at mid length of the lip is

$$M = -EI_L \frac{d^2 v_1}{dx^2} \tag{5.12}$$

Differentiating Equation 5.11 twice with respect to x and substituting into Equation 5.12, along with Equation 5.10, the mid-span moment is

$$M = \frac{\pi^2 EI_L}{L^2} v_1 = \frac{\pi^2 EI_L}{L^2} v_o \left(\frac{1}{1 - \frac{\sigma_A}{\sigma_{crL}}} - 1 \right) \tag{5.13}$$

Rearranging Equation 5.13 the bending stress at the outer most fibre of the lip caused by the Pw moment is

$$\sigma_B = v_o \frac{\sigma_A A_L \bar{y}}{I_L} \left[\frac{\sigma_E}{\sigma_{crL}} \right] \left[\frac{1}{\left(1 - \frac{\sigma_A}{\sigma_{crL}} \right)} \right] \tag{5.14}$$

The total compressive stress at the outermost fibre of the lip due to axial compression and bending is

$$\sigma_{max} = \sigma_A + \sigma_A \frac{v_o \bar{y}}{r_L^2} \left[\frac{\frac{\sigma_E}{\sigma_{crL}}}{\left(1 - \frac{\sigma_A}{\sigma_{crL}} \right)} \right] \tag{5.15}$$

Rearranging Equation 5.15 and solving for σ_{uL}, with $\sigma_o = \sigma_{max}$ and $\sigma_{uL} = \sigma_A$ the axial resistance of an elastically restrained lip is given by a modified Perry formulation, which is

$$\sigma_{uL} = 0.5 \left[\left(\sigma_d + (1+\eta') \sigma_{crL} \right) - \left[\left(\sigma_d + (1+\eta') \sigma_{crL} \right)^2 - 4 \sigma_d \sigma_{crL} \right]^{1/2} \right] \tag{5.16}$$

where

$$\eta' = \eta \frac{\sigma_{Ez}}{\sigma_{crL}} \tag{5.17}$$

σ_{uL} lip strength

σ_d design strength (the smaller of σ_o or 0.84 σ_u)

σ_{crL} obtained from Equations 5.7 or 5.9

σ_{Ez} Euler buckling stress of effective lip where

$$\sigma_{Ez} = \frac{\pi^2 E r_L^2}{\ell^2} \tag{5.18}$$

ℓ lip half wave length of buckling

η imperfection parameter where

$$\eta = \frac{v_{oL}\,\bar{y}}{r_L^2} \tag{5.19}$$

v_{oL} is the initial hortizontal imperfection of the lip

Because of the relative difference in buckle halfwave length for local and lip buckling no reduction in deformational stiffness is expected. This assumption will be examined by finite element analysis.

5.3.2 NON-LINEAR FINITE ELEMENT ANALYSIS OF DOUBLY LIPPED CHANNEL

Non-linear elasto-plastic finite element analyses were carried out to determine the axial load and moment, and the corresponding lip stress, at first yield and failure for a 122x97x20x20 doubly lipped channel section for various thickness. The same mesh, boundary conditions and loading arrangement used in the critical buckling analyses were again employed. An initial single half-wave outward lip imperfection of v_{oL} = L/1000 was assumed for all 1220mm long members. A single half wave imperfection was chosen to ensure that the torsional stiffness of the web, table and the lip of the channel would have as little an effect as possible on the buckling behaviour of the lip . The lip buckling stress at first yield and failure for a member subjected to axial load was defined as the total force on the effective lip elements divided by the area of the "effective strut" A_L.

The lip buckling resistance given by the numerical analysis and Equation 5.16 with the imperfection parameter η given by Equation 5.17 in which v_{oL} = L/1000, are compared in Figure 5.11. It is observed that Equation 5.16 gives a reasonable estimate of the lip buckling stress for the range of depths considered.

In general, the lip was observed to deflect in the direction of the initial imperfection. However, in the case of the 122mm x 97mm-1.5mm thick section, the deflection was initially outward but then changed direction, and failure occurred by inward buckling. Figure 5.12 shows the load/displacement history for a 1.5mm thick section. The reversal in lip displacement can be explained by the shift in the vertical neutral axis of the effective lip which results from the diminishing effectiveness of

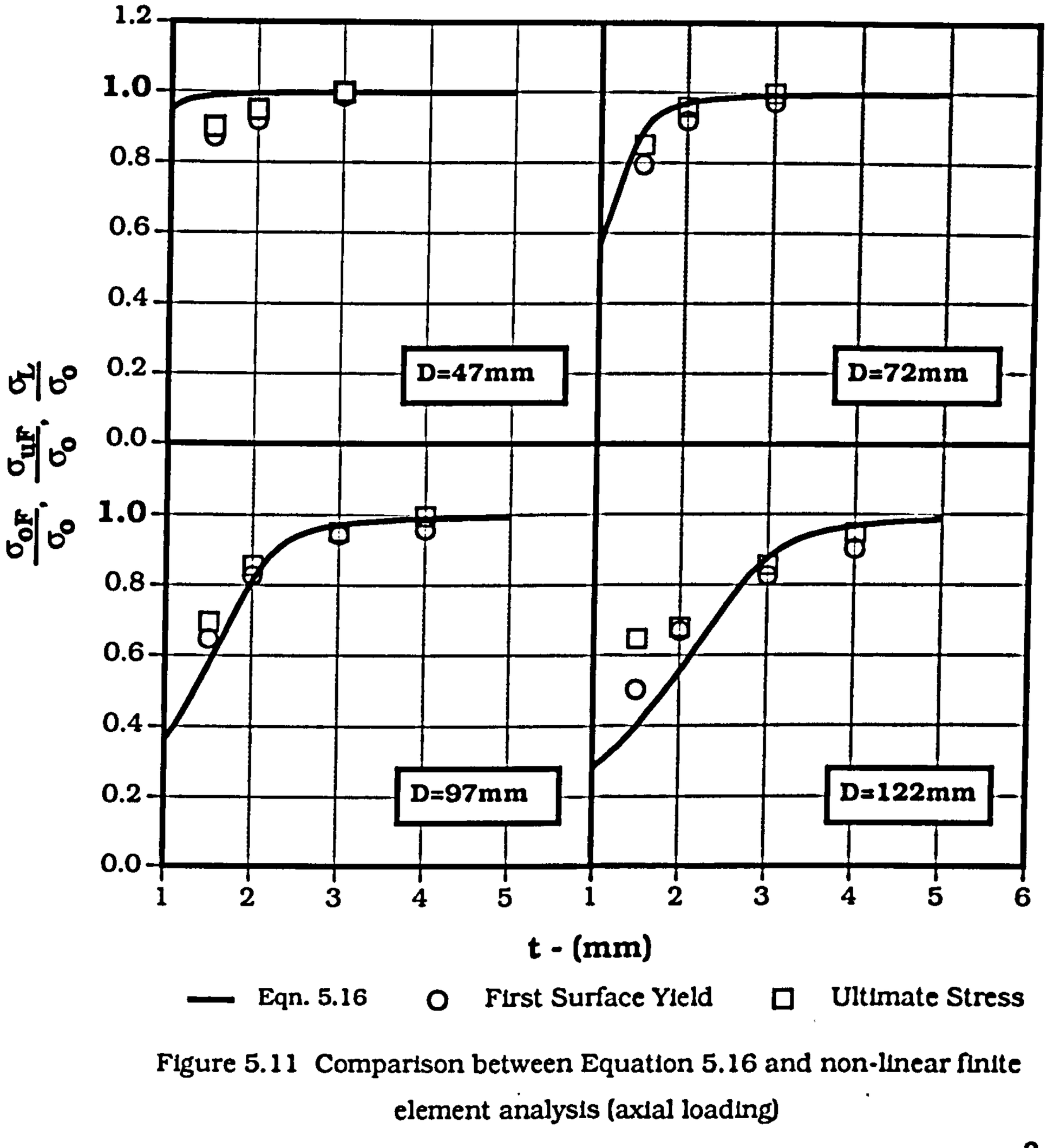


Figure 5.11 Comparison between Equation 5.16 and non-linear finite element analysis (axial loading)

$B = 122mm$, $B_L = 17mm$, $D_L = 18.5mm$, $L = 1220mm$, $\sigma_o = 390\ N/mm^2$

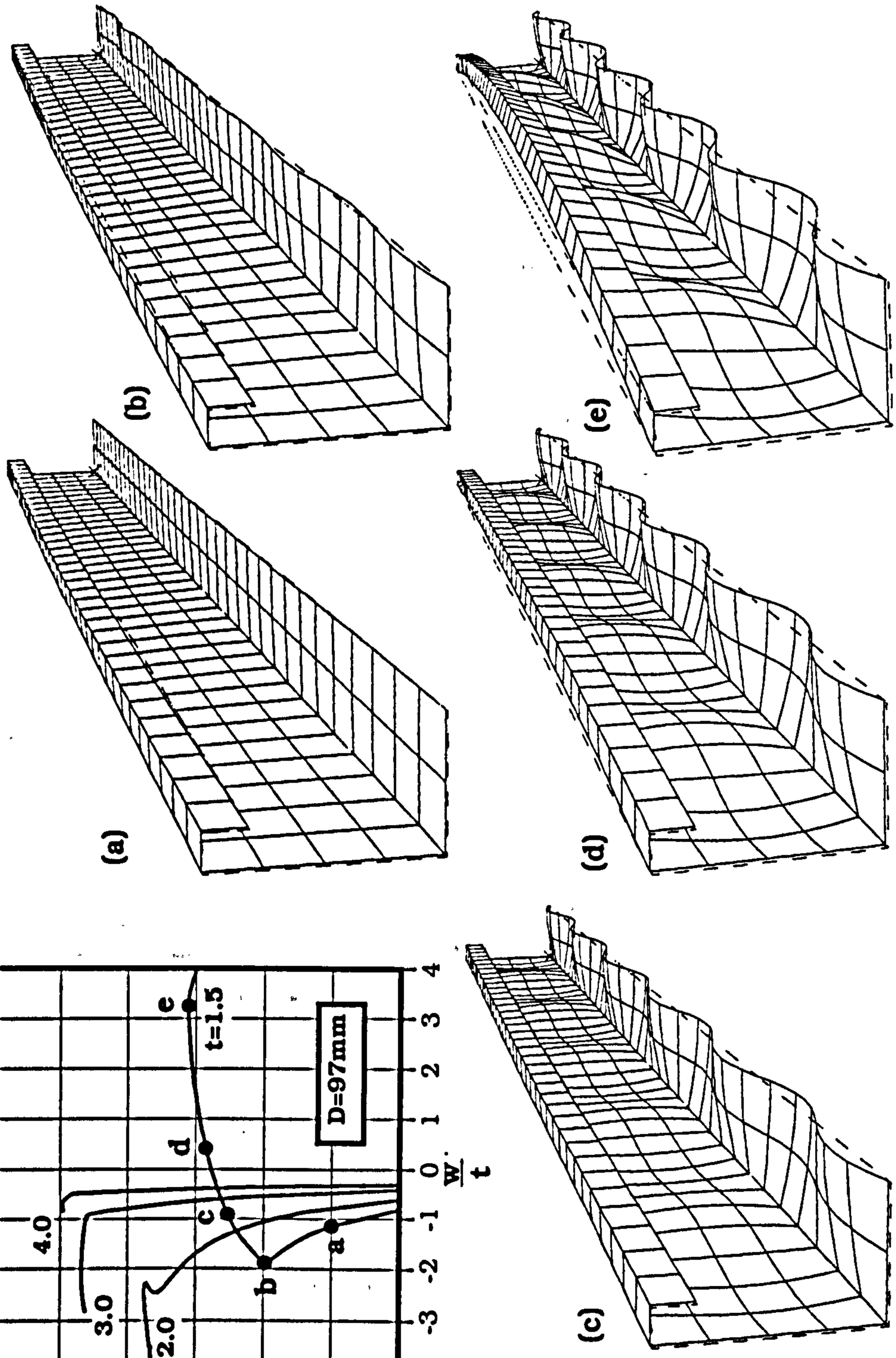


Figure 5.12 Non-linear elasto-plastic analysis - Lip buckling vs lateral displacement
B = 122mm, D = 97mm, B_L = 17mm, D_L = 18.5mm, t = 1.5mm, L = 1220mm, σ_o = 390 N/mm^2

the web as local buckling develops. The applied end force P is uniform, and initially the additional lateral deflection is in the same direction as v_{oL}. The shift in neutral axis results in a countervailing moment which causes the deflection to change direction. When v_{oL} = L/500, reversal of the lip lateral displacement did not occur, suggesting that the moment caused by the initial imperfection was large enough to cancel the eccentric moment caused by the shift in neutral axis position relative to the applied load. The rather large difference between the first yield stress and failure stress for the 1.5mm thick section, as seen in Figure 5.12, is due to the lip reversal. Similar lip buckling behaviour was observed during experiments carried out by Desmond et al (1981) and Hancock (1985).

The sensitivity of the load to cause first yield and failure to initial imperfection levels was investigated by doubling the initial value of v_{oL} from L/1000 to L/500. The results plotted in Figure 5.13 show that both the first yield and failure load are not very sensitive to an increase in imperfection. However, for thin sections (t<2) if v_{oL}-> 0 then it would be expected that σ_{uL}-> σ_o.

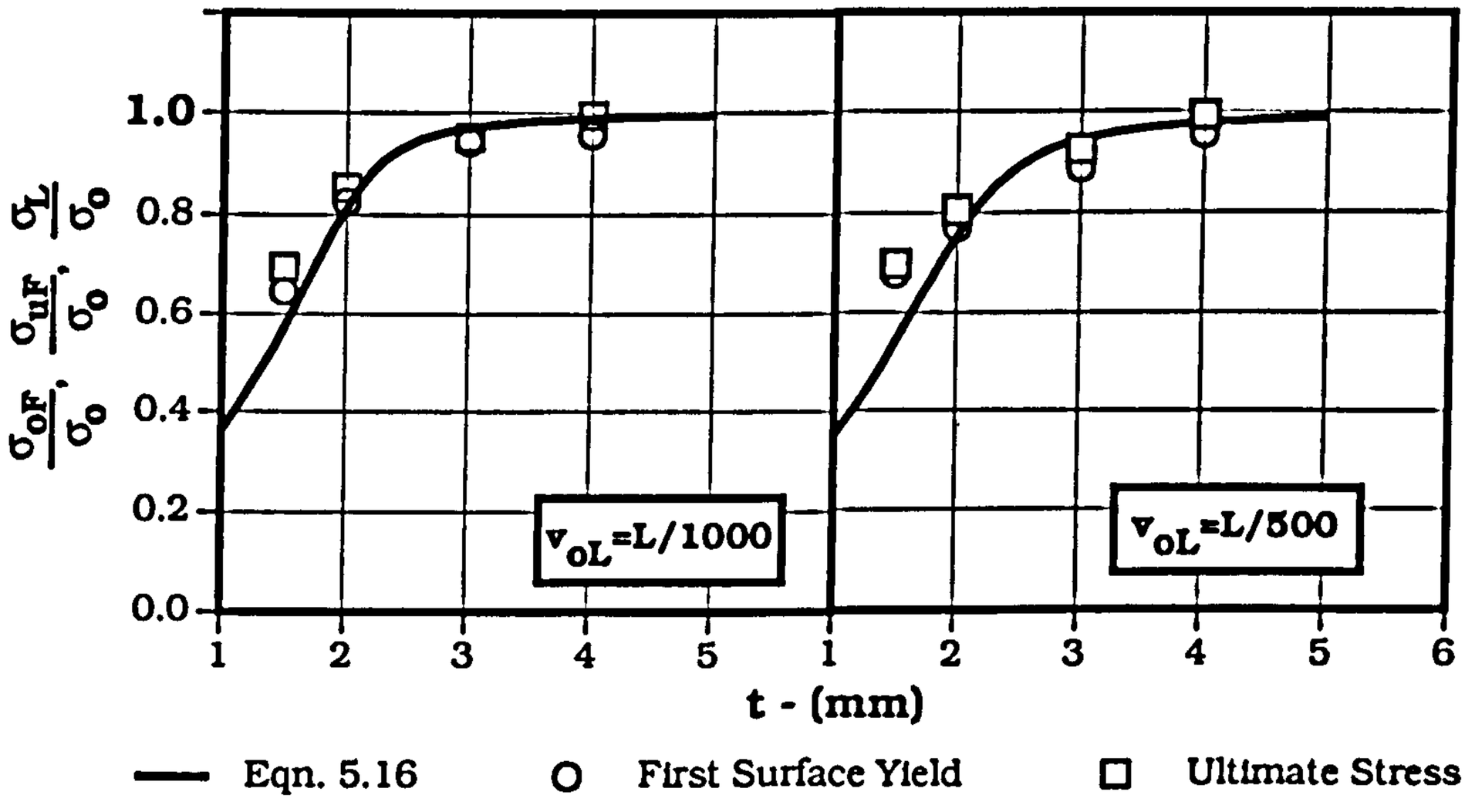


Figure 5.13 Imperfection sensitivity of lip buckling stress (Axial loading)

B = 122mm, B_L = 17mm, D_L = 18.5mm, L = 1220mm, σ_o= 390 N/mm^2

The lip stress at first surface yield and failure caused by equal moments applied to each end of a 1220mm long member, for various thicknesses, were also obtained numerically and are shown in Figure 5.14. The lip stress for bending was taken as the applied moment divided by the gross section modulus at the mid thickness of the lip table element. It can be seen that there is little difference between the first yield and ultimate lip stresses obtained for axial loaded members (Figure 5.11) and members subjected to a uniform moment (Figure 5.14).

A limited study on the effect of mode and magnitude of v_{oL}, on the lip buckling resistance of a 122mm x 97mm-3mm section, 3000mm long, was also carried out. The first and second eigenvectors obtained from the critical buckling analysis, corresponding to a three half wave and four half wave lip buckle along the member, were scaled to obtain the required level of imperfection needed for the non-linear analysis, such that $v_{oL} = L_{cr}/1000$. The load-displacement history for a 3mm thick section can be seen in Figure 5.15. The lip buckling resistance for different modes and levels of imperfection are shown in Table 5.3.

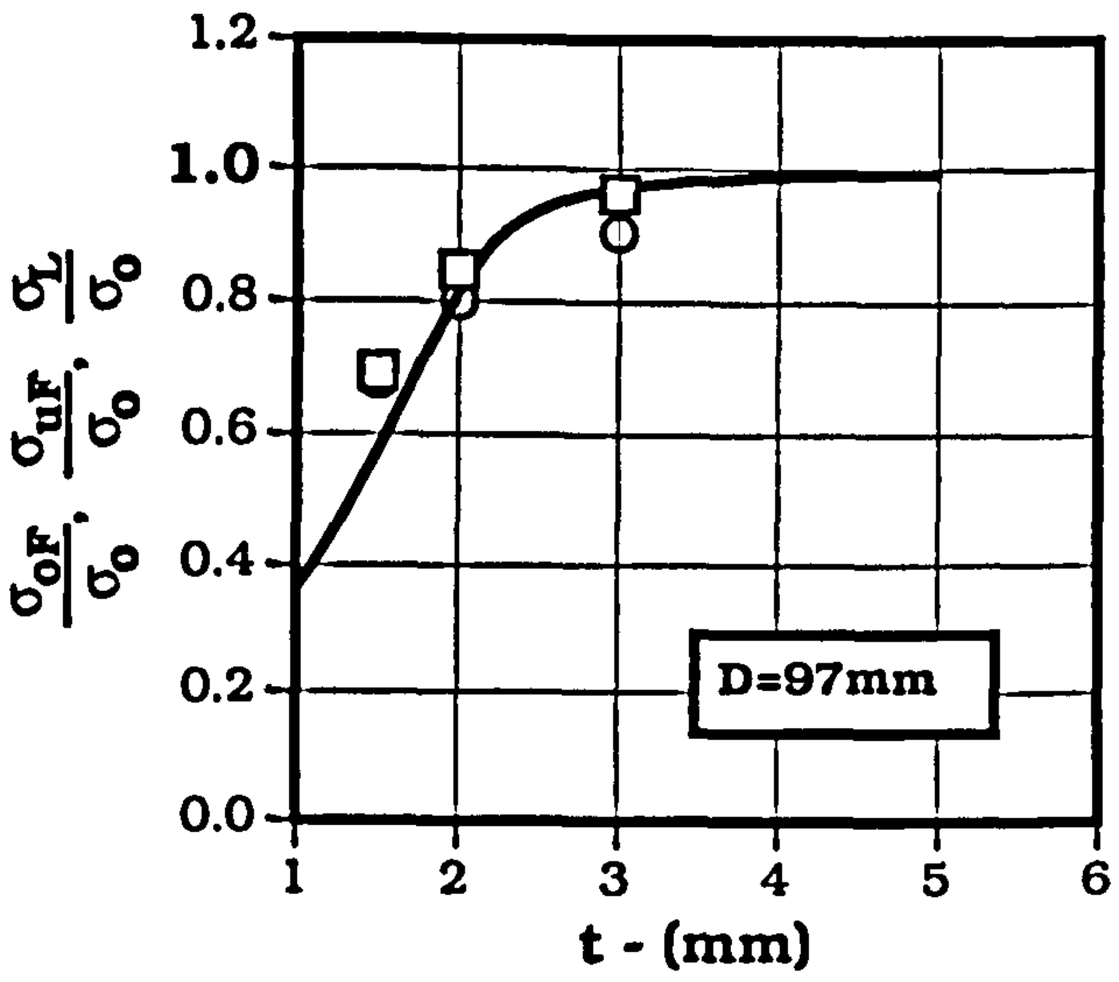


Figure 5.14 Comparison between Equation 5.16 and non-linear finite element analysis, (Bending)

B = 122mm, B_L = 17mm, D_L = 18.5mm, L = 1220mm, σ_o= 390 N/mm^2

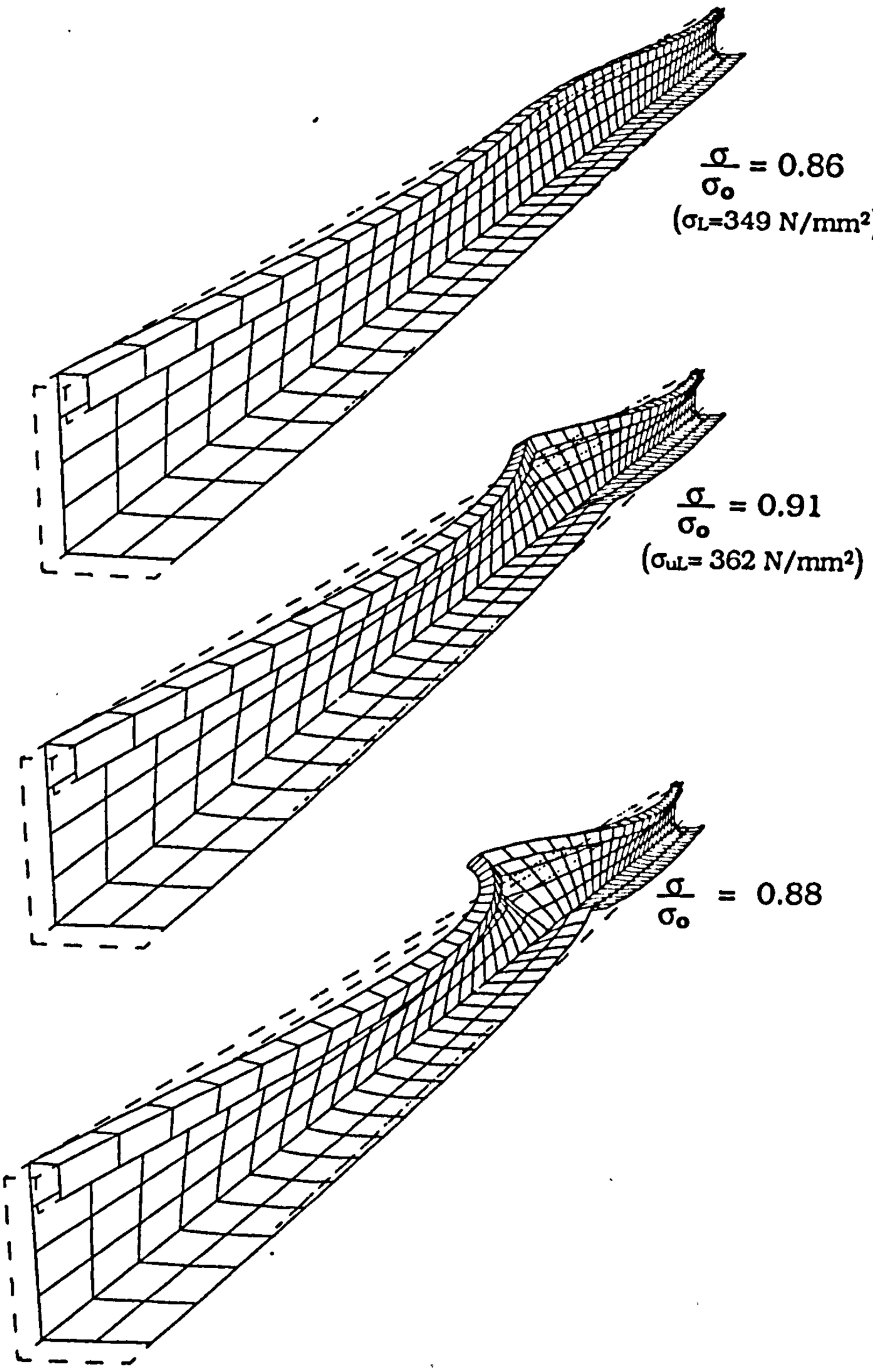


Figure 5.15 Non-linear elasto-plastic analysis - Lip buckling (Axial load)

B = 122mm, D = 97mm, B_L = 17mm, D_L = 18.5mm, t = 3.0mm

v_{oL} = ±1.0mm, L = 3000mm, σ_o = 390 N/mm^2

(Displacement scale x20)

t (mm)	m	v_{oL} (mm)	P_{oF} (kN)	P_{uF} (kN)	σ_{oF} (N/mm^2)	$\frac{\sigma_{oF}}{\text{Eqn. 5.16}}$
3.0	3	-1.0	389	402	352	1.00
	3	+1.0	387	411	350	0.99
	3	-0.6	400	418	356	0.98
	3	+0.6	409	421	367	1.01
	4	0.75	386	393	339	1.05
	4	0.2	422	430	371	1.03

Table 5.3 Sensitivity of lip buckling resistance to initial imperfection obtained from Equation 5.16.

B = 122mm, D = 97mm, B_L = 17mm, D_L = 18.5mm, L = 3000mm, σ_o = 390 N/mm^2

5.3.3 EXPERIMENTS

Experiments on concentrically loaded thin walled cold-formed channel columns were carried out to compare and investigate the following:

(a) The ultimate buckling capacity of the channel sections of various wall thickness.

(b) Load-deformation characteristics.

(c) The possible influence of local buckling on lip buckling

Test	B	D		B_L		D_L		t	σ_o	σ_u	%e
	mm	mm		mm		mm		mm	N/mm^2	N/mm^2	
		D_1	D_2	B_{L1}	B_{L2}	D_{L1}	D_{L2}				
LC1	125.6	99.0	99.0	20.3	20.5	19.3	20.7	1.5	364	494	26.1
LC2	125.0	100.9	100.0	20.5	20.5	18.5	18.0	3.0	490	539	20.8

Table 5.4 Geometric and material properties for 9 metre column test

Tensile coupons 50mm wide and 200mm between gauge marks were taken from each specimen. Tensile tests were carried out to determine the yield and ultimate

stresses (σ_o and σ_u) and percentage elongation (%e) of the material used so that each specimen could be analysed on the basis of the true yield stress. The dimensions and material properties of the specimens tested are given in Table 5.4. All sections were strain gauged at mid length as shown in Figure 5.2. The ends of each section were inspected prior to testing to ensure that an even bearing surface had been obtained.

The test arrangement shown in Figure 5.16 was used to apply axial load through a 50 ton jack to the ends of a 9000mm (3 x 3000mm) long channel column. It is well known that as the applied load is increased, the effective section reduces, and as a result a shift in neutral axis position of the section occurs. In order to ensure that the load was applied axially to the channel in the later stages of loading the knife-edges were located at the effective neutral axis position. Restraint against warping and lip rotation existed at each end of the column; however, by using three spans the effect of restraint on the lip buckling behaviour of the central span is reduced. For the lip buckling experiments flexure about both axes of the section and twisting about the longitudinal axis were restrained along the entire length. This was done to ensure that the lip buckling behaviour would not be affected by overall buckling.

At suitable load intervals, the test was suspended so that lateral lip displacements could be measured at 300mm centres along the entire length of specimen. The longitudinal strains at the four corners of the channel section at mid length of the specimen were also measured. Two thicknesses of channel section were tested to failure. Figure 5.17 shows the lateral displacement at various loads of the 1.5mm thick lip at mid length of the central span. The buckle halfwave length obtained experimentally was L_B = 1100mm which compares well with L_B = 1091mm given by Equation 5.8. Lip buckling for the 1.5mm thick section (LC1) was observed to developed gradually from the outset. Failure occurred at a load of 96 kN caused by sudden collapse of the lip downturn. The resulting failure can be seen in Figure 5.16. The 3.0mm thick section (LC2) failed at a load of 420kN caused by torsional-flexural buckling which occurred between points of flexural restraint.

The variation in longitudinal strain with load, for both tests, is shown in Figure 5.18, where it can be seen that the longitudinal strains at all four corners around the cross-section are similar in magnitude, indicating that the load was predominantly axial. Test results are given in Tables 5.5

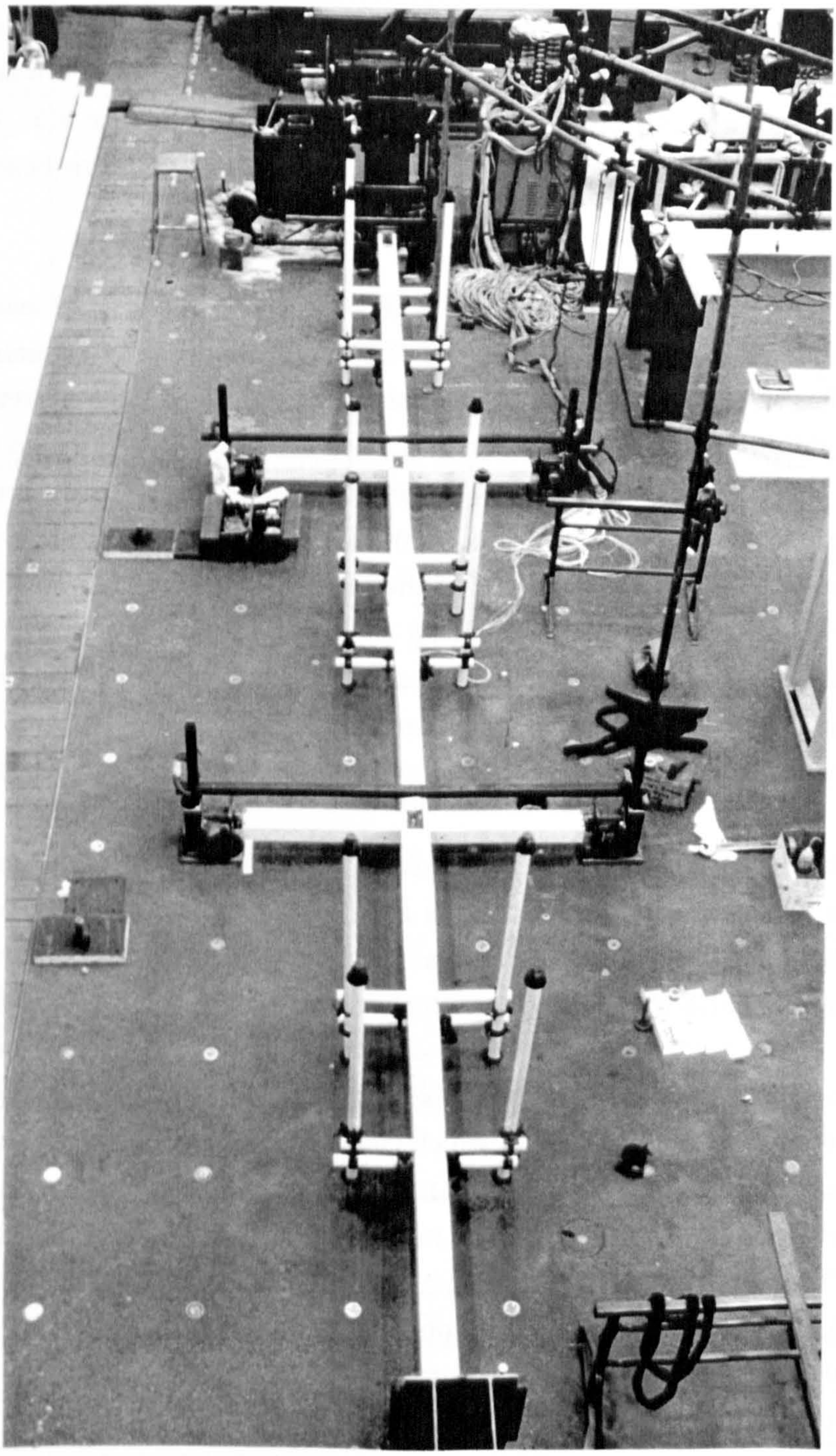


Figure 5.16 Loading arrangement - 9 metre column test

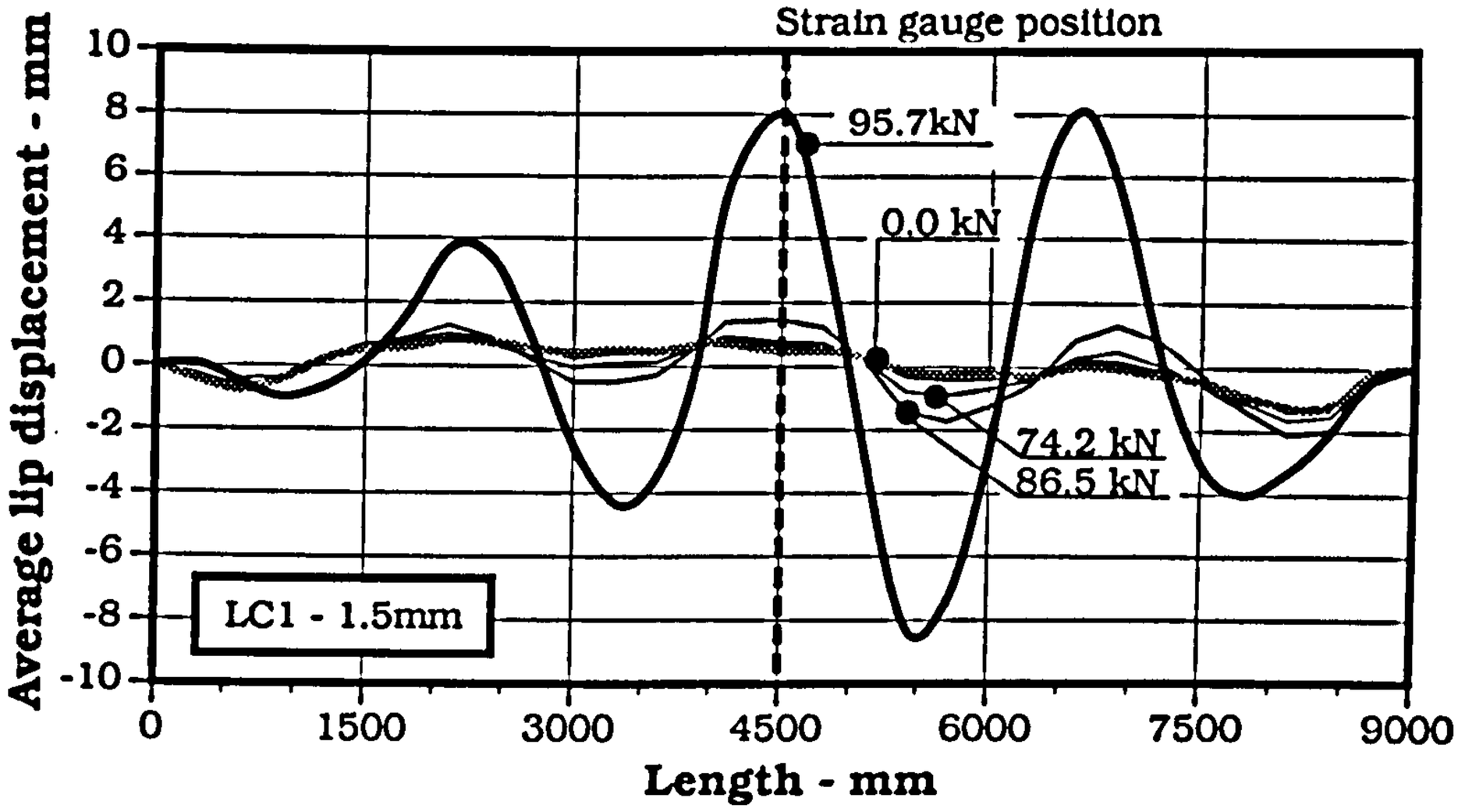


Figure 5.17 Load vs average lateral displacement of lip - 9 metre Column Tests

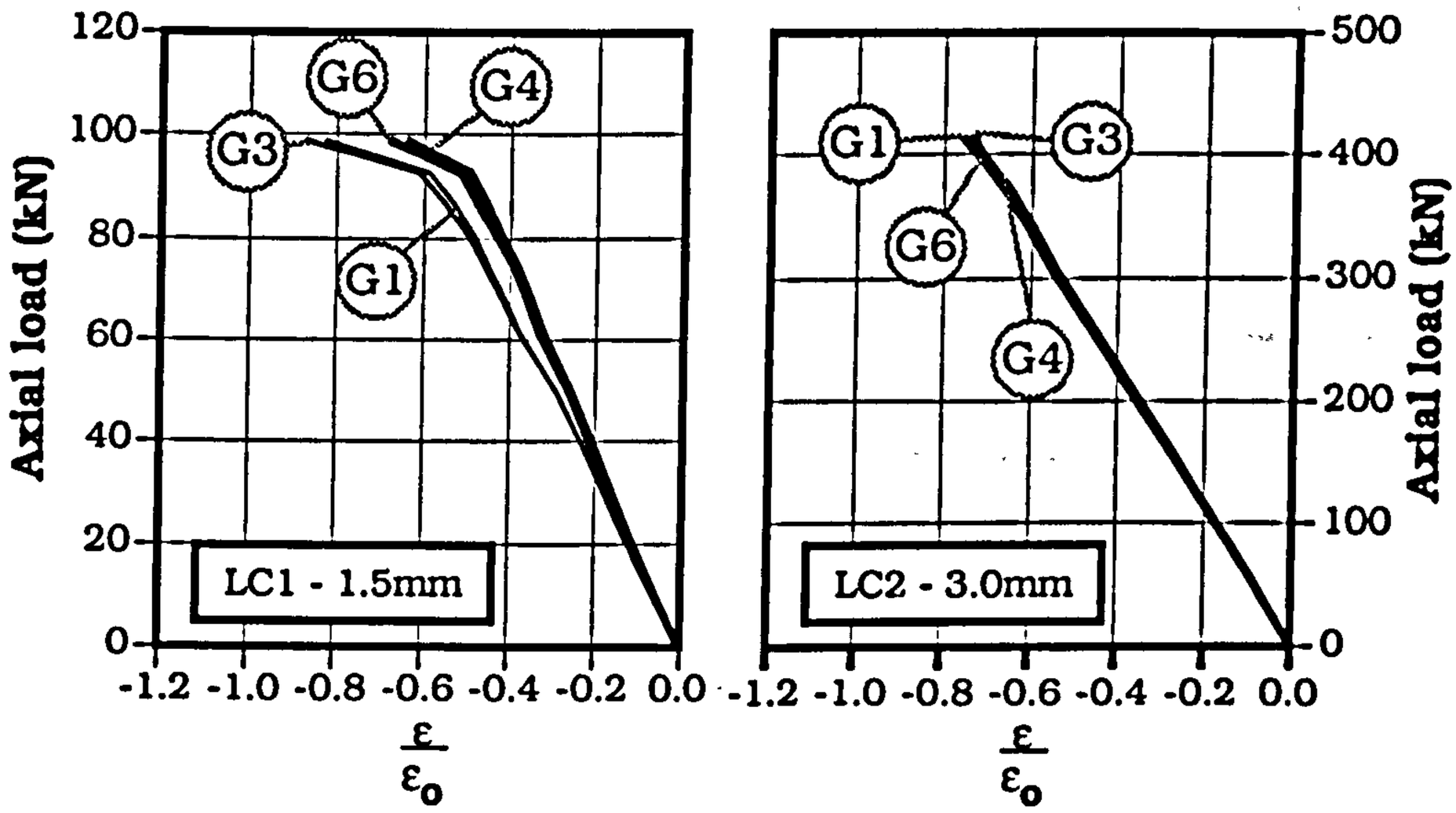


Figure 5.18 Load vs Strain - 9 metreColumn Tests

During Test 3c, described in Chapter Three, it was observed that by introducing transverse stiffeners into the 1.5mm bottom chord lips-down channel at intervals of 600mm it was possible to suppress lip buckling and to substantially increase the load carrying capacity of the doubly lipped channel section.

5.3.4. COMPARISON BETWEEN EXPERIMENTS AND VARIOUS METHODS OF DESIGN

BS5950 Part 5 (1987) does not refer to lip buckling, but does stipulate that the sides of an open section may be supported by a simple lip having a width which is at least one fifth of the width of the adjoining element. For other types of edge stiffening a minimum allowable second moment of area of stiffener (I_s) about the middle surface of the element to be supported is recommended, where

$$I_s \geq \frac{t\,D^3}{375} \qquad (5.20)$$

Similar recommendations are made in AISI (1989) where the stiffener flexural rigidity is based on the slenderness of the plate element (D/t) being supported. Three classes are given, each containing a different definition for lip adequacy.

In order to provide adequate support to the free edge of the web element of a 122mm x 97mm channel section the minimum moment of inertia according to Equation 5.20 for a 1.5mm thick section is $I_s = 3600$ mm^4, and for a 3.0mm thick section is $I_s = 7300$ mm^4. In the channel section shown in Figure 5.1, the moments of inertia for the 1.5mm and 3.0mm thick compound lip, obtained in accordance with recommendations made in BS 5950: Part 5 (1987) are 10476 mm^4 and 20952 mm^4 respectively.

t (mm)	P_{exp} (kN)	$\frac{P_{exp}}{\text{Eqn. 5.16}}$	$\frac{P_{exp}}{P_{uBS}}$
1.5	95.7	1.08	0.76
3.0	420.3	1.07*	0.85

Table 5.5. Comparison of test results with predicted failure loads given by Equation 5.16 and the short strut capacity given by BS5950: Part 5 (1987)

* Torsional-flexural buckling failure observed.

It has been shown both numerically and experimentally that an axially loaded doubly lipped channel section can fail as a result of lip buckling, even when the flexural stiffness of the lip exceeds the minimum required by BS 5950: Part 5 (1987). The experimental results are compared with failure loads obtained from recommendations given in BS 5950: Part 5 (1987) and Equation 5.16 in Table 5.5.

5.4 PROPOSED DESIGN MODEL

It was shown earlier in this chapter that a reasonable estimate of the lip buckling resistance for a doubly lipped channel may be obtained by adopting a procedure where the critical stress is given by a simple strut on elastic foundation model which is then introduced into a modified Perry formulation with an appropriate imperfection parameter η'.

When the member is long and the preferred halfwave length of buckle is free to develop the critical lip stress may be found from Equation 5.7.

$$\sigma_{crL} = 2\, r_L \left(\frac{E\,\beta}{A_L}\right)^{1/2}$$

For a short member the number of halfwaves must be an integer and the critical lip buckling stress may be obtained by minimizing Equation 5.9 with respect to L_{cr}.

$$\sigma_{crL} = \frac{\pi^2 E}{\left(\frac{L_{cr}}{r_L}\right)^2}\left(1 + \frac{\beta\, L_{cr}^4}{\pi^4\, E\, I_L}\right)$$

The lip buckling resistance for the doubly lipped channel section may then be obtained from Equation 5.14, where

$$\sigma_{uL} = 0.5\left[\left(\sigma_d + (1+\eta')\,\sigma_{crL}\right) - \left[\left(\sigma_d + (1+\eta')\,\sigma_{crL}\right)^2 - 4\,\sigma_d\,\sigma_{crL}\right]^{1/2}\right]$$

The accuracy of the solution depends largely on the equation adopted for the imperfection parameter η'. In Table 5.5 and Figure 5.12 it can be seen that a good estimate to the failure load may be obtained when the value of η' is given by Equation 5.16.

The reduction in flexural buckling and bending resistance of a doubly lipped channel caused by lip buckling can be taken into account for the purpose of overall strength assessment by setting the design stress σ_d in the lip table to the lesser of σ_{uL}, σ_o or 0.84 σ_u.

5.5 CONCLUSIONS

1) The lip buckling phenomenon has been studied for a range of C-sections having lips with downturn. For the thinner sections, the lip buckling strength is considerably less than the yield stress. It is therefore essential to consider lip buckling when designing members in which the lips are in compression.

(2) The lip has been treated as a strut supported by an elastic foundation. The stiffness of the foundation depends on the deformational stiffness of the section. The stiffness is assumed to be that of uncoupled transverse strips. The critical buckling stresses so calculated, incorporating an assumed depth of lip and an assumed point of application of the disturbing force, accord satisfactorily with those calculated by finite element models in which the column deflection and rotation are prevented.

(3) For a typical section and length of member (3000mm), the number of lip buckling half waves in the length varies between two and four, depending on the thickness of the section.

(4) Lip buckling strength is estimated by introducing an assumed initial imperfection and applying a modified Perry formulation for column design to determine the average lip stress at which first yield occurs. The imperfection constant η is modified to take account of the relation between critical stress and wavelength for an elastically supported strut. The formulation shows good agreement with experiments and with non-linear finite element analysis.

(5) In the design method, it is assumed that local buckling of the table and/or webs of the section will not diminish the deformational stiffness of the section, provided that the wavelength for local buckling is small compared to

the wavelength of lip buckling. For the sections considered, this assumption is found to be justified.

(6) The effects of lip buckling can be reduced by restraining deformation of the section at intervals which are smaller than the preferred half wavelength.

(7) The influence of lip buckling on flexural, torsional-flexural and lateral-torsional buckling can be approximated by substituting the lip buckling resistance for the yield stress.

Chapter Six

FLEXURAL BUCKLING OF AXIALLY LOADED DOUBLY LIPPED CHANNELS AND TUBES

6.1 INTRODUCTION

Probably no buckling problem has received as much attention over the past 250 years as that of the axially loaded, pin-ended column. The pin ended strut can be considered to be a rather special case, as it is seldom encountered in practice. Real columns are usually loaded eccentrically, are continuous, or restrained to some degree by the connections at their extremities. Notwithstanding this, every structural code has an axially loaded pin ended column curve. This simple model provides a basis for taking into account other important boundary conditions.

This chapter includes a brief account of the development of the Perry column formula. A full appraisal of the historic development of column buckling equations is given by Godfrey (1962), Young (1971) and Dwight (1972). BS 5950: Part5 (1987) adopts a modified Perry-Robertson formulation, applicable to sections symmetrical about both principal axes.

In Chapters Four and Five the effects of local element and lip buckling and their effects on resistance were studied. In this chapter the detrimental effects of local and lip buckling on the overall flexural buckling resistance are discussed with particular reference to experimental and numerical data. Design methods for concentrically and eccentrically loaded doubly lipped channels taking into account the interaction between local, lip and flexural buckling are proposed.

Consideration is also given to the flexural buckling behaviour of the diagonal tubes found in the test frame, with particular attention being given to defining the end

conditions. Design recommendations for estimating the flexural buckling resistance, based on the test frame results, are provided.

6.2 CRITICAL FLEXURAL BUCKLING

Euler (1759) dealt with the critical buckling behaviour of a perfectly straight member subject to axial compression in his famous treatise "Sur la force des colonnes" (Van den Broek 1947). In this treatise he presented the well known formulation for determining the critical buckling stress (Euler stress) for perfect columns, which is

$$\sigma_E = \frac{\pi^2 E}{\left(\frac{L}{r}\right)^2} \qquad (6.1)$$

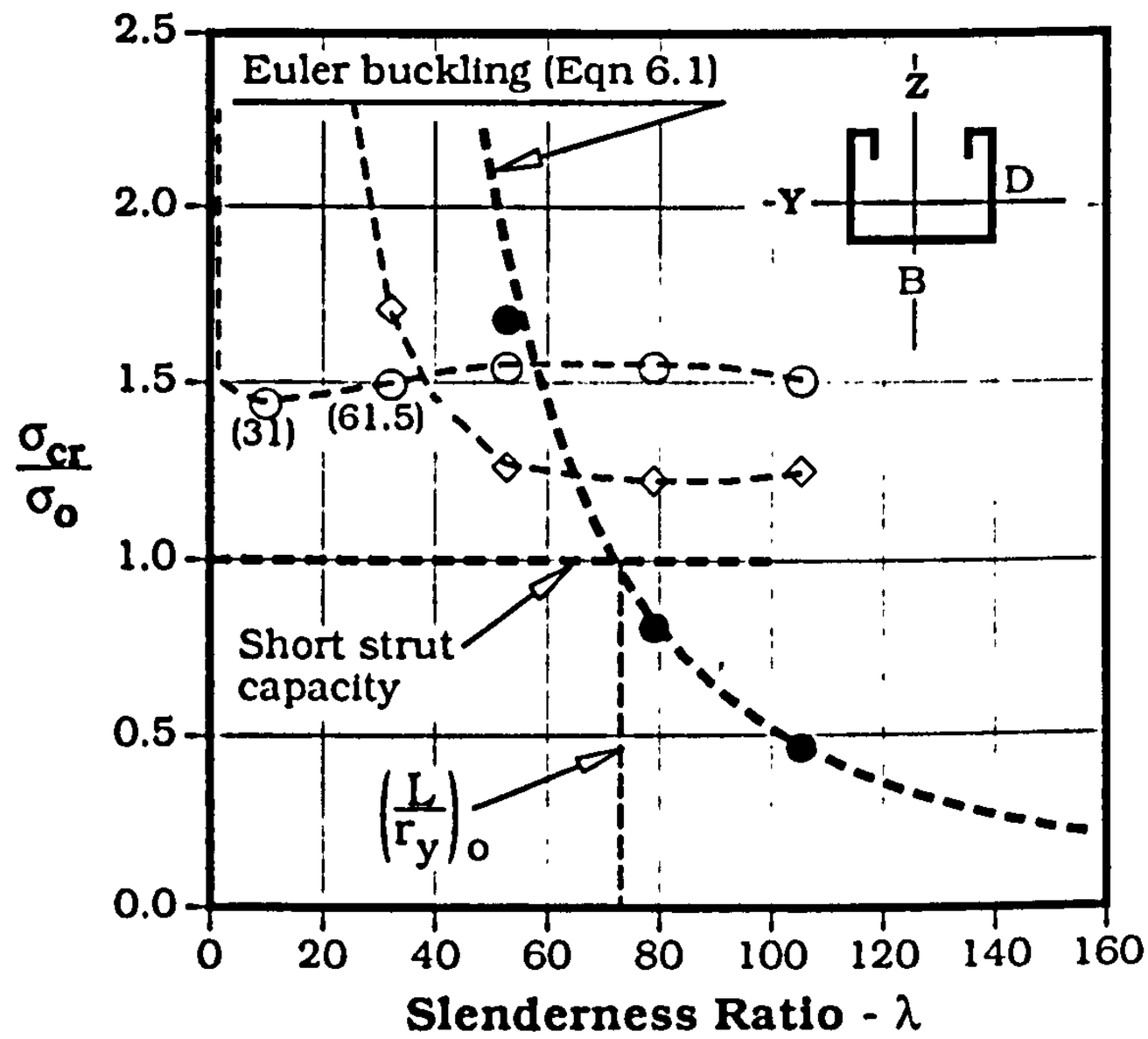


Figure 6.1 Variation in critical buckling stress with slenderness given by Equation 6.1 and critical elastic buckling analysis
B = 122mm, D = 97mm, B_L = 17mm, D_L = 18.5mm, t = 3.0mm, σ_o = 390 N/mm^2

Euler's formula is applicable only to elastic struts; however, it immediately establishes the importance of the slenderness ratio λ (L/r). The relationship

between stress and slenderness given by Equation 6.1, for a 3mm thick doubly lipped channel section is shown in Figure 6.1

The intersection of the Euler curve with the squash load represents the slenderness at which the critical buckling stress equals the yield stress and is commonly referred to as the critical buckling slenderness, which is a function of the material yield stress, and is

$$\left(\frac{L}{r}\right)_o = \pi\left(\frac{E}{\sigma_o}\right)^{1/2} \qquad (6.2)$$

6.2.1 FINITE ELEMENT ANALYSIS OF DOUBLY LIPPED CHANNEL

A series of critical buckling analyses were carried out to determine the accuracy in predicting the critical flexural buckling load for several different finite element meshes used to model the 122x97x17x18.5 doubly lipped channel section. A 3mm thick section was chosen for this investigation, as this ensured that the slenderness ratio (b/t) of each element in the cross-section was sufficiently stocky to prevent the occurrence of local element buckling. This made it possible to use fewer elements than would be required for thinner sections.

Length	No of Elements	P_{crF}	$\frac{\text{Eqn. 6.1}}{P_{crF}}$
4000	1024	209	1.01
	512	209	1.01
3000	768	367	1.03
	384	367	1.03
2000	512	760	1.11
	256	760	1.11
	256	819	1.03†

† lateral displacement of lip prevented

Table 6.1 Comparison between Equation 6.3 and finite element critical buckling analysis for a doubly lipped channel section.
B = 122mm, D = 97mm, B_L = 17mm, D_L = 18.5mm, t = 3.0mm, L = 3000mm

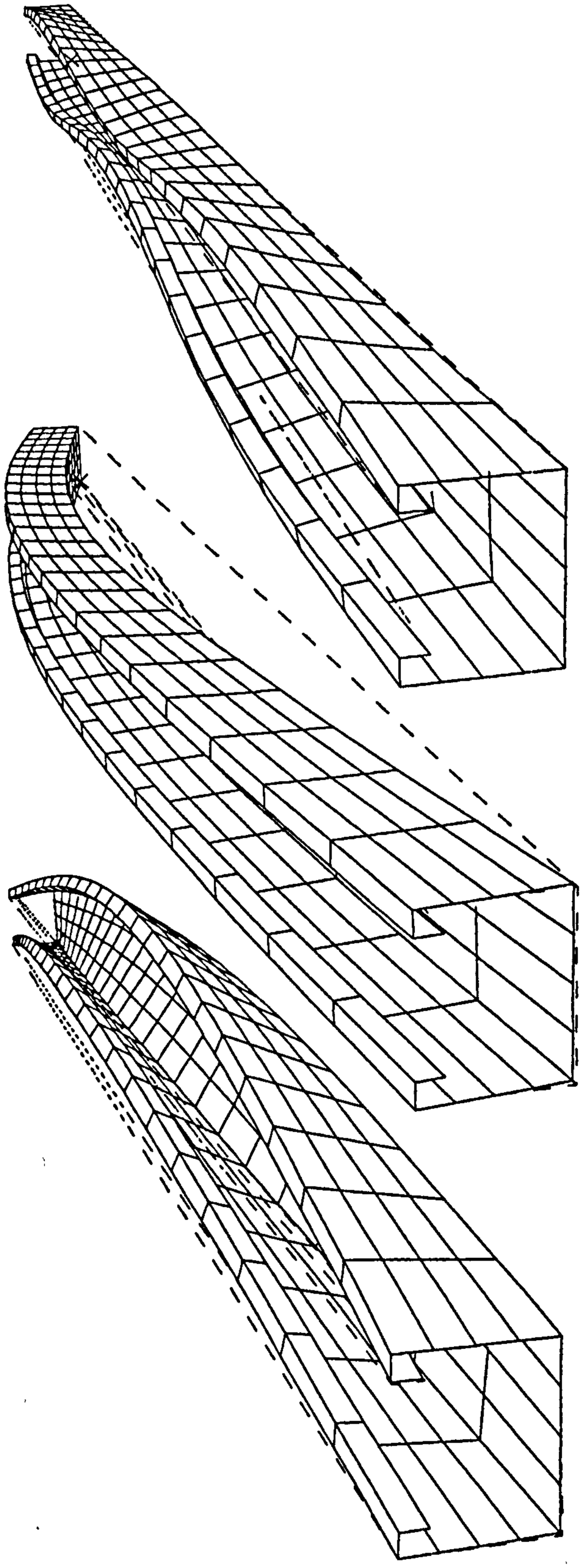
The cross-section of the doubly lipped channel was modelled using sixteen elements: one in the lip downturn, one in the lip table, four in the depth of the web and four in the breadth of the table. The member was subjected to a uniform axial stress. The boundary conditions applied at the ends of the member prevented rotation of the cross-section about the longitudinal (X) axis, but permitted rotations about the Z and Y axes.

A convergence study was conducted where the number of elements around the cross-section was kept constant while varying the length of the finite elements. The finite element critical buckling stresses for the doubly lipped channel section, 2000mm, 3000mm and 4000mm long are compared with Equation 6.1 in Table 6.1 and Figure 6.1.

The lip, flexural and torsional-flexural, critical buckling modes for the channel, where L = 3000mm, are shown in Figure 6.2.

The critical flexural buckling stresses obtained from the finite element analysis are in good agreement with Equation 6.3. However, the correspondence is seen to diminish with diminishing length. Examination of the critical flexural buckling eigenvector for the 2000mm long member revealed that the cross-section had deformed, resulting in outward lateral displacement of the lips. Further analysis where the lip was restrained against lateral displacements showed better agreement between the numerical and theoretical solutions. Halving the number of elements along the length of the member has no effect on the critical flexural buckling stress. The longer length of element (125mm) adequately describes the overall buckling behaviour of the doubly lipped channel member and will be adopted for subsequent non-linear elasto-plastic analysis.

This mesh would however not be adequate for thin sections where the interaction between local element and overall flexural buckling may freely occur and a much more refined mesh along the length of the member would have to be employed if the true buckling behaviour of the channel were to be described. It should be said that the numerical analyses presented in this chapter focus on the combined lip and flexural buckling behaviour on the 3mm thick doubly lipped channel section.



$\frac{\sigma_{cr}}{\sigma_o} = 1.22$

$\frac{\sigma_{cr}}{\sigma_o} = 0.81$

$\frac{\sigma_{cr}}{\sigma_o} = 0.27$

Figure 6.2 Critical buckling modes. (Axial Compression)
B = 122mm, D = 97mm, B_L = 17mm, D_L = 18.5mm, t = 3.0mm, L = 3000mm, σ_o = 390 N/mm^2

6.3 FLEXURAL BUCKLING RESISTANCE OF IMPERFECT CHANNEL MEMBERS

It was not until the nineteenth century, that the design of struts began to be placed on a practical or logical basis. Young (1807) pointed out that the Euler theory was correct if applied to perfect, elastic slender columns, but real columns were different in that they suffered from geometric imperfections and that loads were not necessarily applied axially. Young was responsible for the first column formulae to allow for initial imperfections and eccentricity of load. Young deduced that if a strut is initially bent in the form of a sine curve with maximum eccentricity w_o at mid length, then the total deflection for any value of axial stress σ_A is given by

$$w = \frac{w_o}{\left(1 - \frac{\sigma_A}{\sigma_E}\right)} \tag{6.3}$$

Young's work did not receive much attention and progress in designing axially loaded columns was slow.

6.3.1 THE PERRY FORMULATION

Young's equation forms the basis of the joint paper by Ayrton and Perry (1886) on the buckling of axially loaded struts. Perry's equation for determining the axial resistance to flexural buckling is based on the following assumptions

(a) the strut is pinned and centrally loaded at it's ends
(b) it has an initial sinusoidal imperfection
(c) there are no residual stresses
(d) it behaves elastically up to yield
(e) failure occurs when the stress in the extreme fibre of the concave side of the strut reaches yield

Consider the symmetrical imperfect rectangular bar shown in Figure 6.3. The maximum compressive stress occurs on the concave side of the bar, where

$$\sigma = \frac{P}{A} + \frac{Pw}{Z_y} \tag{6.4}$$

w is the total displacement at any load obtained from Young's equation (Equation 6.3)

Z_y section modulus about the Y axis

$$\frac{r_z^2 A}{\bar{y}} \tag{6.5}$$

in which

$\bar{y}$ is the distance to the outermost fibre

A the gross area of the section

r_z radius of gyration about the Z axis

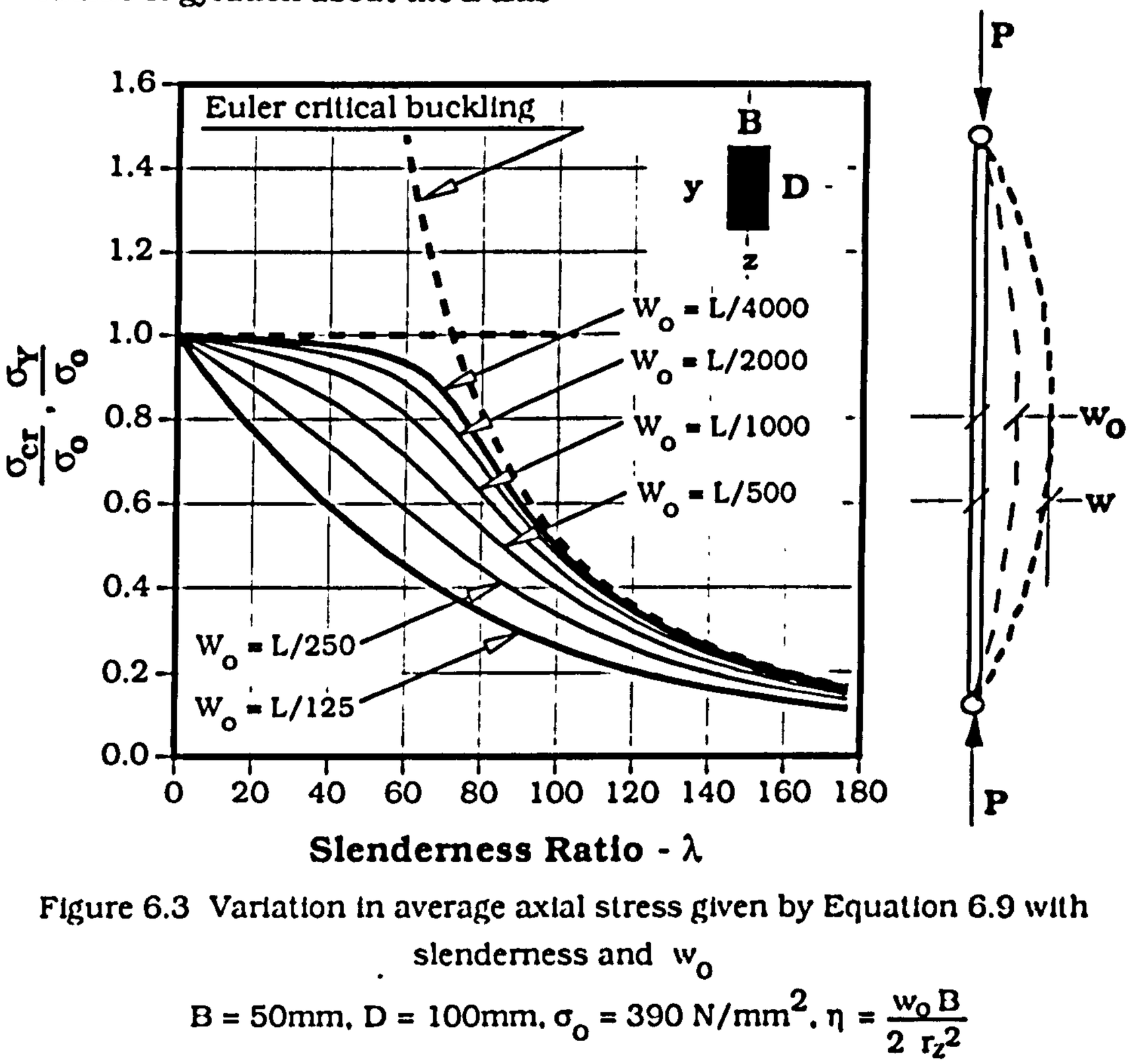


Figure 6.3 Variation in average axial stress given by Equation 6.9 with slenderness and w_o

B = 50mm, D = 100mm, σ_o = 390 N/mm^2, $\eta = \frac{w_o B}{2\ r_z^2}$

The average axial stress to cause first yield can be obtained by substituting Equations 6.3 and 6.5 into Equation 6.4 and is

$$\sigma_Y = \frac{\sigma_o}{\left(1 + \left(\frac{w_o \bar{y}}{r_z^2}\right)\left(\frac{\sigma_E}{\sigma_E - \sigma_Y}\right)\right)} \tag{6.6}$$

From which the following quadratic equation may be obtained

$$\sigma_Y{}^2 - \sigma_Y \{\sigma_o + (1 + \eta)\sigma_E\} + \sigma_Y \sigma_E = 0 \qquad (6.7)$$

where the non dimensional quantity η the "Perry constant" is a measure of the assumed initial imperfection w_o at the mid length expressed as

$$\eta = \frac{w_o y}{r_z^2} \qquad (6.8)$$

The smaller root obtained from Equation 6.7 provides the average axial stress to cause first surface yield, and is the Perry column equation, which is

$$\sigma_Y = 0.5\left[\{\sigma_o + (1 + \eta)\sigma_E\} - \left[\{\sigma_o + (1 + \eta)\sigma_E\}^2 - 4\sigma_o \sigma_E\right]^{1/2}\right] \qquad (6.9)$$

Figure 6.3 shows the relationship between Equations 6.3 and 6.9, and the variation in the average axial stress to cause first yield with slenderness for a solid rectangular section, for various initial values of w_o. The average axial stress to cause first yield is seen to be most sensitive to the initial value of w_o in the region of critical slenderness ($\sigma_{cr} = \sigma_o$). Equation 6.9 forms the basis for comparison between numerical and experimental results presented in this chapter.

6.3.2 BUCKLING RESISTANCE OF SINGLY SYMMETRIC SECTIONS

BS 5950: Part 5 (1987) adopts a modified Perry-Robertson formulation which assumes that the bending stresses induced by the PΔ moment are distributed linearly about the mid-depth of the section, but this is not correct for asymmetric sections.

Consider a 'Tee' section; the variation in the average axial stress to cause first surface yield in the 'Tee' section either in the flange or the tip of the stem, with slenderness is shown in Figure 6.4. The percentage variation in the stress to cause first yield, compared to that based on a mid-depth neutral axis, depending on the direction of the imperfection w_o is shown in Figure 6.5. Equation 6.9, based on a mid-depth neutral axis is non conservative by up to 10%. For very slender members, tensile yield occurs first.

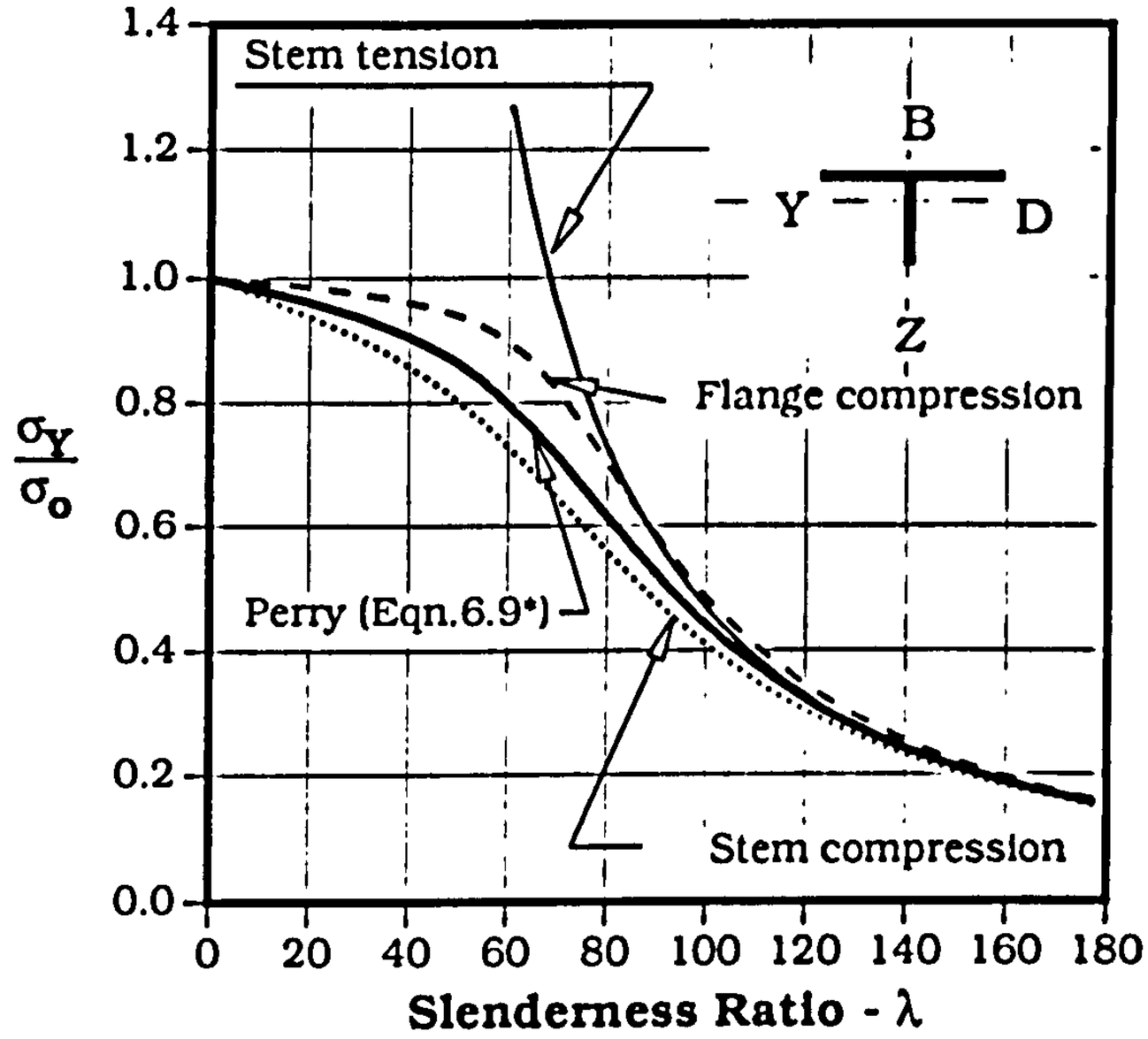


Figure 6.4 Variation in average axial stress to cause first surface yield given by Equation 6.9*, and Equation 6.4 with slenderness for 'Tee' section (Equation 6.9* with $\bar{y} = D/2$)

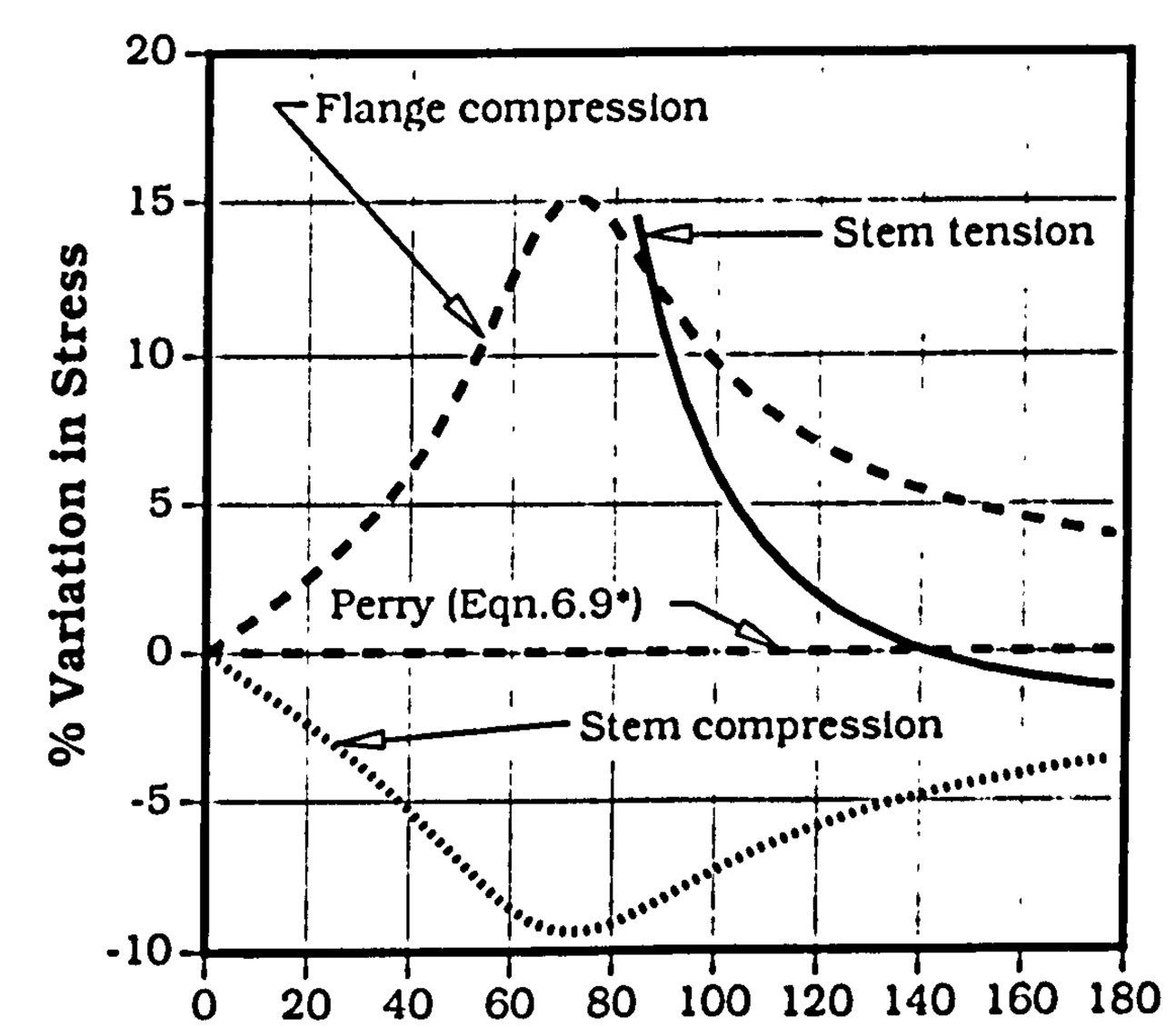


Figure 6.5 Percentage variation in average axial resistance relative to Equation 6.9* , given by Equation 6.4 (Equation 6.9* with $\bar{y} = D/2$)

Assuming that amplification of the initial imperfection always causes the greater compressive stress in the fibre furthest from the neutral axis of the cross-section, then the imperfection constant η can be written as

$$\eta = \frac{w_o \bar{z}_{max}}{r_y^2} \qquad (6.10)$$

where

$\bar{z}_{max}$ is the greatest distance from the neutral axis to the extreme fibre on the section.

It is possible to ensure a conservative estimate of the flexural buckling resistance of singly symmetric sections by adopting Equation 6.9 with η given by Equation 6.10, where amplification of the initial imperfection w_o causes compressive bending stresses, in the plane of buckling, at a point on the section having the greatest distance from the neutral axis.

6.3.3 BUCKLING RESISTANCE OF DOUBLY LIPPED CHANNELS IN THE PRESENCE OF LOCAL AND LIP BUCKLING

The flexural buckling resistance of sections made up of a number of slender plate elements, may be greatly reduced due to the effects of local element and lip buckling. Equation 6.9 can be adapted to account for the effects of local buckling by using the short strut capacity based on the effective cross-sectional area, while the full section properties are used to determine the Euler critical buckling stress. This ensures that in the case of short struts which fail through yielding the full effects of local buckling are taken into account since the critical local element buckling stress is less than the corresponding Euler stress. For long columns the effects of local buckling are minimised because the Euler stress is smaller than the local element buckling stress (Figure 6.1).

Equation 6.9 may be rewritten as

$$\sigma_Y = 0.5\left[(Q\sigma_o + (1+\eta)\sigma_E) - \left[(Q\sigma_o + (1+\eta)\sigma_E)^2 - 4Q\sigma_o\sigma_E\right]^{1/2}\right] \qquad (6.11)$$

where

$$Q = \frac{A_{eff}}{A} \qquad (6.12)$$

in which

A_{eff} is the effective area of the cross-section (Equation 4.11)

A is the gross cross-sectional area

Local buckling also changes the position of the neutral axis. As local buckling progresses the neutral axis of the gross cross-section moves from its original position to that corresponding to the effective section. If the load is applied at the centroid of the gross section it becomes eccentric to the centroid of the effective section, resulting in a bending moment about the effective neutral axis. The magnitude of the moment depends on the distance by which the effective neutral axis is displaced which in turn depends upon the degree of local buckling undergone by the member. The shift in neutral axis position and the magnitude of the induced moment can be estimated by considering the loss of effectiveness for the cross-section assuming that the short strut capacity can be attained. The resulting moment can then be added to any other externally applied end moment and the strut treated as a beam-column.

In Chapter Five it was shown that cold-formed doubly lipped channel columns may fail through lip buckling. It is proposed to account for lip buckling by limiting the maximum stress in the outermost fibre in the cross-section to the lip buckling stress σ_{uL}, given by Equation 5.16. The loss of cross-sectional effectiveness should then be determined for a stress level equivalent to the lip buckling stress.

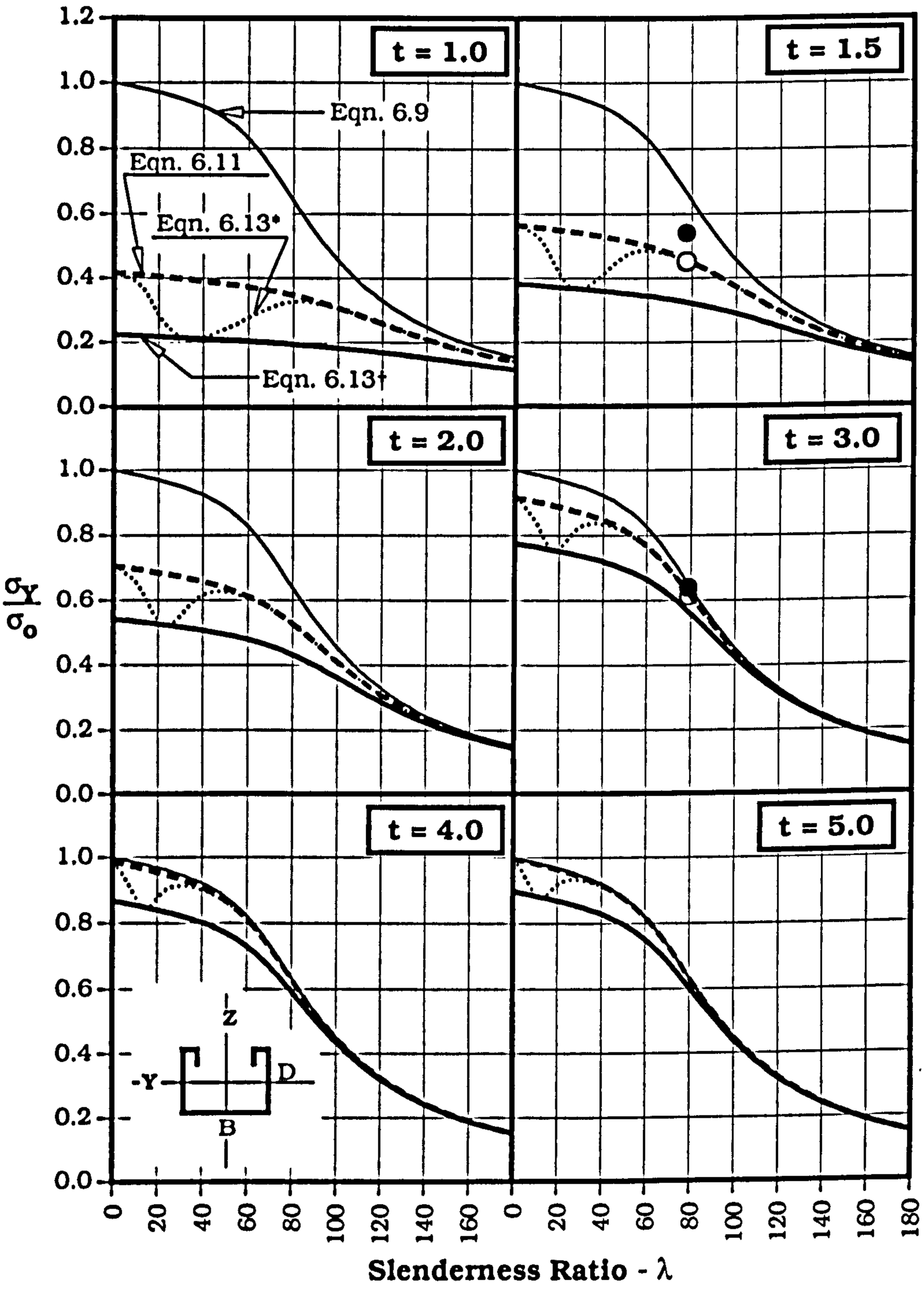
This approach should give a conservative estimate of the flexural buckling stress since in practice a lower compressive stresses will be present in the table of the cross-section due to the reduced PΔ moments cause by migration of the neutral axis. Equation 6.11 can be rewritten as

$$\sigma_Y = 0.5\left[Q\sigma_{uL} + (1 + \eta)\sigma_E - \left[(Q\sigma_{uL} + (1 + \eta)\sigma_E)^2 - 4Q\,\sigma_{uL}\sigma_E\right]^{1/2}\right] \quad (6.13)$$

where

σ_{uL} is the lip buckling resistance (Equation 5.16)

Q is the ratio of the effective area to the gross area of the section, where the effective cross-section is determined for σ_{uL}



● Flexural and Local Buckling O Flexural, Local and Lip buckling

Figure 6.6 Variation in average axial stress to cause first surface yield given by Equations 6.9, 6.11 and 6.13 (η given by Equation 6.10) with thickness and slenderness ratio.

† lip buckling stress based on L_{cr}, * lip buckling stress based on $L_B = L$

B = 125mm, D = 100mm, B_L = 20, D_L = 20, σ_o = 390 N/mm^2

(External dimensions)

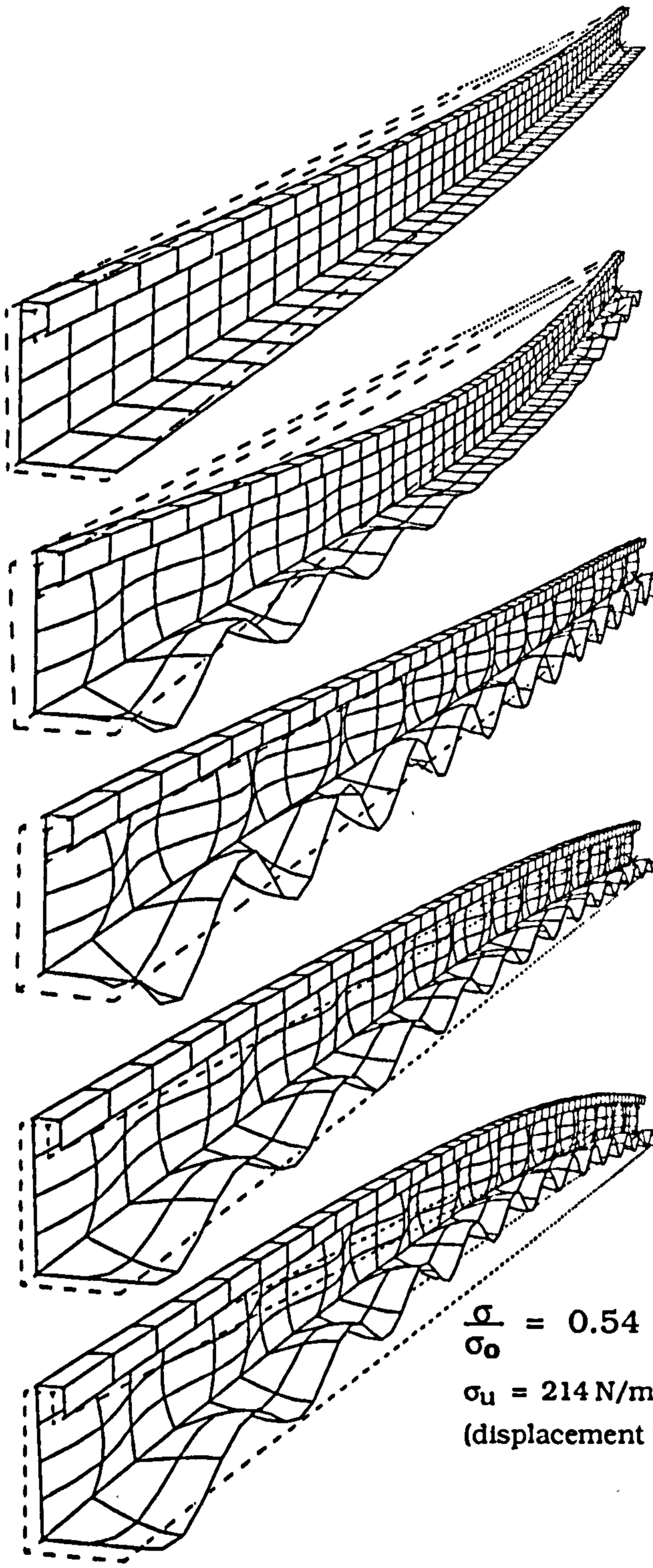
The variation in average axial stress to cause first surface yield in the lip table of the doubly lipped channel given by Equations 6.9, 6.11 and 6.13, (η given by Equation 6.10 and an initial out of plane imperfection w_{ov} = L/1000) with slenderness, for various thicknesses of channel section is shown in Figure 6.6. The curve given by Equation 6.13 accounts for lip buckling by assuming that the critical lip buckling half wave length is free to develop. If the overall length of the member is less than the preferred critical lip buckling half wave length, the flexural buckling resistance will increase as a result of a higher critical buckling stress (Figure 5.4). In Figure 6.6 it can be seen that Equation 6.13 gives a conservative estimate of combined lip and flexural buckling stress when $L/r < 30$. A better estimate may be obtained when $L < L_{cr}$ by evaluating the lip buckling stress for a single half wave lip buckle equivalent to the length of the member and setting the design stress σ_d in Equation 6.13 to the value of the lip buckling stress (σ_{uL}). This approach provides a transition curve between Equations 6.11 and 6.13 (Figure 6.6). A substantial degradation in the flexural buckling stress (Equation 6.11) due to local buckling effects is evident in Figure 6.6 for the thinner sections considered.

6.3.4 NON-LINEAR ELASTO-PLASTIC FINITE ELEMENT ANALYSIS OF IMPERFECT DOUBLY LIPPED CHANNELS

The interaction between lip buckling and overall buckling for the doubly lipped channel section was investigated numerically by carrying out a series of non-linear elasto-plastic finite element analyses. Solutions were obtained for both the 1.5mm and 3.0mm thick sections, with particular emphasis being given to the buckling behaviour of the latter.

The number of elements used to model the cross-section was kept to a minimum by taking advantage of the symmetric nature of the deformations associated with the local element, lip and flexural buckling modes. Half the channel was modelled using a finite element mesh consisting of one element in the lip table, one in the lip downturn, four elements in the depth of the web and two elements across the width of half the table. The finite element length was 62.5mm. Figure 6.7 shows the mesh employed for this investigation.

The solutions obtained for the 1.5mm thick section do not accurately represent the effect of local buckling on flexural buckling due to the length of the finite elements adopted. Nevertheless, the results give an insight into the general buckling



$\frac{\sigma}{\sigma_o} = 0.27$

(displacement mag. x 5)

$\frac{\sigma}{\sigma_o} = 0.47$

(displacement mag. x 5)

$\frac{\sigma}{\sigma_o} = 0.51$

(displacement mag. x 5)

$\frac{\sigma}{\sigma_o} = 0.53$

$\sigma_Y = 211\ N/mm^2$

(displacement mag. x 2

$\frac{\sigma}{\sigma_o} = 0.54$

$\sigma_u = 214\ N/mm^2$

(displacement mag. x 2

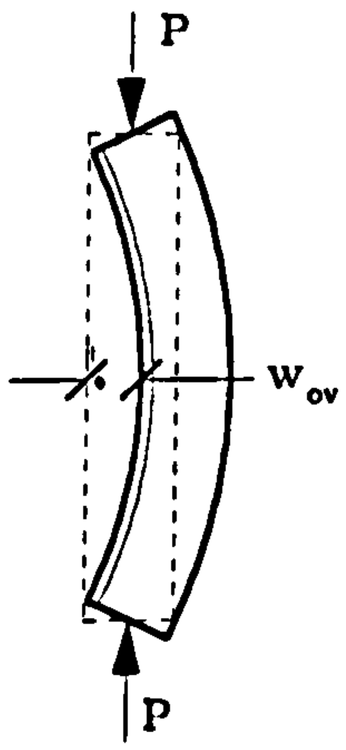


Figure 6.7 Load-displacement history for 1.5mm thick doubly lipped channel section obtained from non-linear, elasto-plastic flexural buckling finite element analysis

(Lip buckling prevented)

B = 122mm, D = 97mm, B_L = 17mm, D_L = 18.5mm,

L = 3000mm, σ_o = 390 N/mm^2, $\dot{w}_{ov}$ = -3.0mm

behaviour of the thin-walled cold-formed channel being considered. An accurate analysis of the 1.5mm thick section taking into account the effects of local buckling would have required twice as many elements. Obtaining a solution for the 1.5mm section with this many elements, using the present computer facilities, was impracticable.

The boundary conditions at the ends of the member were the same as those used in the critical buckling analysis. Additional inplane restraint was provided to the table of the section, ensuring uniform displacement of the table (warping prevented). Rotational restraint about the longitudinal axis along the table centre line was also provided in order to prevent torsional modes of instability. The channel was subjected to uniform axial stress, with the resultant force passing through the neutral axes of the gross cross-section.

Thickness (mm)	w_{ov} (mm)	v_{oL} (mm)	**No. of halfwaves**	σ_{YF} (N/mm^2)	σ_{uF} (N/mm^2)	$\frac{\sigma_{YF}}{\sigma_o}$	$\frac{\sigma_{YF}}{\text{Eqn. 6.13}}$
1.5	-3.0	-	-	211	214	0.54	1.19
	-3.0	-1.00	3	176	177	0.45	1.38
3.0	-3.0	-	-	250	255	0.64	1.05
	+3.0	-	-	261	264	0.67	N.A
	-3.0	+1.00	3	242	247	0.62	1.04
	-3.0	-1.00	3	241	244	0.62	1.04
	+3.0	-1.00	3	263	264	0.67	N.A
	-3.0	±0.75	4	239	243	0.61	1.08

Table 6.2 Variation in flexural buckling stress with initial mode of lip and overall flexural imperfections obtained from finite element analysis and Equation 6.13 where η is given by Equation 6.10 (η for lip buckling given by Equation 5.17)

(Axial Load)

B = 122mm, D = 97mm, B_L =17mm, D_L =18.5mm, L = 3000mm, σ_o = 390 N/mm^2

The initial imperfections used in the analysis were obtained by scaling the appropriate lip buckling and overall critical buckling modes. The magnitude of the flexural buckling (w_{ov}) and lip buckling (v_{oL}) initial imperfections were equivalent to L/1000 and ℓ/1000 respectively. A negative value of w_{ov} in Table 6.2 indicates that the lip table was located on the concave side of the overall flexural imperfection producing higher compressive stresses in the lip. A negative value for v_{oL} indicates

that for a three half wave lip imperfection along the length of the member, the lip downturn, at mid length was located on the concave side of the imperfection.

Flexural buckling analyses were first carried out to establish the sensitivity of the failure load, in the absence of lip buckling, to the overall mode of initial flexural imperfection. Figure 6.7 shows the load-displacement history for an imperfect 1.5mm thick channel for which lip buckling has been inhibited. It is interesting to note the gradual loss of effectiveness with increasing load, resulting in a reversal of the vertical displacements. This is due to a moment caused by the shifting of the neutral axis. The average axial stress corresponding to first yield and failure given in Figure 6.6.

Finite element analysis were also carried out to investigate the interaction between, lip and overall flexural buckling. Various modes of lip imperfection were added to an overall flexural imperfection. The results from this study are given in Table 6.2. In all cases it can be seen that the first yield is closely followed by failure. The average axial stresses corresponding to first surface yield and failure caused by combined lip and flexural buckling for L = 3000mm and t = 1.5mm and 3.0mm are shown in Figure 6.6. It can be seen that good agreement exists between Equations 6.11 and 6.13, and finite element results for the 3mm thick channel. When t = 1.5mm, the numerical results as seen to be underestimated by Equations 6.11 and 6.13. As previously stated, this is due to the coarse finite element mesh adopted along the length of the member which cannot accurately describe local element buckling (Appendix A). Figures 6.8 and 6.9 show the load-displacement history for the 3.0mm thick section for different lip imperfections.

Reversing the initial overall flexural imperfection (w_{ov} = +3.0mm) for the 3.0mm thick channel gives a slight increase (4%) in the flexural buckling stress. The failure load for the 3.0mm thick section is not very sensitive to the mode of the initial lip imperfection. However, this may not be the case in general and further analysis is suggested. The average axial stress for the thinner section is affected to a greater degree by both local element and lip buckling, as can be seen in Figure 6.6, since increasing b/t also reduces β the foundation modulus of the lip.

A limited numerical study investigating the flexural behaviour of the channel section subjected to uniform bending was also carried out. In Chapter Five it was shown that a doubly lipped channel section subject to equal and opposite end moments, where the moment cause more compression in the lip, fails when the average stress

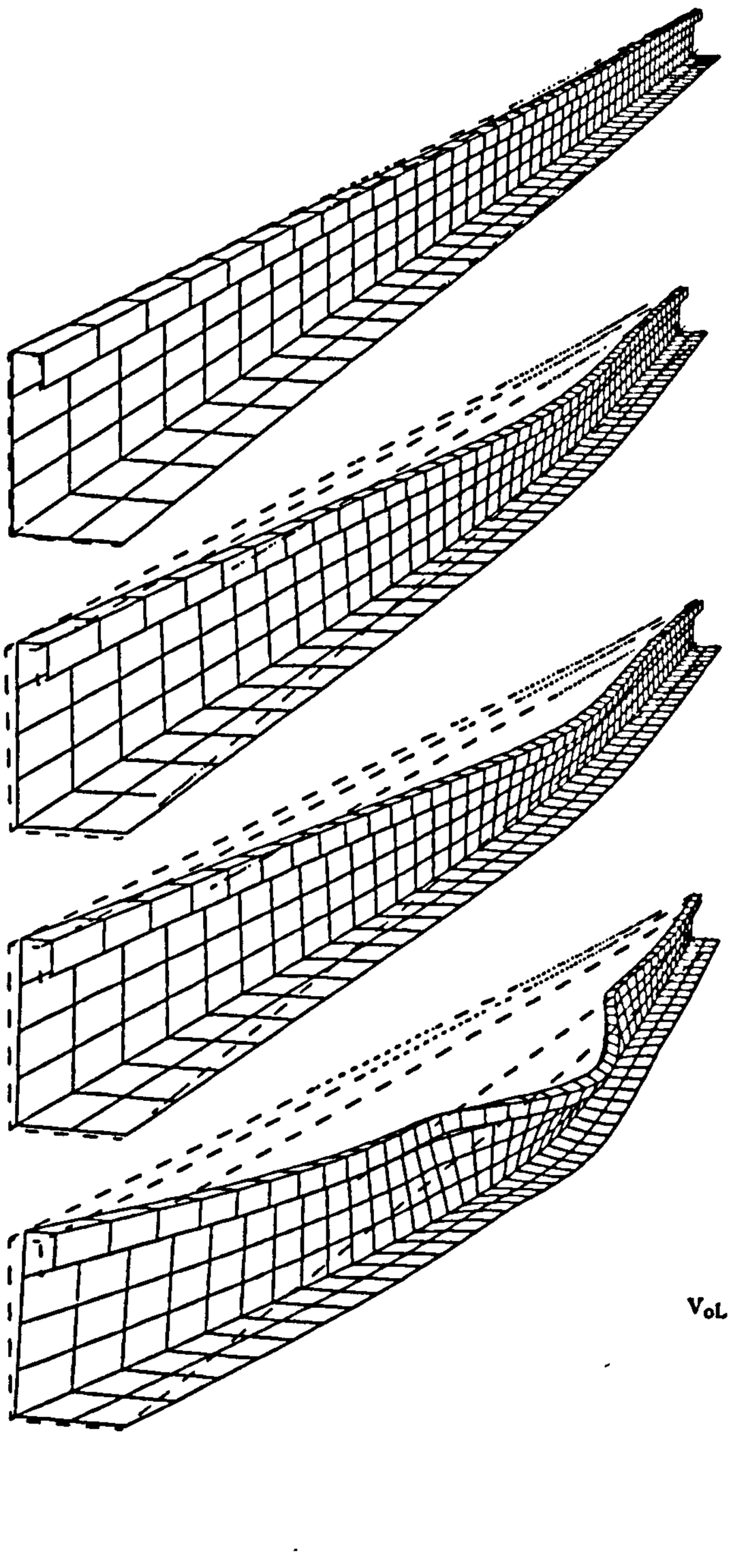


Figure 6.8 Load-displacement history for 3.0mm thick doubly lipped channel section obtained from non-linear, elasto-plastic, combined lip and flexural buckling finite element analysis (displacement mag. x 5).

$B = 122mm$, $D = 97mm$, $B_L = 17mm$, $D_L = 18.5mm$,

$L = 3000mm$, $\sigma_o = 390\ N/mm^2$, $w_{ov} = -3.0mm$, $v_{oL} = \pm 1.0mm$

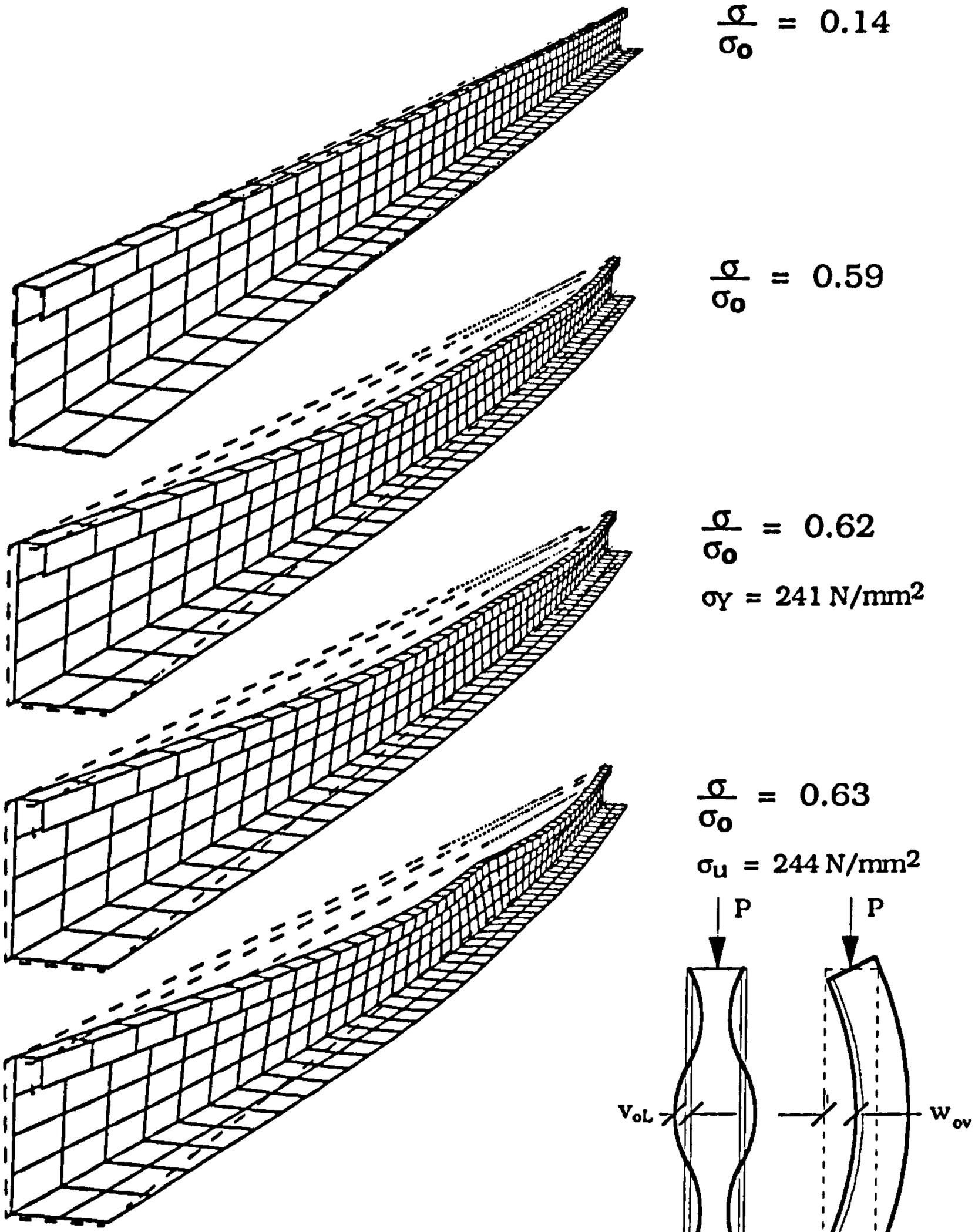


Figure 6.9 Load-displacement history for 3.0mm thick doubly lipped channel section obtained from non-linear, elasto-plastic, combined lip and flexural buckling finite element analysis (displacement mag. x 5).

$B = 122mm$, $D = 97mm$, $B_L = 17mm$, $D_L = 18.5mm$,

$L = 3000mm$, $\sigma_o = 390\ N/mm^2$, $w_{ov} = -3.0mm$, $v_{oL} = \pm 1.0mm$

in the lip becomes equal to the lip buckling stress (Equation 5.16).

The bending resistance of the channel may be conservatively estimated by taking the product of the section modulus at the lip table Z_ℓ and the lesser of the yield stress σ_o and the lip buckling stress σ_{uL}, such that

$$M_u = Z_\ell \sigma_d \qquad (6.14)$$

A comparison between Equation 6.14 and the finite element results given in Table 6.3 shows reasonable agreement.

Thickness (mm)	v_{oL} (mm)	No. of halfwaves	M_{YF} (kNm)	M_{uF} (kNm)	σ_{YF} (N/mm^2)	$\frac{\sigma_{YF}}{\sigma_o}$	$\frac{M_{YF}}{\text{Eqn. 6.14}}$
3.0	+1.00	3	10.6	13.2	355	0.91	1.03
	±0.75	4	11.6	12.6	388	0.99	1.23

Table 6.3 Comparison between Equation 6.14 and finite element results.
(Uniform bending)
B = 122mm, D = 97mm, B_L =17mm, D_L =18.5mm, L = 3000mm
σ_o = 390 N/mm^2, Z_ℓ = 29755 mm^3

6.3.5 EXPERIMENTS

A series of concentrically and eccentrically loaded cold-formed channel section columns were tested to investigate the following:

(a) The ultimate buckling capacity in the presence of local element, lip and flexural buckling of the doubly lipped channel sections of various wall thickness.

(b) Load-deformation characteristics.

Singly and doubly lipped cold-folded and cold-rolled channels, shown in Figure 5.1, were tested to failure. The cross-sectional geometry of each specimen is given in Table 6.4. Tensile coupons 50mm wide and 200mm between gauge marks were taken from the web and table of each specimen. Tensile tests were carried out to determine the yield and ultimate stresses (σ_o and σ_u) and percentage elongation (e%), the results are given in Table 6.5.

Specimen	L† (mm)	t (mm)	B (mm)	D (mm)		B_L (mm)		D_L (mm)	
3 METRE BEAM/COLUMN (P located 65mm from table of section)									
EC1	3172	1.00	126.3	101.4	102.4	20.2	20.7	19.8	20.2
EC2	3172	1.86	124.4	100.4	100.5	20.3	20.5	19.8	20.2
EC3	3172	3.00	125.0	99.0	99.6	22.6	22.7	19.0	17.8
3 METRE BEAM/COLUMN (P located at neutral axis of section)									
C1	3172	1.5	125.7	99.0	99.0	20.5	20.5	18.5	20.5
C2	3172	3.0	125.5	100.2	100.7	20.6	20.5	18.3	18.2

† distance between knife edge supports

Table 6.4 Cross-sectional geometry

Specimen	σ_o (N/mm^2)	σ_u (N/mm^2)	e%
EC1	295	377	25
EC2	360	390	22
EC3	346	425	23
C1	364	494	26
C2	489	539	21

Table 6.5 Material properties

A general view of the test rig is shown in Figure 6.10. Two loading arrangements were used; the first arrangement shown in Figure 6.11a was used to eccentrically load the channel columns. The knife edges were located 65mm from the outer surface of the table. This arrangement permitted the member to bend freely about the weak axis, but provided restraint against strong axis bending, and prevented rotation about the longitudinal axis. This arrangement gave a similar combination of axial force and bending moment to that found in the test frame except that warping was prevented, hence no torsional-flexural buckling. Channels tested using this load arrangement are denoted as **EC**-(eccentrically loaded column) in Table 6.4 through to Table 6.6.

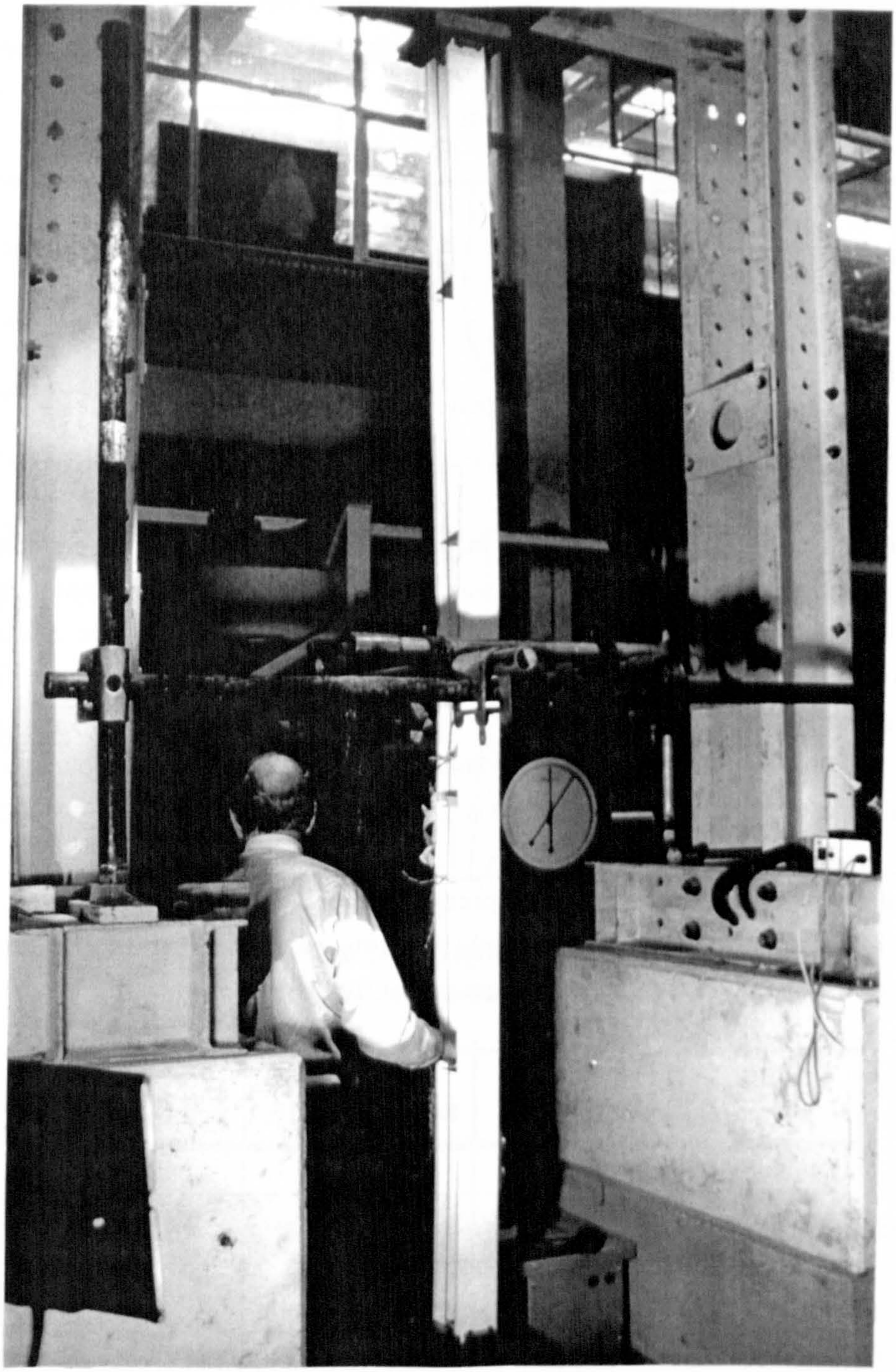


Figure 6.10 Lip buckling / flexural buckling - 3 metre test arrangement

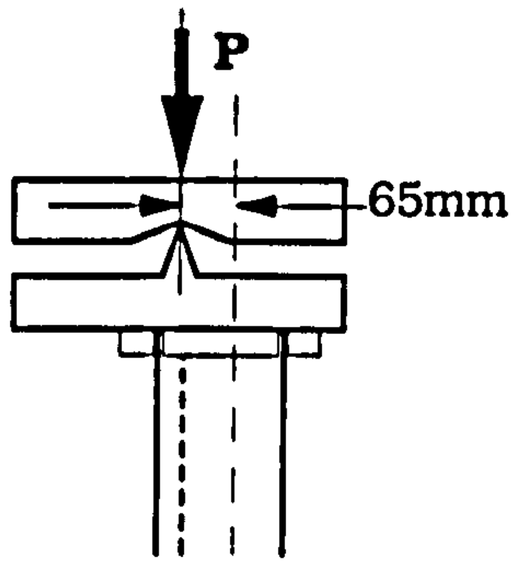


Figure 6.11a - (EC)

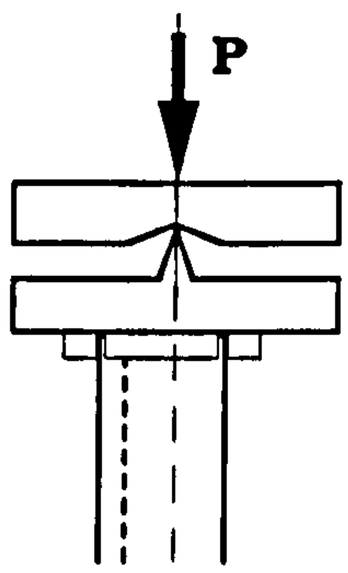


Figure 6.11b - (C)

Figure 6.11 Loading arrangement used in 3 metre column tests

The alternative arrangement shown in Figure 6.11b was used to apply concentric load to the ends of the member. It was shown earlier on in this chapter that, the effective section reduces with increasing load, causing a shift in the neutral axis position of the section. In order to reduce the effects of bending due to the shifting neutral axis, the knife-edge supports were located at the theoretical neutral axis position for the effective section. These tests are denoted as **C**-(axially loaded column) Table 6.4 through to Table 6.6.

The ends of each member were inspected to ensure that an even bearing surface had been obtained before accurately locating each member in the knife edge supports. Each member was strain gauged at mid length as shown in Figure 5.1.

Specimen	P_{exp} (kN)	$\frac{P_{exp}}{\text{Eqns 6.13, 6.16*}}$	$\frac{P_{exp}}{\text{Eqns 6.11, 6.16**}}$
EC1	30	1.32	0.84
EC2	98	1.36	1.08
EC3	150	1.13	1.12
C1	80	1.09	0.84
C2	275	1.04	1.01

Table 6.6 Experimental results for concentrically (**C**) and eccentrically loaded (**EC**) double lipped channel sections.
Equation 6.16*: $\sigma_d = \sigma_{uL}$, Equation 6.16**: $\sigma_d = \sigma_o$

At suitable load intervals, loading was suspended so that out-of-plane deflections of the lip relative to one another could be taken, along with strain measurements at mid-length of the specimen. The experimental results are given in Tables 6.6 and Figures 6.12.

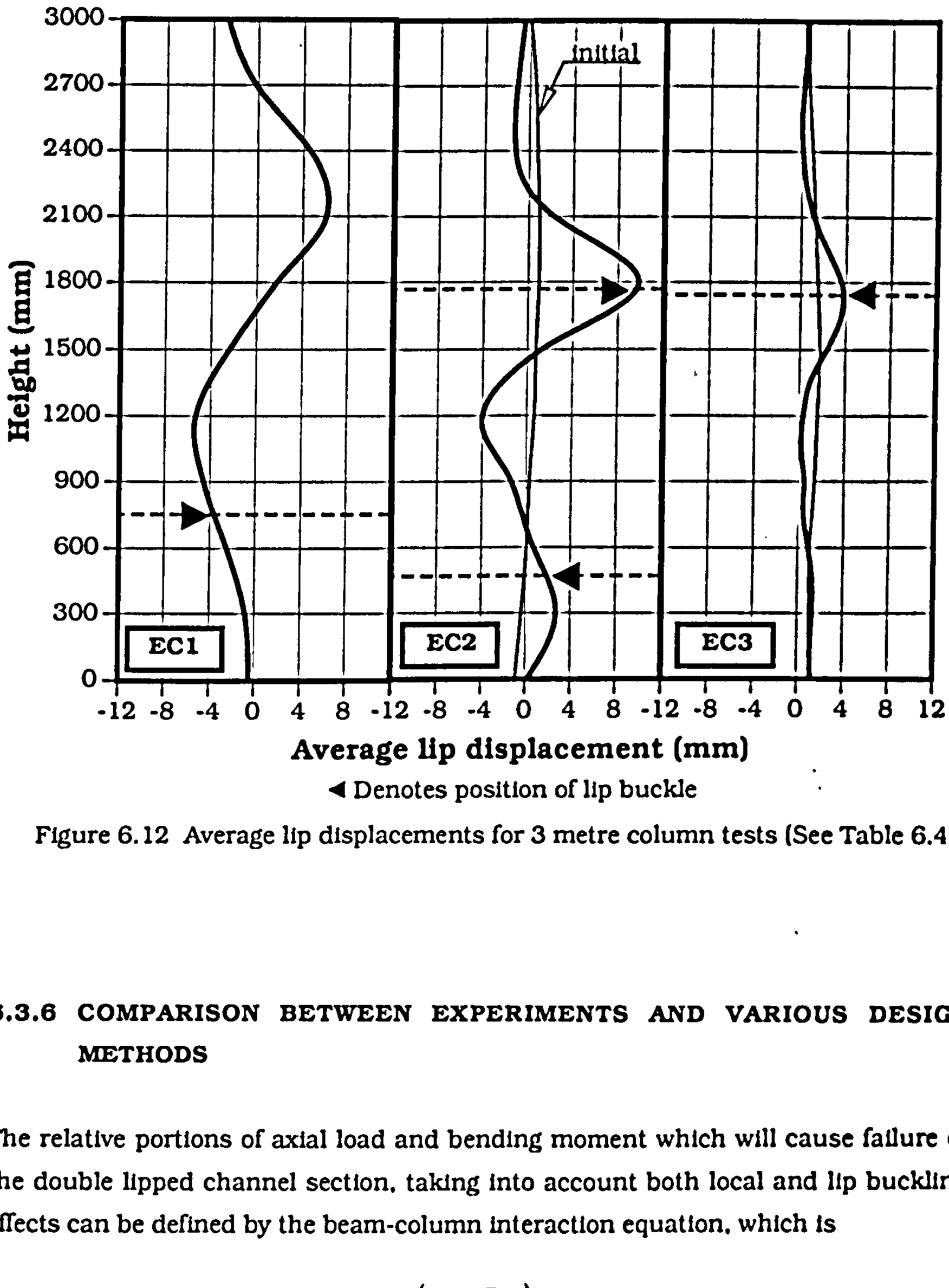


Figure 6.12 Average lip displacements for 3 metre column tests (See Table 6.4)

6.3.6 COMPARISON BETWEEN EXPERIMENTS AND VARIOUS DESIGN METHODS

The relative portions of axial load and bending moment which will cause failure of the double lipped channel section, taking into account both local and lip buckling effects can be defined by the beam-column interaction equation, which is

$$\frac{P}{P_Y} + \frac{(M \pm Pe_c)}{M_{uy}\left(1 - \frac{P}{P_{Ey}}\right)} \leq 1.0 \qquad (6.15)$$

where

e_c is the distance between the gross and effective neutral axis positions

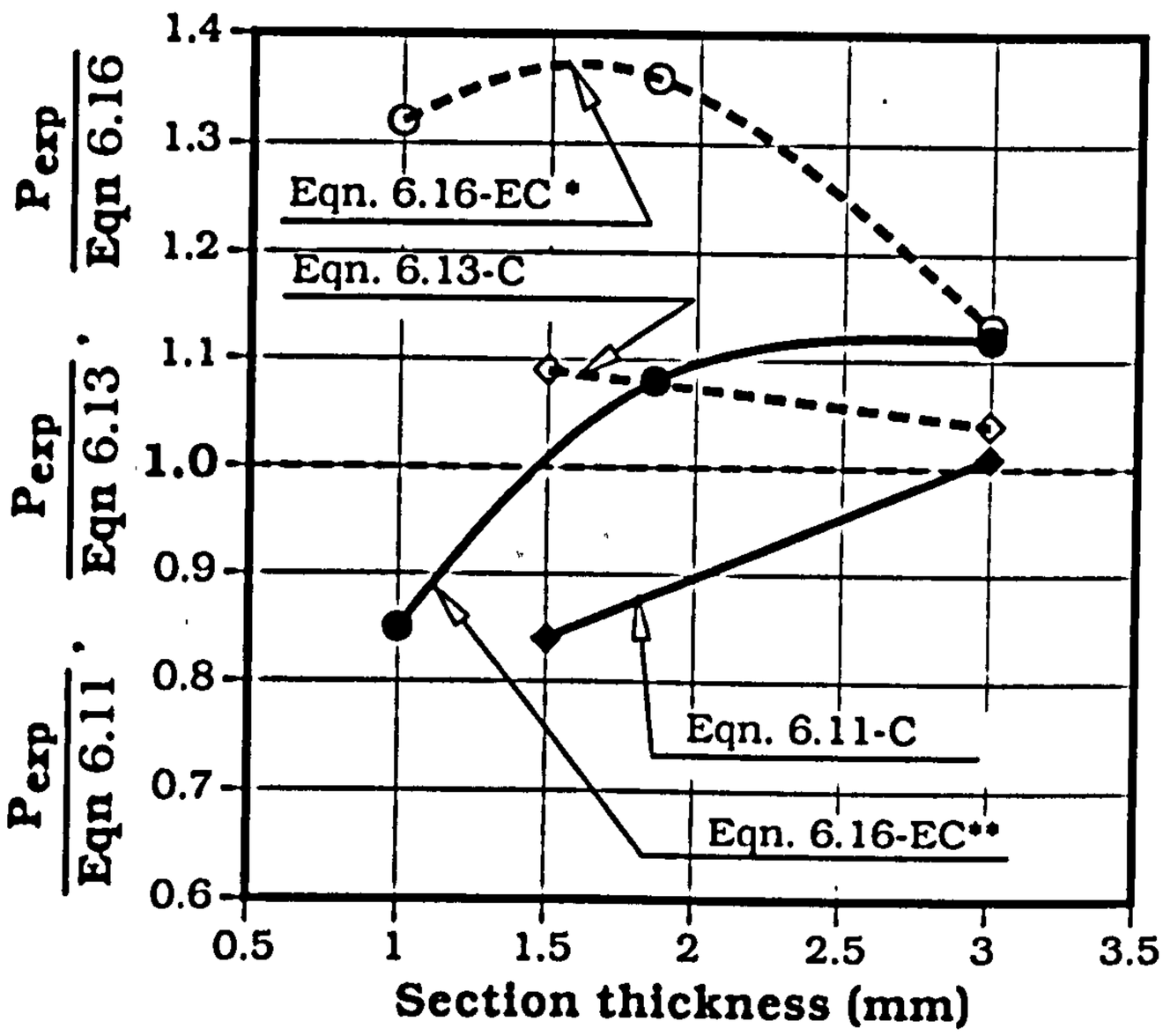
P is the applied axial load

P_{Ey} is the Euler critical buckling load of the section about the Y axis

P_Y is the axial resistance of the section based on a design stress σ_d, the lesser of σ_{uL} or σ_o (Equation 6.11)

M is the applied end moment (obtained from linear analysis)

M_{uy} is the bending resistance of the section based on a design stress σ_d, the lesser of σ_{uL} or σ_o (Equation 6.13)



Equation 6.16* with $\sigma_d = \sigma_{uL}$, Equation 6.16** with $\sigma_d = \sigma_o$

Figure 6.13 Ratio of experimental to calculated failure loads for doubly lipped channel

The estimated failure loads for the channel tests were obtained by replacing the applied moment M in Equation 6.15 with the product of the applied axial load P, and the distance between the point of application and the gross neutral axis position, denoted by 'e', and solving for P. Due regard should be given to the direction of moment generated by the shifting of the neutral axis as the section becomes less effective. Equation 6.15 may be rewritten as

$$\frac{P}{P_Y} + \frac{P(e \pm e_c)}{M_u\left(1 - \frac{P}{P_{Ey}}\right)} \leq 1.0 \qquad (6.16)$$

The failure loads obtained from Equations 6.11, 6.13 and 6.16 are compared with experimental data in Table 6.6 and Figure 6.13. The experimental results given in Table 6.6 correspond to ultimate failure load for each specimen. It can be seen that for thin sections susceptible to lip buckling, setting the design stress σ_d equal to σ_o in Equations 6.13 and 6.14, which are then introduced into Equation 6.16 before solving for P, gives a non-conservative estimate of the ultimate load carrying capacity of channel members as would be expected. By limiting σ_d to σ_{uL} it is possible to obtain a reasonably conservative estimate of the ultimate failure load. The rather conservative predictions for the beam-column tests given by Equation 6.16, with $\sigma_d = \sigma_{uL}$ (Table 6.6), are probably due to the non uniform lip stress due to bending. In using Equations 6.13 and 6.14 it is assumed that failure occurs when the stress in the outermost fibre is equal to the lip buckling stress.

Table 6.7 shows a comparison between lip-table stress measurements (gauges 4 and 6 in Figure 5.1) at mid length of the column and Equation 5.16. It can be seen that in all cases the lip buckling stress is conservatively estimated by Equations 5.16.

Specimen	P_{exp} kN	σ_{exp}‡ N/mm2	$\frac{\sigma_{exp}}{\text{Eqn.5.16}^*}$
EC1	30	151	1.02
EC2	98	325	1.28
EC3	150	358	1.04
C1	80	276	1.26
C2	275	409	1.08

Table 6.7 Comparison between stress measurements at lip-table for concentrically (C) and eccentrically loaded (EC) doubly lipped channel sections and Equations 5.16.

Eqn. 5.16*: Imperfection parameter given by Eqn 5.17 with $v_{oL} = \ell/1000$.

σ_{exp}‡ : stresses obtained from strain gauge readings

6.4 PROPOSED DESIGN MODEL FOR SINGLY SYMMETRIC CHANNELS

In this chapter it has been shown that the degradation of the flexural buckling stress of the doubly lipped channel section shown in Figure 5.1, due to local and/or lip buckling can be accounted for by using Equation 6.13, which is

$$\sigma_Y = 0.5\left[\left(Q\sigma_d + (1+\eta)\sigma_E\right) - \left[\left(Q\sigma_d + (1+\eta)\sigma_E\right)^2 - 4Q\sigma_d\sigma_E\right]^{1/2}\right]$$

where

$$\eta = \frac{w_{ov}\bar{z}_{max}}{r_y^2}, \qquad Q = \frac{A_{eff}}{A}$$

σ_d is the design stress, equal to σ_{uL} (Equations 5.16).

σ_E Euler buckling stress

Alternatively, the imperfection constant η given by BS 5950: Part 5 (1987) may be used, where

$$\text{For } \frac{L}{r} \leq 20, \eta = 0.0 \tag{6.17}$$

$$\text{For } \frac{L}{r} > 20, \eta = \frac{2\bar{z}_{max}}{B}\,0.002\left(\frac{L}{r} - 20\right) \tag{6.18}$$

The bending resistance of a doubly lipped channel, where the lips are in compression can be obtained from Equation 6.14 with $\sigma_d = \sigma_{uL}$.

6.5 FLEXURAL BUCKLING RESISTANCE OF IMPERFECT TUBULAR MEMBERS

The diagonal tubes in the test frames are formed by a fabrication procedure which involves; the tube firstly being cut to length, the tabs being pressed with the creases at an angle of 38° relative to one another with bolt holes punched simultaneously during formation of the tab. The final stage in the process requires that both tabs be bent, about their crease, to a seating angle of 49.7° to the axis of the tube (Figure 6.14). Connection between the chord members and the diagonals is achieved by clamping the tabs between the back-to-back channel sections as shown in Figure 1.2.

The end conditions of the diagonals in this type of connection are difficult to define. The bottom crease is supported along its entire length by the bottom chord lips-down section, while the top chord tab, because of the angle of entry into the connection, is only partially supported over its length (Figure 1.2). When subjected to compression the inclined top tab crease tends to cause the top of the tube to deflect in a direction which is inclined to the direction at the bottom end, where the crease is normal to the axis of the tube. This induces some twisting of the tube. The tube deflects predominantly in a vertical plane due to the bottom chord crease being clamped over its full width.

It is assumed that the axial force at the top end has an eccentricity e_B (Figure 6.14) in the vertical plane of the diagonal owing to the partially supported top crease. This eccentricity increases the deflection at the mid length of the tube. The tab eccentricity e_B is given by

$$e_B = \frac{(D_C - D_S)}{2} \sin \psi \qquad (6.19)$$

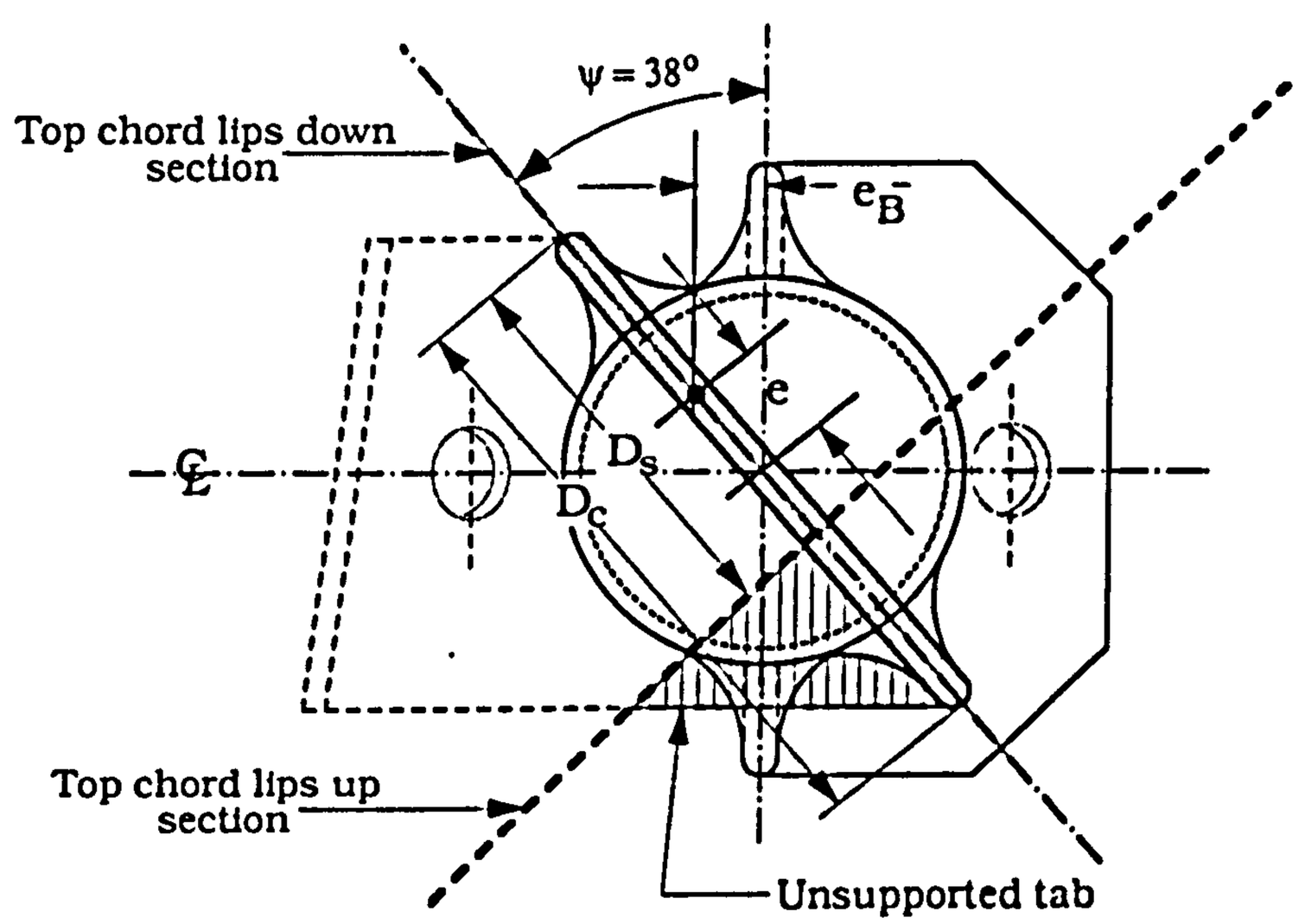


Figure 6.14 Tab geomerty (View along longitudinal axis of tube)
D_S = supported crease length, D_C = crease length

The moment at the top crease is the product of the diagonal force and the eccentricity e_B. The diagonals are concentrically loaded through the bottom crease. Table 6.7 gives the tab geometry for the various tubes used in the frame tests.

Specimen	Area (mm^2)	Crease length (D_c-mm)	Supported length (D_s-mm)	e_B (mm)
48 x 2.0	289.03	84.6	57.4	8.4
60 x 2.5	451.60	105.8	68.0	11.6
60 x 4.0	703.72	105.8	68.2	11.6
70 x 3.0	631.46	123.4	76.9	14.4
76 x 3.0	688.00	134.0	82.1	15.9

Table 6.7 Geometric properties of tubes and tab creases

In order to ensure that the diagonals are adequate for the combination of applied axial load and bending they must satisfy both an overall buckling check and a local capacity check.

Overall Buckling Check

It is natural to assume that the ends of the tube are hinged; however, the rotational restraint due to the crease bending resistance can have a significant effect on the axial resistance of the member.

When a member is subjected to a bending gradient along its length, the end moments can be converted to an effective moment, which may be determined in accordance with recommendations found in BS 5950: Part5 (1987), where

$$\overline{M} = \frac{P e_B}{C_b} \qquad (6.20)$$

where

$$C_b = 1.75 - 1.05\beta + 0.3\beta^2 < 2.3 \qquad (6.21)$$

$\overline{M}$ equivalent moment

C_b equivalent moment coefficient

e_B top chord tab eccentricity in the vertical plane of the diagonal (Figure 6.14)

β is the ratio of the smaller end moment to the larger end moment M. β is taken to be positive in the case of single curvature bending and negative in the case of double curvature bending ($\beta = 0$).

The diagonal tubes in the test frames are subjected to an effective moment in the vertical plane of 0.58 times the eccentric end moment. The effective length is taken to be the distance along the centre of the member between crease lines (L_{eff} = 2100).

The relationship between the applied load and equivalent moment for the diagonal tubes can be expressed in terms of the interaction equation given in BS5950: Part 5 (1987) where

$$\frac{P}{P_Y} + \frac{\overline{M}}{M_p\left(1 - \frac{P}{P_E}\right)} \leq 1.0 \qquad (6.22)$$

where

P_Y the flexural buckling capacity of the diagonal (Equation 6.13 with $\sigma_d = \sigma_o$ and Q = 1.0)

M_p plastic moment capacity of diagonal

The diagonal tube failure loads can be estimated by taking into account the partial rotational restraint provided by major axis bending capacity of the top crease resolved into the vertical plane of the diagonal. Consider the tab crease shown in Figure 6.15. The presence of axial load in the crease reduces the crease moment capacity and should therefore be taken into account. Assuming that the supported portion of the crease in the connection resists the eccentric moment, then the bending resistance of the crease in the vertical plane of the diagonal can be obtained from

$$M_{ec} = \frac{t D_s^2}{3}\left[\sigma_o - \frac{P}{2 t D_s}\right] \sin\psi \,, \qquad (6.23)$$

where

ψ is the relative angle between the bottom and top creases

D_s the length of crease supported in the joint

Equation 6.21 may be rewritten as

$$\frac{P}{P_Y} + \frac{(P e_B - M_{ec})}{M_p C_b\left(1 - \frac{P}{P_E}\right)} \leq 1.0 \qquad (6.24)$$

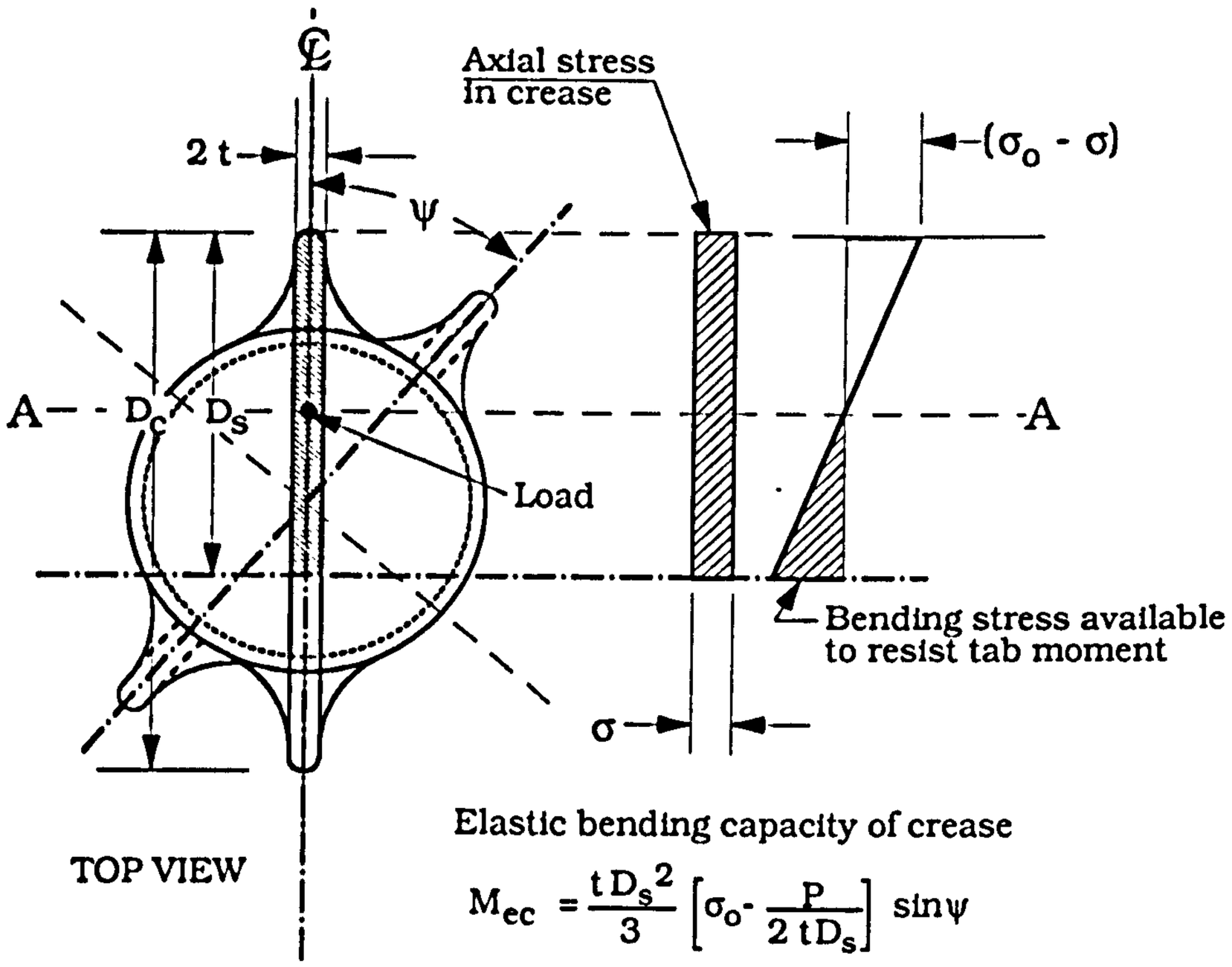


Figure 6.15 Bending resistance of top chord crease resolved into plane of bottom chord crease

If $P/(2t\ D_s) = \sigma_o$, then $M_{ec} = 0$, and the tab crease no longer provides any restraint to the tube. When this happens Equation 6.22 and 6.24 become identical.

Local Capacity Check

The end section must also be checked for possible local yielding due to the combined axial force and bending. Assuming that the axial force acts at the middle of the supported crease, then the following equation must be satisfied

$$\frac{P}{P_Y} + \frac{P e}{M_u} \leq 1.0 \qquad (6.25)$$

The section modulus of the crease about a line perpendicular to the supported crease (line A-A in Figure 6.15) is slightly greater than that of the circular tube ($Z_{flat} = 1.05\ Z_{tube}$), so the moment M_u at the end of the tube may be assumed to act on the circular section.

6.5.1 EXPERIMENTS

The buckling behaviour of the diagonal tubes was observed during several of the frame tests. In order to induce a diagonal buckling failure smaller diameter tubes were located in the test frames along grids B3-F7 and B3-F8 (Figure 3.3). Prior to failure, the diagonal members were observed to displace appreciably in an approximately vertical plane. Failure of the smaller diameter tubes was gradual with visible deflections occurring at mid length, while failure of larger diameter tubes was sudden with little or no deflection prior to failure. In all cases failure through localised yielding at the mid length of the diagonal was observed (Figure 3.17). Figure 6.16 shows a failed 76mm dia- 3mm thick tube.

Specimen	σ_o (N/mm^2)	σ_u (N/mm^2)	$\frac{\sigma_o}{\sigma_u}$	e%
48 x 2.0	426	450	0.95	22.5
	415	491	0.85	19.0
	415	491	0.85	20.0
60 x 2.0*	395	439	0.90	18.5
	427	453	0.94	21.0
60 x 2.5	421	450	0.94	26.0
60 x 4.0	497	577	0.86	14.5
70 x 3.0	475	554	0.86	22.0
76 x 3.0	451	520	0.87	14.5

* tube used in tension only

Table 6.8 Tube material properties

Tensile tests were carried out to determine the yield and ultimate stresses of the material, along with the percentage elongation (e%). Specimens 450mm long were prepared from the existing stock of tubes, each specimen was plugged at both ends prior to testing. Gauge marks 200mm apart were scribed on the tube at mid length of the specimen. The material properties for each of the tubes enable the theoretical failure loads given by existing and proposed design methods to be estimated using the actual material properties. The geometric and material properties for each of the various tubes used during testing are given in Tables 6.7 and 6.8 respectively.

BS 5950: Part5: (1987) recommends that the design stress σ_d should not exceed $0.84\sigma_u$. This done to ensure a ductile mode of failure. The ratio of yield stress σ_o to ultimate stress σ_u in Table 6.8 exceeds this limit. This may be one explanation for the suddenness of the observed mode of failure.

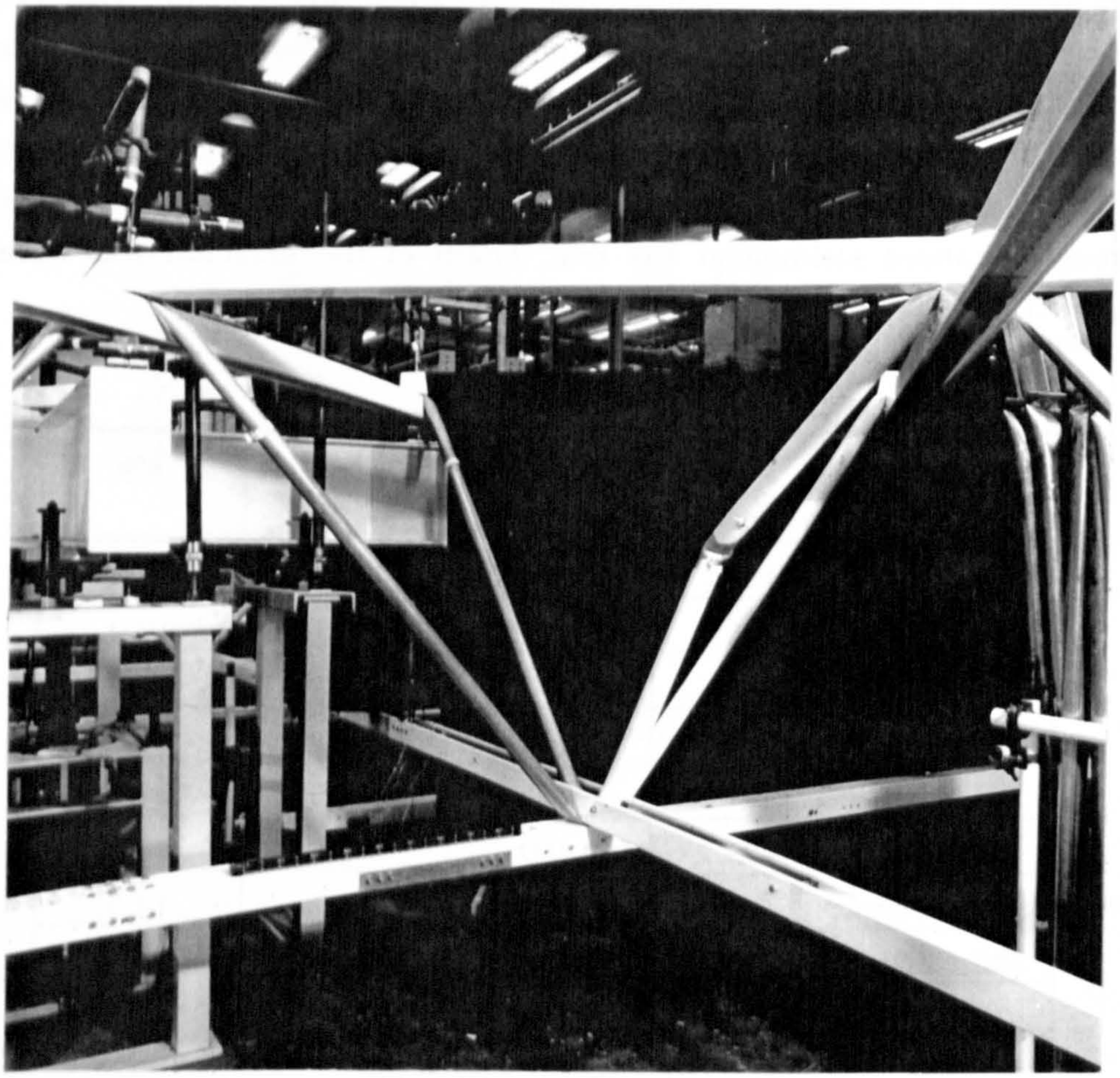


Figure 6.16 Diagonal buckling failure (76mm dia-3.0mm thick, tube)

The failure loads for the various tube diameters and thicknesses observed during the frame tests are given in Table 6.9. Several diagonal failures were obtained in Test 6c (Chapter Three). During this test it was possible to find the failure load of three 70mm dia-3.0mm thick compressive diagonals by replacing each failed 70mm diagonal with a larger diameter tube, and then reloading the frame. The failure load increased only slightly for each successive test. The diagonal forces P_{exp}^* in

Table 6.9 have been obtained from a linear frame analysis of diagonal-on-square frame, for the measured jack load (Chapter Two).

TUBE	TEST	Load (kN)	P_{exp}‡ (kN)	P_{exp}* (kN)	$\frac{P_{exp}^*}{\text{Eqn. 6.13}^*}$	$\frac{P_{exp}^*}{\text{Eqn. 6.22}}$	$\frac{P_{exp}^*}{\text{Eqn. 6.24}}$
48x2	3e	200	24	35	1.08	1.41	1.08
60x2.5	2b	374†	64	66	0.87	1.22	1.01
	5c	440	N.A	77	1.01	1.42	1.17
60x4	7b	630	115	111	0.95	1.31	1.03
70x3	6c	600	N.A	106	0.74	1.08	0.95
		630	N.A	110	0.77	1.12	0.98
		650	N.A	114	0.80	1.16	1.02
76x3	7d	760	145	132	0.75	1.12	1.02

Table 6.9 Diagonal failure loads (Frame tests)

Eqn. 6.13*: $\eta = 0.002(L/r\text{-}20)$, P_{exp}*: forces calculate from linear frame analysis .

P_{exp}‡ : Loads obtained from strain gauge readings prior failure. (Chapter Two), † diagonal replaced due to excessive deflection.

6.5.2 COMPARISON BETWEEN EXPERIMENTS AND VARIOUS DESIGN METHODS

A comparison between failure loads predicted by Equations 6.13, 6.22 and 6.24 and those obtained experimentally, is given in Table 6.7 and Figure 6.17. Equation 6.13 assumes that the diagonal is pin ended and concentrically loaded. This has been included to illustrate the reduction in strength compared to that of a concentrically loaded strut caused by the end eccentricity.

If the diagonal member is assumed to be eccentrically loaded at the top chord tab the failure load can be estimated from the beam-column equation, Equation 6.22, which gives conservative estimates of the failure stress. Equation 6.24 assumes that the top chord tab eccentric moment is reduced on account of the rotational resistance provided by the supported length of crease. Equation 6.24 gives a good estimate of the failure load for the diagonals considered, as can be seen in Table 6.9.

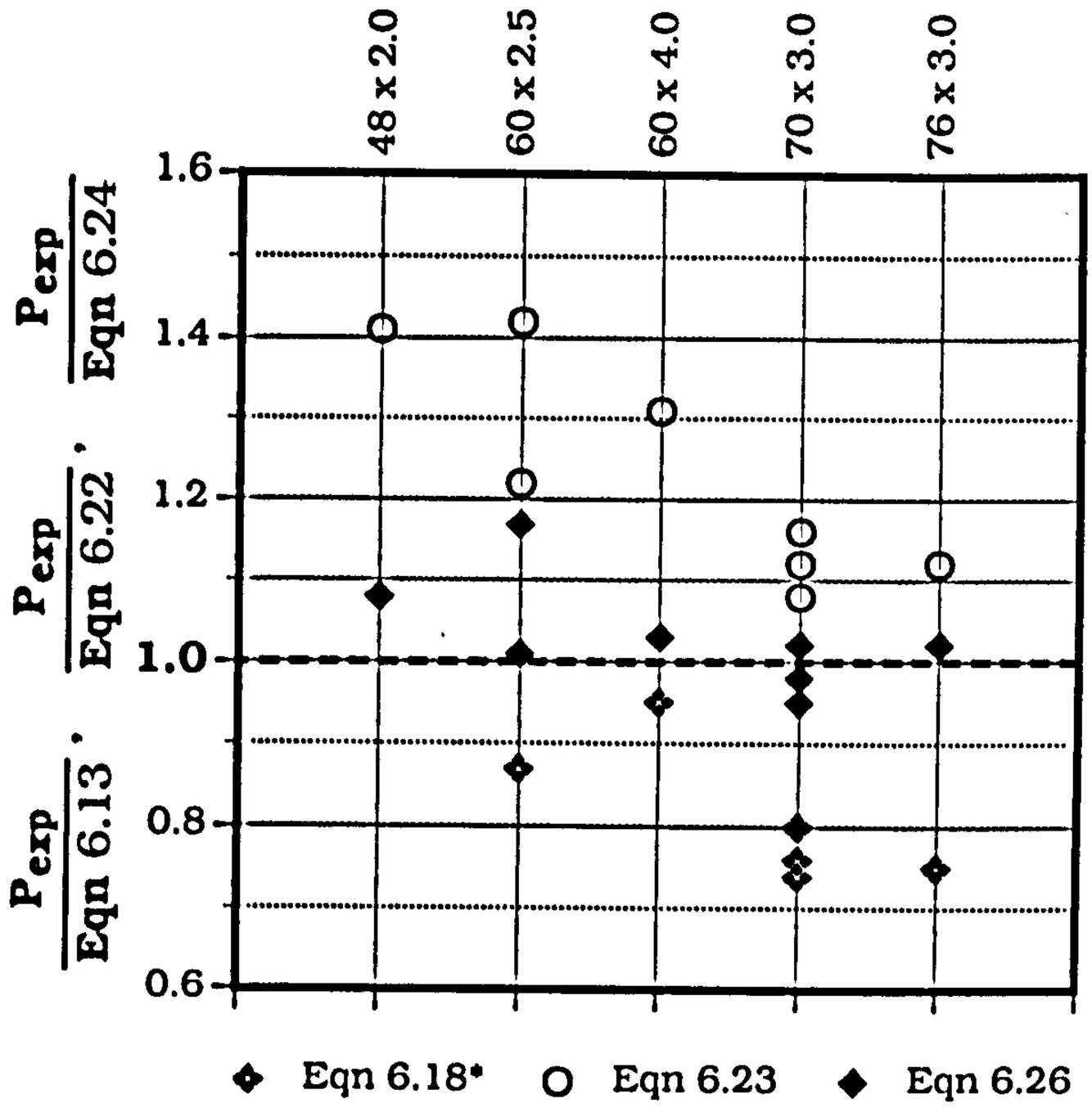


Figure 6.17 Comparison between failure loads predicted by Equations 6.13, 6.22 and 6.24 with experimental results

6.6 PROPOSED DESIGN MODEL FOR TUBULAR DIAGONALS

It has been shown (Figure 6.17 and Table 6.9) that a conservative estimate of the failure load for the diagonal members can be obtained from Equation 6.26 which is

$$\frac{P}{P_Y} + \frac{(P\,e_B - M_{ec})}{M_p\ C_b\left(1 - \frac{P}{P_E}\right)} \leq 1.0$$

where

C_b equivalent moment coefficient

e_B top chord tab eccentricity in the vertical plane of the diagonal (Equation 6.14)

P is the applied axial load

P_E diagonal tube critical buckling load

P_Y the axial resistance of the tube is given by

$$P_Y = 0.5\left[(P_o + (1+\eta)P_E) - \left[(P_o + (1+\eta)P_E)^2 - 4P_o P_E\right]^{1/2}\right]$$

P_o is the short strut capacity ($A\,\sigma_o$)

The imperfection constant η is

$$\eta = 0.002\left(\frac{L}{r} - 20\right)$$

The bending resistance of the tube is

$$M_p = \sigma_o Z_p$$

Z_p plastic section modulus of tube

The elastic bending capacity of the crease in the presence of axial load is

$$M_{ec} = \frac{t D_s^2}{3}\left[\sigma_o - \frac{P}{2\,t\,D_s}\right] \sin\psi$$

ψ is the relative angle between the bottom and top creases

D_s the length of crease supported in the joint

t thickness of tube

A better prediction of the diagonal tubing failure loads might be obtained by modelling more accurately the axial forces and the moments at both ends of the tube. This would almost certainly complicate the design equation.

6.7 CONCLUSIONS

(1) The current column design formulation found in BS5950: Part5 (1987) may give rise to non conservative design when applied to singly symmetric sections.

(2) The failure load for singly symmetric sections depends on the direction of the initial imperfection and the location of the neutral axis position with respect to the outermost fibres in the cross-section. The imperfection parameter η

used in the Perry equation should take into account the distance between the neutral axis position and the outermost fibre such that $\bar{y} = \bar{y}_{max}$

(3) Like local element buckling, lip buckling can have a detrimental affect on the overall flexural buckling resistance of the double lipped channel section. The interaction between lip and overall flexural buckling can be accounted for by limiting the design stress- σ_d, in the column formulation to the lip buckling stress - σ_{uL} (Chapter Five). A comparison between this proposal and numerical and experimental data shows good agreement. The proposed method is shown to give a conservative estimate of the average axial stress to cause first surface yield.

(4) The diagonal members in the test frame are incompletely supported in the top chord connection. The diagonal forces can be assumed to act at the centre of the supported crease length, which generates an end moment.

(5) Because of the large bending stiffness of the bottom chord crease about an axis perpendicular to the crease the diagonal tends to buckle in a plane perpendicular to the crease. This was confirmed by observations made during the frame tests where the diagonals buckled in an approximately vertical plane perpendicular to the bottom chord crease. The eccentricity at the top chord connection was therefore resolved in that direction. The existing beam-column interaction equations given in BS 5950: part 5 (1987) then gives a conservative estimate of the failure load.

(6) An estimate which compares favourably with the experimental failure loads was obtained when the elastic bending capacity of the supported length of the upper crease resolved in the direction of buckling, was taken into account.

Chapter Seven

TORSIONAL-FLEXURAL BUCKLING OF DOUBLY LIPPED CHANNELS

7.1 INTRODUCTION

The preceding chapter dealt with flexural buckling of axially loaded singly symmetric channels taking into account the effects of both local element and lip buckling. Because of their low torsional rigidity thin-walled compression members may also buckle torsionally. Cold-formed sections frequently lack double symmetry, due to the forming processes employed. In singly symmetric or non-symmetric sections the centroid and shear centre do not coincide and therefore torsion and flexure interact to produce a mode of failure commonly termed "torsional-flexural buckling".

The theory of critical torsional-flexural buckling is well developed (Bleich 1952, Timoshenko and Gere 1961 and Galambos 1968). The behaviour of imperfect, concentrically and eccentrically loaded thin-walled sections has been extensively researched by Chajes and Winter (1965) and, Pekoz and Winter (1969). Yu (1991) gives a through summary of the design approach adopted for use in the AISI (1989) code based on this work, where the ultimate torsional-flexural buckling resistance of a section is obtained by using the column flexural buckling formulation with the critical torsional-flexural buckling stress substituted for the Euler buckling stress.

Rhodes (1991) summarises the design approach adopted in BS5950: Part5 (1987) where the ultimate torsional-flexural buckling resistance of a section is obtained by using the same assumptions as in the AISI recommendations-that is the flexural buckling clauses are used with the proviso that the effective length of the member under consideration is multiplied by a factor to account for the difference in critical buckling loads applicable to purely flexural buckling and torsional-flexural buckling

respectively. The critical torsional-flexural buckling load (P_{TF}) can then be substituted directly into the Perry-Roberston equation for the Euler buckling load (P_E) (in this respect BS 5950: Part 5 differs from AISI).

The adaptation of the Perry-Robertson equation for determining the ultimate torsional-flexural capacity of an open thin-walled cross-section provides a convenient basis for design. This is rational inasmuch as it ensures that neither the short strut capacity nor the critical buckling load is exceeded. However, it assumes that the imperfections have the same effect on torsional-flexural buckling as for purely flexural buckling, and takes no account of the different stress distributions which prevail in torsional buckling.

In this chapter it is shown that the Perry equation cannot correctly give the load at which first surface yield occurs and an alternative design method for concentrically loaded singly symmetric channel sections is proposed in which Young's magnification factor is employed to describe the effects of both translation and rotation of the section, and to predict more correctly the stress distribution and the load to cause first yield. Validation of the proposed design method is provided through comparisons with numerical and experimental results.

7.2 CRITICAL TORSIONAL AND TORSIONAL-FLEXURAL BUCKLING

If a symmetrical I-section is free to twist along its length, but not at each end, the resistance to twisting is derived partly from the torsional stiffness GJ, and partly from the bending of the flanges in their own planes. The latter effect, sometimes called the "flange bending effect", is expressed by the warping rigidity EC_w. In open thin-walled sections, EC_w is usually much greater than GJ. If on the other hand the ends are free to twist and to warp, the flanges remain straight, and the warping rigidity is not mobilised. "Warping" denotes that a plane cross-section distorts out of its plane. In the case of an I-section prevented from twisting at each end, but free to warp, when twisting occurs along the member the flanges bend and slope in opposite directions, so the end sections warp. The warping displacements diminish towards the mid length, where warping is zero because of symmetry. Where the end sections twist freely relative to each other without warping restraint, warping is uniform along the length of the member and the flanges remain straight; there is no warping resistance to buckling, and the buckling load will be greatly reduced.

7.2.1 GOVERNING EQUATIONS FOR TORSIONAL-FLEXURAL BUCKLING

Consider the open thin-walled cross-section shown in Figure 7.1, subjected to a concentric axial load. Assuming that during buckling the cross-section will not deform but will translate and rotate it is possible to derive the differential equilibrium equations for the strut. (Appendix B)

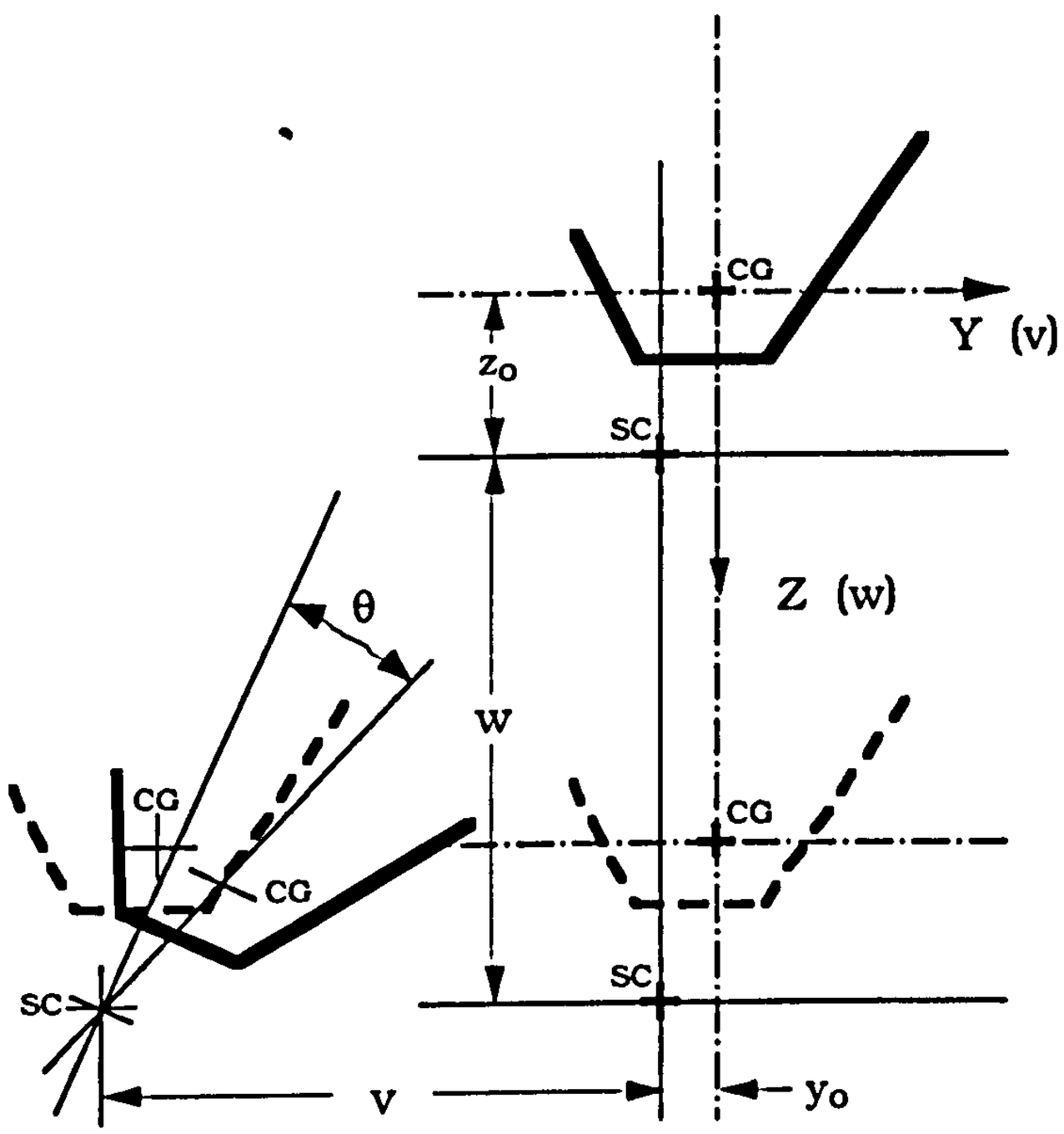


Figure 7.1 Displacement of section during torsional flexural buckling
[Chajes and Winter (1965)]

For a concentrically axial loaded strut Equations B.8 to B.10 become

$$E I_z \frac{d^4 v}{dx^4} + P\frac{d^2 v}{dx^2} + P z_o \frac{d^2 \theta}{dx^2} = 0 \qquad (7.1)$$

$$E I_y \frac{d^4 w}{dx^4} + P\frac{d^2 w}{dx^2} - P y_o \frac{d^2 \theta}{dx^2} = 0 \qquad (7.2)$$

$$E C_w \frac{d^4 \theta}{du^4} - (GJ - P r_o^2)\frac{d^2 \theta}{du^2} - P y_o \frac{d^2 w}{du^2} + P z_o \frac{d^2 v}{du^2} = 0 \qquad (7.3)$$

where

C_w Warping constant (Equations 7.21 and 7.22)

G shear modulus

J St. Venant torsion constant, given by

$$J = \frac{1}{3}\sum_{i=1}^{n} b_i t_i^3 \qquad (7.4)$$

i is the element number

r_o polar radius of gyration about the shear centre, given by

$$r_o = \left(r_z^2 + r_y^2 + z_o^2 + y_o^2 \right)^{1/2} \qquad (7.5)$$

y_o y co-ordinate of shear centre

z_o z co-ordinate of shear centre

r_z radius of gyration about the Z axis

r_y radius of gyration about the Y axis

Assuming that the rotation θ and the translations v and w of the buckled section are described by sinusoidal displacement functions, then the rotation and displacement of any point along the member are given by

$$\theta = \theta_{max} \sin\frac{\pi x}{L}, \qquad v = v_{max} \sin\frac{\pi x}{L}, \qquad w = w_{max} \sin\frac{\pi x}{L} \qquad (7.6)$$

where

v_{max}, w_{max} are initial deflections (imperfections)

θ_{max} initial rotation

Differentiating Equations 7.6 with respect to x, twice

$$\frac{d^2\theta}{dx^2} = -\theta_{max}\left(\frac{\pi}{L}\right)^2 \sin\frac{\pi x}{L}, \qquad \frac{d^2v}{dx^2} = -v_{max}\left(\frac{\pi}{L}\right)^2 \sin\frac{\pi x}{L}, \qquad \frac{d^2w}{dx^2} = -w_{max}\left(\frac{\pi}{L}\right)^2 \sin\frac{\pi x}{L} \qquad (7.7)$$

and twice again

$$\frac{d^4\theta}{dx^4} = \theta_{max}\left(\frac{\pi}{L}\right)^4 \sin\frac{\pi x}{L}, \qquad \frac{d^4v}{dx^4} = v_{max}\left(\frac{\pi}{L}\right)^4 \sin\frac{\pi x}{L}, \qquad \frac{d^4w}{dx^4} = w_{max}\left(\frac{\pi}{L}\right)^4 \sin\frac{\pi x}{L} \qquad (7.8)$$

7.2.2 CRITICAL BUCKLING OF AN I-SECTION

For doubly symmetric sections, such as the I-section shown in Figure 7.2 the shear centre and centroidal axes coincide, hence $y_o = z_o = 0$. Substituting $y_o = z_o = 0$ into Equations 7.1 to 7.3 uncouples the rotation θ and the displacements v and w. Three independent buckling modes are therefore possible, one mode involving displacement in the Z direction, the second involving displacement in the Y direction and the third involving rotation about the X axis of the section. The critical stress for each mode may be obtained by substituting Equations 7.7 and 7.8 into Equations 7.1 to 7.3 and solving for P. The resulting critical buckling stresses are;

Euler buckling about the Z axis

$$\sigma_{E\,z} = \frac{\pi^2 E r_z^2}{L^2} \tag{7.9}$$

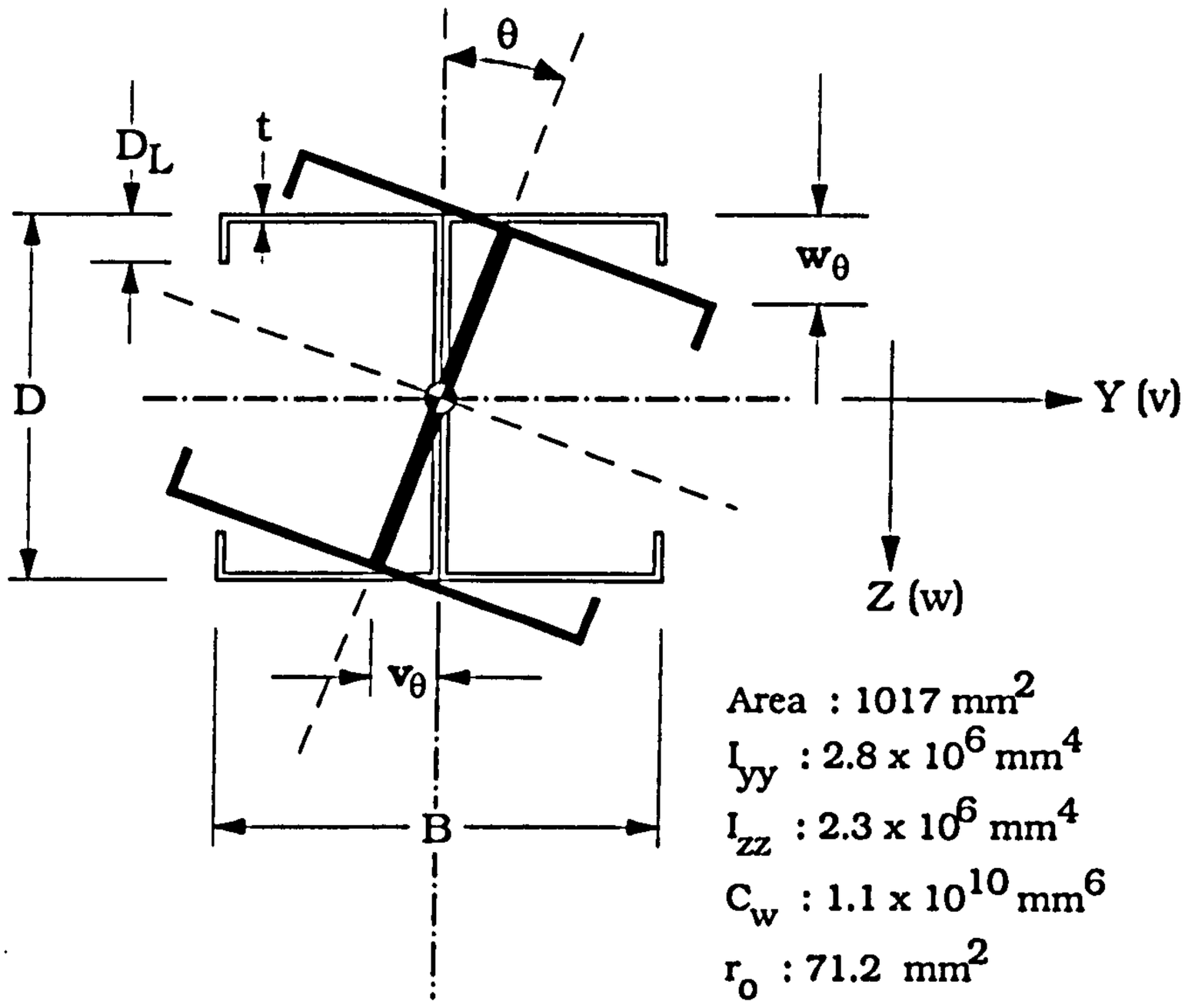


Figure 7.2 Torsional buckling of back to back channel section
B = 180mm, D = 125mm, D_L = 20mm, t = 1.5mm

Euler buckling about the Y axis

$$\sigma_{Ey} = \frac{\pi^2 E r_y^2}{L^2} \qquad (7.10)$$

Torsional buckling about the X axis

$$\sigma_T = \frac{1}{A r_o^2}\left[GJ + K_w \frac{\pi^2 E C_w}{L^2} \right] \qquad (7.11)$$

where

K_w is a warping restraint factor. K_w = 4.0 for fixed ends, K_w = 1.0 for simply supported ends

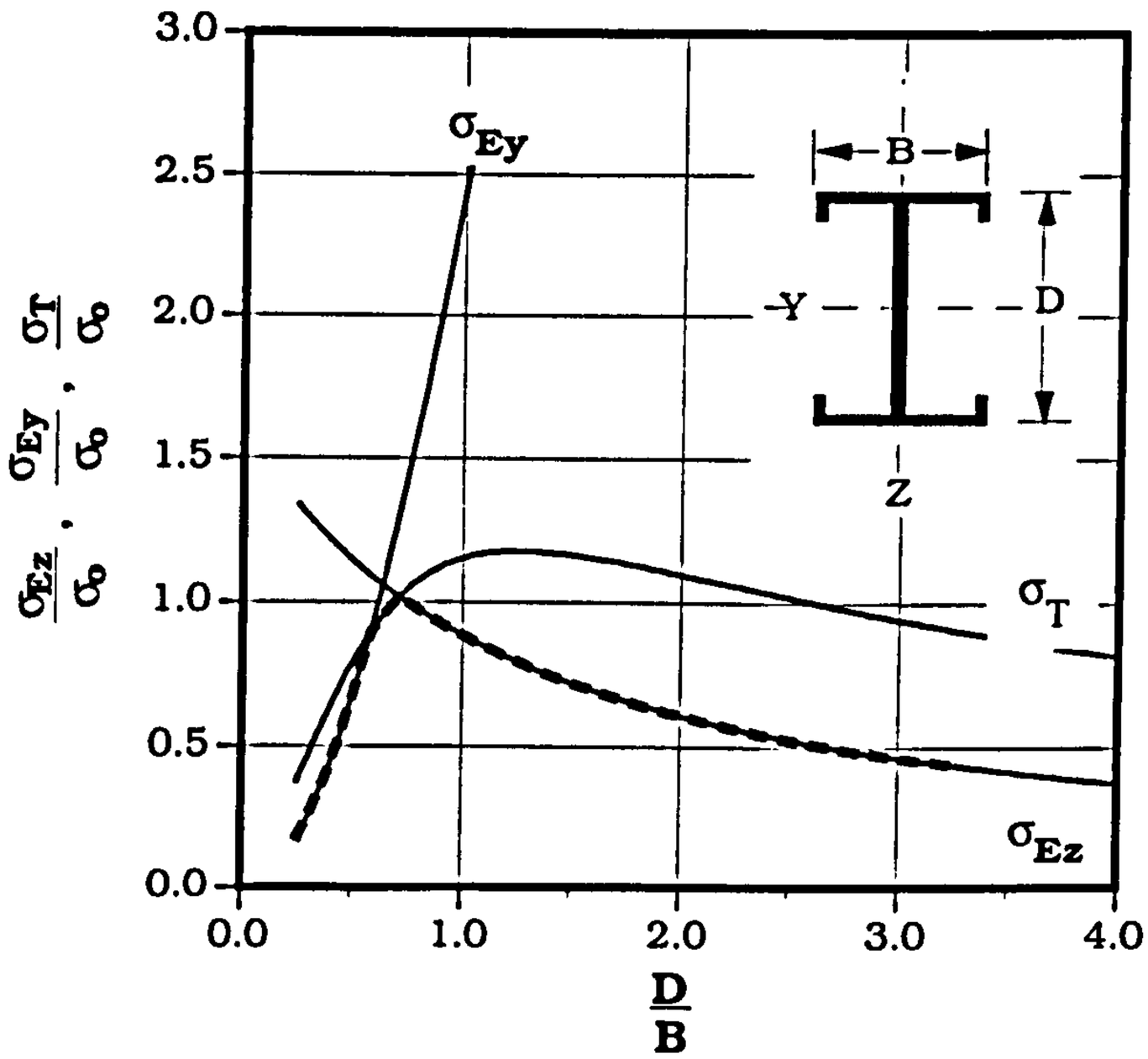


Figure 7.3 Variation in critical buckling stress with depth of section for doubly symmetric I-Section

$B = 180mm, D_L = 20mm, t = 1.5mm, L = 3400mm, \sigma_0 = 390\ N/mm^2$

The lowest critical buckling stress for a doubly symmetric section is the lowest value obtained from Equations 7.9 to 7.11. Figure 7.3 shows the effect of varying the depth (D) of the I-section on the critical buckling stresses σ_{Ey}, σ_{Ez} and σ_T for a given length. Flexural buckling about the Y axis occurs first for D/B ratios less than 0.58, while for ratios greater than 0.71 flexural buckling about the Z axis occurs

first. It can be seen that critical torsional buckling occurs first only when $0.58 < D/B < 0.71$ and is then only slightly smaller than σ_{Ey} or σ_{Ez}. In this region the buckling mode which actually develops will also depend on the mode and magnitude of the initial imperfection. It is evident that for the doubly symmetric I-section, torsional instability is restricted to a very small range of D/B ratios, and is not a major effect.

7.2.3 CRITICAL BUCKLING OF DOUBLY LIPPED CHANNELS

If the Z axis is the axis of symmetry as for the doubly lipped channel section shown in Figure 7.4, then the distance y_o between the shear centre and the centroid in the direction of the Y axis is equal to zero. The critical buckling stresses for such a section may be obtained from Equations 7.1 to 7.3 by substituting $y_o = 0$. One solution is simply the Euler buckling stress about the Y axis obtained from Equation 7.2, given by Equation 7.10.

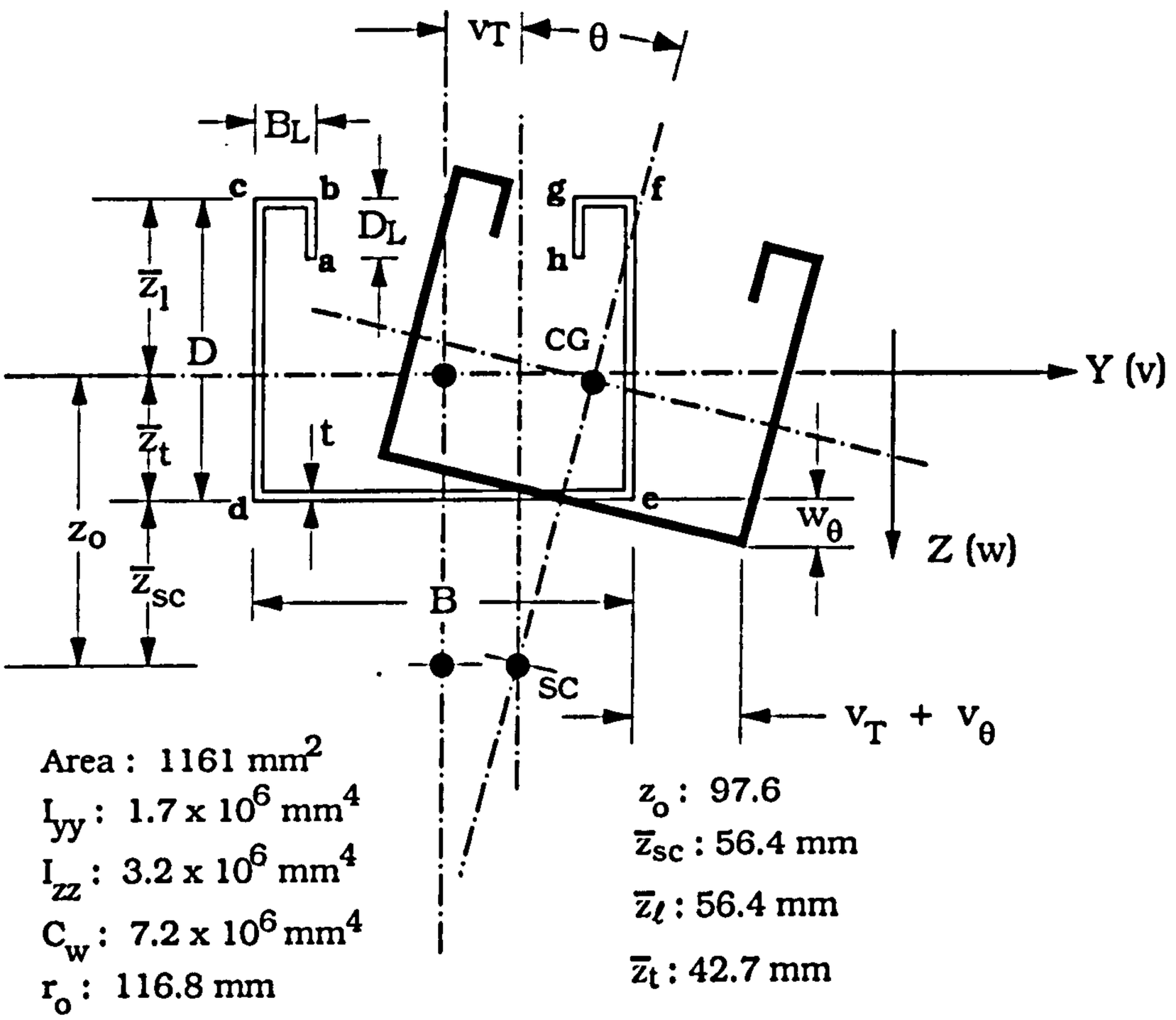


Figure 7.4 Displacements caused by torsional flexural buckling
B = 122mm, D = 97mm, B_L = 17mm, D_L = 18.5mm, t = 3.0mm

However, substitution of $y_o = 0$ into Equations 7.1 and 7.3 does not uncouple the rotation θ and displacement v as for the doubly symmetric I-section. The resulting buckling mode consists of a translation v_T and rotation θ about the shear centre. Assuming that the relation between the θ and v_T can be expressed as the ratio

$$a = \frac{z_o \theta}{v_T} \tag{7.12}$$

Then differentiating Equation 7.12 with respect to x twice, the derivatives may be expressed in terms of θ and v_T as

$$\frac{d^2\theta}{dx^2} = \frac{a}{z_o}\frac{d^2v}{dx^2} \tag{7.13}$$

$$\frac{d^2v}{dx^2} = \frac{z_o}{a}\frac{d^2\theta}{dx^2} \tag{7.14}$$

Substitution of Equations 7.7, 7.8 and 7.13 into Equation 7.1 yields an expression defining the relationship between the rotation θ and displacement v in terms of the critical buckling loads P_{Ez} and P_{TF}. If $v = v_T$, then

$$\frac{z_o \theta}{v_T} = \left(\frac{P_{Ez}}{P_{TF}} - 1\right) \tag{7.15}$$

Similarly substituting Equations 7.7, 7.8 and 7.14 into Equation 7.3 gives

$$\frac{z_o \theta}{v_T} = \frac{z_o^2}{r_o^2}\left(\frac{P_{TF}}{P_T - P_{TF}}\right) \tag{7.16}$$

The critical torsional-flexural buckling load, P_{TF}, may be obtained by equating Equations 7.15 and 7.16 and solving for P_{TF}. Two solutions are obtained,

$$\sigma_{TF} = \frac{1}{2\beta}\left[(\sigma_{Ez} + \sigma_T) + \left\{(\sigma_{Ez} + \sigma_T)^2 - 4\beta\sigma_T\sigma_{Ez}\right\}^{1/2}\right] \tag{7.17}$$

$$\sigma_{TF} = \frac{1}{2\beta}\left[(\sigma_{Ez} + \sigma_T) - \left\{(\sigma_{Ez} + \sigma_T)^2 - 4\beta\sigma_T\sigma_{Ez}\right\}^{1/2}\right] \tag{7.18}$$

where

$$\beta = 1 - \left(\frac{z_o}{r_o}\right)^2$$

σ_{TF} critical torsional-flexural buckling resistance

σ_T torsional buckling resistance (Equation 7.11)

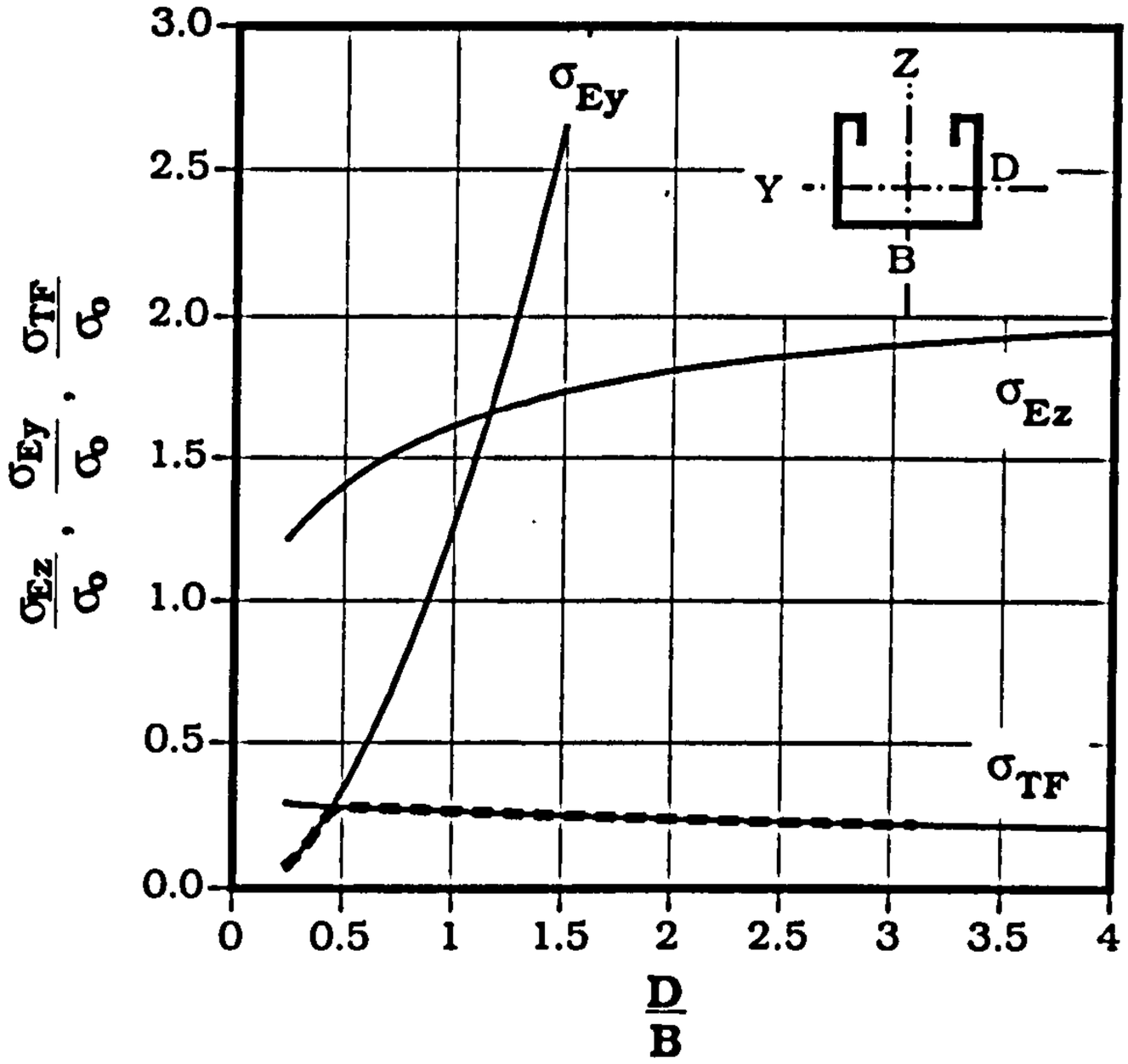


Figure 7.5 Variation in critical buckling stress with depth of section for a singly symmetric doubly lipped channel section

B = 125mm, B_L = 20mm, D_L = 20mm, t= 3.0mm, L = 3000mm, σ_o = 390 N/mm^2

The critical buckling load obtained from Equation 7.18 is less than 7.17 and is always smaller than P_{Ez}, but may be either smaller or larger than P_{Ey}. The lowest critical buckling stress for a singly symmetric open section is given by the smaller of Equations 7.10 or 7.18 (given in BS 5950: Part 5 1987). Figure 7.5 shows the variation of the three critical stresses with D/B for a doubly lipped channel section. It can be seen that critical torsional-flexural buckling is the preferred mode when $D \geq 0.5B$.

7.2.4 SHEAR CENTRE AND WARPING CONSTANT

The location of the shear centre position $\bar{z}_{sc}$ and the warping constant C_w are section properties which must be evaluated before the critical torsional or torsional-flexural buckling resistance of a thin-walled section can be obtained. Formulae for a variety of commonly used structural sections may be found in Appendix D, BS5950: Part 5 (1987) but the doubly lipped channel is not included. The shear centre for the I-section of Figure 7.2 coincides with the centroidal axes of the section, the warping constant C_w given in BS5950: Part 5 (1987) Appendix D is

$$C_w = \frac{B^3 D^2 t}{24}\left[1 + 6\frac{D_L}{B}\left\{1 + 2\frac{D_L}{B} + \frac{4}{3}\left(\frac{D_L}{B}\right)^2\right\}\right] \qquad (7.19)$$

Equations 7.20, 7.21 and 7.22, which give the shear centre location and warping constant for the doubly lipped channel of Figure 7.4 have been obtained using the general theory presented by Timoshenko and Gere (1961).

The shear centre of a singly symmetric section is located along the axis of symmetry (Z axis). The distance $\bar{z}_{sc}$ from the shear centre to the mid thickness of the table for the doubly lipped channel in Figure 7.4 is given by;

$$\bar{z}_{sc} = \frac{t}{I_{zz}}\left[\frac{B^2(D^2 - D_L{}^2)}{4} + \frac{DB^2(B_L + D_L)}{2} - \frac{2DB_L{}^3}{3} - BB_L D_L{}^2 - B_L{}^2(2DD_L - D_L{}^2)\right] \qquad (7.20)$$

Equation 7.20 represents the point about which the first moment of the shear forces around the section are in equilibrium. The position of the shear centre $\bar{z}_{sc}$ given by Equation 7.20 has been validated numerically using FINASIC (1990), by applying a force in the Y direction through the table and two equal and opposite forces in the Z direction at the web/table junctions. The magnitude of the forces in the Z direction were adjusted till the channel translated in the Y direction without rotating about the shear centre. The location of the shear centre could then be found by taking the ratio of the moment about the centre line of the table, to the applied force in the Y direction.

The warping constant C_w for the doubly lipped channel is given by

$$C_w = \sum_{i=1}^{7} t\left[(\omega_{av} - A_i)^2 (X_i - Y_i) + B_i (A_i - \omega_{av})(X_i{}^2 - Y_i{}^2) + \frac{B_i{}^2}{3}(X_i{}^3 - Y_i{}^3)\right] \qquad (7.21)$$

where

i	denotes the segment and A,B,X and Y are constants found in Table 7.1
ω_{av}	is the average value of the warping displacement

	i	A_i	B_i	X_i	Y_i
ab	1	0	$\left(\frac{B}{2} - B_L\right)$	DL	0
bc	2	$\left(\frac{B}{2} - B_L\right) D_L + (D + \bar{z}_{sc}) D_L$	$-(D + \bar{z}_{sc})$	DL + BL	DL
cd	3	$\left(\frac{B}{2} - B_L\right) D_L - (D + \bar{z}_{sc}) B_L + \frac{B}{2}(D_L + B_L)$	$-\frac{B}{2}$	DL + BL + D	DL + BL
de	4	$\left(\frac{B}{2} - B_L\right) D_L - (D + \bar{z}_{sc}) B_L - \bar{z}_{sc}(B_L + D_L + D) - \frac{B}{2} D$	$\bar{z}_{sc}$	DL + BL + B + D	DL + BL + D
ef	5	$\left(\frac{B}{2} - D_L\right) B_L - (D + \bar{z}_{sc}) B_L + \bar{z}_{sc} B - \frac{B}{2} D + \frac{B}{2}(D_L + B_L + D + B)$	$-\frac{B}{2}$	DL + BL + 2D + B	DL + BL + B + D
fg	6	$\left(\frac{B}{2} - B_L\right) D_L - (D + \bar{z}_{sc}) B_L + \bar{z}_{sc} B - DB + (D + \bar{z}_{sc})(B_L + D_L + 2D + B)$	$-(D + \bar{z}_{sc})$	2DL + BL + 2D + B	DL + BL + 2D + B
gh	7	$\left(\frac{B}{2} - B_L\right) D_L - 2(D + \bar{z}_{sc}) + \bar{z}_{sc} B - DB + \left(\frac{B}{2} - B_L\right)(D_L + 2B_L + 2D + B)$	$\left(\frac{B}{2} - B_L\right)$	2DL + 2BL + 2D + B	DL + 2BL + 2D + B

Table 7.1 A, B, X and Y constants used in evaluating Equation 7.21 and 7.22.

where

$$\omega_{av} = \sum_{i=1}^{7} \left[\frac{A_i (X_i - Y_i) + \frac{D}{2}(X_i^2 - Y_i^2)}{B + 2D + 2B_L + 2D_L} \right] \qquad (7.22)$$

The numerical values for $\bar{z}_{sc}$ and C_w for the doubly lipped channel section, where t = 3.0mm are given in Figure 7.4.

For more complex shapes general computer algorithms capable of automatically calculating the complete section properties for any geometry are available (Roberts 1985 and Murray and Attard 1987).

7.2.5 FINITE ELEMENT CRITICAL BUCKLING ANALYSIS OF DOUBLE LIPPED CHANNEL.

The critical torsional-flexural buckling stress for three lengths of 3mm thick 122x97x17x18.5mm doubly lipped channel section, where L = 2000mm, 3000mm and 4000mm were obtained numerically using FINASIC (1990). In Chapters Four, Five and Six the critical buckling modes for local, lip and flexural buckling were all symmetrical, so only half of the cross-section needed to be modelled. The critical torsional-flexural buckling mode is asymmetric about the longitudinal axis of the member, so the whole cross-section needed to be modelled.

Two different finite element meshes were tested for convergence and compared with the theoretical values for the critical torsional-flexural buckling load P_{TF} obtained from Equation 7.18. The number of elements (16) used to describe the whole cross-section was the same as that used in Chapters Four through to Six. The first mesh had the an element length of 62.5mm. The second mesh was coarser, with an element length of 125mm.

Boundary conditions at the ends of the member permitted inplane bending in each of the element (warping), but prevented distortion and torsional rotation of the cross-section. The members were subjected to uniform axial load. The results from the numerical analyses are given in Table 7.2. It can be seen that making the mesh coarser along the length of the member has no effect on the critical buckling load, and good agreement with calculated values is shown for both meshes.

As a result of this study it was decided to use the coarser of the two meshes for further numerical analysis. This substantially reduced the computational time needed to obtain a solution.

Figure 7.6 shows the lowest two critical buckling modes for the doubly lipped channel section where L = 3000mm

Length (mm)	**No of Elements**	P_{crF} (kN)	$\frac{\text{Eqn. 7.18}}{P_{crF}}$
4000	1024	74.4	1.00
	512	74.4	1.00
3000	768	120.3	1.01
	384	120.3	1.01
2000	512	247.1	1.03
	253	247.1	1.03

Table 7.2 Comparison between Equation 7.18 and critical torsional-flexural buckling stresses for a 3mm thick doubly lipped channel obtained numerically.

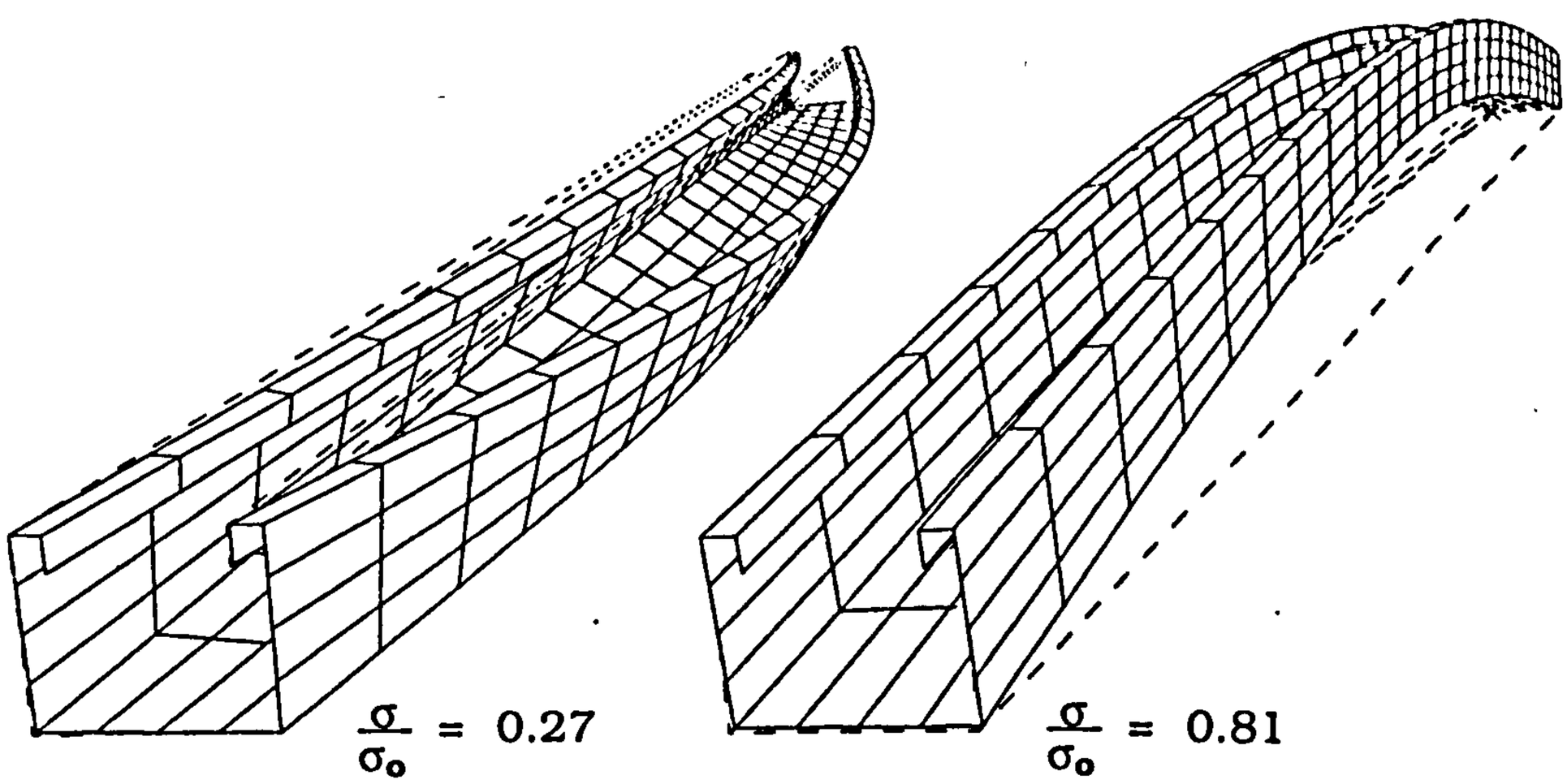


Figure 7.6 First and second critical buckling modes (axial compression).
B = 122mm, D = 97mm, B_L = 17mm, D_L = 18.5mm, t = 3.0mm
L = 3000mm, σ_o = 390 N/mm^2

The ratios between $z_o\,\theta$ and displacement v_T obtained from the critical buckling analysis are compared with Equation 7.15 for different lengths of channel in Table 7.3. In all cases the ratios obtained from Equation 7.15 are slightly higher than those obtained numerically.

Length (mm)	FINASIC θ (rad)	FINASIC v_T (mm)	FINASIC $\frac{z_o\,\theta}{v_T}$	Eq. 7.15 $\frac{z_o\,\theta}{v_T}$	$\frac{\text{Eq. 7.15}}{\text{FINASIC}}$
4000	0.06543	1.515	4.21	4.27	1.01
3000	0.04915	1.023	4.69	4.77	1.02
2000	0.03277	0.648	4.94	5.21	1.05

Table 7.3 Comparison between critical mode ratio given by Equation 7.15 and results obtained from a critical buckling analysis of a 3mm thick doubly lipped channel (z_o = 97.61mm)

7.3 ULTIMATE TORSIONAL-FLEXURAL BUCKLING RESISTANCE

The ultimate torsional-flexural buckling resistance of a thin-walled member is influenced by geometrical imperfections, eccentricity of load and residual stresses, so that the theoretical critical stress based on perfect conditions is not realized in practice, in the same way that the Euler buckling stress is not realized in flexural buckling of struts. In the case of flexural buckling, the effect of imperfections is accounted for by using the Perry-Robertson formulation presented in Chapter Six (Equation 6.18). The torsional-flexural buckling resistance is also influenced by the degree of warping restraint provided at the ends of the member.

Several design codes use a flexural buckling formulation to determine the ultimate torsional-flexural resistance of open thin-walled sections, where the critical torsional-flexural buckling stress is substituted in place of the flexural critical buckling stress. This approach presupposes that any imperfections have the same effect on torsional-flexural buckling as on purely flexural buckling, but the stress distribution and displacements obtained using this approach bear no resemblance to the actual stress distribution and displacement of a member which buckles torsionally.

An alternative approach to determining the ultimate torsional-flexural resistance is proposed. The method is based on Young's equation (Equation 6.3) applied to the initial displacement v_T and rotation θ, which are given in Equations 7.24 and 7.25. In design, loss of effectiveness would be taken into account in the same way as for flexural buckling.

7.3.1 TORSIONAL BUCKLING OF IMPERFECT DOUBLY SYMMETRIC SECTIONS

Consider the doubly symmetric I section shown in Figure 7.2. Torsional buckling is resisted by both the St. Venant and the warping stiffness of the section. However, for thin-walled open sections the St. Venant torsional stiffness GJ is small compared to the warping stiffness EC_w. It may be assumed that torsional buckling is primarily resisted by the flexural stiffness of each flange "flange bending" caused by warping.

If the initial imperfection is assumed to be affine to the critical torsional buckling mode, only torsional displacements will occur. Also, for a given maximum imperfection at a corner of the section, the average axial stress to cause first yield, σ_Y, will be a minimum for affine initial rotation θ_o. The lateral displacement of the flange due to an initial rotation θ_o is

$$v_{\theta o} = \frac{\theta_o D}{2} \qquad (7.23)$$

Assuming that each flange behaves as an axially loaded strut with an initial lateral imperfection equivalent to $v_{\theta o}$, it is reasonable to assume that any increase in lateral displacement will be amplified according to Young's equation (Equation 6.3) such that

$$v_{1\theta} = \frac{v_{\theta o}}{\left(1 - \frac{\sigma_A}{\sigma_T}\right)} - v_{\theta o} \qquad (7.24)$$

where

σ_A the average axial stress
σ_T the critical torsional buckling resistance

Since θ and v are proportional (Equation 7.23) the additional rotation θ, about the shear centre for any level of load σ_A/σ_T is given by Equation 7.24, which is

$$\theta_1 = \frac{\theta_o}{\left(1 - \frac{\sigma_A}{\sigma_T}\right)} - \theta_o \qquad (7.25)$$

Referring to Figure 7.2, for small values of θ, θ causes displacements at the corners of the I-section

$$v_{1\theta} = \frac{\theta_1 D}{2} \qquad (7.26)$$

and

$$w_{1\theta} = \frac{\theta_1 B}{2} \qquad (7.27)$$

The horizontal curvature in the flanges caused by $v_{1\theta}$ is

$$\frac{1}{R} = v_{1\theta} \frac{\pi^2}{L^2}$$

and the corresponding corner stress may be expressed as

$$\sigma = \frac{E}{R} \frac{B}{2} = v_{1\theta} \frac{\pi^2}{L^2} \frac{B}{2} E \qquad (7.28)$$

The stress increment from a corner to the tip of the downturn is

$$\sigma = w_{1\theta} \frac{\pi^2}{L^2} D_L E \qquad (7.29)$$

Equations 7.28 and 7.29 enable the warping stress distribution to be plotted around the section at any value of σ_A/σ_T and θ_o, as shown in Figure 7.7, where θ has been assumed to be given by

$$\theta = \frac{2L}{1000 D}$$

This assumption is consistent with the imperfection tolerance being in the direction of minor axis flexural buckling . It should be noted however that for purely torsional imperfection, $w_{\theta o}$ is greater than $v_{\theta o}$, for the section considered.

The maximum, total compressive stress occurs at diagonally opposite tips of the flange downturn, and is given by

$$\sigma = \sigma_A + \frac{\pi^2 E}{L^2}\left(\frac{v_{1\theta}}{2} B + w_{1\theta} D_L\right) \qquad (7.30a)$$

whilst the stress at opposing flange downturns is

$$\sigma = \sigma_A - \frac{\pi^2 E}{L^2}\left(\frac{v_{1\theta}}{2} B + w_{1\theta} D_L\right) \qquad (7.30b)$$

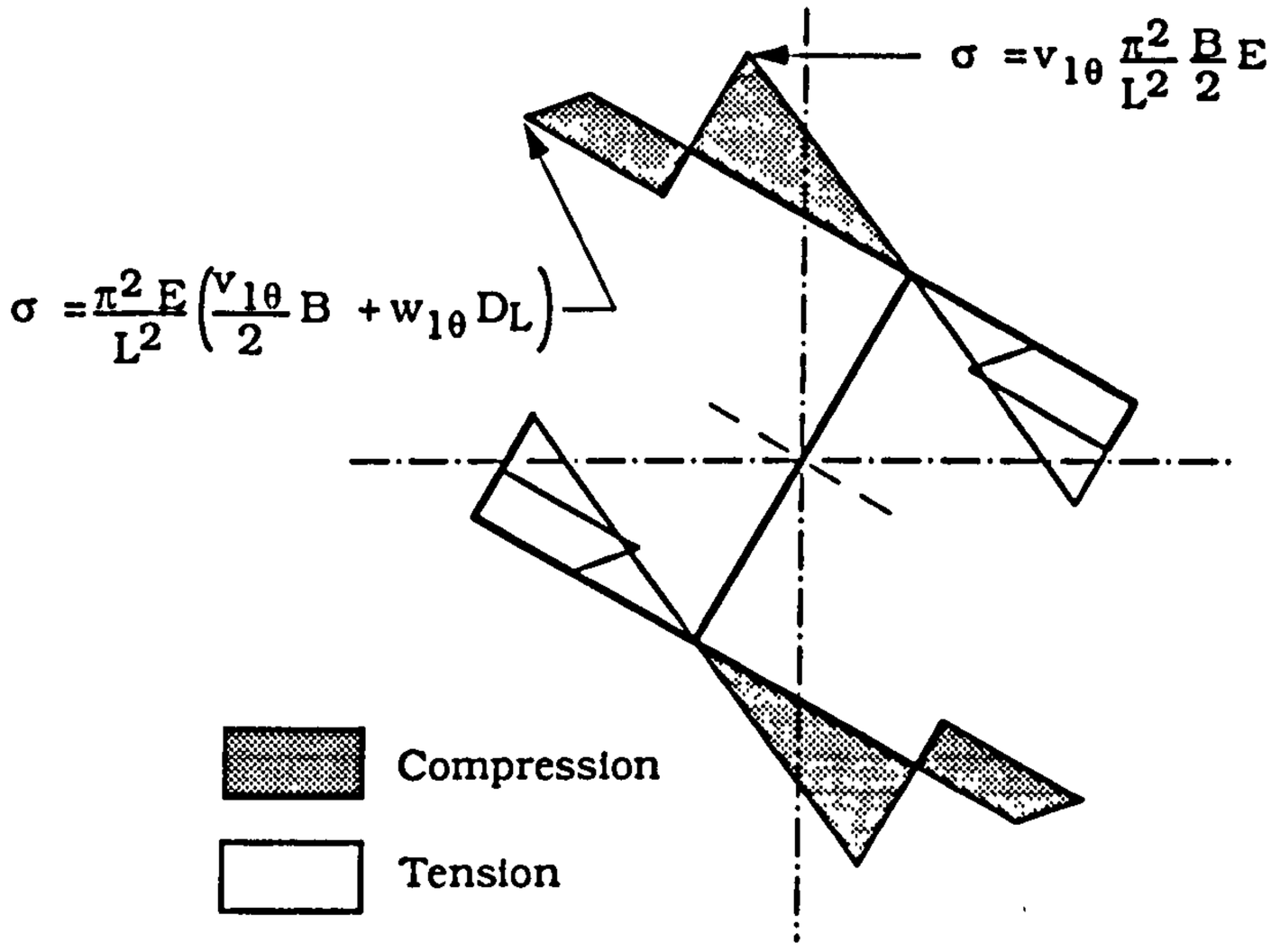


Figure 7.7 Warping stress caused by Torsional Buckling

Equations 7.30 enable the stress to be found for any value σ_A/σ_T and θ_o. The average axial stress σ_Y that causes first yield can be written in a form which is similar to the Perry equation for flexural buckling by substituting Equations 7.26 and 7.27 into Equation 7.30a. Setting $\sigma = \sigma_o$ and $\sigma_A = \sigma_Y$, and solving for σ_Y

$$\sigma_Y = \frac{1}{2}\left[(\sigma_o + \sigma_T + \eta\,\sigma_{Ez}\,\alpha) - \{(\sigma_o + \sigma_T + \eta\,\sigma_{Ez}\,\alpha)^2 - 4\,\sigma_o\,\sigma_T\}^{1/2}\right] \qquad (7.31)$$

where

$$\eta = \frac{v_{\theta o} B}{2\ r_z^2}, \qquad \alpha = \left(1 + \frac{2 D_L}{D}\right)$$

Equation 7.31 displays a general resemblance to the Perry equation as well as some important differences. The stress distribution at first yield for the I-section of

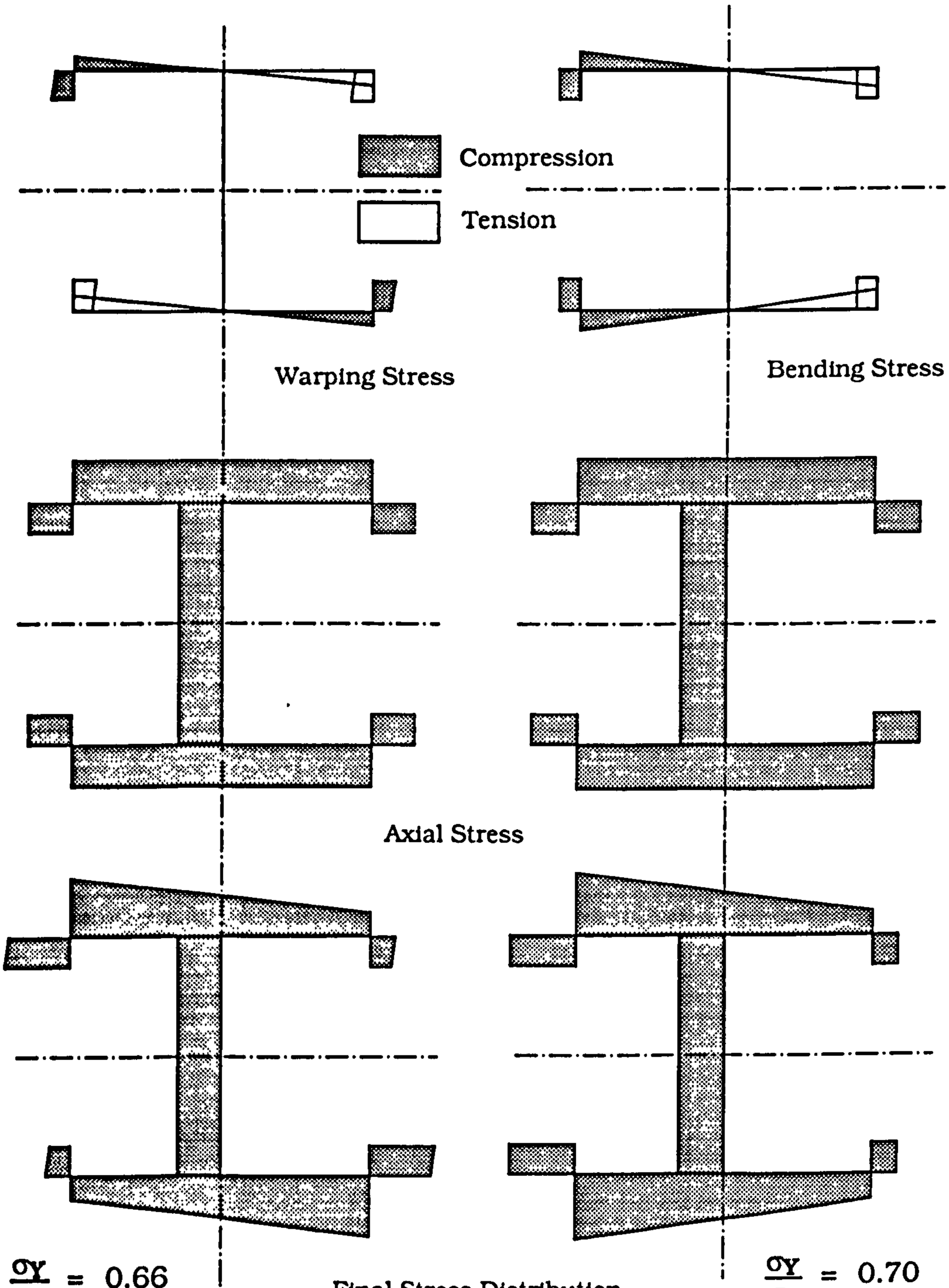


Figure 7.8 Warping, axial and total stress distributions at first surface yield (Equations 7.28 to 7.31)

Figure 7.9 Bending, axial and total stress distributions at first surface yield (Equation 7.32)

B = 180mm, D = 125mm, D_L = 20mm, t = 1.5mm, L = 3400mm, σ_o = 390 N/mm^2

critical length, L = 3400mm, is shown in Figure 7.8. The corresponding average axial stress given by Equation 7.31, is $\sigma_Y = 257\ N/mm^2$.

Currently BS 5950:Part5 (1987) assumes that the average axial stress to cause first yield is given by a modified Perry-Robertson equation, with P_T substituted for P_E, (that is the smaller of P_{Ey} and P_{Ez}). The Perry equation (Equation 6.11, where Q = 1.0) then becomes

$$\sigma_Y = \frac{1}{2}\left[(\sigma_o + \sigma_T + \eta\sigma_T) - \{(\sigma_o + \sigma_T + \eta\sigma_T)^2 - 4\,\sigma_o\sigma_T\}^{1/2}\right] \qquad (7.32)$$

In order to obtain a realistic comparison between Equation 7.31 and 7.32 the imperfection constant η has been taken in accordance with the original Perry equation that is

$$\eta = \frac{v_{\theta o} B}{2\ r_z^2} \qquad (7.33a)$$

$$v_{\theta o} = \frac{L}{1000} \qquad (7.33b)$$

The stress distribution for the I-section determined by Equation 7.32 is shown in Figure 7.9, for which $\sigma_Y = 271\ N/mm^2$. It can be seen the stress distribution given by Equation 7.32 differs from the actual stress distribution given by Equations 7.28 to 7.30, and that the average axial stress to cause first yield, obtained from Equations 7.31 and 7.32 are different. This is because the warping effects are not described by the Perry equation. For any given section, the difference between the values of σ_Y given by Equations 7.31 and 7.32 will depend on the relative magnitudes of σ_{Ez} and σ_T and the magnitude of α. For the particular case where $\sigma_T = \sigma_{Ez}$ and $\alpha = 1$, Equations 7.31 and 7.32 become identical.

Equation 7.32, becomes identical to equation 7.31 if η' is substituted for η, where

$$\eta' = \alpha\frac{\sigma_{Ez}}{\sigma_T}\ \eta \qquad (7.34)$$

This would suggest that it is rational to increase η for torsional buckling by the ratio (σ_{Ez}/σ_T), rather than $(\sigma_E/\sigma_T)^{1/2}$ as suggested in BS5950: Part 5 (1987), where σ_E is the smaller flexural buckling stress.

7.3.2 TORSIONAL-FLEXURAL BUCKLING OF IMPERFECT DOUBLY LIPPED CHANNEL SECTIONS

Because of the interaction between the rotation θ and the translation v_T for singly symmetric sections, torsional-flexural buckling is the likely mode of failure. Consider the doubly lipped channel section shown in Figure 7.4. If the initial deformation is assumed to be affine to the critical torsional-flexural buckling mode then the displacements of such a strut are given by

$$\theta = \frac{\theta_o}{\left(1 - \frac{\sigma}{\sigma_{TF}}\right)} \tag{7.35}$$

where θ is the total rotation about the shear centre, and

$$v_T = \frac{v_{To}}{\left(1 - \frac{\sigma}{\sigma_{TF}}\right)} \tag{7.36}$$

where v_T is the total horizontal translation of the shear centre. Consider a small rotation θ about the shear centre; this causes displacements v_θ and w_θ at the corners of the section. The horizontal displacement v_θ of the table due to θ is

$$v_\theta = \bar{z}_{sc}\,\theta \tag{7.37}$$

and at the lip table

$$v_\theta = (\bar{z}_{sc} + D)\,\theta \tag{7.38}$$

In the plane of the webs

$$w_\theta = \frac{B\theta}{2} \tag{7.39}$$

Warping stresses in the section are caused by the additional displacements $v_{1\theta}$ and $w_{1\theta}$, where

$$v_{1\theta} = v_\theta - v_{\theta o}, \qquad w_{1\theta} = w_\theta - w_{\theta o} \tag{7.40}$$

The horizontal curvature of the table caused by the additional displacement $v_{1\theta}$ is

$$\frac{1}{R} = v_{1\theta}\frac{\pi^2}{L^2} \tag{7.41}$$

The corresponding stress at the corner of the web/table junction (point **d**, Figure 7.4) is

$$\sigma = v_{1\theta} \frac{\pi^2}{L^2} \frac{B}{2} E = \bar{z}_{sc}\, \theta_1 \frac{\pi^2}{L^2} \frac{B}{2} E \qquad (7.42)$$

Similarly the stress increment over the depth of the web is

$$\sigma = w_{1\theta} \frac{\pi^2}{L^2} D\, E = \frac{B\theta_1}{2} \frac{\pi^2}{L^2} D\, E \qquad (7.43)$$

and the stress increments over the width, and the depth of the lip are obtained from Equations 7.44 and 7.45 respectively

$$\sigma = v_{1\theta} \frac{\pi^2}{L^2} B_L\, E = (D + \bar{z}_{sc})\, \theta_1 \frac{\pi^2}{L^2} B_L\, E \qquad (7.44)$$

$$\sigma = w_{1\theta} \frac{\pi^2}{L^2} D_L\, E = \left(\frac{B}{2} - B_L\right) \theta_1 \frac{\pi^2}{L^2} D_L\, E \qquad (7.45)$$

Amplification of v_{To} results in an additional translation v_{1T} where

$$v_{1T} = v_T - v_{To} \qquad (7.46)$$

The corresponding bending stress in the web is

$$\sigma = v_{1T} \frac{\pi^2}{L^2} \frac{B}{2} E \qquad (7.47)$$

The bending stress in the lip table/lip downturns

$$\sigma = v_{1T} \frac{\pi^2}{L^2} \left(\frac{B}{2} - B_L\right) E \qquad (7.48)$$

For the section shown in Figure 7.4, for L = 3000mm, σ_{TF} = 105 N/mm^2. The relation between rotation θ and the translation v_T for torsional flexural buckling, in the critical mode, is given by Equations 7.16 and 7.17. Figure 7.10 shows the variation of Equation 7.16 with varying D/B, where L = 3000mm.

The initial imperfection $w_{\theta o}$ at the web/table junction is assumed to be ± L/1000, so that the initial rotation about the shear centre is

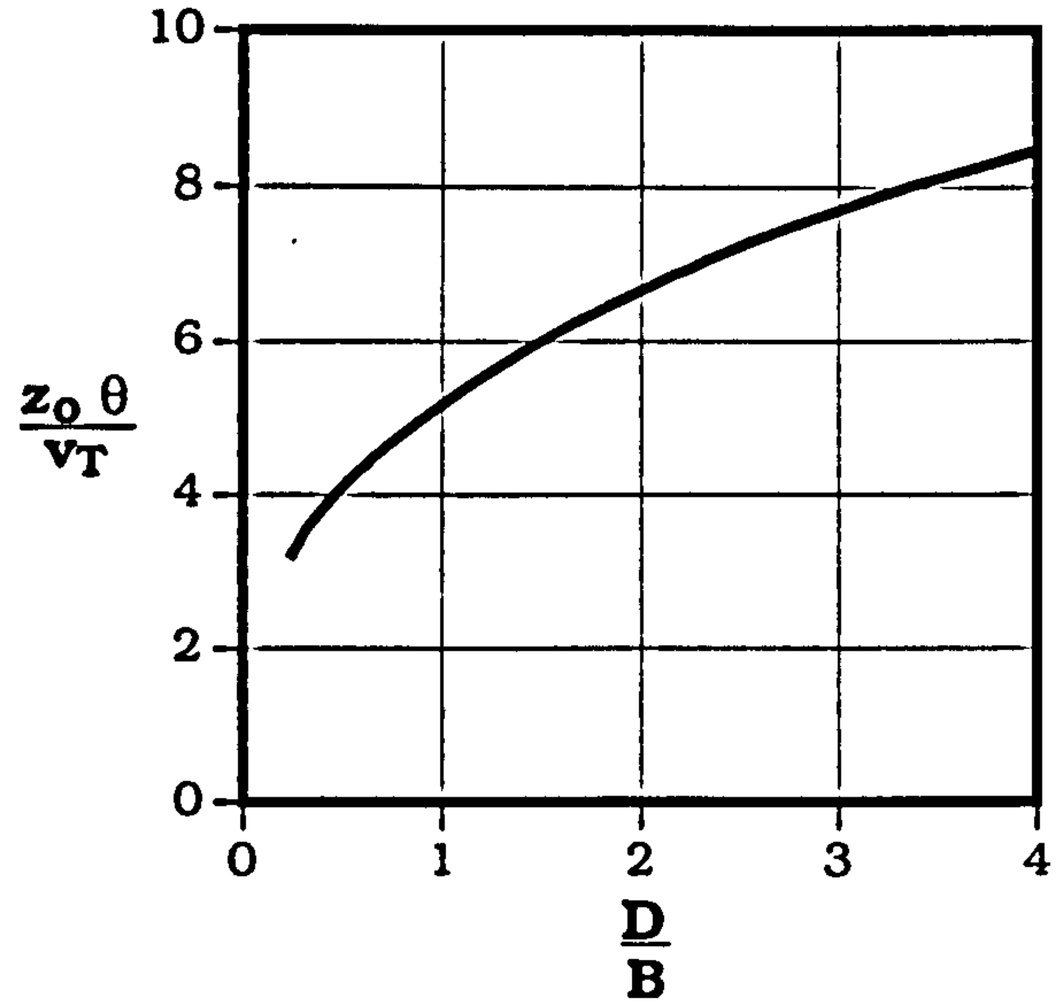


Figure 7.10 Variation in critical mode ratio (Equation 7.16)
with depth of section
B = 122mm, B_L = 20mm, D_L = 20mm, t = 3.0mm, L = 3000mm

$$\theta_o = \frac{2\,L}{1000\,B} \tag{7.49a}$$

If the initial imperfection is affine to the critical torsional-flexural buckling mode, the initial translation is given by Equation 7.16

$$v_{To} = \frac{z_o\ \theta_o\ P_{TF}}{(P_{Ez}\ -\ P_{TF})} \tag{7.49b}$$

The assumed value of θ_o (for which $w_{\theta o}$ = L/1000) is directionally consistent with the usual design assumption that the strut buckles flexurally about the minor axis. It should be remarked that the initial deformation v_o (v_{To} + $v_{\theta o}$) at the level of the lip table is much greater, and exceeds the tolerance specification, if the specification is taken to apply to the four corners of the section.

If the initial deformation were only in the direction normal to the minor axis, as implied by the Perry equation, then the initial displacement w_o would be magnified according to

$$w = \frac{w_o}{\left(1 - \frac{\sigma}{\sigma_{Ey}}\right)} \tag{7.50}$$

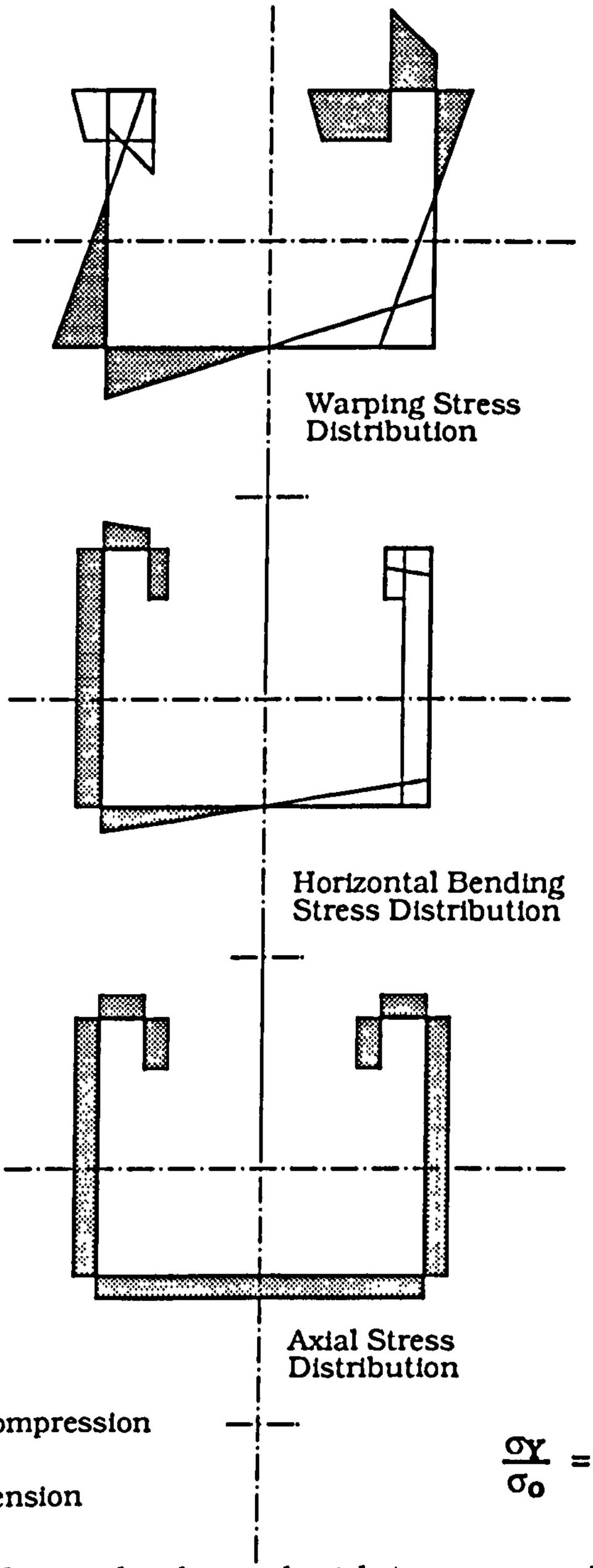


Figure 7.11 Warping, bending and axial stresses caused by torsional flexural buckling (Eqns 7.42 to 7.45)

B = 122mm, D = 97mm, B_L = 17, D_L = 18.5, t = 3.0mm,

L = 3000mm, σ_o = 390 N/mm^2

The critical flexural buckling stress for the channel section where L = 3000mm, is $\sigma_{Ey} = 324$ N/mm^2, while the average axial stress to cause first yield in the section caused by flexural buckling is $\sigma_Y = 237$ N/mm^2. As the critical torsional-flexural buckling stress σ_{TF} is less than the ultimate flexural buckling capacity of the section, critical torsional buckling would occur without prior twisting (because $\theta_o = 0$) at an average stress equal to $\sigma_{TF} = 105$ N/mm^2. However, the code design method implies that an increased flexural deformation occurs, such that when σ_{TF} is substituted for σ_{Ey} into the Perry equation, the displacement w is then given by

$$w = \frac{w_o}{\left(1 - \frac{\sigma}{\sigma_{TF}}\right)} \tag{7.51}$$

The average axial stress to cause first yield is then reduced to 100 N/mm^2. The recommended design procedure given in BS 5950: Part5 (1987) incorporates a modified imperfection constant η, such that

$$\eta = 0.002\left[\left(\frac{L}{r_y}\left(\frac{\sigma_{Ey}}{\sigma_{TF}}\right)^{1/2}\right) - 20\right] \tag{7.52a}$$

Equation 7.52a gives $\eta = 0.28$ compared to $\eta = 0.12$ given by Equation 7.52b

$$\eta = \frac{w_o \bar{z}_{max}}{r_y^2} \tag{7.52b}$$

Substitution of Equation 7.52a into 7.32 causes further reduction in σ_Y to 95 N /mm^2.

The warping stresses obtained from Equations 7.42 to 7.45, the horizontal bending stresses from Equation 7.47 and 7.48 and the axial stress, are shown in Figure 7.11. The total stress distribution is shown in Figure 7.12, at first yield, which occurs at the web/table junction. The average axial stress at first yield is $\sigma_Y = 89$ N/mm^2. Figure 7.12 also shows the displaced shape obtained from Equations 7.35 and 7.36. The variation of stress and displacement determined in accordance with the Perry equation are shown in Figure 7.13. The stress distribution in Figure 7.13, which is the distribution implied by the current design method, may be contrasted with the distribution of Figure 7.12, which takes account of torsional flexural buckling.

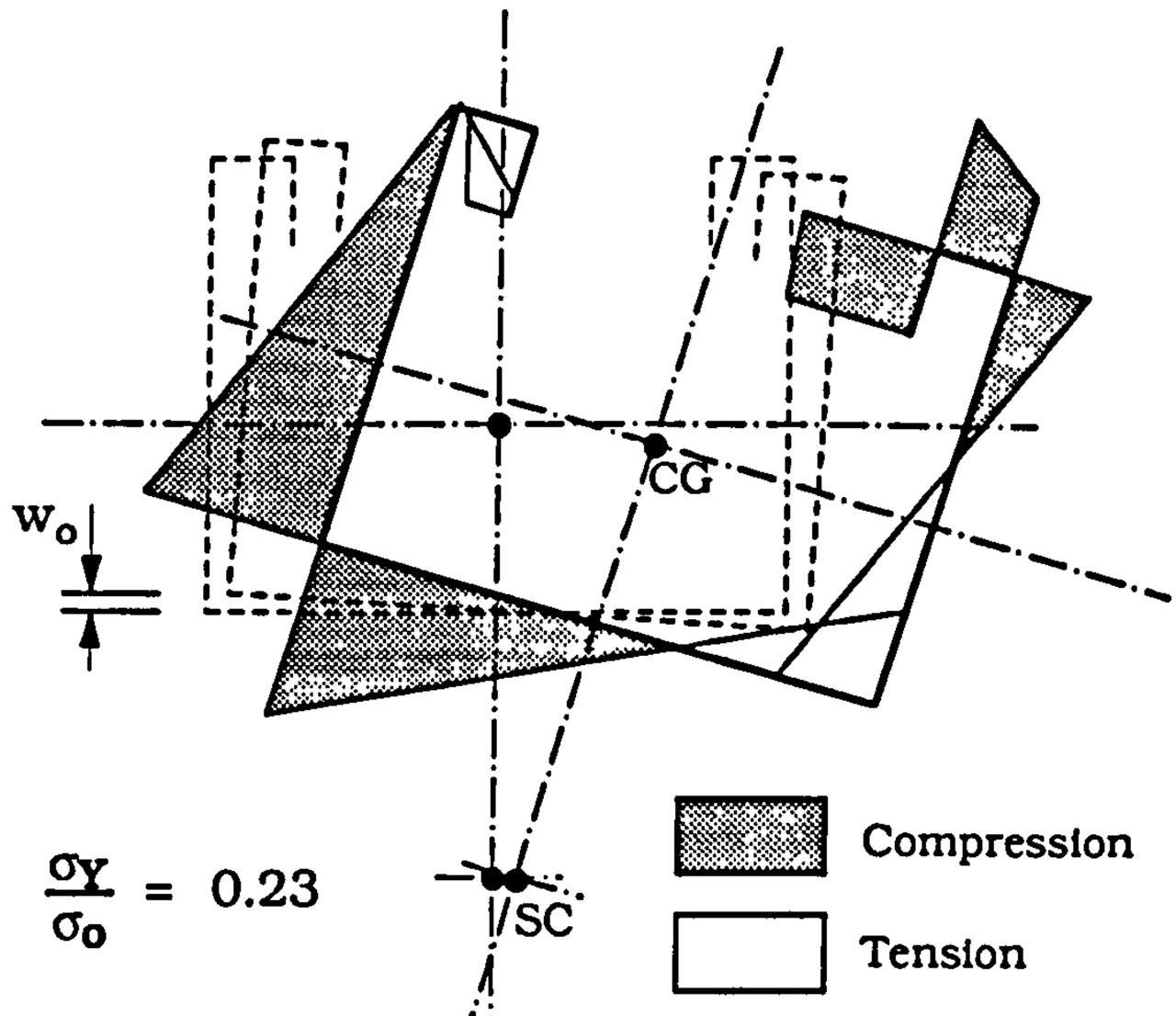


Figure 7.12 Stress Distribution and Displacements at First Surface Yield (Eqns 7.42 to 7.48)

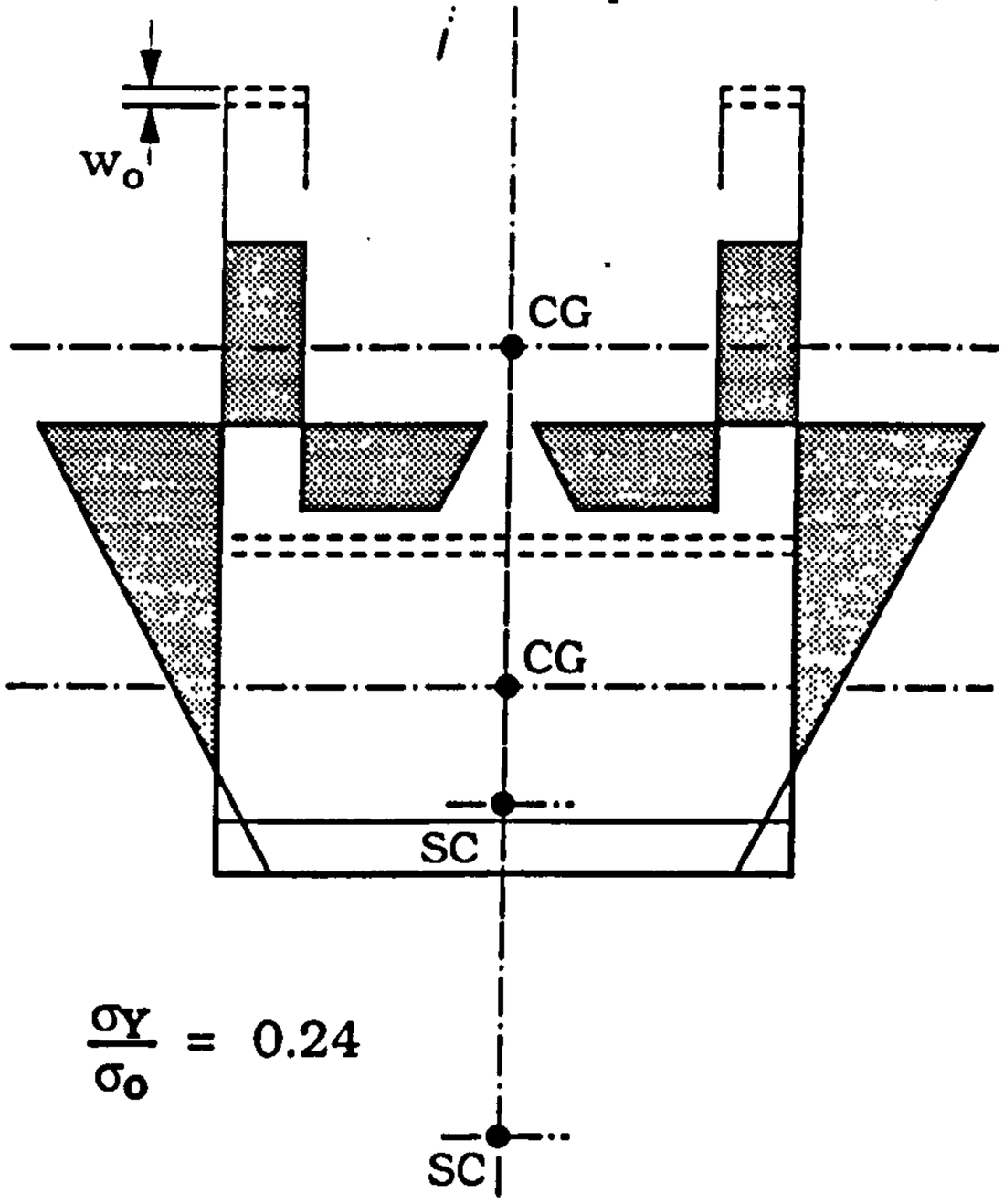


Figure 7.13 Stress distribution given by Perry equation with P_{TF} substituted for P_E

B = 122mm, D = 97mm, B_L = 17, D_L = 18.5, t = 3.0mm,
L = 3000mm, σ_o = 390 N/mm^2

The point at which first yield occurs depends on the shape of the section. For the doubly lipped channel first yield will occur either at the web/table junction (point **d**, Figure 7.4) at an axial stress given by

$$\sigma_Y = \sigma_o - \frac{B\pi^2}{2L^2} E\,(v_{1T} + \theta_1 \bar{z}_{sc}) \tag{7.53}$$

or at the lip table/downturn junction (point **g**, Figure 7.4)

$$\sigma_Y = \sigma_o + \frac{\pi^2}{L^2} E\left[v_{1T}\left(\frac{B}{2} - B_L\right) - \left[(D - \bar{z}_{sc})\frac{B}{2} + (D + \bar{z}_{sc})B_L\right]\theta_1\right] \tag{7.54}$$

If first yield occurs at the web/table junction, then the total additional horizontal displacement v_1 may be expressed as

$$v_1 = (v_{1T} + \theta_1 \bar{z}_{sc}) \tag{7.55}$$

The total additional displacement v_1 for any σ_A/σ_{TF} may be expressed as

$$v_1 = \frac{v_o}{\left(1 - \frac{\sigma_A}{\sigma_{TF}}\right)} - v_o \tag{7.56}$$

where

$$v_o = v_{To} + v_{\theta o}$$

If $\sigma_A = \sigma_Y$, then Equation 7.53 can be rewritten as

$$\sigma_Y = \sigma_o - \frac{B\pi^2}{2L^2} E\left[\frac{v_o}{\left(1 - \frac{\sigma_Y}{\sigma_{TF}}\right)} - v_o\right] \tag{7.57}$$

and solving for σ_Y

$$\sigma_Y = \frac{1}{2}\left[(\sigma_o + \sigma_{TF} + \eta\sigma_{Ez}) - \left((\sigma_o + \sigma_{TF} + \eta\sigma_{Ez})^2 - 4\,\sigma_o\sigma_{TF}\right)^{1/2}\right] \tag{7.58}$$

where

$$\eta = \frac{v_o B}{2 r_z^2}$$

Equation 7.58 gives the average axial stress to cause first yield at the web/table junction. The equation has the same form as Equation 7.31 if $\alpha = 1.0$ and if σ_{TF} is substituted for σ_T

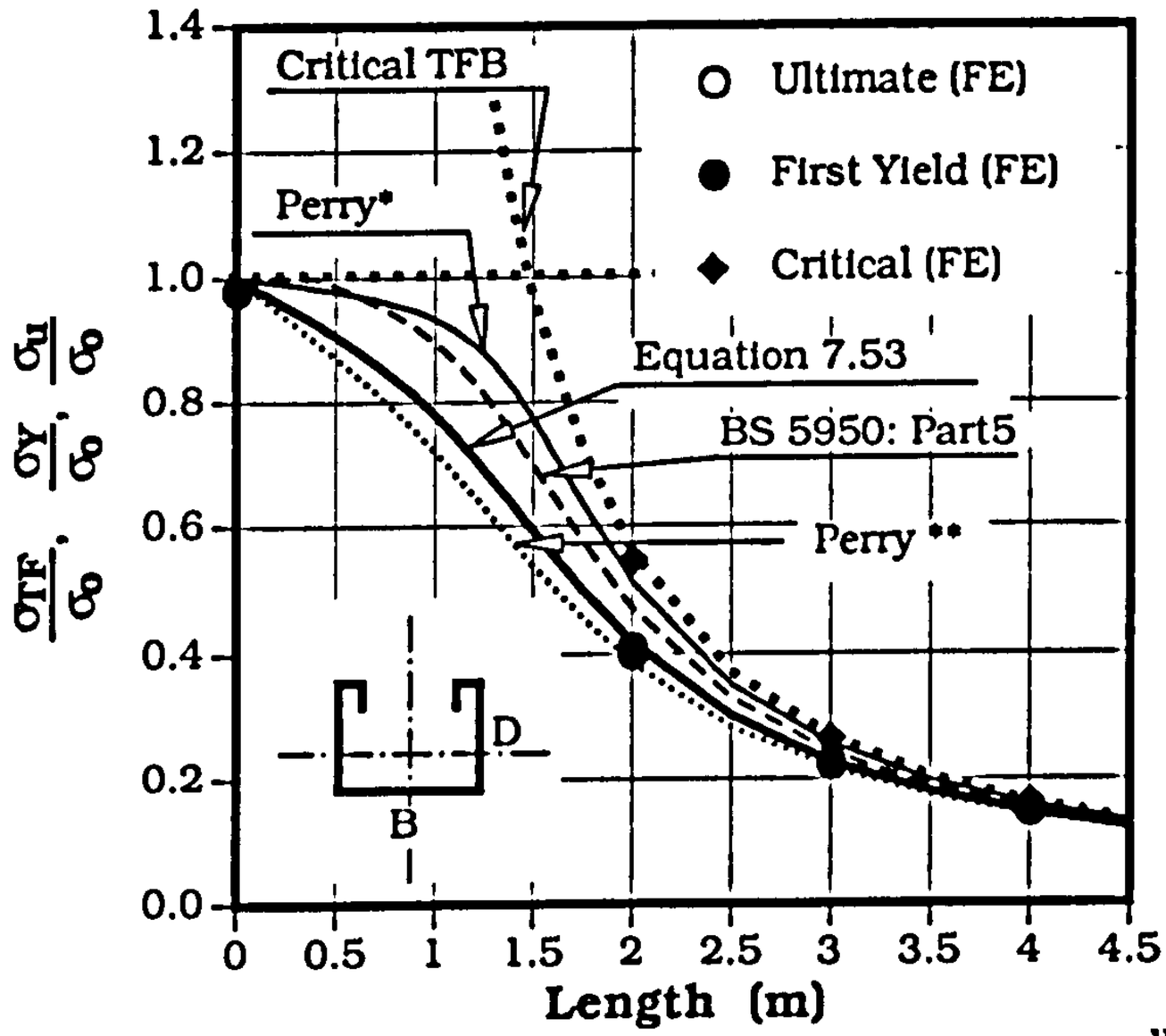
If η' is substituted for η, where

$$\eta' = \frac{\sigma_{Ez}}{\sigma_{TF}} \eta \qquad (7.59)$$

Then Equation 7.58 becomes

$$\sigma_Y = \frac{1}{2}\left[(\sigma_o + (1 + \eta')\sigma_{TF}) - \{(\sigma_o + (1 + \eta')\sigma_{TF})^2 - 4\,\sigma_o \sigma_{TF}\}^{1/2}\right] \qquad (7.60)$$

which is identical to the Perry equation for flexural buckling about the Z axis (major axis), with σ_{TF} substituted for σ_{Ez} and η' substituted for η. The critical flexural buckling stress σ_{Ez} would not of course be the smaller flexural buckling stress, which would be the usual design basis. It should also be pointed out that the position of first yield depends on the shape of the section and will not necessarily be at the web/table junction.



Perry*-σ_{TF} is substituted for σ_E in Equation 6.9 with $\eta = \frac{w_o \bar{z}_{max}}{r^2}$

Perry**-σ_{TF} is substituted for σ_E in Equation 6.9 with $\eta = \frac{w_o \bar{z}_{max}}{r^2}\frac{P_{Ez}}{P_{TF}}$

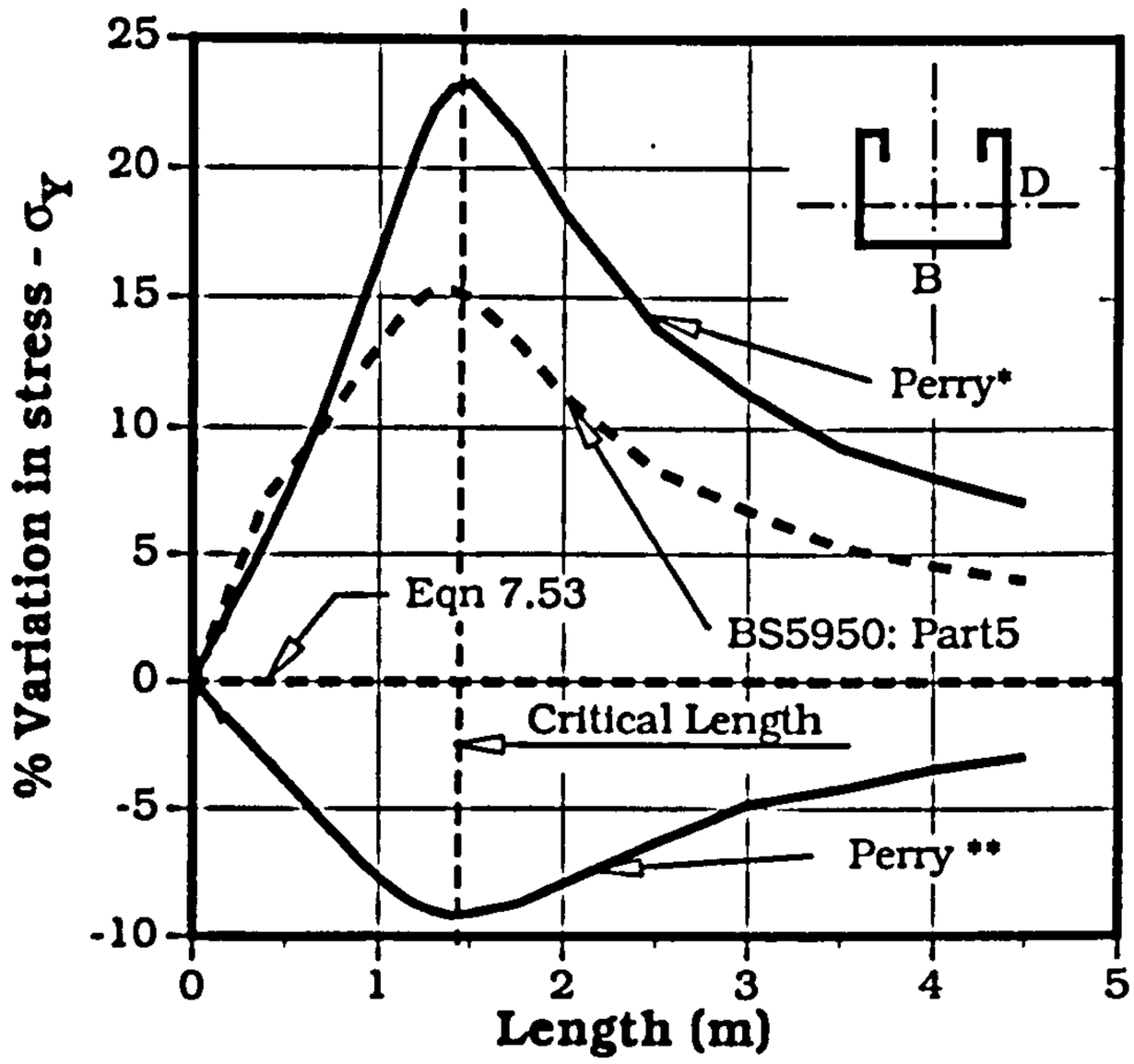
Figure 7.14 Average stress to cause first surface yield and failure according to Equation 6.9 Equation 7.53, BS5950: Part5 and finite element analysis.
B = 122mm, D = 97mm, B_L = 17mm, D_L = 18.5, t = 3.0mm,
σ_o = 390 N/mm^2 w_o = L/1000

The above reasoning explains the significance and validity limits of the substitution of η' for η. As already noted in section 7.3.1 (page 7-20), the multiplier should be

the ratio of a critical flexural buckling stress to the torsional-flexural buckling stress not the square root of the ratio, which is the current design practice.

When L = 3000mm, $\eta' = 5.8\eta$ and the original Perry equation with η' substituted for η, and σ_{TF} substituted for σ_{Ey} (Equation 7.60) then gives $\sigma_Y = 89 N/mm^2$, which is identical to the result obtained from Equation 7.53.

It should be noted that the imperfection implied by the minor axis flexural Perry equation is about the Y axis of the channel whereas in Equations 7.53 and 7.60 the imperfection is about the Z axis. Curves derived according to the original Perry equation (Equation 6.9), with σ_{TF} substituted for σ_{Ey} (Perry*), and the Perry equation with σ_{TF} substituted for σ_{Ey} and η' given by Equation 7.59 (Perry**), in which the constant η is assumed to be have an initial imperfection about the Y axis, are included in Figures 7.14 to 7.16. Figure 7.14 shows the variation of average stress to cause first yield, σ_Y, given by Equation 7.53 and BS 5950: Part5 (1987) with length, for the doubly lipped channel shown in Figure 7.4.



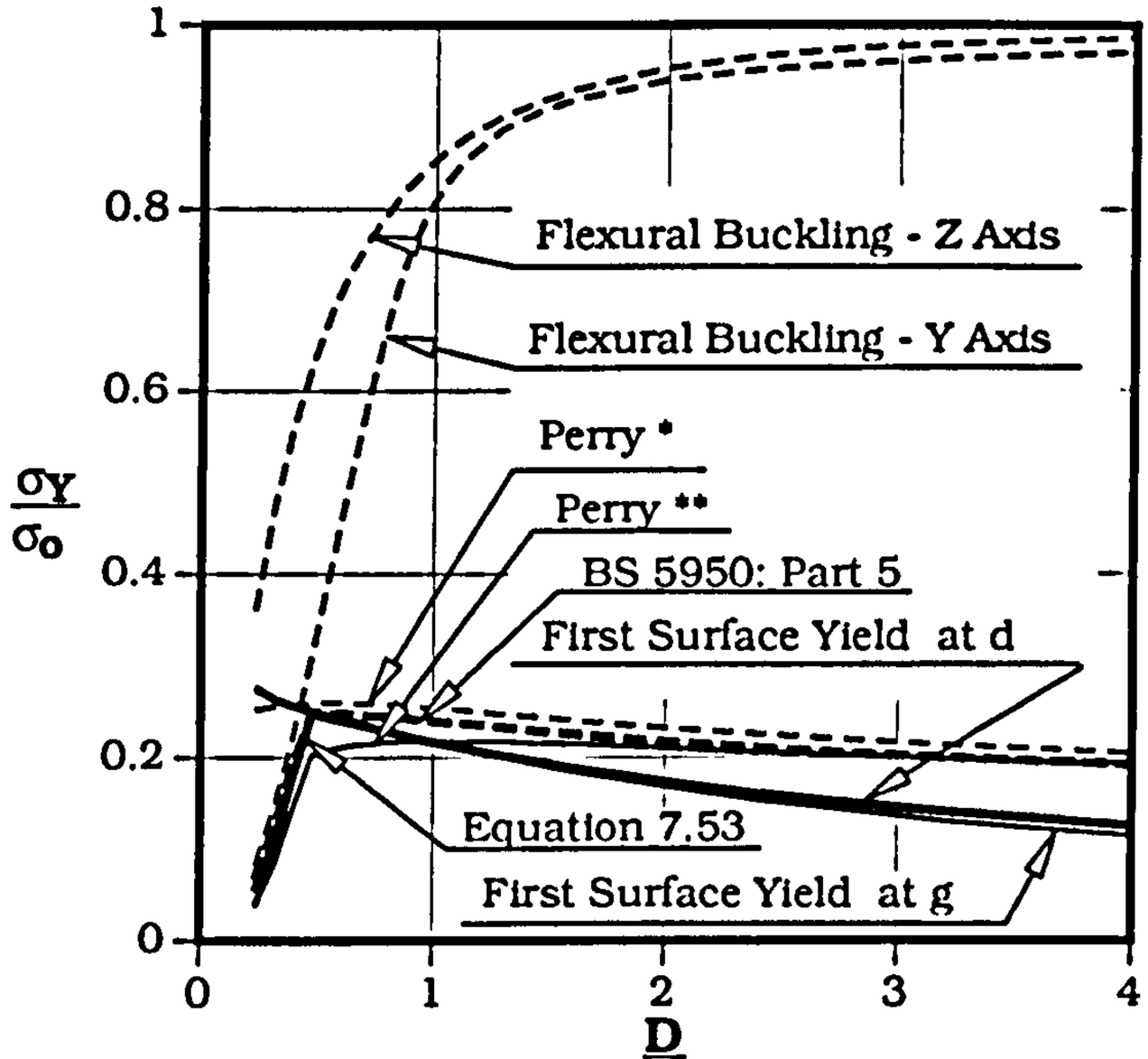
Perry*-σ_{TF} is substituted for σ_E in Equation 6.9 with $\eta = \frac{w_o \bar{z}_{max}}{r^2}$

Perry**-σ_{TF} is substituted for σ_E in Equation 6.9 with $\eta = \frac{w_o \bar{z}_{max}}{r^2} \frac{P_{Ez}}{P_{TF}}$

Figure 7.15 Percentage variation in axial stress according to Equation 6.9 and BS5950: Part5 relative to Equation 7.53

B = 122mm, D = 97mm, B_L = 17mm, D_L = 18.5, t = 3.0mm, $\sigma_o = 390 N/mm^2$

The percentage variation in axial stress σ_Y given by Equations 7.53 relative to the axial stress given by substituting σ_{TF} for σ_{Ey} in the Perry equation for buckling about the minor axis and by BS 5950: Part 5 (1987), is shown in Figure 7.15. Perry* overestimates the first yield load by 23% when compared with Equation 7.53, while BS 5950 overestimates the first yield load by 15%. If σ_{TF} is substituted for σ_{Ey}, and η is multiplied by σ_{Ez}/σ_{TF}, then Perry** underestimates the first yield load by up to 9%.



Perry*-σ_{TF} is substituted for σ_E in Equation 6.9 with $\eta = \frac{w_o \bar{z}_{max}}{r^2}$

Perry**-σ_{TF} is substituted for σ_E in Equation 6.9 with $\eta = \frac{w_o \bar{z}_{max}}{r^2} \frac{P_{Ez}}{P_{TF}}$

Figure 7.16 Variation in axial stress σ_Y with depth given by Equation 6.9, BS 5950: Part 5 and Equation 7.53

B = 122mm, B_L = 17mm, D_L = 18.5mm, t = 3.0mm,

L = 3000mm, σ_o = 390 N/mm^2, w_o = L/1000

(Section assumed to remain fully effective)

The variation in average axial stress (assuming the section remains fully effective) to cause first surface yield σ_Y, with D/B, for L = 3000mm is shown in Figure 7.16. It can be seen that for sections where D/B > 1.0, first yield occurs at the lip table/downturn junction. For this particular cross-section the difference in the average axial stress to cause first yield at either point **d** or **g** on the cross-section is small.

If first yield occurs at the table/web junction, then it is possible to estimate the ultimate torsional-flexural resistance from either Equation 7.53 or 7.60. These equation leads to an over estimation of the torsional-flexural resistance when $D/B \geq 2$. The average axial stress to cause first yield would be overestimated by 2%, while this increases to about 10% for $D/B = 5$. However, from Figure 7.15 it can be seen that this assumption is conservative when compared to the Perry* formulation and BS 5950: Part 5 (1987). In practice, D/B is unlikely to be greater than 1.0. It should not be assumed that the above criteria will apply for all channel proportions.

The value of σ_Y depends on the values of θ_o and v_o. Comparisons with existing methods also depend on the interpretation of the tolerance specifications. If for example, the Perry formulation for flexural buckling were applied using the imperfection assumed for the torsional-flexural analysis (Equations 7.49), for which the flexural imperfections at the centroid are $w_o = 0$, $v_o = L/3000$, flexural buckling would occur about the major axis. First yield due to flexural buckling would occur at $\sigma_Y = 312$ N/mm^2. If σ_{TF} is substituted for σ_{Ez}, the value of σ_Y for torsional-flexural buckling would be 102 N/mm^2.

7.3.3 NON-LINEAR ELASTO-PLASTIC ANALYSIS OF IMPERFECT MEMBERS

A series of non-linear elasto-plastic analyses were carried out to determine the ultimate torsional-flexural buckling capacity of various lengths of channel section. The finite element mesh used for this series of analyses is shown in Figure 7.6. The boundary conditions adopted for the critical buckling analysis were also employed for the non-linear elasto-plastic analysis.

The lowest critical torsional-flexural buckling mode for each length was scaled to provide initial deformations in accordance with the assumed theoretical imperfections described in the previous section. The vertical imperfection w_o at the web/table junctions was set to $\pm$ L/1000 in all cases. Numerical solutions were obtained for the three lengths of member, 2000mm, 3000mm and 4000mm.

The variation in rotation θ about the shear centre, and the translation v_T, with load, obtained from the numerical analysis, are compared with values given by Equations 7.35 and 7.36 in Figure 7.17, for L = 3000mm.

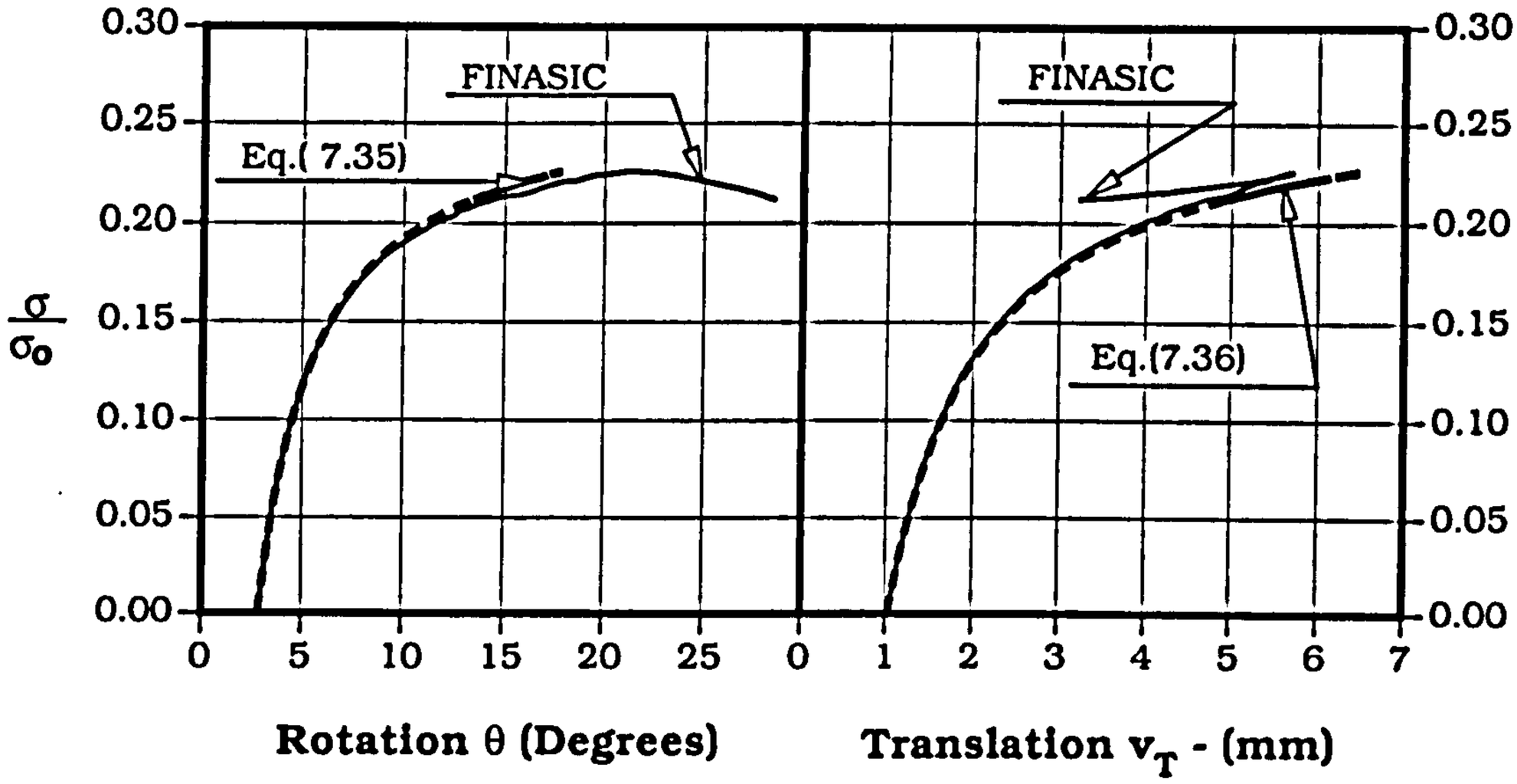


Figure 7.17 Rotation and translation given by Young's equation and by FE analysis

B = 122mm, D = 97mm, B_L = 17mm, D_L = 18.5mm, t = 3mm

L = 3000mm, σ_o = 390 N/mm^2

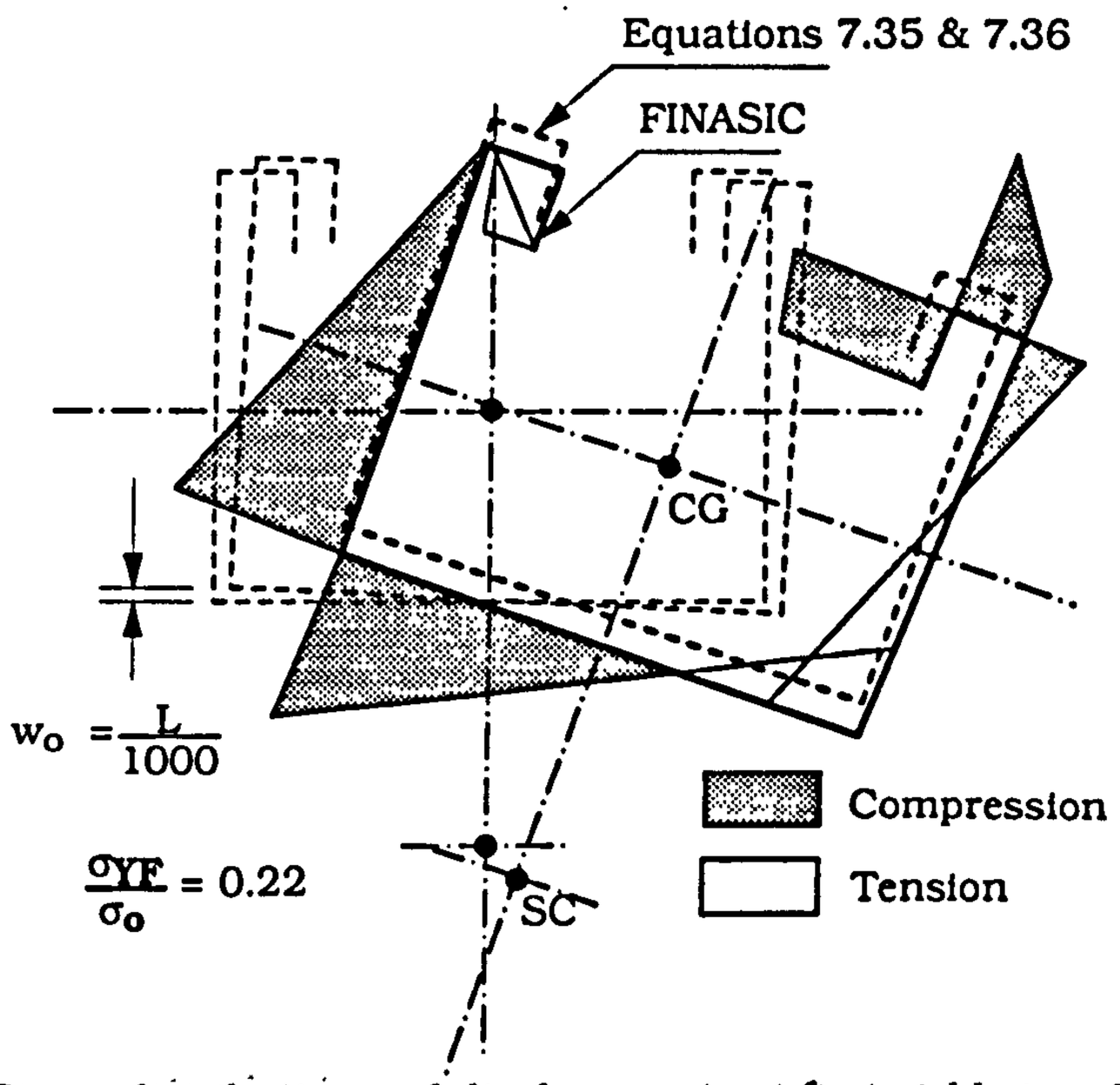


Figure 7.18 Stress distribution and displacements at first yield given by FE analysis

B = 122mm, D = 97mm, B_L = 17.5mm, D_L = 18mm, t = 3mm

L = 3000mm, σ_o = 390 N/mm^2

The magnitudes of the assumed initial imperfections can be seen in these diagrams. Agreement is good even though the total rotation θ at first yield is 17°. The stress distribution given by finite element analysis for L = 3000mm, at first yield is shown in Figure 7.18, which also compares the deformations with Equations 7.35 and 7.36. The average axial stress σ_Y = 87 N/mm^2, compared to σ_Y = 89 N/mm^2 given by Equation 7.60. The finite element solutions confirm that for this particular cross-section, first surface yield occurs at the web/table junction. In all three cases analysed, first yield was followed closely by failure. (Table 7.4)

Figure 7.18 shows that the cross-section also deforms. This can be attributed to the magnification of the v displacement of the lip with the higher axial compressive stress. The preferred half wave length of lip buckling for the 3000mm long, 3mm thick channel is 725mm, but the assumed imperfections and the subsequent translation and rotation of the section impose a predominantly single half wave deflection of the lip. The magnification of this mode depends on the critical lip buckling stress for a single half wave, which is much greater than for four half waves, 3818 N/mm^2 compared to 445 N/mm^2 (see Figure 5.4).

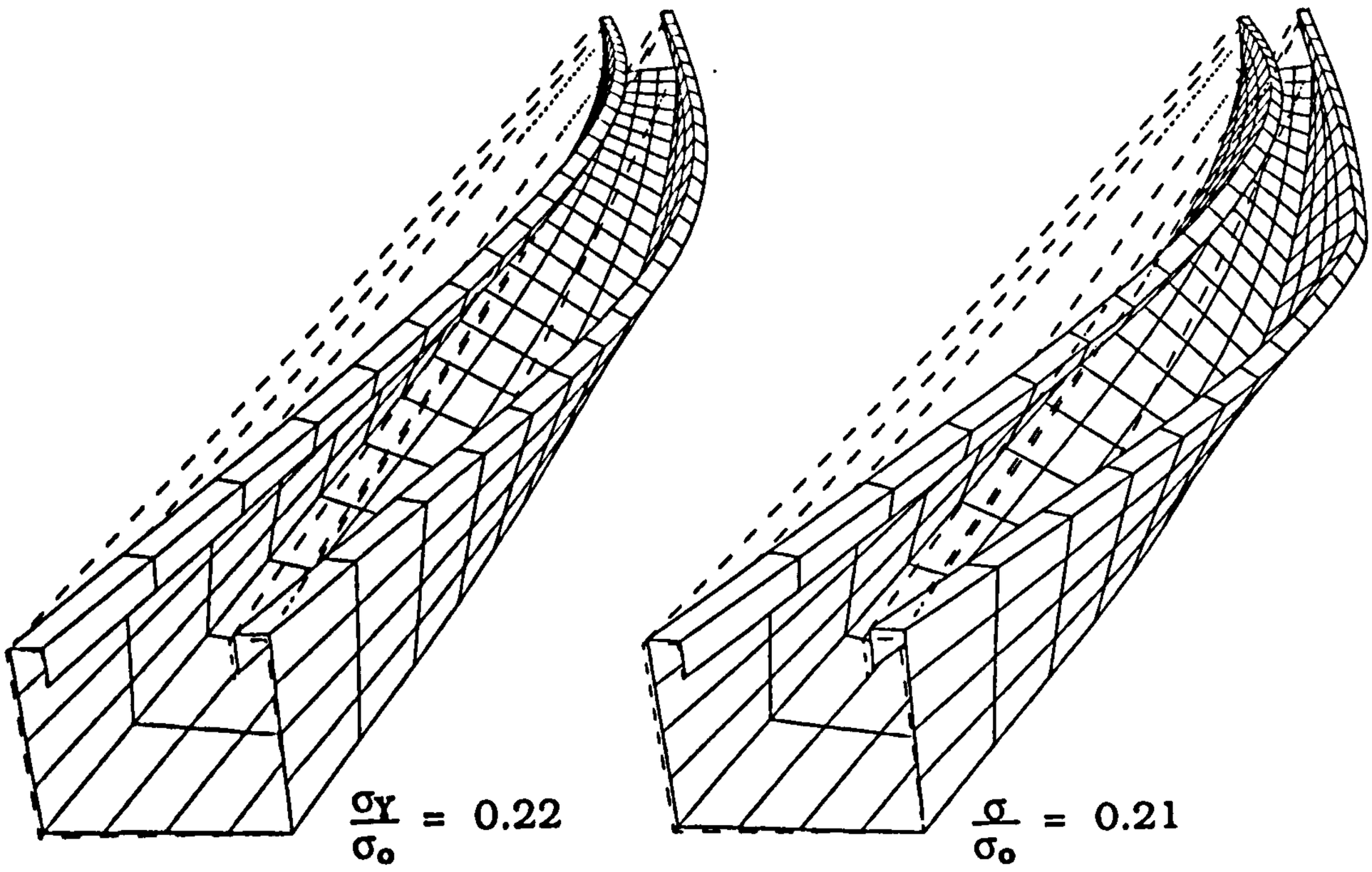


Figure 7.19 Torsional-flexural buckling deformations at failure and post failure
B = 122mm, D = 97mm, B_L = 17mm, D_L = 18.5mm, t = 3.0mm,
L = 3000mm, σ_o = 390 N/mm^2

However, the lip buckling deformations also depend on the deformation which in this case results from the rotation of the section, and becomes much larger than v_o at the lip. On the other hand the lip buckling resistance is increased by the increased deformational stiffness caused by unequal axial forces in the lips. Figure 7.19 shows the torsional-flexural buckling deformations at failure and post failure for a 3000mm length of section.

Length (m)	Method	$\frac{\sigma_Y}{\sigma_o}$	$\left(\frac{\sigma}{\sigma_o}\right)_d$	$\left(\frac{\sigma}{\sigma_o}\right)_g$	$\frac{\sigma_Y}{\sigma_Y(\text{ FINASIC})}$	$\frac{\sigma_u}{\sigma_Y}$
2.0	**FINASIC**	0.40	0.99	1.00	1.00	1.02
	Eq 7.30a	0.42	1.00	0.96	1.05	
	PERRY*	0.51	0.15	1.00	1.28	
	PERRY**	0.39	-0.06	1.00	0.98	
	BS 5950†	0.47	0.08	1.00	1.18	
	BS 5950‡	0.42	-0.01	1.00	1.05	
3.0	**FINASIC**	0.22	1.00	0.93	1.00	1.01
	Eq 7.30a	0.23	1.00	0.91	1.05	
	PERRY*	0.26	-0.29	1.00	1.18	
	PERRY**	0.22	-0.36	1.00	1.00	
	BS 5950†	0.25	-0.31	1.00	1.14	
	BS 5950‡	0.23	-0.34	1.00	1.04	
4.0	**FINASIC**	0.15	1.00	0.84	1.00	N/A.
	Eq 7.30a	0.15	1.00	0.86	1.00	
	PERRY*	0.16	-0.47	1.00	1.07	
	PERRY**	0.14	-0.49	1.00	0.93	
	BS 5950†	0.15	-0.48	1.00	1.00	
	BS 5950‡	0.15	-0.48	1.00	1.00	

A negative sign indicates a tensile stress * σ_{TF} substituted for σ_{Ey} in Eqn 6.9, with η given by Equation 7.52b. ** σ_{TF} substituted for σ_{Ey} in Eqn 6.9 with η' substituted for η. † σ_{TF} substituted for σ_{Ey} with η given by Equation 7.52a

‡ σ_{TF} substituted for σ_{Ey} with $\frac{\sigma_{Ey}}{\sigma_{TF}} L$ instead of $\left(\frac{\sigma_{Ey}}{\sigma_{TF}}\right)^{1/2}$ in Eqn. 7.52a

Table 7.4 Comparison between FE analysis and existing and proposed methods
B = 122mm, D = 97mm, B_L = 17mm, D_L = 18.5mm, t = 3.0mm, σ_o = 390 N/mm^2

For the lengths investigated it would seems that some interaction between lip and overall buckling does take place, because lateral displacement of the more

compressive lip is observed in the numerical analysis. Further numerical investigation into the interaction between lip and torsional-flexural buckling is necessary before the effect can be evaluated. A comparison between results obtained from the non-linear elasto-plastic analyses and various design methods is given in Table 7.4

7.3.4 EXPERIMENTAL BEHAVIOUR

Experiments on concentrically loaded doubly lipped channel sections, 1.5mm and 3.0mm thick were carried out to observe the torsional-flexural buckling behaviour, and to determine the failure load. The axial load was applied to the ends of the three span channel through thick end blocks attached to crossed knife edges, which permitted flexure about both the Y and Z axis, but which prevented torsional rotation, warping, and rotation of the lip in plan at the end section. The member was located in the end blocks such that the resultant axial load passed through the effective neutral axis of the cross-section. Prior to testing, each specimen was carefully aligned both vertically and horizontally along it's length to eliminate any eccentricity. By using three spans, the effect of warping restraint at the ends of the member on the torsional-flexural buckling behaviour of the central span is much less than it would be if a single span were loaded through rigid flat ends.

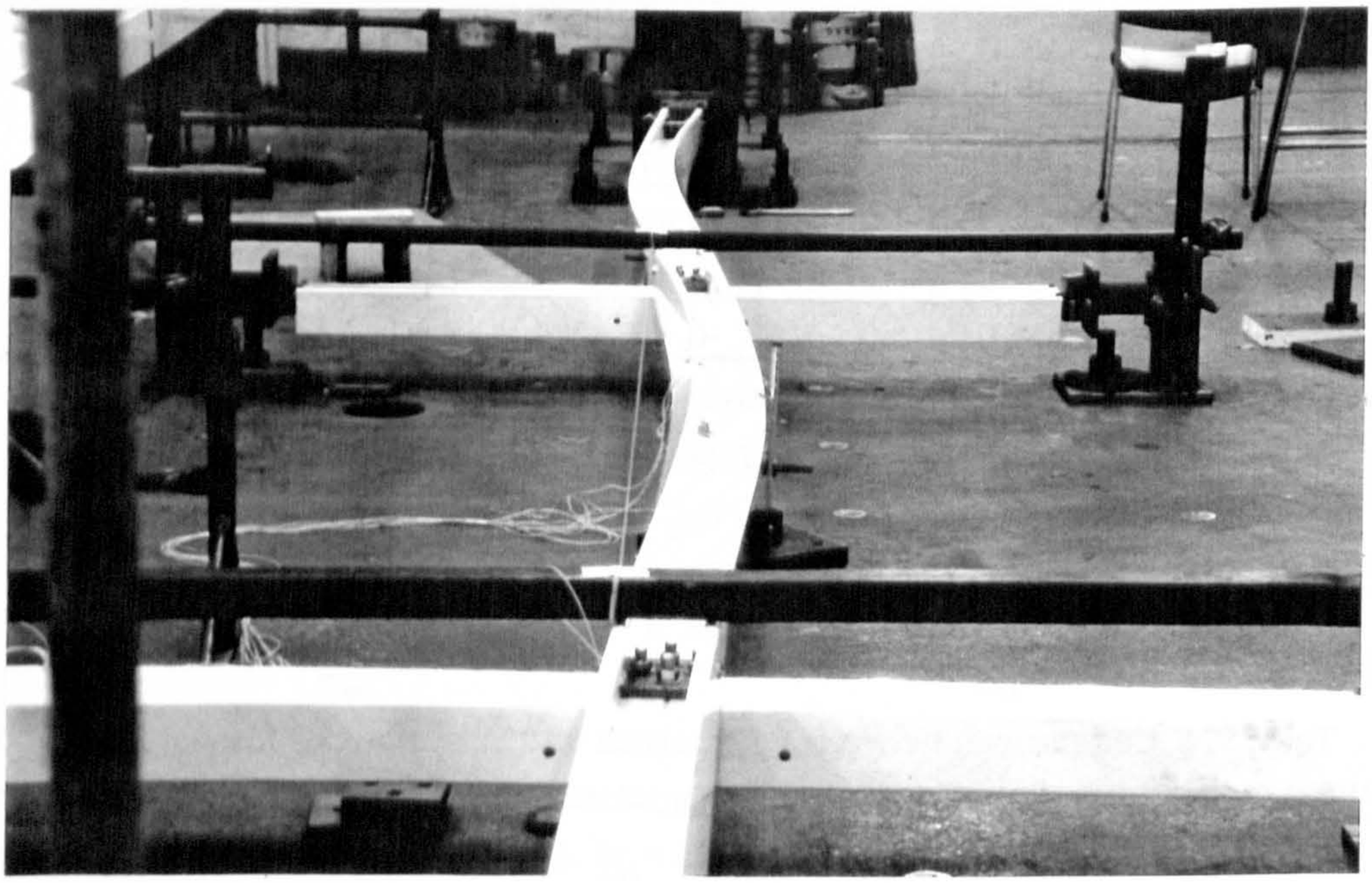
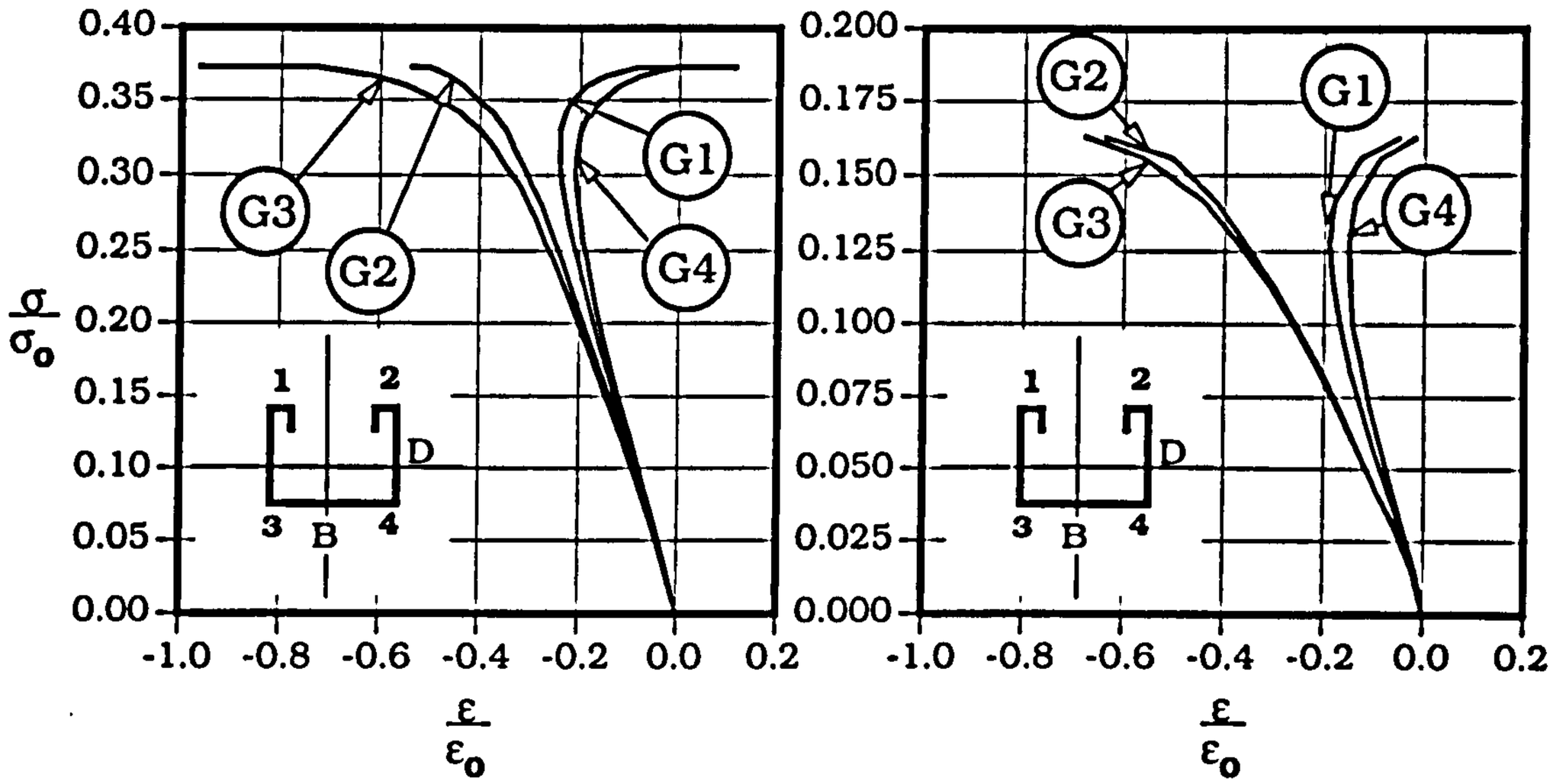


Figure 7.20 3 x 3 metre chord member.
Incipient torsional-flexural buckling failure



3mm section/15mm plates/sleeved 1.5mm section/10mm plates/sleeved

Figure 7.21 Variation in axial strain with load measured at mid span, of central span, for the 3 x 3 span, 9 metre column tests

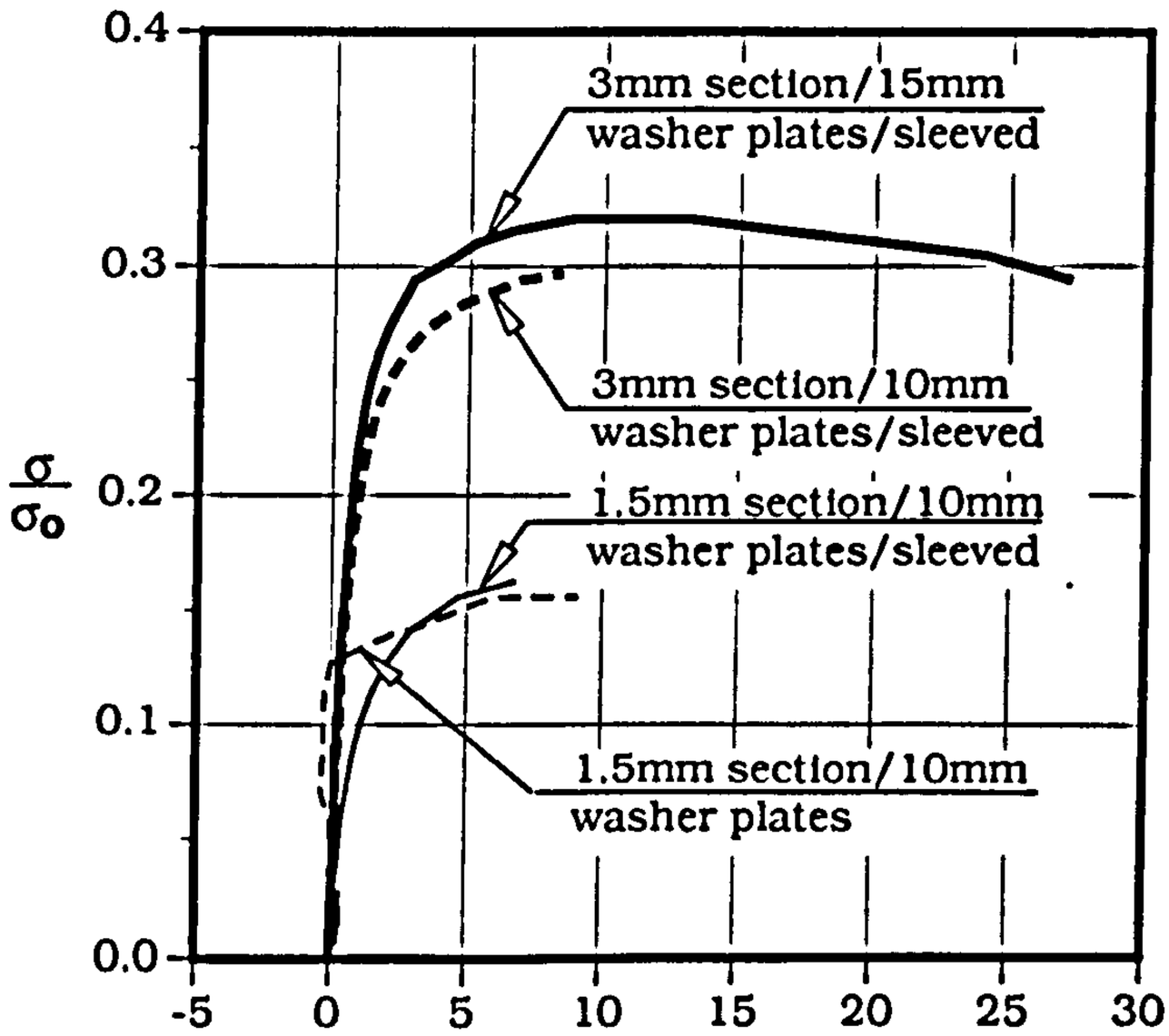


Figure 7.22 Variation in rotation with load measured at mid span, of central span, for 3 x 3 span, 9 metre column tests

A 3 x 3 span, 9 metre column under concentric axial load, located in the test rig, is shown in Figure 7.20. The test arrangement chosen provided a means of assessing the torsional restraint provided by 10mm thick washer plates in a 1.5mm thick channel section and 15mm thick washer plates in a 3.0mm thick channels section. Axial strains and torsional rotations were measured at mid length of the central span. Figures 7.21 and 7.22 show the variation of strain and rotation with load for the tests carried out. The experimental results for the two 3 x 3 span, 9 metre column tests with 340 x 125, 3mm sleeve inserts, are given in Table 7.5.

t_s (mm)	t_w (mm)	σ_o N/mm^2	P_{exp} (kN)
1.5	10	364	71
3.0	15	489	176

Table 7.5 Test Results 3 x 3 span, 9 metre column tests torsional-flexural buckling resistance

7.3.5 EFFECT OF WARPING RESTRAINT ON THE ULTIMATE TORSIONAL-FLEXURAL BUCKLING RESISTANCE .

The torsional effective length is a function of the warping restraint provided at the ends of the member, and this can be taken into account in determining the torsional-flexural buckling resistance of a member. For a 3000mm length of 3mm thick doubly lipped channel, the average axial stress to cause first surface yield given by Equation 7.60 for $L_{eff} = 0.5L$, that is for full warping restraint is σ_Y = 211 N/mm^2 compared to σ_Y = 90 N/mm^2 when $L_{eff} = L$. The degree of warping restraint present in different types of end connection depends on several factors. In the absence of any quantified estimate of warping restraint, it should be assumed that $L_{eff} = L$.

In the AISI specification, no allowance is made for warping restraint, and so the torsional-flexural buckling resistance of a section is assessed on the assumption that $K_w = 1.0$ in Equation 7.11. In the UK, prior to BS5950: Part5 (1987) the design rules given for torsional-flexural buckling (BS 449: Part 2: Addendum No.1 1975) were based on full warping restraint i.e. $K_w = 4.0$ (Rhodes 1991). The

recommendations were in agreement with the bulk of column tests results published by Chilver (1951) and Harvey (1953). It should be noted that the tests were generally carried out by loading the columns through heavy end plates, which prevented warping of the end section, and as a result the effects of torsional-flexural buckling were minimized. Full warping restraint is very unlikely to occur in practice. On the other hand the assumption of zero warping restraint may be conservative in most practical situations.

BS 5950: Part 5 (1987) recommends the use of a general torsional effective length of 0.7L (K_W = 2.0). EC3: Part 1.3 (1992), clause 5.2.1 acknowledges the possibility of warping restraint by allowing for a torsional effective length, but does not offer any guidance.

In this section a proposed design method for determining the warping restraint provided by the washer plates in the diagonal on square frame connection and chord continuity is given.

K_W For Connection Torsional Stiffness

In order to establish the effect of variations in warping restraint on the critical torsional-flexural buckling resistance a series of finite element solutions were obtained. Warping restraint was induced at the ends of a 3000mm long, 3mm thick channel section, by varying the thickness (t_e) of the table elements at each end over a length approximating to the length of the washer plates. The element thickness t_e given by Equation 7.61 was taken to represent the sum of the torsional stiffness of the washer plates and of the table acting separately. No account of the sleeve inserts is made in determining t_e.

The equivalent thickness was taken to consist of two washer plates and the table thicknesses of both orthogonally intersecting chords such that

$$t_e = (2\,t_w^3 + 2\,t_s^3)^{1/3} \qquad (7.61)$$

where

t_e equivalent element thickness
t_w washer plate thickness
t_s thickness of channel table

The finite element results for various washer plate thickness are given in Table 7.6. for which the values of K_w have been obtained by equating Equation 7.18 to the finite element results and solving for K_w.

t_w (mm)	P_{TF} (FINASIC) (kN)	P_T (FINASIC) (kN)	K_w
0	120.3	137.7	1.00
5	127.7	147.6	1.07
10	162.4	196.5	1.40
15	209.4	271.7	2.11
20	244.6	336.0	2.65
30	277.0	403.2	3.22
40	288.3	428.8	3.43
∞	293.5	441.1	3.54

Table 7.6 Variation in warping restraint K_w with t_w for 122x97x17x18.5, 3mm thick doubly lipped channel section obtained from numerical analysis.

Assuming that the torsional stiffness in a connection affects the torsional-flexural buckling load of a member in the same way that the elastic rotational restraint effects the critical flexural buckling load of an axially loaded strut, then by analogy, the methods for determining the critical buckling load for elastically restrained columns described by Allen and Bulson (1980) can be employed to find the torsional effective length. Bulson equates the ratio of the stiffness of the elastic spring restraint at the end of the member to the flexural stiffness of the member, to a function involving the ratio of the critical buckling load (P_{cr}) for the restrained member to the Euler critical buckling load (P_E) of the same member.

$$\frac{K_R}{K_M} = -2\left(\frac{\pi\rho/2}{\tan(\pi\rho/2)}\right) \qquad (7.62a)$$

where

$$\rho = \left(\frac{P_{cr}}{P_E}\right)^{1/2} \qquad (7.62b)$$

and

K_R is the stiffness of the elastic rotational restraint

K_M is the flexural stiffness of the member, EI/L

P_{cr} is the buckling load of the restrained column

P_E is the Euler buckling load

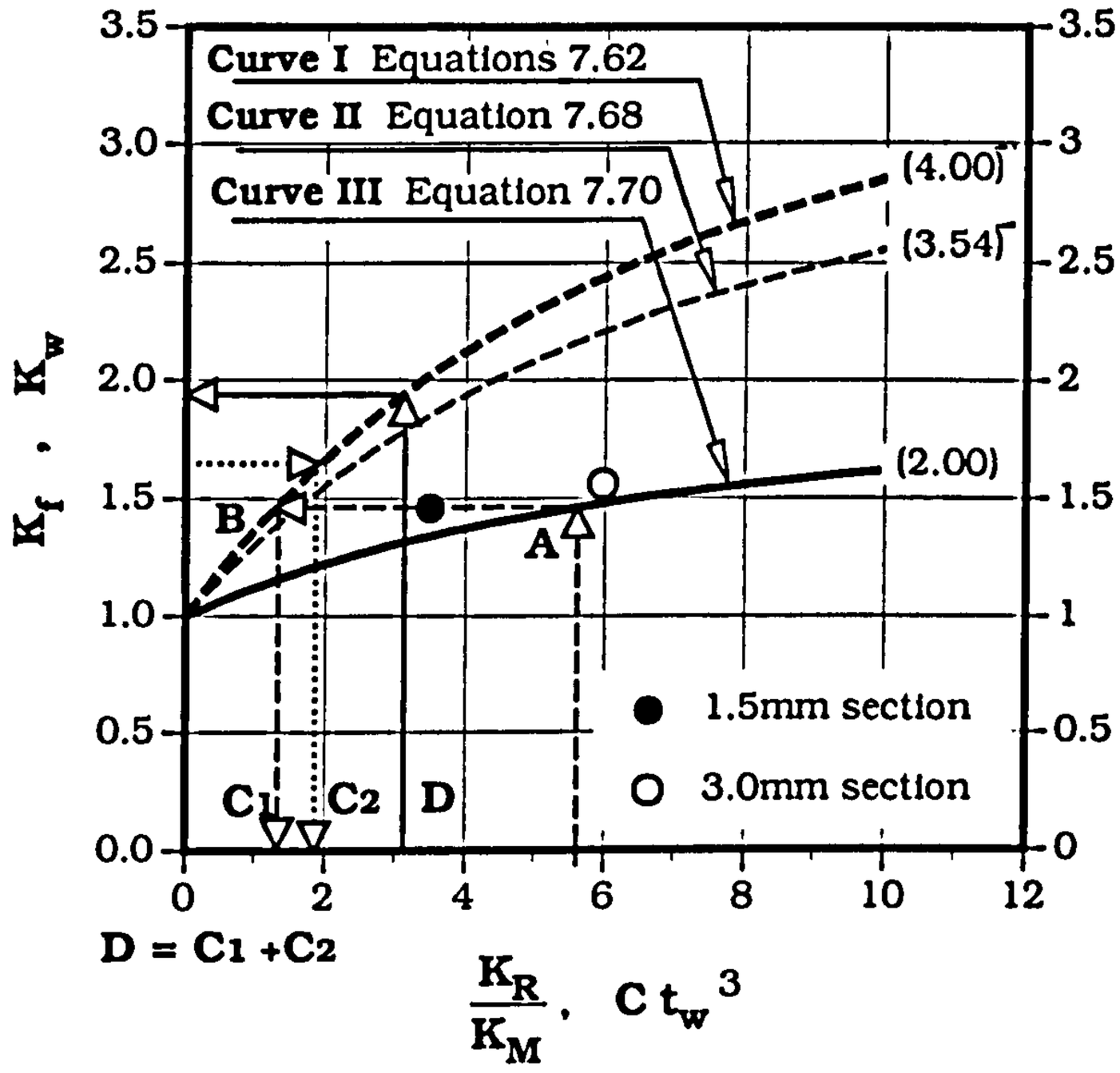


Figure 7.23 Comparison between proposed design curve III, Equations 7.62, 7.68 and 7.70 with 3 x 3 span, 9 metre experiments

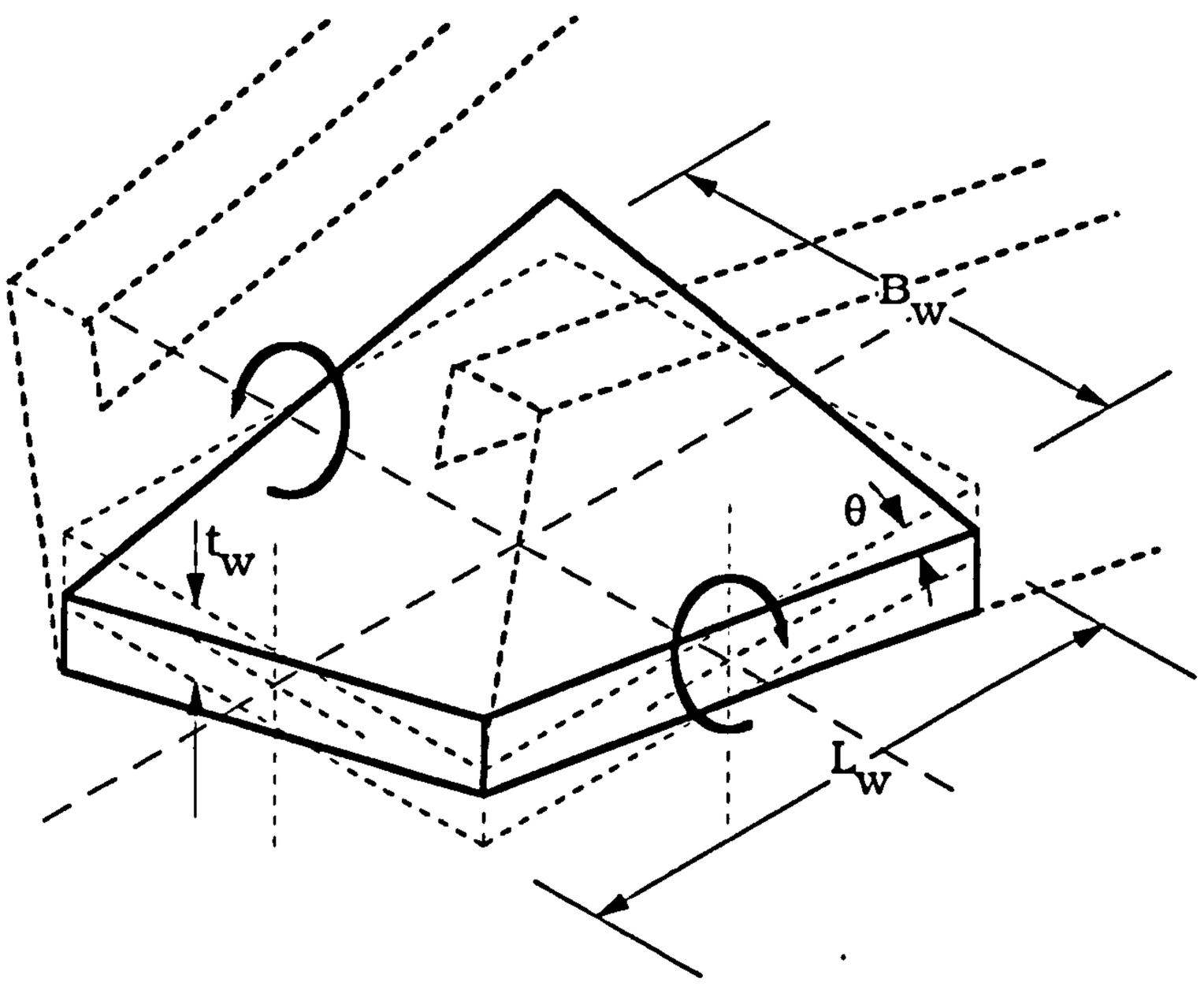


Figure 7.24 Torsional Deformation of Washer Plate

The critical load ratio ρ has a minimum value of 1.0 and is asymptotic to a value of 4.0, corresponding to a variation in effective length from 1.0L (simply supported end conditions) to 0.5L (full fixity) (**Curve I** -Figure 7.23). The increase in the critical torsional-flexural buckling load P_{TF} of the channel due to the torsional restraint provided by the washer plates and the table of the channel may then be estimated by analogy with Equation 7.62a. The connection stiffness ratio is

$$\frac{K_c}{K_T} = -2\left(\frac{\pi\,\rho/2}{\tan(\pi\,\rho/2)}\right) \qquad (7.63a)$$

where

$$\rho = (f(K_w))^{1/2} \qquad (7.63b)$$

and

K_c is the torsional stiffness of the connection

K_T is the torsional stiffness of the member

K_w is the warping restraint factor

The elastic torsional restraint provided by the washer plates can be considered to be equivalent to a rotational spring of stiffness K_c applied to each web of the channel at the ends of the member. The stiffness ratio is then the ratio of K_c to the torsional stiffness of the member K_T. If the washer plate shown in Figure 7.24 is assumed to stabilises two adjacent spans and that each joint consisted of two plates, then the torsional stiffness of the connection is given by

$$K_c = \frac{2\,\Omega\,G\,L_w t_w^3}{3\left(\frac{B_w}{2}\right)} \qquad (7.64)$$

The warping stiffness of the member K_T is given by

$$K_T = \frac{E\,C_w}{L\,r_o^2} \qquad (7.65)$$

The stiffness ratio is then

$$\frac{K_c}{K_T} = \frac{\frac{2\,\Omega\,G\,L_w t_w^3}{3\left(\frac{B_w}{2}\right)}}{\frac{E\,C_w}{L\,r_o^2}} = C\,t_w^3 \qquad (7.66)$$

Where the constant C is

$$C = \frac{4\,\Omega\, L\, r_o^2\, L_w}{3\, B_w\, C_w (1 + \nu)} \tag{7.67}$$

in which

B_w breadth of washer plate

L_w is the length of washer plate

Ω is the ratio of the length of the washer plate restraining one span to the actual length of washer plate (Ω may be reasonably taken to equal 0.5 for the particular connection being considered)

The results in Table 7.6 show that the warping restraint factor K_w corresponding to full torsional restraint of the table (i.e. torsional displacement prevented) is asymptotic to 3.54, equivalent to a reduction in torsional effective length from 1.0L to 0.53L. The torsional effective length can be further reduced to 0.5L if inplane longitudinal displacements are prohibited from occurring in the web, lip table and lip downturn of the channel.

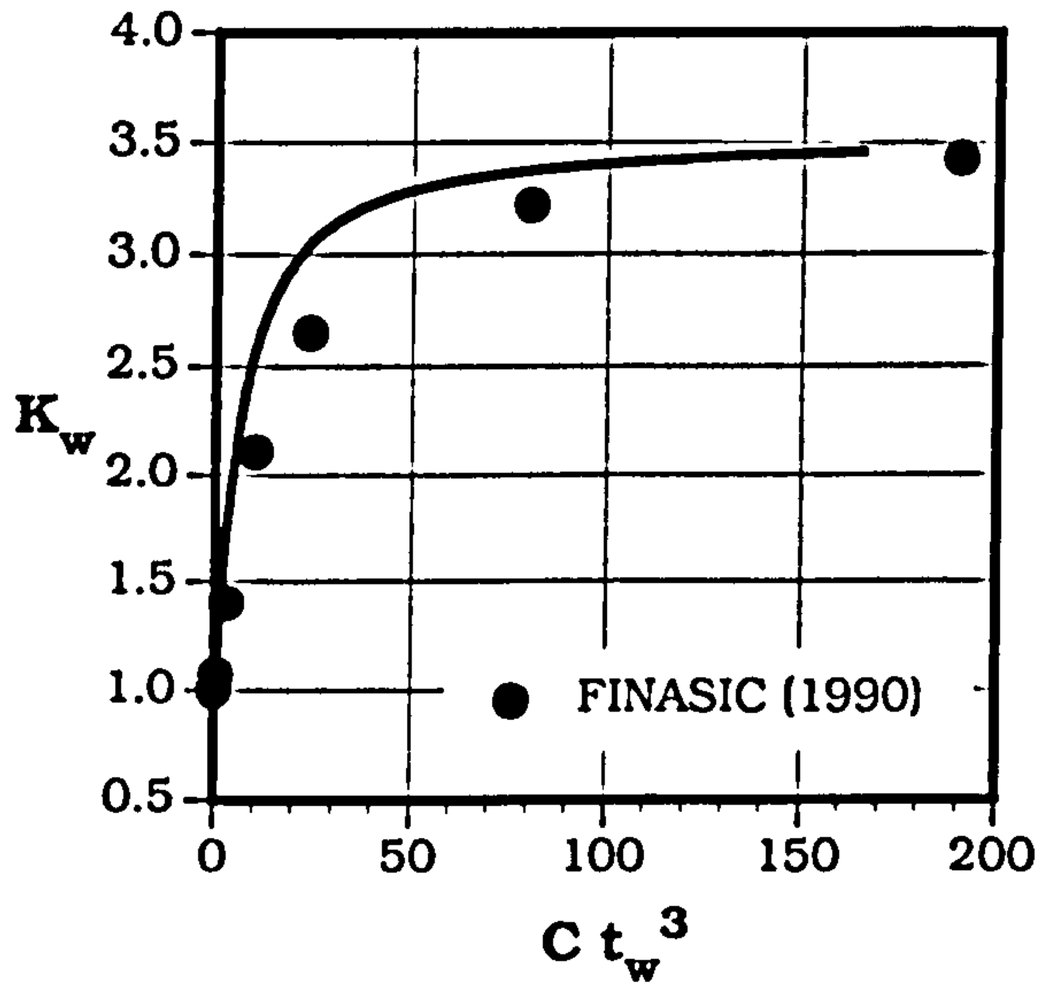


Figure 7.25 Comparison between numerical results and Equations 7.63a and 7.68

A function for ρ which satisfies the limits obtained from the finite element analysis such that

$$\rho^2 = 1 \text{ when } K_w = 1$$

and

$$\rho^2 = 4 \text{ when } K_w = 3.54$$

is given by

$$\rho = (1.1811\, K_w - 0.1811)^{1/2} \qquad (7.68)$$

A comparison between the numerical results and Equation 7.63a with ρ given by Equation 7.68 is shown in Figure 7.25 (**Curve II**-Figure 7.23). It should be remarked that Equation 7.68 has been obtained for a perfect connection where the "washer plate" extends over the full width of the member and is fully connected to the webs. In practice the washer plates stop short of the webs, and the corner of the channel is curved.

K_w For Continuous Members With End Warping Restraint.

The torsional-flexural buckling resistance of the critical central span in a three span continuous member is influenced by the end conditions, and the load level in each of the spans. By analogy with the axially loaded three bay chord member discussed in Chapter Two, K_w for the central span may be obtained from Figure 2.8 for simply supported end conditions, and Figure 2.9 for fully fixed end conditions.

K_w For Combined Connection Torsional Stiffness And End Warping Restraint.

In order to be able to interpret accurately the experimental results, a method for determining K_w for the combined effects of the torsional stiffness of the connection and end boundary conditions is needed. The two effects can be combined to give a single value of K_w. This is possible by transforming the connection stiffness ratio K_c/K_T to an equivalent member flexural stiffness ratio K_R/K_M.

The connection stiffness ratio obtained from Equation 7.66 is projected vertically from the abscissa to point **A** on **Curve III** (Equation 7.70). A line is then taken horizontally from point **A** to point **B** on **Curve I** (Equations 7.62). The equivalent member stiffness ratio is then obtained by projecting down to point **C1** on the abscissa of Figure 7.23.

The reduction in effective length due to the different loads in each span and end conditions of the member may be obtained from Figures 2.8 or 2.9. The flexural stiffness K_R/K_M ratio, point **C2** can be then obtained directly from **Curve I** in Figure 7.23, where

$$K_f = \left(\frac{L}{L_E}\right)^2 \qquad (7.69)$$

The total flexural stiffness ratio is the summation of the two individual stiffnesses **C1** and **C2**. The warping restraint factor K_w applicable to the central span is then found by projecting the total flexural stiffness ratio, from point **D** (where D = C1+C2) vertically to **Curve I** and then horizontally to ordinate axis of Figure 7.23. The torsional effective length can then be found from Equation 7.69.

Equations 7.63 and Equation 7.68 were modified on the basis of experimental results (Table 7.5). **Curve II** in Figure 7.23 is observed to overestimate the reduction in effective length when compared with experimental results. An empirical fit to the test results was obtained by setting the asymptotic value to 2.0.

The critical load ratio ρ is then

$$\rho = (3K_w - 2)^{1/2} \qquad (7.70)$$

The torsional effective lengths for the central span of the bottom chord lips down channel, obtained from Figure 7.23, using the method outlined in section 7.3.4, for the 1.5mm thick section with 10mm washer plates, and the 3.0mm thick section with 15mm plates are $K_w = 1.73$ and $K_w = 1.87$ respectively. The failure stress given by Equation 7.70 for a 1.5mm thick section where $K_w = 1.0$, and $\sigma_o = 364$ N/mm^2, is $\sigma_Y = 76$ N/mm^2, compared to $\sigma_Y = 110$ N/mm^2 when Kw = 1.73. Similarly, for a 3mm thick section, when $K_w = 1.0$, and $\sigma_o = 490$ N/mm^2, the average stress to cause first yield is $\sigma_Y = 93$ N/mm^2, compared to $\sigma_Y = 144$ N/mm^2 when $K_w = 1.87$.

7.5 PROPOSED DESIGN METHOD

In section 7.3.2 it was shown that the torsional-flexural buckling resistance of a 3mm thick doubly lipped channel section obtained from Equation 7.60 was in good agreement with finite element results. Before any rational comparison between the 9 metre column experimental results and predicted failure loads given by Equation 7.60 can be made some modifications are needed to account for interaction between local element buckling, lip buckling and overall torsional-flexural buckling.

The interaction between local, lip and overall buckling can be taken into account by determining the effective area of the section, using the method described in Chapter Four, and limiting the short strut capacity to the product of the effective cross-sectional area A_{eff}, and yield stress σ_o. Lip buckling can be taken into account by limiting the short strut capacity to the product of the lip buckling stress σ_{uL} obtained from Equations 5.16, and the corresponding effective cross-sectional area.

The ultimate torsional-flexural buckling stress, based on first yield occurring at the web/table junction, taking into account the effects of local element and lip buckling can be found from

$$\sigma_{TFY} = \frac{1}{2}\left[Q\sigma_d + (1+\eta')\sigma_{TF} - \left\{(Q\sigma_d + (1+\eta')\sigma_{TF})^2 - 4Q\sigma_d\sigma_{TF}\right\}^{1/2}\right] \quad (7.71)$$

where

A_{eff} is the effective area of the section.
Q is A_{eff}/A
η' imperfection constant (Equation 7.59)

$$\eta' = \frac{\sigma_{Ez}}{\sigma_{TF}}\,\eta$$

in which

$$\eta = \frac{v_o B}{2 r_z^2}$$

v_o is the initial lateral imperfection of the table ($v_{\theta o} + v_{To}$)
B is the breadth of the channel
r_z is the radius of gyration about the Z axis
σ_d the design limiting stress σ_{uL} (Equation 5.16) or σ_o
σ_{TF} the critical torsional-flexural buckling resistance (Equation 7.18)
σ_{TFY} the axial load to cause first yield due to torsional-flexural buckling

7.5.1 COMPARISON BETWEEN EXPERIMENTS AND CURRENT AND PROPOSED DESIGN METHODS

The predicted torsional-flexural buckling resistance (P_{TFY}) for the 1.5mm and 3.0mm thick section, with 10mm and 15mm washer plates respectively, obtained from Equation 7.71 and BS5950: Part 5 (1987) are compared in Tables 7.7 with the

experimental results (Table 7.5). In applying Equation 7.70 the effects of local element and lip buckling, end warping restraint and connection torsional stiffness have been accounted for in determining the failure loads. The torsional-flexural buckling resistance has been obtained in accordance with BS5950: Part 5 (1987), with a warping restraint factor, $K_w = 2.0$.

From Table 7.7a it is observed that a conservative estimate of the failure load is obtained from Equation 7.71 for the 1.5 and 3.0mm thick sections if lip buckling is assumed to occur. If lip buckling is neglected then a better estimate to the experimental failure load is obtained. This would seem to suggest that there is little or no interaction between lip buckling and torsional-flexural buckling. In Table 7.7b BS 5950: Part5 (1987) is seen to be marginally conservative when taking into account the effects of local buckling. Lateral displacement and rotation of the cross section and the overall lip curvature, cause stress gradients in the web and table elements (Figure 7.18). In Table 7.7a it appears that the loss of effectiveness of the cross-section is less for higher levels of load than would be predicted for pure flexural buckling.

t_s (mm)	t_w (mm)	K_w	P_{exp} (kN)		Eqn. 7.71 (kN)	$\frac{\text{Eqn 7.71}}{P_{exp}}$
1.5	**10**	1.73	71	(a)	74	1.03
				(b)	59	0.84
				(c)	48	0.68
3.0	**15**	1.87	176	(a)	163	0.92
				(b)	158	0.90
				(c)	148	0.83

Table 7.7a Comparison between Equation 7.71 where η' is given by Equation 7.59 and 3 x 3 span, 9000mm column tests
(a) gross cross-section, (b) effective section, (c) Lip buckling

For the sections investigated it would be safe to conclude that Equation 7.71, neglecting the effects of lip buckling gives a reasonable estimate to the failure load. However, it must be stressed that this observation may not be generally applicable over a wide range of slenderness (L/r) and further investigation in the form of a parametric study is recommended.

t_s (mm)	t_w (mm)	K_w	P_{exp} (kN)		P_{uBS} (kN)	$\frac{P_{uBS}}{P_{exp}}$
1.5	**10**	2.0	71	(a)	88.9	1.25
				(b)	73.9	1.04
3.0	**15**	2.0	176	(a)	182.3	1.06
				(b)	178.4	1.01

Table 7.7b Comparison between BS 5950: Part 5: (1987)
and 3 x 3 bay 9metre column tests
(a) gross cross-section, (b) effective section

7.6 CONCLUSIONS

(1) Young's equation provides the basis for the Perry equation, which correctly describes the flexural buckling behaviour of a strut having flexural imperfections. Through a finite element study it has been possible to show that Young's equation is also applicable to rotational displacements. This provides the basis for a design method which correctly describes the torsional or torsional-flexural buckling behaviour of a strut with torsional imperfections.

(2) Current design for torsional and torsional-flexural buckling is based on the flexural buckling formulations in which the Euler buckling stress is replaced by the torsional or torsional-flexural buckling stress. This method takes no account of the differences in the stress distribution associated with the flexural and torsional buckling modes. Young's equation used for flexural buckling of imperfect struts can also be applied to the rotations are translations occurring during torsional and torsional-flexural buckling. Within the limits of linear elastic theory, the torsional and flexural displacements and the corresponding stress distributions, are correctly described.

(3) The initial rotational and translational imperfections are assumed to be affine to the critical torsional-flexural buckling mode, which can be determined from the differential equations for equilibrium. Young's equation can then be

applied to the initial imperfections to give the total displacements which together cause first surface yield at one corner of the channel section.

(4) Notwithstanding the major differences in stress distribution, the application of the original Perry equation for flexural buckling, with P_{TF} substituted for P_E, gives a reasonable estimate of the failure load. The magnitude of the difference depends on the mode and magnitude of the initial imperfection, and on the member slenderness (L/r) as well as the geometry of the cross-section. For the sections investigated, the Perry equation incorporating P_{TF}, overestimates the force that causes first yield by up to 23%, depending on the value of the slenderness (L/r). The BS5950: Part5 (1987) adaptation of the Perry equation, in which the imperfection parameter η depends on the slenderness, over estimates the load to cause first surface yield by up to 15%.

(5) For torsional buckling of a doubly symmetric section, the force which causes first yield is correctly given by the Perry equation P_T is substituted for P_{Ey}, and η is multiplied by P_{Ez}/P_T, in which η it is assumed that the initial imperfection is about the Z axis. If P_{TF} is substituted for P_{Ey}, and η is multiplied by P_{Ez}/P_{TF} where η is the imperfection constant usually taken for flexural buckling load, then the load to cause first yield is underestimated by up to 9%.

(5) It was observed during the numerical investigation that first surface yield due to torsional-flexural buckling was closely followed by failure of the member.

(6) The torsional-flexural buckling resistance of a section depends on the degree of warping restraint present at the ends of the member. BS 5950: Part 5 (1987) assumes a general reduction in torsional effective length equivalent to $L_{eff} = 0.7L$ ($K_W = 2.0$). This may overestimate the warping restraint and caution should be exercised in using the code recommendations. In the absence or numerical of experimental verification, no warping restraint should be assumed ($K_W = 1.0$).

(7) A comparison between the displacements obtained from the proposed design method (Equation 7.60) and the numerical results shows that the cross-section deforms laterally at the level of the lip table. This can be attributed

to the magnification of the rotational lateral displacement of the lip, caused by axial compression, which is much greater in one lip than in the other.

(8) For the lengths investigated experimentally it was observed that interaction between lip buckling and overall torsional-flexural buckling was insignificant. However, for short lengths of member where the preferred halfwave length of the same order as the member length, interaction occurs between the two modes of buckling. Further investigations in the form of a numerical parametric study is recommended before general conclusions can be made.

Chapter Eight

LATERAL-TORSIONAL BUCKLING OF DOUBLY LIPPED CHANNELS

8.1 INTRODUCTION

The lateral-torsional buckling phenomenon is best explained by considering a beam subjected to a uniform bending moment about the major axis. The compressive flange, if sufficiently slender, tends to buckle sideways like a column. The tensile flange has no tendency to buckle. The beam as a whole deforms primarily by twisting, together with a lateral displacement, coupled with vertical displacements caused by in-plane bending.

The main factors affecting lateral-torsional instability in a beam are the St.Venant and warping torsional stiffnesses, the type and level of loading, and the support conditions. The determination of the lateral-torsional buckling strength is quite complex. Consequently, this form of buckling still attracts much attention, and extensive research continues to date. The theory and design applications are covered by Bleich (1952), Timoshenko and Gere (1961), Nethercot and Rockey (1971, 1973), Nethercot and Trahair (1976, 1983), Brush and Almroth (1975), Allen and Bulson (1980), Trahair and Bradford (1988) and Attard (1990).

Lateral-torsional buckling is closely related to torsional-flexural buckling. The similarity of these two forms of buckling is also reflected in the way current codes of practice estimate the lateral-torsional buckling resistance of a member. The resistance is generally obtained by using a column flexural buckling formulation with the major axis critical lateral-torsional buckling stress substituted for the Euler buckling stress.

BS5950: Part 5 (1987) states that lateral torsional buckling about the minor axis need not be considered. For the cross section used in the test frame, it seemed that this assumption might not be justified. A simple approximate formulation for minor axis critical lateral torsional buckling stress suggested that minor axis buckling does occur, and was introduced to provide an interim basis for design.

Contrary to popular belief, it is not a necessary condition for lateral-torsional buckling that bending takes place about the major axis and it can be shown that in some cases singly symmetric beams bent about the minor axis may be prone to this type of buckling behaviour. The occurrence of minor axis lateral torsional-buckling has been shown to exist both theoretically (Timoshenko and Gere 1961, Attard 1990) and experimentally (Seah and Khong 1990, Rhodes and Seah 1992). The possibility of minor axis lateral-torsional buckling of singly symmetric sections has been recognised in the recently published addendum to AISI (1989), and design guidance for determining both the critical and ultimate buckling moments is provided. EC3: Part 1.3 (1992) does not address this phenomenon.

This chapter deals with the critical buckling behaviour of doubly and singly symmetric beams subjected to uniform moment. The effects of initial pre-buckling bending curvature on the critical buckling mode and critical stress for the channel section are discussed. The lateral-torsional buckling behaviour of initially imperfect doubly and singly symmetric beams is dealt with and a design method for channel beams subjected to uniform bending about the minor axis is proposed in which Young's amplification factor is used to determine separately the translation and rotation of the member. A method for estimating the stress distribution and moment to cause first yield is then described. The method can also be used for major axis bending. The various theoretical formulations and design proposals are verified numerically by means of critical elastic and non-linear elasto-plastic finite element analyses.

8.2 CRITICAL LATERAL-TORSIONAL BUCKLING

The governing equations for critical lateral-torsional buckling for a thin walled open cross section subjected to equal end moments can be obtained from Equations B.8 to B.10 given in Appendix B, by setting the axial load P equal to zero. It should be mentioned that the differential equations given in Appendix B do not take into account initial deflections caused by the applied moment.

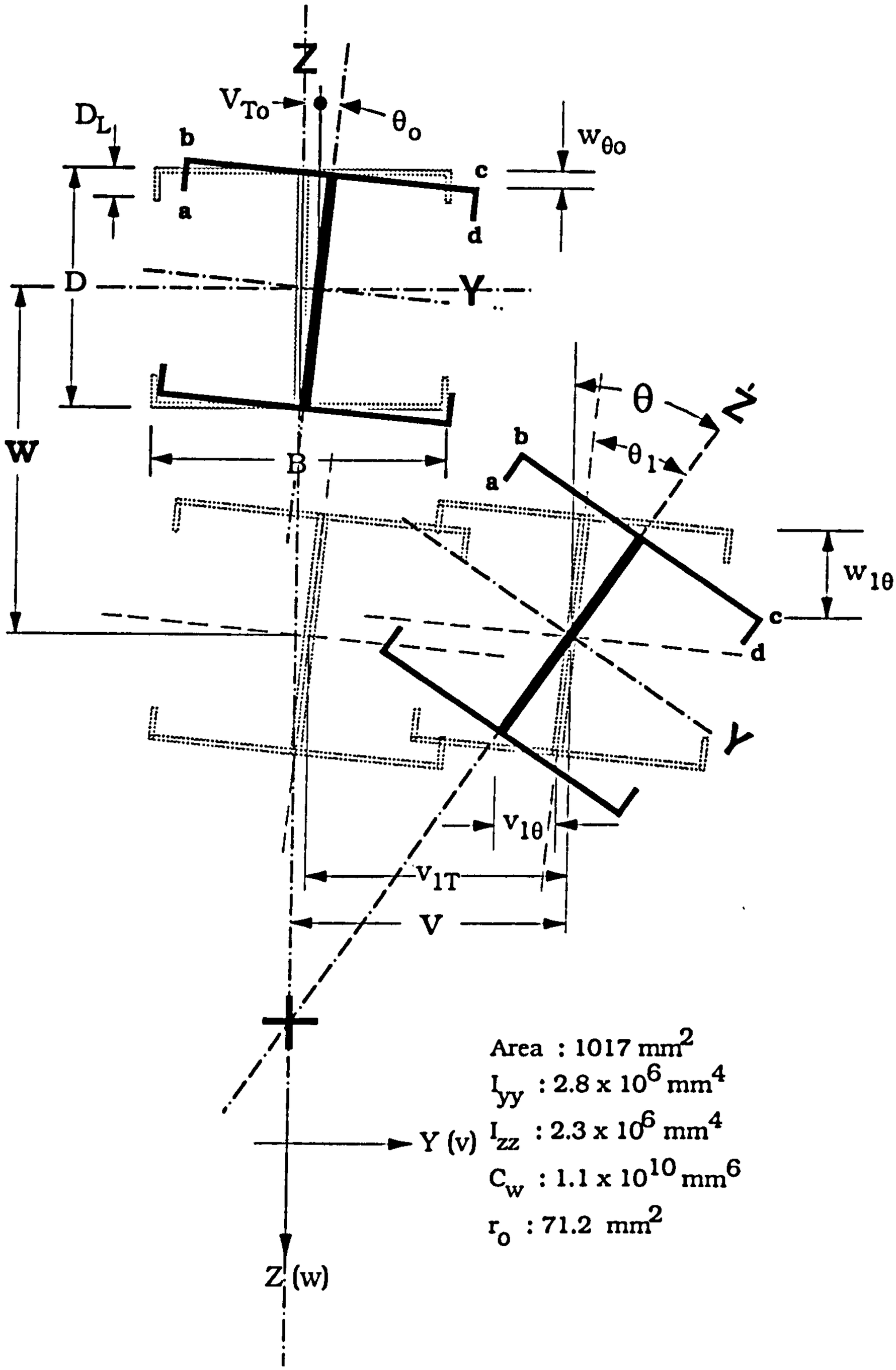


Figure 8.1 Lateral-torsional buckling deformation of back to back channel section
B = 180mm, D = 125mm, D_L = 20mm, t = 1.5mm

8.2.1 CRITICAL BUCKLING OF DOUBLY SYMMETRIC SECTIONS

Consider the doubly symmetric I-section shown in Figure 8.1 where the centre of gravity and shear centre coincide, and both the geometric constants β_y and β_z are equal to zero (Appendix B). If the I-section is bent about the Y axis (M_z=0) then the governing Equations B.8 and B.10 can be rewritten as

$$E I_z \frac{d^4 v}{d x^4} + M_y \frac{d^2 \theta}{d x^2} = 0 \qquad (8.1)$$

$$E C_w \frac{d^4 \theta}{d x^4} - G J \frac{d^2 \theta}{d x^2} + M_y \frac{d^2 v}{d x^2} = 0 \qquad (8.2)$$

where

C_w	the warping constant (Equation 7.19)
E	modulus of elasticity (205 kN/mm^2)
G	shear modulus
J	St. Venant torsion constant (Equation 7.4)
I_z	second moment of area about Z axis
M_y	applied the moment about the Y axis

Assuming that the rotation θ and the displacement v due to buckling are described by sinusoidal functions, then at any point along the length of the member the rotation and displacement is given by

$$\theta = \theta_{max} \sin\frac{\pi x}{L}, \quad v = v_{max} \sin\frac{\pi x}{L} \qquad (8.3)$$

The critical mode ratio defining the relationship between the rotation θ and the displacement v may be obtained by differentiating the displacement functions (Equation 8.3) with respect to length, and substituting into Equations 8.1 and 8.2.

The critical mode ratio at mid span of the member is given by

$$\frac{\theta}{v} = \frac{P_{Ez}}{M_{LTy}} \qquad (8.4)$$

or

$$\frac{\theta}{v} = \frac{M_{LTy}}{r_o^2 P_T} \qquad (8.5)$$

where

P_{Ez} Euler buckling load about Z axis

P_T critical torsional buckling load (Equation 7.11)

r_o polar radius of gyration about the shear centre

As the critical mode ratios θ/v given by Equations 8.4 and 8.5 are equal, an expression for the critical moment may be found by equating Equation 8.4 to 8.5 and solving for M_{LTy}

$$M_{LTy} = \frac{\pi}{L}\left[E I_z GJ\left(1 + \frac{\pi^2 E C_w}{GJL^2} \right)\right]^{1/2} \qquad (8.6)$$

where

M_{LTy} critical lateral torsional buckling moment about the Y axis

BS 5950: Part5 (1987) gives an approximate equation based on Equation 8.6 which is

$$M_{LTy} = \frac{\pi^2 AED}{2\left(\frac{L}{r_z}\right)^2}\left\{ 1 + \frac{1}{20}\left(\frac{L}{r_z}\frac{t}{D}\right)^2\right\}^{1/2} \qquad (8.7)$$

D refers to the depth of the element located in the plane of bending. Equation 8.7 may be obtained by substituting approximate equations for the I-beam section properties into Equation 8.6, the code also permits the use of Equation 8.7 for channels subject to major axis bending. Trahair and Bradford (1988) point out that the accuracy of Equation 8.7 is quite variable and care should be taken when using it for sections other than an I-section.

If the flexural rigidities about both principal axes are of the same order then it can be expected that pre-buckling displacements will be of greater importance and if large enough will affect the value of the critical moment. This phenomenon was reported by Baker et al (1956), in which reference is made to the transcendental equations derived by Davidson (1952), which take into account pre-buckling bending deformations. The equation given by Baker et al (1956) for determining the smallest critical buckling moment for doubly symmetric sections is

$$M_{LTy} = \frac{\pi}{L} \frac{\left[E I_z G J \left(1 + \frac{\pi^2 E C_w}{G J L^2} \right) \right]^{1/2}}{\left[\left(1 - \frac{I_z}{I_y} \right) \left[1 - \frac{G J}{E I_y} \left(1 + \frac{\pi^2 E C_w}{G J L^2} \right) \right] \right]^{1/2}} \qquad (8.8)$$

If I_y is reduced till it approaches I_z, then the value of M_{LTy} obtained from Equation 8.8 approaches infinity (Figure 8.2). This indicates that lateral-torsional buckling for doubly symmetric sections bent about their minor axis will not occur. This conclusion cannot however be drawn from Equations 8.6 or 8.7.

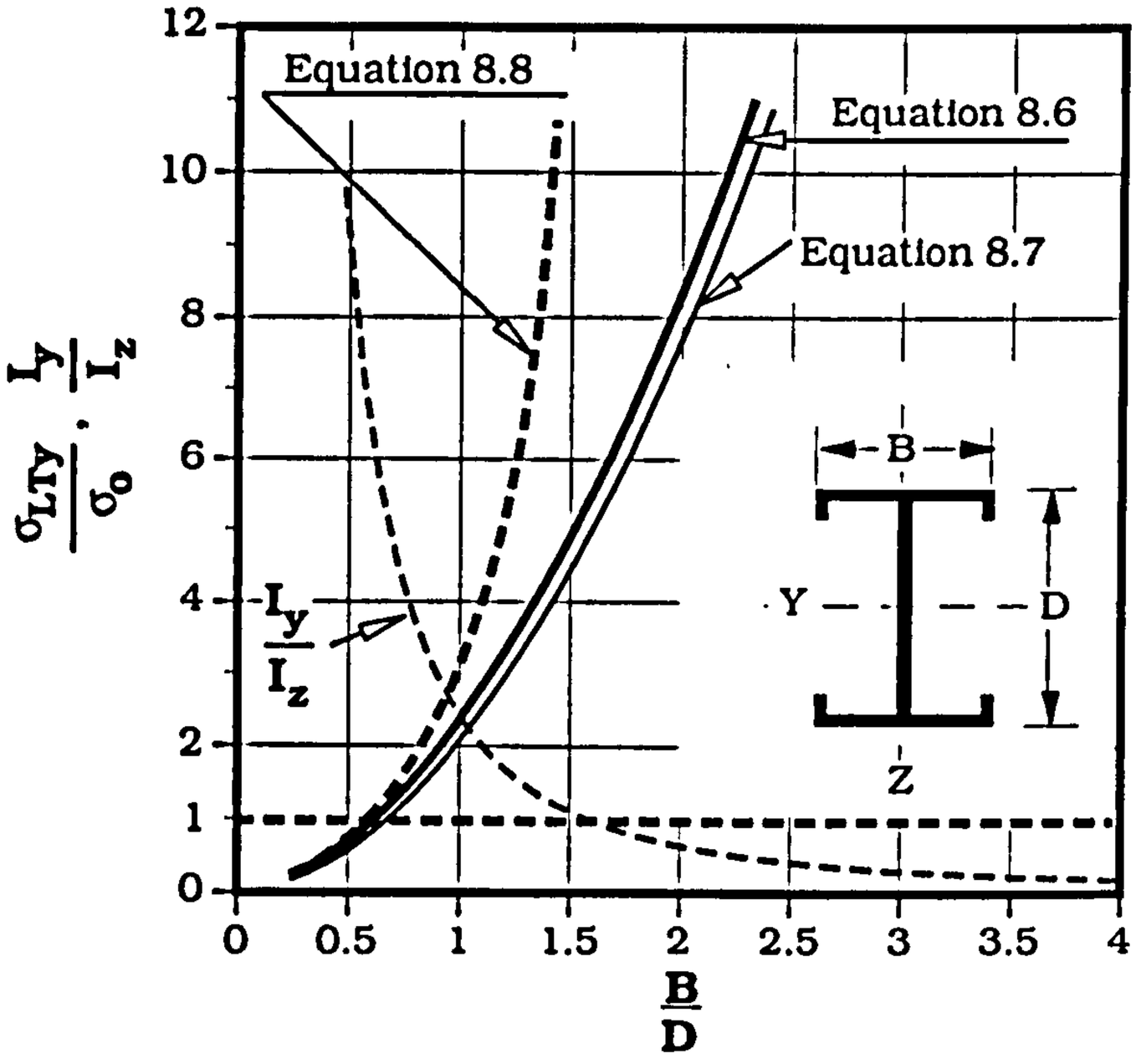


Figure 8.2 Variation in critical lateral-torsional buckling stress with breadth for doubly symmetric I-section

$D = 125mm$, $D_L = 20mm$, $L = 2000mm$, $t = 1.5mm$, $\sigma_o = 390\ N/mm^2$

Equation 8.6 presupposes that the beam is straight at the instance of buckling. It therefore gives the correct result for a beam which is initially curved by an amount equal and opposite to the pre-buckling curvature. Equation 8.8 on the other hand gives a higher buckling stress than does Equation 8.6, the difference increasing rapidly as $I_z/I_y \rightarrow 0$. It could be argued that a pre-buckling curvature which is of opposite sign to the bending curvature, may reduce the critical stress.

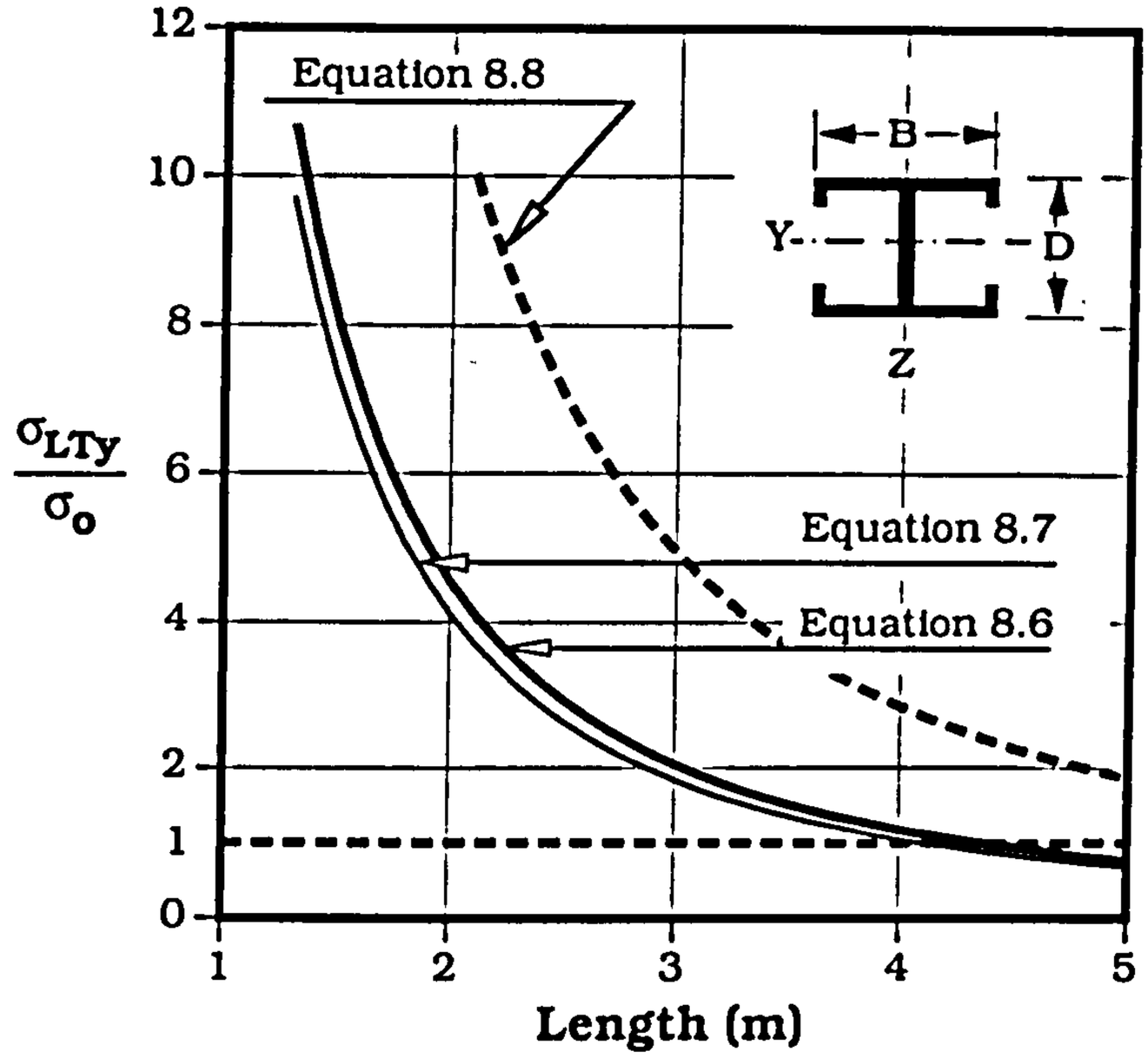


Figure 8.3 Variation in critical lateral-torsional buckling stress with length for doubly symmetric I-section.

B = 180mm, D = 125mm, D_L = 20mm, t = 1.5mm, σ_o = 390 N/mm^2

Further investigation into this phenomenon has been carried out by Trahair and Woolcock (1973), Vacharajittiphan et al (1974), and Attard (1990).

The variation in critical bending stress with breadth is shown in Figure 8.2 where it can be seen that the critical bending stresses increase rapidly with increasing B/D. When the initial pre-buckling curvatures are taken into account (Equation 8.8) the critical bending stress tends to infinity at a value of B/D = 1.5, corresponding to I_z/I_y = 1.0. This result is not given by Equations 8.6 and 8.7; nevertheless, BS 5950: Part 5 (1987) (Equation 8.7) states that buckling will not occur when $I_y \leq I_z$. Figure 8.3 shows the variation of σ_{LT} with length for a section shown in Figure 8.1, having B/D = 1.44, I_z/I_y = 0.82. The difference between 8.8 and 8.6 or 8.7 is large for this section.

The variation in the non-dimensional critical mode ratio $D\theta/2v$ with B/D for the I-section is shown in Figure 8.4. The mode ratio is seen to increase slightly with increasing B/D.

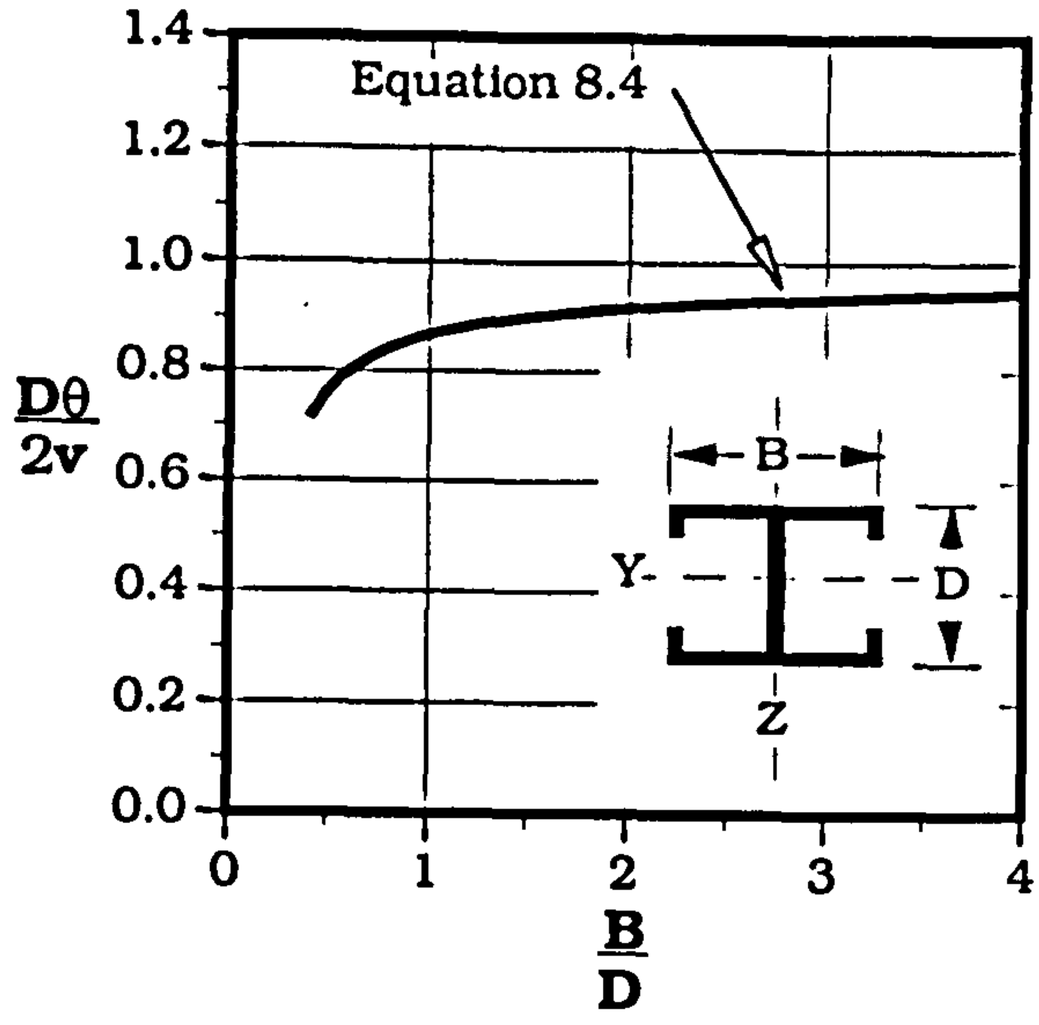


Figure 8.4 Variation in critical mode ratio D θ/2v with breadth for back to back channel. (pre-buckling curvature excluded)
D = 125mm, D_L = 20mm, t = 1.5mm, L = 2000mm

8.2.2 CRITICAL BUCKLING OF DOUBLY LIPPED CHANNELS

Singly symmetric channel sections are prone to critical lateral-torsional buckling. about the minor axis even if curved when buckling occurs. Consider the channel section shown in Figure 8.5. The distance y_o between the shear centre and the centroid in the direction of the Y axis is equal to zero, $\beta_z = 0$ (Appendix B). If the channel section is bent about the Y axis ($M_z = 0$) such that the lips are in compression, then the governing Equations B.8 and B.10 can be rewritten as

$$E I_z \frac{d^4 v}{dx^4} + M_y \frac{d^2 \theta}{dx^2} = 0 \qquad (8.9)$$

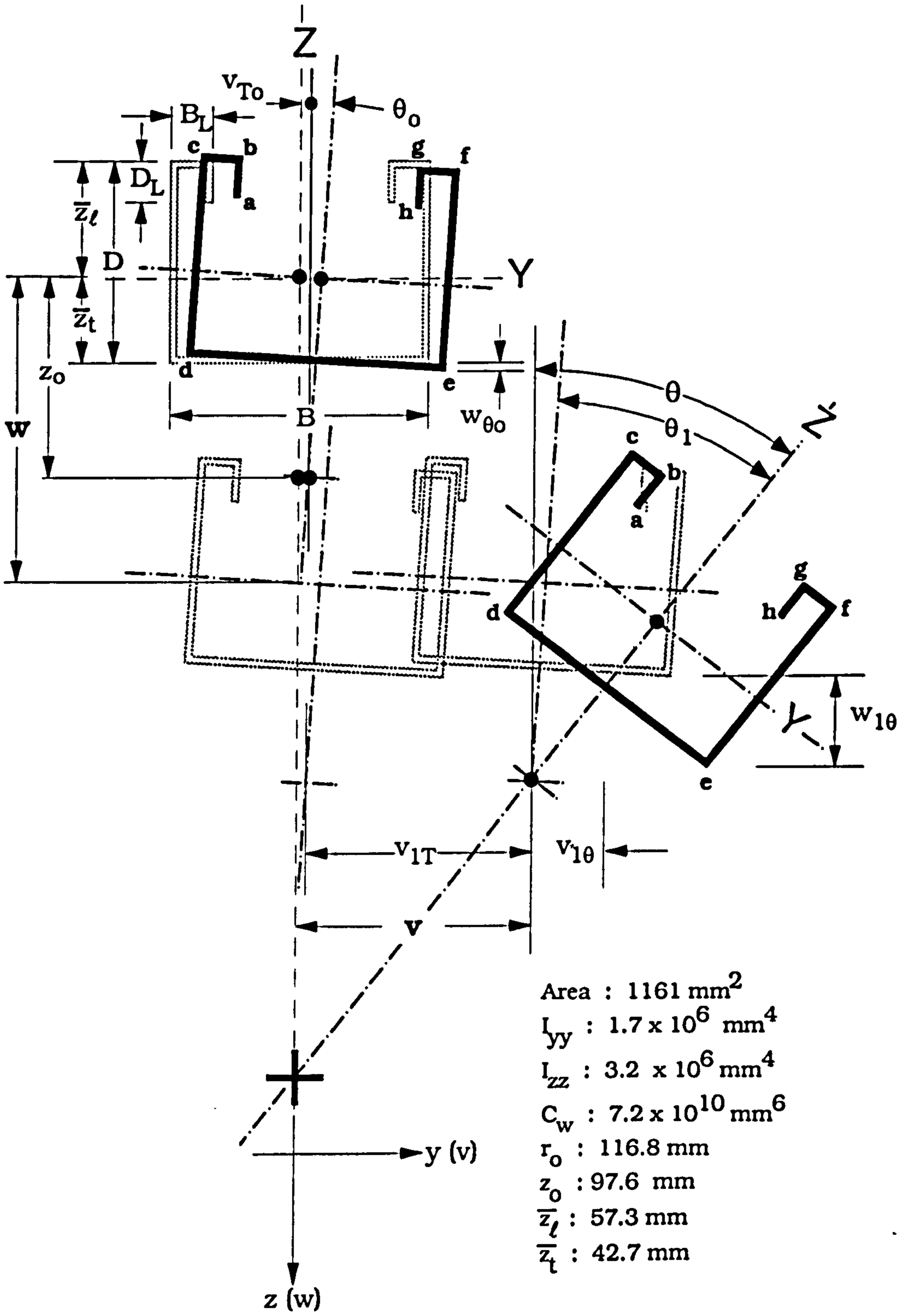
$$E C_w \frac{d^4 \theta}{dx^4} - (GJ + M_y \beta_y) \frac{d^2 \theta}{dx^2} + M_y \frac{d^2 v}{dx^2} = 0 \qquad (8.10)$$

where

β_y geometric parameters

in which

$$\beta_y = \frac{1}{I_y} \left(\int_A z^3 \, dA + \int_A y^2 z \, dA \right) - 2 z_o \qquad (8.11)$$



Area : 1161 mm^2
I_{yy} : 1.7×10^6 mm^4
I_{zz} : 3.2×10^6 mm^4
C_w : 7.2×10^{10} mm^6
r_o : 116.8 mm
z_o : 97.6 mm
$\overline{z}_\ell$: 57.3 mm
$\overline{z}_t$: 42.7 mm

Figure 8.5 Lateral-torsional buckling deformations of a doubly lipped channel section.

B = 122mm, D = 97mm, B_L = 17mm, D_L = 18.5mm, t = 3.0mm

The geometric parameter β_y defined in Equation 8.11 is required before being able to determine the critical moment M_{LTy} for the channel section. The value β for a number of singly symmetric sections may be obtained from equations given by Yu (1991), based on earlier work carried out by Pekoz and Celebi (1969). The value of β_y for the doubly lipped channel section shown in Figure 8.5, may be obtained by evaluating Equation 8.11, and is

$$\beta_y = \frac{[\beta_B + \beta_D + \beta_{BL} + \beta_{DL}]t}{I_y} - 2z_o \qquad (8.12)$$

where

$$\beta_B = \frac{1}{12}\bar{z}_t B^3 + \bar{z}_t{}^3 B$$

$$\beta_D = \frac{1}{2}[(D + \bar{z}_t)^4 - (\bar{z}_t)^4] + \frac{1}{4}B^2[(D + \bar{z}_t)^2 - (\bar{z}_t)^2]$$

$$\beta_{BL} = 2B_L(\bar{z}_t + D)^3 + \frac{2}{3}(\bar{z}_t + D)\left[\left(\frac{B}{2}\right)^3 - \left(\frac{B}{2} - B_L\right)^3\right]$$

$$\beta_{DL} = \left(\frac{B}{2} - B_L\right)^2\{(D + \bar{z}_t - D_L)^2 - (D + \bar{z}_t)^2\} + \frac{1}{2}\{(D + \bar{z}_t - D_L)^4 - (D + \bar{z}_t)^4\}$$

where

B	breadth of section
B_L	breadth of lip
D	depth of section
D_L	depth of lip downturn
I_y	second moment of area about Y axis
$\bar{z}_t$	is the distance between the neutral axis of the section and the mid thickness of the table element, in which

$$\bar{z}_t{}' = -\frac{\left[D\left(D + 2B_L + 2D_L - \frac{D_L{}^2}{D}\right)\right]}{[B + 2D + 2B_L + 2D_L]} \qquad (8.13)$$

Assuming that the rotation θ about the shear centre and displacement v of the shear centre at any point along the channel during buckling can be described by the sinusoidal functions given by Equations 8.3, then the relationship between the θ and v can be obtained by differentiating Equations 8.3 with respect to length and

substituting into Equations 8.9 and 8.10. The critical mode ratios θ/v for the channel are

$$\frac{\theta}{v} = \frac{P_{Ez}}{M_{LTy}} \tag{8.14}$$

or

$$\frac{\theta}{v} = \frac{M_{LTy}}{\left(r_o^2 P_T - M_{LTy} \beta_y \right)} \tag{8.15}$$

The minor axis critical bending moment (M_{LTy}) for the doubly lipped channel section can be obtained by equating Equation 8.14 to 8.15. Solving for M_{LTy} gives

$$M_{LTy} = - \frac{P_{Ez} \beta_y}{2} \pm \left[\left(\frac{P_{Ez} \beta_y}{2} \right)^2 + r_o^2 P_{Ez} P_T \right]^{1/2} \tag{8.16}$$

Equation 8.16 is also given by Timoshenko and Gere (1961).

When bending occurs about the Z axis ($M_y = 0$, $\beta_z = 0$) the governing equations for critical lateral torsional buckling are

$$E I_y \frac{d^4 w}{dx^4} + M_z \frac{d^2 \theta}{dx^2} = 0 \tag{8.17}$$

$$E C_w \frac{d^4 \theta}{dx^4} - GJ \frac{d^2 \theta}{dx^2} + M_z \frac{d^2 w}{dx^2} = 0 \tag{8.18}$$

Assuming that the displacement w, in the plane of bending can be described by

$$w = w_{max} \sin \frac{\pi x}{L}$$

Differentiating w with respect to length and substituting into Equations 8.17 and 8.18, the critical mode ratio θ/w is then given by

$$\frac{\theta}{w} = \frac{P_{Ey}}{M_{LTz}} \tag{8.19}$$

or

$$\frac{\theta}{w} = \frac{M_{LTz}}{r_o^2 P_T} \tag{8.20}$$

The critical lateral-torsional buckling moment (M_{LTz}) for the channel section bent about the Z axis can be obtained by equating Equations 8.19 to 8.20, and solving for M_{LTz}

$$M_{LTz} = \frac{\pi}{L}\left[E I_y GJ\left(1 + \frac{\pi^2 E C_w}{GJL^2} \right)\right]^{1/2} \qquad (8.21)$$

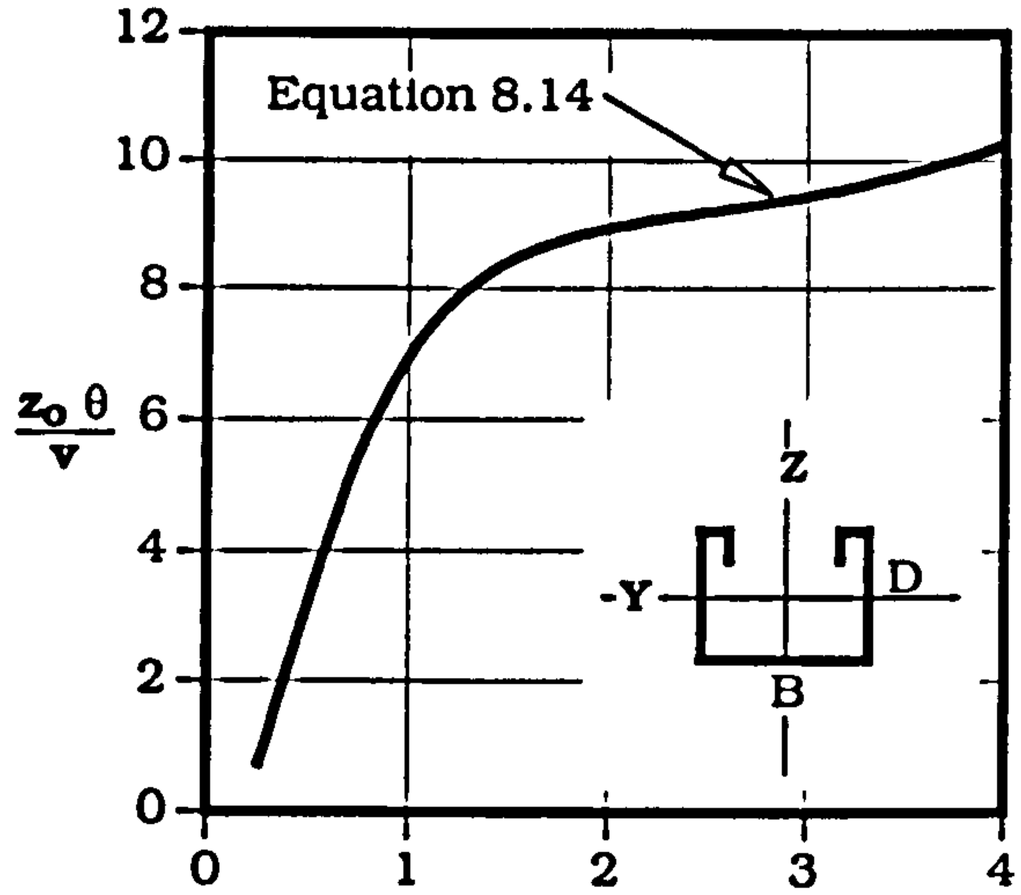


Figure 8.6 Variation in non-dimensional mode ratio $z_0\theta/v$ with breadth for doubly lipped channel section. (pre-buckling curvature excluded)
D = 97mm, B_L = 17mm, D_L = 18.5mm, t = 3.0mm, L = 3000mm

It is interesting to note the similarity in the critical mode ratio for the I-section bent about the Y axis (Equations 8.4 and 8.5) and the critical mode ratio for the channel bent about the Z axis (Equations 8.19 and 8.20), and also the similarity in Equations 8.6 and 8.21. The similarities occur because the geometric parameter β_z for the channel section is equal to zero and the governing equations for the channel are then the same as those for the I-beam. The variation in the non-dimensional critical mode ratio $z_o\theta/v$ (Equation 8.14), with breadth, for the channel section is shown in Figure 8.6. For the usual range of sections ($2 > B/D > 1$) the variation is not very great. According to Equation 8.16 σ_{LTy} is finite for any I_y/I_z ratio.

Attard (1990) derives an approximate general equation for determining the critical lateral-torsional buckling moment for singly symmetric sections taking into account the effects of initial pre-buckling curvatures. This will be called the "curved beam"

solution; the beam is curved at the critical moment, but is initially straight. For a simply supported member subjected to uniform moment the critical moment given by Attard (1990) can be written in the same form as Equation 8.16,

$$M_{LTy} = -\frac{P_{Ez}^{*}\beta_y}{2} \pm \left[\left(\frac{P_{Ez}^{*}\beta_y}{2}\right)^2 + r_o^2 P_{Ez}^{*} P_T\right]^{1/2} \qquad (8.22a)$$

where

$$P_{Ez}^{*} = \frac{P_{Ez}}{\left(1 - \frac{I_z}{I_y}\right)} \qquad (8.22b)$$

If $I_z \neq I_y$ and β_y is non-zero, a solution to Equation 8.22a may still be obtained even though the values given by Equation 8.22b is non-zero and negative, that is $I_z > I_y$. When $I_z = I_y$, there is no solution to Equation 8.22a; Attard (1990) points out however, that critical lateral-torsional buckling may still occur and is given by

$$M_{LTy} = \frac{r_o^2 P_T}{2\beta_y} \qquad (8.23)$$

If in Equation 8.22a the term in the square brackets becomes negative (B/D = 2.45, I_z/I_y = 6.9 for the doubly lipped channel, where D = 97mm) then a positive real solution can not be found, and critical lateral-torsional buckling will not occur.

The variation in critical bending stress σ_{LTy} with B/D for D = 97mm and L = 3000mm is shown in Figure 8.7a. It can be seen that the critical bending stress given by Equations 8.16 and 8.22a both increase as the section becomes wider. The critical stress given by Equation 8.22a, which accounts for pre-buckling bending curvatures (curved beam), increases at a greater rate than that given by Equation 8.16. Equation 8.22a is seen to become asymptotic to a value of B/D = 2.45. For the section used in the present investigation, B/D = 1.25, the difference between Equations 8.16 and 8.22a is not very great.

Figure 8.7b shows a comparison between the critical lateral-torsional buckling moment for a channel bent about the Z axis, given by Equations 8.21 and Equations 8.7 and 8.8, in which I_y and I_z have been interchanged. Equation 8.7, given in BS 5950: Part5: (1987) is seen to be non-conservative when compared to Equation 8.8 and 8.21 for channels where B/D > 2.5. Equation 8.8 tends to infinity when

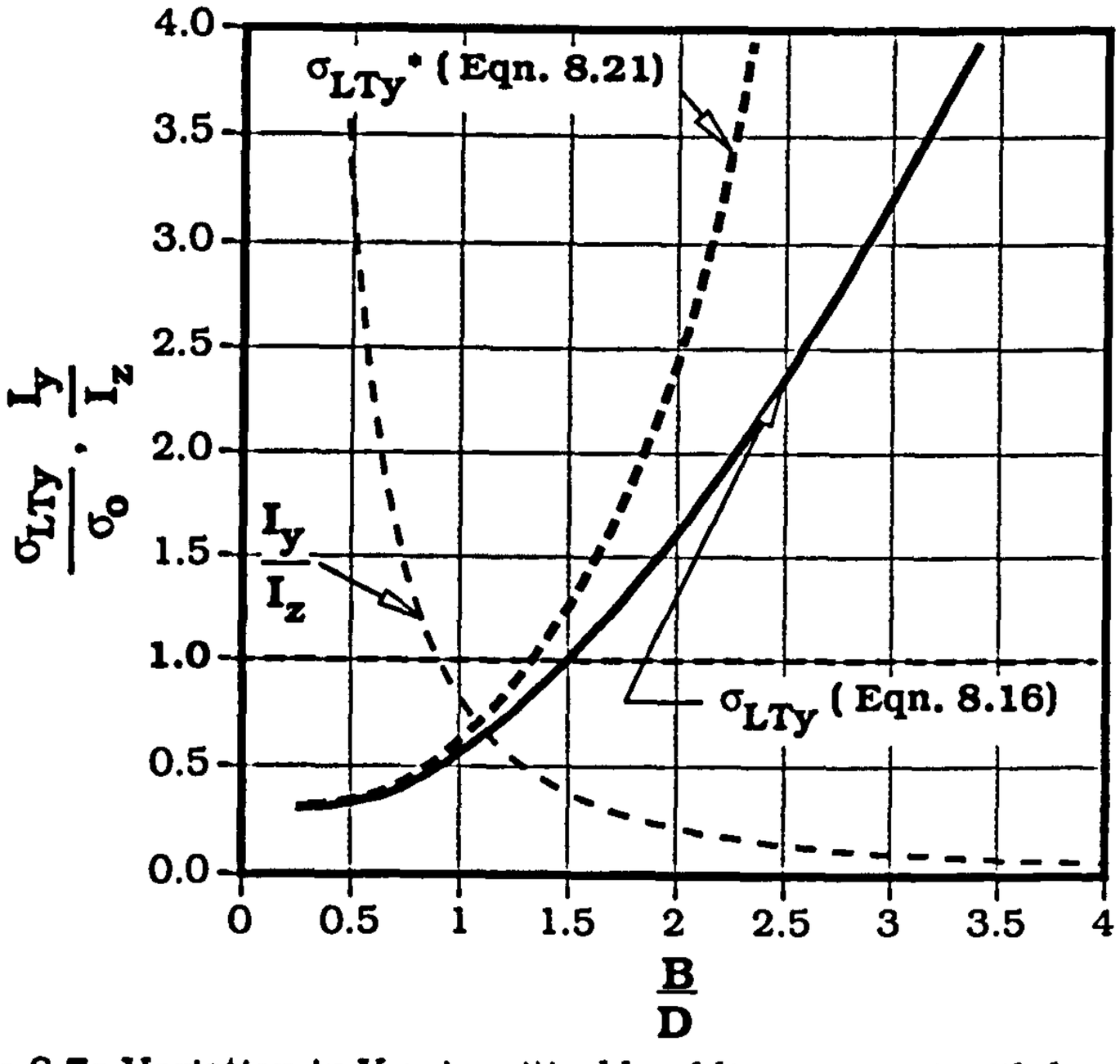


Figure 8.7a Variation in Y axis critical buckling moment with breadth for doubly lipped channel section. (* pre- buckling curvatures included)
D = 97mm, B_L = 17.0, D_L = 18.5, t = 3.0mm, L = 3000mm

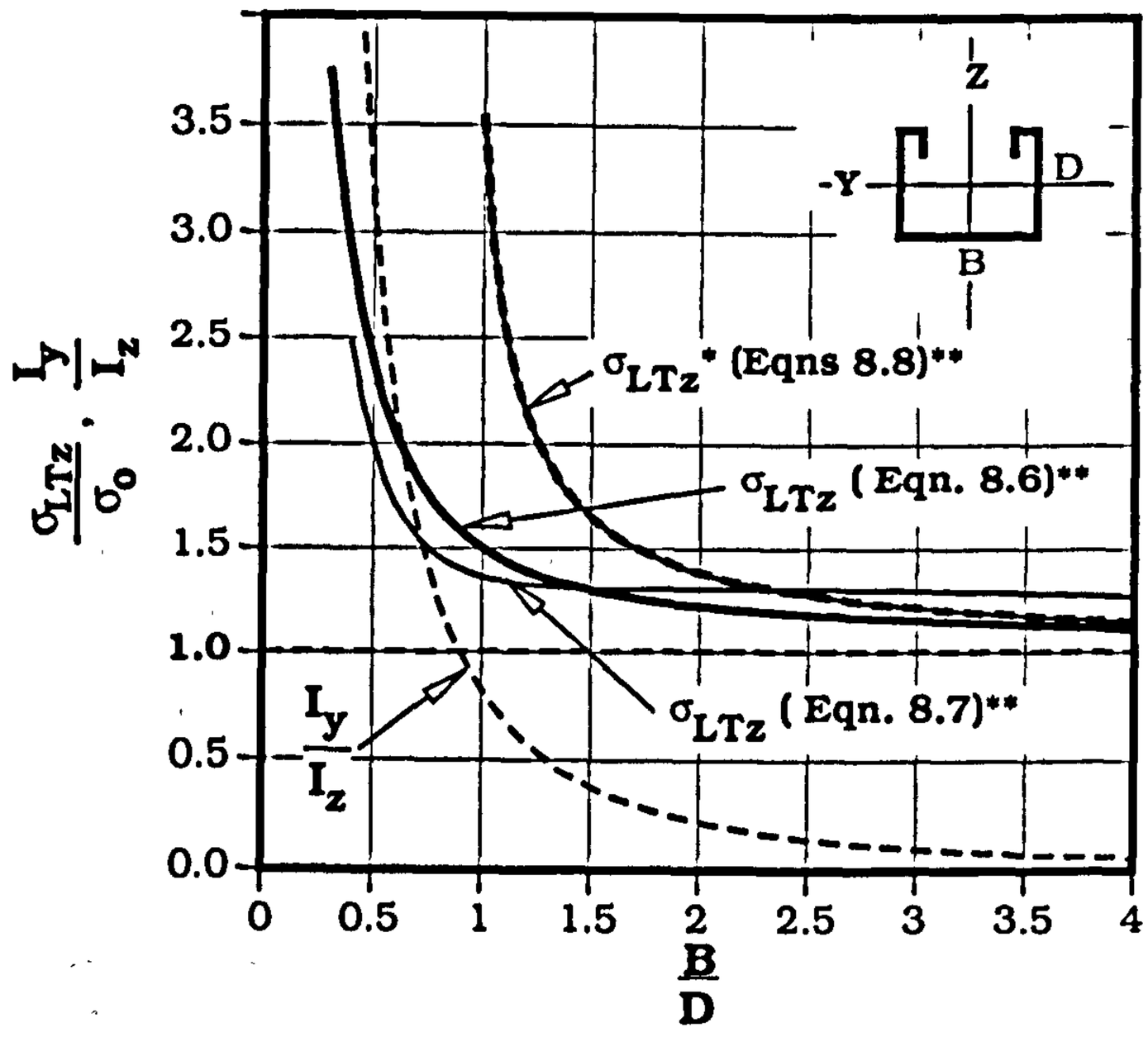


Figure 8.7b Variation in Z axis critical buckling moment with breadth for doubly lipped channel section. (* pre- buckling curvatures included. ** I_z substitued for I_y)
D = 97mm, B_L = 17.0, D_L = 18.5, t = 3.0mm, L = 3000mm

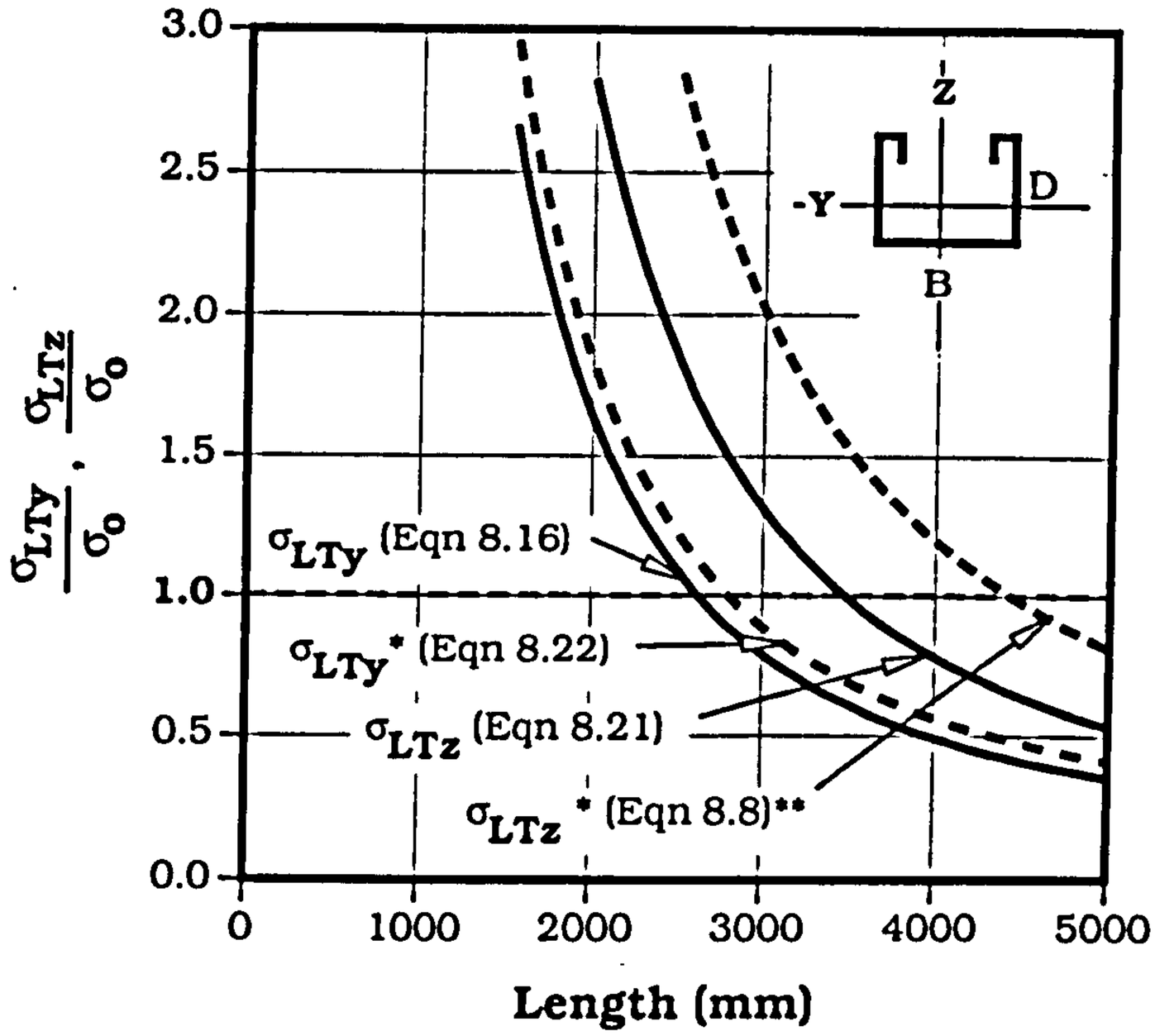


Figure 8.8 Varitation in critical buckling moment with length for doubly lipped channel section. (σ_{LTy}* : pre-buckling curvatures included. ** I_z substituted for I_y)
B = 122mm, D = 97mm, B_L = 17.0, D_L = 18.5, t = 3.0mm

B/D = 0.9 ($I_y = I_z$) indicating that critical lateral-torsional buckling will not occur for cross-sectional geometries where B/D < 0.9 ($I_y/I_z > 1.0$).

Figure 8.8 shows the variation in the critical lateral-torsional bending stresses σ_{LTy} and σ_{LTz} with length, where B/D = 1.25. The critical lateral-torsional buckling stress for Y axis bending given by Equations 8.16 and 8.22a falls below σ_o at approximately L = 2500mm, for all practical spans, therefore, lateral-torsional buckling must be considered. A conservative and satisfactory estimate of the minor axis critical lateral-torsional buckling stress can be obtained from Equation 8.16. In Figure 8.8 σ_{LTz} given by Equation 8.21 falls below the yield stress when L = 3500mm.

8.2.3 FINITE ELEMENT BUCKLING ANALYSIS OF DOUBLY LIPPED CHANNEL.

In order to validate Equations 8.16 and 8.22a, finite element critical buckling solutions were obtained for a 3mm thick doubly lipped channel of lengths 2000mm,

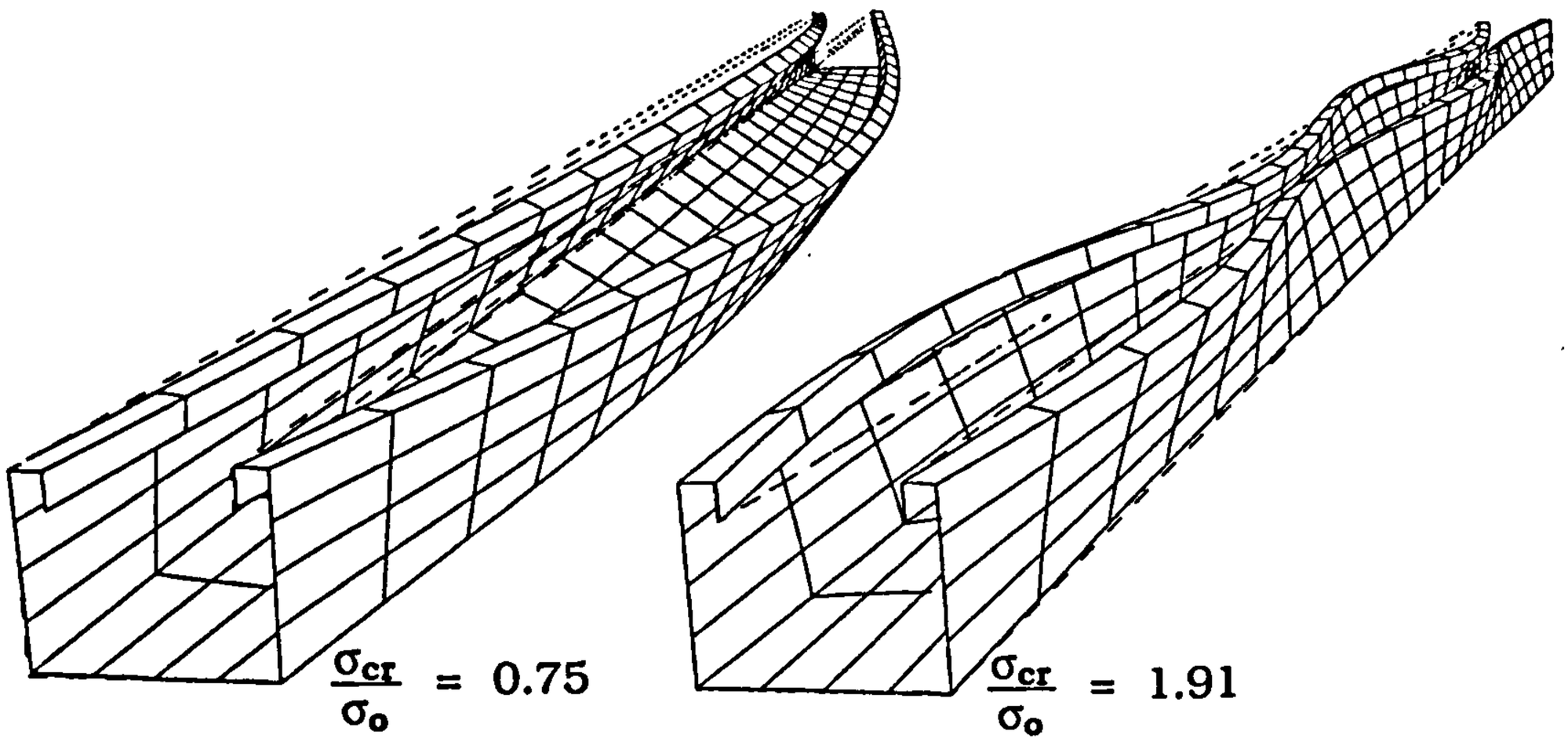


Figure 8.9 First and second critical buckling modes

(Bending - Lip compression)

B = 122mm, D = 97mm, B_L = 17mm, D_L = 18.5mm, t = 3.0mm

L = 3000mm, σ_o = 390 N/mm^2

Length (mm)	$\frac{\theta}{v}$			$\frac{\sigma_{LTy}}{\sigma_o}$		
	FINASIC	Eq 8.14	$\frac{\text{Eq 8.14}}{\text{FINASIC}}$	FINASIC	Eq 8.16	$\frac{\text{Eq 8.16}}{\text{FINASIC}}$
2000	0.0796	0.0872	1.09	1.42	1.59	1.12
3000	0.0844	0.0805	0.95	0.75	0.76	1.02
3000†	-0.109	N/A.	N/A.	0.86†	0.85†	0.99†
4000	0.0782	0.0728	0.93	0.48	0.48	1.00

† pre-buckling curvatures taken into account in Equation 8.22 and in finite element solution

Table 8.1 Comparisons between the critical buckling mode ratio θ/v and Equations 8.14, and numerical results for critical lateral-torsional buckling and Equations 8.16 and 8.22.

B= 122mm, D = 97mm, B_L = 17mm, D_L = 18.5mm, t = 3.0mm, σ_o = 390 N/mm^2

3000mm and 4000mm. The mesh and boundary conditions used in the critical torsional-flexural buckling analysis presented in Chapter Seven were again employed. Figure 8.9 shows the mesh, and the first and second modes of deformation, for a 3000mm long member. Lateral-torsional buckling was the lowest critical mode observed in all cases investigated. It should be noted that the linear eigen solver in FINASIC does not take into account the effects due to pre-buckling curvature.

Finite element and analytical values for the mode ratio θ/v and for the critical stress σ_{LTy} are compared in Table 8.1.

The influence of in-plane pre-buckling bending curvature on the critical moment for a 3000mm long channel was also investigated numerically. An initial bending displacement in the direction of the moment was applied prior to buckling, which was obtained from

$$w = \frac{M L^2}{8 E I_y} \tag{8.24}$$

where M was equal to the critical moment M_{LTy} obtained from the straight beam analysis. The central displacement prior to buckling was 27.9mm. The critical lateral-torsional buckling stress obtained from the numerical analysis showed an increase from $\sigma_{LTy} = 0.75\sigma_o$ obtained from the straight beam analysis to $\sigma_{LTy} = 0.86\sigma_o$ an increase of 14%. It is interesting to note the difference in sign of the critical mode ratio, for the initially straight and curved beams, when L = 3000mm, in Table 8.1. The negative value of θ/v indicates that the lateral displacement v_θ due to rotation θ about the shear centre and the lateral translation v_T are in opposing directions, resulting in a reduced horizontal bending curvature. Depending on the section geometry, the lateral displacement of the shear centre due to the moment components about both principal axes at mid span may be larger and in the opposite direction, to the lateral translation due to rotation of the section about its shear centre, which leads to a negative critical mode ratio.

In Table 8.1 it can be seen that the minor axis critical buckling moments obtained from Equation 8.16 compare well with those obtained numerically. However, for the 2000mm long member Equation 8.16 overestimates the critical lateral-torsional buckling moment by 12%. This is probably due to interaction between the lip buckling and the overall lateral-torsional buckling modes. A member length of

2000mm is closer to the preferred lip buckling halfwave length 750mm, and the interaction would be expected to be greater for this length of member than for the longer members. A similar interaction was noted for torsional-flexural buckling in Chapter Seven. The results in Table 8.1 also indicate that the chosen finite element mesh size is satisfactory for subsequent solutions for imperfect members in the elastic range. After yielding however, the accuracy of the solution will diminish because of the high strain gradients which occur in areas of localized plasticity.

8.3 LATERAL-TORSIONAL BUCKLING RESISTANCE OF IMPERFECT MEMBERS

Real beams are not perfectly straight, but have small initial curvatures and twists which cause them to displace as soon as external loads are applied. The amplification of these initial imperfections lead to a failure moment which is lower than the critical moment. This section sets out to provide a physical appreciation of the lateral-torsional buckling phenomenon. A method for determining both the displacements and stress distribution based on Young's equation similar to that described in Chapter Seven is discussed and compared with results obtained from a numerical parametric study.

8.3.1 BUCKLING RESISTANCE OF IMPERFECT DOUBLY SYMMETRIC SECTIONS

When the doubly symmetric thin-walled I-section, of Figure 8.1, is subject to equal end moments about the horizontal Y axis (major axis), failure may occur through either flexural yield or lateral-torsional buckling. The type of failure depends on the mode and magnitude of the initial imperfection as well as the D/B and L/r ratios of the section. If the section is initially imperfect such that the imperfections are affine to the critical lateral-torsional buckling mode, then under load the cross-section displaces horizontally v, as well as rotating θ about the shear centre. The bending stress to cause first yield will be a minimum for affine initial displacements v_{To} and θ_o.

In Chapter Seven it was shown that Young's equation (Equation 6.3) described the increase in displacement v_T and the rotation θ with load for a member prone to torsional-flexural buckling. Analogously for an imperfect beam susceptible to

lateral-torsional buckling, the displacement v_{1T} and rotation θ_1 may be obtained from

$$v_{1T} = \frac{v_{To}}{1 - \frac{\sigma_B}{\sigma_{LT}}} - v_{To} \tag{8.25}$$

where v_{1T} is the additional lateral displacement of the shear centre, and

$$\theta_1 = \frac{\theta_o}{1 - \frac{\sigma_B}{\sigma_{LT}}} - \theta_o \tag{8.26}$$

where θ_1 is the additional rotation about the shear centre. The horizontal bending stress caused by the amplification of v_{1T} at the lip/flange junction is

$$\sigma = v_{1T} \frac{\pi^2}{L^2} E \frac{B}{2} \tag{8.27}$$

A small additional rotation θ_1 about the shear centre causes displacements $v_{1\theta}$ and $w_{1\theta}$. The resulting warping stress at the lip/flange junctions are

$$\sigma = \pm v_{1\theta} \frac{\pi^2}{L^2} \frac{B}{2} E \tag{8.28}$$

The warping stresses at the free edge of the lip downturn at each end of the flange are

$$\sigma = \pm \frac{\pi^2 E}{L^2} \left(\frac{B}{2} v_{1\theta} + D_L w_{1\theta} \right) \tag{8.29}$$

in which

$$v_{1\theta} = \frac{\theta_1 D}{2}, \quad w_{1\theta} = \frac{\theta_1 B}{2}$$

The warping stress distribution can be plotted around the I-section at any value of σ_B/σ_{LT} and θ_o from Equations 8.28 and 8.29.

The central vertical displacement w for any value of end moment can be obtained from Equation 8.24. The longitudinal stresses caused by vertical bending, at the free edge of the lip (point **a**) and at the lip/flange junction (point **b**) on the section (Figure 8.1) are

$$\sigma = \frac{M}{Z_a} = \sigma_B \left(\frac{z_a}{z_b}\right) \tag{8.30}$$

and

$$\sigma = \frac{M}{Z_b} = \sigma_B \tag{8.31}$$

where

Z_a, Z_b are the section modulii at point **a** and **b** on the cross-section

z_a, z_b are the distances from the neutral axis to point **a** and **b** on the cross-section

The total stress at any point may be obtained by adding together the three individual stress components, that is, the vertical bending stresses, the horizontal bending stresses and warping (Equations 8.27 to 8.31). The total compressive stress at point **a**, the free edge of the lip, due to bending about the Y axis is

$$\sigma = \sigma_B\left(\frac{z_a}{z_b}\right) + \frac{\pi^2}{L^2} E \frac{B}{2} v_{1T} + \frac{\pi^2}{L^2} E\left[\frac{B}{2} v_{1\theta} + D_L w_{1\theta}\right] \tag{8.32}$$

while the stress at point **b**, the lip/flange junction is

$$\sigma = \sigma_B + \frac{\pi^2}{L^2} E \frac{B}{2} v_{1T} + \frac{\pi^2}{L^2} E \frac{B}{2} v_{1\theta} \tag{8.33}$$

Substituting Equations 8.25 and 8.26 into Equation 8.33 and rearranging, Equation 8.33 may be rewritten in a form similar to the Perry equation:

$$\sigma_{By} = 0.5\left[(\sigma_o + \sigma_{LTy} + \eta\sigma_{Ez}) - \left\{(\sigma_o + \sigma_{LTy} + \eta\sigma_{Ez})^2 - 4\sigma_o\sigma_{LTy}\right\}^{1/2}\right] \tag{8.34}$$

where

$$\eta = \frac{B}{2 r_z^2}[v_{To} + v_{\theta o}] = \frac{B v_o}{2 r_z^2} \tag{8.35a}$$

in which

$$v_o = v_{To} + v_{\theta o} \tag{8.35b}$$

Equation 8.34 becomes identical to the original Perry formulation when the imperfection parameter η in Equation 8.34 is

$$\eta' = \frac{\sigma_{Ez}}{\sigma_{LTy}}\eta \qquad (8.36)$$

Consider the I-section shown in Figure 8.1, where L = 2000mm (span/depth ratio L/D = 16) and σ_o = 390 N/mm^2. The yield moment is M_{uy} = 17.9 kNm, and the critical moment (Equation 8.16), M_{LTy} = 81.5 kNm. The bending stress to cause first yield at the free edge of the lip, given by Equation 8.32 is σ_{By} = 506 N/mm^2, while the moment to cause first yield at the lip/flange junction, given by Equation 8.33, is σ_{By} = 366 N/mm^2.

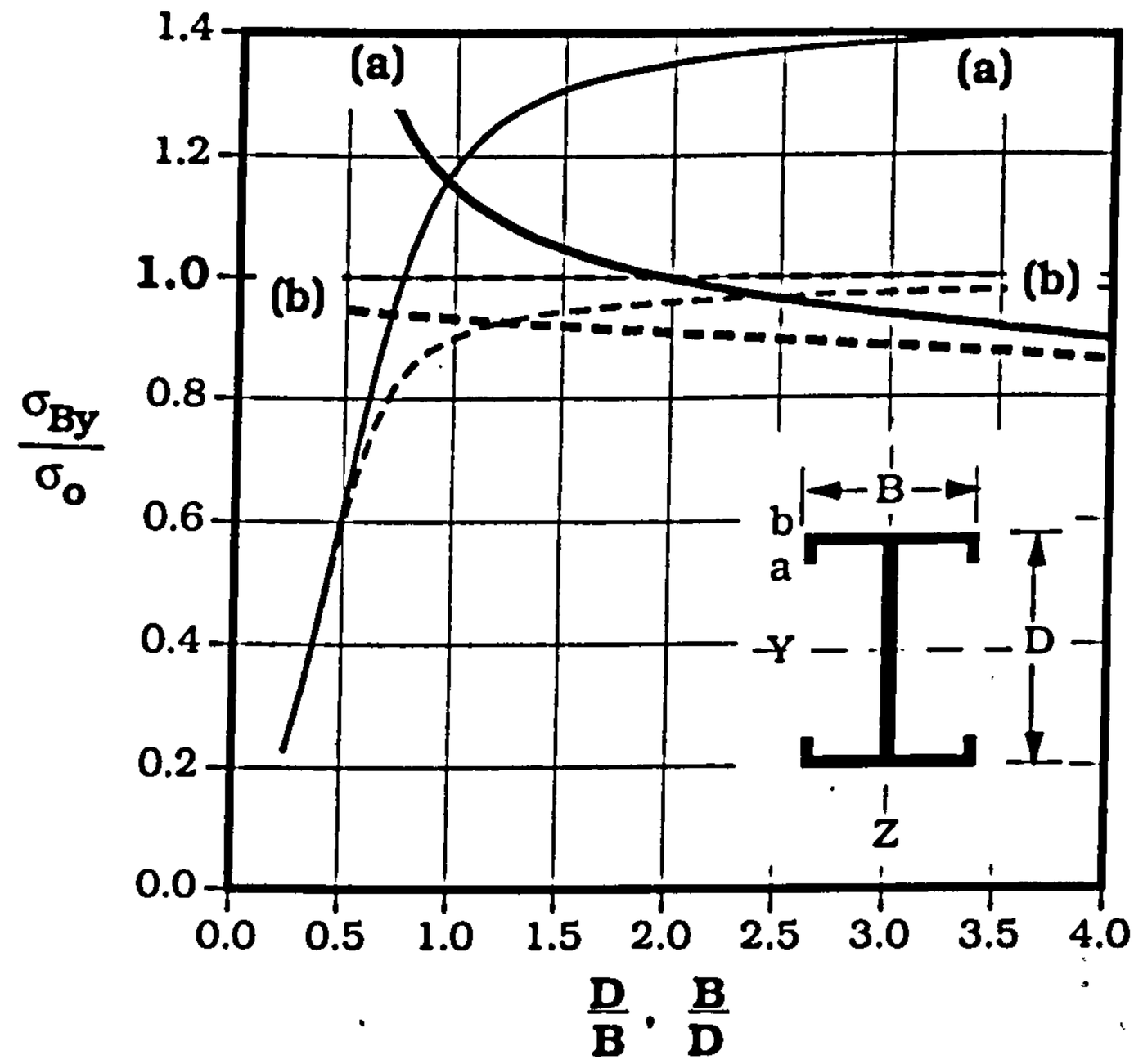


Figure 8.10 Variation in bending stress to cause first surface yieldwith depth and breadth, given by Equations 8.32 and 8.33.

D_L = 20mm, t = 1.5, L = 2000mm, σ_o = 390 N/mm^2

Figure 8.10 shows the variation in bending stress to cause first yield with depth and breadth for the I-section, obtained from Equations 8.32 and 8.33. It is observed that first yield always occurs at the lip/flange junction.

The bending stress to cause first yield as a result of lateral-torsional buckling, according to BS 5950: Part 5 (1987), is given by a modified Perry formulation, where the lateral-torsional buckling stress σ_{LTy} is substituted for the critical Euler buckling stress σ_E. The Perry equation is then written as

$$\sigma_{By} = 0.5\left[(\sigma_o + \sigma_{LTy} + \eta\,\sigma_{LTy}) - \left\{(\sigma_o + \sigma_{LTy} + \eta\,\sigma_{LTy})^2 - 4\,\sigma_o\,\sigma_{LTy}\right\}^{1/2}\right] \qquad (8.37a)$$

where the imperfection parameter η is

$$\eta = 0.002\left(\frac{L_e}{r_z} - 40\right) \qquad (8.37b)$$

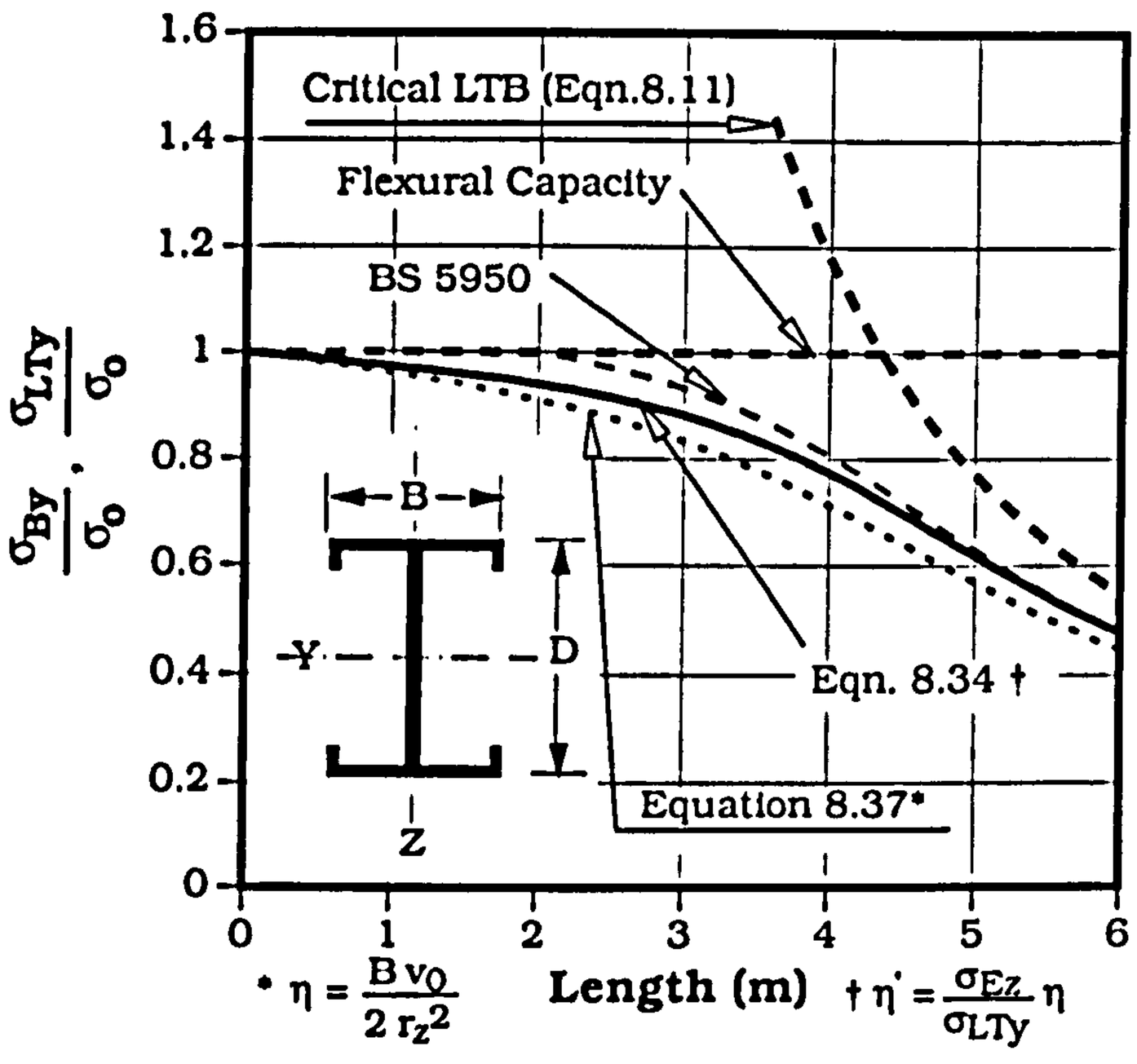


Figure 8.11 Variation in bending stress to cause first yield according to Equations 8.34, 8.37* and BS 5950: Part5

B = 180mm, D = 125mm, D_L = 20mm, t = 1.5, σ_o = 390 N/mm^2

In order to provide a representative comparison between Equations 8.34 and 8.37 the imperfection constant η for both equations is assumed to be given by Equations 8.35a. The ultimate bending stresses obtained from Equations 8.34 and 8.37a, where $v_o = L/1000$, are $\sigma_{By} = 366$ N/mm^2 and $\sigma_{By} = 355$ N/mm^2 respectively. It seems rational to adjust η for lateral-torsional buckling in Equations

8.37a with η' given in Equation 8.36, effectively reducing the magnitude of the assumed initial imperfection and subsequently increases the ultimate bending stress, as can be seen in Figure 8.11. BS 5950: Part 5 (1987) presently recommends Equations 8.37 which gives a bending stress equal to $\sigma_{By} = 388\ N/mm^2$. Figure 8.11 shows the variation in bending stress to cause first yield with length given by Equations 8.34 and 8.37 with various formulations for η.

8.3.2 BUCKLING RESISTANCE OF IMPERFECT DOUBLY LIPPED CHANNELS

Consider an initially imperfect doubly lipped channel section (Figure 8.5), where θ_o and v_{To} are affine to the critical lateral-torsional buckling mode. Young's equation can again be used to determine the increase in displacement v_T and rotation θ with load. If the initial imperfection $w_{\theta o}$ at the web/table junction is assumed to be $\pm$ L/1000, the rotation θ_o about the shear centre is

$$\theta_o = \frac{2\,L}{1000\,B} \tag{8.38}$$

The initial horizontal translation v_{To} of the shear centre can then be found from the critical mode ratio given by Equation 8.14, which can be rewritten as

$$v_{To} = \frac{M_{LTy}\,\theta_o}{P_{Ez}} \tag{8.39}$$

The longitudinal stresses caused by the additional lateral displacement v_{1T} (Equation 8.25) can be obtained by consideration of the resulting curvatures. The stress at the lip/web junction caused by a horizontal displacement is

$$\sigma = \pm v_{1T}\,\frac{\pi^2}{L^2}\,E\,\frac{B}{2} \tag{8.40}$$

While the stress at the lip table/lip downturn junction is

$$\sigma = \pm\, v_{1T}\,\frac{\pi^2}{L^2}\left(\frac{B}{2} - B_L\right)E \tag{8.41}$$

Consider a small rotation θ about the shear centre; this causes displacements v_θ and w_θ at the corners of the section. The horizontal displacement v_θ of the table due to θ is

$$v_\theta = \bar{z}_{sc}\,\theta \tag{8.42}$$

and at the lip table

$$v_\theta = (\bar{z}_{sc} + D)\,\theta \tag{8.43}$$

In the plane of the webs

$$w_\theta = \frac{B\theta}{2} \tag{8.44}$$

Warping stresses in the section are caused by the additional displacements $v_{1\theta}$ and $w_{1\theta}$, where

$$v_{1\theta} = v_\theta - v_{\theta o}, \qquad w_{1\theta} = w_\theta - w_{\theta o} \tag{8.45}$$

The horizontal curvature of the table caused by the additional displacement $v_{1\theta}$ is

$$\frac{1}{R} = v_{1\theta}\frac{\pi^2}{L^2} \tag{8.46}$$

The corresponding stress at the corner of the web/table junction (point **d**, Figure 8.5) is

$$\sigma = v_{1\theta}\frac{\pi^2}{L^2}\frac{B}{2}E = \bar{z}_{sc}\,\theta_1\frac{\pi^2}{L^2}\frac{B}{2}E \tag{8.47}$$

Similarly the stress increment over the depth of the web is

$$\sigma = w_{1\theta}\frac{\pi^2}{L^2}D\,E = \frac{B\theta_1}{2}\frac{\pi^2}{L^2}D\,E \tag{8.48}$$

and the stress increments over the width, and the depth of the lip are obtained from Equations 8.49 and 8.50 respectively

$$\sigma = v_{1\theta}\frac{\pi^2}{L^2}B_L\,E = (D + \bar{z}_{sc})\,\theta_1\frac{\pi^2}{L^2}B_L\,E \tag{8.49}$$

$$\sigma = w_{1\theta}\frac{\pi^2}{L^2}D_L\,E = \left(\frac{B}{2} - B_L\right)\theta_1\frac{\pi^2}{L^2}D_L\,E \tag{8.50}$$

The longitudinal stress caused by vertical bending at the web/table junction is

$$\sigma = \frac{M}{Z_t} = -\sigma_{Bt} \tag{8.51}$$

and at the web/lip junction

$$\sigma = \frac{M}{Z_\ell} = \sigma_{B\ell} \tag{8.52}$$

where

Z_t, Z_ℓ are the section modulii of the channel section taken at the table and lip

σ_{Bt}, $\sigma_{B\ell}$ are the bending stresses in table and lip table of the section

The warping stress distribution for the doubly lipped channel section can be obtained from Equations 8.47 to 8.50, with v_{1T} and θ_1 given by Equations 8.25 and 8.26. The total stress at the junction of any two elements in the cross-section, for any level σ_B/σ_{LT} and $w_{\theta o}$ may be obtained from the summation of individual stress components.

When the channel is bent about the Y axis such that the lips are in compression, tensile yield (denoted by a negative sign) will occur at the web/table junction (point e), given by

$$-\sigma_{Bt} = \sigma_B = -\sigma_o + \frac{B}{2} E \frac{\pi^2}{L^2}(v_{1T} + \theta_1 \bar{Z}_{sc}) \tag{8.53}$$

Similarly, compressive yield occurs at the intersection of lip table/lip downturn (point g) , when

$$\sigma_{B\ell} = \sigma_B = \sigma_o + \left(\frac{B}{2} - B_L\right) E \frac{\pi^2}{L^2} v_{1T} - \frac{\pi^2}{L^2} E \theta_1 \left[\left(\frac{B}{2} + B_L\right) D - \left(\frac{B}{2} - B_L\right) \bar{Z}_{sc}\right] \tag{8.54}$$

Consider the doubly lipped channel section (Figure 8.5), where L = 3000mm and w_o = L/1000. Tensile yield (Equation 8.53) occurs when M_{By} = 7.12 kNm, corresponding to a table stress of σ_{Bt} = 182 N/mm^2, and $\sigma_{B\ell}$ = 244 N/mm^2 at the lip. Compressive yield (Equation 8.54) occurs when the M_{By} = 6.16 kNm, where σ_{Bt} = 157 N/mm^2 and $\sigma_{B\ell}$ = 211 N/mm^2.

Figure 8.12 shows the variation between σ_{By} with breadth obtained at points **e**, **f**, **g** and **h** around the channel section. For this particular cross-section first yield always occurs at point **g**, the lip table/lip downturn junction, which is defined by Equation 8.54.

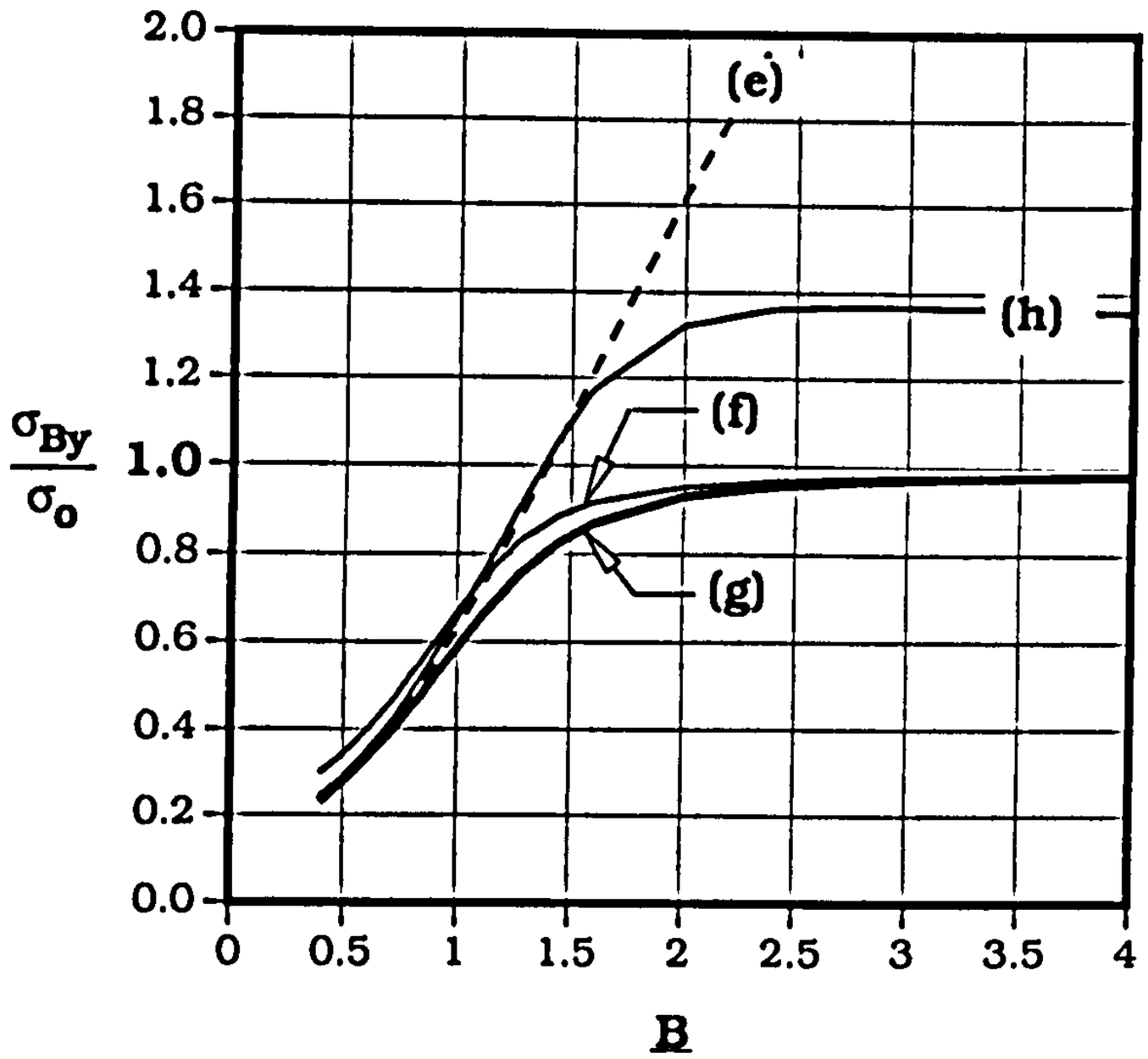


Figure 8.12 Nominal lip bendng stress σ_{By} which causes first yield at points around the channel section (see Figure 8.5). Stress at point **(e)** is tensile (σ_{LTy} corresponding to "straight beam" solution)

D = 97mm, B_L = 17mm, D_L = 18.5mm, t = 3.0mm, L = 3000mm, σ_o = 390 N/mm^2

The three individual stress components at first yield due to rotation about the shear centre, horizontal displacement of the shear centre and vertical displacement due to bending and are shown in Figure 8.13. It can be seen that the vertical bending and torsional warping stresses make the largest contributions to the failure stress, while the horizontal bending stress has little effect on the final stress distribution.

Figure 8.14 shows the final stress distribution and displaced shape of the channel section, assuming the initial imperfections to be affine to the "curved beam" critical buckling mode which were obtained from the finite element critical buckling analysis.

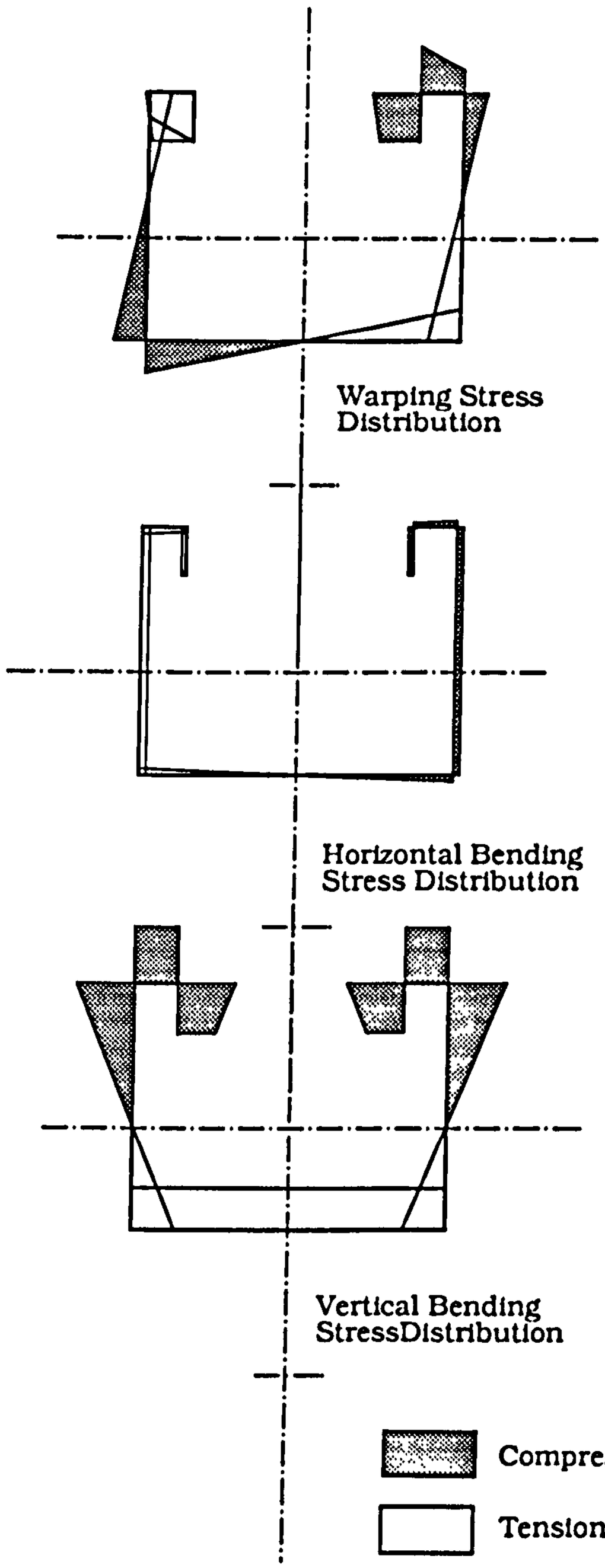


Figure 8.13 Warping, horizontal bending and vertical bending stress distributions at first yield caused by lateral torsional buckling.
(curved beam critical mode)
B = 122mm, D = 97mm, B_L = 17mm, D_L = 18.5mm, t = 3.0mm
σ_o = 390 N/mm^2, L = 3000mm

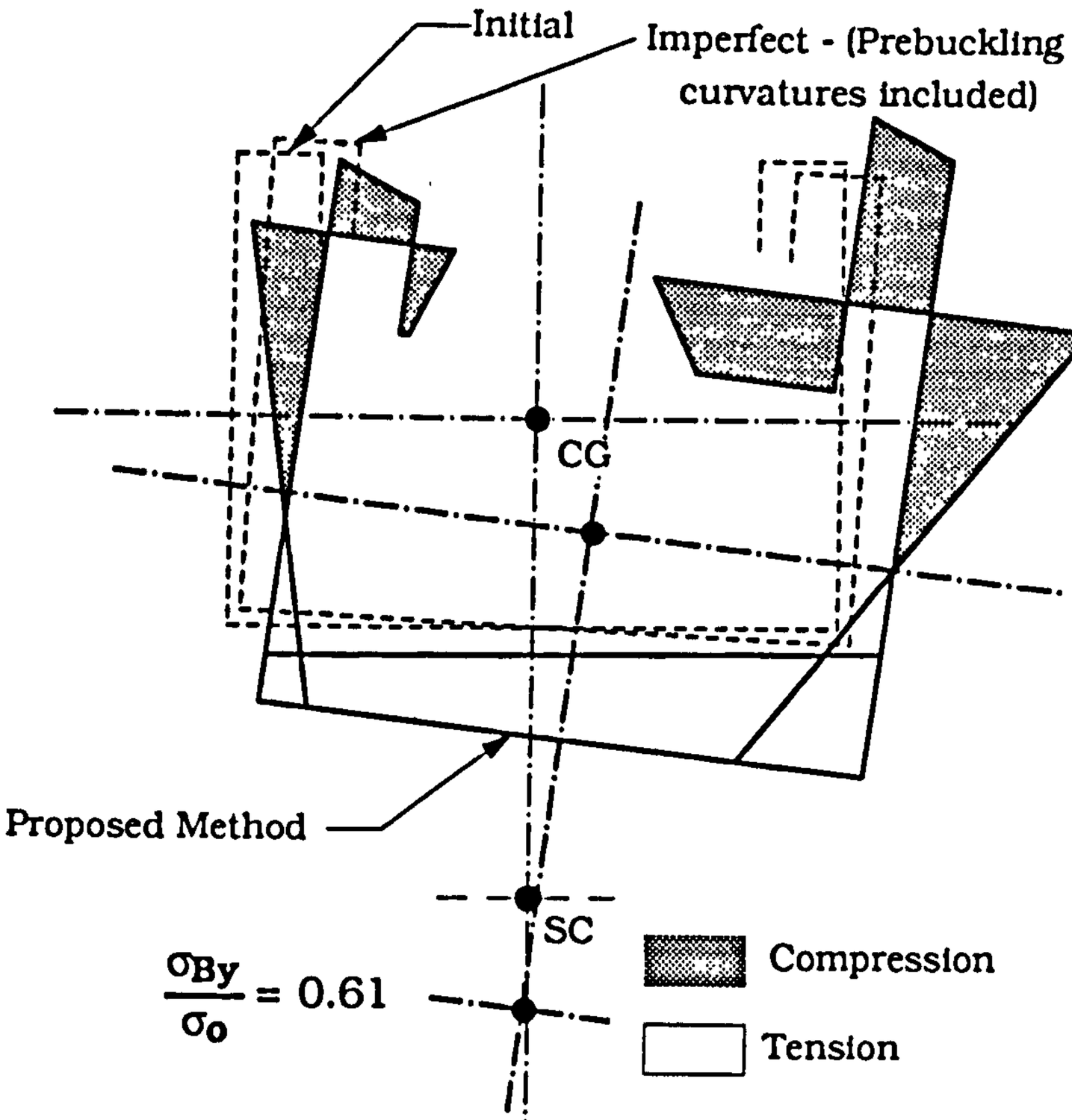


Figure 8.14 Stress distribution and displacements at first surface yield based on Young's equation.

8.3.3 NON-LINEAR ELASTO-PLASTIC FINITE ELEMENT ANALYSIS OF DOUBLY LIPPED CHANNELS

The ultimate lateral-torsional buckling resistances for 2000mm, 3000mm and 4000mm long 122x97x17x18.5-3mm thick channel sections were obtained by means of non-linear elasto-plastic finite element analyses. The boundary conditions, loading and mesh arrangements used in the critical lateral-torsional buckling analysis were again employed. The initial mode of imperfection necessary for each non-linear analysis was scaled from the corresponding eigenvector obtained during the critical buckling analysis for members without pre-buckling deflections. The level of imperfection introduced into the non-linear analysis, based on the critical buckling mode, was equivalent to an up/down vertical displacement at the web/table junctions of ± L/1000. When L = 3000mm, the initial imperfections were alternatively taken to be affine to the critical mode for the initially "straight beam" and "curved beam" solutions. It was then possible to determine the effects of

different modes of initial imperfection on the first yield and failure moments. The bending moments to cause first yield and failure are given in Table 8.2, along with the first yield moments predicted by equation 8.54.

Length (m)	FINASIC (1990)		Equation 8.54
	$\frac{\sigma_B}{\sigma_o}$	$\frac{\sigma_{By}}{\sigma_o}$	$\frac{\sigma_B}{\sigma_o}$
2	0.81	0.86	0.80
3	0.62	0.64	0.58
3†	0.63†	0.66†	0.61†
4	0.49	0.63	0.40

† initial imperfection affine to the "curved beam" critical buckling mode

Table 8.2 Minor axis lateral-torsional buckling resistance obtained from numerical analysis and Equation 8.54 of doubly lipped channel section.
B = 122mm, D = 97mm, B_L = 17mm, D_L = 18.5mm,
t = 3.0mm, σ_o = 390 N/mm^2

The numerical analysis shows that first yield is closed followed by failure except for L = 4000mm. In this case the rotations were so large that there was a major component of bending about the major axis. It is observed that when L = 3000mm the first yield moment is a minimum for initial imperfections affine to the critical mode for the "straight beam", such that σ_{By} = 242 N/mm^2, compared to σ_{By} = 247 N/mm^2 for the "curved beam" critical mode. This slight difference in bending stress suggests that the buckling behaviour is not very sensitive to the direction of the initial horizontal imperfection.

The variation in moment with translation v_T and rotation θ about the shear centre obtained from the non-linear elasto-plastic analysis of a 3000mm long member, with initial imperfections affine to the curved beam critical buckling mode, along with displacements given by Equations 8.25 and 8.26 are plotted in Figure 8.15. The lateral displacement v_T and rotation θ predicted by Young's equation agree well with those obtained numerically. A similar comparison was also carried out on a beam with initial imperfections affine to the straight beam critical buckling mode. The cross-sectional displacements obtained numerically, and those given by Equations 8.25 and 8.26 are shown in Figure 8.16. It is observed that Equation 8.26 overestimates the rotation θ, while the shear centre position is seen to displace laterally to the left of the vertical neutral axis, even though the initial horizontal

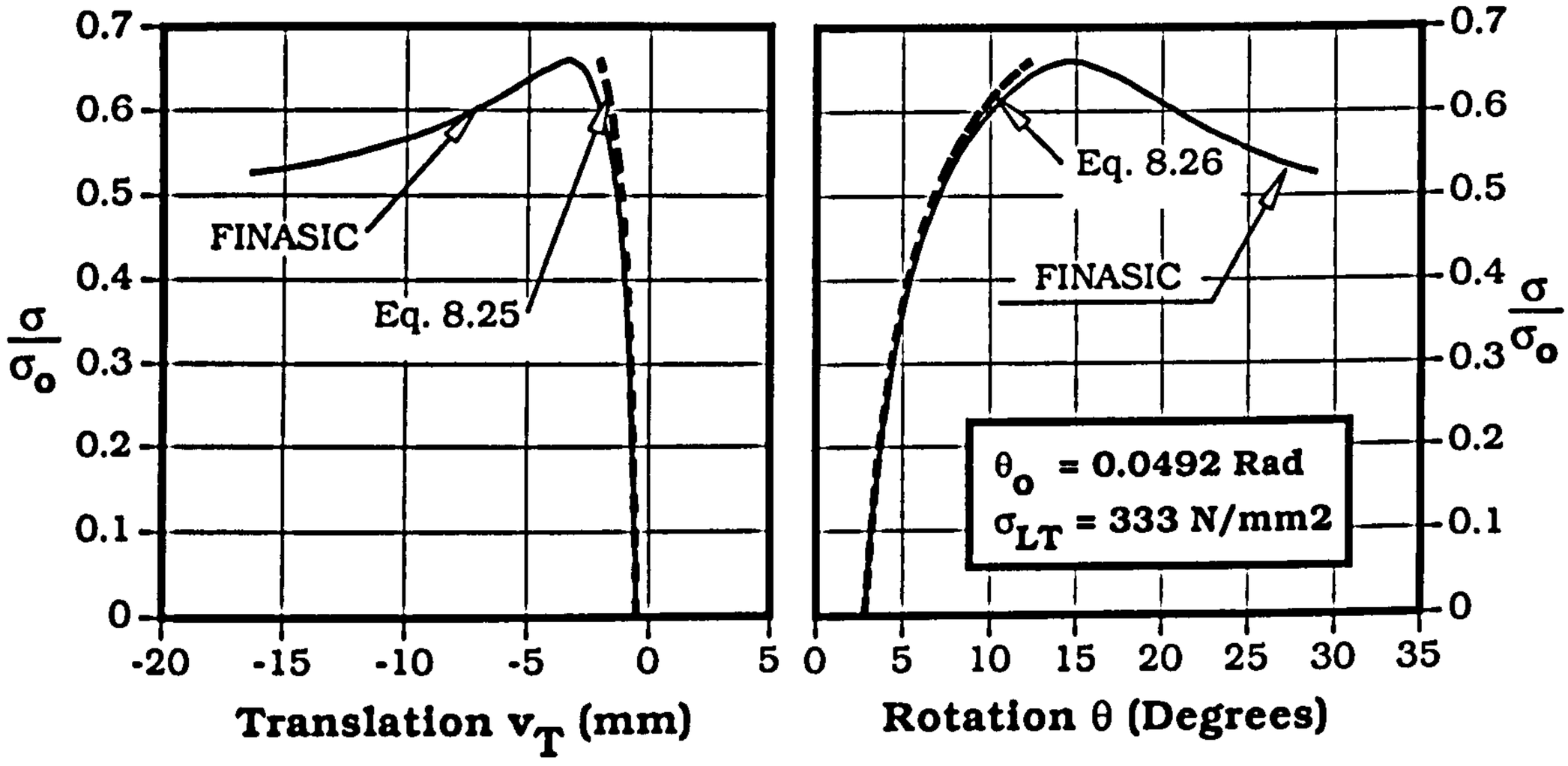


Figure 8.15 Variation in displacementand rotation, with moment given by Equations 8.25 and Equation 8.26 and FE analysis (curved beam critical mode)

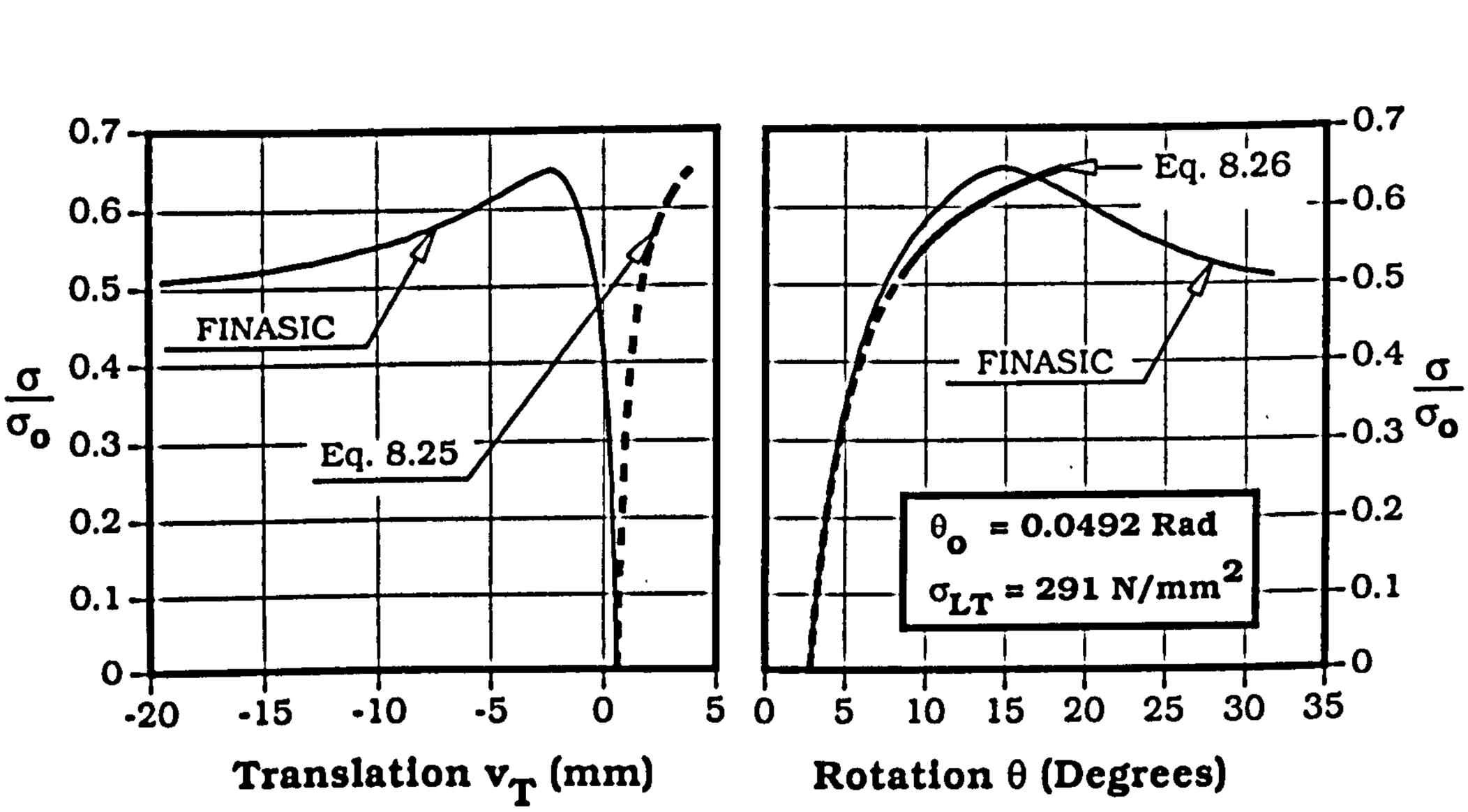


Figure 8.16 Variation in displacement and rotation, with moment given by Equations 8.25 and Equation 8.26 and FE analysis (straight beam critical mode)

imperfection was to the right (Equation 8.14). The variation of lateral displacement with moment obtained from Equation 8.25 is seen to increase to the right.

This inconsistency in behaviour is due to the occurrence of a relatively large mid-span cross-sectional rotation which violates the small deformation assumptions. When the section rotates, the minor axis moment applied to the ends of the member is resisted by the flexural rigidity in both principal planes of bending. The applied moment can be resolved into two component moments, one about each of the principal axes of the displaced cross-section. These moments cause in-plane displacements, which may then be resolved to give the final position of the cross-section. Figure 8.17 shows the mid-span location of the shear centre obtained at first yield by considering solely the displacements caused by bending. It can be seen that the shear centre position lies to the left of the original vertical plane; this is due to the large rotation of the cross-section.

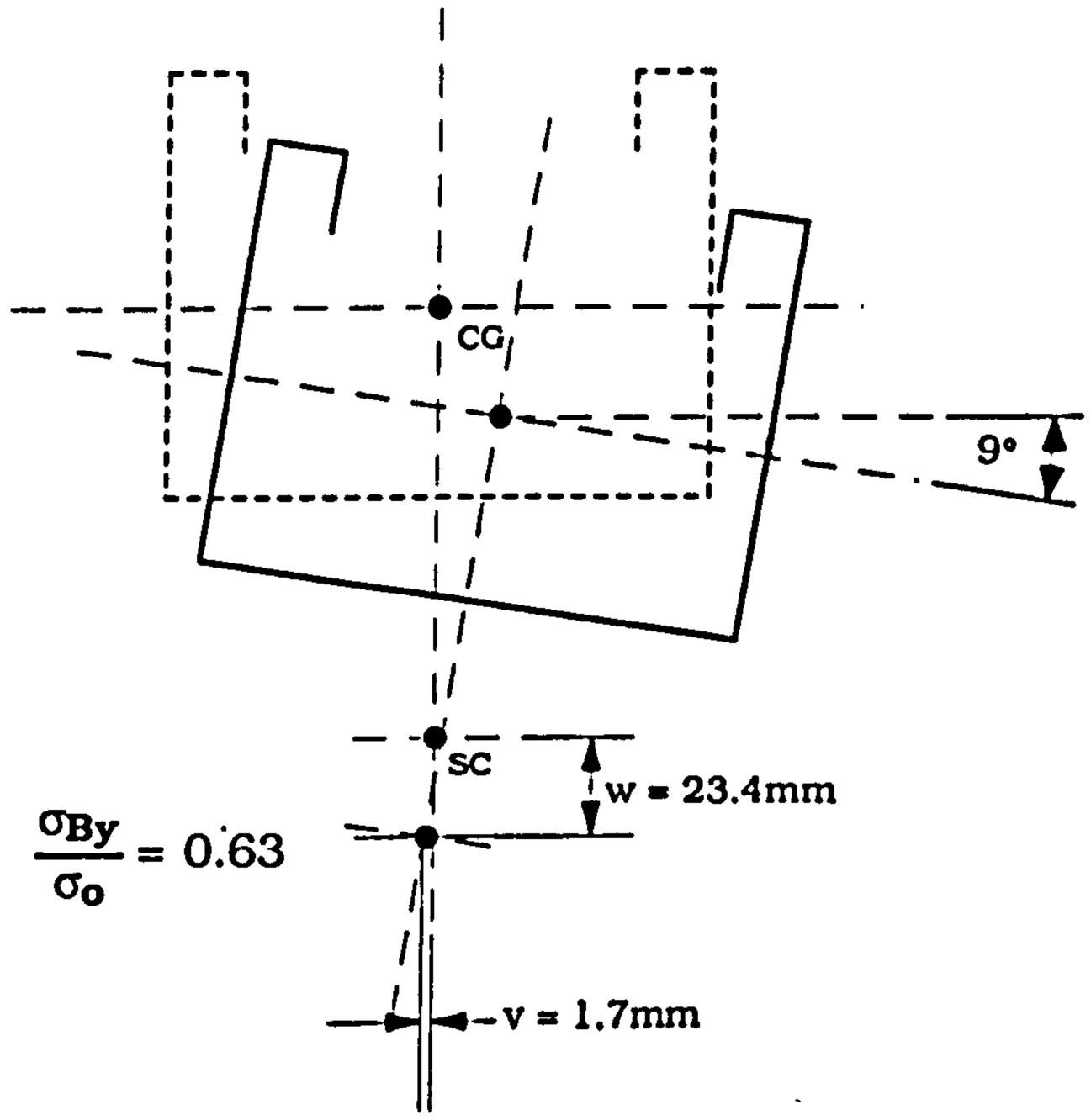


Figure 8.17 Shear centre position after bending of rotated cross-section (curved beam solution)

The mid-span stress distribution, for L = 3000mm, with initial imperfections affine to the curved beam critical buckling mode ($w_{\theta o}$ = L/1000) obtained numerically is shown in Figure 8.18, which also compares the cross-section displacements obtained numerically and from Equations 8.25 and 8.26. A small amount of cross-sectional deformation is observed and it was found that the lips of the section had moved apart by 4mm, resulting in additional lip stresses across the width of the lip table element, equal to 7.5 N/mm^2. A similar occurrence was also noted for torsional-flexural buckling analysis previously discussed in Chapter Seven.

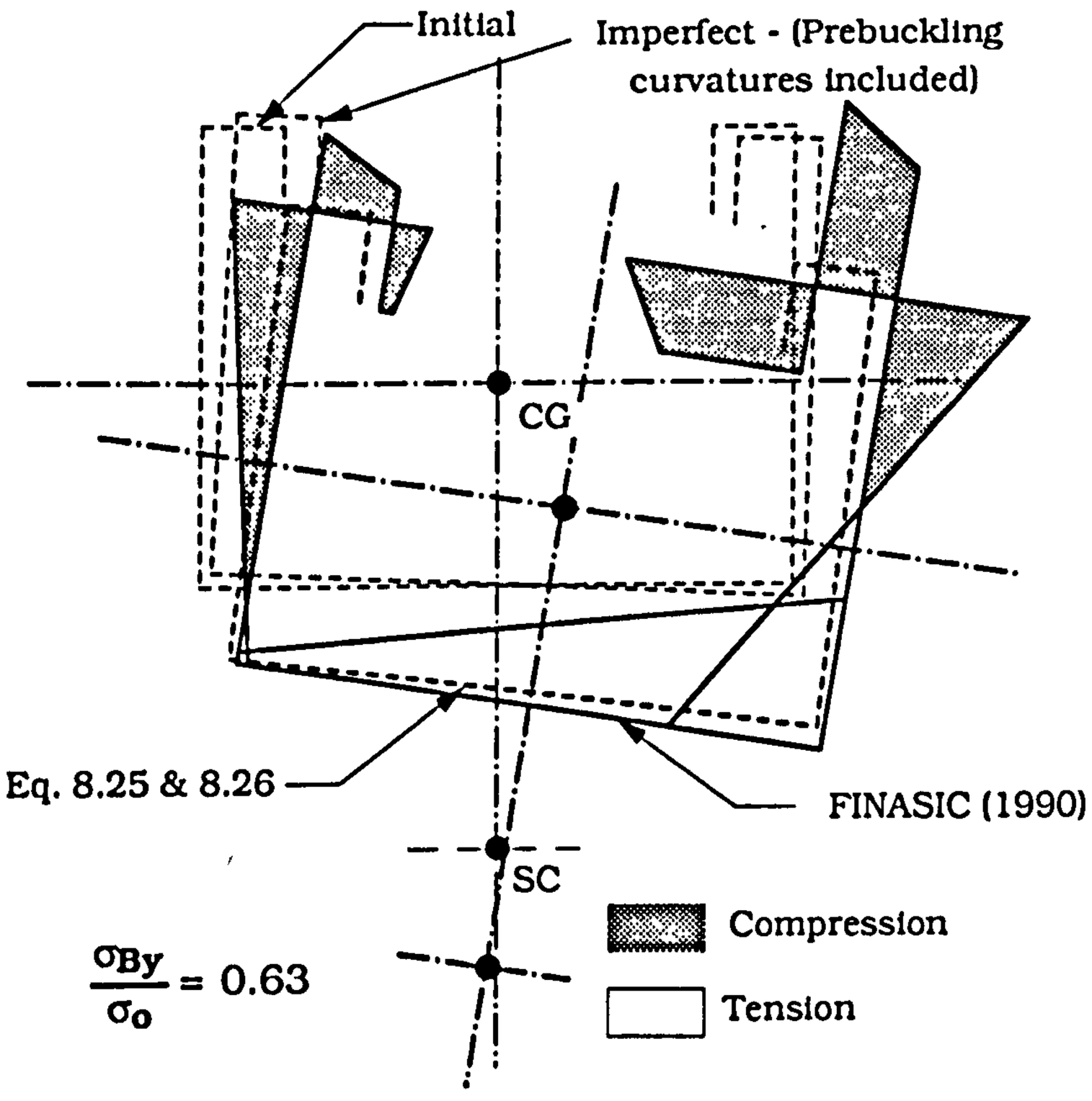


Figure 8.18 Stress distribution and displacements at first surface yield given by FE analysis (FINASIC 1990)

In Table 8.2 it is observed that Equation 8.54 predicts the first yield moment with sufficient accuracy, but on comparing Figures 8.14 with 8.18 it is evident that the stress distributions are slightly different. Given that the rotation and lateral translation obtained from Equations 8.25 and 8.26, and those obtained numerically, are in good agreement (Figure 8.15), it would be expected that similar agreement exists between stress distributions. The differences in stress distribution are due to the assumptions made regarding the vertical bending stresses. The vertical bending

stress distribution shown in Figure 8.13 was obtained by assuming that the applied moment is resisted solely by the flexural rigidity about the horizontal axis of the channel (EI_y). This is in keeping with the assumptions associated with the application of small displacement behaviour, but is not strictly correct for large rotational deformation as observed in the finite element analysis. A more accurate representation of the final stress distribution may be obtained by considering the displacements caused by the two components of bending generated by the global deformations incurred.

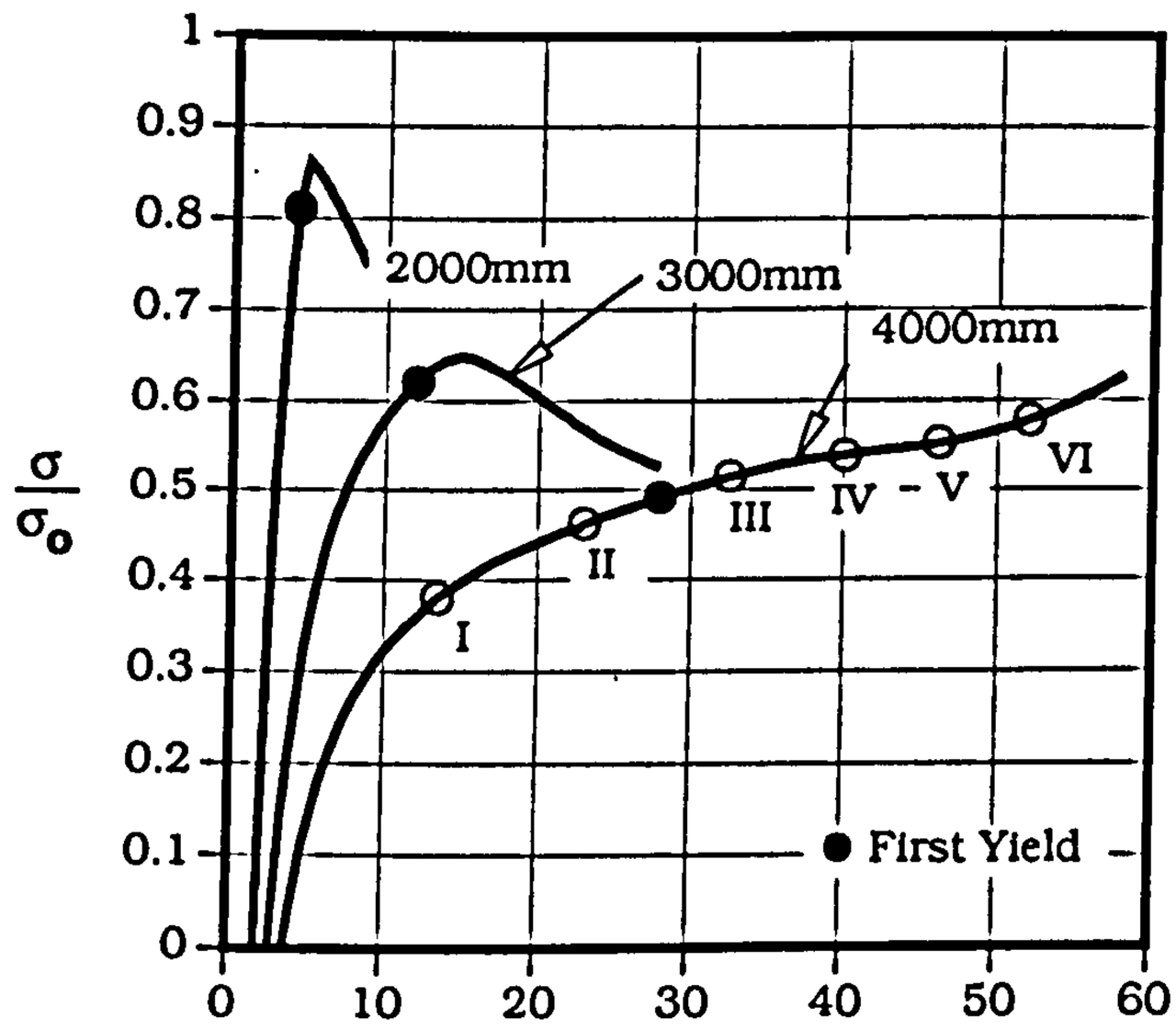


Figure 8.19 Bending stress vs rotation θ about the shear centre obtained from FE analysis for doubly lipped channel section for various member length (see Figure 8.20).

B = 122mm, D = 97mm, B_L = 17mm, D_L =18.5mm, t = 3.0mm,

L = 3000mm, σ_o = 390 N/mm^2

Figure 8.19 shows the variation in applied moment with rotation θ about the shear centre for all three lengths. When L = 4000mm, failure was not obtained, even though first yield had occurred. This increase in moment resistance is due to the large mid-span rotation, which causes further mobilization of the major axis flexural stiffness. Figure 8.20 shows the moment/deformation history for the 4000mm long member obtained from the finite element analysis.

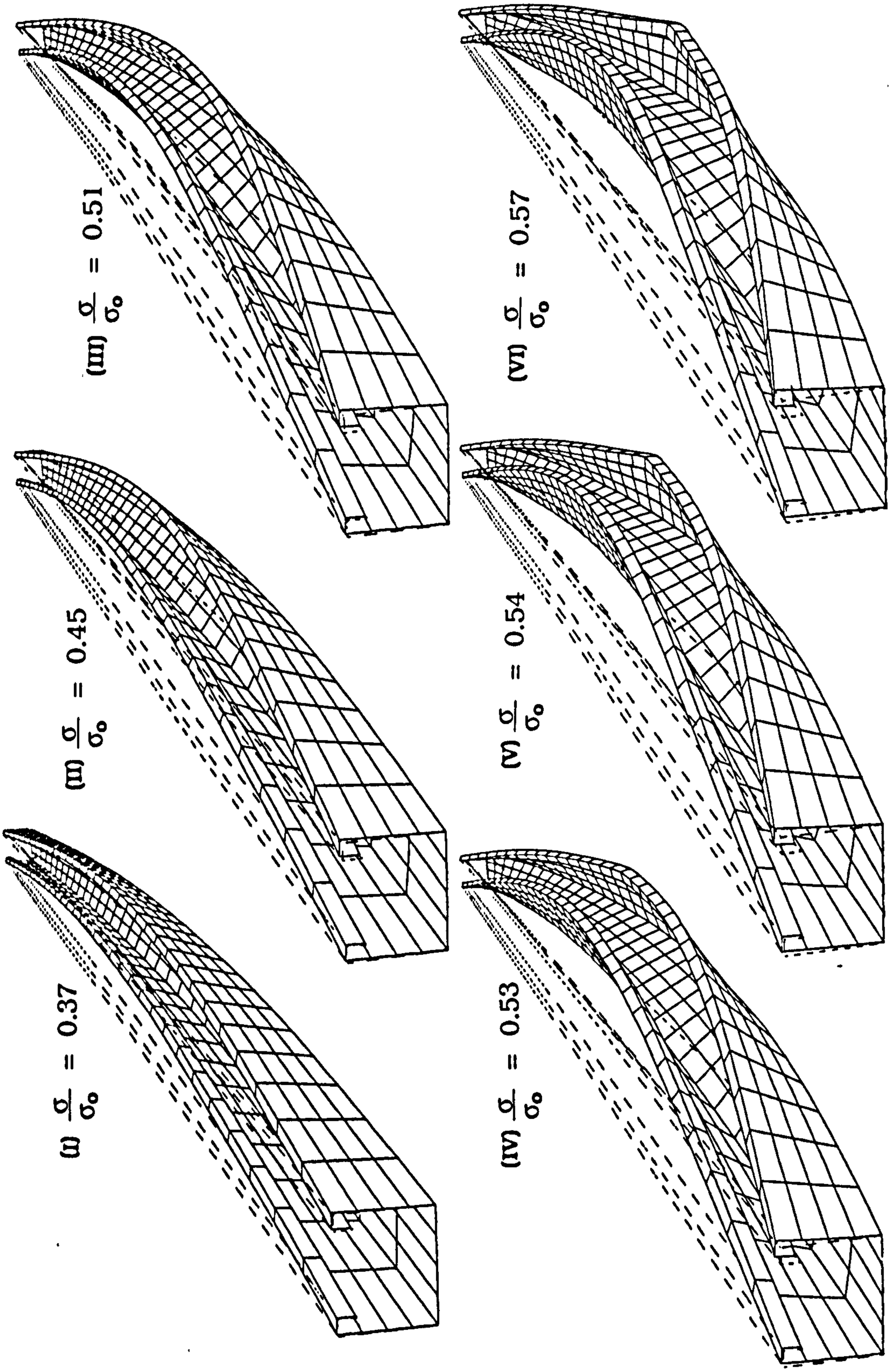


Figure 8.20 Load vs. deformation history of doubly lipped channel subjected to uniform minor axis bending (See Figure 8.19).
B = 122mm, D = 97mm, B_L = 17mm, D_L = 18.5mm, t = 3.0mm, L = 4000mm, σ_o = 390 N/mm^2, M_o = 11.6kNm
(Displacments x 2)

8.4 PROPOSED DESIGN METHOD

The major axis critical lateral-torsional buckling moment M_{LTz} for the doubly lipped channel obtained according to BS 5950: Part5 (1987) was shown to lead to somewhat non-conservative design (Figure 8.7). BS 5950: Part 5 does not take account of minor axis lateral-torsional buckling. Design methods are now proposed for determining the critical lateral-torsional buckling moment M_{LT} and the lateral-torsional buckling moment to cause first surface yield, M_B, for singly and doubly symmetric sections bent about their major or minor axes.

8.4.1 CRITICAL LATERAL-TORSIONAL BUCKLING

In BS 5950: Part 5 (1987) the recommendations for determining the critical elastic lateral-torsional buckling resistance are confined to I, C, Z and T beams. The critical buckling formulations do not presently account for pre-buckling curvatures prior to buckling. In this chapter it has been shown that the critical lateral-torsional buckling moment for a thin-walled section of arbitrary shape subjected to bending about either of the two principal axes, taking into account the effects of pre-buckling curvatures, may be obtained from the following general equations (Attard 1990);

For bending about the Y axis

$$M_{LTy} = -\frac{P_{Ez}\beta_y}{2\left(1-\frac{I_z}{I_y}\right)} \pm \left[\left(\frac{P_{Ez}\beta_y}{2\left(1-\frac{I_z}{I_y}\right)}\right)^2 + \frac{r_o^2 P_{Ez} P_T}{\left(1-\frac{I_z}{I_y}\right)}\right]^{1/2} \tag{8.55}$$

or

$$M_{LTy} = \frac{r_o^2\ P_T}{2\ \beta_y} \quad \text{for } I_y = I_z \tag{8.56}$$

For bending about the Z axis

$$M_{LTz} = -\frac{P_{Ey}\beta_z}{2\left(1-\frac{I_y}{I_z}\right)} \pm \left[\left(\frac{P_{Ey}\beta_z}{2\left(1-\frac{I_y}{I_z}\right)}\right)^2 + \frac{r_o^2 P_{Ey} P_T}{\left(1-\frac{I_y}{I_z}\right)}\right]^{1/2} \tag{8.57}$$

or

$$M_{LTz} = \frac{r_o^2 \, P_T}{2 \, \beta_z} \quad \text{for } I_z = I_y \tag{8.58}$$

The minor axis critical lateral-torsional buckling moment for the doubly lipped channel section, obtained from the finite element analysis are compared with Equations 8.16 and 8.55 in Figure 8.21. Good agreement between the two can be seen. Equations 8.55 to 8.58 are recommended for obtaining the critical lateral-torsional buckling moment for any arbitrary cross-section.

8.4.2 MINOR AXIS LATERAL-TORSIONAL BUCKLING RESISTANCE

Consider the singly symmetric doubly lipped channel section (Figure 8.5) subject to bending about the Y axis. It was previously shown that first yield always occurs at the junction between the lip table and lip downturn (Equation 8.54) for sections where $0.4 < B/D < 4.0$. An equation for determining the bending stress σ_{By} to cause first surface yield may be obtained by substituting Equations 8.25 and 8.26 into Equation 8.54 and solving for σ_B. The solution can then be expressed in terms of the Perry column equation:

$$\sigma_{By} = 0.5\left[(\sigma_o + \sigma_{LTy} + \eta\sigma_{Ez}) - \left[(\sigma_o + \sigma_{LTy} + \eta\sigma_{Ez})^2 - 4\sigma_o\sigma_{LTy}\right]^{1/2}\right] \tag{8.59}$$

where

$$\eta = (\eta_T + \alpha\eta_\theta) \tag{8.60}$$

in which

$$\eta_T = \frac{v_{To} \, B}{2 \, r_z^2} \tag{8.61}$$

and

$$\eta_\theta = \frac{\theta_o(D + \bar{z}_{sc}) \, B}{2 \, r_z^2} \tag{8.62}$$

α is a geometric constant which defines the position where first surface yield occurs. For the doubly lipped channel, α is

$$\alpha = \frac{(D - \bar{z}_{sc})}{\bar{z}_{sc}}\left[1 + \frac{2B_L}{B}\frac{(D + \bar{z}_{sc})}{(D - \bar{z}_{sc})}\right] \tag{8.63}$$

where

$\bar{z}_{sc}$ is the distance between the shear centre and the mid-thickness of the table element.

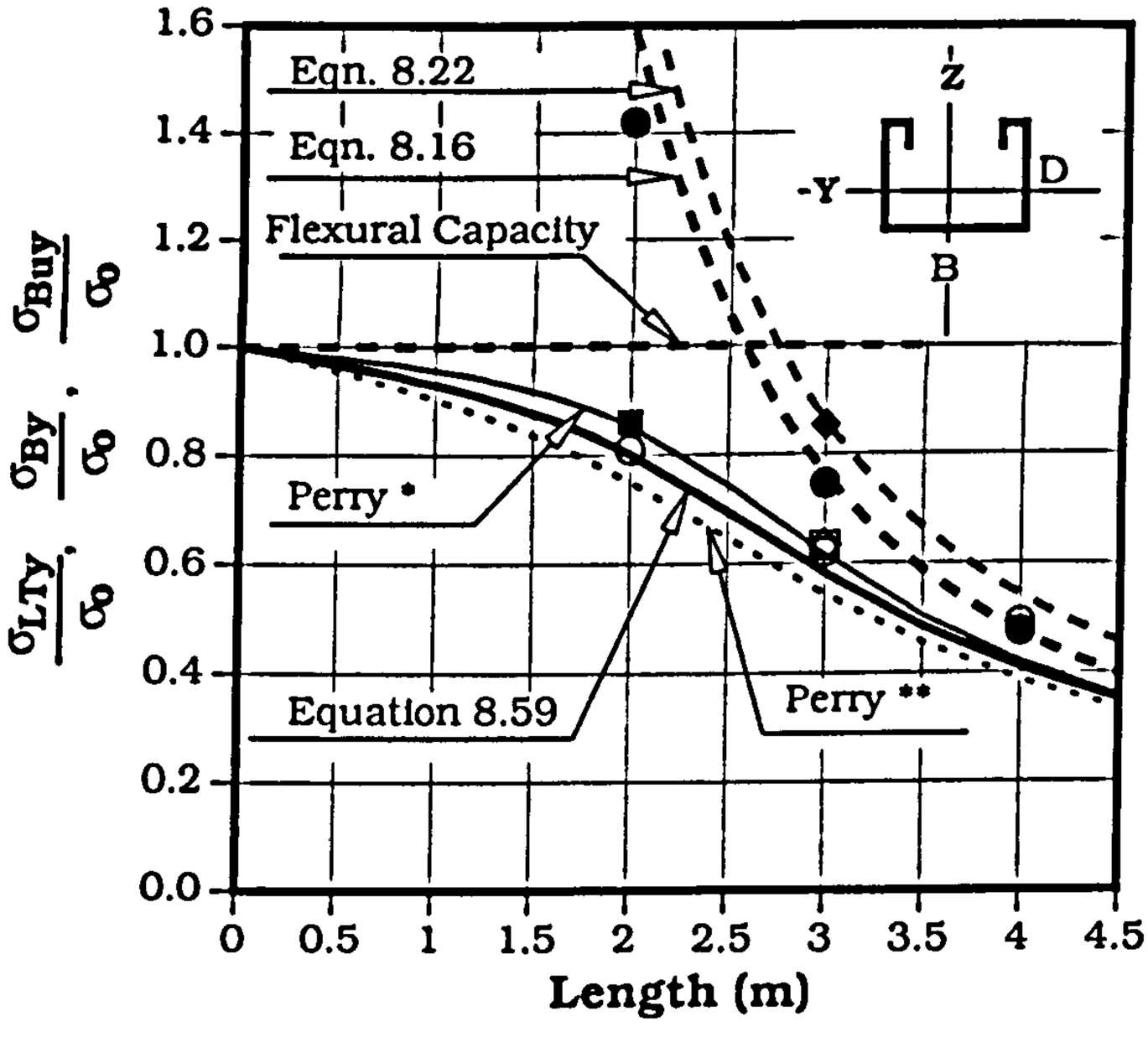


Figure 8.21 Bending stress to cause first yield and failure according to Equations 8.59, 8.64 and 8.65 and FE analysis.

B = 122mm, D = 97mm, B_L = 17mm, D_L = 18.5, t = 3.0mm, σ_o = 390 N/mm^2

Figure 8.21 shows the variation in allowable bending stress with length given by Equations 8.59 where η is given by Equation 8.60, and also Equation 8.37a with η given by Equations 8.64 and 8.65.

$$\eta = \frac{w_{\theta o}\,\bar{z}_{max}}{r_y^2} \qquad \text{(Perry *)} \qquad (8.64)$$

$$\eta = \frac{w_{\theta o}\,\bar{z}_{max}}{r_y^2}\,\frac{\sigma_{Ez}}{\sigma_{LTy}} \qquad \text{(Perry **)} \qquad (8.65)$$

The initial imperfection assumed in Equations 8.64 and 8.65 is in the vertical plane. This assumption is rational in as much as the web element incurs the largest vertical displacements and it is therefore likely, that first surface yield will occur at or near to the web/lip table junction.

In Figure 8.21 the finite element results given in Table 8.2 are compared with various lateral-torsional buckling formulations. The percentage variation in ultimate bending stress to cause first surface yield, given by the Perry equations (Equation 8.37a) with η given by Equation 8.64 and 8.65 relative to Equation 8.59 with η given by Equation 8.60 is shown in Figure 8.22. The Perry* approach overestimates the ultimate bending stress given by Equation 8.37a by 7%. If the correction factor σ_{Ez}/σ_{LT} is applied to the imperfection parameter η then the ultimate moment obtained from Perry ** is conservative by about 7%.

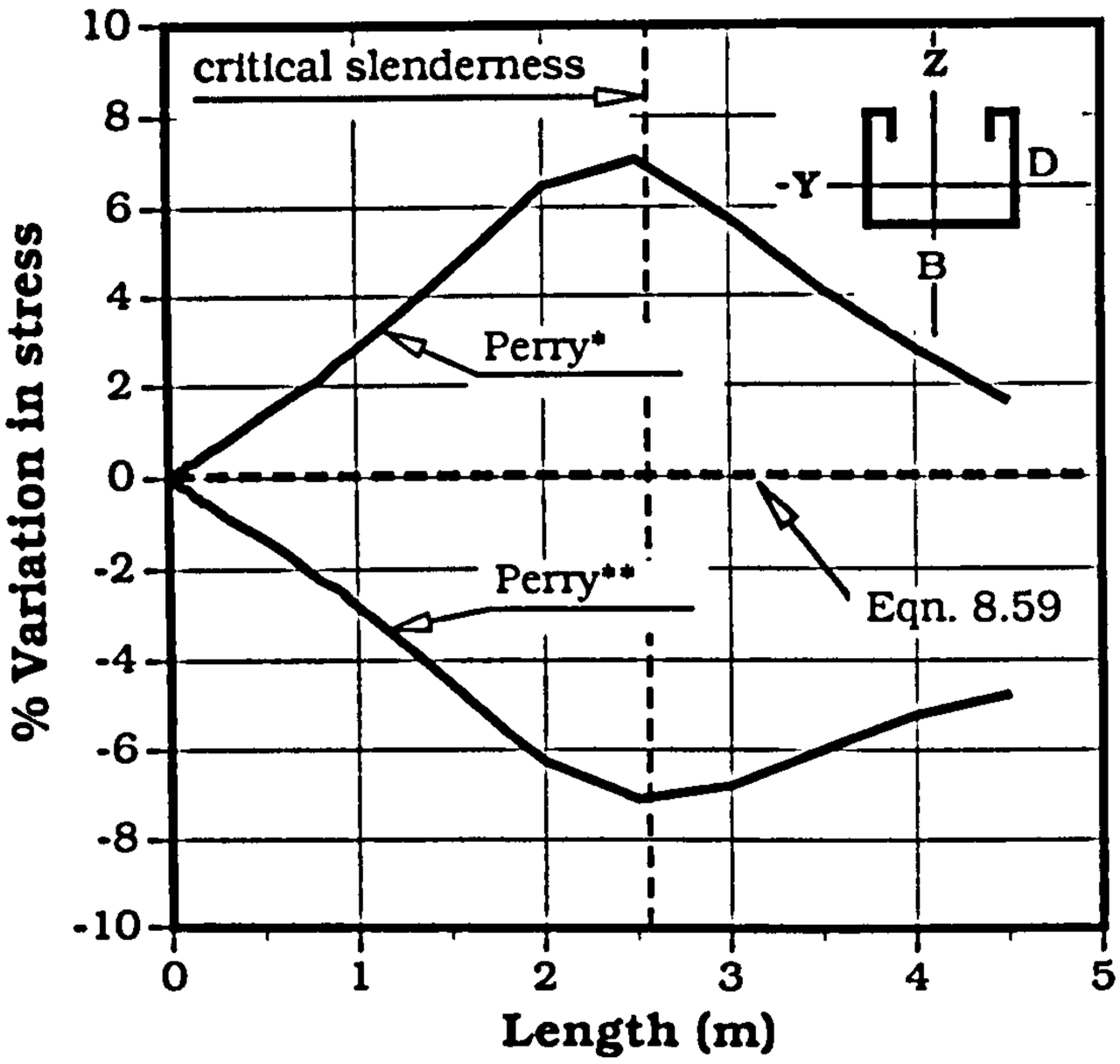


Figure 8.22 Percentage variation in ultimate bending stress according to Equations 8.37 with η given by Equations 8.64 and 8.65 relative to Equation 8.59. B = 122mm, D = 97mm, B_L = 17mm, D_L = 18.5mm, t = 3.0mm, σ_o = 390 N/mm^2

If, as stated in BS5950, it were assumed that singly symmetric sections are not prone to lateral-torsional buckling when bent about the minor axis, then the

ultimate moment would be overestimated by between 20% and 60% when 2000mm < L < 4000mm (Figure 8.21).

Equation 8.59 may be used to obtain the minor axis lateral-torsional buckling stress for any cross-section so long as an appropriate geometric constant α is used. Alternatively, a conservative estimate of the minor axis lateral-torsional buckling resistance for the doubly lipped channel section may be obtained from Equation 8.37a with the imperfection parameter η given by Equation 8.65.

8.5 CONCLUSIONS

(1) The design formulation given by several codes of practice, for determining the critical lateral-torsional buckling moment of doubly symmetric sections subjected to major axis bending is based on the assumption that the inplane bending deformation prior to buckling is small, and that its effect on the critical moment is deemed to be negligible. This assumption provides a simple formulation giving a conservative estimate of the critical moment. When the pre-buckling deformation is taken into account, the value of the critical moment was shown to increase.

(2) The equation currently given in BS 5950: Part 5 (1987) for critical lateral-torsional buckling of I-sections can be used for channels subject to major axis bending. However, this can lead to somewhat non-conservative estimates of the major axis critical lateral-torsional buckling moment for wide doubly lipped channel sections where B/D > 2.45. Equations 8.57 and 8.58 can be used to obtain the critical major axis moment for any cross-section.

(3) According to BS 5950: Part 5 (1987), lateral-torsional buckling about the minor axis does not occur. This is correct for doubly symmetric sections because when Iz = Iy, the critical stress becomes infinite for an initially straight beam. General approximate equations given for determining the critical lateral-torsional buckling moment for any open thin-walled beam (Equations 8.55 and 8.56) show that minor axis bending of certain singly or non-symmetric section does occur. A finite element study has confirmed the

existence of minor axis lateral-torsional buckling of singly symmetric channel sections.

(4) The design recommendations generally used for assessing the major axis lateral-torsional buckling resistance of imperfect sections are based on the flexural buckling formulation (Perry) in which the Euler buckling stress is replaced by the critical lateral-torsional buckling stress. This method takes no account of the differences in stress distribution and displacements associated with the flexural and lateral-torsional buckling modes.

(5) As BS 5950: Part 5 (1987) does not consider the possibility of minor axis lateral-torsional buckling, the minor axis bending resistance of the doubly lipped channel section has been shown numerically to be overestimated by up to 40%, when L = 3000mm.

(6) It has been shown that Young's equation can be used to obtain the displacements and rotations associated with lateral-torsional buckling for singly and doubly symmetric section up to first yield. Young's equation can be applied to the initial imperfections to give the total displacements which together cause first surface yield in the section. This provides the basis for a design method which describes the major and minor axis lateral-torsional buckling behaviour.

(7) Application of the original Perry formulation for flexural buckling with σ_{LTy} substituted for σ_{Ey} overestimates the lateral-torsional buckling moment by 7%. The lateral-torsional buckling moment to cause first surface yield is correctly given by the Perry formulation with σ_{LTy} substituted for σ_{Ey}, and with η multiplied by σ_{Ez}/σ_{LTy} and by a geometric constant α. If σ_{LT} is substituted for σ_E and η is multiplied by σ_{Ez}/σ_{LTy}, and η assumes an initial imperfection in the plane of bending, then the failure moment to cause first surface yield is underestimated by up to 7%, for the channel section considered.

Chapter Nine

INTERACTION BETWEEN AXIAL FORCE AND MINOR AXIS BENDING

9.1 INTRODUCTION

The strength of a beam-column subjected to any combination of axial load P, major axis moment M_z, and minor axis moment M_y can be displayed in the form of a three dimensional interaction diagram of the type shown in Figure 9.1. The end points represent the resistance to axial load P, and moments M_z and M_y. The interaction between the three components can be expressed as a formulation of the type

$$\frac{P}{P_u} + \frac{M_y}{M_{uy}} + \frac{M_z}{M_{uz}} \leq 1.0 \qquad (9.1)$$

which provides a smooth transition between end points. The geometrical properties, material strength, end support conditions and member slenderness will all have an effect on the shape of the interaction curve, that is, their degree of concavity or convexity. Initial out-of-plane deformations and/or residual stress will also influence the component strengths as well as the shape of the interaction.

This chapter is concerned with the interactive buckling behaviour and strength of doubly lipped channels subjected to axial compression and minor axis bending causing lip compression or lip tension. A brief account of current code design methods is also presented. In the case of a doubly symmetric section such is that in Figure 8.1 the interaction between P and M_y is the same whether My is positive or negative. In the case of the channel however, M_y has a destabilizing effect if it causes lip compression, but a stabilizing effect if it causes lip tension. The linear interaction indicated by Equation 9.1 provides a good representation of the true interaction when M_y causes lip compression, but is over conservative when My

causes lip tension. If M_y causes tension and is sufficiently large, torsional buckling does not occur. The most intriguing objective addressed in this chapter is determining the shape of the interaction curve when M_y causes tension.

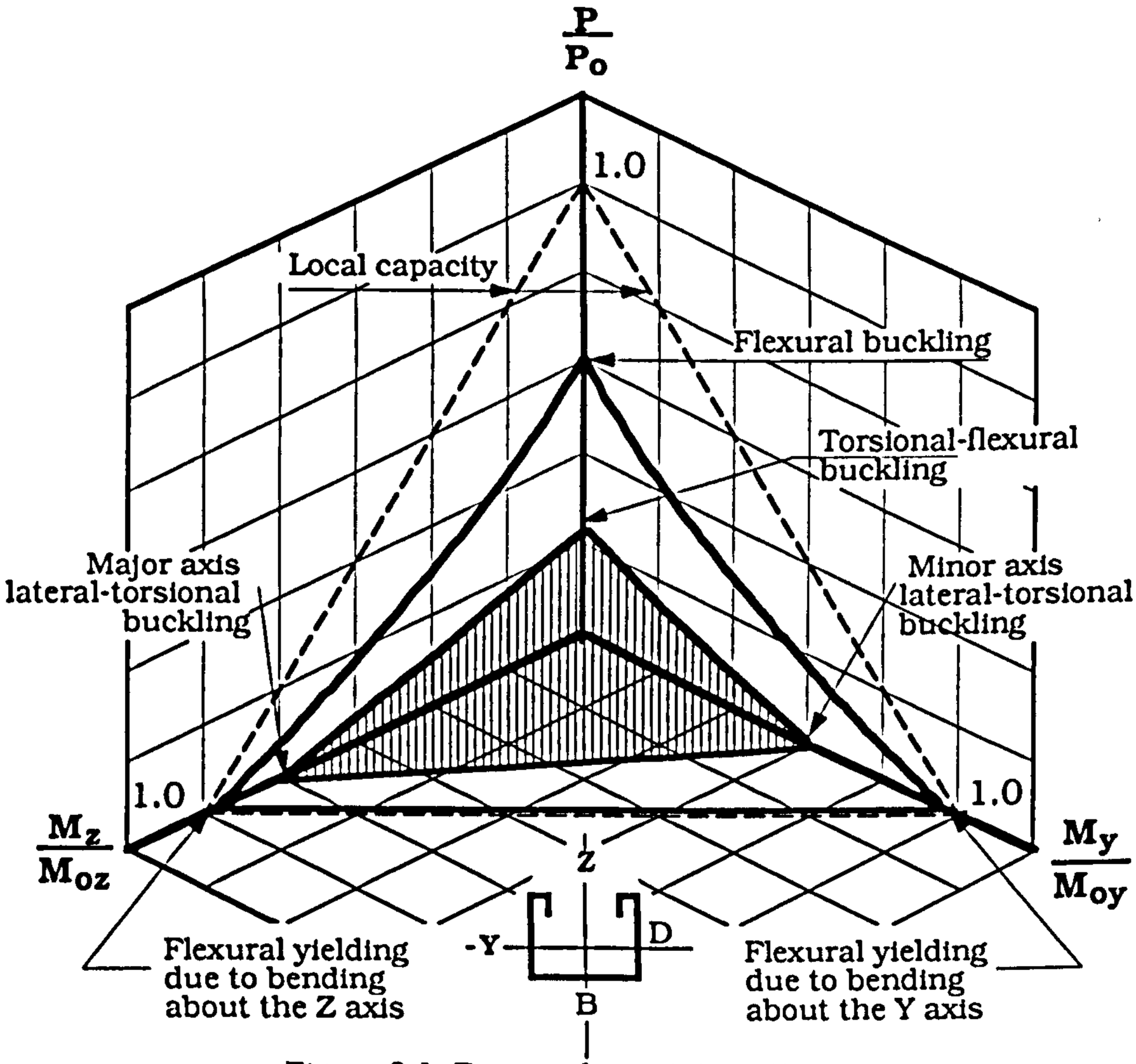


Figure 9.1 Beam-column interaction curves

A series of non-linear elasto-plastic finite element analyses were carried out to determine the shape of the interaction curves and to investigate the effects of different modal imperfections. Design equations describing the interactive buckling behaviour of the doubly lipped channel are proposed, based on the results obtained from the numerical analysis. Validation against available experimental data is provided.

9.2 COMBINED BENDING AND COMPRESSION

The analysis of axially loaded biaxially bent members has formed the subject of many research investigations. The interactive buckling behaviour of thin-walled

cold-formed channel columns subjected to eccentric loading has been investigated by Pekoz and Winter (1969), Loughan and Rhodes (1979) and Loughan (1983).

There are two different possible modes of failure for thin-walled cold-formed sections which should be examined when dealing with the interaction between axial compression and bending. These are

(a) yielding due to the section capacity being exceeded at points of greatest bending moment (usually at the ends of a member)
(b) Overall buckling

9.2.1 LOCAL CAPACITY CHECK

The local capacity of a section subject to combined loading can be described by a linear interaction equation, which ensures that any combination of axial load and bending will not cause the section to yield locally. The local capacity check given in BS 5950: Part 5: (1987) is

$$\frac{P}{P_{cs}} + \frac{M_y}{M_{uy}} + \frac{M_z}{M_{uz}} \leq 1.0 \qquad (9.2)$$

Interaction between local element buckling and overall buckling caused by the axial and bending loads are taken into account by introducing the short strut capacity P_{cs}, and moment capacities M_{uy} and M_{uz}, based on the geometrical properties of the effective cross-section, into Equation 9.2.

9.2.2 OVERALL BUCKLING CHECK

A suitable overall buckling check for thin-walled open sections should include the effects of:

(a) Local element buckling
(b) Lip buckling
(c) Flexural or torsional-flexural buckling due to axial compression
(d) Flexural yield or lateral-torsional buckling due to bending

Current design recommendations found in BS 5950: Part 5 (1987), AISI (1989) and EC3: Part 1.3 (1992) deal with the interaction between local element, flexural buckling and major axis lateral-torsional buckling. BS 5950: Part 5 (1987) prescribes two interaction equations to deal with overall buckling, the particular equation to be used in any given situation being dependent on whether or not lateral-torsional buckling is a possibility. If a section is not prone to lateral-torsional buckling, and is subjected to a combination of axial load and uniform moment about both principal axes, then the governing interaction equation is

$$\frac{P}{P_Y} + \frac{M_y}{M_{uy}\left(1 - \frac{P}{P_{Ey}}\right)} + \frac{M_z}{M_{uz}\left(1 - \frac{P}{P_{Ez}}\right)} \leq 1.0 \qquad (9.3)$$

The moment magnification factor $(1\text{-}P/P_E)$ included in the denominator of the moment ratios accounts for the additional curvature arising from the reduction in stiffness caused by the axial load.

If the section is prone to major axis lateral-torsional buckling and subjected to a combination of axial load and uniform moment, the following equation is given in place of Equation 9.3

$$\frac{P}{P_Y} + \frac{M_y}{M_{uy}\left(1 - \frac{P}{P_{Ey}}\right)} + \frac{M_z}{M_{Bz}} \leq 1.0 \qquad (9.4)$$

The moment magnification factor for major axis bending causing lateral-torsional buckling of the section is omitted since it's effect on the interaction is considered to be negligible, because it is assumed that P_Y will be much smaller than P_{Ez} and consequently, the value of the amplification factor $(1\text{-}P/P_{Ez})$ will be approximately equal to unity. The interaction between P, M_y and M_z given by Equations 9.3 and 9.4 can be seen in Figure 9.1.

AISI (1989) and EC3: Part 1.3 (1992) both recommend a similar approach but include the moment magnification factor for major axis bending causing lateral torsional buckling of the section, and is

$$\frac{P}{P_Y} + \frac{M_y}{M_{uy}\left(1 - \frac{P}{P_{Ey}}\right)} + \frac{M_z}{M_{Bz}\left(1 - \frac{P}{P_{Ez}}\right)} \leq 1.0 \qquad (9.5)$$

Except for EC3: Part 1.3 (1992), no account of the interaction between lip buckling and the overall modes of buckling is made. EC3: Part 1.3 (1992) includes the effects of lip buckling in the interaction equation by reducing the effective area of the section which in turn influences the axial resistance of the section. The interaction between torsional-flexural and lateral-torsional buckling, and torsional-flexural buckling and bending is considered by both AISI (1989) and EC3: Part 1.3 (1992). Both codes use the interaction equation for flexural buckling and lateral-torsional buckling in which the torsional-flexural buckling capacity is substituted for the flexural buckling capacity. BS 5950: Part 5 (1987) prohibits the use of the current beam-column design recommendations for members subject to either torsional-flexural or a combination of torsional-flexural and lateral-torsional buckling. Many other national codes of practice have adopted the recommendations given in the AISI (1989) specification.

In practice singly symmetric sections prone to lateral-torsional buckling may also be susceptible to torsional-flexural buckling in the presence of axial loads. The displacements resulting from torsional-flexural and lateral-torsional buckling are similar and therefore it would seem reasonable to expect that these two modes interact. A previous study carried out by Pekoz and Winter (1969), investigated the critical elastic torsional-flexural buckling behaviour of thin-walled sections subjected to eccentric axial load. Simple design aids for channel sections prone to torsional-flexural buckling and bending in the plane of symmetry were provided. It was also noted that the direction of the end moment influenced the mode of failure.

Consider the singly symmetric doubly lipped channel section shown in Figure 7.4, subjected to axial compression and uniform minor axis bending (M_y). If the section does not buckle laterally, then the overall buckling checks, Equations 9.3 and 9.4, given in BS 5950: Part 5 (1987) reduce to the same equation, that is

$$\frac{P}{P_Y} + \frac{M_y}{M_{uy}\left(1 - \frac{P}{P_{Ey}}\right)} \leq 1.0 \qquad (9.7)$$

In Chapter Eight it was shown that the doubly lipped channel section is prone to lateral-torsional buckling when bent about its minor axis in a direction which causes compression in the lip. Analogously with Equation 9.7 a beam-column interaction which includes the effects of flexural and minor axis lateral-torsional buckling may be expressed as

$$\frac{P}{P_Y} + \frac{M_y}{M_{By}\left(1 - \frac{P}{P_{Ey}}\right)} \leq 1.0 \qquad (9.8)$$

Figure 9.2 shows a comparison between Equations 9.7 and 9.8. It can be seen that neglecting minor axis lateral-torsional buckling will result in non-conservative design.

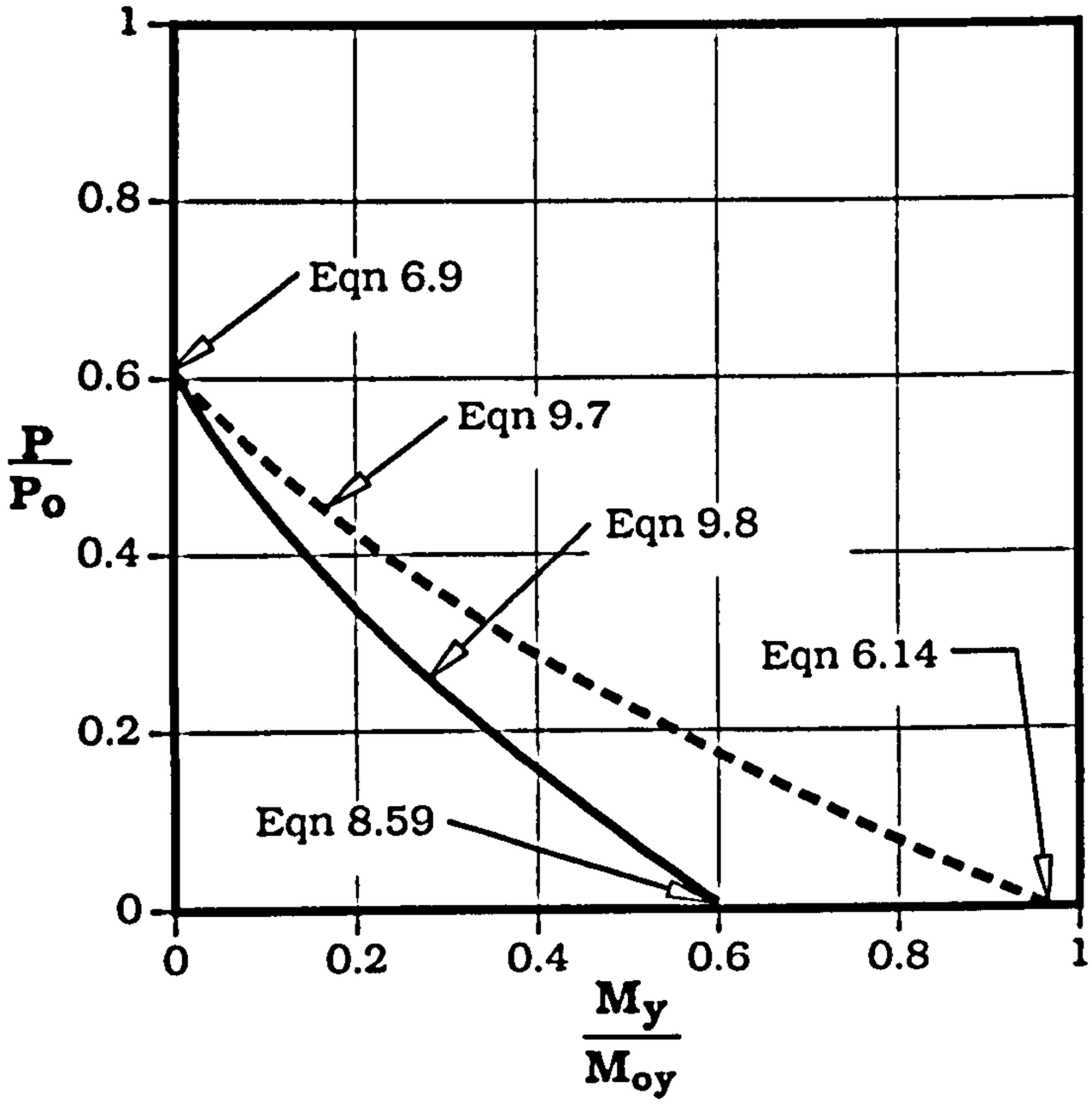


Figure 9.2 Beam-column interaction curves given by Equations 9.7 and 9.8
B = 122mm, D = 97mm, B_L = 17mm, D_L = 18.5mm, t = 3.0mm
L = 3000mm, σ_o = 390 N/mm^2

If the applied moments cause tension in the lip the section is inherently more stable, and failure of slender members will probably occur through yielding of the channel table, while for stocky sections lip buckling may govern. Equation 9.7 may be used to assess the adequacy of laterally restrained doubly lipped channel for any combination of axial load and minor axis bending.

The effects of local element buckling are taken into account by using the effective area of the cross section, and lip buckling can be accounted for substituting the lip buckling stress σ_{uL} for the yield stress.

9.3 NON-LINEAR, ELASTO-PLASTIC FINITE ELEMENT ANALYSIS OF DOUBLE LIPPED CHANNELS

A series of non-linear elasto-plastic finite element analyses were carried out for the 3mm thick, 3000mm long doubly lipped channel section, with the purpose of obtaining a better understanding of the interaction between torsional-flexural and lateral-torsional buckling and between torsional-flexural buckling and bending. The finite element mesh adopted for this numerical study was identical to that used for the torsional-flexural and lateral-torsional buckling analyses given in Chapters Seven and Eight. The boundary conditions imposed at the ends of the member prevented distortion of the cross-section, lateral movement in both the Z and Y planes as well as inplane rotation; warping was permitted. Two different load combinations were applied to the section- axial loading at the neutral axis of the gross cross-section, with hogging or sagging bending moment about the Y axis. A hogging moment (acting alone) puts the lip in tension, while a sagging moment causes the lip to be in compression. An interaction curve was obtained for the channel by systematically varying the proportion of axial load and bending moment.

The initial imperfections necessary for the non-linear analysis were obtained by scaling the torsional flexural buckling mode from the critical buckling analyses given in Chapters Seven. In all cases the magnitude of the total initial vertical imperfection ($w_{\theta o}$) at the web/table junctions was ± L/1000. This is in line with the initial imperfections used in Chapters Six, Seven and Eight.

The deformations corresponding to first surface yield obtained from the finite element analysis are shown in Figures 9.3 for various combinations of P and M_y. The changing mode of deformation, as P/M_y varies, can be clearly seen.

Figure 9.4 shows the resistance of the channel for various combinations of axial load and moment. The right hand quadrant of Figure 9.4 shows the interaction between the torsional-flexural and the lateral-torsional buckling resistance. The squash load P_o and the first yield moment M_o have been obtained for a fully effective section from Equations 4.10 and 6.14 respectively. There is good agreement between the torsional-flexural buckling and lateral-torsional buckling values obtained from the finite element analyses (Chapters Seven and Eight) and those given by Equations 7.71 and 8.59. The finite element results suggest an almost linear interaction. First surface yield is observed to be closely followed by failure.

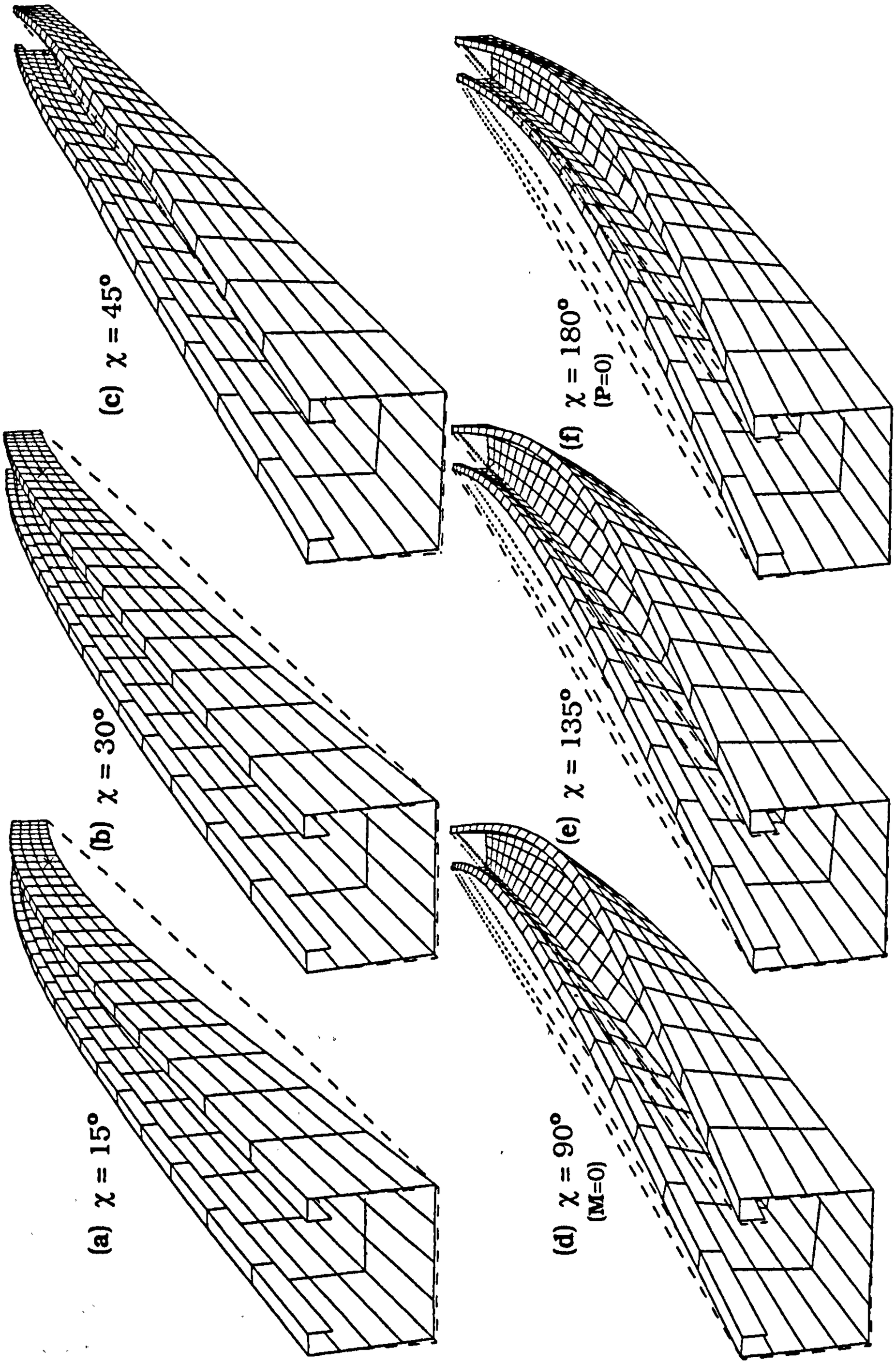


Figure 9.3 Overall deformation at first yield for various combinations of axial load and bending moment (see Figure 9.4)
B = 122mm, D = 97mm, B_L = 17mm, D_L = 18.5mm, t = 3.0mm, L = 3000mm, σ_o = 390 N/mm^2
$\chi = \mathrm{Tan}^{-1}$ (P/M_y)

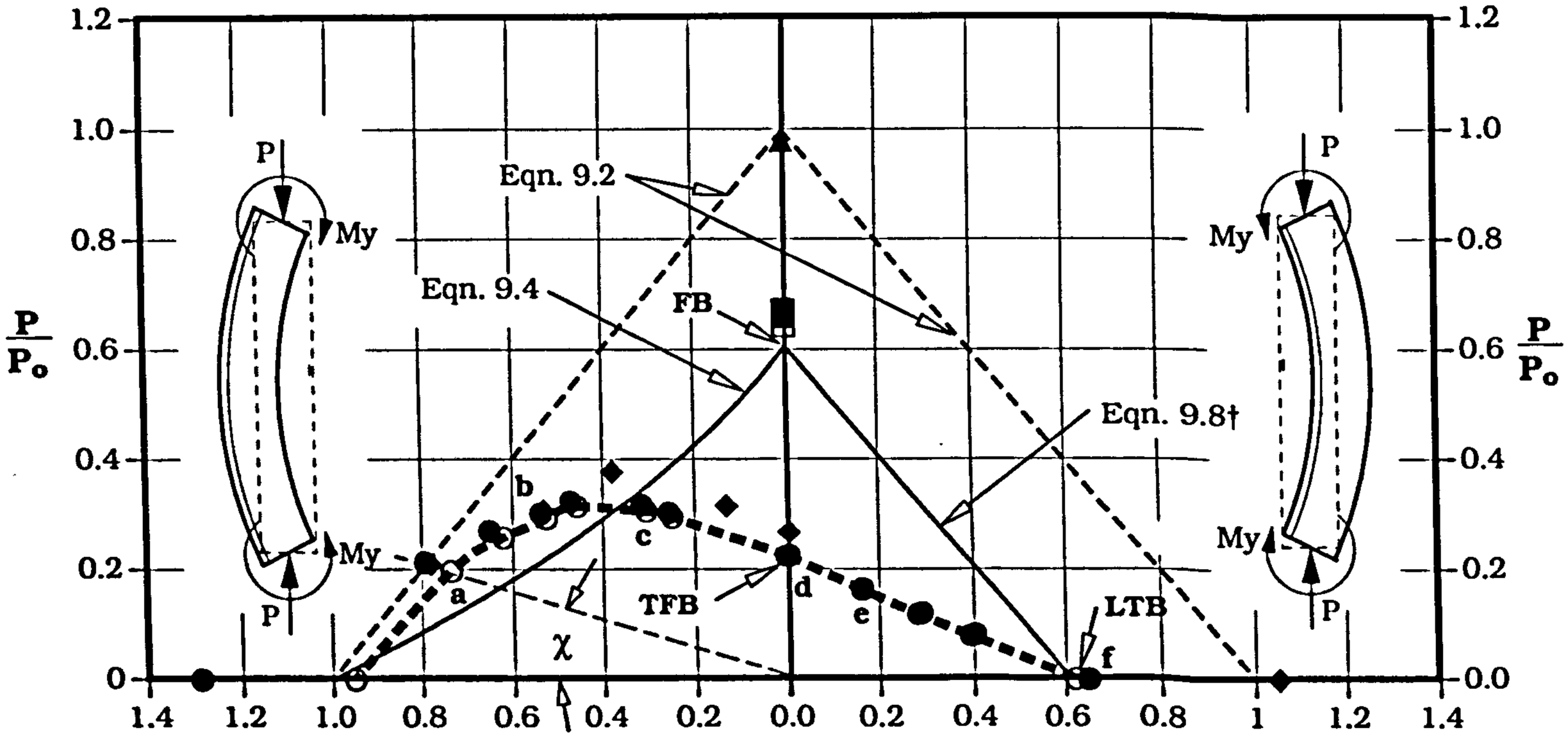


Figure 9.4 Axial load, minor axis bending - interaction diagram

B = 122mm, D = 97mm, B_L = 17mm, D_L = 18.5mm, L = 3000mm, σ_o= 390 N/mm^2, w_o= L/1000 - (TF)&(F)

† $(1-P/P_E)$ neglected in accordance with BS 5950: Part 5 (1987)

The left hand quadrant of Figure 9.4 shows the interaction between torsional-flexural buckling and bending causing lip tension. The end points of the interaction have been obtained from Equations 7.71 and 6.14. Again good agreement between the finite element values and Equations 7.71 and 6.14 can be seen. Several analyses were carried out, where, for any given combination of axial load and bending the initial imperfections were affine to either flexural or to torsional-flexural modes of buckling.

When a channel with an initial flexural imperfection was subjected to axial load (P), it was observed that as P increased, the overall flexural displacement of the section changed to a deformed shape corresponding to that of a torsional-flexural buckle. This change in displacement occurred at a load approximately equal to the critical torsional-flexural buckling load for the channel. When $M/M_o \leq 0.5$ the lowest failure loads were obtained for those analyses where the imperfection was affine to the torsional-flexural mode. As the applied moment increases to $M/M_o = 0.5$ the overall displacement of the section at failure, changes from a predominantly torsional-flexural to a flexural mode, as can be seen in Figure 9.3. When the moment is further increased, then the initial mode of imperfection had little effect on the interaction. When the mode of failure is flexural the buckling behaviour becomes less sensitive to the initial mode of imperfection.

The numerical results shown in Figure 9.4 clearly show how the direction of the applied moment determines the buckling behaviour of the channel. When the moment causes lip compression, torsional-flexural buckling is seen to interact with lateral-torsional buckling, displaying a near linear interaction. However, when the moment causes tensile stresses in the lip the failure the interaction is seen to be convex, with failure loads above the torsional-flexural buckling resistance of the channel.

Any design proposal should give due regard to the direction of the applied moment in order to obtain a true picture of interactive buckling behaviour of the channel.

9.4 PROPOSED DESIGN METHOD

Current application of an interaction formula implies that each term will be separately satisfied. The different responses to tension or compression, and to positive or negative moment, are recognised, but the different shapes of the

interaction curves are not. Linear interaction is assumed regardless of the direction of the axial force and moments.

This section gives a simple method based on the finite element analysis, which enables the direction of bending about the minor axis to be taken into account. This was an important requirement for the design of the structure being investigated. It is a first step towards defining the interaction shape in all quadrants of the interaction surface.

Members subject to Torsional-Flexural Buckling and Bending causing lip tension.

The finite element results and the beam-column interaction given by Equations 9.2 and 9.7 are compared in Figure 9.5. The failure loads exceed the torsional-flexural buckling capacity of the channel over part of the interaction because the moment inhibits twisting of the section. AISI (1989) and EC3: Part 1.3 (1991) assume that the interactive buckling behaviour is governed by Equation 9.7 where the axial resistance P_Y is taken to be equal to the torsional-flexural buckling resistance of the channel (equation 7.71). Equation 9.6 is rational except in as much as it fails to recognise the effect of lip tension on twisting of the section. It is evident that for the doubly lipped channel, Equation 9.6 gives a very conservative estimation of the actual buckling behaviour, when the moment causes lip tension.

In view of the limited amount of numerical data available, the beam-column interaction for the channel subject to torsional-flexural buckling and bending may be defined by a bi-linear approximation, where Equation 9.6 is truncated to prevent the applied load exceeding the torsional-flexural buckling resistance P_{TFY} of the section. If $P < P_{TFY}$ and

$$\frac{M_y}{M_{uy}} > \left(1 - \frac{P}{P_y}\right)\left(1 - \frac{P}{P_{Ey}}\right) \qquad (9.9a)$$

then the interaction may be obtained from Equation 9.7.

If

$$\frac{M_y}{M_{uy}} \leq \left(1 - \frac{P}{P_y}\right)\left(1 - \frac{P}{P_{Ey}}\right) \qquad (9.9b)$$

then

$$P = P_{TFY} \qquad (9.9c)$$

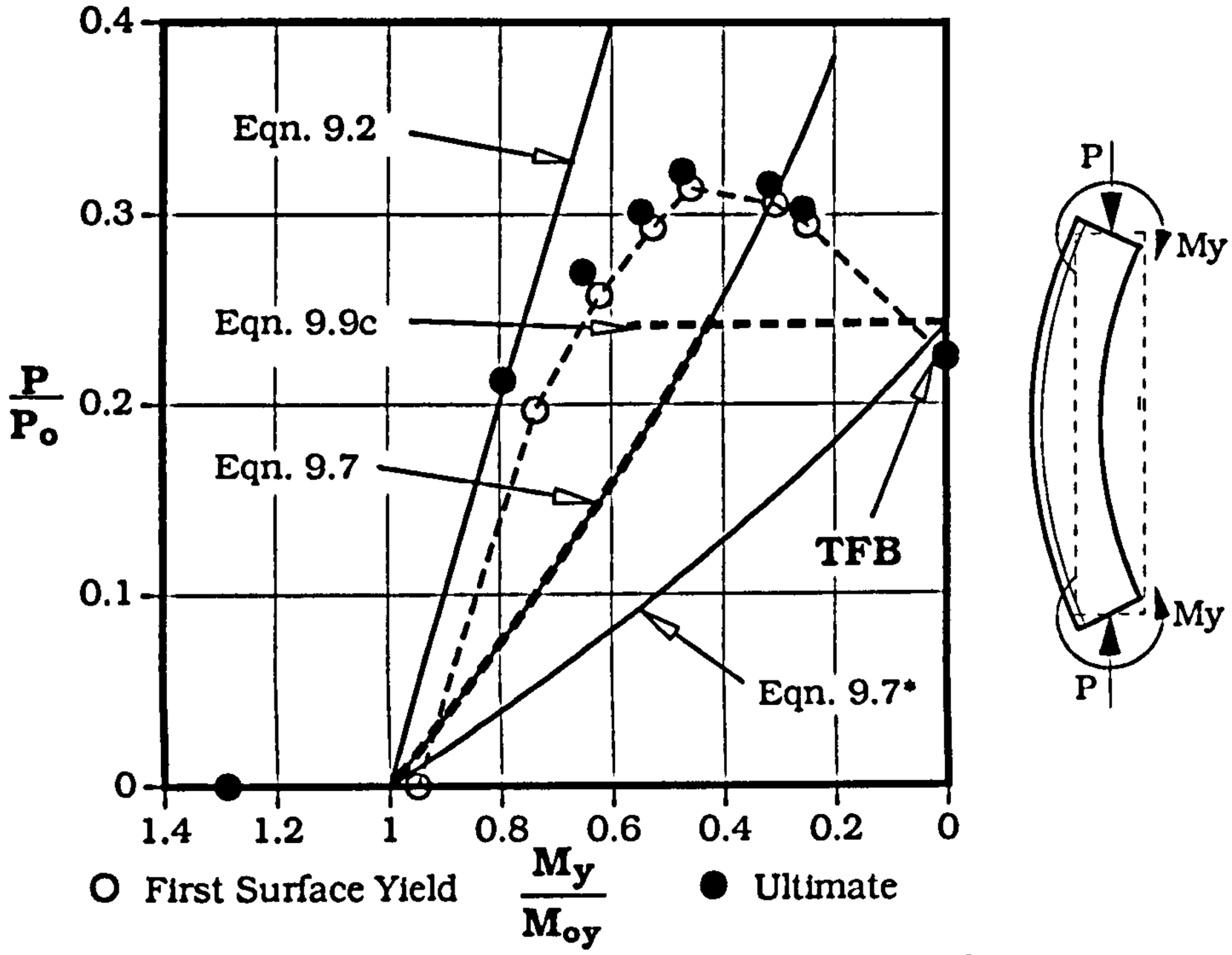


Figure 9.5 Comparison between finite element analysis and Equations 9.2, 9.7 and 9.9c

B = 122mm, D = 97mm, B_L = 17mm, D_L = 18.5mm, t = 3.0mm, L = 3000mm, σ_0= 390 N/mm^2, w_0= L/1000 (* P_{TFY} substituted for P_Y in Equation 9.7)

It is observed in Figure 9.5 that Equations 9.9 gives a conservative prediction of the beam-column buckling behaviour for the channel section. Local and lip buckling effects on the interactive buckling behaviour can be taken into account by evaluating the short strut and bending capacities of the member using the effective section properties and the lip buckling stress in place of the yield stress.

Members subject to Torsional-Flexural & Lateral-Torsional Buckling causing lip compression.

It can be seen in Figure 9.6 that the failure loads obtained from the finite element analysis show a slightly convex interaction. This behaviour can be modelled by modifying Equation 9.8 such that the axial resistance P_Y corresponds to the torsional-flexural buckling resistance P_{TFY} of the channel, given by Equation 7.71.

Equation 9.8 can be rewritten as

$$\frac{P}{P_{TFY}} + \frac{M_y}{M_{By}\left(1 - \frac{P}{P_{Ey}}\right)} \leq 1.0 \qquad (9.10)$$

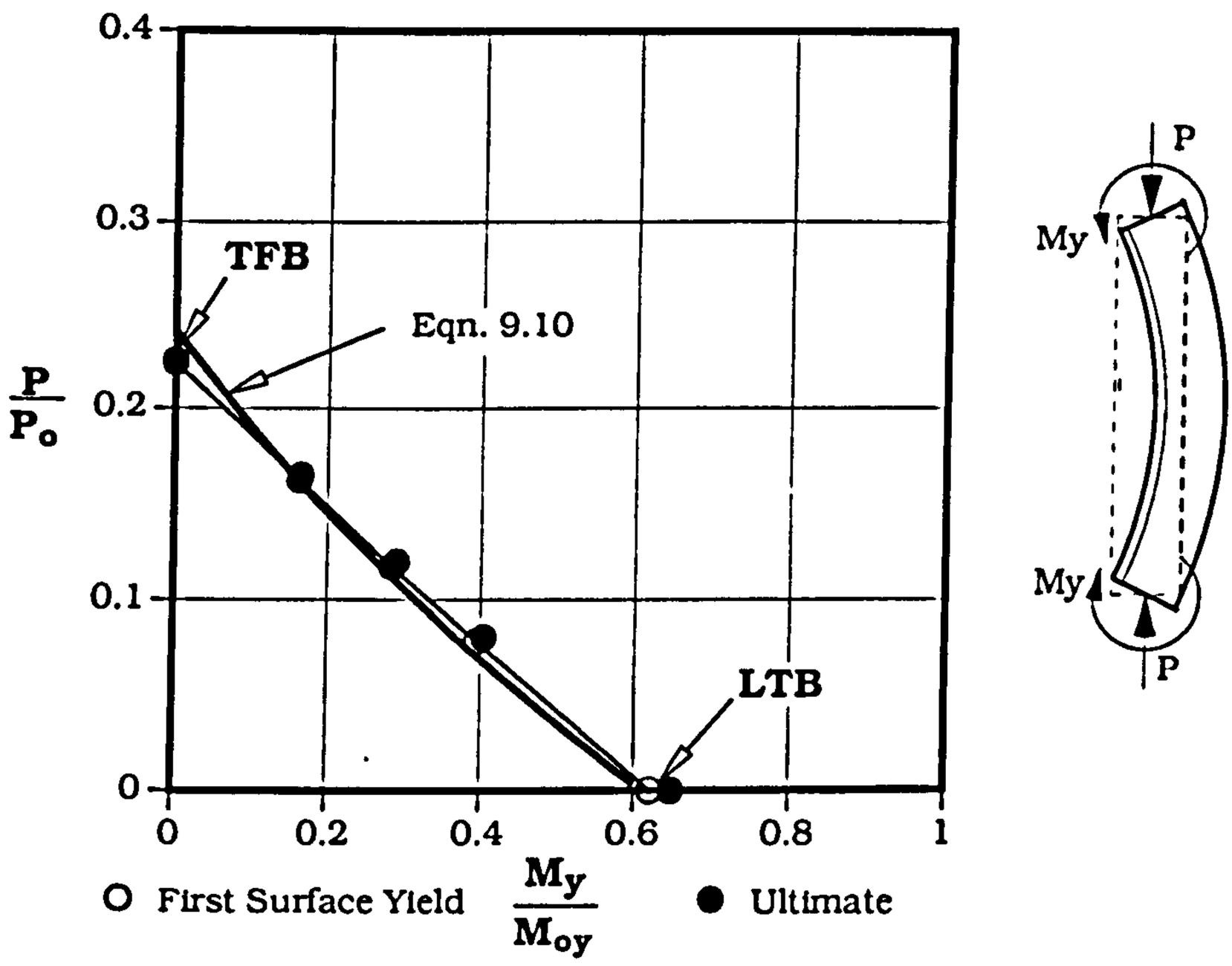


Figure 9.6 Comparison between finite element analysis and Equation 9.10

B = 122mm, D = 97mm, B_L = 17mm, D_L = 18.5mm, t = 3.0mm

L = 3000mm, σ_o= 390 N/mm^2, w_o= L/1000

Good agreement between the beam-column interaction equation, Equation 9.10 and the numerical results is observed. The influence of local and lip buckling on the interactive buckling behaviour may be accounted for in the manner described in the preceding section.

9.5 COMPARISON BETWEEN THE PROPOSED DESIGN METHOD AND EXPERIMENTS

The bottom chord members of the test frame are subjected to a combination of axial load, minor and major axis bending. Several chord failures were observed during testing (Chapter Three-Table 3.2). Before being able to carry out a comparison between the failure loads given by Equations 9.9 and 9.10 and the experimental results, the members forces need to be established. The central bay bottom chord

member forces can be obtained from the linear frame analysis presented in Chapter Two, and are given in Table 9.1, expressed in terms of a unit central load P_{JK}.

LOAD		Bottom chord lips-up	Bottom chord lips down
Axial load (P)	kN	0.3179 P_{JK}	0.3587 P_{JK}
Minor axis moment (M_y)	kNm	0.008575 P_{JK}	0.003810 P_{JK}
Major axis moment (M_z)	kNm	0.000325 P_{JK}	0.001425 P_{JK}

Table 9.1 Chord member forces for a unit central load P_{JK}

In Chapter Two it was shown that the axial load along the continuous bottom chord varies between spans and that the more lightly loaded member offers some flexural restraint to the heavily loaded central bay member. The effective length of the central member can be reduced on account of this flexural restraint. Similarly, a reduction in the torsional effective length due to torsional restraint provided by the adjoining members caused by different loads in each span and the torsional stiffness of the washer plates were also taken into account in determining the frame failure loads.

The effective length for flexural buckling found from Figure 2.8 has been taken to be is L_{eff} = 0.794L (2380mm). The torsional effective length, obtained using the method described in Section 7.3.5 was found to be equal to L_{eff} = 0.73L (2190mm), and for the 1.5mm doubly and·2.0mm singly lipped channels, L_{eff} = 0.76L (2280mm).

The average yield stress for each channel section (Table 3.1) was used to determine the axial and bending resistance of the sections given in Table 9.2. The effects of local element and lip buckling on the axial and bending resistance of the member have also been taken into account where necessary. The experimental frame test failure loads are given in Table 9.2.

The predicted frame failure loads given in Table 9.2 neglect the effects of the major axis bending moments present in the test frame. The frame failure loads have been obtained by substituting the appropriate member capacities and loads from Tables 9.1 and 9.2, into Equations 9.9 and 9.10 and solving for P_{JK}. Where the member is subject to minor axis bending, causing tensile bending stresses in the lip, no account of lip buckling has been taken A comparison between the experimental and

Section		P_{Ey} kN	P_Y kN	P_{TFY}	M_{uy} kNm	M_{By} kNm	P_{TEST} kN	Eqn. 9.9 / P_{TEST}	Eqn.9.10 / P_{TEST}
127x65x12.5-2	LU	108	82	N.A	2.3	N.A	163	0.67	N.A
125x100x20x20-1.5	LU	317	109	N.A	4.5	N.A	188	1.01	N.A
	LD		N.A	60	N.A	3.8	161	N.A	0.87
	LD[1]		N.A	72	N.A		205	N.A	0.80
	LD[2†]		109	N.A	4.5	N.A	240	0.94	N.A
125x100x20x20-3[3]	LU	598	384	N.A	13.5	N.A	510	1.08	N.A
	LD		N.A	179	N.A	8.8	510	N.A	0.82

(1) Load corresponding to first surface yield in section (no lip buckling) (2) Section fitted with anti-twist battens (no lip buckling)

(3) Maximum load reached without failure, LU Lips up section, LD Lips down section. N.A not applicable.

Table 9.2 Comparison between the test frame results and the predicted failure loads given by Equations 9.9 and 9.10

predicted failure loads given by Equations 9.9 and 9.10 is made in Table 9.2 where it can be seen that reasonable agreement between the interaction equations and the experimental results was obtained.

9.6 CONCLUSIONS

(1) BS 5950: Part 5 (1987) does not consider the possible interaction between either torsional-flexural and lateral-torsional buckling, or torsional-flexural buckling and bending; nor does it recognise the possibility of minor axis lateral-torsional buckling. In this chapter it has been shown experimentally and numerically that a doubly lipped channel section subject to combined axial compression and minor axis bending will buckle both lateral-torsionally and torsional-flexurally.

(2) Numerical results show that the mode of initial overall imperfection and the direction of the applied minor axis end moments influence the interactive buckling behaviour of the 3000mm long channel section. If the moment causes the lip stress to be more compressive, then the section will failure as a result of combined lip, torsional-flexural and lateral-torsional buckling. If the moment reduces lip compression to a sufficient extent, the section is stable and failure is caused by bending and compression without twisting.

(3) From the finite element analysis it can be seen that when the applied loads cause the doubly lipped channel to buckle in a combined torsional-flexural and lateral-torsional mode, the resulting interaction is slightly convex, starting at the torsional-flexural buckling resistance and ending at the lateral-torsional buckling resistance of the section. If the moment causes lip tension then the resulting curve is seen to be concave, with a considerable increase in member resistance as the moment increases.

(4) The interactive buckling behaviour of members prone to combined torsional-flexural and lateral-torsional buckling can be described by a convex, geometric non-linear relationship between the torsional-flexural resistance and the lateral-torsional buckling resistance of the section.

(5) The interactive buckling behaviour of members prone to torsional-flexural buckling in the presence of a bending moment causing lip tension, can be conservatively approximated by a bi-linear relationship.

(6) When the moment causes lip tension, the resistance under combined moment and axial force, when $M/M_Y > 0.4$, is about twice the value given by Equation 9.7 with P_{TFY} substituted for P_Y.

Chapter Ten

DESIGN OF FRAME CONNECTION

10.1 INTRODUCTION

The tensile and compressive forces in the diagonals are resolved into horizontal tab forces and vertical forces applied directly or indirectly to the edges of the washer plates. The washer plates transfer moments to the chords by vertical forces applied to the channel tables by the washer plates. Separation of the washer plates from the channel table is prevented by tensile forces in the bolts. Horizontal forces are transferred from the tabs to the bolts which bear upon the tables of the channels. The washer plates serve to redistribute the forces applied by the individual tabs.

The detailed behaviour of the connection is exceedingly complex and to achieve a feasible design procedure, simplifying assumptions about the action of the components must be made. In this chapter the assumptions will be described and discussed, and design formulations will be given. The following actions will be considered:

(a) Combined web crippling, bending and compression
(b) Table shearing at the web/table junction
(c) Bearing stress in the tension diagonal tabs
(d) Tensile and shear forces in bolts
(e) Washer plate bending

Design proposals will be related to experimental data obtained from component and frame tests.

10.2 WEB CRIPPLING OF CHANNEL SECTIONS

An important effect which must be avoided in the use of cold-formed steel sections is local crippling at points of support or concentrated load. Web crippling in channel sections differs from that in welded plates because it is strongly influenced by the corner radius. It also differs from that which occurs in channels clamped back-to-back, which arrangement was used in most of the previously reported tests. A special feature of the connection now discussed is that the local edge force is not uniform, but varies from zero to maximum over half the length of the washer plate.

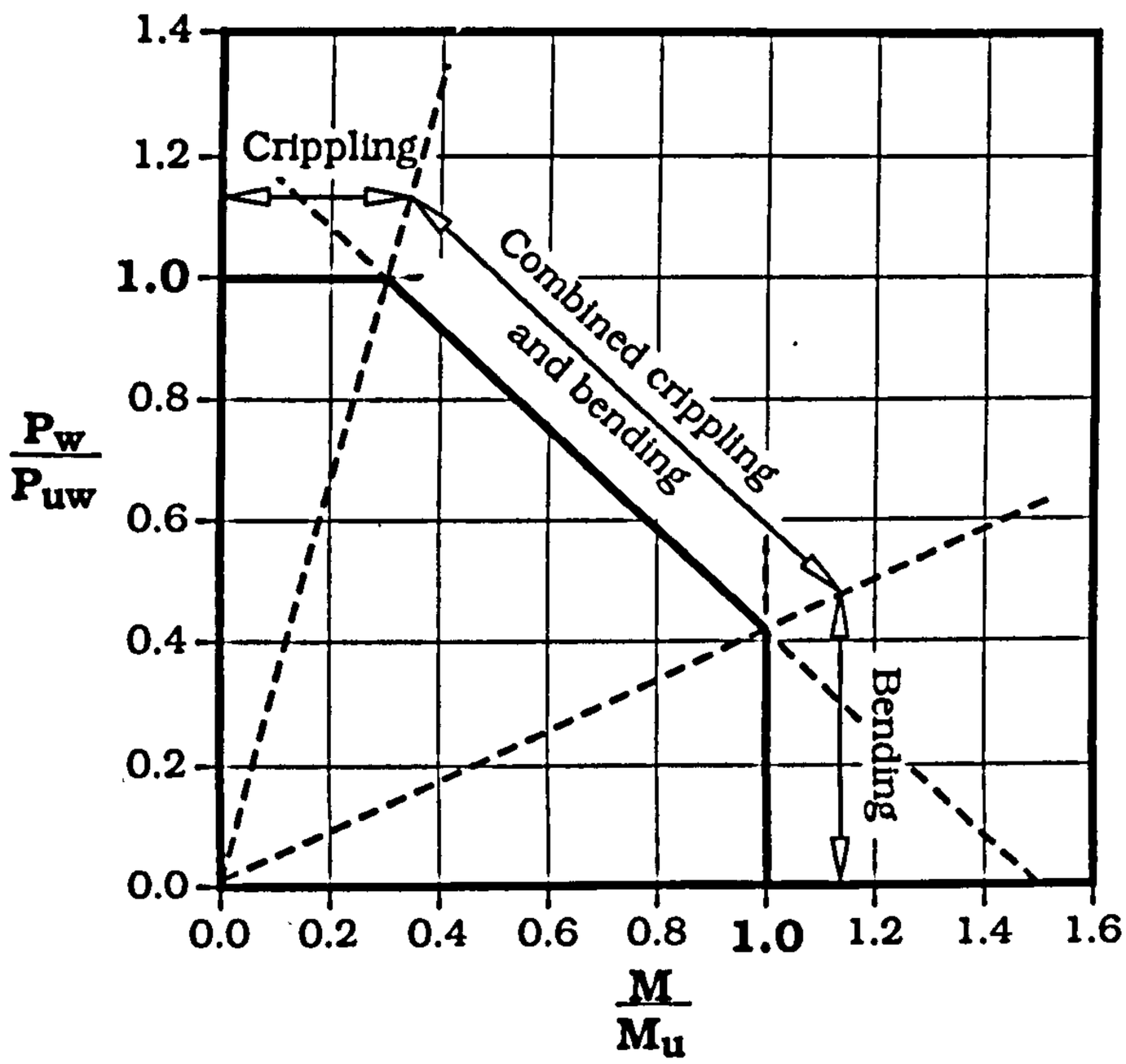


Figure 10.1 Interaction between web crippling and bending given by Equation 10.1

This buckling phenomenon is similar to that observed for rectangular simply supported plates under locally distributed edge forces, which has been extensively researched by numerous investigators (Zetlin 1955, Khan and Walker 1972, Khan et al 1977). A comprehensive summary of research on crippling in cold-formed sections is given by Yu (1991). Extensive experimental work initially carried out at Cornell University (Winter and Pian 1946, Zetlin 1955), and more recently at the University of Missouri-Rolla (Santaputra et al 1986, 1988) forms the basis for the current AISI recommendations which provide a number of equations dealing with various load cases. Several national codes of practice including BS 5950: Part 5

(1987) have adopted the AISI (1989) recommendations for the design of thin-walled sections against crippling. These recommendations are, based on a parametric analysis of test results. The equations for resistance include 12 empirical coefficients, which can be found in BS 5950: Part 5 (1987). Only the coefficients which are relevant to the connection now under consideration will be referred to here.

The crippling capacity of an element will be reduced by coexistent inplane compressive forces due to axial loads and or bending moments. The interaction between crippling and bending has been studied for example by Rocky et al (1972) and Hetrakul and Yu (1980) amongst many.

The web crippling/bending interaction equation given by AISI (1989) and BS 5950: Part 5 (1987) for combined web crippling and bending, shown in Figure 10.1, is

$$1.2\frac{P_w}{P_{uw}} + \frac{M}{M_u} \leq 1.5 \qquad (10.1a)$$

where

P_w the patch load

P_{uw} the crippling capacity in the absence of bending moments (obtained from BS 5950 Part 5 (1987), Table 7 where $c > 1.5D$, $D/t \leq 200$)

$$P_{uw} = t^2 k C_1 C_2 C_{12}\left\{3350 - 4.6\left(\frac{D}{t}\right)\right\}\left\{1 + 0.007\left(\frac{N}{t}\right)\right\} \qquad (10.1b)$$

$$C_1 = (1.22 - 0.22k) \qquad (10.1c)$$

$$C_2 = \left(1.06 - 0.06\frac{r}{t}\right) \leq 1.0 \qquad (10.1d)$$

$$C_{12} = 0.7 + 0.3\left(\frac{\theta}{90}\right)^2 \qquad (10.1e)$$

c distance from the end of the member to the load or reaction

D the depth of the section

k $\sigma_d/_{228}$, in which σ_d is the design stress

M the applied moment

M_u moment capacity of the section corresponding to first yield

N is the length of the bearing ($L_w/3$)

r the inside bend radius ($r/t \leq 6$)

t web thickness

θ is the angle between the plane of the web and the bearing surface

In this section the web crippling behaviour of the doubly lipped channel section subjected to coexisting bending moment and vertical shear will be discussed considering experimental results. Design recommendations are given for determining the stress levels at which reinforcing inserts are required, and for assessing the crippling capacity of a channel reinforced by sleeves.

10.2.1 UNREINFORCED CONNECTION

Consider the space frame connection shown in Figure 10.2. The vertical components of the force in the diagonals are transmitted through the washer plates to the channel table. The vertical shear along the transverse edge of the washer plates will be relatively small owing to the flexibility of the table remote from it's junction with the webs. When the deformations become large, the shear forces generated by the washer plate will be partially resisted by longitudinal inclined tensile forces, as well as some additional resistance which develops across the ends of the washer plate. The webs must be checked for their ultimate crippling resistance, and to ensure that at working loads excessive out-of-plane web deformations which may render the connection unserviceable do not occur. The table/web junction must also be checked for shearing.

Consider first the bottom chord connection in a diagonal on square frame. If it is assumed that the vertical component of the smaller diagonal force is approximately equal to that of the larger force, the couple acting on the pair of washer plates (Figure 10.2) can be expressed as

$$M = V L_c \qquad (10.2)$$

in which

L_c the distance between diagonal creases measured at mid thickness of the tab.

V the greater vertical force at the ends of the washer plate where

$$V = P_{Dmax} \sin \phi$$

P_{Dmax} the greater diagonal force

ϕ the angle between the diagonal and the bottom chord

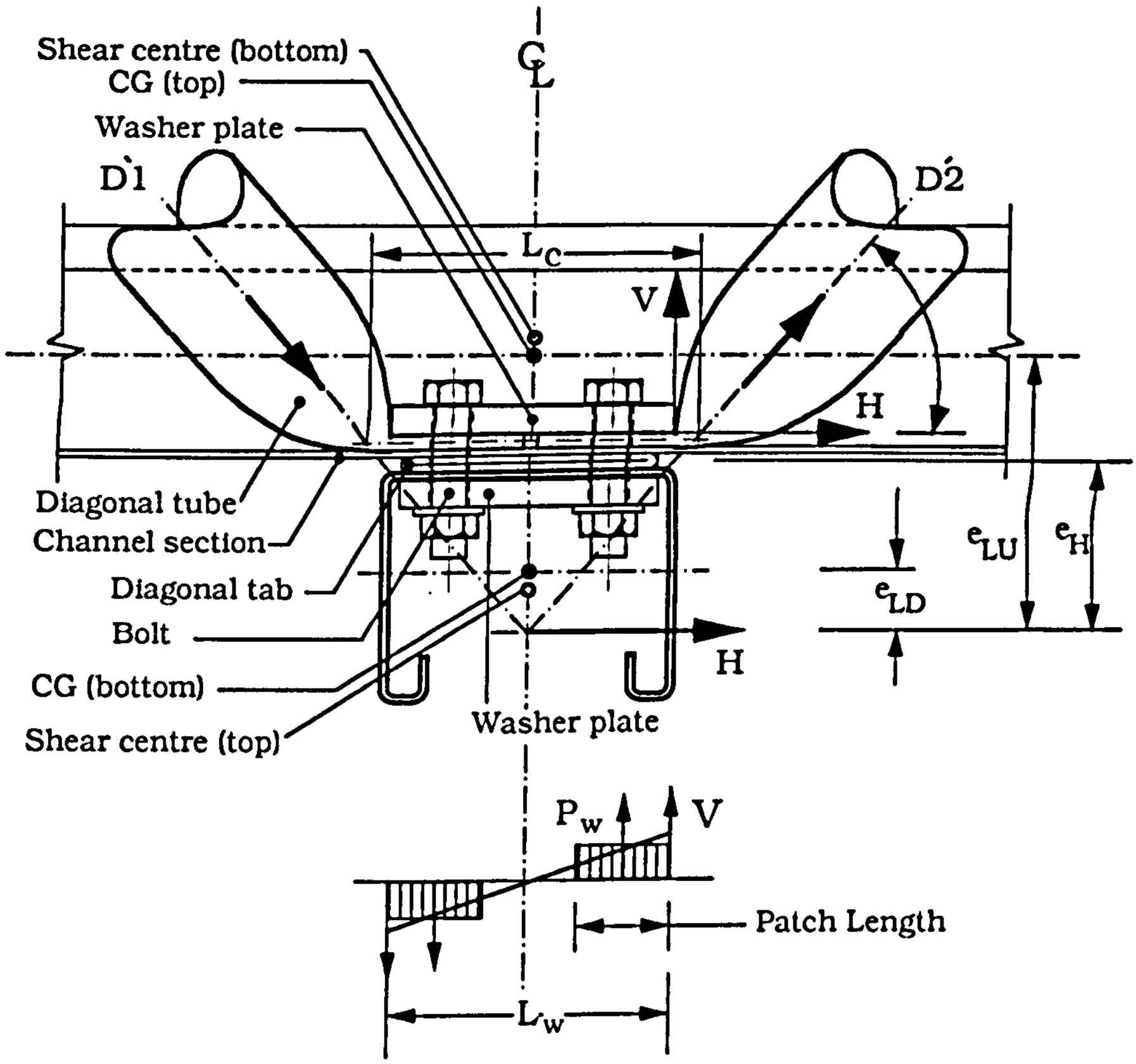


Figure 10.2 Space frame connection - bottom chord diagonal on square.

Assuming that the moment produces a linear distribution of vertical shear stress in the table along the edges of the plate and a similar distribution of vertical stress in the web, the vertical resultant patch forces P_w is assumed to act at a distance $2L_w/3$ apart and to be distributed uniformly over a patch length $L_w/3$ (Figure 10.2). The patch force per web is

$$P_w = \frac{3VL_c}{4L_w} \qquad (10.3)$$

and if $L_c \approx L_w$

$$P_w = \frac{3V}{4} \qquad (10.4)$$

where

L_w is the length of the washer plate

In the top chords, the vertical crippling force is estimated by first assuming that both diagonal forces are equal to the greater force in the connection. The horizontal force components are resolved in the direction of each chord member. The resultant forces are assumed to act at the diagonal intersection. The moment at the connection in each chord is then obtained by multiplying the vertical distances to the respective neutral axes by the horizontal force. The moment in each chord may also be obtained from the LUSAS (1992) analysis.

The total moment is also equal to the sum of the moments caused by the horizontal component of the diagonal force acting at the mid plane of the connection, and the moment caused by the vertical components acting at a distance L_c. If the horizontal moment about the centroidal axis of the chord is subtracted from the total moment the difference is the moment caused by the notional vertical forces V at a distance L_w apart, applied at each end of the washer plate. The vertical force at the ends of a washer plate located in a top chord lips up member (Figure 10.3) is given by

$$V = \frac{H_{LU}(e_{LU} + e_H)}{L_w} \qquad (10.5a)$$

and in the top chord lips down member

$$V = \frac{H_{LD}(e_{LD} - e_H)}{L_w} \qquad (10.5b)$$

where

e_H the distance between the centroid of the section and the mid plane of the connection

e_{LD}, e_{LU} the distances between the intersection point of the diagonals and the centroidal axes of the lips up and lips down top chord members

H_{LU}, H_{LD} the horizontal forces resolved in the direction of the lips up and lips down top chord members respectively, given by

$$H_{LU} = 2\,P_{Dmax}\cos\alpha\cos\phi$$

$$H_{LD} = 2\,P_{Dmax}\sin\alpha\sin\phi$$

where

α is the angle between the diagonal and the top chord viewed, in plan.

The patch load in each web may then be obtained from Equation 10.4.

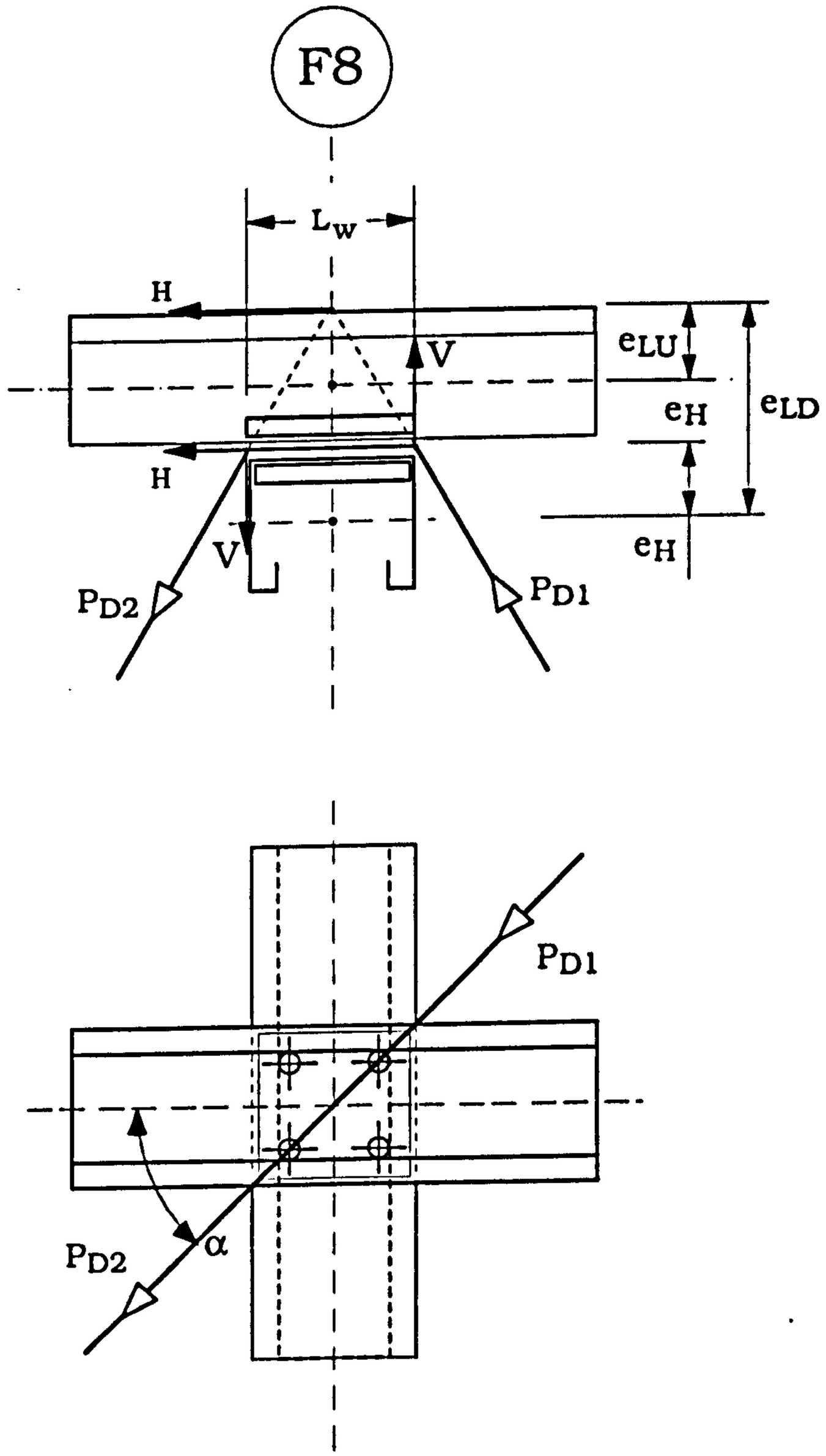


Figure 10.3 Top chord force diagram

If the chord members are subjected to a combination of minor axis bending, major axis bending and axial force an approximate interaction equation may be obtained by modifying Equation 10.1

$$1.2\frac{P_w}{P_{uw}} + \left[\frac{M_y}{M_{uy}} + \frac{M_z}{M_{uz}} + \frac{P}{P_{cs}}\right] \leq 1.5 \qquad (10.6a)$$

where

$$\frac{P_w}{P_{uw}} \leq 1.0 \qquad (10.6b)$$

and

$$\frac{M_y}{M_{uy}} + \frac{M_z}{M_{uz}} + \frac{P}{P_{cs}} \leq 1.0 \qquad (10.6c)$$

in which

P	the applied axial load
P_{cs}	the short strut capacity of the section
M_y, M_z	the applied moments
M_{uy},M_{uz}	the fully effective elastic moment capacities of the section

If the axial force is tensile, the axial term (P/P_{cs}) in Equations 10.6 may be omitted since it can be assumed to have neither a beneficial nor a detrimental affect on the crippling capacity of the section.

A further check is required to ensure that the connection does not failure through "punching" shear at the table/web junction. If the vertical force acts over a patch length $L_w/3$, then the total shear resistance of the section at both edges of the washer plate P_{us} is

$$P_{us} \leq \frac{2 L_w t \sigma_o}{3\sqrt{3}} \qquad (10.7a)$$

and

$$\frac{P_w}{P_{us}} \leq 1.0 \qquad (10.7b)$$

10.2.2 CONNECTION WITH REINFORCING SLEEVES

If the cross-section is unable to resist the vertical forces it may be necessary to reinforce the connection by introducing short angle inserts, as shown in Figure 10.4. Angles are used in preference to channels to assist insertion, and to

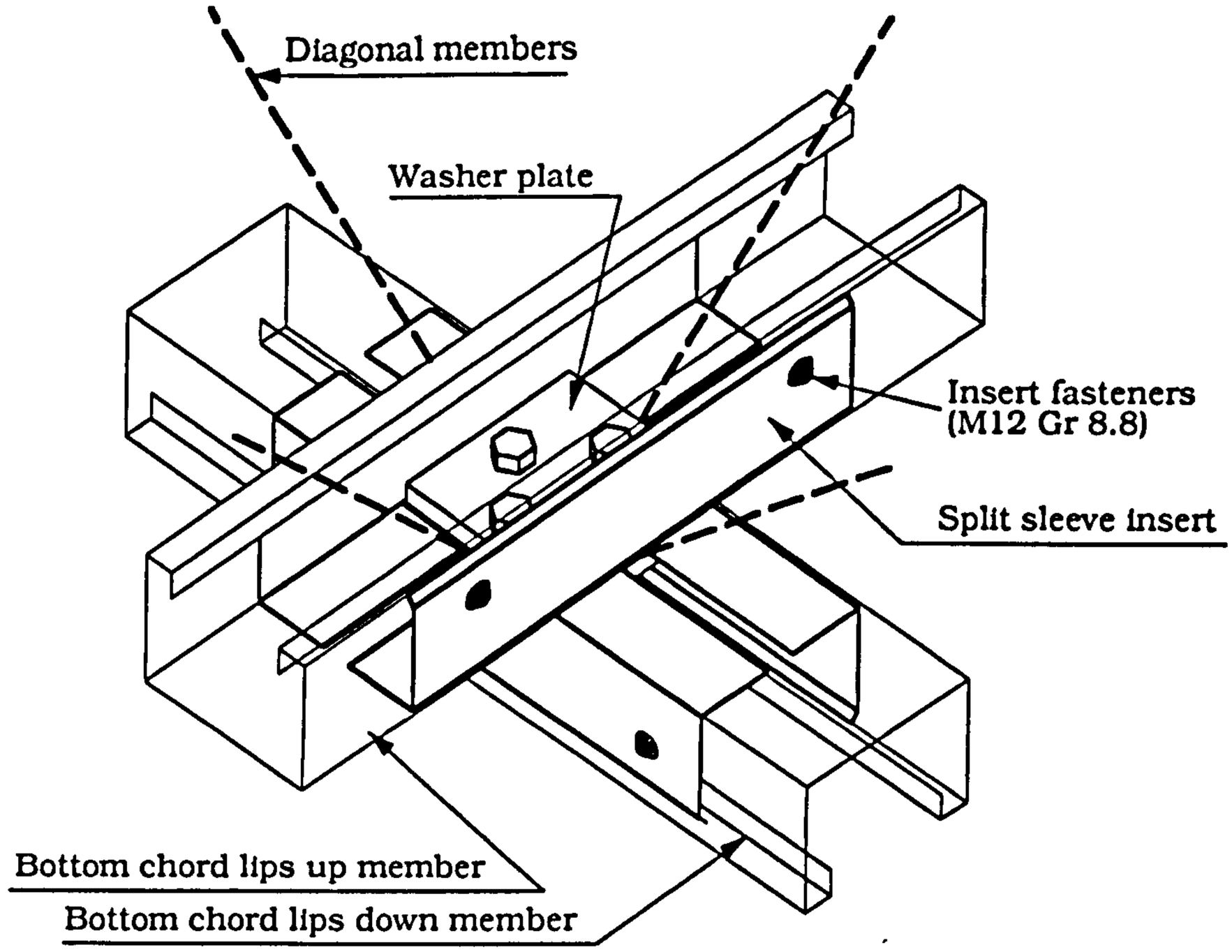


Figure 10.4a Reinforced bottom chord connection

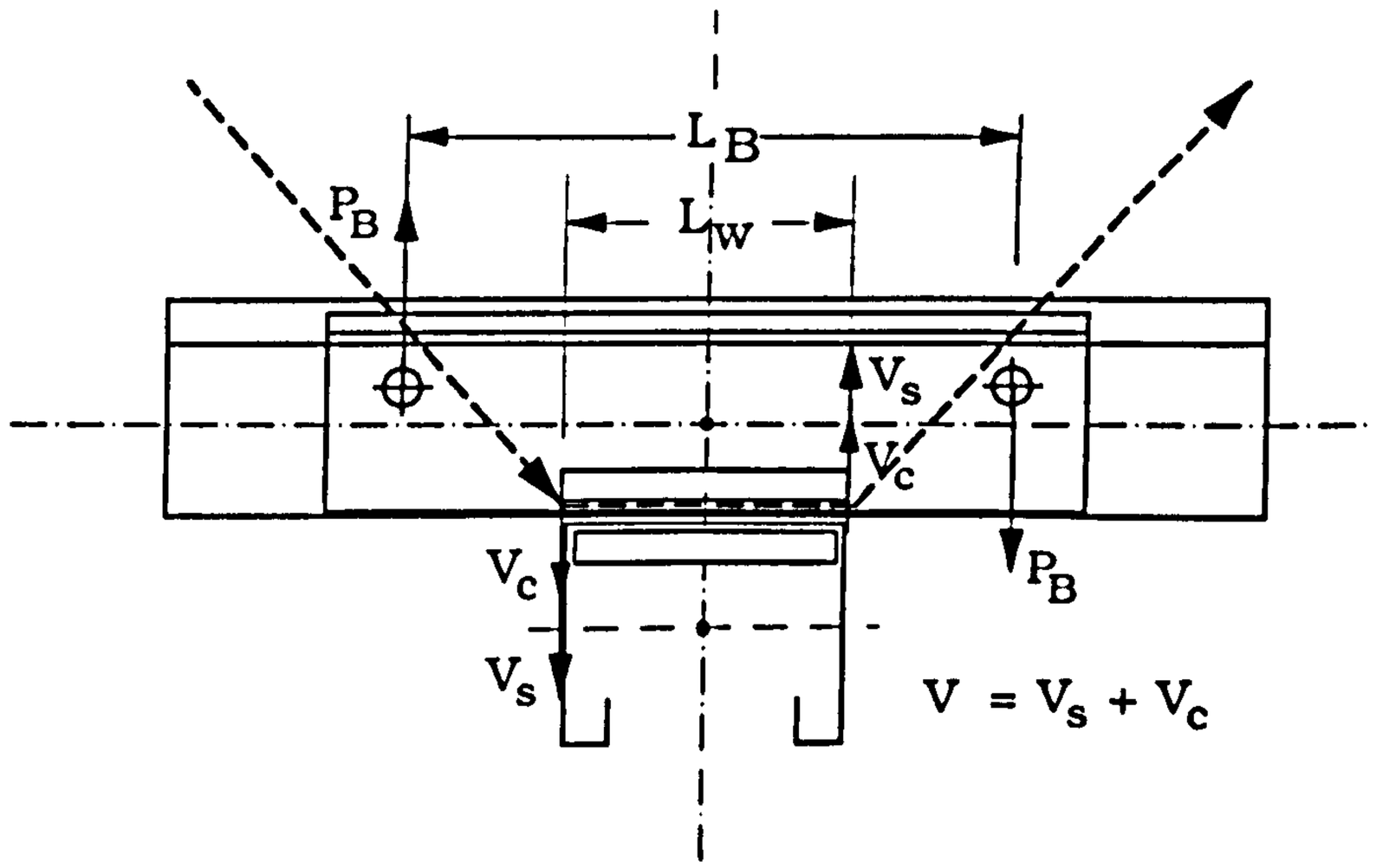


Figure 10.4b Bottom chord lips up sleeve insert forces

enable the same components to be used for any chord section. Web fasteners connecting the sleeve inserts to the web of the channel will attract small forces caused by axial straining and chord bending. However, it seems reasonable to neglect these forces provided that the chord sections under axial forces and bending moments are designed to derive no advantage from the sleeve. The fasteners are then assumed to be fully available to resist vertical forces which tend to cause crippling of the web elements and shearing of the table.

The fastener resistance is the lesser of the single shear capacity of the bolt or the bearing resistance of the thinner ply, determined according to section eight of BS 5950 Part 5 (1987). The bolts exert a moment equivalent to $P_B L_B$ so that the vertical forces V_s carried by the sleeve is

$$V_s = \frac{P_B L_B}{L_w} \qquad (10.8)$$

where

P_B the bolt force (the lesser of the shear capacity of the bolt or the bearing capacity of the thinner ply)

L_B the distance between bolts

The forces V_s resisted by the sleeve are transmitted by the patch forces P_{ws}, through the bolts and thence to the web of the channel. The total vertical force V is given by

$$V = V_c + V_s \qquad (10.9)$$

The patch force on the channel insert is

$$P_{ws} = \frac{3V_s}{2} \leq P_{uws} \qquad (10.10)$$

The sleeve is assumed to have no coexistent stress, so that the crippling capacity of the sleeve P_{uws} can be found from Equation 10.1b. The patch load P_w' resisted by the channel is

$$P_w' = P_w - P_{ws}$$

The interaction between web crippling, axial force and bending incorporating the additional web crippling resistance of the sleeve insert may be obtained from Equation 10.4 by replacing P_w with P_w' such that

$$1.2\left[\frac{P_w'}{P_{uw}}\right] + \left[\frac{M_y}{M_{uy}} + \frac{M_z}{M_{uz}} + \frac{P}{P_{cs}}\right] \leq 1.5 \qquad (10.11a)$$

where

$$\left[\frac{P_w'}{P_{uw}}\right] \leq 1.0 \qquad (10.11b)$$

and

$$\left[\frac{M_y}{M_{uy}} + \frac{M_z}{M_{uz}} + \frac{P}{P_{cs}}\right] \leq 1.0 \qquad (10.11c)$$

10.2.3 EXPERIMENTS

A series of crippling tests were carried out to examine the validity of existing design guidance and also to observe the web crippling behaviour of single and doubly lipped, unsleeved and sleeved channel sections of various thickness. The test arrangement shown in Figure 10.5 was used to carry out twenty-three component tests. Crippling was also observed in the frame tests.

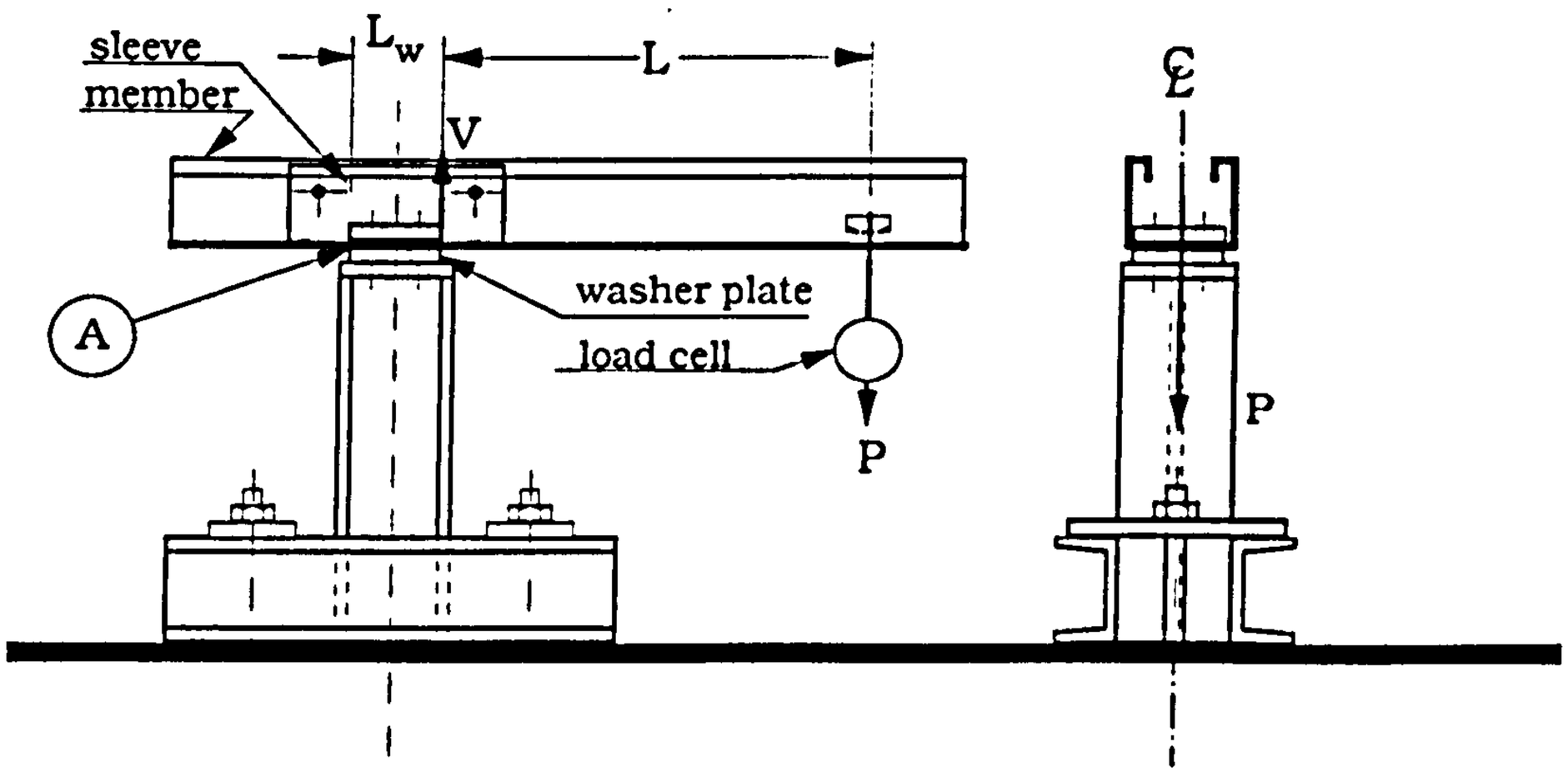


Figure 10.5 Combined web crippling and bending test rig

Each section was subjected to a combination of vertical force and bending induced by applying a vertical load P at the end of a cantilever member, where L = 1170mm. The vertical force V at the edge of the washer plate of length L_w = 120mm can be obtained by taking moments about point A (Figure 10.5), where

$$V = P\left(\frac{L}{L_w} + 1\right) \tag{10.12}$$

It has been assumed in Equation 10.12, that the overall vertical reaction in the system has little effect on the stress distribution, consequently it has been neglected. The bending moment M expressed in terms of the vertical force, V, can be written as

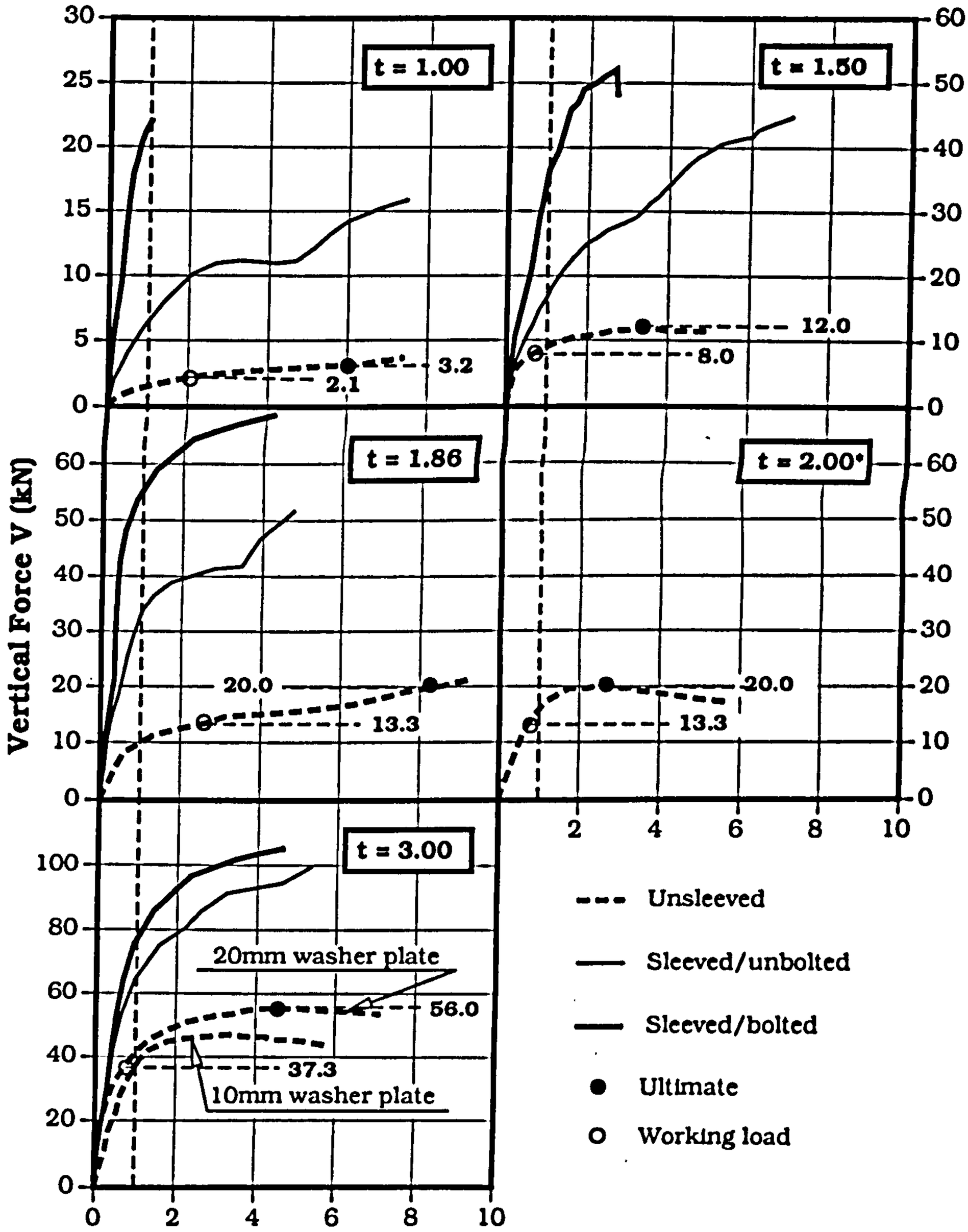
$$M = PL = \frac{L}{\left(\frac{L}{L_w} + 1\right)} V \tag{10.13}$$

During the tests, out-of-plane web displacements were measured at a distance of 0.2D from the underside of the table. The variations in lateral displacement with load for several of the tests are shown in Figure 10.6. The thin unsleeved sections were observed to sustain rather large web displacements before failing. Some of the tests were terminated, when the lateral web displacements became visually excessive before reaching the ultimate capacity. Several tests were also carried out to determine the crippling resistance of sections reinforced by 340 x 100-3mm thick split sleeves. The inserts were either bolted to the webs of the channel or simply clamped between the channel table and the washer plates.

Specimen	t (mm)	σ_o (N/mm^2)	σ_u (N/mm^2)	$\frac{\sigma_o}{\sigma_u}$	e%
127 x 67 x 12.5	2.00	363	468	0.78	22
125 x 100 x 20 x 20	1.00†	292	373	0.78	32
	1.86†	360	390	0.93	22
	3.00†	346	425	0.81	23
125 x 100 x 20 x 20	1.5*	364	494	0.74	26
	3.0*	485	554	0.88	21

†Cold-formed sections *cold rolled sections (yield and ultimate stress values are averages)

Table 10.1 Material properties of cold-formed and cold rolled sections



Patch Load : P_w = 0.75 V kN/web, Coexistant Moment: M = 0.1088 V kNm

B = 125mm, D = 100mm, B_L = 20mm, D_L = 20mm (external dimensions)

* 127x65x12.5-2.0mm thick section

Figure 10.6 Variation in average out-of-plane web displacement with vertical force.

Specimen coupons 50mm wide and 200mm between gauge marks were taken from all sections to be tested. Tensile tests were carried out to obtain yield and ultimate stresses (σ_o and σ_u) and percentage elongation (%e). The results are given in Table 10.1.

Specimen	t (mm)	Configuration	V_{exp} kN		$\frac{V_{exp}}{\text{Eqn. 10.1, 10.11}}$
127 x 67 x 12.5	2.00	US	20.0		1.28
125 x 100 x 20 x 20	1.00†	US	3.2	(3.6)*	0.75
	1.00†	SL/UB	11.0	(16.0)*	-
	1.00†	SL/B	22.5		1.19
125 x 100 x 20 x 20	1.50	US	12.0		0.92
	1.50	SL/UB	28.0	(44.0)	-
	1.50	SL/B	52.0		1.26
125 x 100 x 20 x 20	1.86†	US	15.3	(20.2)*	1.01
	1.86†	SL/UB	41.2	(51.8)*	-
	1.86†	SL/B		(68.2)*	1.21
125 x 100 x 20 x 20	3.00†	US	56.0		1.18
	3.00†	SL/UB	94.0	(100.0)*	-
	3.00†	SL/B		(106.0)*	1.17

†Cold-formed sections *values given in brackets are maximum loads recorded

US-unsleeved, SL-sleeved, UB-unbolted, B-bolted.

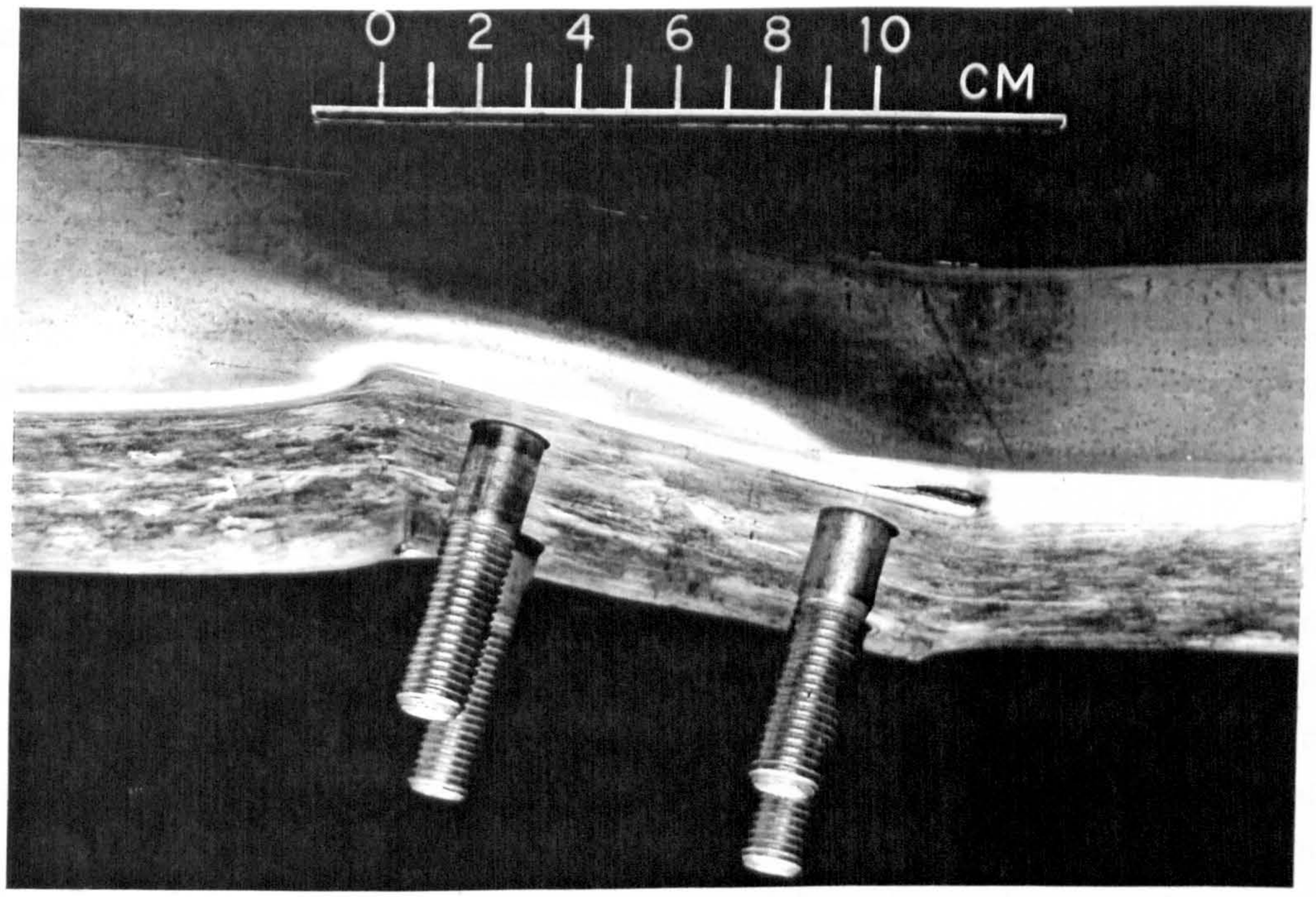
Table 10.2 Combined web crippling and bending test results

Specimen	t (mm)	TEST (Node)	P_{TEST} kN	$\frac{P_{TEST}}{\text{Eqn. 10.6}}$	$\frac{P_{TEST}}{\text{Eqn. 10.6*}}$
127 x 67 x 12.5	2.0	1b (F8)	250	0.86	1.00
125 x 100 x 20 x 20	1.5†	3a (B3)	85	0.61	1.14
	1.5†	4a (F8)	140	0.73	1.35
	3.0†	2a (B3)	330	0.56	0.66
	3.0†	5a (B3)	340	0.58	0.68

†Failure note obtained, test terminated due to excessive lateral deformation of web

* P_{uw}' used in place of P_{uw}

Table 10.3 Web crippling frame test results



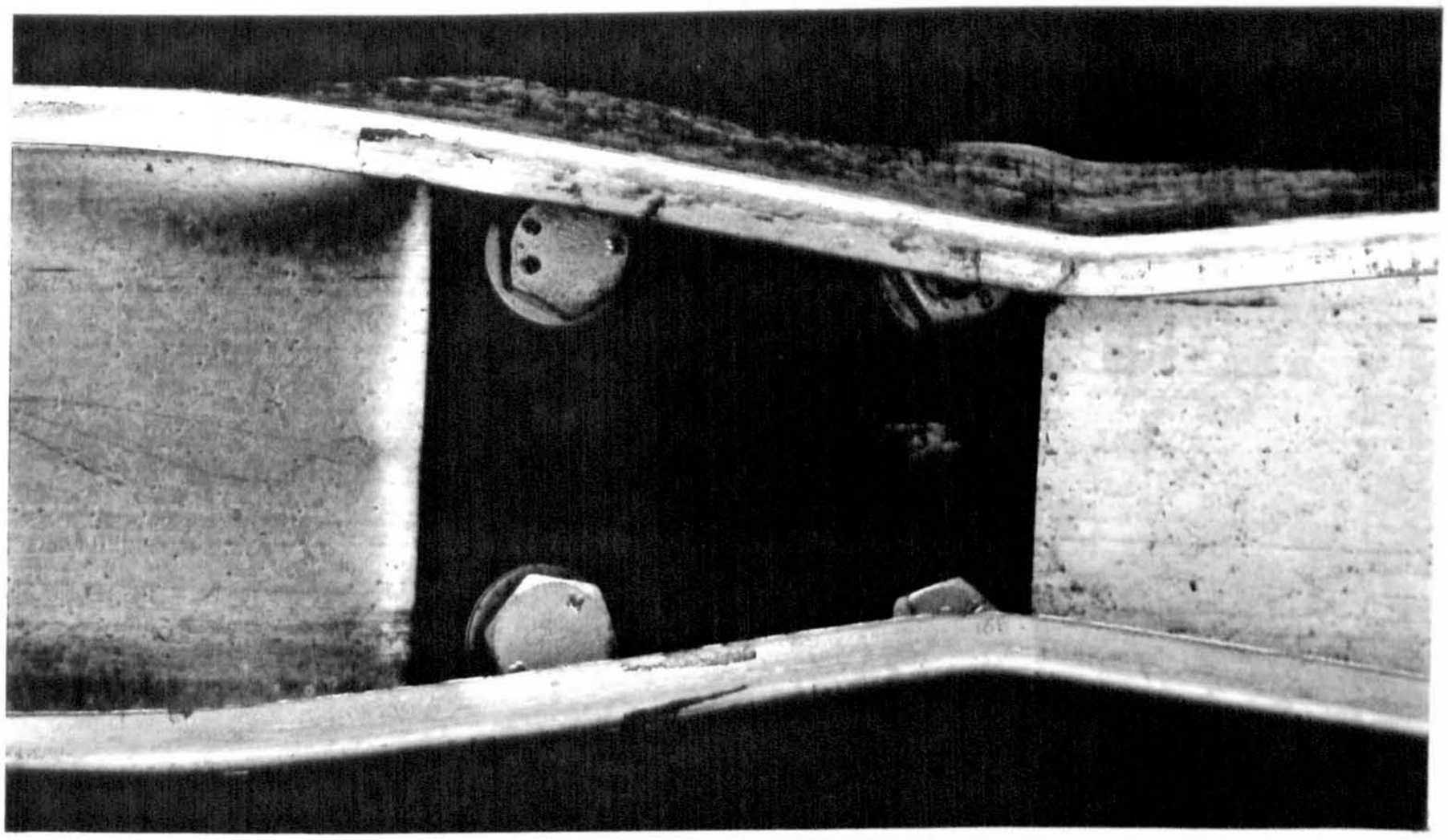


Figure 10.7 Top chord lips up web crippling failure and table tearing

The ultimate loads V_u at the edge of the washer plate obtained from Equation 10.12 are given in Table 10.2. Figure 10.6 shows a substantial increase in the crippling resistance for those sections with bolted sleeve inserts.

Web crippling failures were also observed during the frame tests, the failure loads are given in Table 10.3. Figure 3.13 and 10.7 show a top chord web crippling/table shearing failure for the 127 x 65 x 12.5-2.0mm thick single lipped channel section. The large deformations associated with this form of localized buckling can be clearly seen in Figure 10.7.

A comparison between Equations 10.1a and 10.11a, and the cantilever results given in Table 10.2 shows reasonably good agreement. If the working load is assumed to be equal to two thirds of the failure load ($V_{wk} = 2/3\ V_u$), then from Figure 10.6 it can be seen that the out-of-plane web displacement, is generally about a millimetre. In order to ensure that undue deformations do not occur at working loads, it was decided to limit the nominal web crippling resistance of the section so that the vertical force in the section did not exceed V_{wk}. The crippling resistance P_{uw} (Equation 10.1b) was therefore reduced by a factor K_{cr}. The reduction factor K_{cr} expressed in terms of the web slenderness ratio t/D was obtained by substituting the patch load P_w (Equation 10.4) and the moment M (Equation 10.12) with the crippling capacity given by $K_{cr}\ P_{uw}$ into Equation 10.1a. Making K_{cr} the subject of the equation

$$K_{cr} = 1.2\ \frac{\frac{3}{4}V}{P_w\left(1.5 - \frac{LV}{\left(\frac{L}{L_w} - 1\right)}\right)} \qquad (10.14)$$

Specimen	t (mm)	t/D	P_w kN	V_u kN	V_{wk} kN	K_{cr}	Eqn 10.15
127 x 67 x 12.5	2.0	0.0307	18.7	20.0	13.3	0.745	0.82
125 x 100 x 20 x 20	1.0	0.0100	3.5	3.2	2.1	0.394	0.40
	1.5	0.0150	9.9	12.0	8.0	0.556	0.50
	1.86	0.0186	15.6	15.3	13.3	0.446	0.57
	3.0	0.0300	41.0	56.0	37.3	0.750	0.80

L = 1170mm, Lw = 120mm

Table 10.4 Web crippling resistance reduction factors K_{cr}

Substitution of the experimental values of V_{wk}, L and L_w into Equation 10.14 gives the values of K_{cr} in Table 10.4. A linear regression analysis for the values of K_{cr} corresponding to V_{wk} given in Table 10.4, was carried out, the resulting linear equation for K_{cr} is given by

$$K_{cr} = 20\frac{t}{D} + 0.2 \qquad (10.15)$$

The crippling capacity of the singly and doubly lipped channel sections given by Equation 10.1b is consequently modified, and can be rewritten as

$$P_{uw} = K_{cr}\left[t^2\, k\, C_1\, C_2\, C_{12}\left\{3350 - 4.6\left(\frac{D}{t}\right)\right\}\left\{1 + 0.007\left(\frac{N}{t}\right)\right\}\right] \qquad (10.16)$$

A comparison between the working loads obtained experimentally and those predicted by Equations 10.1a, with Equation 10.16 can be found in Table 10.5. Good agreement is observed.

Specimen	t (mm)	V_{wk}	$\frac{V_{wk}}{\text{Eqn. 10.1a}^*}$
127 x 67 x 12.5	2.00	13.3	0.95
125 x 100 x 20 x 20	1.00	2.1	0.97
	1.50	8.0	1.09
	1.86	13.3	1.05
	3.00	37.3	0.96

* P_{uw}' used in place of P_{uw}

Table 10.5 Comparison between component tests and predicted working loads.

A similar line of reasoning can be used to determine the load at which split sleeve inserts may be provided in a connection in order to prevent excessive web deformations. Failure of the test frame due to web crippling/table shearing was observed during Test 1b (Figures 3.13 and 10.7), all the other test results given in Table 10.3 correspond to the load level at which the web deformation became visible. In Table 10.3, it can be seen that Equation 10.6 with P_{uw} given by Equation 10.1b overestimate the working load for the frame tests. Limiting the crippling capacity to that given by Equation 10.16 provides a better estimate of the working load. However, considerable variation in the actual failure load is observed especially for thicker channel sections. This is due to the fact that the frame tests

may have been suspended prematurely in order to prevent permanent damage to the frame, which would have rendered it unsuitable for further testing.

10.2.4 PROPOSED DESIGN METHOD FOR COMBINED WEB CRIPPLING AND BENDING

Because of the limited number of component and frame tests carried out and the complex behaviour of the connection, a design method is proposed which ensures that the load does not produce unacceptable out-of-plane web displacements at working loads and which is within the ultimate capacity of the web. This has been achieved by curtailing the web crippling capacity of the cross-section to that given by Equation 10.16.

The combined web crippling/bending resistance of the bottom chord connection is then governed by

$$1.2\frac{P_w}{K_{cr}\,P_{uw}}+\left[\frac{M_y}{M_{uy}}+\frac{M_z}{M_{uz}}+\frac{P}{P_{cs}}\right]\leq 1.5 \qquad (10.17a)$$

where

$$\frac{P_w}{K_{cr}\,P_{uw}}\leq 1.0 \qquad (10.17b)$$

and

$$\left[\frac{M_y}{M_{uy}}+\frac{M_z}{M_{uz}}+\frac{P}{P_{cs}}\right]\leq 1.0 \qquad (10.17c)$$

If the applied axial force P is tensile then P/P_{cs} may be omitted.

The web crippling capacity of a connection with reinforcing inserts can be found from Equation 10.11 with $K_{cr}P_{uw}$ in place of P_{uw}. The section should also be checked against possible failure through bolt/section bearing and bolt shear. It must be emphasized that the recommendations made in this section pertain to the connection considered.

10.3 BEARING STRENGTH OF CONNECTED ELEMENTS

Unlike bolted connections commonly found in conventional steel structures fabricated from hot-rolled sections where the bolt diameter is of similar magnitude to the thickness of the individual connected parts, the thickness of cold-formed steels is usually only a small fraction of the diameter of the fastener. Four possible modes of failure may occur in bolted connections made in thin cold-formed steels; shear failure at the end of the joint, bearing failure of the sheet, tensile failure of the sheet and shearing of the bolt.

The design of connections prone to tensile failure of the connected components and shear failure of the bolt are the same as those for hot rolled steels. However, because of the relative thinness of the material, the design of connections in thin cold-formed steels tends to be dictated by considerations of end distance. With regard to bearing failure, BS 5950: Part 1 (1990) and Part 5 (1987) give different design expressions for hot-rolled and cold-formed steels. Davies (1991) points out that this is in part due to the different design philosophies adopted in each part of the code, where the design criteria for connections made in hot-rolled steels, is that of limiting the amount of slip that occurs in a connection, while for connections in cold-formed steels the criteria is one of adequate reserve of strength against ultimate load.

Experimental work carried out by Winter (1956), Dhalla et al (1971), Chong and Matlock (1975), Gilchrist and Chong (1979), Zadanfarrokh and Bryan (1989) and Bryan and Zadanfarrokh (1992) has been concerned with obtaining an appreciation of the behaviour of single and multiple bolt single lap joints, with or without washers, and to provide design guidance for connections made in thin gauge steels.

For a sufficient end distance and thickness of ply, BS 5950: Part 5 (1987) permits an ultimate bearing stress equal to three times the yield strength, or 0.84 times the ultimate strength, whichever is smaller. This is a higher stress than has been used hitherto, and it seemed desirable to provide substantiation, both in respect of the ultimate strength, and in respect of the amount of deformation occurring at service loads. Also the expression given in the code for variation of bearing resistance with end distance is linear, but does not approach zero resistance for zero end distance (Figure 10.8). It seemed therefore likely that the expression might not correctly represent actual behaviour, especially for small end distances close to the specified minimum (1.5d).

For ply thickness ≤ 3.0mm the code requires that the bearing strength be reduced. This is presumably because local out-of-plane deformation of a thin ply can occur in the vicinity of the bolt. Also, for single lap joints more general deformation of the plies can occur owing to bolt tilting. In the test frame connections, compressive wrinkling and bolt titling are both restrained by the washer plates, and it appeared that the reduction required by the code might not be necessary. For the above reasons a series of bearing tests were conducted, with the constraints prevailing in the test frames.

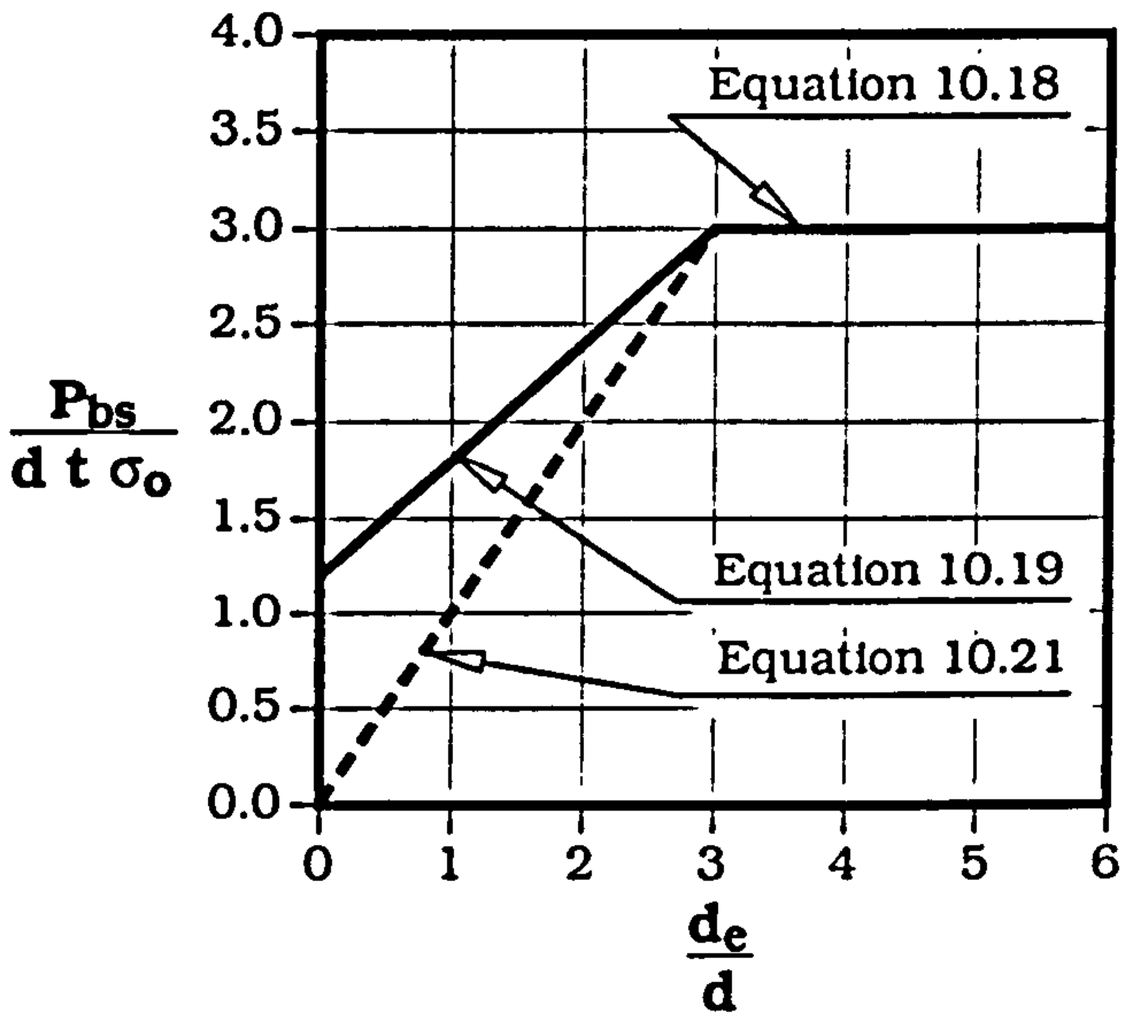


Figure 10.8 Comparison between bearing resistance given by Equations 10.18, 10.19 and 10.21

10.3.1 EXPERIMENTS

A series of single bolt bearing tests were carried out to investigate the following:

(a) The ultimate bearing capacity of strips of various thicknesses, end distances and bolt diameters

(b) The end bearing capacity of tube end tabs having varying end distance and bolt diameter

(c) The influence of the tube seam weld on bearing capacity

(d) The influence on bearing capacity of corner cut-outs at the tab end

(f) The effect of chamfered ends on bearing capacity.

(e) Load - deformation characteristics

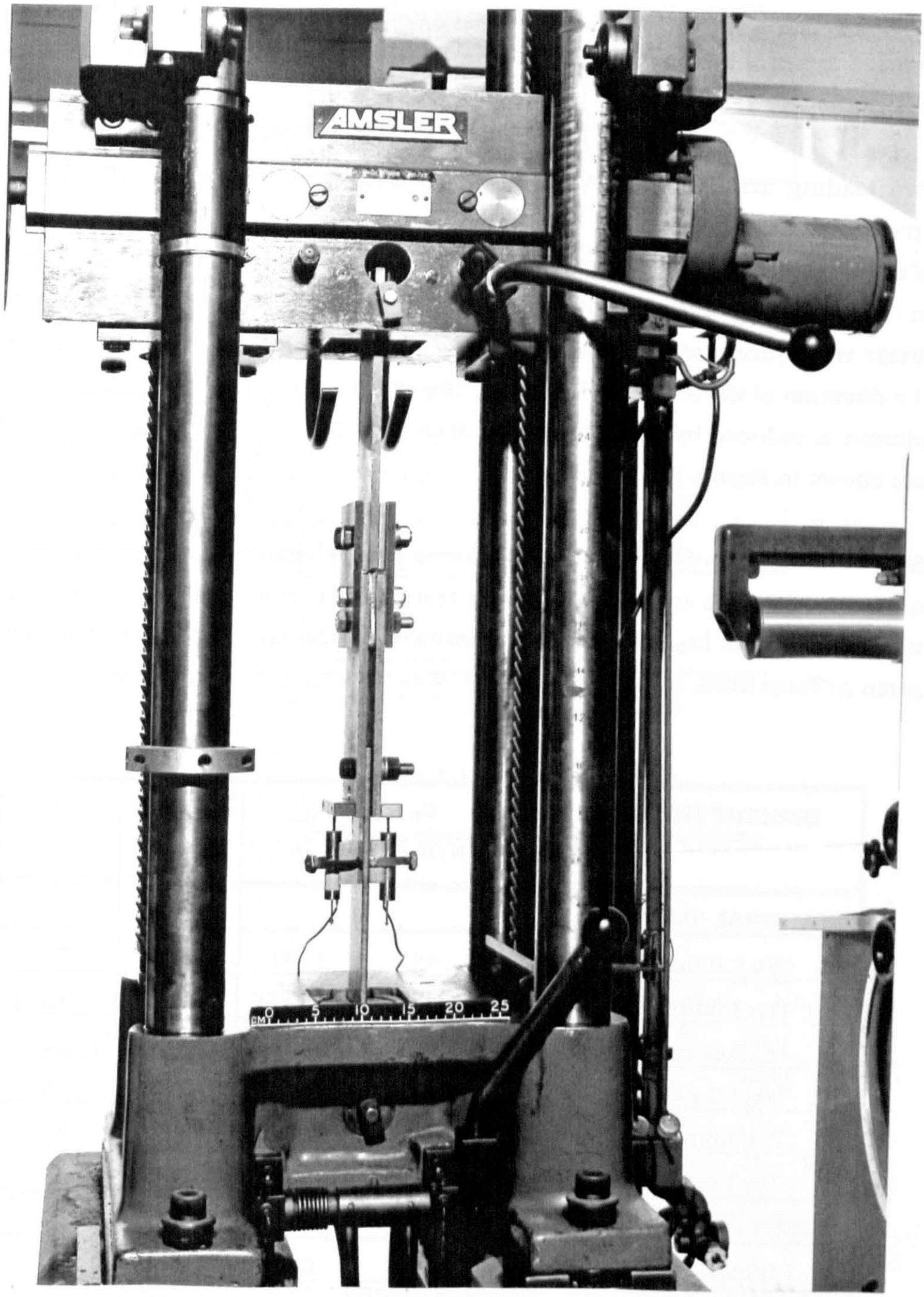


Figure 10.9 Bearing test arrangement

All tests were conducted in a tensile testing machine, the load being controlled manually. Loading rates were controlled by following a timing device (the load rates for each series of tests are given in Tables C.1 to C.5). Figure 10.9 shows a general view of the test set up.

Two loading arrangements were used, as shown in Figures 10.10. The first arrangement (Figure 10.10a) has the advantage that the strength obtained is that of the weaker of two specimens. The second arrangement (Figure 10.10b) was used in the latter part of the bearing tests to test single specimens. In some cases two linear transducers were introduced to measure the amount of hole elongation in the direction of the load. All bolts were finger tight, since in the frame the bolt pre-tension is reduced by the force in the diagonal. The specimen end configurations are shown in Figure 10.11.

Specimen coupons 50mm wide and 200mm between gauge marks were taken from all materials to be tested, and tensile tests were carried out to obtain yield and ultimate stresses (σ_o and σ_u) and percentage elongation. Material test results are given in Table 10.5.

DESCRIPTION	σ_o N/mm^2	σ_u N/mm^2	$\frac{\sigma_o}{\sigma_u}$	0.78 σ_u N/mm^2	e%
DIAGONAL TUBES					
48x 2.0mm	429	447	0.96	349	21
60x2.0mm	395	439	0.90	342	19
60x2.5mm	425	451	0.94	352	23
60x4.0mm	497	577	0.86	450	15
70x3.0mm	425	451	0.94	352	22
76x3.0mm	444	451	0.98	352	12
SHEET MATERIAL					
1.00mm strip	310	368	0.84	287	27
2.00mm strip	363	468	0.77	363	22
3.00mm strip	278	359	0.77	278	18

Table 10.5. Material properties for diagonal tubes and strip

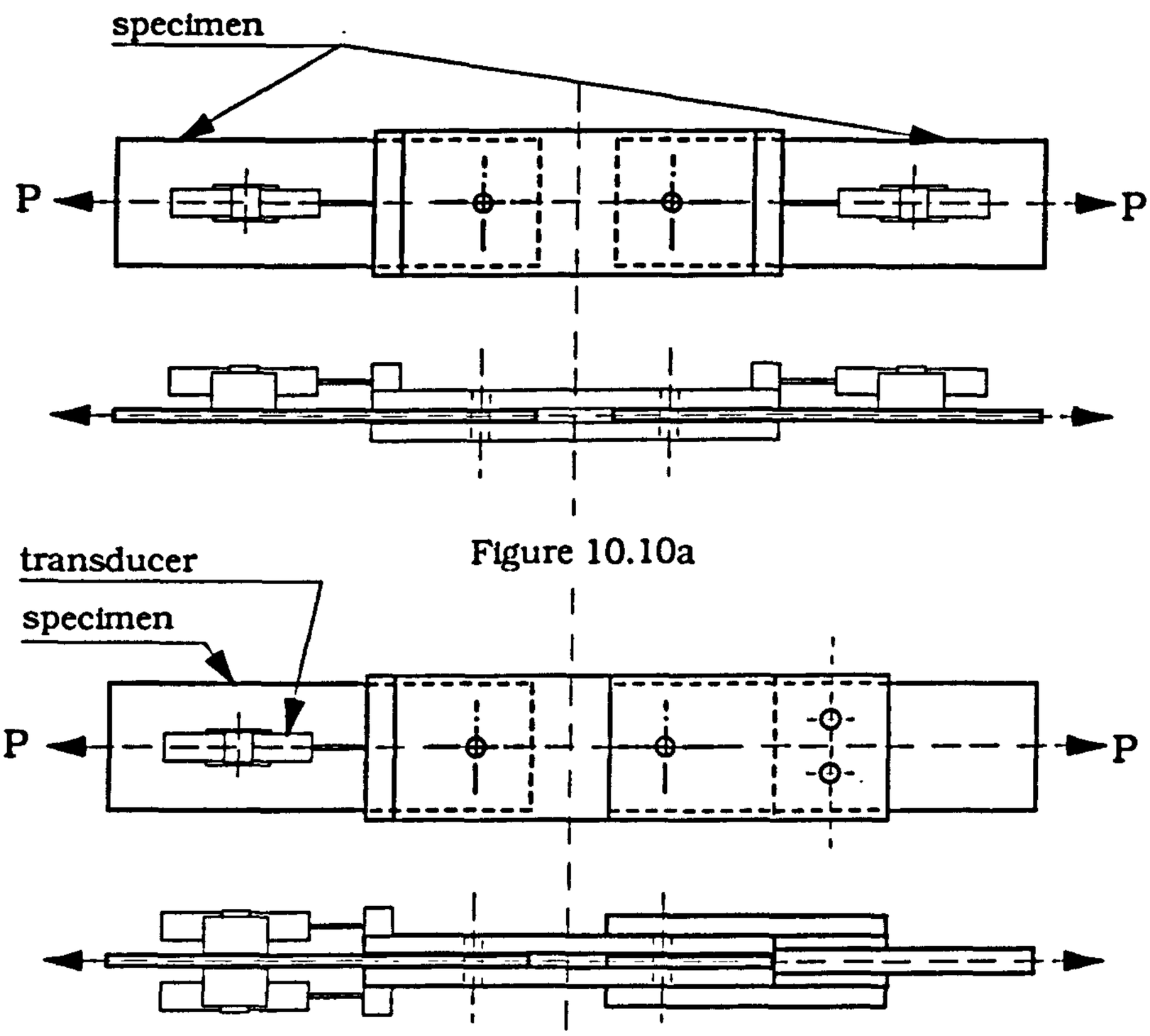


Figure 10.10a

Figure 10.10b

Figure 10.10 Test arrangement of bearing specimens

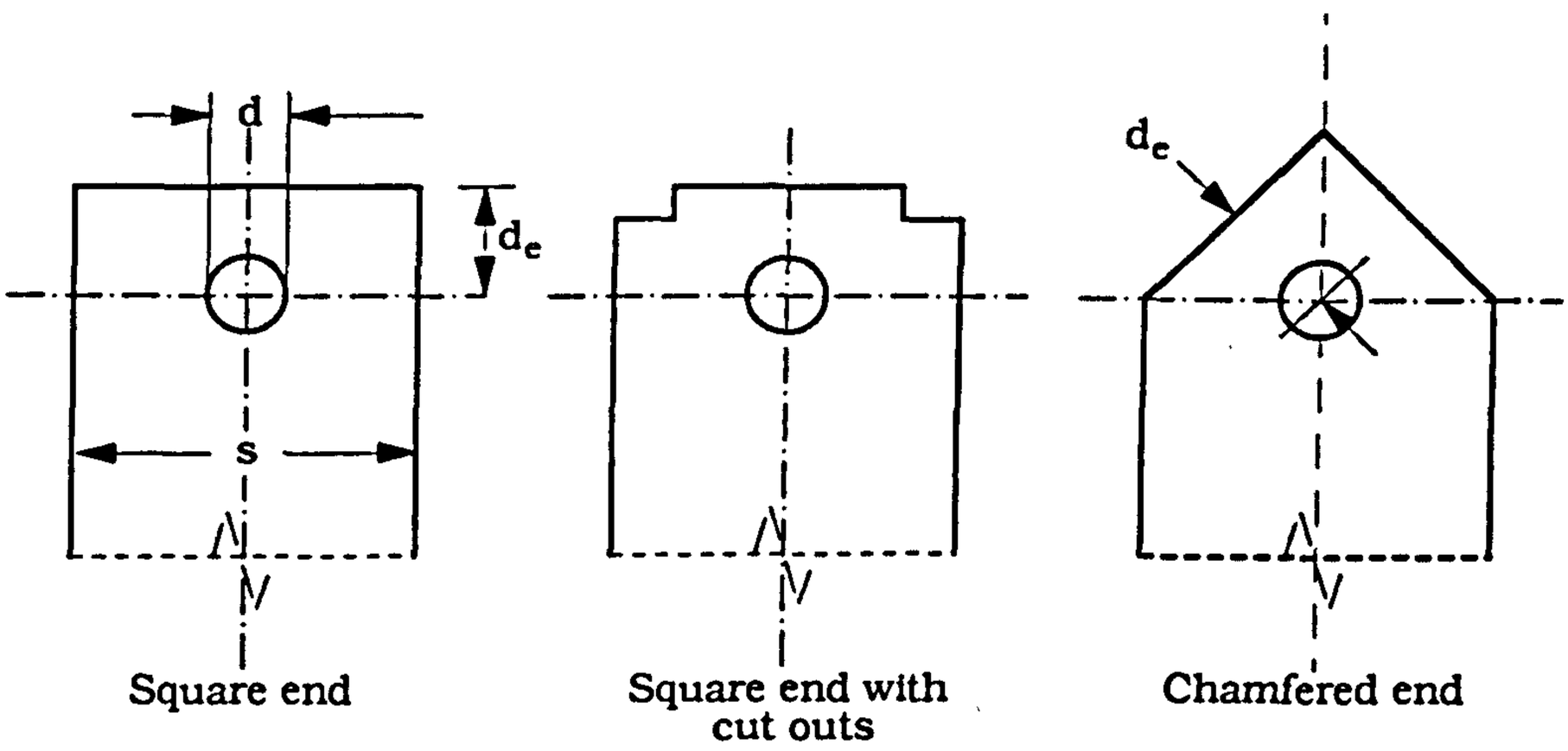


Figure 10.11 Tab end geometries

The bearing test results and the various observed failure modes are given in full in Appendix C, Tables C.1 to C.6, and Figure C.1. The variation in bearing resistance with bolt hole elongation for the 48mm dia-2.0mm thick, and 60mm dia-2.5mm thick tube tabs are shown in Figures 10.12 and 10.13. Figures 10.14 and 10.15 show the variation in bearing resistance with end distance for various thickness of sheet and tube. From the results given in Tables C.1 to C.6 the following observations may be made:

(a) For end distance/bolt diameter (d_e/d) ratios of 0.7 to 3.0 the bearing resistance varies approximately linearly with d_e/d. On a P_{bs} versus d_e/d plot, a line passing through $3\sigma_o$ when $d_e/d = 3$ and zero when $d_e/d = 0$ gives a satisfactory representation of the actual behaviour.

(b) Ultimate resistance depends principally on σ_u. The deformation at service load is influenced by σ_o

(c) Provided that the tube seam weld is not cracked during tab forming, then the weld seam does not influence the ultimate bearing capacity of the tab. Nevertheless the weld seam should be placed away from the bolt hole.

(d) Corner cut-outs of the given dimensions do not significantly affect the ultimate end bearing capacity of the tabs.

(e) At two thirds of ultimate load, hole deformations for $d_e/d = 1.5$ ranged between 0.4 and 0.8 mm.

(f) For the small number of results available for chamfered ends, if the end distance is taken to be the normal distance from the hole centre to the chamfered end, the end bearing resistance is approximately the same as that for tabs with square ends having the same end distance.

(g) For de/d > 3.0 the ultimate load carrying capacity increases, hole elongation prevents a higher design stress being used.

Several tab failures were observed during the frame tests. The resulting failure loads are given in Appendix C, Table C.6 and Figure 10.15. Failure was sudden and resulted in complete dislocation of the tab from within the connection. In all cases the bolt was torn out of the end of the tab. This is probably due to a reduction in

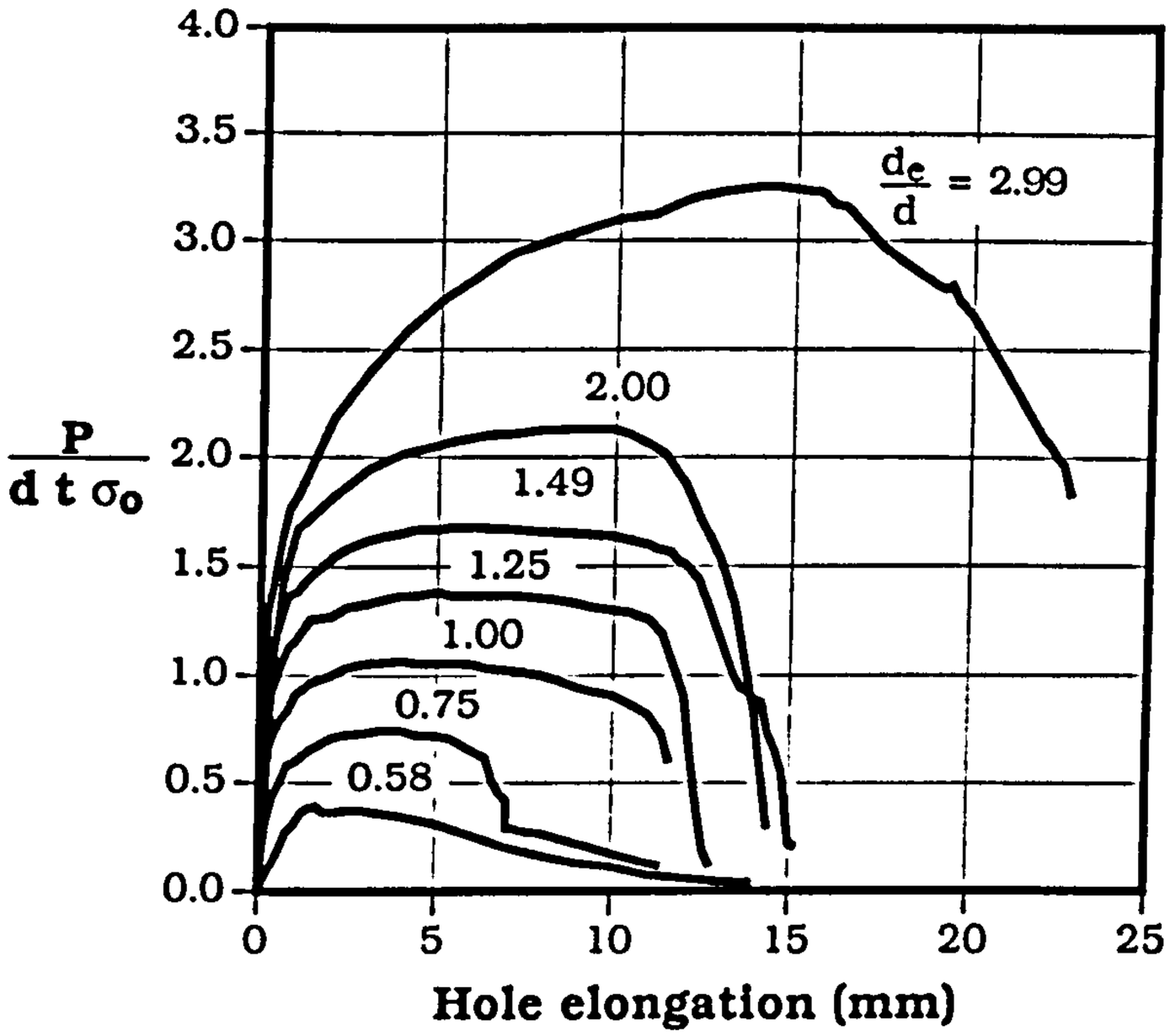


Figure 10.12 Variation in applied load with hole elongation for 48mm dia 2.0mm thick tubes, with M16 Gr 8.8 bolts

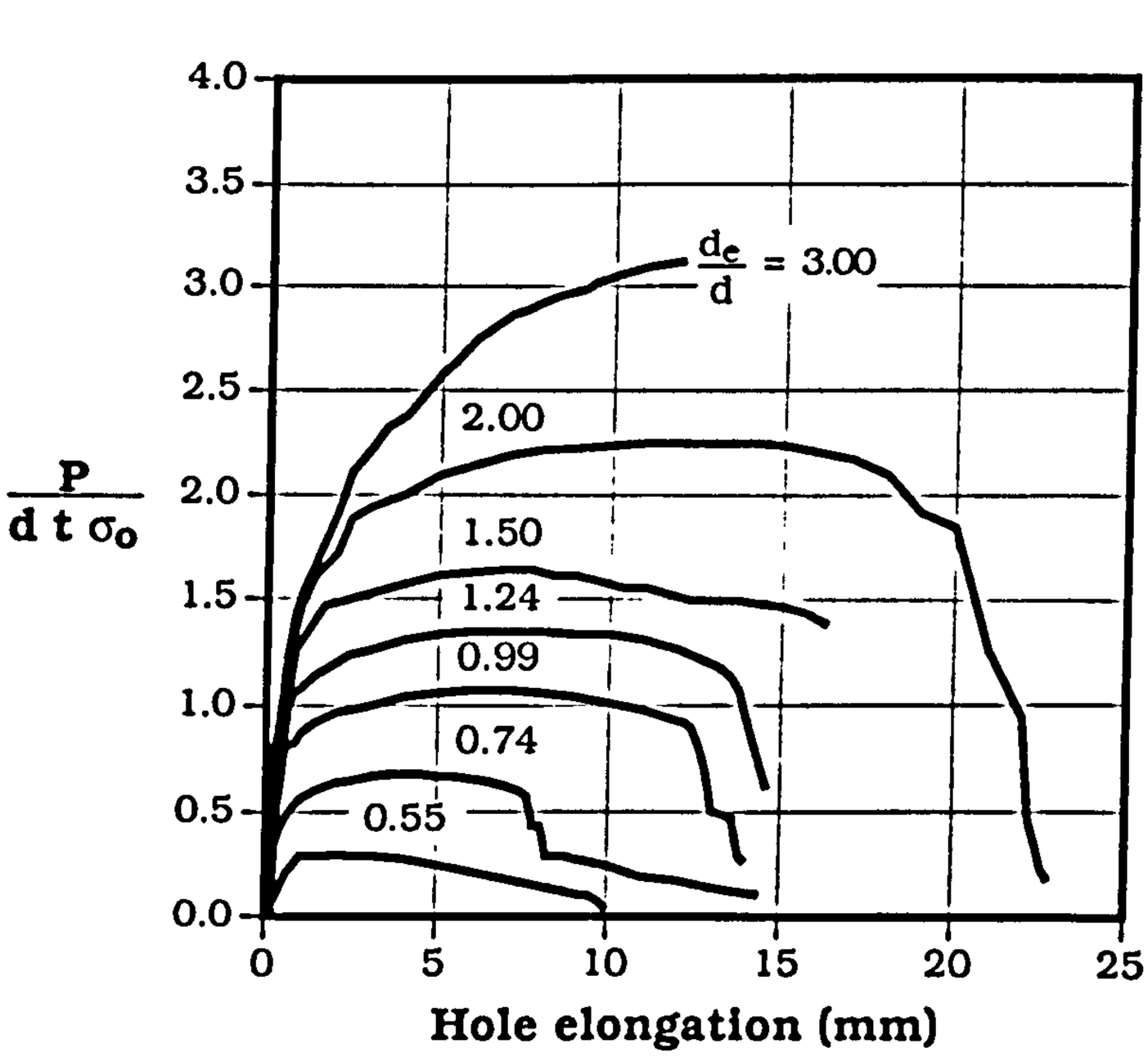


Figure 10.13 Variation in applied load with hole elongation for 60mm dia 2.5mm thick tubes, with M20 Gr 8.8 bolts

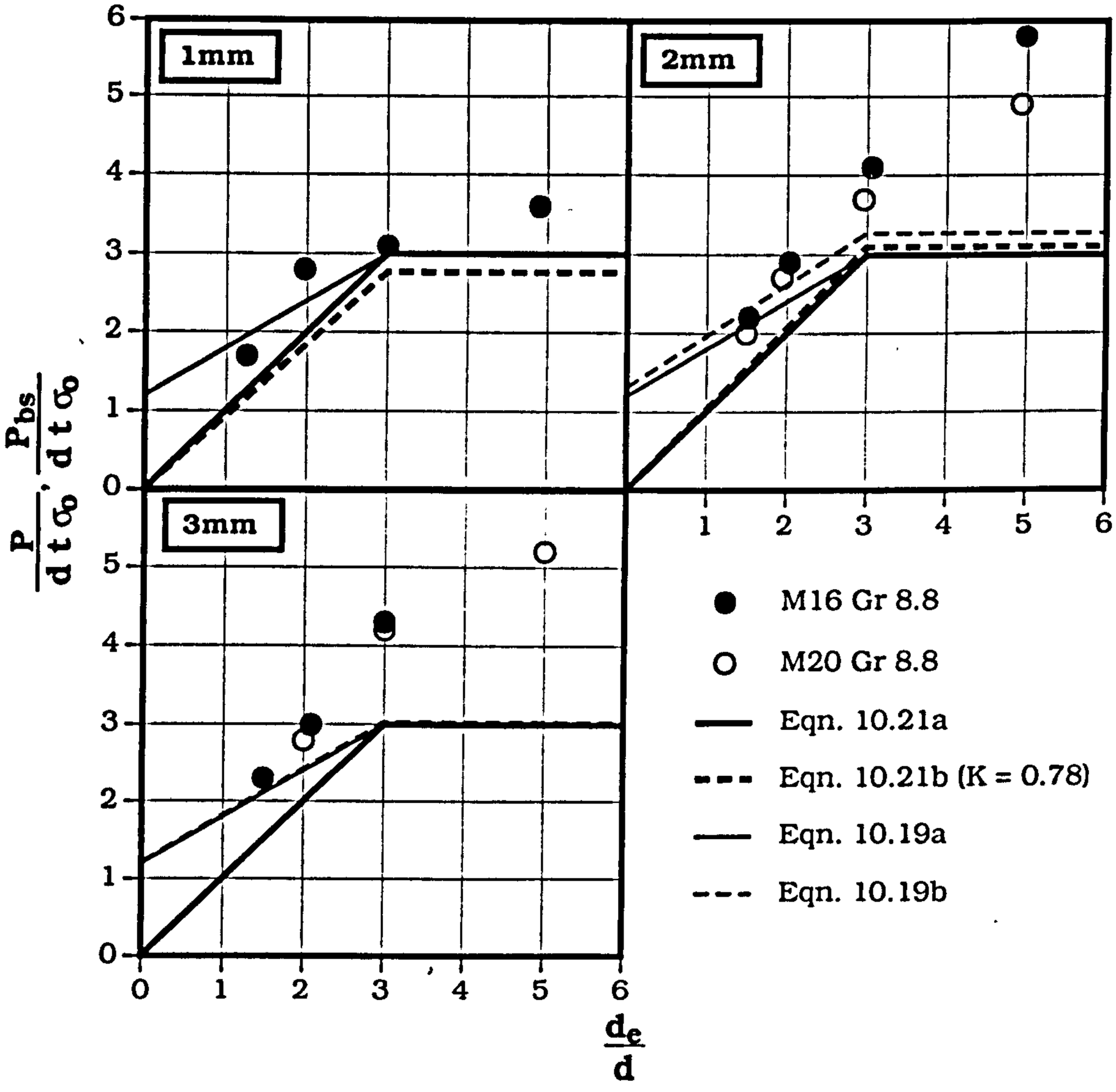


Figure 10.14 Bearing results for sheet metal speciemens with square ends

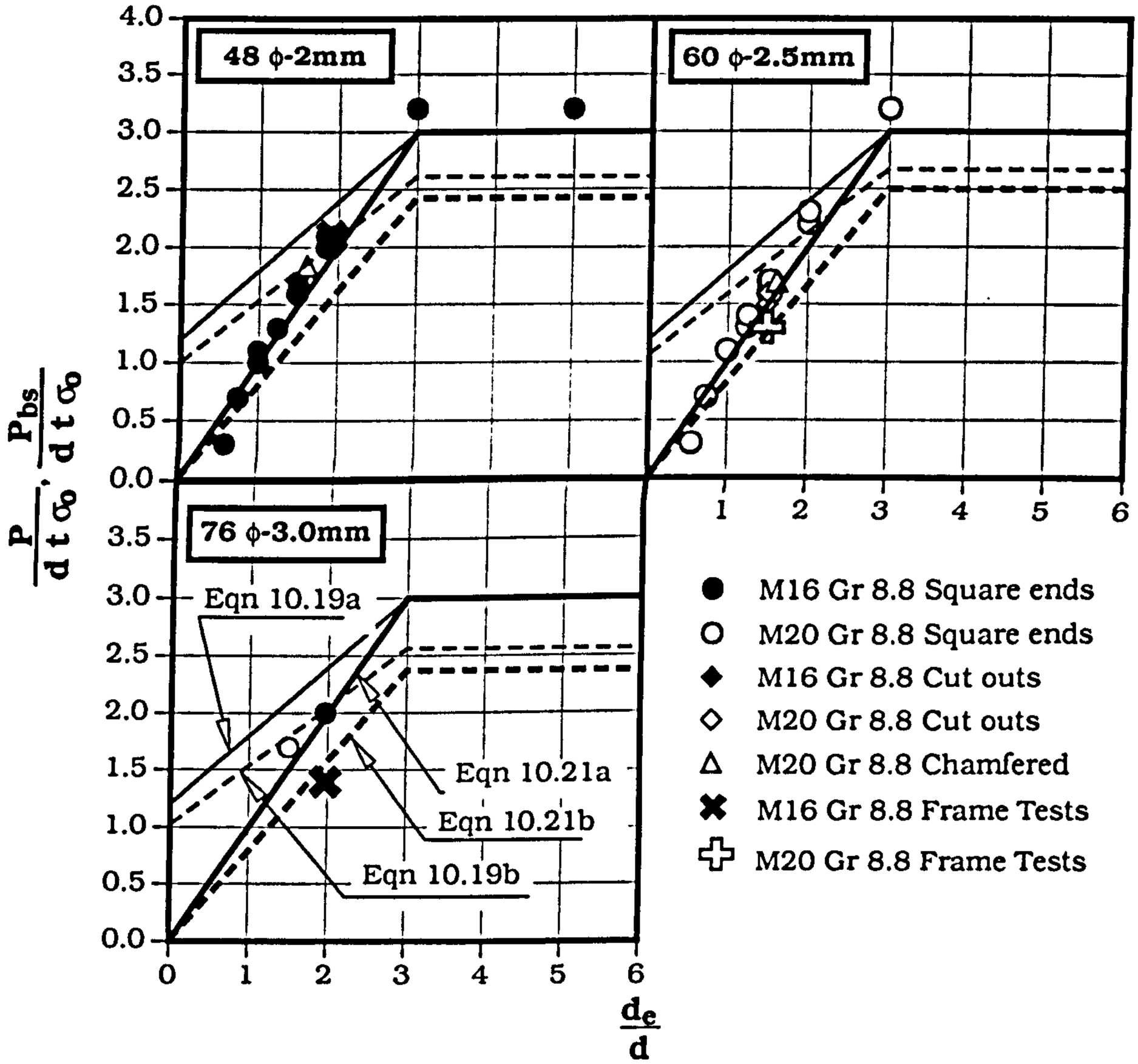


Figure 10.15 Variation in Bearing capacity with edge distance fro tube specimens and frame tests

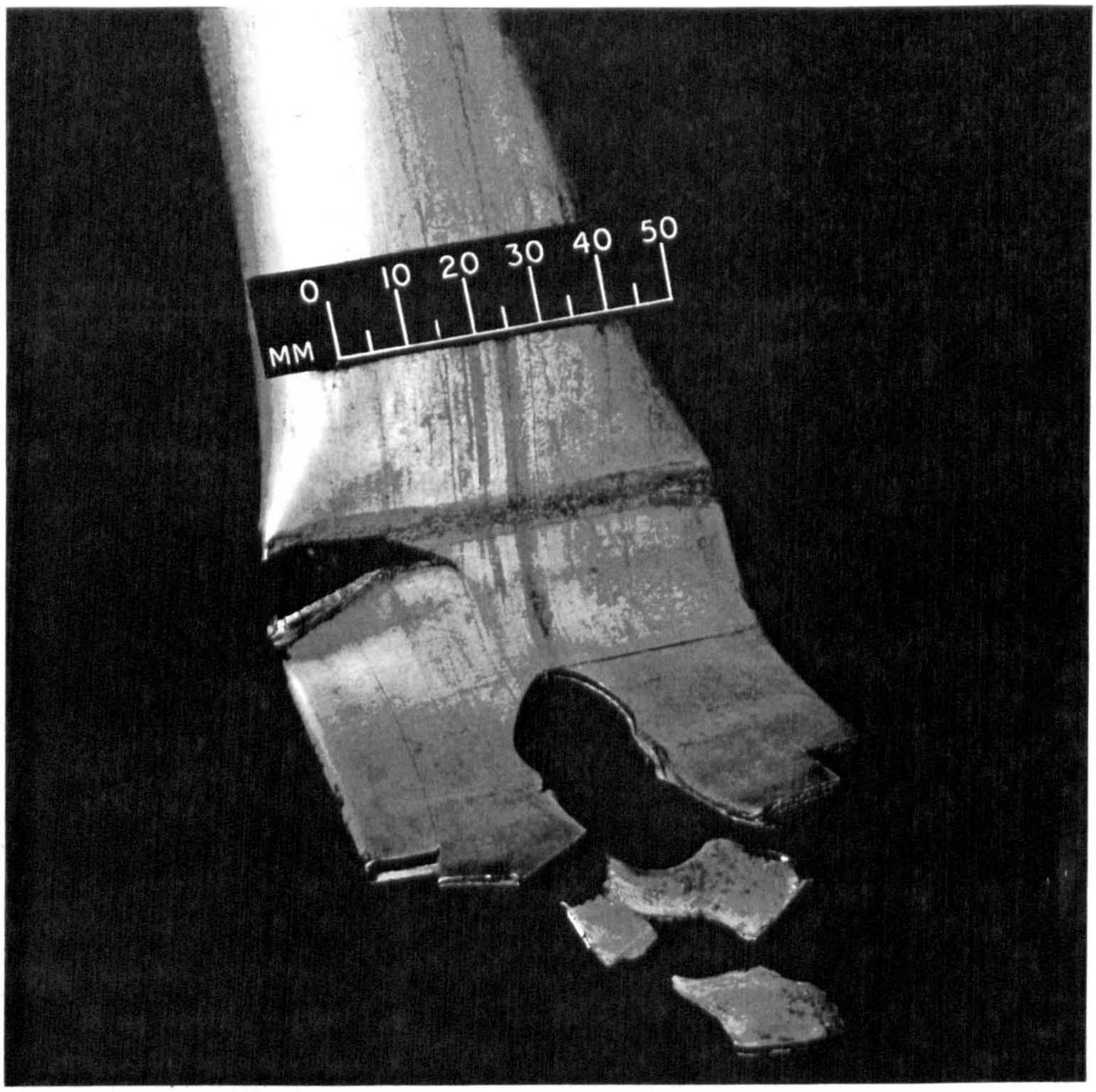


Figure 10.16 Tab failure 60mm dia-2.5mm thick tube

shear resistance caused by substantial bearing deformations in front of the bolt hole.

In the frame tests, tab failure was accompanied by partial cracking of the inner crease. During Test 5b it was observed that where the edge folds of the 76mm dia. tubes had been machined away to allow entry between joint inserts, crease cracking caused premature failure. The crack developed to an extent that caused the upper ply to be completely detached, so that bearing was resisted only by the lower ply. This effect was prevented by welding the machined edges. Presumably, when the tab edges are joined (as they will always be in practice), the propagation of the crack is controlled by the tab force on the lower ply being partly transferred to the upper

ply. The unequal partition of force between the two plies may contribute to the reduction in the tab bearing strength in the frame tests compared to the strength found in bearing tests. The reduced bearing capacity may also be due to the connections rotating and opening up under increasing load, consequently the tabs no longer remain horizontal and this causes an increase in the tab tensile forces.

Figure 10.16 shows failure of a 60mm dia tube tab. Opening of the tab crease caused by the inclination of the diagonal force with respect to the horizontal tab force and tearing of the crease developing from both ends of the crease can also be seen.

10.3.2 COMPARISON BETWEEN EXPERIMENTS AND DESIGN METHODS

Where the connected plies are confined against out-of-plane deformations by washer plates, and when $d_{e/d} > 3$, the tensile bearing tests have shown that the ultimate bearing resistance can be taken as:

$$P_{bs} = 3\,d\,t\,\sigma_o \qquad (10.18)$$

where

P_{bs} the bearing strength
d the diameter of bolt

This is in accordance with BS 5950: Part 5 (1987) for material thickness of $t > 3$mm. The reduction in bearing capacity for thinner material required by the code is not necessary when the plies are confined. For $d_e/d < 3$ the code recommends the use of the following equations:

$$P_{bs} = \left(1.2 + 0.6\frac{d_e}{d}\right) d\,t\,\sigma_o \qquad (10.19a)$$

or

$$P_{bs} = \left(1.2 + 0.6\frac{d_e}{d}\right) d\,t\,0.84\sigma_u \qquad (10.19b)$$

whichever is the smaller.

It can be seen from Figure 10.8 that when $d_e/d = 0$, $P_{bs} = 1.2\ dt\sigma_o$, which suggests that the equations might not be accurate for small values of d_e/d. Supposing that the failure is induced by shear along two longitudinal planes of length d_e, then the resistance at yield can be expressed as:

$$P_{bs} = 2\, d_e\, t\, \frac{\sigma_o}{\sqrt{3}} = 1.15\, d_e\, t\, \sigma_o \qquad (10.20)$$

If the bearing strength is assumed to be $3\sigma_o$ when $d_e/d = 3$ then the following adaptation of Equation 10.20 seems appropriate, because $P_{bs} = 0$ when $d_e = 0$ and the equation is identical to Equation 10.18 when $d_e = 3\ d$. For very small values of d_e it can be expected that Equation 10.20 will be non conservative, because if $d_e < d/2$, the hole is no longer enclosed. Alternative stress limits can be introduced:

$$P_{bs} = d_e\, t\, \sigma_o \qquad (10.21a)$$

or

$$P_{bs} = d_e\, t\, K\, \sigma_u \qquad (10.21b)$$

whichever is the smaller.

The constant K in Equation 10.21b can be found from the experiments. When $K = 0.78$ a satisfactory fit to the experimental data is obtained. Equations 10.19 and 10.21, are compared with test results in Figures 10.14 and 10.15. Equations 10.21 are generally satisfactory, remembering that the lesser of the two governs for design. For $d_e/d > 3$, the experimental resistance continues to increase, but the hole elongation at failure is then very large, and if P_{bs} were assumed to be greater than $3d_et\sigma_o$ the elongation at service loads could be excessive. Equations 10.19 and 10.20 are seen to be non-conservative only when $d_e \leq 0.7d$. The type of failure at $d_e/d \leq 0.7$ is not described by Equations 10.21 because failure then occurs by transverse tension at the end (Type II, Figure C.1, Appendix C).

The tab end bearing strength observed in the frame tests, where the horizontal tab force is calculated on the basis of computed diagonal forces and the original frame dimensions, were below the corresponding values for tensile tab tests. Some reduction in end bearing capacity can be expected as a result of rotation of the joint under load and local deformations of the connection, as these effects may increase the horizontal component of the diagonal force.

10.3.3 PROPOSED DESIGN METHOD

From the small number of failures which have occurred in the frame tests, coupled with tensile tests on similar material, it appears that Equations 10.21 can be adopted if K is taken as 0.78. A partial safety factor $\gamma_m = 1.1$, should be introduced in recognition of the sensitivity of the tab strength to material defects, to possible differences between calculated and actual forces, and in recognition of the importance of the tab end connection to the integrity of the system. For design purposes, the end bearing resistance of the diagonal tube tabs may be taken as the lesser of

$$P_{bs} = \frac{d_e\, t\, \sigma_o}{\gamma_m} \qquad (10.22a)$$

or

$$P_{bs} = \frac{d_e\, t\, 0.78\, \sigma_u}{\gamma_m} \qquad (10.22b)$$

where

γ_m partial material safety factor equal to 1.1

10.4 BOLT AND WASHER PLATE DESIGN

The number of elements located at different planes in the connection makes it difficult to trace and to apportion the horizontal and vertical forces. In this section an attempt has been made to determine the principal force paths from the diagonals into the bolts and washer plates and to provide rational design recommendations based on the limited test data available.

10.4.1 TRANSFER OF FORCES

The resultant of the vertical components of force in the four diagonal tubes meeting at a bottom node will normally be close to zero. However, opposite members do not necessarily have equal forces. Consider first the bottom chord connection shown in Figure 10.2. The tensile diagonal tube, P_{D2}, whose tab enters between the upper washer plate and the table of the lips up chord tends to lift one edge upwards. This upward force is transferred through a single bolt to the lower washer plate, which

bears on the webs of the upper channel. It is this force which tends to cause crippling of the webs of the upper channel.

The vertical force of the compressive diagonal, P_{D1}, in the same plane bears upon the lower washer plate. The bolt transfers this force back into the upper washer plate which in turn exerts a downward force to the table of the upper channel which applies a tensile force to the webs of the upper channel. Figure 10.17 shows the assumed distribution of forces under a pair of washer plates. A similar line of reasoning can be applied to the diagonal members in the plane of the bottom chord lips down section. It is evident from Figure 10.17 and the above that all four bolts are in tension.

The bolt forces in a bottom chord connection, if equally torqued should in principal remain equal as the load is increased. If the diagonal forces in a pair of tubes are greater than in the other pair some degree of force redistribution between bolt pairs may take place through bending of the washer plate, but this should be ignored due to the relative flexibility of the washer plate compared to that of the bolts.

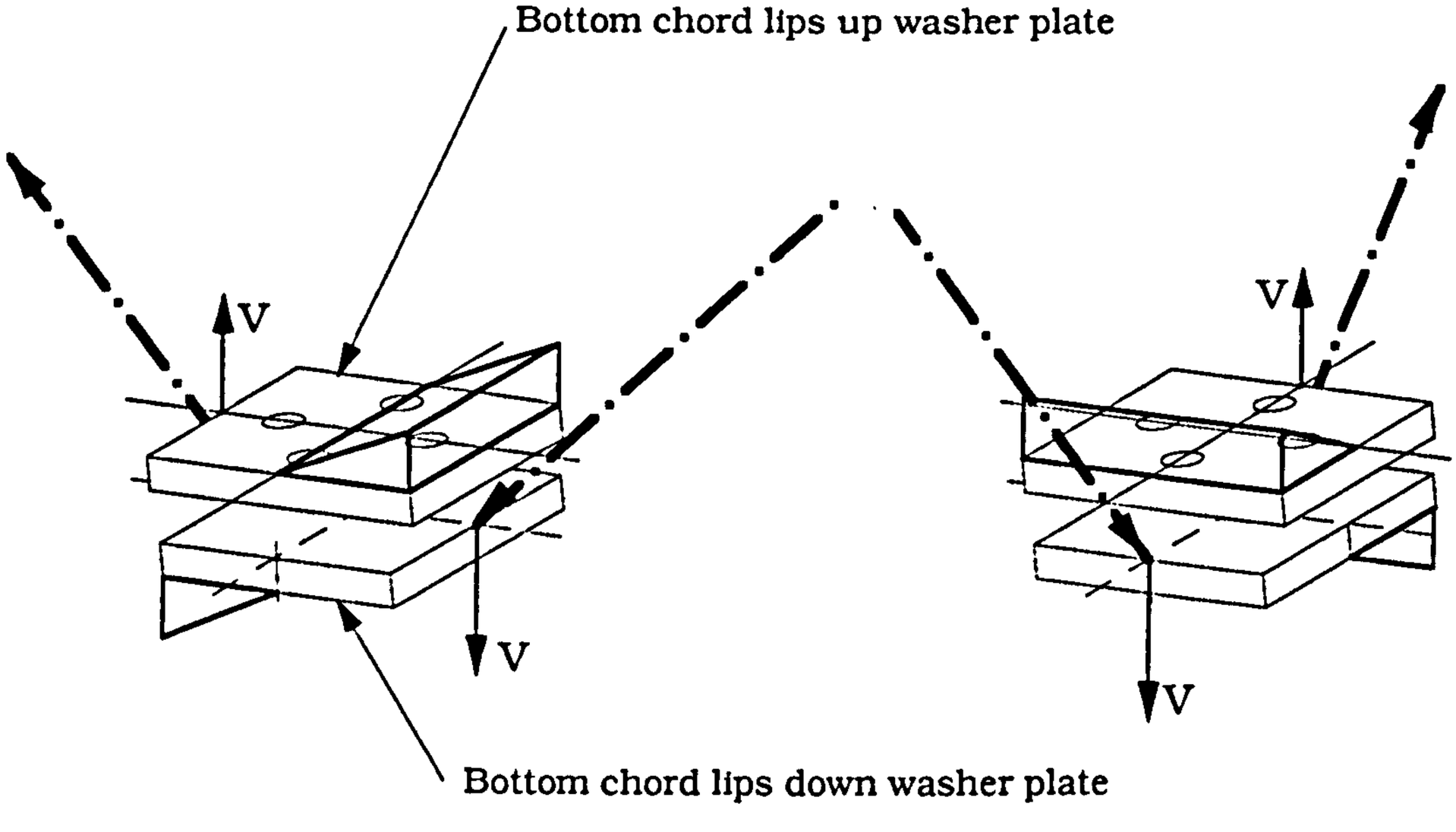


Figure 10.17 Force distribution under washer plates in bottom chord

10.4.2 JOINT MODEL FOR BOLT DESIGN

Figure 10.18 shows the bolt forces, the vertical component of the diagonal tubes and the reactive force between the washer plate and the chord table. If the force distribution is linear along the edges of the washer plate (L_W), the distance between the resultant forces is 2/3 L_W, and it can be seen that the tensile force in the bolt will be greater than the vertical force at the edge of the plate.

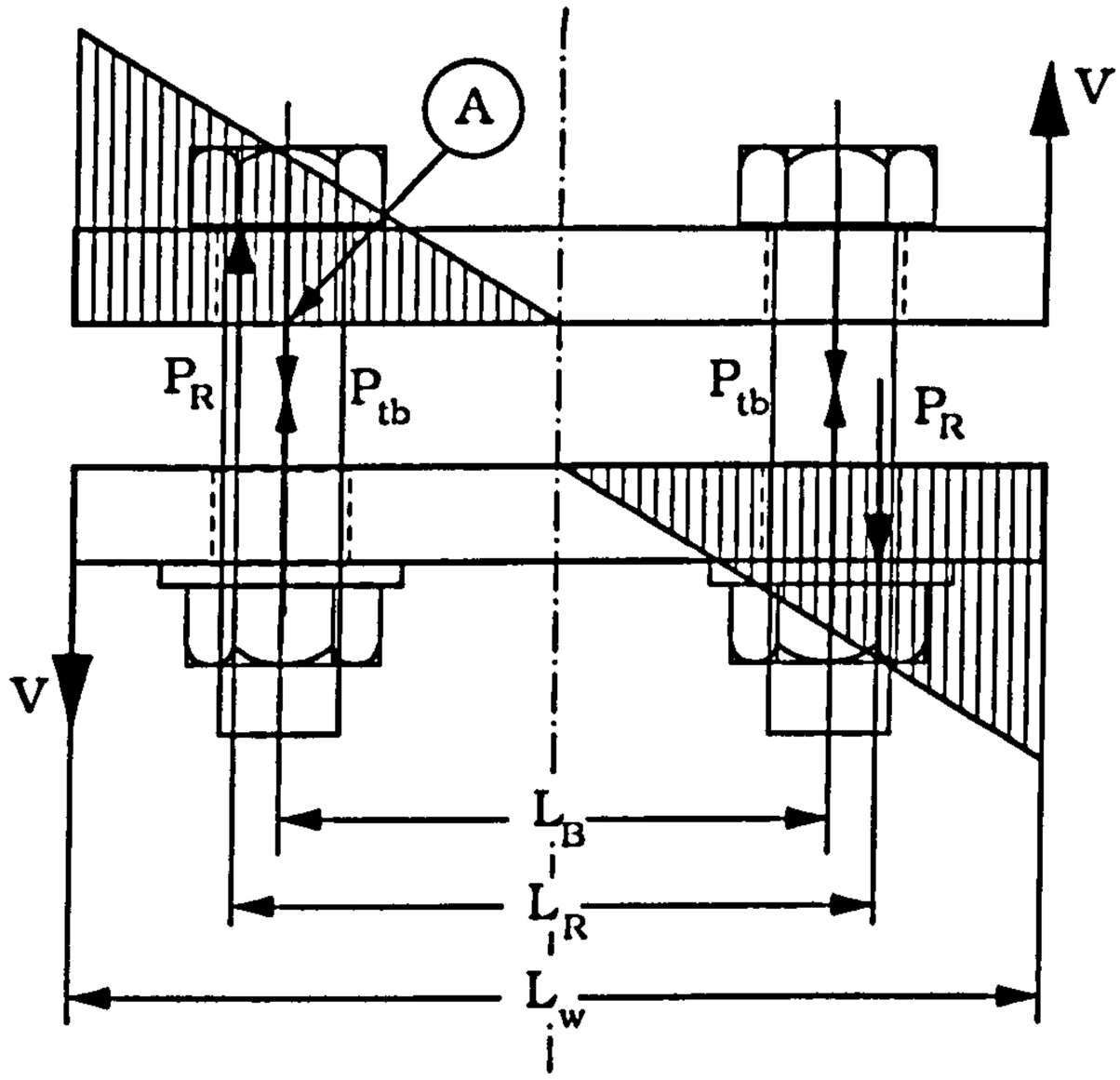


Figure 10.18 Assumed bolt and washer plate force distribution

Bolt Tension

Consider equal upward and downward forces acting on a pair of bottom chord washer plates. The bolt forces can be expressed in terms of the distance between the reactions L_R; the effect of any departure from the assumed stress distribution can then be clearly seen. From moment equilibrium of the external and internal forces

$$L_w V = L_R P_R \qquad (10.23a)$$

from which

$$P_R = V \frac{L_w}{L_R} \qquad (10.23b)$$

where

L_R distance between reactions

P_R reaction between washer plate and channel

Consider moments about point A of the forces acting on the upper plate

$$\frac{V}{2}(L_W + L_B) - L_B P_{tb} - \frac{P_R}{2}(L_R - L_B) = 0 \qquad (10.24)$$

Substituting for P_R

$$\frac{V}{2}(L_W + L_B) - L_T P_{tb} - \frac{V}{2}\frac{L_W}{L_R}(L_R - L_B) = 0 \qquad (10.25)$$

Rearranging

$$P_{tb} = \frac{V}{2}\left(1 + \frac{L_W}{L_R}\right) \qquad (10.26a)$$

For a linear stress distribution

$$L_R = \frac{2}{3} L_W \qquad (10.26b)$$

and the tensile force in the bolt is

$$P_{tb} = 1.25\,V \qquad (10.26c)$$

It can be seen that P_{tb} is dependent on L_R but independent of L_B.

Suppose now that the vertical forces are unequal, and are of magnitudes $(V+2V_1)$ upwards and V downwards. The forces can be represented as a couple having end forces $(V+V_1)$ and two forces V_1 both in the same direction. The bolt forces caused by the couple are found from Equations 10.26 by substituting $(V+V_1)$ for V. The symmetrical force V_1 cause equal bolt forces. Combining the two gives

$$P_{tb} = \frac{V}{2}\left(1 + \frac{L_W}{L_R}\right) + \frac{V_1}{2}\left(3 + \frac{L_W}{L_R}\right) \qquad (10.27)$$

Consider a connection with an upward force of 2V and a downward force V. The additional force at one end is

$$V_1 = \frac{V}{2} \qquad (10.28)$$

The tensile force in the bolt given by Equation 10.17 is

$$P_{tb} = 1.25\,V + 1.125\,V_1 = 2.375\,V \qquad (10.29a)$$

when

$$\frac{L_W}{L_R} = \frac{3}{2} \qquad (10.29b)$$

If it is assumed that the tensile force would be approximately the same as for a couple having forces 2V, the bolt forces given by Equation 10.26 would then be

$$P_{tb} = 2.5\,V \qquad (10.30)$$

If on the other hand a couple having the average force 3/2V had been assumed, then

$$P_{tb} = 1.875\,V \qquad (10.31)$$

It can be seen that the first approximation (Equation 10.30) overestimates the tensile force by 5%, whilst the second (Equation 10.31) gives a 21% underestimation. Thus it would seem conservative to assume that the vertical forces are both equal to the greater for the purpose of estimating the tensile force in the bolt.

Consider now the top chord joint. Assuming that the diagonal force is applied on the centre line of the diagonal tube, which enters the top chord connection close to the corners of the plate (Figure 10.3), and that the flexural stiffness of the plate is small compared to the axial stiffness of the bolt, then the forces will be reacted principally by the two bolts nearest the tube axes. The bolt forces can be found from Equations 10.26 (which assumes that the diagonal forces in the connection are both equal to the larger of the two diagonal forces) or 10.27 (which uses the actual diagonal forces) and if $L_W/L_R = 3/2$ then the top chord bolt forces have the same magnitude as the bolt forces in the bottom chord.

Bolt Shear

The shear force applied to each bolt is equal to the horizontal component of the force in a diagonal. Figure 10.19 shows the shear planes to be considered in the bottom chord connection. Consider bolts A and C, the horizontal forces from the diagonals

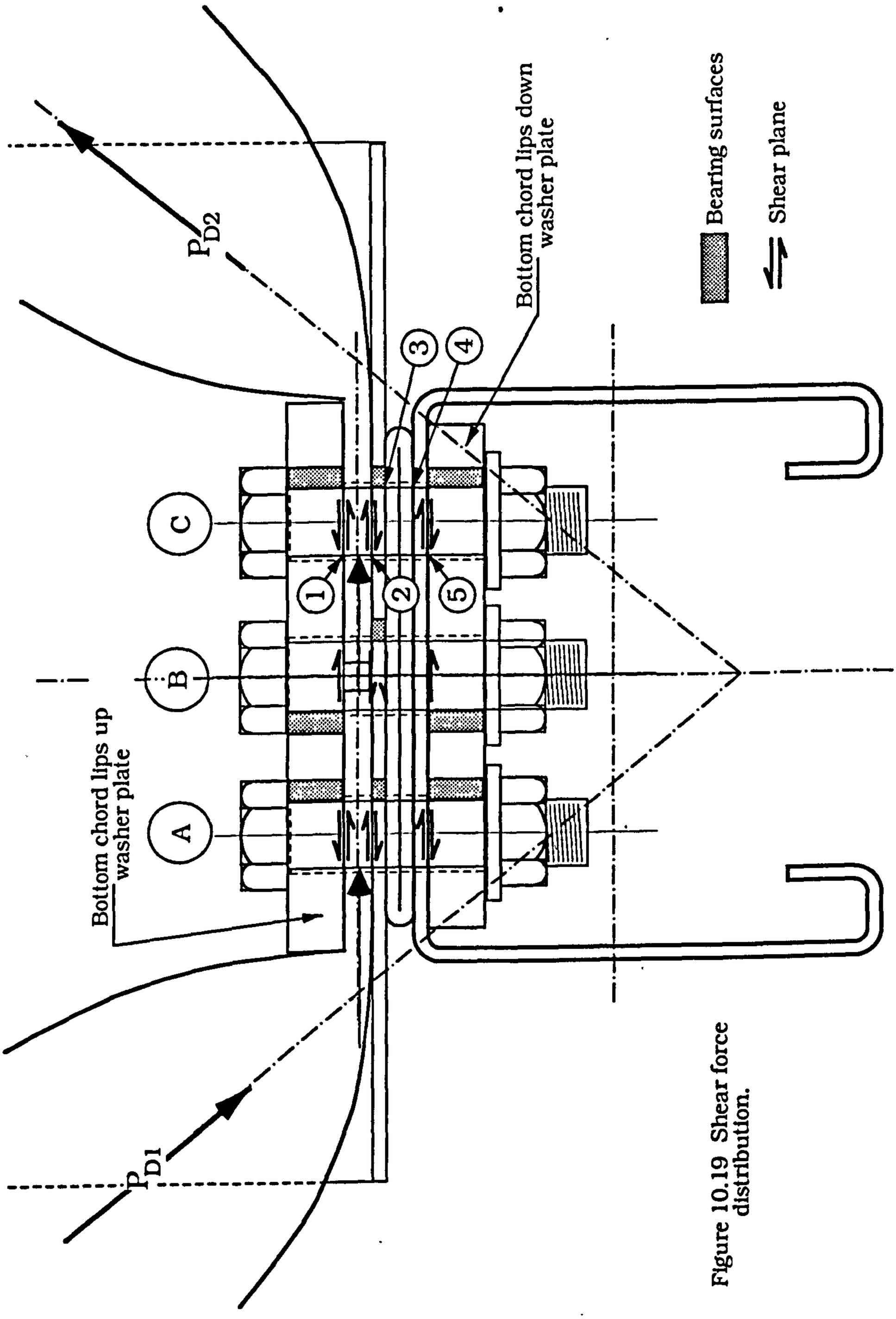


Figure 10.19 Shear force distribution.

are transmitted through the bolts by dowel action into the table of the channel. The chord perpendicular to the direction of the applied horizontal force is assumed to exert no resistance to the bolt group in the direction of the diagonal being considered. The bolt can be conservatively considered to be in single shear along the diagonal tab/channel table interface (point 2 in Figure 10.19).

Bolt B, the unloaded bolt, also provides resistance to the shear forces in Bolts A and C. A second shear plane between the upper washer plate and the diagonal tab (point1) can be partially mobilized. The shear force is also resisted by a third shear plane located at the lower washer plate/table interface, denoted by point 5 in Figure 10.19. The relative distribution of shear forces between the shear planes would depend on the bending stiffness of the bolts and on hole clearances. It would seem rational to assume that most of the shear force would be resisted by the shear planes closest to the level of the applied horizontal load. This suggests that the bolt is subjected to *quasi* double shear. In practice it would be prudent and conservative to assume that the bolts act in single shear.

In the top chord, the shear force in a bolt is again equal to the horizontal component of the force in the diagonal, but the bolt is clearly subjected to double shear. This is because the applied force is reacted equally by both chords, and because the tab enters the connection between the chord tables. It should be noted however, that the two chords exert reactive components perpendicular to the direction of the horizontal force. These forces are applied respectively above and below the tab, resulting in a tendency for some lateral tilting of the bolt group to occur.

Because the bolt and tab are critical elements of the system, a partial safety factor $\gamma_m = 1.1$ on the yield stress has been introduced.

For a shear plane located in the threaded part of the bolt the shear capacity is

$$P_{usb} = \frac{A_t \sigma_o}{\gamma_m \sqrt{3}} \qquad (10.32)$$

where

A_t tensile area of the bolt

P_{usb} single shear capacity of bolt

and for a shear plane in the unthreaded part of the bolt

$$P_{usb} = \frac{A_b \sigma_o}{\gamma_m \sqrt{3}} \qquad (10.33)$$

A_b shank area

To reduce deformation, to enhance bolt bearing resistance by restraining out of plane deformations of the connected plies, and to prevent progressive slackening of the bolts, it is necessary to pre-tension the bolts to a specified torque. The pretension in the bolts should not be less than the calculated bolt tension at working loads.

10.4.3 JOINT MODEL FOR WASHER PLATE DESIGN

Several practical constraints dictate the maximum thickness of the washer plate. If it is too thick it may make it difficult to insert the bolts in the connection which may necessitate reducing the length of the lip downturn, thereby affecting the load carrying capacity of the section. It is also advantageous to keep the washer plate as thin as possible so that the bolt lengths can be kept to a minimum. A washer plate must posses sufficient bending capacity to resist the moment caused by the vertical component of the diagonal tube acting about the bolt centre. The washer plate moments are difficult to determine, as the distribution of the applied forces is influenced by the stiffness of the channel. Also, design assumptions for web crippling depend on the washer plate having adequate stiffness. However, one end of the upper washer plate in the bottom chord connection is loaded directly by the tab of a tension diagonal, and in this case the moment in the washer plate can be estimated.

Assuming that yielding occurs along a line a-a, (Figure 10.20) parallel to the edge, across a line passing through the centre of the bolt hole, the magnitude of the vertical component of the diagonal force at which washer plate failure occurs is

$$V = \frac{\sigma_o (B_w - d)\, t_w^2}{2\,(L_w - L_B)} \qquad (10.34)$$

where

B_w width of washer plate

t_w thickness of washer plate

The washer plate thickness required to resist the moment can be found from Equation 10.35, which is

$$t_w = \left(\frac{2\,V(L_w - L_B)}{\sigma_o(B_w - d)}\right)^{1/2} \qquad (10.35)$$

The bending moment on the top chord washer plates is difficult to estimate, because the diagonal forces are in part transmitted directly to the channel webs. It was found from the frame tests that the by using top chord washer plates of equal thickness to the adjacent bottom chord plates, the performance was satisfactory.

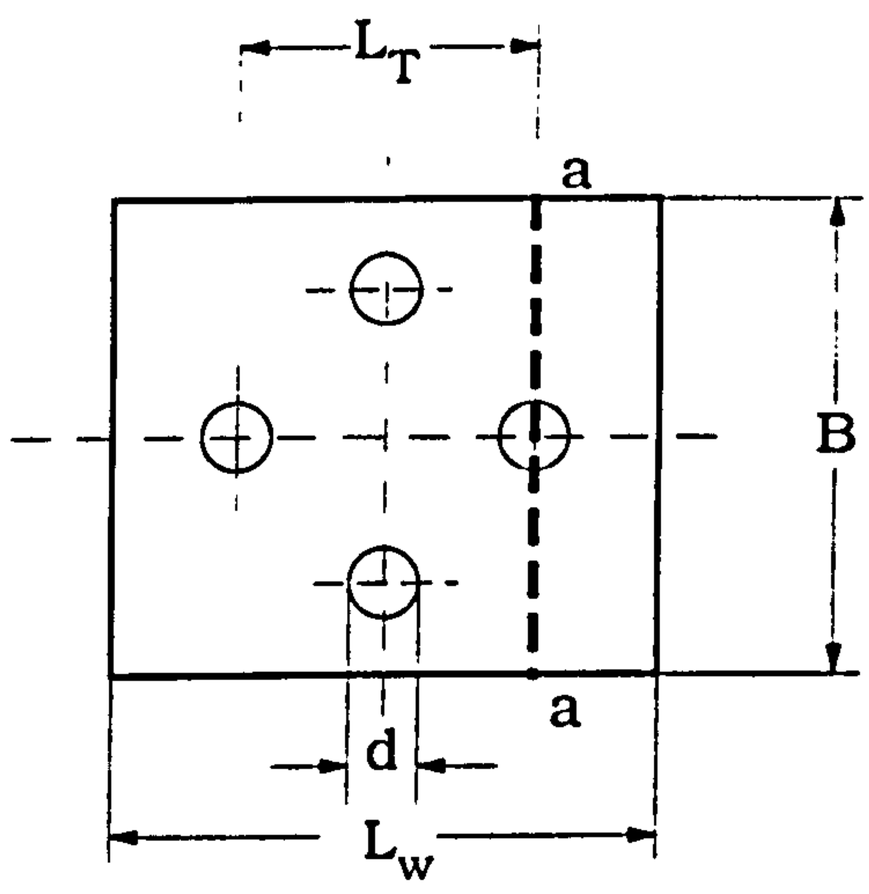


Figure 10.20 Bottom chord washer plate yield line

10.4.4 EXPERIMENTS

Bolt tensile forces were measured during several of the frame tests described in Chapter Three. Tensile bolts forces were obtained from strain gauges bonded within small concentric holes as shown in Figure 10.21. Strain readings, the frame loads and tensile forces P_{tb} in the bottom and top chord joints are given in Tables 10.7 and 10.8 respectively.

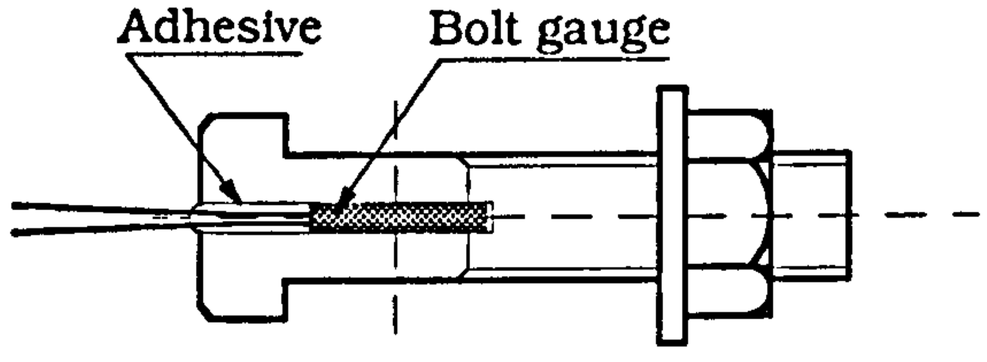


Figure 10.21 Strain gauged bolt

TEST	P_{TEST} kN	ε_{max} με	P_{tb} kN	$\frac{P_{tb}}{\text{Eqn. } 10.26}$
1b	250	1354	44	1.13
2a	330	1331	43	0.84
2b	374	1354	44	0.76
2c	470†	1393	70	0.96
3b*	140	892	29	1.31
3e*	200	1255	41	1.32

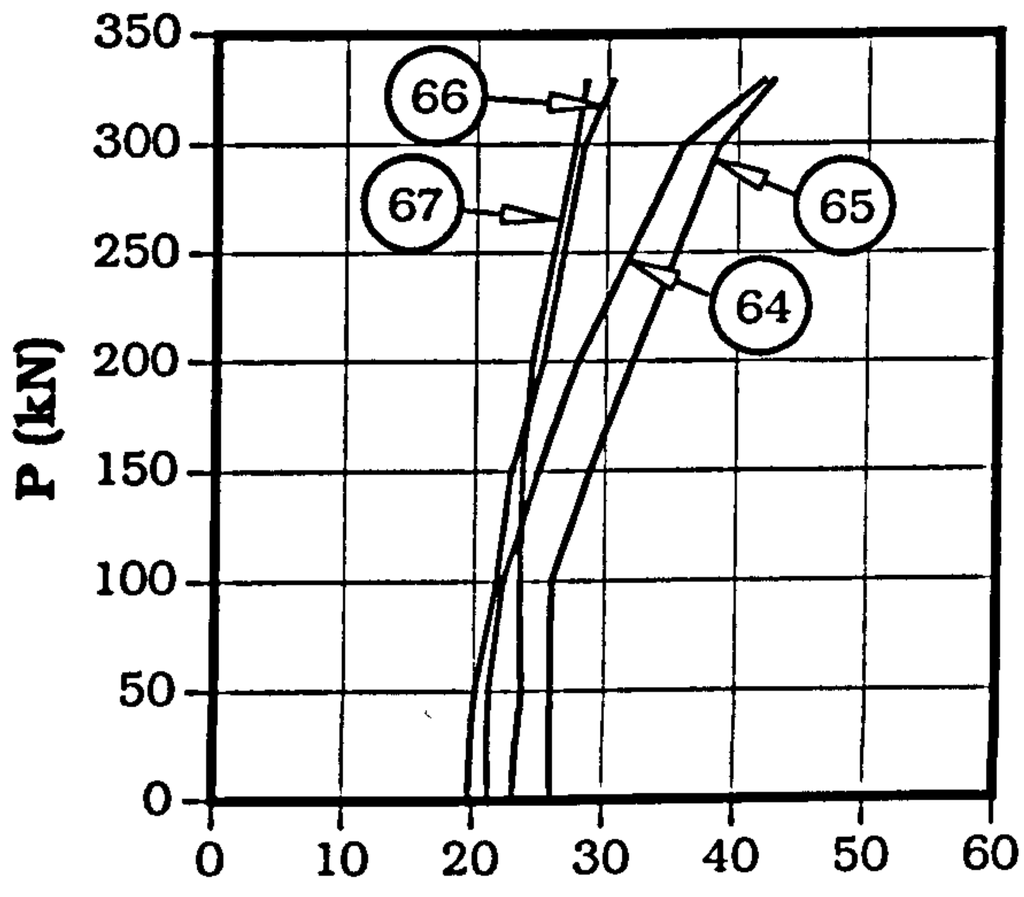
†M20 Gr 8.8 *Sleeved joint

Table 10.7. Experimental bottom chord bolt strains - M16 Gr8.8

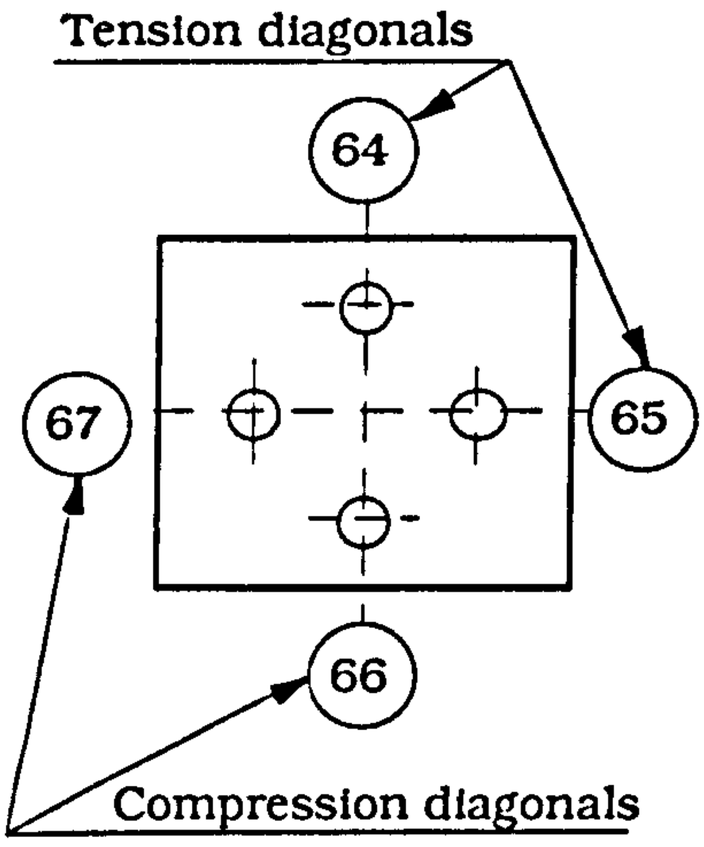
TEST	P_{TEST} kN	ε_{max} με	P_{tb} kN	$\frac{P_{tb}}{\text{Eqn. } 10.26}$
1b	250	1135	37	0.95
2a	330	1306	43	0.85
2b	374	1675	54	0.93
2c	470†	1499	79	1.07
3b*	140	1158	38	1.68
3e*	200	1465	48	1.52

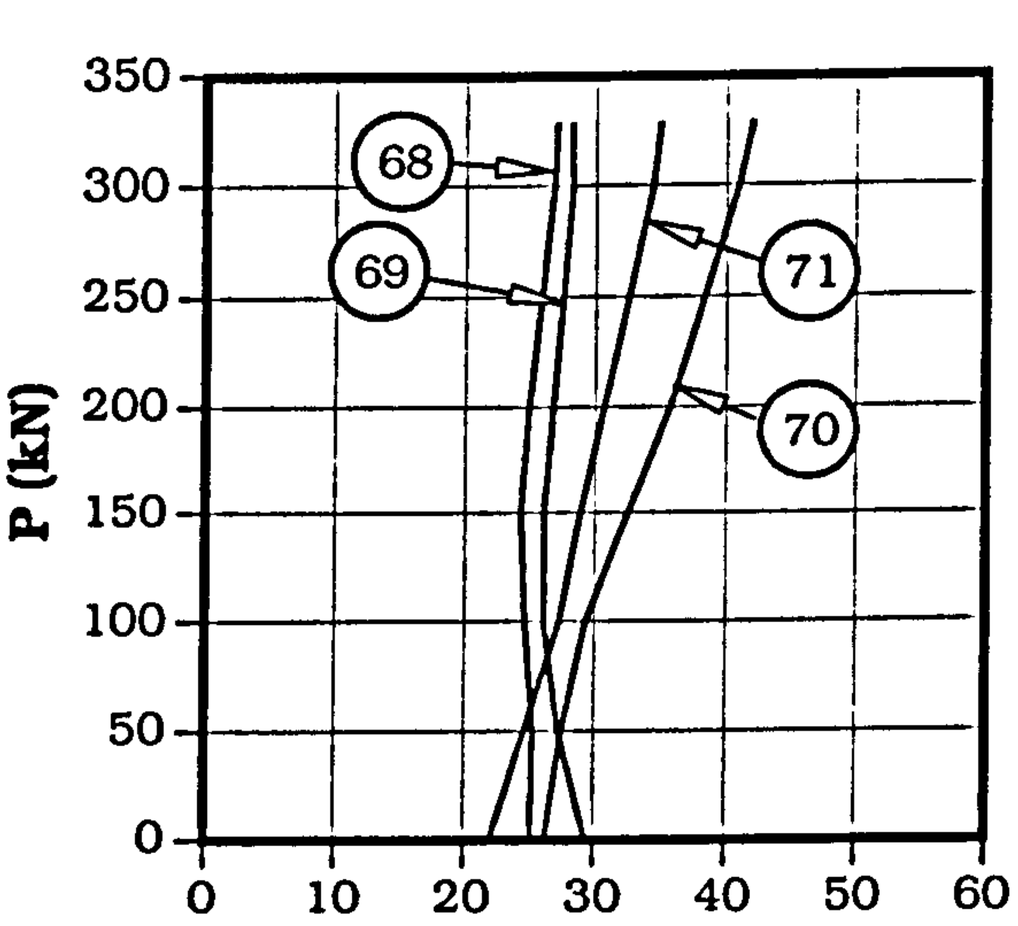
†M20 Gr 8.8 *Sleeved joint

Table 10.8. Experimental top chord bolt strains - M16 Gr 8.8



Bolt forces bottom chord P_{tb} - kN





Bolt forces top chord P_{tb} - kN

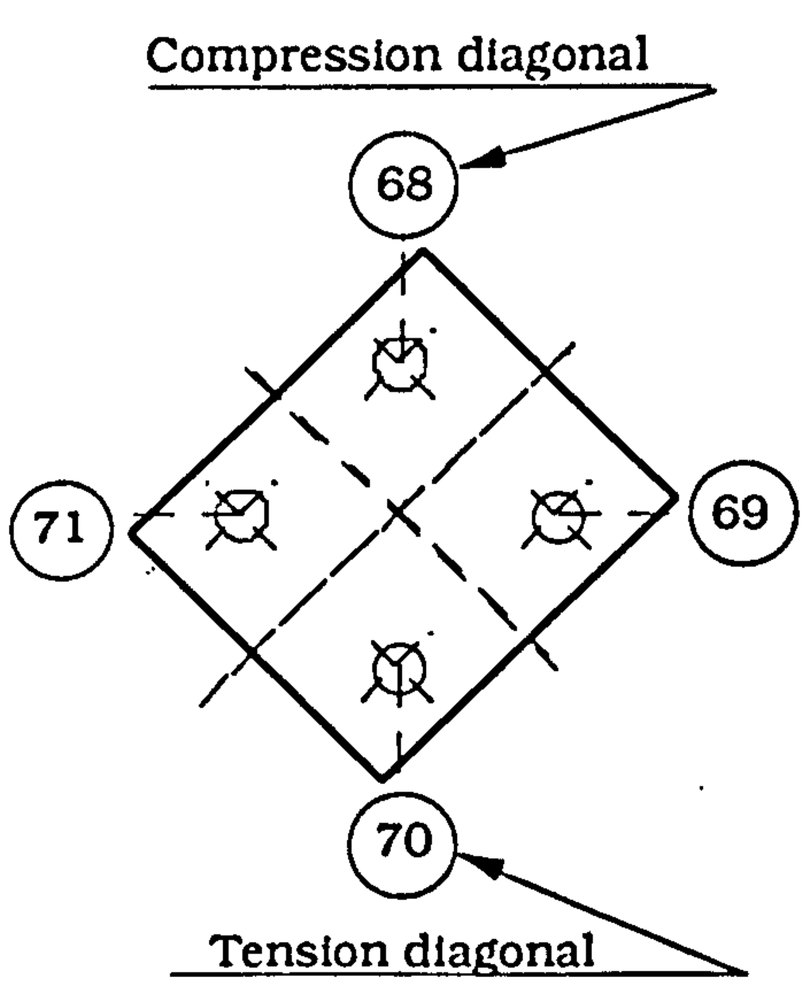


Figure 10.22 Variation in bolt forces with central frame load

Figure 10.22 shows the variation in bolt strains with load for the bottom chord connection, B3, and the top chord connection F8, in Test 2b. The bolts with the higher strains were located at the ends of the tensile diagonals, while the bolts in the tabs of the compression diagonals are seen to have smaller strains. The variation in bolt strain around the connection is similar to the variation in the diagonal forces observed in the numerical analysis, described in Chapter Two. Frame failure due to combined tension and shear failure of the bolt was not observed. Test 7d, which consisted entirely of connections with M16 Gr 8.8 bolts, sustained a central load of 760 kN, substantial bending deformation of the bolt was observed on dismantling the frame (Figure 10.23).

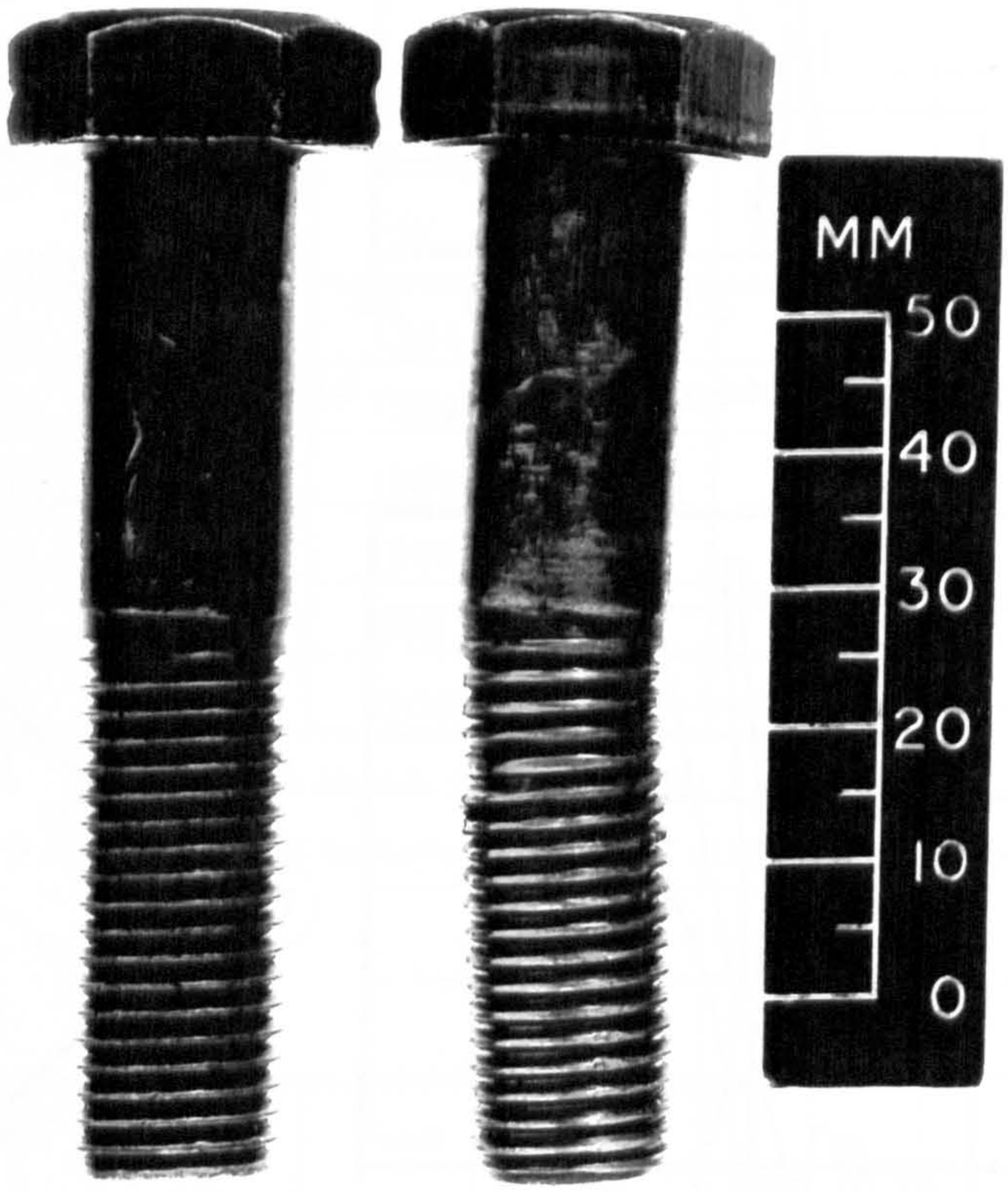


Figure 10.23 M16 Gr. 8.8 bolt failure

A comparison between the bolt tensile forces given by Equation 10.26 and those obtained experimentally is given in Table 10.8. Good agreement between the experimental results and Equation 10.26 for the top and bottom chords can be seen, except that an increase in tensile bolt strain is evident for sections reinforced with split sleeve inserts.

The washer plates used in the frame tests were fabricated from hot rolled mild steel plate. Tensile tests were carried out to obtain the yield and ultimate stress of the washer plate material, where it was found that σ_o = 250 N/mm^2 and σ_u = 297 N/mm^2. Washer plate bending was recorded during two of the test, the frame loads are given in Table 10.9.

TEST (Node)	**t** (mm)	P_{TEST} kN	**V*** kN	$\frac{V}{\text{Eqn. } 10.34}$
2a - (B3)	10	330	35	1.8
4b - (F8)	6	300	37	6.1

* vertical force based on LUSAS /cruciform analysis

Table 10.9. Washer plate test results

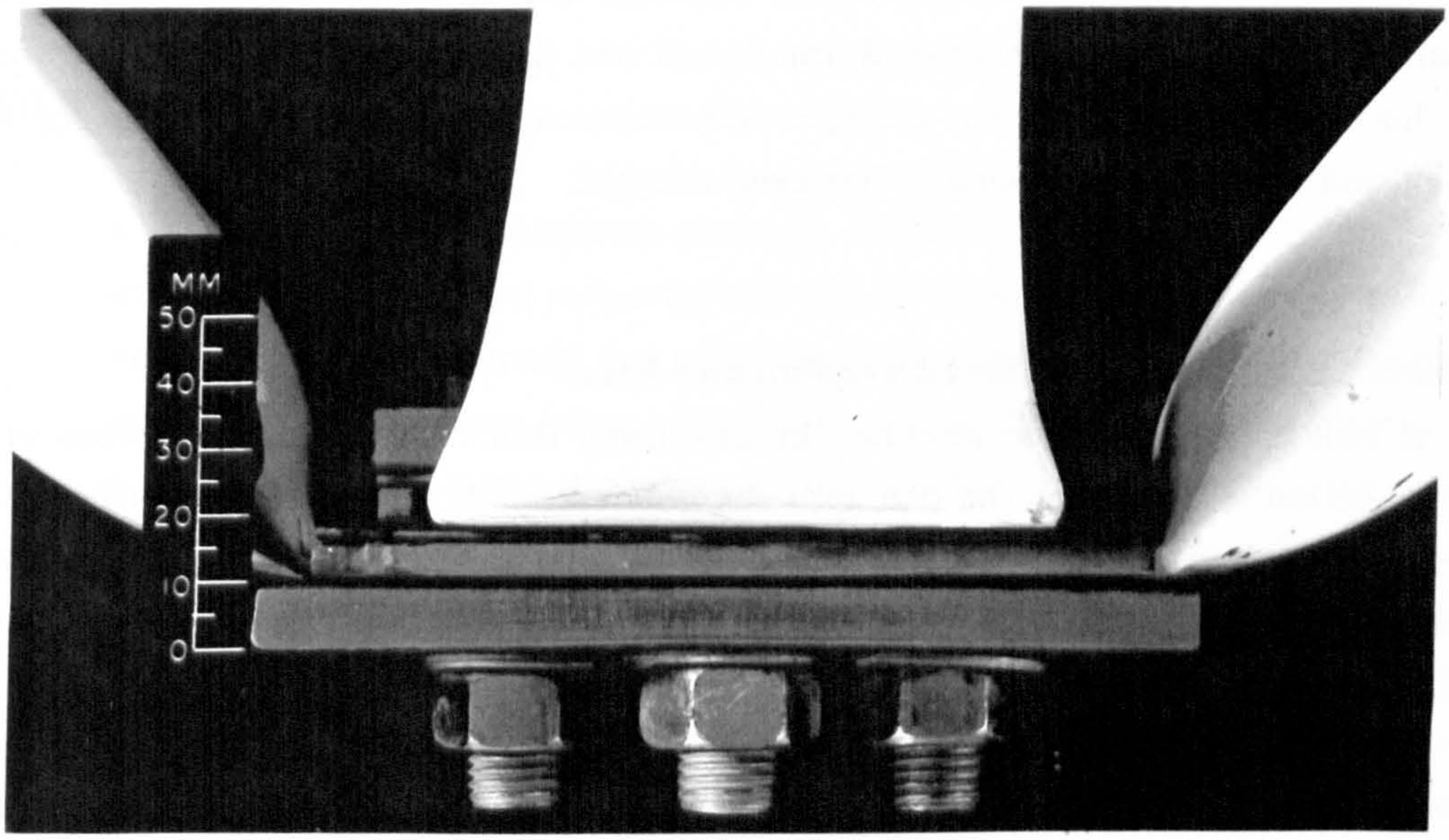


Figure 10.24 10mm bottom chord washer plate failure
(Channels sections removed)

Equation 10.34 is seen to give a very conservative estimate of the limiting load for the 6mm top chord and 10mm bottom chord washer plates. The load at which the 6mm plates were replaced exceeded the estimated limit load by a factor of six. This increase in load is due to the top chord diagonal tab, which enters the connection between the backs of the channels, which consequently mobilizes the web crippling

capacity of the section simultaneously with the bending resistance of the washer plate. This is confirmed by the fact that during Test 4b an out-of-plane web deformation of 1.5mm was observed in the top chord connection along with permanent bending deformations in the 6mm washer plates.

A better estimate for the bottom chord washer plate is obtained from Equation 10.26, since the diagonal tab is directly reacted by the upper washer plate in the connection. After removal of the 10mm washer plates it was observed that failure occurred by yielding along a line parallel to the edge, across the centre line of the plate. This implies some opening of the joint under load, which is evident in Figure 10.24.

10.4.5 PROPOSED DESIGN METHOD

The structural integrity of the frame depends largely on the robustness of the connections. Due to the limited amount of test data available and the complex behaviour of the connection, a simple and conservative approach to estimating the bolt and washer plate capacities has been adopted.

Bolts Subjected to Combined Tension and Shear

The bolt capacity can be obtained by assuming that all the diagonal forces in a connection are equal to the one with the greatest load. It was shown earlier that Equation 10.26 can be used to obtain the tensile bolt force in the bottom chord connection. The horizontal shear force is resisted by the bolt by single shear. The interaction between tension and shear in a bolt is governed by

$$\frac{P_{tb}}{P_{utb}} + \frac{P_{sb}}{P_{usb}} \leq 1.4 \qquad (10.36)$$

where

$$\frac{P_{tb}}{P_{utb}} \leq 1.0 \qquad (10.37)$$

and

$$\frac{P_{sb}}{P_{usb}} \leq 1.0 \qquad (10.38)$$

The bolt forces in the top chord connection are slightly smaller than those in the bottom chord, and a similar procedure to that adopted for the bottom chord connection may be used, with the shear capacity equal to the double shear capacity

of the bolt. In practice it would be convenient and preferable to use the same grade and diameter of bolt as that in the corresponding bottom chord connection.

It is advisable to pre-tension the bolts so as to eliminate the possibility of the joint opening at working loads. Successive applications of the torquing procedure are required in order to ensure that all bolts have reached the required level of torque.

Washer Plate Bending

A linear force distribution, consistent with the one adopted for web crippling has been shown to give conservative estimates of the required washer plate thickness. The thickness needed to resist the vertical force along the edge of the washer plate can be obtained from Equation 10.35. Again it would be desirable to have the same washer plates in the top chord connection as that in the corresponding bottom chord connection.

10.5 CONCLUSIONS

(1) Current design formulations given in BS 5950: Part 5 (1987) for web crippling and combined web crippling and bending are empirically based. A series of test were carried out to validate the code recommendations when applied to the sections being considered. If a linear distribution of stress is assumed to exist along the edges of the washer plate, then a patch load length equal to one third of the washer plate length used in conjunction with the code formulation is seen to give a reasonable estimate of the experimental failure loads. However, unacceptably large out-of-plane web deformations were observed during testing. The code formulation was therefore modified to prevent excessive web displacement. Good agreement between the modified equation and the test results has been obtained.

(2) The web crippling capacity of a section can be enhanced by introducing split sleeve inserts into the connection.

(3) Shearing of the table/web junction by the washer plate should be checked. The patch load length used in assessing the web crippling capacity should be used to determine the shear capacity of the table. The shear capacity of the connection can be enhanced by introducing split sleeve inserts.

(4) The bearing capacity calculated according to BS 5950: Part 5 (1987) is non conservative for small end distances similar to those encountered in the test frame. A series of end bearing tests showed that the bearing resistance decreases linearly to zero, as the end distance decreases to zero. The proposed design equations, Equations 10.19 and 10.20 are satisfactory.

(5) The reduction in bearing stress for thin plies required by the code is not necessary when the plies are confined, as in the test frame where the tabs are enclosed between the washer plates and the table of the bottom chord channel, or between the tables of intersecting channels.

(6) The efficiency of the tension diagonals could be improved if the tab strength were increased. This could be achieved increasing the thickness of the diagonals or by lengthening the tab.

(7) By using the same force distribution adopted for web crippling, it has been shown that the bolt forces given by vertical resolution of the diagonal forces are magnified by 25% for the washer plate and bolt centres used in the test frames. This increase in bolt tensile force has also been observed experimentally. The magnification effect is not prying in the usual sense since it is statically calculable. The increase in bolt tension must be taken into account when determining the bolt resistance.

(8) Having increased the bolt forces by calculation, the 25% increase in tensile force to account for prying recommended by BS 5950: Part 5 (1987) need not be included.

(9) The horizontal shear forces in the connection are resisted by dowel action of the bolts. Because of the many different levels through which the load must be transferred, it was shown that the bottom chord bolts are in quasi double shear; however, it would be prudent to assume single shear. The bolts in the top chord connection are in double shear. In practice the same grade and diameter of bolt should be used at both ends of a diagonal.

(10) Pre-tensioning the bolts will reduce the possibility of the joint opening at working loads which could reduce the bearing capacity of the tab due to loss of confinement and also increase the tensile force in the tab.

(11) Bending actions on the washer plates are extremely complex, because the forces depend on the flexural stiffness of the cross-section at the joint and also on the web crippling behaviour of the webs. In the test frame, one of the tabs enters between the washer plate and the table of the bottom chord channel, and in this case the bending moment on the plate is readily found. A conservative estimate of the required washer plate thickness can be obtained by assuming that yielding occurs along a line parallel to the loaded edge, passing through the centre of the bolt hole. It can be conservatively assumed that the washer plate moments are obtained in the same manner even when the tab enters between the chords, as in the top chord.

(12) Because the bolt and tabs are critical elements of the system a partial safety factor γ_m=1.1, on the yield stress is recommended.

(13) More tests are required to elucidate connection behaviour.

Chapter Eleven

GENERAL COMMENTS AND CONCLUSIONS

The initial purpose of this investigation was to produce design methods for a space frame system consisting of back to back cold-formed doubly lipped channel chords with tubular diagonals. Several points can be made regarding the manufacture, efficiency and design of this type of space frame.

(1) The system studied was designed to minimise production and construction costs. It is not surprising therefore that it is not structurally efficient.

(2) Production efficiency is achieved at the cost of considerable analytical complexity which becomes acceptable only by virtue of computer aided design which expedites analysis, detailing, scheduling and production control.

(3) The design methods which have been formulated, lend themselves to computerization, and enable the structure to be designed with reasonable economy. There is however scope for refinement of the design methods, for optimisation of the section dimensions, and for improvements in the connection design.

Interim design methods were initially developed on the basis of frame and component tests. Clarification and/or modification to the existing or proposed design methods was provided through numerical results obtained from a series of non-linear elasto-plastic analyses. Notwithstanding the exigencies of the development programme, the research has led to several new insights to improve methods of design/analysis of members and connections.

In this thesis the local and overall buckling behaviour of the doubly lipped channel subject to axial compression and/or uniform bending has been investigated experimentally and numerically. The design of the connection is also discussed. The investigations provide a basis for further advances in the design of thin-walled cold-formed members.

Local buckling: Effectiveness in compression can be estimated on the assumption that the web and table elements of the doubly lipped channel section are simply supported. In fact, the cross-section has a single critical stress, and various approximations may be made to estimate the strength of the section. The assumption permitted in BS 5950: Part 5 (1987), that the increased strength of the more slender side, resulting from restraint in the strength of the less slender sides, was not adopted.

Web crippling: The eccentricity moments cause vertical forces in the webs of the channels. The lever arm of the couple is based on an assumed linear distribution; the intensity and length of equivalent uniform forces are then found such that the lever arm and moment are unchanged. BS 5950: Part 5 (1987) treats web crippling but the equation was found to be non conservative compared to the experimental results obtained and a correction was therefore introduced. The load application in the tests on which the code method is based was not the same as in the test frame. The coexisting compression caused by axial force and bending is taken into account assuming linear interaction. Where the local strength of the channel at a connection is insufficient, split channel inserts are provided.

Lip buckling: When the lips of the section are subject to compression, they may buckle as struts on an elastic foundation. The buckling wavelength is determined by the deformational stiffness of the cross-section. The lip buckling resistance can be found from the Perry strut equation for an assumed imperfection over the buckling halfwave length. The lip buckling behaviour is found to be similar for lip compression caused by axial force or by bending. Modal interaction between local buckling and lip buckling does not occur, because the buckling wavelengths are sufficiently different. The reduction in the resistance to axial force and bending caused by lip buckling can be taken into account by reducing the design stress.

Torsional-flexural buckling: For singly symmetric sections, torsional flexural buckling can occur. Whereas for flexural buckling, compressive yielding occurs first at both lips, for torsional-flexural buckling yielding occurs first at one of two

diagonally opposite corners, while the stress at the other two corners is relatively small. This difference in behaviour is not recognised in current design codes, in which the design procedure implies that flexural buckling occurs but with an effective length which in increased on the basis of the square root of the ratio of the flexural and torsional-flexural buckling stresses. The governing equations for critical torsional-flexural buckling enable the relative values of the rotation and translation to be determined. These values can be used to determine assumed imperfections. Young's equation for buckling of an imperfect strut can then be applied to the translational and rotational imperfections to find the lateral translation of the shear centre and the rotation about the shear centre at any given load level. Curvatures and stresses around the section caused by rotations about the shear centre, and by translation of the shear centre can then be found and added to the axial stress for a given load. Non-linear elasto-plastic finite element studies confirm that the stress distribution and load to cause first surface yield are given with good accuracy by the above method.

Lateral-torsional buckling: According to BS 5950: part 5 (1987), lateral torsional buckling about the minor axis does not occur. This is correct for initially straight doubly symmetric beams. However, this thesis shows that singly symmetric sections subject to minor axis bending are in fact prone to lateral-torsional buckling. A similar approach to that adopted for torsional-flexural buckling can be applied to a beam having imperfections affine to the critical mode, to give the stresses caused by rotations about the shear centre and horizontal translation of the shear centre. The total stresses are then given by adding the these stresses to those caused by vertical bending. The deformations and stresses so determined agree closely with those given by non-linear finite element analysis.

Interaction between buckling modes: When the doubly lipped channel section is subjected to a combination of axial compression and moment, causing lip compression, there is a strong interaction between the two torsional buckling modes, because both modes have a wavelength equal to the span. The modes do differ somewhat in respect of the relative magnitudes of rotation and translation, and the critical stress for bending is much higher than for compression. For the doubly lipped channel section used in the tests frame, modal interaction with lip buckling is a minor effect, because the lip buckling wavelength is much less than the distance between lip buckling nodes. When the moment causes lip tension, there is no tendency for lateral-torsional buckling to occur, and the moment reduces the tendency for torsional buckling to develop. The interaction curve is then

bounded approximately by the torsional flexural buckling resistance and by the interaction curve for bending and flexural buckling. For smaller moments, the resistance varies little with moment.

Bearing stresses in connections: End bearing stresses according to BS 5950: Part 5 (1987) appeared to be non conservative for small end distances. This supposition was confirmed by tests on flat bars and on flattened tubes, and the design formula was adjusted accordingly. However, the reduction in bearing stress required by the code for thin plies was not applied, because the plies are confined by the washer plates in the connection.

Advantages and disadvantages of the system: The system is competitive in respect of cost, delivery time, aesthetic appeal, function, and corrosion protection. The connection is architecturally neat, but limits the choice of chord and diagonal sections. The tab end distance is limited by the width of the chord, and the tensile resistance of the tube is therefore reduced. The tube diameter is limited by the necessity of enclosing the greater part of the crease. The unsupported portion of the crease causes a reduction in the compressive resistance of the tube. The bending of the tab after flattening necessitates the use of very formable steel. The tab crease is rather vulnerable during assembly.

REFERENCES

AISI (1989) *"Specification for the* Design of Cold-Formed Steel Structural Members" *American Iron and Steel Institute. Washington, DC.*

ALLEN H.G. & BULSON P.S. (1980) "Background to Buckling" *McGraw Hill Book Co. Ltd, London*

ATTARD M.A. (1990) "General Non-Dimensional Equation for Lateral Buckling" *Thin-walled Structures*, Vol. 9, pp. 417-435

AYRTON W.E & PERRY J. (1886) "On Struts: *The Engineer* Vol **62** pp. 464-465

BAKER J.F., HORNE M.R. and **HEYMAN J. (1956)** "The Steel Skeleton" Vol.II. *Cambridge University Press*, Cambridge. pp. 228-248

BATES D.N. (1987) "The Mechanics of Thin-Walled Structures with Special Reference to Finite Rotations" *Ph.D. Thesis Presented to the University of London*, Imperial College London.

BLEICH F. (1952) "Buckling Strength of Metal Structures" *McGraw-Hill, New York*

BRUSH D.O. and **ALMROTH B.O. (1975)** " Buckling of Bars, Plates and Shells" *McGraw-Hill*, New York

BRYAN E.R. and **ZADANFARROKH F. (1992)** " Testing and Design of Bolted Connections in Cold-formed Steel Sections" *Eleventh International Specialty Conference on Cold-Formed Steel Structures*, St. Louis, Missouri, U.S.A. pp. 625-661

BRYAN G.H. (1891) "On the Stability of a Plane Plate under Thrust in its own plane, with application to the Buckling of the sides of a ship" *Proc.Lond. Math. Soc.*, Vol **22**

BS 18 (1987) "Tensile Testing of Metals" *British standards institute.* London

BS 449 Addendum No.1 (1975) "Specification for the Use of Cold-Formed Steel Sections in Building" *British Standards Institution, London*

BS 5950: Part 1 (1990) "Code of Practice for Design in Simple and Continuous Construction: hot rolled sections" *British Standards Institution, London*

BS 5950: Part 5 (1987) "Code of Practice for the Design of Cold-Formed Sections" *British Standards Institution, London*

BULSON P.S. (1970) "*The Stability of Flat Plates*" Chatto & Windus. London

CESLIC Report CFS1 (1991) "Bearing Resistance of Connected Elements" Civil Engineering Department. Imperial College.

CHAJES A. & WINTER G. (1965) "Torsional-Flexural Buckling of Thin-Walled Members" *ASCE J.Structural Division* Vol **91** pp. 103-24

CHILVER A.H. (1951) "Behaviour of Thin-Walled Structural Members in Compression" *Engineering 31st August 1951* Vol **172** pp. 281-282

CHONG K.P. and **MATLOCK R.B. (1975)** "Light-Gage Steel Bolted Connections without Washers" *ASCE J.Structural Division* **Vol.101**, ST7, pp. 1381-1391

CODD B.E. (1991) "Conder Introduces Harley Space Frame to Europe" *Steel construction today*. Steel construction Institute. London.

DAVIDSON J.F. (1952) "The Elastic Stability of Bent I-Section Beams" *Proceedings of the Royal Society* ,Vol **212**. pp. 80-95

DAVIDSON P.C. (1989) "Design of Plate Panels under Biaxial Compression, Shear and Lateral Pressure" *Ph.D. Thesis Presented to the University of London*, Imperial College London.

DAVIES J. (1991) " Connections for Cold-Formed Steelwork" *Design of Cold-Formed Steel Members* .(Ed) Rhodes J Elsevier Applied Science, Essex. UK. pp. 265-292

DESMOND, T. P, PEKOZ, T. and WINTER, G. (1981), "Edge Stiffeners for Thin-Walled Members" *Journal of the Structural Division*, ASCE Vol. **107**, No. ST2. pp. 329-353

DHALLA A.K, SAMUEL J.E. and **WINTER G. (1971)** "Connections in Thin Low-Ductility Steels" *ASCE J.Structural Division* Vol.**97**, ST10, pp. 2549-2566

DOUTY R.T. (1962), "A Design Approach to the Strength of Laterally Unbraced Compression Flanges" *Bulletin No. 37*, Cornell University

DWIGHT J.B. (1972) "Use of Perry Formula to Represent the New European Strut-Curves" *Report CUED/C-Struct/TR.30, Department of Engineering, University of Cambridge.*

EC3: Part 1.3 (1992) "Design of Steel Structures-Cold Formed Thin Gauge Members and Sheeting " *Draft version* (April 1992)

ENV 1993-1 (1992) "Eurocode 3: Design of steel structures. Part 1.1 General rules and rules for buildings" *British standards institute.* London.

EULER L. (1759) "Sur la force des colonnes" *Memoires de l'Academie de Berlin,* Berlin.

FAULKNER D. (1975) "A Review of Effective Plating for use in the Analysis of Stiffened Plating in Bending and Compression" *Journal of Ship Research,* Vol **19.** pp. 1-7

FINASIC (1990), "User Manual", *Department of Civil Engineering, Imperial College,* London

GALAMBOS T.V. (1968) "Structural Members and Frames" *Prentice-Hall, International. U.K.*

GILCHRIST R.T. and **CHONG K.P. (1979)** "Thin Light-Gage Bolted Connections without Washer" *ASCE J.Structural Division* Vol.**105**, ST1, pp. 175-183

GODFREY B. (1962) "The Allowable Stresses in Axially-Loaded Steel Struts" *The Structural Engineer. Vol 40 No. 3. Institution of Structural Engineers. London.* pp. 97-112

HANCOCK G.J. (1985), "Distortional Buckling of Steel Storage Rack Columns" *Journal of the Structural Division,* ASCE Vol. **111,** No. ST12. pp. 2770-2783

HARVEY J.M. (1953) "Structural Strength of Thin-Walled Channel Sections" *Engineering* Vol **175** pp. 291-292

HAUSSLER R.W. (1964), "Strength of Elastically Stabilised Beams" *Journal of the Structural Division,* ASCE Vol. **90,** (ST3) pp. 219-264

HETRAKUL N. and **YU W.W. (1980)** "Cold-Formed Steel I-beams Subjected to Combined Bending and Web Crippling" *Thin-Walled Structures, International Conference at the University of Strathclyde,* Glasgow, (Eds.) Rhodes J and Walker A.C.

KHAN M.Z. and **WALKER A.C. (1972)** "Buckling of Plates Subjected to Localised Edge Loading", *The Structural Engineer*, Vol.**50**, No 6. pp. 225-232

KHAN M.Z, JOHNS K.C. and **HAYMAN B. (1977)** "Buckling of Plates With Partially Loaded Edges", *ASCE J.Structural Division* Vol.**103**, ST3, pp. 547-558

LA BOUBE R.A. (1986) "Literature Survey of Cold-Formed Sections" *Proc. Eighth International Specialty Conference on Cold-Formed Steel Structures.* St.Louis Missouri. U.S.A.

LAU, S.C.W. and HANCOCK, G.J., (1987), "Distortional Buckling Formulas for Channel Columns" *Journal of the Structural Division,* ASCE Vol. **113,** No. ST5. pp. 1063-1078

LAU, S.C.W. and HANCOCK, G.J., (1988), " Distortional Buckling Tests of Cold-Formed Channel Sections" *Proc. Ninth International Specialty Conference on Cold-Formed Steel Structures.* St. Louis, Missouri, U.S.A.

LOUGHLAN J. (1983) "The Ultimate Load Sensitivity of Lipped Channel Columns to Column Axis Imperfection" *Thin-Walled Structures* **Vol 1** No 1 Applied science Publishers England.

LOUGHLAN J. and **RHODES J. (1979)** "The Interactive Buckling of Lipped Channel Columns Under Concentric and Eccentric Loading" *Thin-Walled Structures* Eds. J. Rhodes and A.C.Walker Granada Publishing

LUSAS (1992) "User Manual" *Finite Element Analysis Ltd, London*

MURRAY N.W. & **ATTARD M.M. (1987)** "A Direct Method of Evaluating the Warping Properties of Thin-Walled Spans and Closed Profiles" *Thin-walled Structures,* (5) pp. 351-64

NETHERCOT D.A. and **ROCKEY K.C. (1971)** " A Unified Approach to The Elastic Lateral Buckling of Beams" *The Structural Engineer,* **Vol. 49**, No.7, July 1971, pp. 321-330

NETHERCOT D.A. and **ROCKEY K.C. (1973)** "Lateral Buckling of Beams With Mixed End Conditions" *The Structural Engineer,* **Vol.51** , No.4

NETHERCOT D.A. and **TRAHAIR N.S. (1976)** "Lateral Buckling Approximations for Elastic Beams" *The Structural Engineer,* **Vol.54** , No.6 pp. 197-204

NETHERCOT D.A. and **TRAHAIR N.S. (1983)** " Design of Laterally Unsupported Beams. " In Developments in the Stability of Structures, Ed. R.Narayanan. *Applied Science Publishers*, London, pp. 71-93

PEKOZ T. and CELEBI N. (1969) "Torsional-Flexural Buckling of Thin-Walled Sections Under Eccentric Load" *Engineering research bulletin* 69-1. Cornell University.

PEKOZ T.B. and **WINTER G. (1969)** "Torsional-Flexural Buckling of Thin-Walled Sections under Eccentric Load" *ASCE J.Structural Division* **95** pp. 941-963

RHODES J. (1982) "Effective Widths in Plate Buckling" *In Developments in Thin-Walled Structures-1. Applied Science Publishers*, London

RHODES J. (1984) "Some Thoughts on Future Cold-Formed Steel Design Rules" *Behaviour of thin-walled structures* Rhodes J and Spence J (Eds). Elsevier Applied Science Publishers, London. pp. 125-142

RHODES J. (1987) "Secondary Local Buckling in Thin Walled Sections" *Acta Technica Academiae Scientarum, Hungaricae* ***87 (1-2)*** pp. 143-153

RHODES J. (1991) "Design of Cold-Formed Steel Members" *Elsevier Science Publisher, Essex*, UK.

RHODES J. and **SEAH L.K. (1992)** "Buckling of Edge-Stiffened Thin-Walled Beam Sections" , Proc. Institution of Civil Engineers, Structures & Buildings. pp. 323-334

ROBERTS T.M. (1985) "Section Properties of Thin-Walled Bars of Open Cross-Section." *Structural Engineer*, **63B** (3) pp. 63-67

ROCKY K.C, EL-GAALY M.A. and **BAGCHI D.K. (1972)** "Failure of Thin-Walled Members under Patch Loading" *ASCE J.Structural Division* **Vol.98**, ST12, pp. 2739-2752

SANTAPUTRA C, PARKS M.B. and **YU W.W. (1986)** "Web Crippling Strength of High Strength Steel Beams" *Eight International Specialty Conference on Cold-Formed Steel Structures*, St. Louis, Missouri, U.S.A. pp. 111-140

SANTAPUTRA C, PARKS M.B. and **YU W.W. (1988)** "Web Crippling Strength of Cold-Formed Steel Beams", *ASCE J.Structural Division* **Vol.115**, ST10, pp. 2511-2526

SEAH L.K. and **KHONG P.W. (1990)** " Lateral-Torsional Buckling of Channel Beams" *J.Constructional Steel Research*, Vol 17, pp. 265-282

SEAH L.K. and RHODES, J., (1990) "Behaviour of Channel Beams with Unbraced Compression Flanges" *Tenth International Specialty Conference on Cold-Formed Steel Structures*. St. Louis, Missouri, U.S.A.

SEAH L.K., RHODES J. and LIM B.S., (1991), "Collapse of Edge Stiffened Thin-Walled Sections" *International Conference on Steel and Aluminium Structures ICSAS*, Singapore. pp. 433-242

SERRETTE R. and PEKOZ T. (1992) "Local and Distortional Buckling of Thin-Walled Beams" *Proc. Eleventh International Specialty Conference on Cold-Formed Steel Structures*. St.Louis Missouri. U.S.A. pp. 63-73

SERRETTE R. and PEKOZ T., (1991), "Strength of Laterally Unsupported Compression Flanges and Panels" *Fourth International Colloquium on Structural Stability*, Istanbul. pp. 232-242

TIMOSHENKO S.P. and **GERE J.M. (1961)** "Theory of Elastic Stability, 2nd Ed." *McGraw Hill*, London.

TRAHAIR N.S. and **BRADFORD M.A. (1988)** "The Behaviour and Design of Steel Structures" *Chapman and Hall*, London

TRAHAIR N.S. and **WOOLCOCK S.T. (1973)** "The Effect of Major Axis Curvature on I-Beam Stability", *ASCE J.Engineering Mechanics*, **1**, pp. 85-98

TREUB U. (1983) "Stability Problems of Elasto-Plastic Frames and Shells by Finite Elements" *Ph.D. Thesis Presented to the University of London*, Imperial College London.

TSUI F. (1993) *Ph.D. Thesis yet to be submitted to the University of London*, Imperial College London.

VACHARAJITTIPHAN P, WOOLCOCK S.T. and **TRAHAIR N.S. (1974)** " Effect of In-plane Deformations on Lateral Buckling", *Journal of Structural Mechanics*, **3**, pp. 29-60

Van DEN BROEK, J. A. (1947) "Euler's classic paper 'On the strength of columns,' " *American Journal Physics*, pp. 309-318

Von KARMAN, SECHELER E.E. and DONELL L.H. (1932) "The strength of thin plates in compression. *ASME Transactions* Vol 54 No.2

WALKER A.C. (1969) "The Post-Buckling Behaviour of Simply-Supported Square Plates *Aero Quarterly* Vol **XX** pp. 203-219

WINTER G. (1946) "Strength of Thin-Steel Compression Flanges" *ASCE Transactions.* Vol 112, pp. 527-554

WINTER G. (1956) "Tests on Bolted Connections in Light Gage steel" *ASCE J.Structural Division* **Vol.82**, ST2, paper 920/pp. 1-25

WINTER G. and **PIAN R.H.J. (1946)** "Crushing Strength of Thin Steel Webs" Bulletin No.35, Part1, *Cornell University Engineering Experiment Station.*

YOUNG B.W. (1971) "Axially Loaded Steel Columns" *C.I.R.I.A. Technical Note 33,* London

YOUNG, T. (1807) " A Course of Lectures on Natural Philosophy and Mechanical Arts" *Royal Institution of Great Britain, London* **Vol.I** on Passive strength and friction, **Vol.II** ix, Theorems pp. 320-324.

YU W.W. (1991) " Cold-Formed Steel Design" 2nd Ed. *John Wiley and Sons, Chichester.* UK.

ZADANFARROKH F. and **BRYAN E.R. (1989)** "Bearing Strength of Bolted Connections in Cold-Formed Steel" *Department of Civil Engineering Report,* University of Salford. UK

ZETLIN L. (1955) "Elastic Instability of Flat Plates Subjected to Partial Edge Loads", *ASCE J.Engineering Mechanics,* **Vol.81**, paper 795/pp. 1-24

Appendix A

DESCRIPTION OF THE FINITE ELEMENT PROGRAM FINASIC, THE ELEMENTS USED AND THE INITIAL CONVERGENCE STUDY

FINASIC (1990)

The program FINAS developed by Trueb (1983) at Imperial College has been recently modified by Tsui (1993) to run under the UNIX operating system and is currently designated FINASIC. It is a general purpose non-linear (material and geometric) finite element program particularly suited to structural stability problems. The program is linked to a number of element modules all of the isoparametric type. Each of the element modules can be linked to a variety of material laws. These include linear elastic, single- or multi-layer elasto-plastic and also user defined material behaviour. The treatment of plasticity is based on the von Mises yield criterion and associated Prandtl-Reuss flow rule with linear isotropic hardening.

Several solution strategies based on the Newton-Raphson technique are available for dealing with geometric and materially non-linear structural behaviour. The various strategies differ in the stage at which the stiffness matrix is reformed. They include; the initial stiffness method where the initial stiffness matrix is used for all load increments, the modified Newton-Raphson method where the structure stiffness matrix is reformed at the beginning of each load increment, the full Newton-Raphson method where the stiffness matrix is updated at the beginning of each iteration at each iteration cycle. No single solution strategy is suitable for the whole non-linear solution path. The user specifies the initial solution strategy, and FINASIC adjust the strategy automatically during the solution if convergence problems are encountered.

Load can be applied to a structure by means of force vectors or by imposing nodal displacements. The later of these approaches is require if the unloading paths are

to be obtained. The size of each load increment is dynamically controlled with in the program.

The simplest method for crossing limit points which is available in FINASIC and one used in all the analyses presented in this thesis, consists of controlling the change of a displacement component within the member. In some problems it is difficult to select the most suitable node and degree of freedom on the member to control the incrementation procedure. For this reason FINASIC provide an algorithm which enables the program to automatically control the most rapidly growing displacement component at each load increment.

Shell Element

A shell element developed by Bates (1987) was used to model the channels sections for all the analyses presented in this thesis. The shell element is a doubly-curved eight noded isoparametric shell element with six degrees of freedom per node. The element formulation is based on the Mindlin shell theory where the transverse direct stress is neglected and the transverse shear stress is assumed to be constant through the shell thickness. Since the shear rigidity of a plate is proportional to its thickness while its flexural rigidity is proportional to the cube of the thickness, the global stiffness matrix may become ill-conditioned for very thin plates and shells. This problem of numerical instability, known as 'shear locking' has been eliminated by Bates (1987) by resorting to reduced integration schemes.

The element includes large displacement and rotation effects by coupling of membrane and bending terms. Bates (1987) has also included an appropriate penalty function in order to avoid spurious zero-energy modes which may arise in continuous shells with six degrees of freedom per node.

Finite Element Modelling

Throughout this thesis a number of buckling phenomena were examined with the aid of FINASIC (1990). The accuracy of the solutions obtained depends largely on the adequacy of the mesh to model the buckling phenomenon being considered. Local element buckling described in Chapter Four has the shortest wavelength of all the buckling modes considered. A mesh convergence study on the critical plate

buckling parameter K was carried out to determine the number of elements needed to adequately model the critical buckling load for plates of varying aspect ratio. The number of elements across the width and along the length of a plate a/b = 1 were systematically varied. The ratio of the critical buckling factors K_F obtained from the buckling analyses to the buckling factor K for a square plate given by

$$K = \frac{\sigma_{cr}\, 12\,(1-\nu^2)}{\pi^2\, E \left(\frac{t}{b}\right)^2} \qquad \text{(A.1)}$$

are shown in Figure A.1. The critical buckling ratio K' is expressed as

$$K' = \frac{K_F}{K} \qquad \text{(A.2)}$$

The results in Figure A.1 are confirmed by a similar study conducted by Davidson (1989) (Figure A.1).

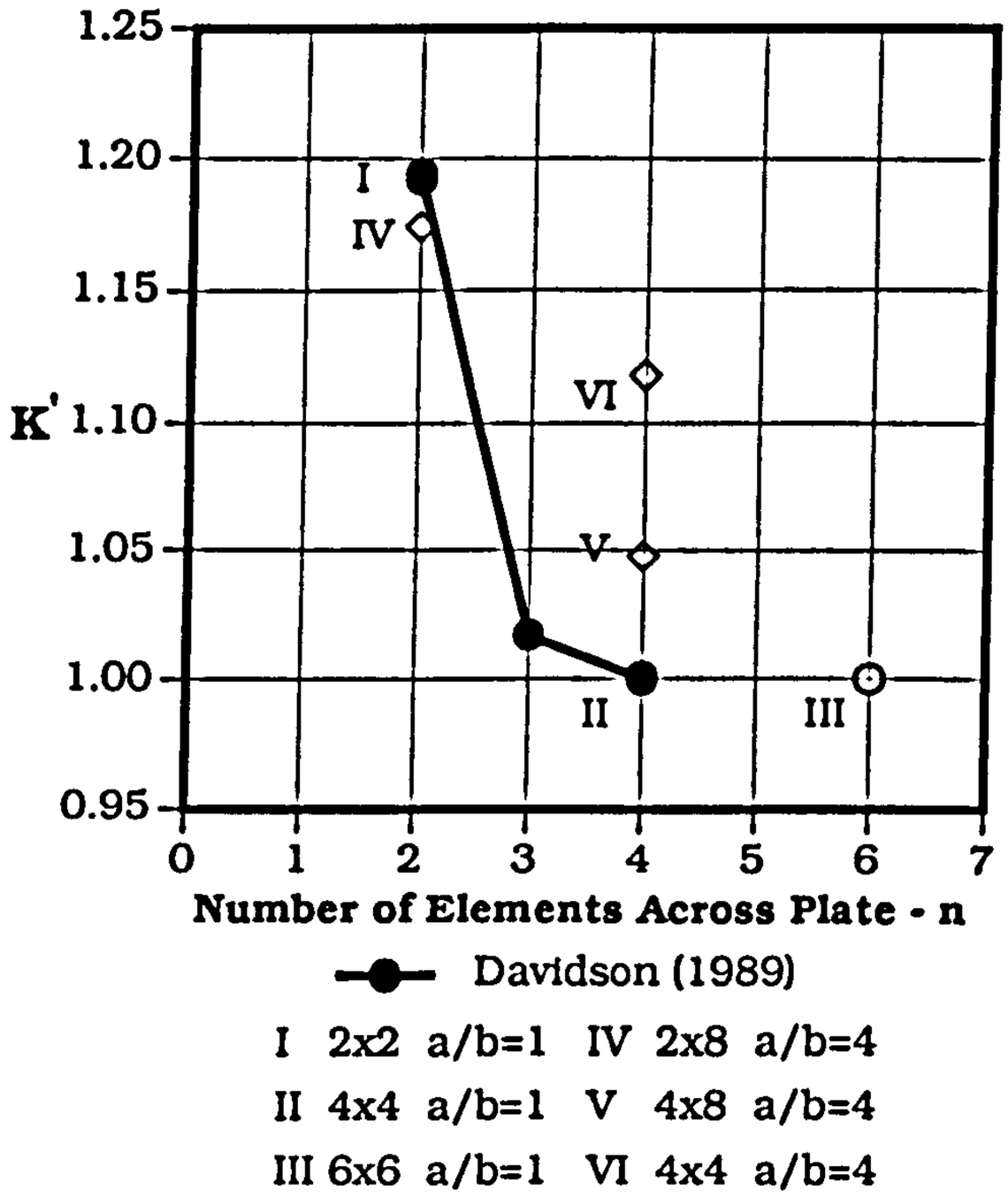


Figure A.1 Plate convergence study

It can be seen that a 4x4 mesh is sufficiently converged for the square plate. A similar investigation was carried out on a plate with an aspect ratio of a/b = 4.

where the number of elements along the length were varied. In Figure A.1 it is observed that the error in the critical buckling ratio K_F/K for a plate a/b = 4 with a 4x8 mesh is about 5%, this increases to 12 % for similar plate with a 4x4 mesh.

From the plate convergence study it is apparent that if the table and webs of the channel are susceptible to local element buckling, then a mesh having the same proportions as that used in the 4x4 critical buckling analysis for the square plate (a/b=1) would be needed to adequately describe the local buckling behaviour of the section. When the predominant mode of buckling involves overall deformation of the member without local buckling, then a mesh similar to that used in the plate a/b = 4, with a 4x1 mesh should be adequate. In most cases separate convergence studies were carried out for the various overall buckling mode being considered in order to determine the minimum number of element needed to adequately describe the buckling phenomenon. The results can be found in the relevant Chapters.

In all cases the doubly lipped channel section was modelled using one element in the lip downturn, one in the lip table, four in each web element and four in the table. It is recommended (Bates 1987) that the length to width ratio of the shell element should not exceed a factor of ten. The minimum number of elements used along the length of the member was predetermined by the limitation in aspect ratio and the lip table dimension.

The non-linear elasto-plastic analyses described in this thesis were carried out using a 2x2 Gaussian integration scheme with the stresses and stress resultants evaluated at seven stations through the thickness of the shell.

Appendix B

THE DIFFERENTIAL EQUATIONS OF STATIC EQUILIBRIUM

The differential equations of static equilibrium for a thin-walled open cross section subject to axial load and end moments can be found in many standard texts dealing with the buckling of bars (Timoshenko and Gere 1963, Galambos 1968). Consider the irregular section shown in Figure B.1a subjected to end moments M_y and M_z and an axial load P. If it is assumed that the effects of the axial load P on the bending stresses are negligible, then the longitudinal stress at any point in the channel is independent of the length and is given by the equation

$$\sigma = -\frac{P}{A} - \frac{M_y z}{I_y} - \frac{M_z y}{I_z} \qquad (B.1)$$

where

A	cross-sectional area
P	the applied axial load
Iy, Iz	second moment of area about y and z axes
My, Mz	applied moments about y and z axes
z, y	co-ordinates of point being considered

Assuming that the initial deflections of the channel due to moments M_y and M_z are small, then they can be neglected. During buckling the cross-section will undergo translation and rotation. The translations are defined by the deflections v and w in the y and z directions respectively, of the shear centre denoted as **SC** in Figure B.1b.

During translation of the cross-section, point **SC** moves to **SC'** and point **CG**, the centroid of the section, moves to **CG'**. Rotation of the cross-section about the shear

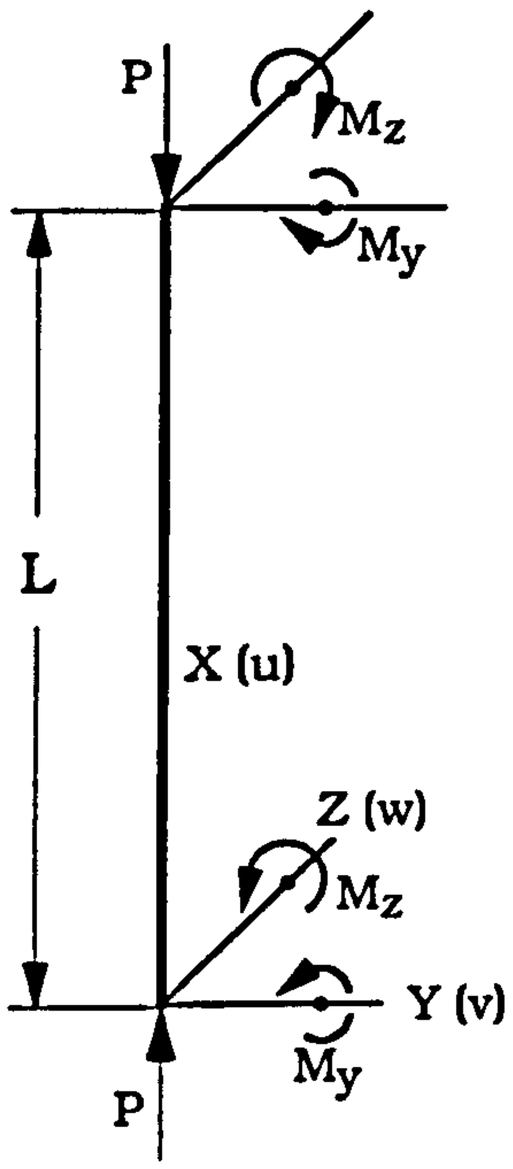


Figure B.1(a)

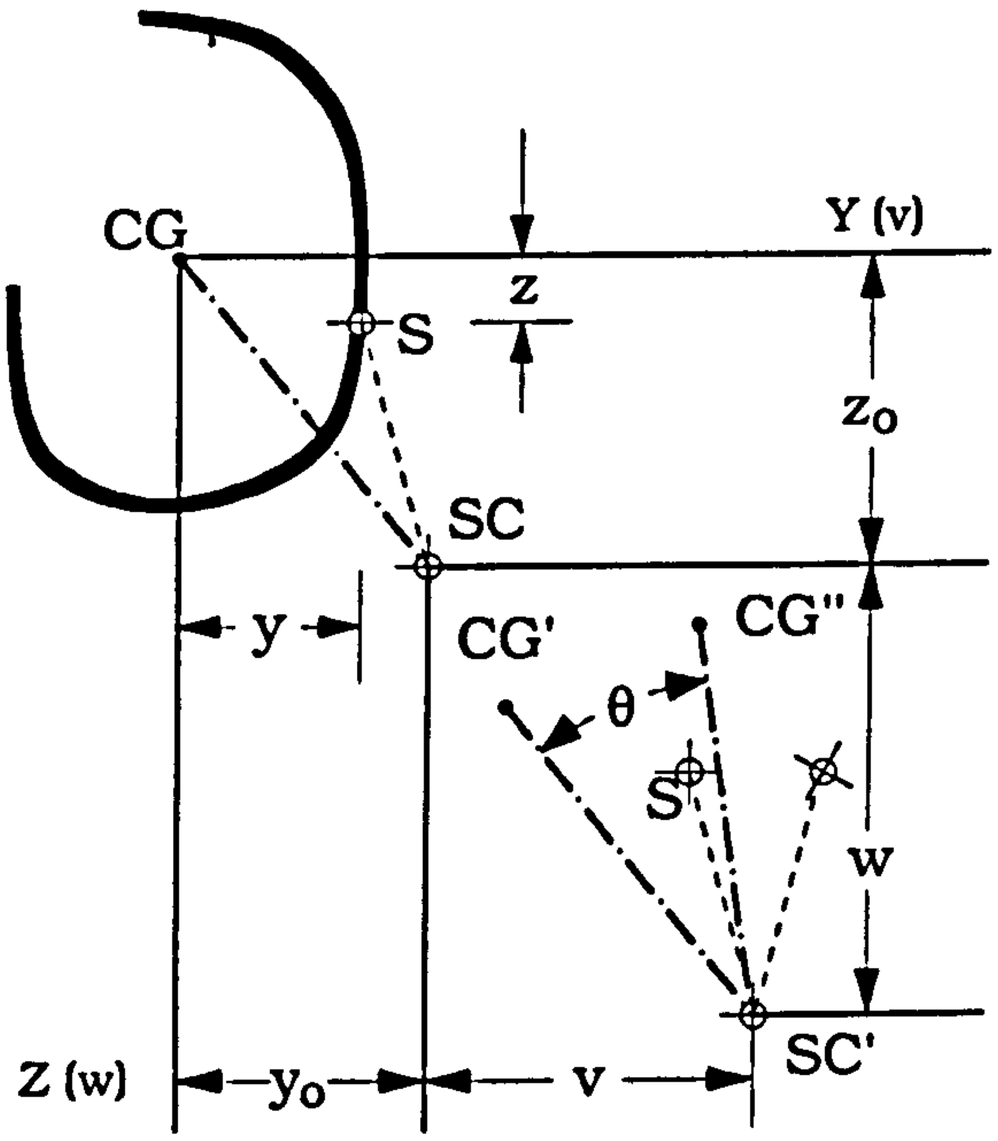


Figure B.1 (b)

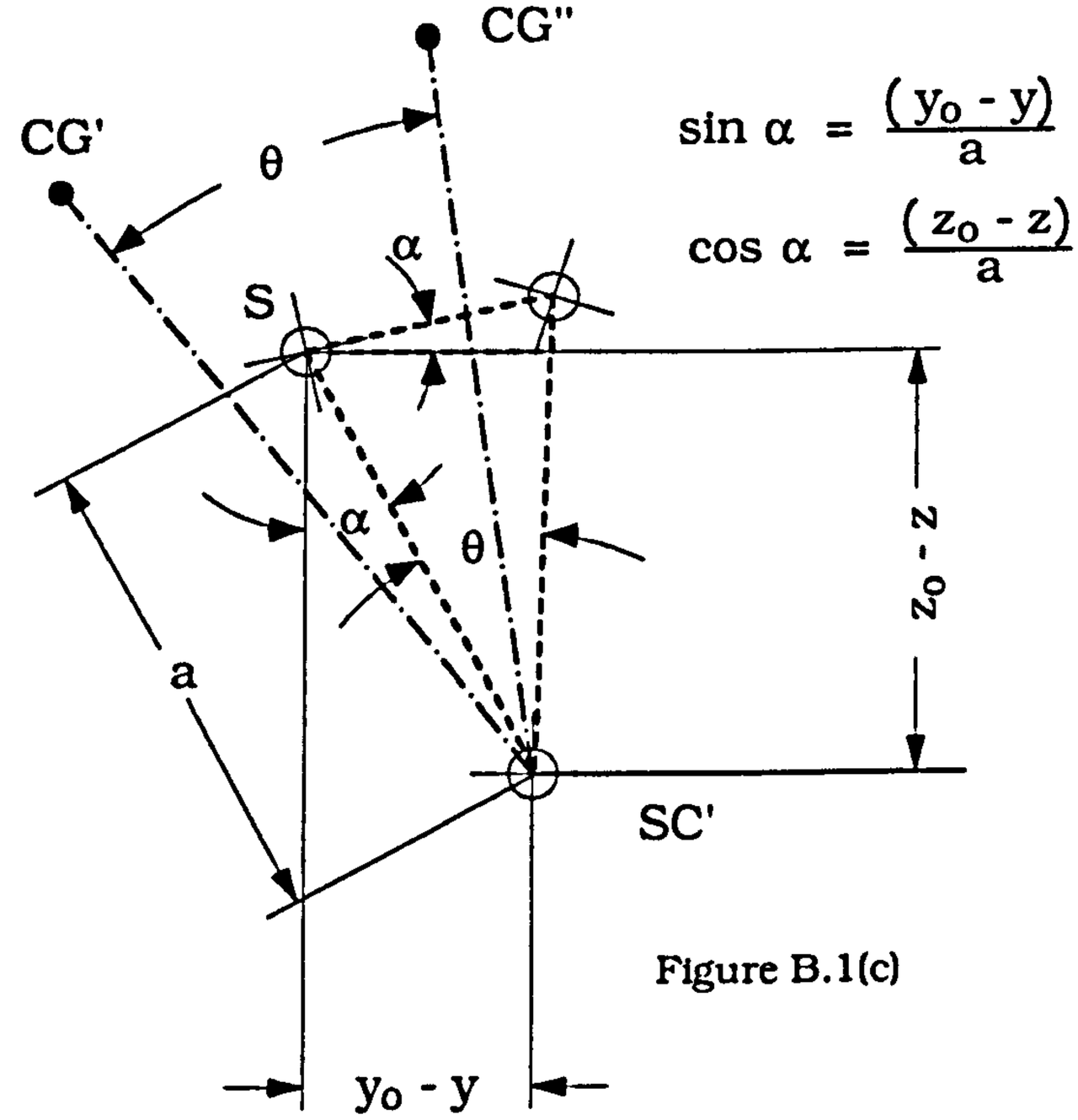


Figure B.1(c)

Figure B.1 End forces and displacements in cross section

centre by an angle θ puts the final position of the centroid at **CG"**. If the angle θ is assumed to be small, then the deflections of the centroid **CG** during buckling are

$$v + z_o \theta \tag{B.2a}$$

$$w - y_o \theta \tag{B.2b}$$

The equation for the angle of twist θ can be found by considering a longitudinal strip of the cross-section tds, at point S on the section (Figure B.1). The displacements of point S in the y and z directions are

$$v + a \theta \sin \alpha \tag{B.3a}$$

$$w + a \theta \cos \alpha \tag{B.3b}$$

where a is the distance between the shear centre and any point on the cross-section.

From Figure B.1c

$$\sin \alpha = \frac{(z_o - z)}{a} \tag{B.4a}$$

$$\cos \alpha = \frac{(y_o - y)}{a} \tag{B.4b}$$

Substituting Equations B.4 into B.3 and taking the second derivatives of Equation B.3 with respect to u over an element length du, the compressive forces σtds acting on the slightly rotated ends of the element give forces in the Y and Z directions of intensity

$$dq_y = -(\sigma t ds)\frac{d^2}{du^2}(v + (z_o - z)\theta) \tag{B.5a}$$

$$dq_z = -(\sigma t ds)\frac{d^2}{du^2}(w + (y_o - y)\theta) \tag{B.5b}$$

Taking moments about the shear centre of the forces given in Equation B.5, the torque per unit length of the section is

$$dm_z = -(\sigma t\, ds)(z_o - z)\left[\frac{d^2 v}{du^2} + (z_o - z)\frac{d^2\theta}{du^2}\right] + (\sigma t\, ds)(y_o - y)\left[\frac{d^2 w}{du^2} + (y_o - y)\frac{d^2\theta}{du^2}\right] \quad \text{(B.6)}$$

Integrating Equations B.5 and B.6 over the whole cross-section

$$q_y = EI_z\frac{d^4 v}{du^4} = -\int_A \sigma t\, ds\, \frac{d^2}{du^2}(v + (z_o - z)\theta) \quad \text{(B.7a)}$$

$$q_z = EI_y\frac{d^4 w}{du^4} = -\int_A \sigma t\, ds\, \frac{d^2}{du^2}(w + (y_o - y)\theta) \quad \text{(B.7b)}$$

$$m_z = E C_w\frac{d^4\theta}{du^4} = -\int_A (\sigma t\, ds)(z_o - z)\left[\frac{d^2 v}{du^2} + (z_o - z)\frac{d^2\theta}{du^2}\right] + \int_A (\sigma t\, ds)(y_o - y)\left[\frac{d^2 w}{du^2} + (y_o - y)\frac{d^2\theta}{du^2}\right] \quad \text{(B.7c)}$$

Substituting Equation B.1 into Equations B.7 and remembering that

$$\sigma\int_A t\, ds = P \qquad \int_A y\, t\, ds = \int_A z\, t\, ds = 0$$

$$\int_A y^2\, t\, ds = I_z \qquad \int_A z^2\, t\, ds = I_y$$

$$I_o = I_y + I_z + A(y_o^2 + z_o^2)$$

The three differential equations for bending and torsion of a thin-walled cross section subject to axial load and moment can be expressed as

$$EI_z\frac{d^4 v}{du^4} + P\frac{d^2 v}{du^2} + (Pz_o - M_y)\frac{d^2\theta}{du^2} = 0 \quad \text{(B.8)}$$

$$EI_y\frac{d^4 w}{du^4} + P\frac{d^2 w}{du^2} - (Py_o - M_z)\frac{d^2\theta}{du^2} = 0 \quad \text{(B.9)}$$

$$EC_w\frac{d^4\theta}{du^4} - \left(GJ - M_y\beta_y - M_z\beta_z - P\frac{I_o}{A}\right)\frac{d^2\theta}{du^2} + (Pz_o - M_y)\frac{d^2v}{du^2} - (Py_o - M_z)\frac{d^2w}{du^2} = 0 \qquad \text{(B.10)}$$

where the geometric parameters β are

$$\beta_y = \frac{1}{I_y}\left(\int_A z^3\,dA + \int_A y^2\,z\,dA\right) - 2z_o$$

$$\beta_z = \frac{1}{I_z}\left(\int_A y^3\,dA + \int_A z^2\,y\,dA\right) - 2y_o$$

The value β for a number of singly symmetric sections may be obtained from equations given by Yu (1991), based on earlier work carried out by Pekoz and Celebi (1969). It is worth mentioning that β about an axis of symmetry is equal to zero.

Appendix C

END BEARING TEST RESULTS

The test results shown in Figures 10.14 and 10.15 were obtained from seventy-six end bearing tests and four frame test. Figure C.1 depicts the observed failure modes, while Tables C.1 to C.6 give the test results.

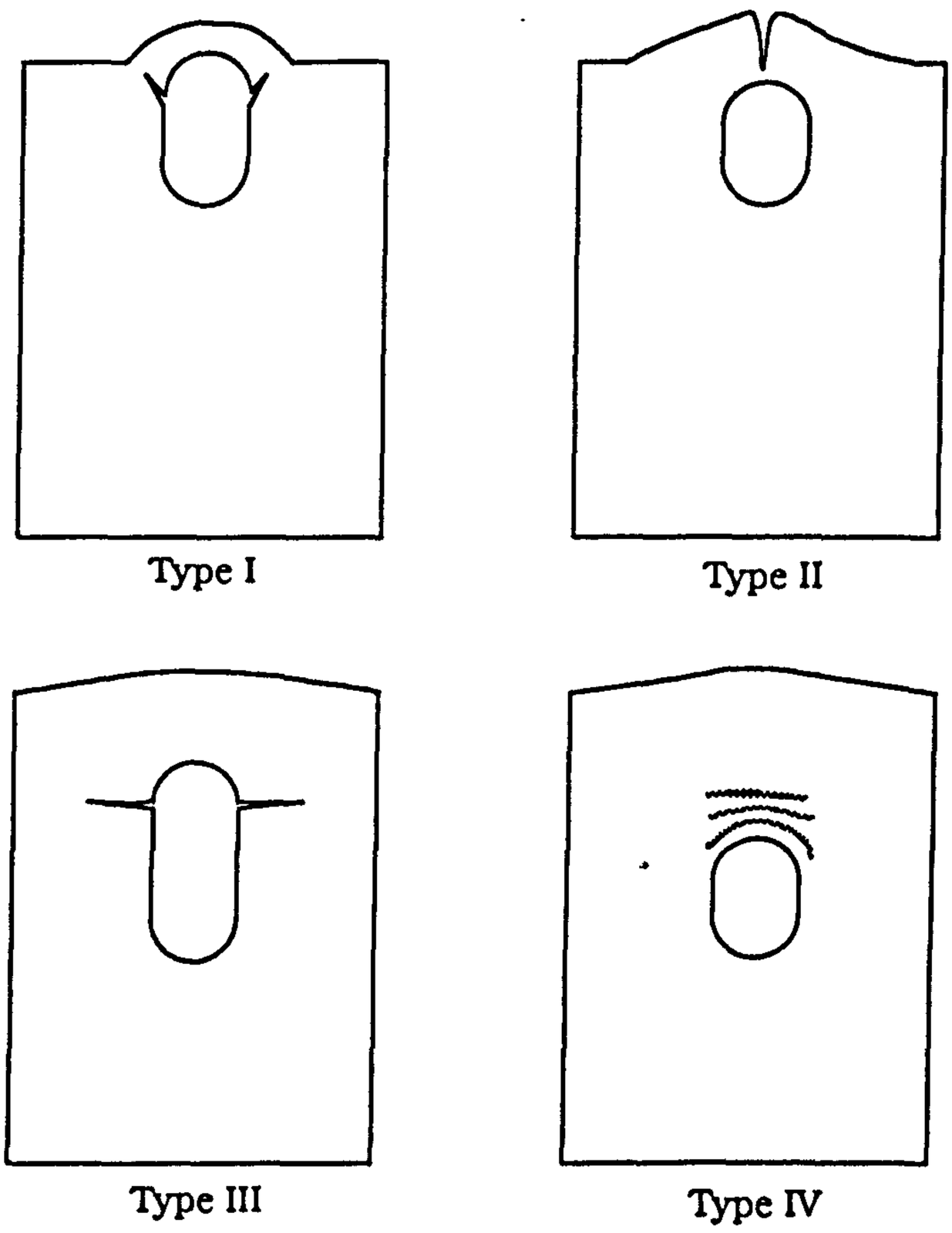


Figure C.1 Tab end failure modes

DESCRIPTION	d_h (mm)	d_e (mm)	$\frac{d_e}{d}$	s (mm)	P (kN)	$\frac{P}{d\,t\,\sigma_o}$	$\frac{P}{\text{Eqn. 10.20}}$	$\frac{P}{\text{Eqn. 10.17}}$	FAILURE MODE	COMMENTS
3mm/M16	16.8	24.4	1.5	99	**30.4**	2.3	1.5	1.1	I	
	16.8	33.2	2.1	100	**40.5**	3.0	1.5	1.2	II	
	17.0	48.0	3.0	100	**57.3**	4.3	1.4	1.4	II + IV	
	17.0	80.2	5.0	99	**85.3**	6.4	2.1	2.1	I + IV	
3mm/M20	21.0	30.5	1.5	100	**37.9**	2.3	1.5	1.1	II	
	21.0	39.0	2.0	100	**47.4**	2.8	1.5	1.2	II	
	21.0	60.8	3.0	100	**70.0**	4.2	1.4	1.4	II + IV	
	21.0	99.5	5.0	100	**87.4**	5.2	1.7	1.7	III +IV	
2mm/M16	17.0	24.5	1.53	101	**25.4**	2.2	1.4	1.0	I	
	17.0	32.5	2.03	101	**33.9**	2.9	1.4	1.2	II	
	17.00	48.90	3.06	101	**47.4**	4.1	1.4	1.4	III + IV	
	17.00	79.70	4.98	101	**67.3**	5.8	1.9	1.9	IV	
2mm/M20	21.70	29.85	1.49	101	**28.9**	2.0	1.3	1.0	N.A	
	21.00	38.80	1.94	99	**39.9**	2.7	1.4	1.2	II	
	21.00	59.10	2.96	100	**54.4**	3.7	1.3	1.3	IV	
	21.00	98.50	4.93	100	**71.3**	4.9	1.6	1.6	IV	
1mm/M16	17.20	20.10	1.26	100	**8.5**	1.7	1.5	0.9	II	
	17.20	31.60	1.98	100	**14.0**	2.8	1.5	1.2	II	
	17.00	48.10	3.01	100	**15.2**	3.1	1.1	1.0	IV	
	17.00	78.50	4.91	99	**18.0**	3.6	1.3	1.2	IV	

Table C.1 Tab bearing test results, specimen dimensions for square ended sheet metal specimens

DESCRIPTION	d_h (mm)	d_e (mm)	$\frac{d_e}{d}$	s (mm)	P (kN)	$\frac{P}{d\,t\,\sigma_o}$	$\frac{P}{\text{Eqn. 10.20}}$	$\frac{P}{\text{Eqn. 10.17}}$	FAILURE MODE	COMMENTS
2 x 2mm/M16	17.0	9.3	0.58	73.0	**9.07**	0.3	0.7	0.2	II	(a)
	17.0	9.3	0.58	73.0	**9.07**	0.3	0.7	0.2	II	(a)
	17.0	9.3	0.58	72.8	**9.17**	0.3	0.7	0.2	II	(a)
	17.0	11.8	0.74	73.0	**19.44**	0.7	1.2	0.5	II	(a)
	17.0	12.0	0.74	73.0	**19.94**	0.7	1.2	0.5	II	(a)
	17.0	12.0	0.75	73.0	**19.44**	0.7	1.2	0.5	II	(a)
	17.0	15.9	0.99	73.0	**28.02**	1.0	1.3	0.7	I	(a)
	17.0	15.9	0.99	73.0	**29.41**	1.1	1.3	0.7	I	(a)
	17.0	16.0	1.00	73.0	**28.81**	1.0	1.3	0.7	I	(a)
	17.0	19.8	1.24	73.0	**36.29**	1.3	1.3	0.8	I	(a)
	17.0	19.8	1.24	73.0	**36.49**	1.3	1.3	0.8	I	(a)
	17.0	19.8	1.24	73.0	**36.88**	1.3	1.3	0.8	I	(a)
	17.0	23.7	1.48	73.0	**45.36**	1.6	1.4	0.9	I	(a)
	17.0	23.9	1.49	73.0	**45.36**	1.6	1.4	0.9	I	(a)
	17.0	23.9	1.49	73.1	**46.46**	1.7	1.4	0.9	I	(a)
	17.6	29.5	1.84	73.0	**55.33**	2.0	1.3	1.0	I	(c) + (b)
	17.2	29.8	1.84	72.9	**57.23**	2.1	1.4	1.0	I	(c) + (b)
	17.7	29.5	1.85	72.7	**55.83**	2.0	1.3	1.0	I + II	(d) + (b)
	17.4	29.7	1.86	73.3	**53.84**	2.0	1.3	1.0	I	(d) + (b)
	17.6	30.1	1.88	73.1	**56.33**	2.0	1.3	1.0	I	(d) + (b)
	17.6	30.8	1.93	73.0	**57.73**	2.1	1.3	1.0	I	(c) + (b)
	17.0	47.9	2.99	73.0	**87.34**	3.2	1.3	1.2	II + IV	(c) + (b)
	17.0	79.9	4.99	73.1	**88.73**	3.2	1.3	1.2	IV	(c) +(b)

(a): load rate 20kN/min (b): load rate 10kN/min (c): tube weld seam through bolt hole (d): tube weld seam to side of bolt hole

Table C.2 Tab bearing results, specimen dimensions for flattened 48mmdia-2mm thick tubes with square ends

DESCRIPTION	d_h (mm)	d_e (mm)	$\frac{d_e}{d}$	s (mm)	P (kN)	$\frac{P}{d\,t\,\sigma_o}$	$\frac{P}{\text{Eqn. 10.20}}$	$\frac{P}{\text{Eqn. 10.17}}$	FAILURE MODE	COMMENTS
2 x 2 mm/M16	**SQUARE ENDS, CUT OUT CORNERS, STRAIGHTENED TABS**									
	17.30	31.25	1.95	72.4	**56.83**	2.1	1.3	1.0	I +II	(f) + (b)
	17.40	31.30	1.95	72.4	**57.83**	2.1	1.3	1.0	I + II	
	17.40	31.30	1.96	72.5	**55.83**	2.0	1.3	1.0	I + II	(g)
	17.50	31.15	1.96	72.3	**57.33**	2.1	1.3	1.0	I + II	(b)
2 x 2mm/M20	**CHAMFERED ENDS**									
	21.00	32.20	1.61	73.1	**63.31**	1.84	1.4	0.97	I	(a)

(a): load rate 20kN/min (b): load rate 10kN/min (f): tubes plugged, tabs straightened and load (g): cyclic loading, 10cycles under load, then held for 10 mins

Table C.3 Tab bearing results, specimen dimensions for flattened 48mmdia-2mm thick tubes

DESCRIPTION	d_h (mm)	d_e (mm)	$\frac{d_e}{d}$	s (mm)	P (kN)	$\frac{P}{d\,t\,\sigma_o}$	$\frac{P}{\text{Eqn. 10.20}}$	$\frac{P}{\text{Eqn. 10.17}}$	FAILURE MODE	COMMENTS
2 x 2.5mm/M20	21.0	11.0	0.55	91.8	**11.72**	0.3	0.6	0.2	II	(a)
	21.0	11.0	0.55	91.9	**12.46**	0.3	0.6	0.2	II	(a)
	21.0	11.0	0.55	91.7	**12.96**	0.3	0.7	0.2	II	(a)
	21.0	14.8	0.74	91.9	**28.42**	0.7	1.1	0.5	II	(a)
	21.0	14.8	0.74	91.8	**30.41**	0.7	1.2	0.5	II	(a)
	21.0	14.5	0.73	91.6	**30.91**	0.7	1.2	0.5	II	(a)
	21.0	19.8	0.99	91.7	**46.36**	1.1	1.3	0.7	I	(a)
	21.0	20.0	1.00	91.9	**45.17**	1.1	1.3	0.7	I	(a)
	21.0	20.0	1.00	91.6	**45.86**	1.1	1.3	0.7	I	(a)
	21.0	24.8	1.24	91.9	**56.33**	1.3	1.3	0.8	I + II	(a)
	21.0	24.8	1.24	91.6	**57.33**	1.3	1.3	0.8	II	(a)
	21.0	25.0	1.25	91.8	**57.43**	1.4	1.3	0.8	II	(a)
	21.0	30.0	1.50	91.8	**67.30**	1.6	1.3	0.8	II	(c) + (b)
	21.0	30.0	1.50	91.8	**71.29**	1.7	1.3	0.9	I + II	(b)
	21.0	30.0	1.50	92.3	**68.89**	1.6	1.3	0.9	I	(b)
	21.1	30.4	1.52	91.9	**69.29**	1.6	1.3	0.9	I	(c) + (b)
	21.1	30.6	1.53	92.0	**70.29**	1.7	1.3	0.9	II	(c) + (e) + (b)
	21.1	30.8	1.54	92.0	**70.29**	1.7	1.3	0.9	I	
	21.0	30.8	1.54	91.8	**67.30**	1.6	1.2	0.8	II	(c) + (b)
	21.0	40.0	2.00	92.0	**91.73**	2.2	1.3	1.0	I + IV	(a)
	21.0	40.0	2.00	91.7	**94.22**	2.2	1.3	1.0	I + IV	(a)
	21.0	40.0	2.00	91.8	**96.71**	2.3	1.4	1.1	I + IV	(a)
	21.0	60.0	3.00	91.9	**134.1**	3.2	1.3	1.2	IV	(a)

(a): load rate 20kN/min (b): load rate 10kN/min (c): tube weld seam through bolt hole (d): tube weld seam to side of bolt hole (e): weld seam split during flattening

Table C.4 Tab bearing results, specimen dimensions for flattened 60mmdia-2.5mm thick tubes with square ends

DESCRIPTION	d_h (mm)	d_e (mm)	$\frac{d_e}{d}$	s (mm)	P (kN)	$\frac{P}{d\,t\,\sigma_o}$	$\frac{P}{\text{Eqn. 10.20}}$	$\frac{P}{\text{Eqn. 10.17}}$	FAILURE MODE	COMMENTS
2 x 2.5mm/M20	**FLATTENED 60 dia TUBES 2.5mm THICK**									
	21.0	29.8	1.49	91.3	**62.41**	1.5	1.2	0.8	I + II	(b)
	21.0	30.0	1.50	91.4	**68.79**	1.6	1.3	0.9	I + II	
	CHAMFERED ENDS									
	21.0	32.2	1.61	92.0	**73.78**	1.7	1.4	0.9	I	(a)
2 x 3.0mm/M16	**FLATTENED 76 dia TUBES 3.0mm THICK**									
	17.0	31.5	1.97	116.1	**92.72**	2.0	1.4	1.1	I	(a)
2 x 3.0mm/M20	**SQUARE ENDS**									
	21.0	30.0	1.50	116.0	**92.23**	1.7	1.5	1.0	I	(a)

(a): load rate 20kN/min (b): load rate 10kN/min

Table C.5 Specimen dimensions and tab bearing results, for flattened 60mm dia-2.5mm thick and 76 mm dia-3mm thick tubes

DESCRIPTION	d_h (mm)	d_e (mm)	$\frac{d_e}{d}$	P (kN)	$\frac{P}{d\,t\,\sigma_o}$	$\frac{P}{\text{Eqn. 10.20}}$	$\frac{P}{\text{Eqn. 10.17}}$	FAILURE MODE	COMMENTS
2x2.0mm/M16	**48mm dia tubes**								
	N.A	30.6	1.91	**56.4**	2.1	1.3	1.0	I + II	
2x2.5mm/M16	**60mm dia tubes**								
	N.A	30.0	1.50	**54.7**	1.3	1.0	0.7	I + II	
2x3.0mm/M16	**70mm dia tubes**								
	22.0	28.0	1.75	**84.22**	2.1	1.4	1.0	I + II	
2x3.0mm/M16	**76mm dia tubes**								
	17.0	31.5	1.97	**59.86**	1.4	0.9	0.7	I + II	(h)

(h): joint packing between channels omitted.

Table C.6 Frame test tab bearing results